Medical Radiology · Diagnostic Imaging
Series Editors: Hans-Ulrich Kauczor · Paul M. Parizel · Wilfred C.G. Peh

Mohamed Fethi Ladeb
Wilfred C. G. Peh *Editors*

Imaging of Tuberculosis

Springer

Medical Radiology

Diagnostic Imaging

Series Editors

Hans-Ulrich Kauczor
Paul M. Parizel
Wilfred C. G. Peh

The book series *Medical Radiology – Diagnostic Imaging* provides accurate and up-to-date overviews about the latest advances in the rapidly evolving field of diagnostic imaging and interventional radiology. Each volume is conceived as a practical and clinically useful reference book and is developed under the direction of an experienced editor, who is a world-renowned specialist in the field. Book chapters are written by expert authors in the field and are richly illustrated with high quality figures, tables and graphs. Editors and authors are committed to provide detailed and coherent information in a readily accessible and easy-to-understand format, directly applicable to daily practice.

Medical Radiology – Diagnostic Imaging covers all organ systems and addresses all modern imaging techniques and image-guided treatment modalities, as well as hot topics in management, workflow, and quality and safety issues in radiology and imaging. The judicious choice of relevant topics, the careful selection of expert editors and authors, and the emphasis on providing practically useful information, contribute to the wide appeal and ongoing success of the series. The series is indexed in Scopus.

Mohamed Fethi Ladeb
Wilfred C. G. Peh
Editors

Imaging of Tuberculosis

Springer

Editors
Mohamed Fethi Ladeb
Department of Radiology
Mohamed Kassab Orthopedic Institute
Tunis, Tunisia

Wilfred C. G. Peh
Department of Diagnostic Radiology
Khoo Teck Puat Hospital
Singapore, Singapore

ISSN 0942-5373 ISSN 2197-4187 (electronic)
Medical Radiology
ISSN 2731-4677 ISSN 2731-4685 (electronic)
Diagnostic Imaging

ISBN 978-3-031-07039-6 ISBN 978-3-031-07040-2 (eBook)
https://doi.org/10.1007/978-3-031-07040-2

© The Editor(s) (if applicable) and The Author(s), under exclusive license to Springer Nature Switzerland AG 2022
This work is subject to copyright. All rights are solely and exclusively licensed by the Publisher, whether the whole or part of the material is concerned, specifically the rights of translation, reprinting, reuse of illustrations, recitation, broadcasting, reproduction on microfilms or in any other physical way, and transmission or information storage and retrieval, electronic adaptation, computer software, or by similar or dissimilar methodology now known or hereafter developed. The use of general descriptive names, registered names, trademarks, service marks, etc. in this publication does not imply, even in the absence of a specific statement, that such names are exempt from the relevant protective laws and regulations and therefore free for general use.
The publisher, the authors and the editors are safe to assume that the advice and information in this book are believed to be true and accurate at the date of publication. Neither the publisher nor the authors or the editors give a warranty, expressed or implied, with respect to the material contained herein or for any errors or omissions that may have been made. The publisher remains neutral with regard to jurisdictional claims in published maps and institutional affiliations.

This Springer imprint is published by the registered company Springer Nature Switzerland AG
The registered company address is: Gewerbestrasse 11, 6330 Cham, Switzerland

This book is dedicated with much grateful appreciation to our parents,
The late Mr. Mohamed Ladeb,
Mrs. Zeineb Ladeb,
The late Dr. Peh Eng Teck, and
Mrs. Libby Tin Peh

Preface

Tuberculosis remains a global health concern despite substantial investment in healthcare services over the recent few decades. The worldwide impact of tuberculosis is extremely important, considering that approximately ten million people develop tuberculosis annually, with more than 1.3 million deaths from this disease. The clinical features of tuberculosis can be nonspecific and often occur insidiously. Imaging has an important role in its early diagnosis, particularly in patients presenting with nonspecific symptoms. It helps to detect disease, guide appropriate laboratory investigation, confirm the diagnosis, and monitor the disease progress and response to treatment, with the aim of achieving effective treatment outcome and prevention of complications.

Radiographs are an excellent screening tool and are typically the initial radiological investigation for suspected pulmonary and musculoskeletal tuberculosis. Computed tomography (CT) is utilized to further evaluate pulmonary, abdominal, urogenital, and head and neck tuberculosis. Magnetic resonance imaging is the modality of choice for assessing tuberculosis of the brain, spine, and musculoskeletal system. Positron-emission tomography/CT has a gradually increasing role in the detection of multifocal tuberculosis lesions and assessment of the response to treatment. Imaging techniques, such as ultrasound and CT, are used to guide diagnostic and therapeutic aspirations and drainages, as well as biopsies for histopathological and bacteriological confirmation of tuberculosis.

Imaging of Tuberculosis, extensively illustrated by 650 images, aims to provide an updated and comprehensive coverage of multimodality imaging of tuberculosis affecting all regions of the human body. This book comprises 15 chapters, with the first 3 chapters dealing with the epidemiology, pathophysiology, bacteriology, and histopathology of tuberculosis. Following a chapter on an overview of imaging techniques, the subsequent chapters are devoted to imaging features of tuberculosis located in all the different body systems. Tuberculosis in patients with human immunodeficiency virus co-infection is also addressed. The last chapter presents decision algorithms relating to diagnosis and management of tuberculosis.

This book is written by a combination of experienced authors from Tunisia, Singapore, Thailand, India, and the Philippines. Besides the various subspecialty radiologists, other authors include experts in bacteriology,

histopathology, infectious disease, respiratory medicine, and otorhinolaryngology—head and neck surgery. *Imaging of Tuberculosis* aims to be a useful and practical reference for all doctors who deal with tuberculosis.

Tunis, Tunisia — Mohamed Fethi Ladeb
Singapore, Singapore — Wilfred C. G. Peh
November 2021

Contents

Epidemiology of Tuberculosis

Lamia Ammari, Aida Berriche, Ikbel Kooli, Wafa Marrakchi, and Mohamed Chakroun

Contents

L. Ammari (✉) · A. Berriche
Department of Infectious Diseases, La Rabta University Hospital, Tunis, Tunisia
e-mail: ammarilamia3@gmail.com

I. Kooli · W. Marrakchi · M. Chakroun
Department of Infectious Diseases, Fattouma Bourguiba Hospital, Monastir, Tunisia

Faculty of Medicine of Monastir, University of Monastir, Monastir, Tunisia
e-mail: chakrounme@gmail.com

Abstract

Tuberculosis (TB) is a life-threatening bacterial disease that is prevalent in several regions of the world. TB usually manifests with pulmonary infection. However, other areas of the body can be affected. The main risk factors for acquiring TB include immunosuppression, diabetes mellitus, lung disease, end-stage renal disease, gastrectomy, malnutrition, tobacco smoking and drug use. Worldwide, the most important risk factor for TB is human immunodeficiency virus infection. Tuberculous lymphadenitis, pleuritis, and spondylodiscitis are the most common forms of extrapulmonary TB. Although central nervous system infections are increasingly rare, they are one of the most devastating clinical forms of TB.

Abbreviations

EPTB	Extrapulmonary tuberculosis
HIV	Human immunodeficiency virus
TB	Tuberculosis

1 Introduction

Tuberculosis (TB) is still prevalent in many regions of the world and is the leading cause of death due to infectious disease. Every year, about

© The Author(s), under exclusive license to Springer Nature Switzerland AG 2022

M. F. Ladeb, W. C. G. Peh (eds.), *Imaging of Tuberculosis*, Medical Radiology Diagnostic Imaging,
https://doi.org/10.1007/978-3-031-07040-2_1

ten million people develop TB disease and approximately 1.3 million people die of it (World Health Organization 2021). Worldwide, the most important risk factor for TB is human immunodeficiency virus (HIV) infection. TB usually affects the lungs. However, other areas of body can be affected, with extrapulmonary TB (EPTB) accounting for 16% of cases worldwide; its incidence varies from region to region (World Health Organization 2021). The main extrapulmonary locations of TB are the lymph nodes, pleura, bones, and meninges.

TB is caused by one of several mycobacterial species that belong to the *Mycobacterium tuberculosis* complex. The human pathogens are *M. tuberculosis*, *M. africanum*, and *M. bovis*. *M. tuberculosis* is the most important of the human pathogens and most often affects the lungs. *M. africanum* causes up to half of human TB in West Africa (De Jong et al. 2010) *M. bovis* is mostly found in cattle and less frequently in other animals such as bison, elk, and deer. *M. bovis* causes TB disease that affects the lungs, lymph nodes and rarely, other parts of the body. *M. tuberculosis* and *M. africanum* spread from person to person through the air and most frequently causes pulmonary TB, while *M. bovis* is transmitted through unpasteurized dairy products and frequently causes lymph node TB.

2 Frequency and Distribution

TB is a ubiquitous and life-threatening bacterial disease that is prevalent in many regions of the world. It is estimated that one-quarter of the world's population are infected with *M. tuberculosis* and have latent TB, which means that they have been infected by *M. tuberculosis* but are not yet ill with the disease and cannot transmit the bacteria. People infected with *M. tuberculosis* have a 5–15% lifetime risk of falling ill with TB (World Health Organization 2021). The global incidence of TB peaked around 2003 and appears to be declining slowly (World Health Organization 2021). According to the World Health Organization (WHO), globally, an estimated 9.9 million people fell ill with TB in 2020. Among them, 5.8 million people were reported to have been newly diagnosed and notified (new and relapsed cases) (World Health Organization 2021). As an impact of the COVID-19 pandemic on TB services in 2020, there was a large global drop in the number of people newly diagnosed with TB and reported, with a fall of 18% between 2019 and 2020. Globally, the cumulative reduction in the TB incidence rate was 11% from 2015 to 2020 (World Health Organization 2021).

Geographically, in 2020, most TB cases were found in the WHO regions of South-East Asia (43%), Africa (25%), and the Western Pacific (18%), with smaller shares in the Eastern Mediterranean (8.3%), the Americas (3.0%), and Europe (2.3%). The 30 high TB burden countries accounted for 86% of all estimated incident cases worldwide, and eight of these countries accounted for two-thirds of the global total: India (26%), China (8.5%), Indonesia (8.4%), the Philippines (6.0%), Pakistan (5.8%), Nigeria (4.6%), Bangladesh (3.6%), and South Africa (3.3%) (World Health Organization 2021). There were 150–400 cases per 100,000 population in most of the 30 high TB burden countries, and more than 500 cases per 100,000 population in the Central African Republic, the Democratic People's Republic of Korea, Lesotho, the Philippines, and South Africa (World Health Organization 2021).

3 Age and Gender

TB can affect anyone, regardless of gender or age. In 2020, men older than 15 years accounted for 56% of the people who developed TB, while women older than 15 years accounted for 33%, and children for 11%. Among all those affected, 8% were people living with human immunodeficiency virus (PLHIV) (World Health Organization 2021). The proportion of TB cases co-infected with HIV was highest in countries in the WHO African Region, exceeding 50% in parts of southern Africa. (World Health Organization 2021). For PLHIV, TB is more frequent in males. A systematic review and meta-analysis noted that TB prevalence is significantly higher among men than women in low- and

middle-income countries (Horton et al. 2016). However, the reasons for the observed gender bias are not clear. Both gender (referring to sociocultural roles and behavior) and sex-related factors (referring to biological aspects) likely contribute to higher TB rates in men (Hertz and Schneider 2018).

4 Risk Factors

It is important to identify the comorbidities and circumstances at risk of acquiring TB to ensure adequate prevention and management of all the diseases that each patient may have. Several medical conditions are risk factors for TB, and TB can complicate the course of some diseases. The risk factors for acquiring TB include immunosuppression, noncommunicable diseases (e.g., diabetes mellitus, lung disease, end-stage renal disease), gastrectomy, malnutrition, tobacco smoking, and drug use. Worldwide, the most important risk factor for TB is HIV infection. PLHIV are 15–22 times more likely to develop TB than persons without HIV. TB is the most common presenting illness among PLHIV, including those on anti-retroviral treatment, and it is the major cause of HIV-related death (World Health Organization 2021). Several immunosuppressive diseases and conditions may increase the occurrence of TB; including head and neck cancers, lung cancer, Hodgkin lymphoma, non-Hodgkin lymphoma, leukemia, prolonged corticosteroid therapy, and immunosuppressive therapy.

The use of tumor necrosis factor (TNF) inhibitors for the treatment of rheumatic diseases has been associated with a significant increase in incident cases of TB. A large retrospective study conducted in Brazil showed that TNF inhibitor exposure was associated with an increased TB incidence of 18 times. Adalimumab and certolizumab were found to be associated with greater and earlier TB diagnosis, compared to etanercept (Sartori et al. 2019). TB and sarcoidosis are chronic granulomatous diseases that rarely exist simultaneously. The relationship between these two diseases is not yet clear, with the hypothesis that mycobacterial antigen in genetically predisposed hosts may cause sarcoidosis being still controversial. Both diseases have clinical, radiological, and histopathological similarities. The differential diagnosis is often challenging but is crucial in treatment decision-making since immunosuppressive treatment of sarcoidosis is undesirable in people having TB (Pedroso et al. 2020).

Diabetes mellitus is one of the most common noncommunicable disease worldwide. The risk of TB among people with diabetes mellitus is 2–3 times higher than among those without diabetes mellitus. Diabetes mellitus can worsen the clinical course of TB, and TB can worsen glycemic control in people with diabetes mellitus (World Health Organization 2021). Malnutrition may occur after gastrectomy or chronic malabsorption syndromes, and it is common in low-income countries. Malnutrition is often highly prevalent in some countries, and there is a relationship between malnutrition and TB. Malnutrition increases the risk of TB and TB can lead to malnutrition (World Health Organization 2021). Chronic obstructive lung disease and some occupational lung diseases are also risk factors for TB. For example, people with silicosis have approximately 30-fold greater risk for developing TB (Centers for Disease Control and Prevention 2000).

Although TB and sickle cell anemia (SCA) may affect the same population in some areas with a high TB prevalence, e.g., Africa, little data on the epidemiological and clinical patterns are available about this comorbid condition affecting both children and adults. A retrospective French cohort study of children with SCA showed no difference regarding the location and evolution of TB. It should be noted that this is likely due to the protective effect of Bacillus Calmette–Guérin (BCG) vaccine, good nutritional state, and low risk of TB exposure of children in this cohort. However, alterations of the efficacy of BCG immunization have not been investigated in the specific context of SCA (Droz et al. 2017).

The available data on TB during pregnancy are of low quality. The WHO recommendation for TB screening, especially in high-burden

areas, is not well implemented and most countries do not report the pregnancy status of female TB cases (Bates et al. 2015). Overall, pregnant women are at increased risk of TB. The immunological changes appearing during pregnancy may promote the occurrence or reactivation of TB. It is known that neonates born to mothers who have active TB disease may contract TB congenitally. However, the incidence of congenital TB seems to be very underestimated. Congenital TB may be subclinical or associated with various birth defects (Bates et al. 2015). One study that included 35 consecutive pregnancies showed that maternal TB is associated with increased risk of prematurity, lower birth weight, and risk of death. Pulmonary location of TB and late start of treatment in infected mothers increase the risk of perinatal death and neonatal morbidity (Figueroa-Damián and Arredondo-García 2001). Thus, it is crucial to identify the comorbidities in people diagnosed with TB in order to ensure appropriate comanagement.

As TB is a contagious disease, people with active TB can infect 10–15 other people through close contact over the course of a year. Therefore, close-contact situations such as case contact of people diagnosed with TB, healthcare workers, and prisoners are high TB risks. The prevalence of TB in prisons is usually much higher than in the general population (Valença et al. 2015).

Without appropriate treatment, about 45% of HIV-negative people with TB and nearly all HIV-positive people with TB will die. In 2019, 1.3 million HIV-negative people died from TB, with addition of another 214,000 deaths among HIV-positive people (World Health Organization 2021). Mortality related to TB can be significant in some situations. A systematic review of risk factors for death in adults during and after TB treatment revealed that risk factors for death in settings with high TB incidence are co-infection with HIV, people with advanced immunodeficiency, sputum smear-negative TB, and malnutrition (Waitt and Squire 2011).

In some countries with low TB incidence and HIV prevalence, risk factors may include non-infectious comorbidities such as diabetes mellitus, cancer, sputum smear-positive TB, tobacco smoking, alcohol and drug abuse (Waitt and Squire 2011). Studies in different areas have also shown that older age, male gender, comorbid medical conditions such as chronic obstructive pulmonary disease and hypertension, drug resistance, and residence in long-term care facilities are significant risk factors of death in patients with TB (Horne et al. 2010; Waitt and Squire 2011). It should be noted that maternal mortality is high among women co-infected with HIV and TB, and TB is associated with increased mortality both during pregnancy and post-partum (Bates et al. 2015).

5 Locations

TB usually affects the lungs, but it can also affect other parts of the body, such as the lymph nodes, pleura, bone (particularly the spine), central nervous system (CNS), and urinary tract. Statistical data about TB locations vary considerably according to countries and regions. EPTB comprised 16% of the 7.1 million incident cases that were notified in 2019, ranging from 8% in the Western Pacific region to 24% in the Eastern Mediterranean region (Ambreen et al. 2021). Because it is a curable and preventable disease, early diagnosis, treatment, and prevention of TB are crucial.

5.1 Pulmonary Tuberculosis

Pulmonary TB is by far the most common form of TB and can be primary or post-primary. Worldwide, 4.8 million people were diagnosed with pulmonary TB in 2020. 59% of these cases were bacteriologically confirmed, with variations among different regions and countries, ranging from the highest percentage in the Americas (77%) to the lowest in the Western Pacific (55%). The ultimate outcome of primary TB infection is dependent on efficacy of the cell-mediated response and/or the initial inoculum. In 90% of cases, the immune system is usually able to control and/or eradicate the infection; and the original and disseminated foci are walled off and

destroyed. However, in 10% of patients, post-primary TB develops when a host is reinfected with TB or probably more commonly when a previously walled-off primary focus reactivates and proliferates. Some of the most important factors which may lead to reactivation are acquired immunodeficiency syndrome (AIDS), malignancy, organ transplant, chemotherapy, steroids, and TNF inhibitors (Eddy et al. 2018).

5.2 Miliary Tuberculosis

Epidemiological data are not available on the true prevalence of miliary TB. Some studies noted that miliary TB is a rare form of TB, occurring in less than 2% of cases. However, the mortality rate may rise to up to 33%, due to delay in diagnosis (Sharma et al. 2012). In autopsy studies in adults, miliary TB has been documented in a higher proportion of patients, accounting for 0.3–13.3% of all autopsies and 11.9–40.5% of all cases of TB. Before 1980, miliary TB was predominantly considered a disease of infants and children but it has since become more frequently recognized in adults, with this epidemiological change being due to the global pandemic of HIV/AIDS and increasing use of immunosuppressive drugs such as TNF inhibitors. Miliary TB also seems to be more frequent in men and among African Americans (Sharma et al. 2012). Several conditions are associated with miliary tuberculosis, namely childhood infections, malnutrition, HIV/AIDS, alcoholism, chronic kidney disease, dialysis, postgastrectomy, organ transplantation, immunosuppressive drug use, connective tissue disorders, pregnancy, post-partum, presence of an underlying malignancy, and silicosis (Sharma et al. 2012).

5.3 Thoracic Extrapulmonary Tuberculosis

Outside the pulmonary parenchyma, TB can invade any structure of the thorax, causing significant clinical disease (Cantres-Fonseca 2020). Thoracic EPTB includes involvement of the pleura, lymph nodes, heart and blood vessels, bone and skin, and even the chest wall. TB can also cause significant disease if it reaches the thoracic spine (Cantres-Fonseca 2020). After tuberculous lymphadenitis, pleural TB is the second most common extrapulmonary presentation of TB disease (Macías et al. 2019; Cantres-Fonseca 2020). 3–25% of patients with TB have tuberculous pleuritis. The incidence of tuberculous pleuritis is higher in PLHIV (Cohen and Light 2015).

Internal thoracic lymphadenopathy has been found to be present in 50 of 137 (36.5%) cases with culture-confirmed active pulmonary TB (Bernheim et al. 2020). The most common extraparenchymal invasion of mycobacteria in the thorax occurs at the supraclavicular, mediastinal, and hilar lymph nodes (Cantres-Fonseca 2020). The incidence of tracheobronchial TB has declined compared with the preantibiotic era but this complication still affects patients with advanced disease, particularly in endemic areas. Mycobacterial implantation to the tracheobronchial wall in patients with TB may originate from infected sputum, extension from adjacent parenchymal infection, regional lymph nodes, or hematogenous spread (Restrepo et al. 2016).

Heart and thoracic blood vessel involvement by TB is rare. Tuberculous involvement of the heart includes infection of the pericardium, cardiac muscle, and large blood vessels such as the aorta (Cantres-Fonseca 2020). Tuberculous pericarditis is the most common cardiovascular complication of TB. It is found in approximately 1% of all autopsied cases of TB (Mayosi et al. 2005; Restrepo et al. 2016) and in 1–2% of patients with pulmonary infection; remaining the most common manifestation in countries with a high prevalence of TB (Agarwal et al. 2005; Mayosi et al. 2005; Restrepo et al. 2016; Cantres-Fonseca 2020). Constrictive pericarditis is one of the most serious complications of tuberculous pericarditis, being reported in as many as half of affected patients with pericardial TB infection (Restrepo et al. 2016). Myocardial involvement by *M. tuberculosis* is less common than pericardial disease. Before the cross-sectional imaging era, it was rarely diagnosed ante-mortem. It is usually due to tuberculomas that are commonly

associated with miliary or extensive TB, which may present as a diffuse infiltrative process or as a nodular or mass-like lesion (Restrepo et al. 2016).

TB of the chest wall is an uncommon manifestation, constituting less than 5% of all musculoskeletal TB. It is far less common than other more commonly-affected skeletal sites, such as the spine, pelvis, hip and knee joints. Excluding the spine, the most affected site is the ribs. It can also affect the sternum, sternoclavicular joints, as well as involve soft tissues, including myositis, cellulitis, and breast infection. It is not clear whether chest wall infection occurs from reactivation of latent foci formed during hematogenous or lymphatic dissemination from the primary infection, or from direct extension contiguous with the lung and pleura (Restrepo et al. 2016; Cantres-Fonseca 2020).

5.4 Head and Neck Tuberculosis

Extrapulmonary involvement can occur in isolation or along with a pulmonary focus in patients with disseminated TB (Yashveer and Kirti 2015). Head and neck TB is quite common in endemic countries but is still misdiagnosed due to its varied presentation and different sites of involvement (Monga et al. 2017). It accounts for 10% of patients with TB. TB can affect most of the organs in the head and neck region, such as cervical lymph nodes, larynx, middle ear, oral cavity, sinonasal region, and pharynx (Das et al. 2016; Monga et al. 2017; Pang et al. 2018).

Adolescents and adults are the most affected by head and neck TB. In a Chinese study consisting of 60 patients, the average age was 44.6 ± 14.8 years (range 5–76 years) (Pang et al. 2018). In two Indian studies, the most common age group affected was 21–30 years and 15–24 years (range 3–70 years old), respectively (Yashveer and Kirti 2015; Das et al. 2016). In a Polish study, the average age was 60.6 years, with the age of men ranging from 36 to 75 years (mean 62.5 years) and of women from 21 to 78 years (mean 59.0 years) (Bruzgielewicz et al. 2014). In a Japanese study, the most commonly affected age group was 50–59 years, with a mean of 52.9 years (Oishi et al. 2016). Male-to-female ratio varied from 0.39 to 0.74 (Oishi et al. 2016; Yashveer and Kirti 2015; Das et al. 2016; Monga et al. 2017; Pang et al. 2018). A male predominance was noted in a one Polish study comprising 43 men and 30 women (Bruzgielewicz et al. 2014).

Because the early manifestations of head and neck TB are often similar to neoplasms or inflammation and because the systemic symptoms of TB may not be obvious, clinical consideration of head and neck TB usually occurs only after ineffective anti-inflammatory treatment, biopsy, or even surgical resection. Cervical lymph node TB (90.5–92.9%), laryngeal TB, oropharyngeal TB, salivary gland (parotid and submandibular) TB, and TB of the paranasal sinuses, skin and oral mucosa are the commonest locations (Bruzgielewicz et al. 2014; Oishi et al. 2016; Yashveer and Kirti 2015; Das et al. 2016; Monga et al. 2017; Pang et al. 2018). 65% of affected patients have no history of contact with known cases of TB while 35% give a definite history of contact with TB (Das et al. 2016).

5.5 Spinal Tuberculosis

Tuberculous spondylodiscitis, known as Pott disease, accounts for less than 5% of all cases of TB cases (Kristensen et al. 2017; Javed et al. 2018; Pu et al. 2019) but it comprises 50–60% of cases of osteoarticular TB and is the one of the most common forms of EPTB (Kristensen et al. 2017; Pu et al. 2019). Diagnosis of tuberculous spondylodiscitis is relatively difficult because it is slowly progressive. When the diagnosis is late, it can lead to irreversible neurological injury (Kristensen et al. 2017; Liu et al. 2019; Pu et al. 2019). Worldwide, 80% of patients with tuberculous spondylodiscitis are in developing countries and poverty-stricken areas (Liu et al. 2019). Spinal TB represents 10–35% of cases of spinal infections (Chen et al. 2016; Menon and Sorour 2016; Javed et al. 2018; Liu et al. 2019). In a Spanish study, an increase in cases of tuberculous spondylodiscitis from 14% to 45.2% among

foreign-born residents in Barcelona over a 10-year period was reported (Javed et al. 2018). In another Spanish study including 108 patients, TB was the second highest cause of spinal infections after *Staphylococcus* spp. (Cebrián Parra et al. 2012). Tuberculous spondylodiscitis is most commonly seen in patients older than 40 years (Batirel et al. 2015; Pu et al. 2019), has a male predominance (Batirel et al. 2015; Erdem et al. 2015), and predominately affects the thoracic and lumbar spine (Chen et al. 2016; Liu et al. 2019).

5.6 Musculoskeletal Tuberculosis

Musculoskeletal TB represents 1–3% of all TB and 5–6% of EPTB. Of these, arthritis accounts for 60%, osteitis for 38%, and bursitis and tenosynovitis for only 2% (De Backer et al. 2009; Ladeb et al. 2013). Concurrent pulmonary TB is observed in approximately 50% of cases (De Backer et al. 2009). Musculoskeletal TB is frequent in TB-endemic regions such as Africa, Asia, and South America. In developed countries, it mainly affects immigrants and immunocompromised people (Ladeb et al. 2013). In the latter, the distribution is approximately equal between male and female patients (Aït Khaled et al. 1997; Pertuiset et al. 1997). The average age of onset is constantly decreasing. In developed countries, it is 50 years of age in native people and 30 years in immigrants (Ladeb et al. 2013). Musculoskeletal TB appears to be uncommon in HIV-infected subjects, with an incidence of 0–9% (Hamza 1993; Aït Khaled et al. 1997; Pertuiset et al. 1997), in contrast to atypical mycobacterial bone infections (Bernard and Perronne 1997).

5.7 Central Nervous System Tuberculosis

Infection of the CNS is one of the most devastating clinical manifestations of TB. CNS involvement occurs in 5–10% of EPTB cases, and accounts for approximately 1% of all TB cases (Cherian and Thomas 2011). In an American epidemiological study of EPTB, up to 10% of cases had CNS involvement (Rieder et al. 1990), while the Centers for Disease Control and Prevention (CDC) data indicated that 6.3% of extrapulmonary cases (1.3% of total TB cases) have CNS TB. Risk factors for CNS TB include age (children > adults), HIV co-infection (Rana et al. 2000), malnutrition, recent measles in children (Yaramiş et al. 1998), alcoholism, malignancies, the use of immunosuppressive agents in adults, and disease prevalence in the community (Phypers et al. 2006).

5.8 Urogenital Tuberculosis

TB affecting the kidneys, ureters, bladder, prostate, urethra, penis, scrotum, testicles, epididymis, vas deferens, ovaries, fallopian tubes, uterus, cervix, and vulva were initially grouped together as genitourinary TB (Kulchavenya et al. 2016; Adhikari and Basnyat 2018). Currently, urinary tract TB occurs more often than genital TB (Kulchavenya et al. 2016), hence the designation of urogenital TB. In females, the genital organs commonly affected are the fallopian tube (95–100%), endometrium (50–60%), ovaries (20–30%), cervix (5–15%), myometrium (2.5%), and vulva/vagina (1%) (Gatongi et al. 2005). Male genital TB is predominantly associated with TB of the kidney and prostate (Kulchavenya and Khomyakov 2006). Renal and prostatic TB are usually due to hematogenous spread of mycobacterium from a chronic latent pulmonary infection. The proportion of urogenital TB among forms of EPTB varies according to geographical region, from 15–20% in Africa, Asia, Eastern Europe, and the Russian Federation to 2–10% in Western Europe and USA (Figueiredo et al. 2008**;** Muneer et al. 2019). The exact prevalence of urogenital TB in various geographical locations and specific patient groups is difficult to estimate because a considerable number of patients remain asymptomatic and are undiagnosed. Urogenital TB has been reported to affect twice as many women as men, but this estimate is controversial owing to the lack of controlled epidemiological and clinical studies. Increased rates of TB are seen in patients who have had a kidney transplant, have

end-stage renal disease, and are undergoing peritoneal dialysis (Rieder et al. 1990; Anand et al. 2017; Muneer et al. 2019).

5.9 Abdominal Tuberculosis

Abdominal TB includes involvement of the gastrointestinal (GI) tract, peritoneum, abdominal lymph nodes, and/or solid organs. Abdominal TB is a rare form of EPTB (Nayagam et al. 2016; Cho et al. 2018), and comprises around 5% of all cases of TB worldwide (Sharma and Mohan 2004; Rathi and Gambhire 2016; Vaid and Kane 2017). Its diagnosis remains one of the most challenging tasks in clinical practice (Khan et al. 2006; Nayagam et al. 2016; Abu-Zidan and Sheek-Hussein 2019). It is difficult to diagnose due to its non-specific clinical presentation, variable anatomical location, and lack of sensitive diagnostic tools (Nayagam et al. 2016; Cho et al. 2018). Abdominal TB may occur anywhere within the abdomen, involving the GI tract, solid organs, or peritoneum (Khan et al. 2006; Cho et al. 2018; Abu-Zidan and Sheek-Hussein 2019). It can affect a single abdominal organ, without chest involvement (Abu-Zidan and Sheek-Hussein 2019).

5.9.1 Gastrointestinal Tuberculosis

GI TB accounts for 1–3% of all TB cases worldwide (Sheer and Coyle 2003) and for about 11–16% of EPTB (Udgirkar et al. 2019). It can occur in the context of active pulmonary disease or as a primary infection without pulmonary involvement. Female predominance of GI TB or equal sex predisposition has been reported (Sreeramareddy et al. 2008). The entire GI tract, from esophagus to anus, can be involved. The ileocecal region is the most common location, being involved in 44–93% of cases (Al-Bahrani and Al-Saleem 1982; Gilinsky et al. 1983; Marshall 1993). The colon and small bowel alone are the next most frequent sites of infection, while the esophagus and stomach are rarely involved. However, any part of the GI tract may be affected (Horvath and Whelan 1998; Rathi and Gambhire 2016).

The increased risk of developing GI TB may be due to a variety of risk factors. GI TB appears to present more frequently and in a more severe form in PLHIV (Donoghue and Holton 2009). In line with this data, a Korean study demonstrated that a higher Charlson comorbidity index (predicts 10-year survival in patients with multiple comorbidities) is associated with development of GI TB (Hong et al. 2013). The prevalence of GI TB appears to vary significantly by geographical location. In North America, GI involvement by TB is one of the least prevalent types of extrapulmonary infection (World Health Organization 2018), whereas it remains a more significant concern in parts of the Middle East, Africa, and Asia. In Saudi Arabia, GI TB represents the most common type of EPTB, with 15.8% of cases affecting the alimentary tract (Al Karawi et al. 1995). However, in Canada, GI TB represents only 4.2% of the cases of EPTB (Akgun 2005). The risk factors of GI TB are immunocompromised people (PLHIV and people using immunosuppressive therapy) and immigrants from regions with a high prevalence of TB (Kawazoe and Nagata 2012). Among immunocompromised patients, several transplant database studies suggest that renal transplant patients appear to be at a particular risk for pulmonary and EPTB. However, in these studies, the absolute numbers of GI TB cases are low (Ulloa et al. 2014). Several reports indicate that female gender may be an additional risk factor for GI TB (Musellim et al. 2005; De Backer et al. 2006).

5.9.2 Abdominal Solid Organ and Peritoneal Tuberculosis

Abdominal TB is a great mimicker (Nayagam et al. 2016; Abu-Zidan and Sheek-Hussein 2019), with single solid organ abdominal TB being able to mimic pancreatic tumor, colonic cancer, gastric cancer, and lymphoma. It can also mimic inflammatory or infectious diseases such as appendicitis, acute cholecystitis, and typhoid fever (Cho et al. 2018; Abu-Zidan and Sheek-Hussein 2019). Solid organ TB represents 3.1–20.4% of all cases of abdominal TB (Sinan et al. 2002; Khan et al. 2006; Nayagam et al. 2016). It is rarely seen in isolation, and is more frequently part of multifocal or disseminated disease (Sinan

et al. 2002). The liver and spleen are the main organs involved (Sinan et al. 2002), with the liver frequently affected in association with miliary TB (Ahmed and Hassan 1994). Liver and spleen TB can occur in the form of microabscesses in miliary TB. Often, the only feature of solid organ TB is organomegaly, with calcified granulomas visible in late-stage disease or after healing (Sinan et al. 2002). Macronodular forms are rare (Ahmed and Hassan 1994). Pancreatic TB is rare and may result from either hematogenous dissemination or direct spread of disease from adjacent nodes. It may also mimic pancreatic tumors (Ahmed and Hassan 1994; Sinan et al. 2002).

Tuberculous peritonitis is usually part of miliary TB, but may be secondary to GI or genital TB (Ahmed and Hassan 1994). It can be acute or chronic (Ahmed and Hassan 1994). Liver cirrhosis, diabetes mellitus, and renal failure requiring continuous ambulatory peritoneal dialysis have all been demonstrated to be significant risk factors in the development of peritoneal TB (Wu et al. 2019). Peritoneal TB can be classified as "wet" or "dry" peritonitis (Palmer et al. 1985; Sinan et al. 2002; Srivastava et al. 2014; Wu et al. 2019). The "wet" (55.3%) and the "dry" (44.7%) types of peritonitis were both commonly found in a Kuwaiti study (Sinan et al. 2002). The peritoneum is the sixth most common extrapulmonary site in the USA; being seen in up to 3.5% of cases of pulmonary TB, 31–58% of cases of abdominal TB (Srivastava et al. 2014), and 0.1–0.7% of all TB cases (Wu et al. 2019). Peritoneal TB represents 30–83% of abdominal TB (Palmer et al. 1985; Wells et al. 1986; Cho et al. 2018; Sinan et al. 2002; Uygur-Bayramiçli et al. 2003; Khan et al. 2006; Nayagam et al. 2016).

6 Treatment Outcomes

Adherence to prescribed TB treatment remains a critical component of clinical care and global TB control. It may strongly influence the outcome of therapy, as well as prevention and control (Vernon et al. 2019; Bea et al. 2021). Poor adherence may result in prolonged disease infectiousness, relapse, drug resistance, worsening of the condition and death. A recent cohort study in South Korea showed that approximately 45% of patients with TB were nonadherent to drug therapy, which is a major concern for treatment outcome (Bea et al. 2021). Hence, healthcare providers should pay special attention to reinforce patients' adherence throughout the course of TB treatment. One of the concerns of the outcome of TB is possible occurrence of relapse after successful treatment. Reported rates of relapse after the standard 6 months of treatment for drug-susceptible pulmonary TB range from 1% to 2% at 24 months (Jo et al. 2014; Cudahy et al. 2020). The main conditions associated with an increased risk of TB relapse are drug resistance, smoking, HIV infection with low CD4 cell count, substance abuse, chronic lung disease, sputum smear-positive disease, and cavitary pulmonary disease (Jo et al. 2014; Cudahy et al. 2020).

Drug-resistant TB continues to be a public health threat. In 2019, close to half a million people worldwide developed rifampicin-resistant TB (RR-TB), of which 78% had multidrug-resistant TB (MDR-TB). The three countries with the largest share of the global burden are India (27%), China (14%), and the Russian Federation (8%). Globally in 2019, 3.3% of new TB cases and 17.7% of previously treated cases had MDR/RR-TB. The highest proportions (>50% in previously treated cases) were found in countries of the former Soviet Union (Liu et al. 2011; World Health Organization 2021).

BCG is currently the only available TB vaccine. While the BCG vaccine has demonstrated significant effectiveness in several populations, protection has not been consistent against all forms of TB and in all age groups (Roy et al. 2014). In a systematic review and meta-analysis of 12 cohort studies, protection against pulmonary TB was found to range from 44% to 99% (Abubakar et al. 2013). Some randomized controlled trials (RCTs) and observational studies of vaccine efficacy support a high protection against pulmonary TB from BCG vaccination of neonates, and moderate protection of school-age tuberculin skin test (TST)-negative children (Mangtani et al. 2013). Evidence from a meta-analysis of six RCTs shows that BCG vaccination confers a high degree of protection against

severe forms of TB, reducing severe TB in vaccinated individuals by 85% (Mangtani et al. 2013). In addition, a systematic review of 14 case control studies indicates a reduction of the incidence of meningeal TB by 73% and of miliary TB by 77% (Trunz et al. 2006).

7 Conclusion

TB is still a global public health problem and is the leading infectious disease killer in the world. The disease is driven by several conditions; among them, HIV infection remains the most important. Pulmonary TB is the most common form. EPTB is dominated by TB of the pleura, lymph nodes, spine, bones and joints, CNS, and urogenital organs. Tuberculous lymphadenitis is regarded as the most common form of EPTB. Although CNS infection accounts for approximately 1% of all cases of TB, it remains one of the most devastating forms. As TB is a curable and preventable disease, early diagnosis, treatment, and prevention of TB are crucial. TB treatment is effective but needs a high level of adherence; this is a critical component of care and important for global TB control. Drug-resistant TB continues to be a public health threat. Prevention is based on immunization and infection controls. The BCG vaccine is effective in several populations but protection has not been consistent against all forms of TB.

References

Abubakar I, Pimpin L, Ariti C et al (2013) Systematic review and meta-analysis of the current evidence on the duration of protection by bacillus Calmette–Guérin vaccination against tuberculosis. Health Technol Assess 17(37):1. (v–vi)

Abu-Zidan FM, Sheek-Hussein M (2019) Diagnosis of abdominal tuberculosis: lessons learned over 30 years: pictorial essay. World J Emerg Surg 14:33

Adhikari S, Basnyat B (2018) Extrapulmonary tuberculosis: a debilitating and often neglected public health problem. BMJ Case Rep 11:e226098

Agarwal R, Malhotra P, Awasthi A et al (2005) Tuberculous dilated cardiomyopathy: an under-recognized entity? BMC Infect Dis 5:29

Ahmed ME, Hassan MA (1994) Abdominal tuberculosis. Ann R Coll Surg Engl 76:75–79

Aït Khaled N, Enarson D, Billo N (1997) Épidémiologie de la tuberculose et de la résistance aux antituberculeux. Rev Mal Respir 14:5S8–5S18

Akgun Y (2005) Intestinal and peritoneal tuberculosis: changing trends over 10 years and a review of 80 patients. Can J Surg 48:131–136

Al Karawi MA, Mohamed AE, Yasawy MI et al (1995) Protean manifestation of gastrointestinal tuberculosis. J Clin Gastroenterol 20:225–232

Al-Bahrani ZR, Al-Saleem T (1982) Intestinal tuberculosis in Iraq: a study of 50 cases. Int Surg 67:483–485

Ambreen A, Tahseen S, Wali A et al (2021) Predictors of slow clinical response and extended treatment in patients with extra-pulmonary tuberculosis in Pakistan. A hospital-based prospective study. PLoS One 16:0259801

Anand M, Nayyar E, Concepcion B et al (2017) Tuberculosis in kidney transplant recipients: a case series. World J Transplant 7:213–221

Bates M, Ahmed Y, Kapata N et al (2015) Perspectives on tuberculosis in pregnancy. Int J Infect Dis 32: 124–127

Batirel A, Erdem H, Sengoz G et al (2015) The course of spinal tuberculosis (Pott disease): results of the multinational, multicentre Backbone-2 study. Clin Microbiol Infect 21:1008.e9–1008.e18

Bea S, Lee H, Kim JH et al (2021) Adherence and associated factors of treatment regimen in drug-susceptible tuberculosis patients. Front Pharmacol 12:625078. https://doi.org/10.3389/fphar.2021.625078

Bernard L, Perronne C (1997) La tuberculose ostéo-articulaire aujourd'hui. Presse Med 26:308–310

Bernheim A, Kempker RR, Hernandez-Romieu AC et al (2020) Internal thoracic lymphadenopathy and pulmonary tuberculosis. Clin Imaging 67:11–14

Bruzgielewicz A, Rzepakowska A, Osuch-Wójcikewicz E et al (2014) Tuberculosis of the head and neck—epidemiological and clinical presentation. Arch Med Sci 10:1160–1166

Cantres-Fonseca JO (2020) Thoracic extrapulmonary tuberculosis in the millennial era. In: Garcia JCH (ed) Update in respiratory diseases. Intech Open. https://doi.org/10.5772/intechopen.90376

Cebrián Parra JL, Saez-Arenillas Martín A, Urda Martínez-Aedo AL et al (2012) Management of infectious discitis. Outcome in one hundred and eight patients in a University Hospital. Int Orthop 36:239–244

Centers for Disease Control and Prevention (2000) Targeted tuberculin testing and treatment of latent tuberculosis infection. https://www.cdc.gov/mmwr/preview/mmwrhtml/rr4906a1.htm, accessed 27 August 2021

Chen CH, Chen YM, Lee CW et al (2016) Early diagnosis of spinal tuberculosis. J Formos Med Assoc 115:825–836

Cherian A, Thomas SV (2011) Central nervous system tuberculosis. Afr Health Sci 11:116–127

Cho JK, Choi YM, Lee SS et al (2018) Clinical features and outcomes of abdominal tuberculosis in southeastern Korea: 12 years of experience. BMC Infect Dis 18:699

Cohen LA, Light RW (2015) Tuberculous pleural effusion. Turk Thorac J 16:1–9

Cudahy PGT, Wilson D, Cohen T (2020) Risk factors for recurrent tuberculosis after successful treatment in a high burden setting: a cohort study. BMC Infect Dis 20:789

Das S, Das D, Bhuyan UT et al (2016) Head and neck tuberculosis: scenario in a tertiary care hospital of North Eastern India. J Clin Diagn Res 10:MC04–MC07

De Backer AI, Mortelé KJ, De Keulenaer BL et al (2006) CT and MR imaging of gastrointestinal tuberculosis. JBR-BTR 89:190–194

De Backer AI, Vanhoenacker FM, Sanghvi DA (2009) Imaging features of extra-axial musculoskeletal tuberculosis. Indian J Radiol Imaging 19:176–186

De Jong BC, Antonio M, Gagneux S (2010) Mycobacterium africanum—review of an important cause of human tuberculosis in West Africa. PLoS Negl Trop Dis 4:e744

Donoghue HD, Holton J (2009) Intestinal tuberculosis. Curr Opin Infect Dis 22:490–496

Droz N, De Lauzanne A, Holvoet L et al (2017) Tuberculosis in children with sickle cell anaemia: a retrospective study in French tertiary care centres. Eur J Pediatr 176:723–729

Eddy J, Khan T, Schembri F (2018) Medical management of drug-sensitive active thoracic tuberculosis: the work-up, radiographic findings and treatment. J Thorac Dis 10:S3378–S3391

Erdem H, Elaldi N, Batirel A et al (2015) Comparison of brucellar and tuberculous spondylodiscitis patients: results of the multicenter "Backbone-1 Study". Spine J 15:2509–2517

Figueiredo AA, Lucon AM, Junior RF et al (2008) Epidemiology of urogenital tuberculosis worldwide. Int J Urol 15:827–832

Figueroa-Damián R, Arredondo-García JL (2001) Neonatal outcome of children born to women with tuberculosis. Arch Med Res 32:66–69

Gatongi DK, Gitau G, Kay V et al (2005) Female genital tuberculosis. Obstet Gynaecol 7:75–79

Gilinsky NH, Marks IN, Kottler RE et al (1983) Abdominal tuberculosis. A 10-year review. S Afr Med J 64:849–857

Hamza M (1993) Tuberculose articulaire et vertébrale. Rev Rhum 60:115–118

Hertz D, Schneider B (2018) Sex differences in tuberculosis. Semin Immunopathol 41:225–237

Hong KS, Kang SJ, Choi JK et al (2013) Gastrointestinal tuberculosis is not associated with proton pump inhibitors: a retrospective cohort study. World J Gastroenterol 19:258–264

Horne DJ, Hubbard R, Narita M et al (2010) Factors associated with mortality in patients with tuberculosis. BMC Infect Dis 10:258

Horton K, MacPherson P, Houben RM et al (2016) Sex differences in tuberculosis burden and notifications in low- and middle-income countries: a systematic review and meta-analysis. PLoS Med 13:1002119

Horvath KD, Whelan RL (1998) Intestinal tuberculosis: return of an old disease. Am J Gastroenterol 93:692–696

Javed G, Laghari AA, Ahmed SI et al (2018) Development of criteria highly suggestive of spinal tuberculosis. World Neurosurg 116:e1002–e1006

Jo KW, Yoo JW, Hong Y et al (2014) Risk factors for 1-year relapse of pulmonary tuberculosis treated with a 6-month daily regimen. Respir Med 108:654–659

Kawazoe A, Nagata N (2012) Intestinal tuberculosis in an HIV-infected patient with advanced immunosuppression. Clin Gastroenterol Hepatol 10:A24

Khan R, Abid S, Jafri W et al (2006) Diagnostic dilemma of abdominal tuberculosis in non-HIV patients: an ongoing challenge for physicians. World J Gastroenterol 12:6371–6375

Kristensen KL, Podlekareva D, Ravn P (2017) Delayed diagnosis of severe tuberculous spondylodiscitis in an asylum seeker; patient or doctors delay? Respir Med Case Rep 21:145–146

Kulchavenya E, Khomyakov V (2006) Male genital tuberculosis in Siberians. World J Urol 24:74–78

Kulchavenya E, Naber K, Bjerklund Johansen TE (2016) Urogenital tuberculosis: classification, diagnosis, and treatment. Eur Urol 15:112–121

Ladeb MF, Chelly-Bouaziz M, Chakroun M (2013) Tuberculose articulaire et extra-rachidienne. Imagerie rhumatologique et orthopédiques, affections générales. Direction JD Laredo Sauramts médical 1:513–522

Liu CH, Li L, Chen Z et al (2011) Characteristics and treatment outcomes of patients with MDR and XDR tuberculosis in a TB referral hospital in Beijing: a 13-year experience. PLoS One 6:e19399

Liu Z, Wang J, Chen GZ et al (2019) Clinical characteristics of 1378 inpatients with spinal tuberculosis in general hospitals in South-Central China. Biomed Res Int 2019:9765253

Macías A, Sánchez-Montalvá A, Salvador F et al (2019) Epidemiology and diagnosis of pleural tuberculosis in a low incidence country with high rate of immigrant population: a retrospective study. Int J Infect Dis 78:34–38

Mangtani P, Abubakar I, Ariti C et al (2013) Protection by BCG vaccine against tuberculosis: systematic review of randomized controlled trials. Clin Infect Dis 58:470–480

Marshall JB (1993) Tuberculosis of the gastrointestinal tract and peritoneum. Am J Gastroenterol 88: 989–999

Mayosi BM, Burgess LJ, Doubell AF (2005) Tuberculous pericarditis. Circulation 112:3608–3616

Menon KV, Sorour TM (2016) Epidemiologic and demographic attributes of primary spondylodiscitis in a Middle Eastern population sample. World Neurosurg 95:31–39

Monga S, Malik JN, Jan S et al (2017) Clinical study of extrapulmonary head and neck tuberculosis in an urban setting. Acta Otorhinolaryngol Ital 37: 493–499

Muneer A, Macrae B, Krishnamoorthy S et al (2019) Urogenital tuberculosis—epidemiology, pathogenesis and clinical features. Nat Rev Urol 16:573–598

Musellim B, Erturan S, Sonmez Duman E et al (2005) Comparison of extra-pulmonary and pulmonary tuberculosis cases: factors influencing the site of reactivation. Int J Tuberc Lung Dis 9:1220–1223

Nayagam JS, Mullender C, Cosgrove C et al (2016) Abdominal tuberculosis: diagnosis and demographics, a 10-year retrospective review from a single centre. World J Clin Cases 4:207–212

Oishi M, Okamoto S, Teranishi Y et al (2016) Clinical study of extrapulmonary head and neck tuberculosis: a single-institute 10-year experience. Int Arch Otorhinolaryngol 20:30–33

Palmer KR, Patil DH, Basran GS et al (1985) Abdominal tuberculosis in urban Britain—a common disease. Gut 26:1296–1305

Pang P, Duan W, Liu S et al (2018) Clinical study of tuberculosis in the head and neck region-11 years' experience and a review of the literature. Emerg Microbes Infect 7:4

Pedroso A, Ferreira I, Chikura T (2020) Tuberculosis and sarcoidosis overlap: a clinical challenge from diagnosis to treatment. Cureus 12:e11662

Pertuiset E, Beaudreuil J, Horusitzky F et al (1997) Aspects épidémiologiques de la tuberculose ostéo-articulaire de l'adulte. Étude rétrospective de 206 cas diagnostiqués en région parisienne de 1980 à 1994. Presse Med 26:311–315

Phypers M, Harris T, Power C (2006) CNS tuberculosis: a longitudinal analysis of epidemiological and clinical features. Int J Tuberc Lung Dis 10:99–103

Pu F, Feng J, Yang L et al (2019) Misdiagnosed and mismanaged atypical spinal tuberculosis: a case series report. Exp Ther Med 18:3723–3728

Rana FS, Hawken MP, Mwachari C et al (2000) Autopsy study of HIV-1–positive and HIV-1–negative adult medical patients in Nairobi, Kenya. J Acquir Immune Defic Syndr 24:23–29

Rathi P, Gambhire P (2016) Abdominal tuberculosis. J Assoc Physicians India 64:38–47

Restrepo CS, Katre R, Mumbower A (2016) Imaging manifestations of thoracic tuberculosis. Radiol Clin North Am 54:453–473

Rieder HL, Snider DE Jr, Cauthen GM (1990) Extrapulmonary tuberculosis in the United States. Am Rev Respir Dis 141:347–351

Roy A, Eisenhut M, Harris R et al (2014) Effect of BCG vaccination against *Mycobacterium tuberculosis* infection in children: systematic review and meta-analysis. BMJ 349:g4643

Sartori NS, Picon P, Papke A et al (2019) A population-based study of tuberculosis incidence among rheumatic disease patients under anti-TNF treatment. PLoS One 14:e0224963

Sharma SK, Mohan A (2004) Extrapulmonary tuberculosis. Indian J Med Res 120:316–353

Sharma SK, Mohan A, Sharma A (2012) Challenges in the diagnosis and treatment of miliary tuberculosis. Indian J Med Res 135:703–730

Sheer TA, Coyle WJ (2003) Gastrointestinal tuberculosis. Curr Gastroenterol Rep 5:273–278

Sinan T, Sheikh M, Ramadan S et al (2002) CT features in abdominal tuberculosis: 20 years experience. BMC Med Imaging 2:3

Sreeramareddy CT, Panduru KV, Verma SC et al (2008) Comparison of pulmonary and extrapulmonary tuberculosis in Nepal—a hospital-based retrospective study. BMC Infect Dis 8:8

Srivastava U, Almusa O, Tung KW et al (2014) Tuberculous peritonitis. Radiol Case Rep 9:971

Trunz B, Fine P, Dye C (2006) Effect of BCG vaccination on childhood tuberculous meningitis and miliary tuberculosis worldwide: a meta-analysis and assessment of cost-effectiveness. Lancet 367: 1173–1180

Udgirkar S, Jain S, Pawar S et al (2019) Clinical profile, drug resistance pattern and treatment outcomes of abdominal tuberculosis patients in Western India. Arq Gastroenterol 56:178–183

Ulloa JG, Parekh J, Hope C et al (2014) Case report of intestinal tuberculosis 6 years after simultaneous pancreas and kidney transplant. Transplant Proc 46:2450–2452

Uygur-Bayramiçli O, Dabak G, Dabak R (2003) A clinical dilemma: abdominal tuberculosis. World J Gastroenterol 9:1098–1101

Vaid U, Kane GC (2017) Tuberculous peritonitis. Microbiol Spectr 5:1–6

Valença MS, Scaini JL, Abileira FS et al (2015) Prevalence of tuberculosis in prisons: risk factors and molecular epidemiology. Int J Tuberc Lung Dis 19: 1182–1187

Vernon A, Fielding K, Savic R et al (2019) The importance of adherence in tuberculosis treatment clinical trials and its relevance in explanatory and pragmatic trials. PLoS Med 16:e1002884

Waitt CJ, Squire SB (2011) A systematic review of risk factors for death in adults during and after tuberculosis treatment. Int J Tuberc Lung Dis 15: 871–885

Wells AD, Northover JM, Howard ER (1986) Abdominal tuberculosis: still a problem today. J R Soc Med 79:149–153

World Health Organization (2018) BCG vaccine: WHO position paper, February 2018—recommendations. Vaccine 36:3408–3410

World Health Organization (2021) Global tuberculosis report 2021. World Health Organization, Geneva. https://www.who.int/teams/global-tuberculosis-programme/tb-reports/global-tuberculosis-report-2021

Wu DC, Averbukh LD, Wu GY (2019) Diagnostic and therapeutic strategies for peritoneal tuberculosis: a review. J Clin Transl Hepatol 7:140–148

Yaramiş A, Gurkan F, Elevli M et al (1998) Central nervous system tuberculosis in children: a review of 214 cases. Pediatrics 102:e49

Yashveer JK, Kirti YK (2015) Presentations and challenges in tuberculosis of head and neck region. Indian J Otolaryngol Head Neck Surg 68:270–274

Pathophysiology of Tuberculosis and Microbiological Diagnosis

Wafa Achour and Yosra Chebbi

Contents

W. Achour (✉) · Y. Chebbi
Laboratory Department, National Bone Marrow Transplantation Center, Rue Djebel Lakhdher, Tunis, Tunisia

Research Laboratory LR18ES39, Faculty of Medicine of Tunis, Tunis-El Manar University, Tunis, Tunisia
e-mail: wafaachour@gmail.com

Abstract

Tuberculosis (TB) is an infectious disease of epidemic proportions, fired not only by poverty and human immunodeficiency virus (HIV) infection but also by incomplete understanding of its pathogenesis and lack of access to accurate and rapid diagnosis. *Mycobacterium tuberculosis* is a highly successful type of bacteria because it produces two distinct disease entities, namely primary TB that mediates protective immunity to disseminated infection; and post-primary TB that causes tissue damage leading to formation of cavities necessary to bacterial transmission. Following exposure to a person with pulmonary TB, the risk of developing infection depends on the capacity of the person infected to transmit the disease and the susceptibility of the person exposed to infection. From exposure to infection to disease, there is a pathogenetic continuum. Individuals may

© The Author(s), under exclusive license to Springer Nature Switzerland AG 2022

M. F. Ladeb, W. C. G. Peh (eds.), *Imaging of Tuberculosis*, Medical Radiology Diagnostic Imaging,
https://doi.org/10.1007/978-3-031-07040-2_2

advance or reverse states within the spectrum of infection. The dissemination of *M. tuberculosis* out of the lungs happens during all infections and results in secondary lesions. The microbiological diagnosis of active TB is based on acid-fast bacillus (AFB) smear microscopy, nucleic acid amplification tests (NAAT), and culture. Culture remains the gold standard for TB diagnosis. It increases the potential of diagnosing TB at early stages of the disease, allows extrapulmonary TB diagnosis, species identification, and drug susceptibility testing. However, it takes weeks before results are available. NAAT have significantly reduced this delay. The identification of individuals with latent TB infection is based on imperfect tests, namely tuberculin skin test and interferon-γ release assay.

Abbreviations

AFB	Acid-fast bacilli
HIV	Human immunodeficiency virus
LTBI	Latent tuberculosis infection
NAAT	Nucleic acid amplification tests
TB	Tuberculosis

1 Introduction

Tuberculosis (TB) is the leading infectious cause of mortality worldwide. The greatest burden of this disease is located in developing countries. However, developed countries are not spared from this threat. The human immunodeficiency virus (HIV) global epidemic and the emergence of multidrug-resistant TB are major obstacles to control this disease (Ankrah et al. 2018). The majority of TB cases are due to *Mycobacterium tuberculosis* (sensu stricto) or *M. africanum*. A minority of cases are due to *M. bovis* or *M. caprae,* the causal agents of bovine and caprine TB, respectively (Pai et al. 2016a, b); and exceptionally to *M. canetti*, *M. microti,* and *M. pinnipedii*. All these species belong to *M. tuberculosis* complex.

Understanding of the pathophysiology of TB, necessary for development of effective treatments and vaccines, continues to evolve. The classical model of distinct latent and active forms of TB disease has been replaced by a spectrum of TB states (Furin et al. 2019). Early diagnosis of TB including drug susceptibility testing (DST), and systematic screening of contacts and high risk groups are essential for ending the TB epidemic (Pai et al. 2016a, b).

2 Chain of Infection

2.1 Reservoir

Humans are the only known reservoir of *M. tuberculosis* (Pai et al. 2016a, b) and *M. africanum*. Unlike humans, most animals infected with *M. tuberculosis* die without developing pulmonary fibrosis and cavitation necessary for transmission of the infection (Ankrah et al. 2018). Almost a third of the world's population harbor *M. tuberculosis* in a quiescent state (Ankrah et al. 2018). *M. africanum* is highly restricted to West Africa, where it causes up to 50% of all TB cases, probably due to an association with patient ethnicity (Asante-Poku et al. 2015).

Major transmitters of TB are infected individuals who test positive for acid-fast bacilli (AFB) smear microscopy or culture, who have cavitary pulmonary or laryngeal TB disease or frequent cough, or who have delayed treatment. Also, the infectiousness of the person with TB disease increases when they fail to cover the mouth and nose when coughing (Bloom et al. 2017). Young children are less of transmitters than adults, because they generally do not produce sputum when they cough (Centers for Disease Control and Prevention et al. 2021).

M. bovis and *M. caprae* have a broad host range and can cause TB in a wide range of domestic and wild animals (Rodríguez et al. 2009). The global burden of TB caused by these

species is higher in African countries (2.8%) than in countries outside Africa (1.4%), with predominance of *M. bovis*. The incidence of human infections with *M. bovis* in developed countries has markedly decreased due to eradication campaigns in animals, and the cases that do appear are likely due to old infection reactivations (Müller et al. 2013).

2.2 Modes of Transmission

M. tuberculosis and *M. africanum* spread by aerosol transmission (Sharma et al. 2016). Infectious droplet nuclei are produced when individuals who have pulmonary or laryngeal TB disease cough, sneeze, shout, or sing. These particles can remain suspended in the air for several hours. Transmission occurs when a person inhales infectious droplet nuclei that traverse the mouth or nasal passages to reach the alveoli of the lungs. The risk of infection among household contacts of TB patients is about 30% (Heemskerk et al. 2015). Human TB caused by *M. bovis* and *M. caprae* is due to consumption of unpasteurized dairy products and close/continuous contact with infected animals (Rodríguez et al. 2009).

2.3 Risk Factors

Risk factors influence the probability of infection, disease, or outcome. They cover physiological, genetic, environmental, and behavioral factors (Bloom et al. 2017).

2.3.1 Risk Factors of *M. tuberculosis* Transmission

Most risk factors reflect the social and environmental determinants of heavy exposure, namely small/enclosed spaces, inadequate local or general ventilation, recirculation of contaminated air, improper specimen handling procedures, positive air pressure in infectious patient's room, high proximity/frequency/duration of exposure, living in densely populated spaces, being incarcerated, and working in occupations involving frequent contact with patients with TB (Bloom et al. 2017; Centers for Disease Control and Prevention et al. 2021). Some genetic loci are linked to increased risk of infection among household contacts exposed to an infectious patient (Bloom et al. 2017).

2.3.2 Risk Factors of Latent TB Infection Progressing to TB Disease

In contrast to infection, disease progression is strongly dependent on host risk factors. HIV infection is the greatest risk factor for the development of TB disease in individuals with latent tuberculosis infection (LTBI) due to immunosuppression. The risk of developing TB disease is 7% to 10% each year for individuals co-infected with HIV (and not receiving highly active antiretroviral therapy) versus 10% over a lifetime for individuals infected only with *M. tuberculosis*. Other important risk factors are low body mass index, exposure to tobacco and biomass fuel, diabetes mellitus, and heavy alcohol use (Bloom et al. 2017).

Individuals are more likely to progress to active TB in the presence of drug abuse, recent infection with *M. tuberculosis* (within the past 2 years), history of untreated or inadequately treated TB disease, fibrotic changes on chest radiograph consistent with prior TB disease, silicosis, chronic renal failure, solid or hematological malignancies, gastrectomy or jejunoileal bypass surgery and immunosuppressive therapy (e.g., tumor necrosis factor-alpha antagonists) (Centers for Disease Control and Prevention et al. 2021). Children younger than 5 years of age are at increased risk for progression of LTBI to TB disease (Centers for Disease Control and Prevention et al. 2021) because of immune response immaturity (Newton et al. 2008).

Populations have increased risk to develop TB disease when they have LTBI, if they have an increased local incidence of TB, or if they are medically underserved or low income (Centers for Disease Control and Prevention et al. 2021).

In vitro studies indicate a role for vitamin D in TB disease. Moreover, there is a correlation between seasonal variation in vitamin D and TB case numbers. The increased susceptibility of dark-skinned individuals to TB infection and more severe disease is linked to the role of melanin to absorb ultraviolet light. Nutritional factors may interact with genetic polymorphisms to increase the risk of TB (Bloom et al. 2017).

2.3.3 Risk Factors of Extrapulmonary TB

Extrapulmonary TB is overrepresented in HIV-infected patients, children, and those who are malnourished. Other risk factors of extrapulmonary TB are homelessness, incarceration, and alcohol abuse (Moule and Cirillo 2020).

2.3.4 Risk Factors Affecting TB Outcomes

Risk factors for poor treatment outcomes are HIV infection, smoking, diabetes mellitus, iron overload, renal dysfunction, and hematological malignancies (Bloom et al. 2017). Infants have a particularly high morbidity and mortality from TB (Newton et al. 2008).

3 Pathophysiology of Tuberculosis

Some individuals exposed to TB do not become infected, whereas others, with minimal exposure, rapidly succumb to infection and disease (Furin et al. 2019). Indeed, there is a complex interaction between the microorganism and the host immune response. The outcome results in a spectrum of TB states (Ankrah et al. 2018).

3.1 Bacterial Infection Determinants

Genomic comparison between *M. tuberculosis* and Bacillus Calmette–Guérin (BCG) has been used to search for the basis of attenuated virulence, uncovering several differences, essentially the region of difference 1. This region contains genes that encode the ESX-1 secretion system, which mediates the delivery of bacterial products into the macrophage cytoplasm. However, the presence of the ESX-1 secretion system in a few atypical mycobacteria reconsiders the primacy of ESX-1 in *M. tuberculosis* virulence. Therefore, ESX-1 seems to be necessary, but not solely responsible, for the full virulence of *M. tuberculosis* (Pai et al. 2016a, b). Whole-genome sequence analysis shows that "modern" *M. tuberculosis* strains induce lower-level and delayed proinflammatory cytokine production, replicate more quickly, and are more pathogenic than more "ancient" TB strains. Therefore, it seems that as human populations expand quickly, *M. tuberculosis* develops traits of more rapid disease progression and increased transmission (Drain et al. 2018).

3.2 Host Determinants of Infection

There is an interaction between *M. tuberculosis* virulence factors and host determinants of susceptibility. Indeed, unremarkable strains, according to genomic and laboratory characterization, have been linked to outbreaks in the appropriate social and epidemiological settings. Conversely, highly virulent strains in Asian populations have a normal clinical and epidemiological presentation in developed countries (Pai et al. 2016a, b). Human resistance to TB infection has a strong genetic basis, involving an evolutionary counter-response to bacterial virulence. Mendelian studies have proved that severe childhood TB could be attributable to single gene inborn errors of interferon-γ immunity (Abel 2018). Also, a chromosome 11 locus has been linked to susceptibility in multiple populations. Conversely, a chromosome 5 locus has been associated with resistance in highly susceptible HIV-positive East African populations (Bloom et al. 2017).

3.3 Infection of Host Cells

While small *M. tuberculosis* aerosol particles are expected to reach the distal airways, larger particles can be trapped in the upper airway or the oropharynx where they can lead to oropharyngeal or cervical lymph node TB (Bussi and Gutierrez 2019). Following inhalation, a number of pathways have been proposed regarding the dissemination of *M. tuberculosis* across the airway epithelia. One hypothesis is that *M. tuberculosis* is carried across the epithelial barrier within infected alveolar macrophages. Another hypothesis is that it directly infects the epithelial cells and translocates across the barrier, without disrupting the epithelium or causing a breach in the barrier by inducing cell death. Alternatively, specialized M cells actively translocate antigens from the alveoli to the interstitium to present them to antigen-presenting cells. Another hypothesis is that dendritic cells in the alveoli transport live mycobacteria to the lymph nodes. Finally, dissemination may involve a combination of several or all of these mechanisms (Moule and Cirillo 2020) (Fig. 1). *M. tuberculosis* actively delays initial T cell priming as well as T cell trafficking into the lung (Pai et al. 2016a, b).

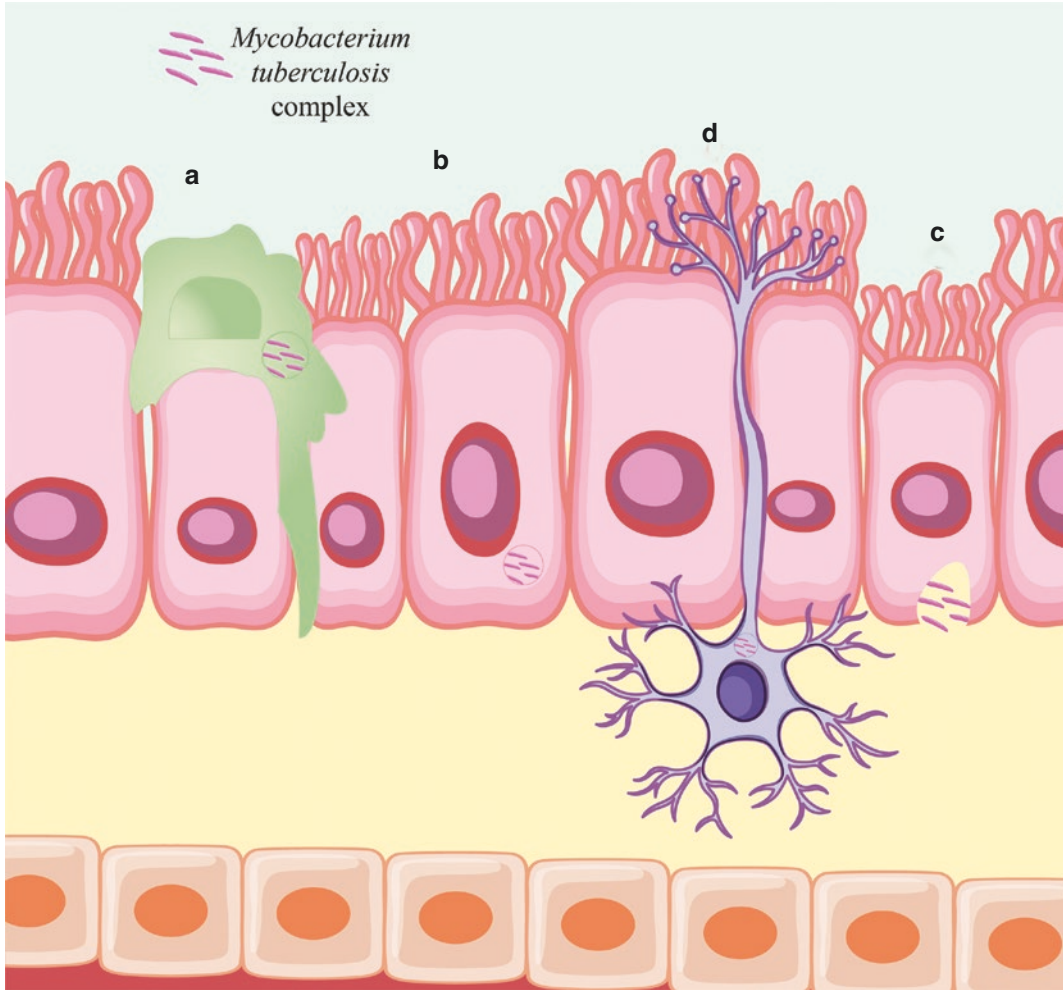

Fig. 1 Schematic diagram illustrates *M. tuberculosis* dissemination mechanisms across the airway epithelia. These comprise of dissemination within infected macrophages (**a**), direct epithelial cell infection (**b**), passage within specialized M cells (**c**), and dendritic cells antigen sampling in the alveoli (**d**) [Adapted from Moule and Cirillo 2020]

HIV infection increases the risk of progression from *M. tuberculosis* infection to active TB disease, as a result of $CD4^+$ T cell depletion and T cell-independent immune response impairment (Pai et al. 2016a, b). In the neonate and infant, mycobacteria overwhelm the effects of the innate immune system because of innate pulmonary defenses impairment. Antigen presentation and the efficiency of naive T cell response to antigen seem less effective and delayed, resulting in development of active disease (Newton et al. 2008).

In patients with no previous exposure to *M. tuberculosis*, pattern recognition receptors expressed by macrophages, dendritic cells, and epithelial cells interact with *M. tuberculosis* ligands. Production of inflammatory cytokines and chemokines recruits new cells to the infection site and initiates granuloma formation by the innate immune system. The adaptive immune response occurs approximately four to six weeks following *M. tuberculosis* antigen presentation by dendritic cells in lymph nodes. Predominantly TH1-delayed-type response sequesters *M. tuberculosis* in a mature granuloma, with rapid bacillary killing power. This prevents *M. tuberculosis* from spreading to other tissues. The innate immune system is less efficient than the adaptive immune system in containing the infection. The early events of *M. tuberculosis* infection influence the ultimate outcome (Ankrah et al. 2018).

Outside the lungs, *M. tuberculosis* can disseminate to any organ. M cells may contribute to dissemination and disease progression. Lymphatic endothelial cells, adipose tissue, and bone marrow provide niches to *M. tuberculosis*, facilitating persistent infection and modulating the local tissue environment (Bussi and Gutierrez 2019).

3.4 Spectrum of Infection

TB can present as a dynamic spectrum, from asymptomatic infection to severe or fatal disease (Pai et al. 2016a, b) (Fig. 2). Drain et al. (2018)

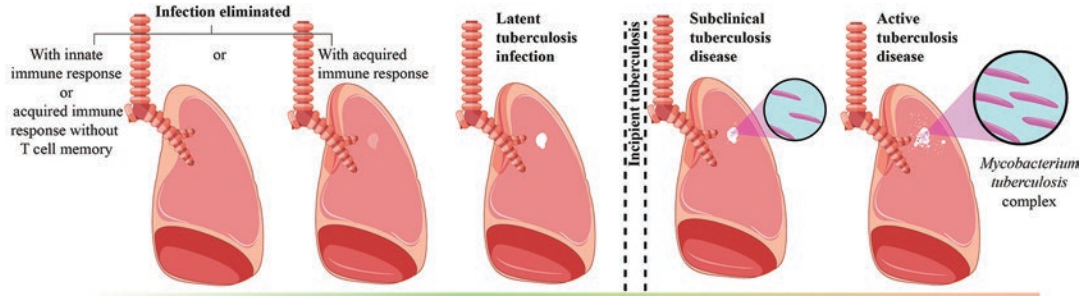

Symptoms	None	None	None	Mild or none	Mild to severe
Infectious	No	No	No	Sporadically	Yes
Sputum smear	Negative	Negative	Negative	Usually negative	Positive or negative
Culture	Negative	Negative	Negative	Intermittenly positive	Positive
TST	Negative	Positive	Positive	Positive	Usually positive
IGRA	Negative	Positive	Positive	Positive	Usually positive
Preferred treatment	None	None	Preventive therapy	Multidrug therapy	Multidrug therapy

Fig. 2 Schematic diagram and accompanying chart show the spectrum of tuberculosis infection and disease. IGRA: interferon-γ release assay. TST: tuberculin skin test. [Adapted from Pai et al. 2016a, b]

divided the pathophysiological spectrum into five categories:

- Eliminated TB infection refers to *M. tuberculosis* infection cleared by innate (in this case, immunological tests might be negative) and/or acquired immune responses (in which case immunological tests might be positive or negative) or cured with anti-TB drugs.
- LTBI is infection with viable *M. tuberculosis* for which progression to TB disease is not expected to occur soon, in the absence of any significant immune deficiency. Immunological tests are typically positive.
- Incipient TB infection is infection with viable *M. tuberculosis* bacteria that is likely to progress to active disease in the absence of further intervention but has not yet caused clinical symptoms, radiographical abnormalities, or microbiological evidence of active TB disease.
- Subclinical TB disease is asymptomatic disease due to viable *M. tuberculosis* with radiographical abnormalities or microbiological evidence of active TB disease.
- Active TB disease is symptomatic disease due to viable *M. tuberculosis* with radiographical abnormalities or microbiological evidence of active TB disease.

In most individuals with LTBI, the immune response is sufficient to maintain control of infection. However, in some cases, for unknown reasons, the infection can progress to clinical disease within weeks to decades. From a bacteriological perspective, presenting intact antigenic proteins contributes to the progression to disease. *M. tuberculosis* genes involved in the production of immunodominant CD4+ T cell antigens are invariable across strains and lineages. From a host perspective, three epidemiological observations inform on essential pathways in controlling infection, namely HIV, anti-TNF drugs, and inborn errors in immunity (Pai et al. 2016a, b). Moreover, immunity to TB varies over time, even within the context of an individual patient. Both local and systemic immune responses seem to be important in controlling TB infection (Furin et al. 2019).

Variations in the cellular compositions and activation levels of immune cells, epithelial cells, and extracellular matrix within granulomas expose *M. tuberculosis* to different microenvironments (nutrient availability, reactive intermediates, cytokine profiles, and drug penetration). In a single human host, different pulmonary and extrapulmonary infection sites induce bacterial phenotypic heterogeneity that can in turn shape the immune response and progression of infection. The types of lesions detectable in asymptomatic individuals correlate with progression to active disease (Drain et al. 2018).

3.5 Primary Versus Post-primary Tuberculosis

M. tuberculosis produces two distinct disease entities, namely primary and post-primary TB. These two entities differ in histopathology, imaging, genetic predisposition and immune status of the host, age of onset, organ distribution, clinical course, and susceptibility to BCG protection (Hunter and Actor 2019). Primary TB results from insufficient immune responses. Conversely, post-primary TB results from strong immune responses.

The early lesion is an accumulation of mycobacterial antigens in alveolar macrophages in association with highly sensitized T cells, forming a massive necrotizing hypersensitivity reaction. This is known as the Koch Phenomenon, which leads to caseous pneumonia, evolving to a pulmonary cavitation or to a focus of post-primary granulomas and fibrocaseous disease. Both granulomas, produced by primary and post-primary TB, surround and isolate infectious foci and protect against disseminated TB. Therefore, after initial sensitization to mycobacterial antigens, all subsequent infections and dissemination occur as post-primary TB. In conclusion, *M. tuberculosis* uses the strongest immune response to produce pulmonary cavities from which it can disseminate to new hosts,

while maintaining a high degree of immunity in the body (Hunter 2020).

Progressive pulmonary TB is due to a continuous host response to mycobacterial products and not to increasing numbers of viable bacilli (Hunter 2020). Subclinical pulmonary lesions frequently develop for months before onset of symptoms. Most early infiltrates resolve completely (Hunter and Actor 2019). This is probably linked to premature development of granulomas, weak immune responses, altered macrophage polarization, and failure of bronchial obstruction (Hunter 2020). TH1 immunity reduces systemic dissemination but does not prevent pulmonary disease (Hunter and Actor 2019).

3.6 Pulmonary Versus Extrapulmonary Tuberculosis

M. tuberculosis is primarily a respiratory pathogen. However, 15% of infections occur at extrapulmonary sites, therefore complicating the disease diagnosis and treatment. The most common forms of extrapulmonary TB are cervical lymph node TB, pleural TB, and gastrointestinal TB (the latter is more commonly associated with *M. bovis)*. A less common but potentially serious form of extrapulmonary TB is central nervous system TB, especially tuberculous meningitis. Miliary TB is the most severe form of extrapulmonary TB. It is a systemic infection caused by hematogenous spread of the bacteria, characterized by numerous small lesions predominating in highly vascularized organs (e.g., lungs, liver, spleen, bone marrow, kidneys).

Lympho-hematogenous spread is the most probable path of disease progression for both pulmonary and extrapulmonary infections. Indeed, the primary pulmonary granuloma can involve the surrounding lymph nodes, creating a Ghon complex. *M. tuberculosis* then spreads from infected lymph nodes into the lymphatic system, most likely entering the circulatory system through the thoracic duct and the subclavian vein. Hematogenous reseeding of the lungs leads to secondary granulomas of the lungs (in apical regions) and/or extrapulmonary organs (Fig. 3). Bacterial virulence factors may be involved in dissemination. Indeed, *M. tuberculosis* strains from different phylogenetic lineages are associated with different rates of extrapulmonary disease, and clinical isolates from extrapulmonary infections are responsible for an increased degree of disseminated disease in animal models (Moule and Cirillo 2020).

4 Microbiological Diagnosis of Active Tuberculosis

Mycobacteria have several unique characteristics as compared to other genera of bacteria. This is essentially due to the higher content of complex lipids, including mycolic acids. In turn, the cell walls are extremely hydrophobic, which impacts staining with colorants and penetration by drugs. These unique bacterial characteristics imply special laboratory considerations for direct staining from specimens, culture, and DST (Caulfield and Wengenack 2016). There are three principal methods for the detection of active TB, namely microscopy, nucleic acid amplification tests (NAAT), and cultures (Pai et al. 2016a, b).

Culture is considered the gold standard for diagnosis. However, it takes weeks before results are available, because of the slow growth of TB bacilli. Furthermore, its sensitivity is only 80% (Ankrah et al. 2018). Pediatric TB diagnosis is challenging because of small amounts of sputum (usually swallowed) and scarcity of bacilli in specimens. In sputum samples, microscopy and culture are positive in around 10–15% and 30%, respectively (Newton et al. 2008).

4.1 Specimen Collection

The specimen type depends on the clinical manifestation of disease. The most common sources are respiratory specimens, including sputum (expectorate or induced sputum), bronchial aspirates, and bronchoalveolar lavage fluid. These are followed by tissues, normally sterile body fluids,

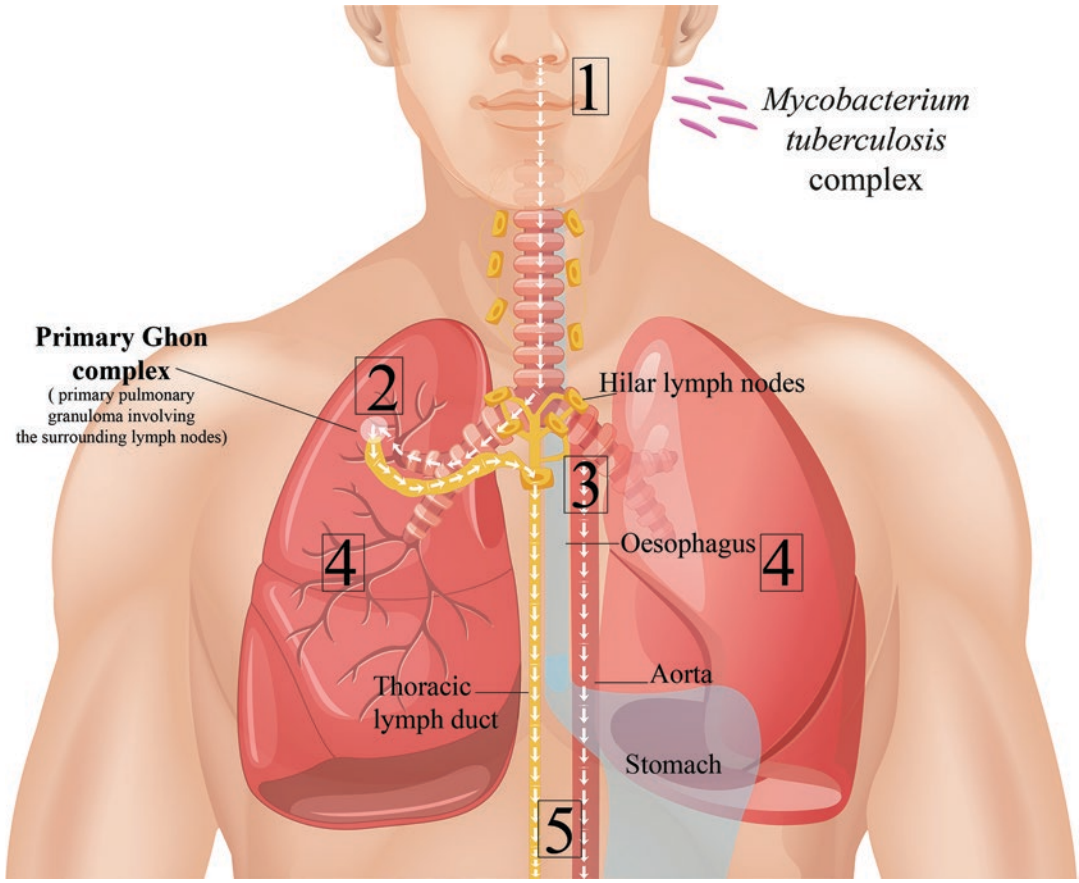

Fig. 3 Schematic diagram shows progression of human *M. tuberculosis* infection. Inhalation of contaminated aerosols (1), followed by primary lung infection forming a Ghon complex (2). Lympho-hematogenous spread (3), with secondary granulomas in the lungs (4) and/or the extrapulmonary organs (5). [Adapted from Moule and Cirillo 2020]

blood, and urine. Specimens should be collected in sterile, leak-proof containers. Tissues may be placed in a small amount of sterile saline solution to avoid dehydration. Most of them should be refrigerated during transport and storage (Caulfield and Wengenack 2016).

4.2 Acid-Fast Bacilli Smear Microscopy

Microscopic examination of stained smears allows rapid screening of mycobacteria in clinical specimens. Mycobacteria resist decolorization by acid alcohol when stained with carbol fuchsin (during Ziehl–Neelsen staining) or auramine (during fluorescent staining). Hence, they are called "acid-fast bacilli" (or "AFB"). The sensitivity of sputum AFB smear varies between 22% and 80%, depending on the concentration of mycobacteria (reliable detection requires 10^3–10^4 CFU/ml), the type of AFB stain used, and the experience of the laboratory technician. Smear-positive predictive value for mycobacteria is >95%. However, it is not specific for *M. tuberculosis* complex and cannot discriminate between mycobacterial species. Positive sputum smears correlate with high infectivity for patients with

pulmonary TB and high AFB concentrations correlate with infection severity (Caulfield and Wengenack 2016).

Examination of Ziehl–Neelsen-stained slides under light microscopy is the most commonly used method in low-resource settings. Fluorescent staining is relatively expensive, but it is more sensitive and allows for more rapid reading of slides. The replacement of conventional fluorescent light sources with light-emitting diodes has considerably reduced cost and maintenance requirements. It also eliminates the necessity of a darkroom. The World Health Organization (WHO) recommends replacing conventional fluorescent and light microscopy by light-emitting diode microscopy (Pai et al. 2016a, b) (Fig. 4). Additionally, it recommends performing two AFB smears (low additional sensitivity gained by performing a third smear after two negative ones). The Centers for Disease Control and Prevention (CDC) recommends reporting AFB staining laboratory results within 24 h of specimen collection (Caulfield and Wengenack 2016).

4.3 Mycobacterial Culture

Culture for mycobacteria is approximately 100 folds more sensitive than AFB smear (reliable detection requires 10–10^2 CFU/ml). However, it requires a more developed laboratory, and needs infrastructure and maintenance to support an adequate biosafety level and uninterrupted power supply (Pai et al. 2016a, b). Mycobacteria are fastidious microorganisms. Culture is traditionally performed on solid egg-based media, such as Lowenstein-Jensen media. It offers good growth of *M. tuberculosis* complex, but is not as reliable for *M. bovis*. While some laboratories still use this media, many have chosen to use more chemically defined agar-based media optimized for faster mycobacterial growth. However, these media are less stable and more prone to deterioration.

M. tuberculosis complex species have a slow growth rate. Colonies become visible on culture plates after several weeks. Generally, cultures are carried on for six to eight weeks before being

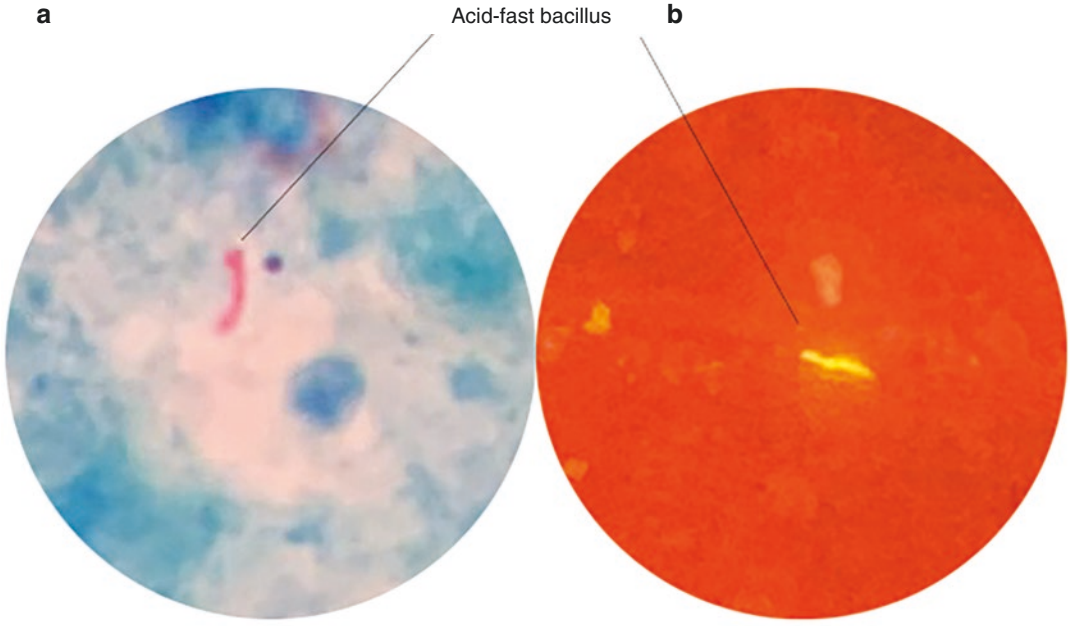

Fig. 4 Photomicrograph of stain sputum smear shows tuberculosis bacilli (Acid-fast bacilli). (**a**) Ziehl–Neelsen (×1,000). (**b**) Auramine O by light-emitting diode fluorescence microscopy (×200)

reported as negative. Plated growth allows for the detection of mixed cultures (containing multiple species) and the identification of mycobacteria (based on morphological characteristics). *M. tuberculosis* colonies are characteristically dry, with a rough texture and a cream/tan color (described as "rough and buff"). Differently, *M. bovis* colonies are flat and smooth. As all *M. tuberculosis* complex species are nonpigmented, the presence of any pigment favors atypical mycobacteria (Caulfield and Wengenack 2016).

Liquid culture is faster and more sensitive than solid culture for mycobacterial isolation. Indeed, *M. tuberculosis* complex from clinical samples is detected faster by automated broth systems (an average of 10 days) than on solid media (20–25 days). However, it must be confirmed with subculture on solid media to detect mixed cultures and to observe colony morphologies. Therefore, optimal recovery of mycobacteria from clinical specimens requires the use of both solid and liquid media (Caulfield and Wengenack 2016).

4.4 Mycobacterial Identification

Rapid discrimination of *M. tuberculosis* complex from other AFB isolated in culture is essential. For this purpose, molecular techniques are faster than traditional biochemical tests. They include nucleic acid hybridization probes, line probe hybridization assays, matrix-assisted laser desorption/ionization time-of-flight mass spectroscopy, and DNA sequencing (Caulfield and Wengenack 2016).

4.5 Direct Molecular Detection from Specimens

NAAT have superior performance to AFB staining in patients with suspected TB. However, they do not differentiate between live and nonviable *M. tuberculosis* complex strains. Respiratory specimens must be cultured for mycobacterial growth in case of negative results by NAAT. It allows detection of false-negative NAAT and atypical mycobacteria. Furthermore, it enables monitoring the treatment response and drug susceptibility testing. The Xpert MTB/RIF tests (Cepheid) are the only U.S. Food and Drug Administration (FDA)-approved automated NAAT that can identify *M. tuberculosis* bacteria (MTB) and resistance to rifampicin (RIF) from respiratory specimens. It is an easy cartridge-based real-time polymerase chain reaction (PCR) method that delivers results in under 2 h. It has a closed amplification system that reduces cross contamination risk. Moreover, it does not require advanced biosafety equipment.

Compared to culture, NAAT have a higher sensitivity from smear-positive (90–99%) than smear-negative (66–74%) respiratory specimens. CDC guidelines recommend performing NAAT on at least one respiratory specimen from each patient (preferably the first) with suspected pulmonary TB (Caulfield and Wengenack 2016). WHO recommends using Xpert MTB/RIF as initial diagnostic test on adults or children suspected to have TB meningitis (on cerebrospinal fluid specimens), multidrug-resistant TB, or HIV-associated TB. If possible, it should be done for all suspected TB cases (Pai et al. 2016a, b).

4.6 Drug Susceptibility Testing

Patients contract drug-resistant TB by two modes, namely infection with a drug-resistant strain (primary resistance) or development of resistance during therapy (secondary resistance). *M. tuberculosis* develops drug resistance through genetic mutations. Multidrug resistance is defined as resistance to at least isoniazid and rifampicin. Extensive drug resistance is defined as multidrug resistance associated with fluoroquinolones and second-line injectable drugs resistance (Dheda et al. 2017). Rifampin resistance is a predictor of multidrug resistance (Caulfield and Wengenack 2016). The detection of resistance is impeded by limitations in both phenotypic and genotypic DST (Pai et al. 2016a, b). WHO recommends establishing laboratory capacity to detect multidrug-resistant TB by national TB control programs (Pai et al. 2016a, b).

4.6.1 Phenotypic Tests

The proportion method is the gold standard test for DST. It counts the number of *M. tuberculosis* colonies that grow on agar without antibiotics, compared with agar containing a critical concentration of antibiotics. For some drugs (e.g., ethambutol), there is important overlap between critical concentrations of wild-type and resistant organisms, which limits the applicability of this method for these drugs. Commercial automated liquid culture systems use a modification of the proportion method. They have reliable results for isoniazid, rifampin, fluoroquinolones, aminoglycosides, and polypeptides, but not to other first-line (ethambutol and pyrazinamide) and second-line drugs. The gold standard for DST for second-line TB drugs is phenotypic testing (liquid or agar proportion) (Pai et al. 2016a, b).

4.6.2 Genotypic Tests

Genotypic tests detect resistance by searching for relevant genes directly by real-time PCR (Xpert MTB/RIF) or DNA sequencing. Conversely, this can be achieved indirectly through line probe assay (LPA) detecting the binding of PCR-amplified DNA to probes targeting the most prevalent mutations encoding resistance or to wild-type probes. Xpert MTB/RIF detects *rpo*B gene mutations responsible for approximately 96% of rifampin resistance in the *M. tuberculosis* complex, with a sensitivity of 94% and a specificity of 98% (Caulfield and Wengenack 2016). However, its positive predictive value is relatively low in countries where rifampin resistance is low.

LPA for drug resistance detection is faster than phenotypic tests, presents lower biosafety risk and increases throughput. LPA for first-line drug resistance detection (rifampin and isoniazid) can be done on cultured isolates or directly from smear-positive sputum samples. As LPA for second-line drug resistance detection (fluoroquinolones and second-line injectable aminoglycosides) has a good specificity (>98%) and a suboptimal sensitivity, it can be used to rule in resistance but cannot be used to completely rule them out. WHO recommends using automated liquid systems and LPA for first-line DST (on isolates or directly on smear-positive sputum) as the current gold standard. It endorses using LPA for second-line DST as the initial test. Confirmation requires conventional culture and phenotypic-based DST for detection of rifampin resistance or multidrug resistance, or resistance on smear-negative sputum (Pai et al. 2016a, b).

5 Testing Methods for Latent *M. tuberculosis* Infection

Testing for LTBI is generally indicated in cases with a high risk of progression to TB disease (e.g., close contact with a patient with TB, immunosuppression). It is based on indirect markers of *M. tuberculosis* exposure, namely tuberculin skin test (TST) and interferon-γ release assay (IGRA). Both tests have reduced sensitivity in children and immunocompromised patients. Additionally, they have low predictive value for progression to active TB. Finally, they are unable to differentiate LTBI from active TB, or to differentiate cleared infection from true infection (Pai and Behr 2016).

5.1 Tuberculin Skin Test

TST is usually performed using the Mantoux method. However, interpretation of the results is complex. It should involve the probability of prior infection and the likely risk of disease in cases of infection. TST has many advantages in low-resource settings (low reagent cost, no hardware costs, limited skill requirement, and no requirement for laboratories). However, its specificity is compromised by late or repeated BCG vaccination, exposure to atypical mycobacteria, or previous cleared infection. Moreover, TST has limited reproducibility, interreader variability, dynamic nature (boosting, conversions, and reversions), and need for patients to return for the reading (Pai and Behr 2016).

5.2 Interferon-γ Release Assays

Two commercial IGRAs are available in many countries, namely QuantiFERON-TB Gold In-Tube assay (an enzyme-linked immunosorbent assay) and T-SPOT.TB assay (an enzyme-linked immunospot assay). IGRAs measure T cell release of interferon-γ after *M. tuberculosis* complex specific antigens stimulation. These antigens are more specific for *M. tuberculosis* than purified protein derivative used for TST because they are produced by only a few atypical mycobacteria and not by BCG vaccine strains. However, IGRAs have highly dynamic natures (inconsistent results, high rates of conversions and reversions in repeated tests) probably related to transitions within the LTBI spectrum or to poor reproducibility. Compared to TST, IGRAs do not add much value, but they are more expensive (Pai and Behr 2016).

6 Conclusion

The global TB elimination is hampered by the huge reservoir of individuals with LTBI. In the absence of overt immune suppression, risk factors of LTBI progression to TB disease are not completely understood. However, many advances have been made in deciphering TB epidemiology and pathophysiology. Finally, multiple laboratory methods are being developed toward a faster, affordable, and accurate diagnosis.

References

Abel L, Fellay J, Haas DW et al (2018) Genetics of human susceptibility to active and latent tuberculosis: present knowledge and future perspectives. Lancet Infect Dis 18(3):e64–e75

Ankrah AO, Glaudemans AWJM, Maes A et al (2018) Tuberculosis. Semin Nucl Med 48:108–130

Asante-Poku A, Yeboah-Manu D, Otchere ID et al (2015) *Mycobacterium africanum* is associated with patient ethnicity in Ghana. PLoS Negl Trop Dis 9:e3370

Bloom BR, Atun R, Cohen T et al (2017) Tuberculosis. In: Holmes KH, Bertozzi S, Bloom BR, Jha P (eds) Disease control priorities, Major infectious diseases, vol 6, 3rd edn. World Bank, Washington DC, pp 233–314

Bussi C, Gutierrez MG (2019) *Mycobacterium tuberculosis* infection of host cells in space and time. FEMS Microbiol Rev 43:341–361

Caulfield AJ, Wengenack NL (2016) Diagnosis of active tuberculosis disease: from microscopy to molecular techniques. J Clin Tuberc Other Mycobact Dis 4:33–43

Centers for Disease Control and Prevention, National Center for HIV/AIDS, Viral Hepatitis, STD, and TB Prevention, Division of Tuberculosis Elimination (2021) Transmission and pathogenesis of tuberculosis. In: Core curriculum on tuberculosis: what the clinician should know, 7th ed. Centers for Disease Control and Prevention, Atlanta, pp. 19–44

Dheda K, Gumbo T, Maartens G et al (2017) The epidemiology, pathogenesis, transmission, diagnosis, and management of multidrug-resistant, extensively drug-resistant, and incurable tuberculosis. Lancet Respir Med 15. S2213-2600(17)30079-6

Drain PK, Bajema KL, Dowdy D et al (2018) Incipient and subclinical tuberculosis: a clinical review of early stages and progression of infection. Clin Microbiol Rev 31:e00021–e00018

Furin J, Cox H, Pai M (2019) Tuberculosis. Lancet 393(10181):1642–1656

Heemskerk D, Caws M, Marais B, Farrar J (2015) Pathogenesis. In: Tuberculosis in adults and children. Springer, London, pp 9–16

Hunter RL (2020) The pathogenesis of tuberculosis—the Koch phenomenon reinstated. Pathogens 9:813

Hunter R, Actor J (2019) The pathogenesis of post-primary tuberculosis. A game changer for vaccine development. Tuberculosis 116S:S114–S117

Moule MG, Cirillo JD (2020) *Mycobacterium tuberculosis* dissemination plays a critical role in pathogenesis. Front Cell Infect Microbiol 25:65

Müller B, Dürr S, Alonso S et al (2013) Zoonotic *Mycobacterium bovis*–induced tuberculosis in humans. Emerg Infect Dis 19:899–908

Newton SM, Brent AJ, Anderson S, Whittaker E, Kampmann B (2008) Paediatric tuberculosis. Lancet Infect Dis 8:498–510

Pai M, Behr M (2016) Latent *Mycobacterium tuberculosis* infection and interferon-gamma release assays. Microbiol Spectr 4(5)

Pai M, Behr MA, Dowdy D et al (2016a) Tuberculosis. Nat Rev Dis Primers 27(2):16076

Pai M, Nicol MP, Boehme CC (2016b) Tuberculosis diagnostics: state of the art and future directions. Microbiol Spectr 4(5)

Rodríguez E, Sánchez LP, Pérez S et al (2009) Human tuberculosis due to *Mycobacterium bovis* and *M. caprae* in Spain, 2004–2007. Int J Tuberc Lung Dis 13:1536–1541

Sharma A, Bloss E, Heilig CM et al (2016) Tuberculosis Caused by Mycobacterium africanum, United States, 2004–2013. Emerg Infect Dis 22(3):396–403

Pathology of Tuberculosis

Soumaya Rammeh and Emna Romdhane

Contents

Abstract

Tuberculous lesions are microscopically heterogeneous and vary depending on the stage of the disease, host immunity response, and phenotypic characteristics of the tuberculous bacillus. The hallmark of tuberculosis infection is necrotizing granulomatous inflammation, composed of epithelioid cells surrounding a central necrotic zone, and accompanied by a variable number of multinucleated giant cells and lymphocytes. Necrosis is typically caseous. Suppurative forms of tuberculosis without granulomas are rare, and mimic pyogenic infection, grossly and microscopically. In immunocompromised persons, tuberculosis may not elicit granulomatous inflammation. The diagnosis of extrapulmonary tuberculosis often requires invasive procedures to obtain cytological and tissue specimens for microbiological, cytological, and histological investigations. Necrosis and granulomas are frequently seen in fine-needle aspiration

S. Rammeh (✉)
Department of Pathology, Charles Nicolle Hospital, Tunis, Tunisia

UR17ES15, Faculty of Medicine of Tunis, Tunis-El Manar University, Tunis, Tunisia
e-mail: soumaya.rammeh@fmt.utm.tn

E. Romdhane
UR17ES15, Faculty of Medicine of Tunis, Tunis-El Manar University, Tunis, Tunisia
e-mail: emnaromdhane90@gmail.com

© The Author(s), under exclusive license to Springer Nature Switzerland AG 2022

M. F. Ladeb, W. C. G. Peh (eds.), *Imaging of Tuberculosis*, Medical Radiology Diagnostic Imaging,
https://doi.org/10.1007/978-3-031-07040-2_3

cytology, but are rarely observed in body fluids. Histological and cytological examinations, notably in endemic areas where molecular tests are unavailable, provide a rapid diagnosis allowing the initiation of the treatment. Ancillary techniques on formalin-fixed paraffin-embedded tissue such as special stains, immunochemistry and molecular tests help to establish the diagnosis. Acid-fast bacilli are identified in specimens containing necrotizing granulomas, especially in areas with suppuration and cavitation. Acid-fast bacilli are less frequently seen in nonnecrotizing granulomas and very rarely seen in nongranulomatous lesions.

Abbreviations

AFB	Acid-fast bacilli
FFPET	Formalin-fixed paraffin-embedded tissue
FNAC	Fine-needle aspiration cytology
HIV	Human immunodeficiency virus
MTB	*Mycobacterium tuberculosis* bacteria
TB	Tuberculosis
ZN	Ziehl–Neelsen

1 Introduction

Unlike pulmonary tuberculosis (TB), the extrapulmonary forms of TB are frequently biopsied. Extrapulmonary TB is often paucibacillary, with negative culture being frequent. In these cases, notably in endemic areas where molecular tests are unavailable, histology provides a rapid diagnosis allowing the initiation of the treatment. The hallmark of TB infection is necrotizing granulomatous inflammation. However, microscopic tuberculous lesions are heterogeneous, being dependent on the disease stage, host immunity response, and phenotypic characteristics of the TB bacillus. This chapter focuses on gross and microscopic features of TB, their pathogenesis, and peculiarities according to locations. The role of ancillary techniques in formalin-fixed paraffin-embedded tissue (FFPET) for the diagnosis of TB is emphasized.

2 Pathogenesis of Tuberculosis Lesions

2.1 Primary Tuberculosis

Primary TB infection refers to the infection of an individual without any previous history of TB (Milburn 2001). It occurs when *Mycobacterium tuberculosis* bacteria (MTB) reach the alveoli of the host and encounter alveolar macrophages. MTB are then phagocytosed and eliminated by alveolar macrophages (Pai et al. 2016). If the defense system of the host fails to eliminate the infection, MTB are not destroyed and the bacilli proliferate inside the alveolar macrophages. The phagocytosed MTB develop various approaches to escape the defense system, such as the inhibition of phagosome maturation, expression of virulence-associated factors, inhibition of phagolysosomal fusion, and protection from reactive oxidative radicals (Cardona 2018; Shim et al. 2020).

Dendritic cells infected by MTB migrate to regional lymph nodes, presenting mycobacterial antigens to lymphocytes. T cells identify MTB antigens and turn into specific T cells, namely CD4 and CD8, leading to the induction of cell-mediated immune response to MTB after a few weeks of infection. These specific lymphocytes return to the lungs, recruit monocytes, and stimulate them by releasing lymphokines including interferon-γ, interleukin 2, and tumor necrosis factor; thus promoting the destruction of mycobacteria (O'Garra et al. 2013). This phenomenon results in the formation of well-defined granulomas consisting of epithelioid cells and giant multinucleated cells surrounded by T lymphocytes, plasma cells, few neutrophils, and a fibrous capsule with collagen (Russell 2007).

Granuloma formation is important to prevent the spread of the infection. In the center of granulomas, there is caseous necrosis, which contains

extracellular bacilli and a high content of lipids and proteins (Kim et al. 2010). Caseous necrosis results not only in tissue destruction but also bacilli destruction. Several mechanisms contribute to the inhibition of MTB replication within necrosis, including low oxygen tension, low pH, and local accumulation of fatty acids (Tomashefski et al. 2008). The Ghon focus is a small focus of granulomatous inflammation that usually occurs in the subpleural parenchyma and affects the mediastinal lymph nodes, forming the Ghon complex. In the majority of patients, the Ghon complex heals with fibrosis and calcifications within weeks or months, with formation of the Ranke complex (Madkour 2004).

In progressive primary TB, the immune system fails to control the multiplication of MTB. Caseous necrosis can become suppurative, containing numerous neutrophils and ultimately leads to cavity formation. The mechanism of suppuration may involve the action of hydrolytic enzymes released from the dead inflammatory cells (Tomashefski et al. 2008). Suppuration has a major action in the progression of disease, causing tissue damage and wide spread to other locations through the blood and lymphatic systems, with resultant extrapulmonary TB (Akhtar and Al Mana 2004).

2.2 Post-primary Tuberculosis

Post-primary TB, also known as secondary TB, is a chronic disease that occurs in immunocompetent individuals who have developed immunity to primary TB. It differs from primary TB in immune response, histopathology, gene predisposition, and clinical presentation (Hunter 2011). In primary TB, caseous necrosis develops within the granulomas; while in secondary TB, granulomas develop around pre-existing foci of caseous pneumonia (Hunter et al. 2014). Post-primary TB is usually due to the reactivation of old lesions by the breakdown of quiescent foci, or to the progression of primary TB into a chronic form (Cardona 2018). The acquisition of a new infection from active cases has been suggested (Hunter et al. 2014).

Post-primary TB is typically restricted to the upper lobes of the lungs and does not involve lymph nodes or other organs. It requires a stronger immune response than primary TB (Hunter et al. 2007). Post-primary TB begins as a lipid pneumonia of foamy alveolar macrophages that undergoes caseation necrosis and fragmentation to produce cavities (Hunter 2011; Hunter et al. 2014). Unlike primary TB that protects the host from disseminated TB, post-primary TB manipulates the immune system through the development of cavities that produce a massive number of bacilli (Hunter and Actor 2019).

3 Pathological Diagnosis

3.1 Specimens for Pathological Diagnosis

The pathological diagnosis of TB is made from cytological and/or tissue specimens. The cytological diagnosis of TB is based on fine-needle aspiration cytology (FNAC) and on cytology of body fluids (Reddy et al. 2013; Sener and Erdem 2019) from specimens such as ascitic fluid, pleural fluid, cerebrospinal fluid, and urine. Cell blocks prepared from FNA material and body fluids are useful for acid-fast staining. Cytology is cost-effective, quick, and relatively non-invasive (Chatterjee and Dey 2014). The diagnosis of TB can be confirmed by a combination of tests performed from FNAC or on body fluids. Necrosis and granulomas are highly suggestive of TB. These features, frequently seen in FNAC material, are rarely observed in body fluids (Reddy et al. 2013). FNAC is a first-line method for the diagnosis of extrapulmonary TB. It is easily applicable to palpable lesions such as peripheral lymphadenopathies. For deep structures, FNAC is guided by radiological examinations such as ultrasound imaging and computed tomography (Handa et al. 2005; Gupta et al. 2011).

The diagnosis of pulmonary TB is mostly based on the isolation of MTB from sputum. Bronchoalveolar lavage and brushings under bronchoscopy are offered mainly in cases with negative sputum to obtain samples for cytology, microbiological, and molecular analyzes. Transbronchial biopsy can play an important role in the diagnosis of pulmonary TB, particularly for patients with negative bacteriology on sputum and on bronchoalveolar lavage fluid. It allows a histological diagnosis suggestive of TB in 42–63% of patients (Lewinsohn et al. 2017). Biopsies and surgical resections are also undertaken in atypical presentations, and in uncontrollable multidrug-resistant diseases (Leong et al. 2016).

Unlike pulmonary TB, the extrapulmonary forms of TB are frequently biopsied. Their diagnosis often requires invasive procedures to obtain tissues for microbiological and histological investigations (Chakravorty et al. 2005). In atypical presentations, notably those mimicking tumors, microbiological analyses may not be performed. In these cases, the diagnosis of TB is based on only histological examination. Furthermore, culture may be negative due to the paucibacillary character of extrapulmonary TB (Gaur et al. 2020). In these cases, histopathology provides a rapid diagnosis of extrapulmonary TB, especially in endemic areas with limited resources, where molecular techniques are unavailable.

3.2 Basic Lesions of Tuberculosis

Microscopically, TB is characterized by heterogeneous and variable lesions depending on the disease stage, host immunity response, and phenotypic characteristics of the TB bacillus (Russell 2007). Microscopically, it is difficult to determine whether a granuloma is primary or secondary, based on only histological features. The hallmark of TB is a necrotizing granulomatous inflammation, composed of epithelioid cells and a peripheral crown of lymphocytes and spindle-shaped fibroblasts, surrounding a central necrotic zone (Fig. 1). Epithelioid granulomas are mostly small, but can present in different range of sizes, reaching several centimeters. They are mostly compact and well delineated, composed of round aggregates of epithelioid cells. These cells have round to oval nuclei, often with irregular contours and abundant eosinophilic cytoplasm (Fig. 2). Several Langhans giant cells are seen in the granulomas. These cells contain many nuclei

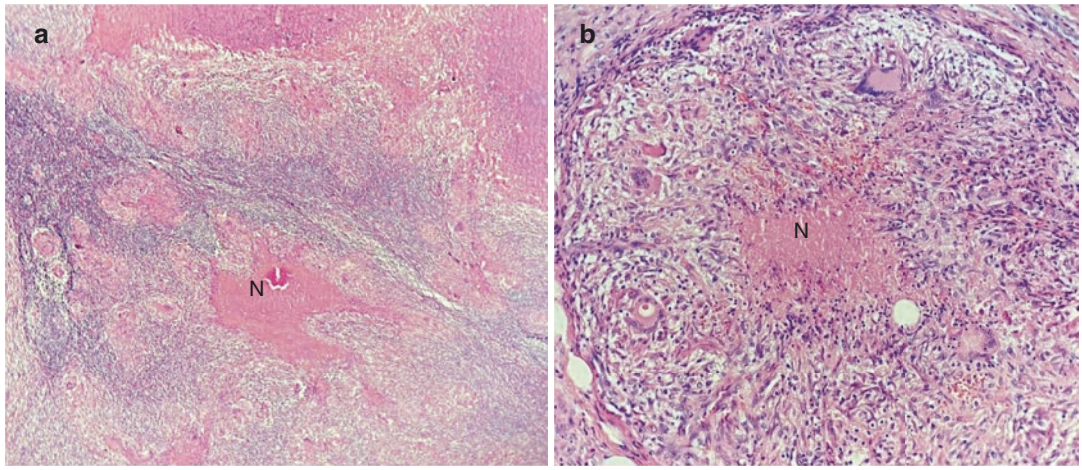

Fig. 1 Photomicrographs show epithelioid granulomas with central caseous necrosis (N). Hematoxylin and eosin stain magnification: (**a**)100× and (**b**) 400×

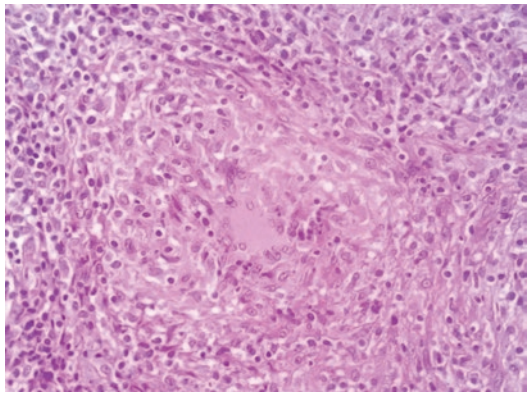

Fig. 2 Photomicrograph shows epithelioid noncaseating granuloma. Epithelioid cells have round to oval nuclei with irregular contours and abundant eosinophilic cytoplasm. Hematoxylin and eosin stain magnification 400×

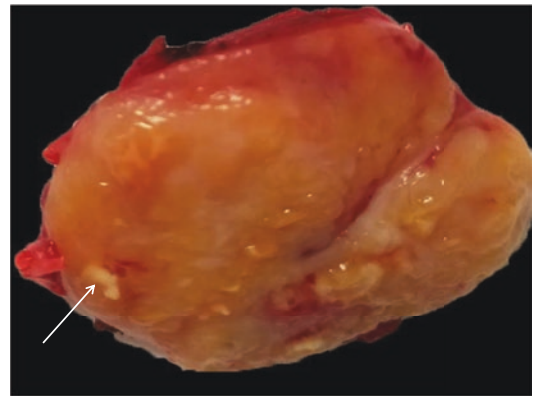

Fig. 4 Caseous necrosis. Specimen photograph of the cut surface of a tuberculous lymph node shows caseous necrosis with a typical white and cheesy appearance (arrow)

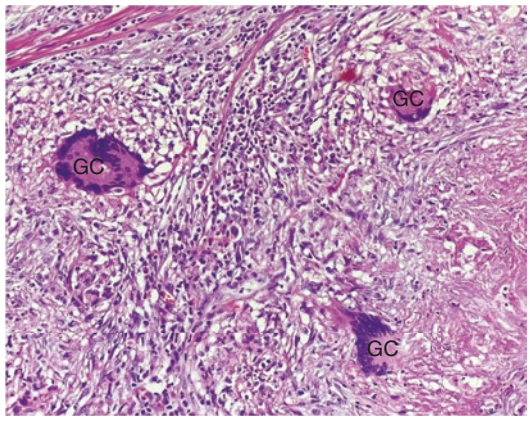

Fig. 3 Photomicrograph shows epithelioid granulomas with Langhans giant cells (GC) with nuclei arranged in a horseshoe-like pattern. Hematoxylin and eosin stain magnification 400×

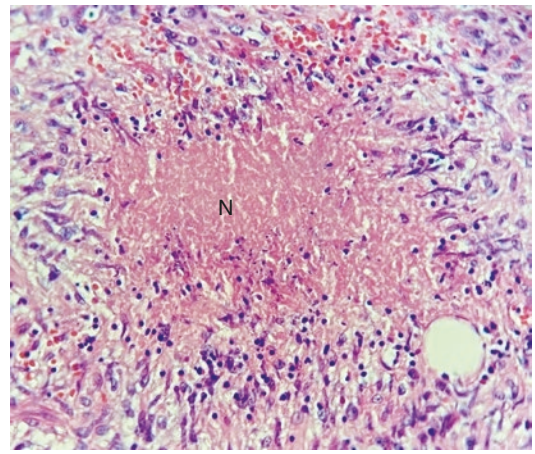

Fig. 5 Caseous necrosis. Photomicrograph shows acellular, granular, and homogeneous eosinophilic necrosis (N) surrounded by palisaded histiocytes. Hematoxylin and eosin stain magnification 400×

arranged in a horseshoe-like pattern at the edge of the cell with abundant cytoplasm (Fig. 3). Langhans giant cells are not specific for TB and are found in various other infectious and non-infectious diseases.

Grossly, caseating necrosis is typically white, soft, and cheesy-looking (Fig. 4). Histologically, in caseating granulomas, epithelioid cells form a palisading arrangement around the central necrosis, which has a fine-grained, homogeneous and eosinophilic necrotic appearance (Fig. 5). In the acute phases of infection, caseous necrosis can become suppurative or liquefactive (Akhtar and Al Mana 2004). Grossly, suppurative and liquefactive necroses are characterized by a yellow creamy appearance. Histologically, liquefactive necrosis has a basophilic appearance containing neutrophils and nuclear debris (Fig. 6). Suppurative necrosis is very rich in neutrophils and is indistinguishable from pus. Unlike caseous necrosis, liquefactive and

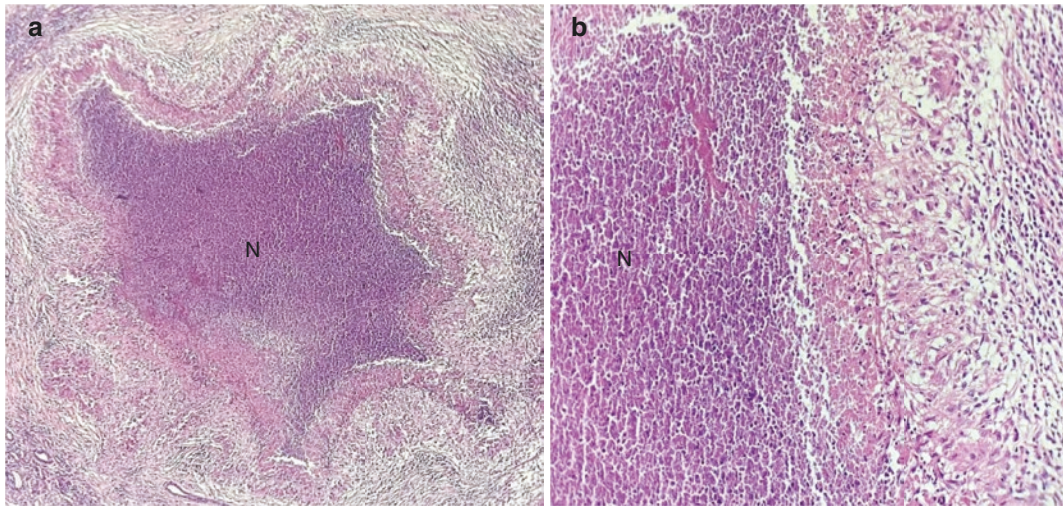

Fig. 6 Liquefactive necrosis. Photomicrograph shows liquefactive basophilic necrosis (N) containing nuclear debris. Hematoxylin and eosin stain magnification: (**a**) 100× and (**b**) 200×

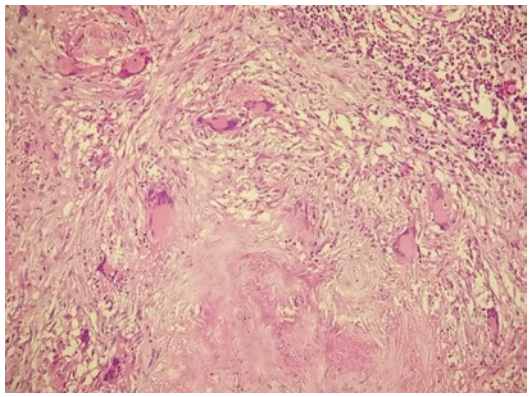

Fig. 7 Photomicrograph shows fibrotic transformation of granuloma. Hematoxylin and eosin stain magnification 400×

suppurative necroses are usually rich in MTB (Tomashefski et al. 2008). Other types of granulomas can be observed in TB infection, including nonnecrotizing granulomas, histiocytic ill-defined granulomas, suppurative necrotic granulomas, and completely fibrotic granulomas (Mattila et al. 2013) (Fig. 7).These lesions reflect the host's immune response to bacterial antigens. Their cell organization and composition depend on the host's immunity.

All types of tuberculous lesions are frequently surrounded by non-specific chronic inflammation called perifocal reaction, which represents a manifestation of delayed hypersensitivity reaction against secreted proteins (Tomashefski et al. 2008). Perifocal reaction occurs in primary and post-primary TB. It is an edematous inflammatory response that contains few or no bacilli, and surrounds a recent active site of infection (Hunter et al. 2014). In pulmonary TB, perifocal reaction is histologically similar to pulmonary alveolar proteinosis which is characterized by many alveoli filled with blood, lipid, plasma, few neutrophils, and many lymphocytes (Fig. 8). Perifocal inflammation is typically associated with vasculitis in small and large arteries and veins, usually the lymphocytic type. Granulomatous vasculitis secondary to TB has also been reported (Pagnoux et al. 2006) (Fig. 9). Thrombosis may be seen in perifocal inflammation, and causes infarction and tissue necrosis (Hunter et al. 2014; Hunter 2020).

The tuberculous changes depend on the balance between the immune response and the infective organisms. In immunocompetent individuals, the infection may be controlled through the development of necrotizing granulomas. MTB may be completely destroyed or reduced to a dor-

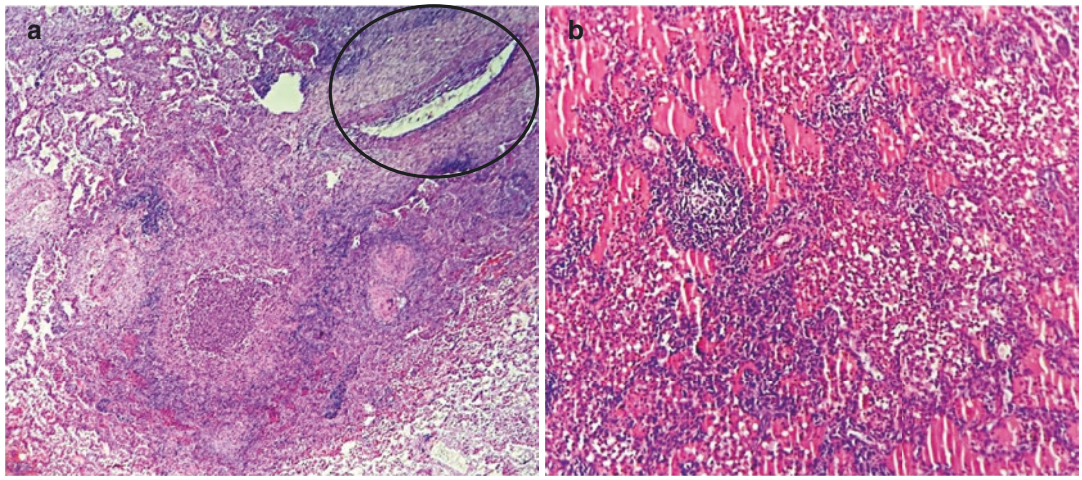

Fig. 8 Perifocal inflammation. (**a**) Photomicrograph shows lymphocytic inflammation with alveolar macrophages and vessel transmural lymphocytic inflammation (circle). Hematoxylin and eosin stain magnification 100×. (**b**) Photomicrograph shows alveolar edema, lymphocytic infiltrate, and alveolar macrophages. Hematoxylin and eosin stain magnification 200×

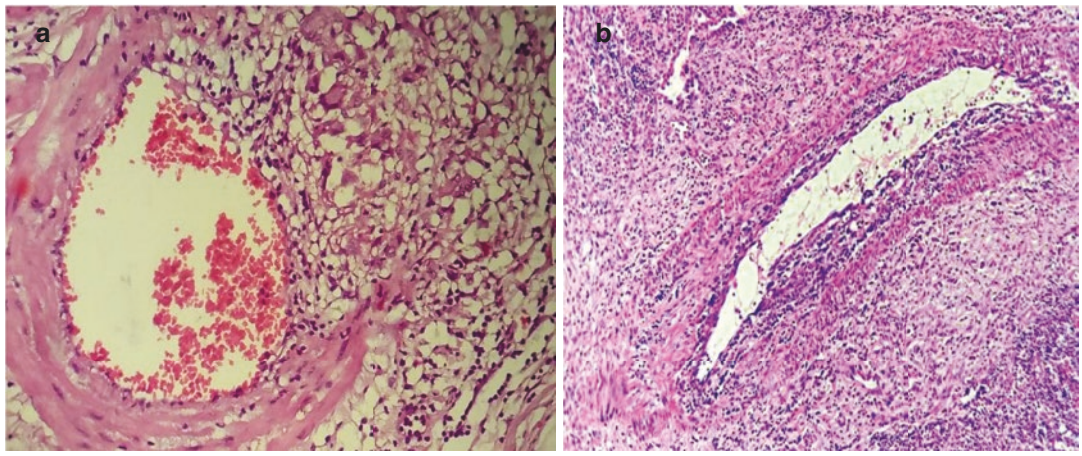

Fig. 9 (**a**) Photomicrograph shows granulomatous vasculitis secondary to tuberculosis. Hematoxylin and eosin stain magnification 400×. (**b**) Photomicrograph shows lymphocytic vasculitis secondary to tuberculosis. Hematoxylin and eosin stain magnification 200×

mant state. Lesions can either be completely resolved or progress to scarring, with no evidence of activity; or leave discrete sequelae where most of the epithelioid cells are gone, with minimal or absent inflammatory cells, fibrosis, and sclerosis. A calcified granuloma generally constitutes a successful immune response (Leong et al. 2016).

Miliary TB usually occurs in immunocompromised individuals. It is characterized by foci of caseating necrosis without granulomas, and is also known as nonreactive miliary TB (Vohra and Dhaliwal 2021). In immunocompromised persons, including patients with human immunodeficiency virus (HIV) infection, TB may either not

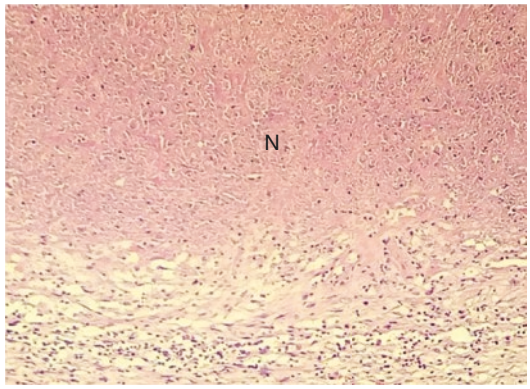

Fig. 10 Tuberculosis in a patient infected by human immunodeficiency virus. Photomicrograph shows necrotic material (N) without epithelioid granuloma. Hematoxylin and eosin stain magnification 400×

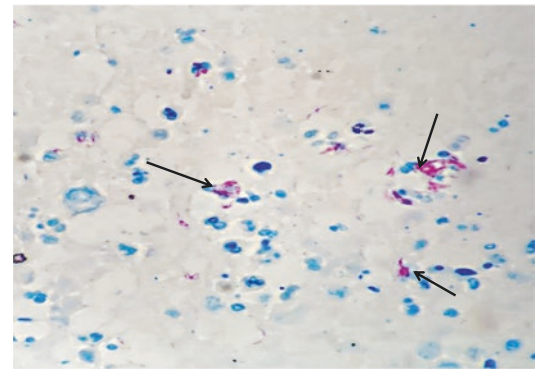

Fig. 11 Ziehl–Neelsen stain on tissue section shows multiple acid-fast bacilli (arrows). Magnification 400×

elicit granulomatous inflammation (Fig. 10), or granuloma formation and reduced function. People living with HIV often fail to develop cell-mediated immunity and may die of disseminated TB. Unlike immunocompetent people, they rarely develop pulmonary cavities and are less able to transmit infection (Hunter et al. 2007). HIV infection causes the apoptosis and depletion of T cells, leading to granuloma disorganization (Ansari et al. 2013). In this situation, granulomas are large and disorganized, and contain a large number of bacilli, plasma cells, and few lymphocytes, with areas of necrosis (Sasindran and Torrelles 2011). As the granulomas enlarge, areas of caseous necrosis expand, causing the rupture of granulomas and the dissemination of MTB. The spread of MTB results in additional formation of new local and nonlocal granulomas.

3.3 Identification of Mycobacteria in Tissue Sections

Special stains for acid-fast bacilli (AFB), immunohistochemistry (Mustafa et al. 2006; Purohit et al. 2017), and molecular tests on FFPET can be helpful to establish the etiological diagnosis of TB (Park et al. 2003; Lee et al. 2011; Budvytiene and Banaei 2020; Romdhane et al. 2020a, b). Histological examination and ancillary techniques are mandatory in establishing an early diagnosis of TB, particularly in extrapulmonary forms, but they do not differentiate among the mycobacteria species (Tomashefski et al. 2008).

3.3.1 Special Stains

Special stains on FFPET for AFB detection are widely used to identify the MTB complex (Johansen et al. 2004; Nassaji et al. 2014). AFB are identified in tissues containing necrotizing granulomas, especially in areas with suppuration and cavitation. AFB are less frequently seen in nonnecrotizing granulomas and poorly formed granulomas (Gupta et al. 2016), and very rarely seen in nongranulomatous lesions (Tomashefski et al. 2008). Three acid-fast stains can be used for the detection of AFB, namely Ziehl–Neelsen (ZN), Kinyoun (cold method), and Auramine–rhodamine.

ZN on FFPET is the most commonly used stain (Fig. 11). It uses carbol fuchsin to stain the lipid wall of the MTB complex. The interpretation of ZN on FFPET requires careful examination because most of lipids from the wall of MTB complex are removed during tissue processing, leading to difficulty in identifying AFB (Fukunaga et al. 2002). The use of oil immersion is mandatory for better visualization and confirmation of MTB. The positivity rate of ZN on FFPET in pulmonary TB can exceed the 50%, but this rate is lower than in sputum smear.

In extrapulmonary TB, which is classically paucibacillary, the sensitivity of ZN on FFPET is much lower, varying from 0% to 44% (Karimi et al. 2014). Therefore, a negative AFB on tissue specimens does not exclude TB infection (Jain et al. 2017). Kinyoun stain is quicker to perform than ZN and does not require heating. In ZN stain, phenol is heated which is toxic to the eyes and respiratory tract.

Auramine–rhodamine staining is applicable on FFPET (Vilchèze and Kremer 2017). It allows rapid screening and it is more sensitive than ZN for mycobacteria detection. But it does not easily localize bacilli within specific lesions (Wöckel 1995). Furthermore, Auramine–rhodamine detection may not be specific, due to the incorporation of fluorochrome dyes by inorganic objects. The cost of fluorescent microscopy is a major limitation, especially in middle- and low-income countries (Tomashefski et al. 2008). Besides, because their low sensitivity on FFPET is due to the influence of formalin fixation and solvents, AFB stains cannot differentiate viable from dead bacilli, and MTB complex from nontuberculous mycobacteria (Tomashefski et al. 2008). False-positive staining can occur in histology laboratories due to the contamination of slides by nontuberculous mycobacteria such as *M. avium* or *M. gordonae*. Contamination is suggested if aggregates of AFB are found in nonnecrotic tissues, out of the tissue plane, or outside the tissue on the slide (Tomashefski et al. 2008).

3.3.2 Immunohistochemistry and In Situ Hybridization

The detection of MTB antigens on FFPET using monoclonal and polyclonal antibodies (PPD, CFP10, ESAT-6, and MPT64) can be used as an alternative to conventional AFB staining (Sumi and Radhakrishnan 2009). An external control is recommended for the adequate processing of immunohistochemistry. The sensitivity of immunohistochemistry on FFPET depends on various factors, including the distribution of mycobacterial antigen, stage of the disease, and specificity of the primary antibody (Kohli et al. 2014). The immunohistochemistry on FFPET targeting anti-MPT64 is very sensitive and specific, and can be used to differentiate MTB complex from nontuberculous mycobacteria (Mustafa et al. 2006; Purohit et al. 2007).

Immunocytochemistry has been also reported for the detection of AFB in aspirated material from lymph nodes and pleural liquid (Tadele et al. 2014; Mustafa et al. 2020), with better sensitivity and specificity than ZN (Hoel et al. 2020). Validated immunohistochemistry and immunocytochemistry offer the advantage of being robust, not sensitive to contamination, and does not require special equipment. In situ hybridization on FFPET has been reported as a useful technique for the identification and differentiation of MTB complex from nontuberculous mycobacteria, with a sensitivity and specificity of 100% and 95%, respectively (Zerbi et al. 2001). However, this technique requires a fluorescence microscope and its cost is a major limitation, especially in countries with limited resources.

3.3.3 Molecular Techniques

Nucleic acid amplification methods offer better sensitivity and specificity for the detection of MTB than conventional techniques (Morel et al. 2020). Unlike culture, molecular tests for the diagnosis of TB do not differentiate viable from dead bacilli (Opota et al. 2019). Molecular tests for TB are routinely performed on fresh tissues. Molecular techniques on FFPET can be an alternative modality for the diagnosis of TB in cases where microbiological investigations have not been performed, mainly because clinical features are in favor of a nontuberculous pathology. Confirmation of TB by molecular tests on FFPET helps these patients avoid another biopsy, which will be impossible in some cases because the lesion has been removed or because of the high risk of anesthesia (Romdhane et al. 2020a, b; Romdhane et al. 2021).

Several molecular tests can be used for the detection of MTB complex on FFPET, including: GeneXpert MTB/RIF (resistance to rifampicin) test, loop-mediated isothermal amplification assays, strand displacement amplification, line probe assay, and digital polymerase chain reac-

tion (PCR) (Johansen et al. 2004; Cao et al. 2020; Romdhane et al. 2020a, b; Romdhane et al. 2021). In paucibacillary TB, nested PCR offers better sensitivity than conventional PCR (Seo et al. 2014; Romdhane et al. 2021). The sensitivity of real-time PCR tests on FFPET varies from 25% to 85.7% (Seo et al. 2014; Polepole et al. 2017; Rindi et al. 2017; Moure et al. 2019; Budvytiene and Banaei 2020), depending on the site of the disease. The sensitivity of these tests on fresh tissues is higher, ranging from 68.6% to 91.9% (Gous et al. 2012; Marouane et al. 2016; Raveendran and Wattal 2016; Mechal et al. 2019; Arora and Dhanashree 2020).

The decrease in sensitivity of molecular tests on FFPET is due to the action of the formalin which induces DNA-tissue protein cross-links, which can inhibit nucleic acid amplification. In addition, nucleic acid fragmentation occurs in FFPET, due to the nature of the specimen and the pH of formalin (Dietrich et al. 2013). For this reason, the selected primer set must be not only specific but also small (<300 pb). Multicopy or repetitive sequences are preferable (Schewe et al. 2005). Some techniques of species typing of MTB have been applied to FFPET (Schaumburg et al. 2017; Carrisoza-Urbina et al. 2019). However, these techniques must be validated before being used for diagnosis.

4 Pathological Features of Tuberculosis in Various Organs

4.1 Pulmonary Tuberculosis

4.1.1 Gross Pathology

Primary pulmonary TB forms a well-limited parenchymal subpleural nodule that is located mostly in the middle and lower pulmonary lobes. It contains caseum in the center and is called a Ghon focus (Dietrich et al. 2013). Rarely, Ghon foci are bilateral or multiple (Leong et al. 2016). Grossly, the Ghon focus is a gray-white, firm solitary nodule measuring 10–15 mm in dimension (Fig. 12). Together with the affected mediastinal lymph node, it forms the Ghon complex. Rarely, a Ghon focus forms a large solitary encapsulated nodule called a tuberculoma that may mimic a neoplasm. On tissue sections, a tuberculoma shows concentric laminations, caseous foci, and cavitation (Leong et al. 2016).

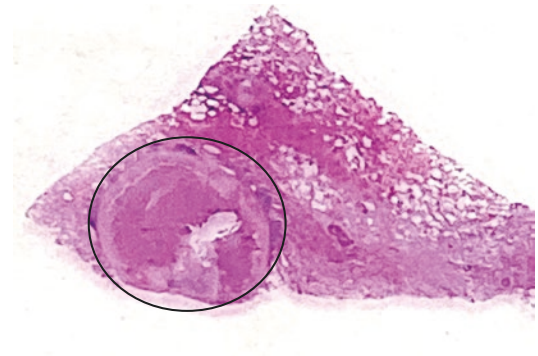

Fig. 12 Subpleural encapsulated pulmonary nodule representing primary tuberculosis. Photomicrograph shows a Ghon focus (circle). Magnification 2×

Healed primary TB is often tiny and easily missed on gross examination. In progressive primary TB, cavitation is characterized by a thin wall that is lined by fibrotic tissue and necrosis. In post-primary TB, lesions are restricted to the upper lung, and characterized by extensive fibrotic and necrotic areas. Cavitations are frequently observed in the lung (Fig. 13) and may be extensive, producing a massive number of MTB (Hunter 2011). In severe situations, the entire lung or a whole lobe may be replaced and destroyed by fibrocaseous pneumonia with cavitation (Tomashefski et al. 2008; Leong et al. 2016).

Rarely, a branch of a pulmonary artery may abut the wall of a cavity. The adventitia and media of the pulmonary arterial wall may be replaced by granulation tissue and then by a fibrin-forming Rasmussen aneurysm, whose rupture into the cavity can cause massive hemoptysis (Tomashefski et al. 2008). Healed progressive post-primary TB is marked by extensive scarring, thick caseous foci, calcifications, bronchiectasis, and emphysema (Tomashefski et al. 2008). When

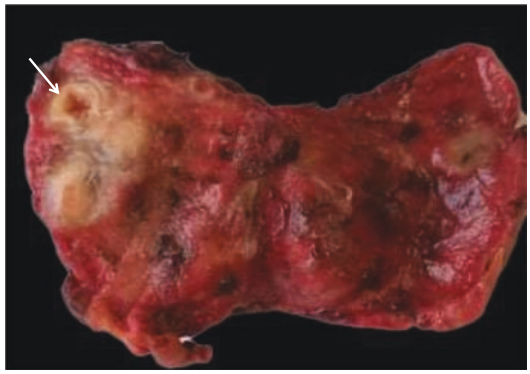

Fig. 13 Photograph of the cut surface of a pulmonary wedge resection specimen shows a subpleural nodule with a cavitary lesion (arrow)

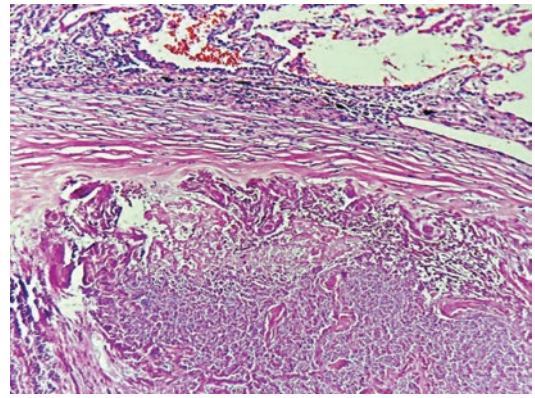

Fig. 14 Photomicrograph shows a fibrotic caseous lesion representing primary tuberculosis. Hematoxylin and eosin stain magnification 100×

the immune system fails to contain TB infection, progressive primary TB and post-primary TB may progress to miliary TB. Grossly, miliary TB is characterized by numerous whitish nodules measuring 1–3 mm in diameter, resembling millet seeds (Sharma and Mohan 2017).

4.1.2 Microscopic Pathology

Microscopically, primary pulmonary TB lesions are not distinctive from those of post-primary TB. The granulomas produced by primary and secondary TB have similar morphological features and similar functions. In primary TB, caseous necrosis develops within the granulomas; while in post-primary pulmonary TB, the granulomas develop around pre-existing foci of caseous pneumonia (Hunter et al. 2014). Primary pulmonary TB is characterized by aggregates of epithelioid cells, leading to formation of the Ghon focus in the apices of the lung (Stephenson and Byard 2020). The Ghon focus is encapsulated by fibrosis, centered by caseous necrosis, and accompanied by a variable number of multinucleated giant cells and lymphocytes (Fig. 14).

In the early stage, post-primary pulmonary TB begins as an endogenous lipid pneumonia associated with bronchial obstruction, characteristic of delayed-type hypersensitivity in which infection is restricted to foamy alveolar macrophages (Hunter et al. 2007). Lipid pneumonia is in part due to intracellular and extracellular accumulation of secreted mycobacterial antigens that can resolve spontaneously in approximately 95% of cases (Hunter 2016). In the other 5%, lesions undergo necrosis to produce a caseous pneumonia that may be expelled to leave a cavity, or remain as a mass that induces granulomas and fibrocaseous disease (Hunter et al. 2014). The wall of the cavity consists of a thin layer of caseous necrotic tissue surrounded by fibrosis with degenerated neutrophils, epithelioid and giant cells, and abundant bacilli (Hunter 2011). Cavitation facilitates dissemination of MTB from the granuloma via the airways to the external environment by breakdown of the fibrous capsule (Subbian et al. 2015).

In pulmonary TB, a mixture of concomitant lesions is usually observed, namely necrotizing and nonnecrotizing granulomas (Fig. 15), fibrotic necrotizing granulomas, and liquefactive and suppurative granulomas (Fig. 16) (Gupta et al. 2016). Suppurative granulomas contain a large number of MTB because the liquefactive milieu constitutes an excellent medium for MTB growth and replication (Leong et al. 2016). Tuberculous cavities may be colonized by Aspergillus fungus, forming an aspergilloma in the pulmonary parenchyma (Fig. 17). Perifocal inflammation is seen in primary and post-primary TB. It surrounds

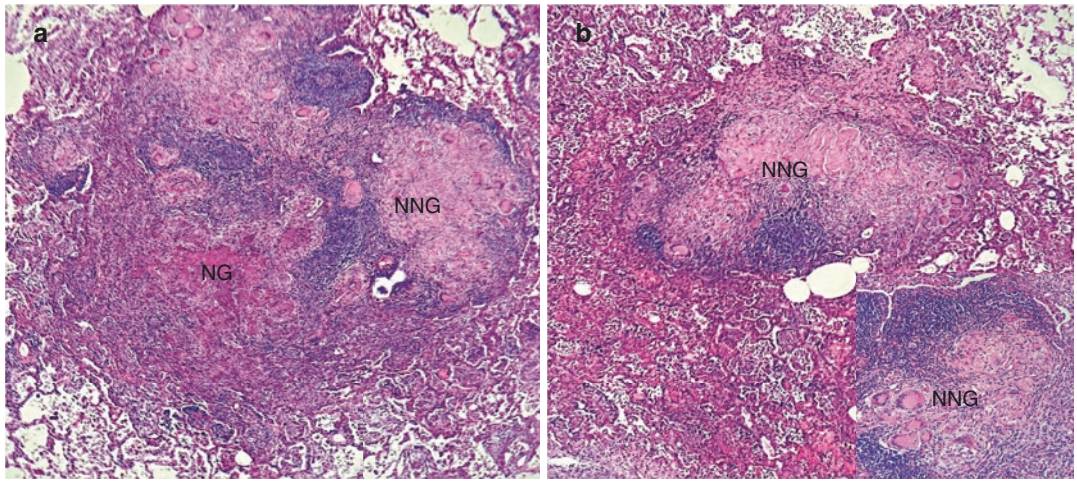

Fig. 15 Pulmonary tuberculosis. (**a** and **b**) Photomicrographs show necrotizing granulomas (NG) and nonnecrotizing granulomas (NNG) with significant perifocal inflammation. Hematoxylin and eosin stain magnification 100×

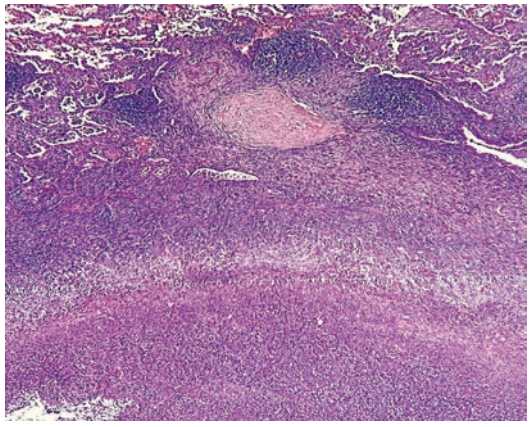

Fig. 16 Pulmonary tuberculosis. Photomicrograph shows a large area of basophilic liquefied necrosis. Hematoxylin and eosin stain magnification 100×

active foci of TB and is microscopically characterized by non-specific inflammation with lipid-rich alveolar edema and inflammatory infiltrate containing plasma cells, few neutrophils and many lymphocytes. Perifocal inflammation typically shows vascular lesions including thrombi, lymphocytic vasculitis, and more rarely granulomatous vasculitis (Pagnoux et al. 2006, Hunter et al. 2014; Hunter 2020) (Fig. 9).

Pulmonary cytological samples correspond mainly to sputum, bronchioalveolar lavage, and FNAC. The most important diagnostic application of bronchioalveolar lavage is for detecting opportunistic infections such as TB in immunocompromised patients. FNAC is mainly performed in pseudotumoral forms of TB, in patients who fail to respond to anti-TB therapy and in immunocompromised patients. A confident diagnosis of a granulomatous process is possible on cytology material. The triad comprising epithelioid histiocytes in cohesive clusters, nonpigmented giant cells, and amorphous or granular necrotic background is suggestive for the diagnosis of TB. Lymphocytes may be plentiful in TB. Unlike the multinucleated histiocytes seen in non-specific pulmonary inflammation, multinucleated cells seen in TB are free of intracytoplasmic pigment or birefringent material.

4.1.3 Differential Diagnosis

The diagnosis of post-primary TB is a challenge for the pathologist. Pulmonary TB can be misdiagnosed as many infectious and non-infectious diseases (Gupta et al. 2016). Granulomatous vascular lesions seen in TB can lead to misdiagnosis of primary vasculitis, particularly Wegener granulomatosis. Pulmonary TB, especially noncaseating forms, can be misdiagnosed as sarcoidosis. Fungal infections (e.g., histoplasmosis, coccidioidomycosis), nocardiosis and nontuberculous infection may display caseous

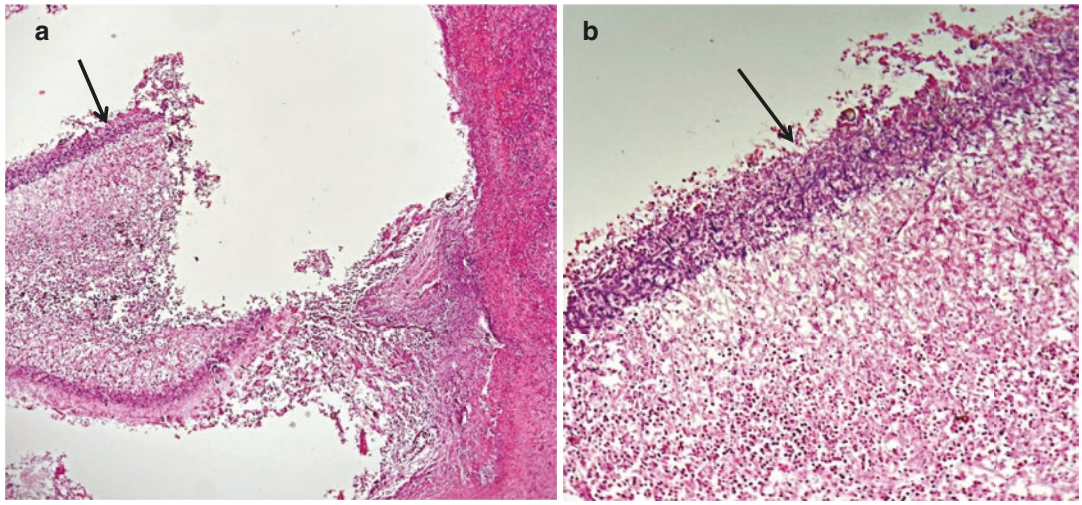

Fig. 17 Pulmonary aspergilloma. Photomicrograph shows a thick layer of Aspergillus hyphae (arrow) occupying the lumen of a tuberculous cavity. Hematoxylin and eosin stain magnification: (**a**) 100× and (**b**) 400×

necrosis, similar to TB (Mukhopadhyay and Gal 2010).

4.2 Pleural Tuberculosis

4.2.1 Gross Pathology

Grossly, tuberculous pleural effusion is typically straw-colored. Pleural TB is grossly characterized by the presence of multiple discrete granulomatous foci, 1–3 mm in size, that may extend to the serosal surface. Subserosal granulomas may heal and leave minimal residual scarring (Tomashefski et al. 2008). Tuberculous involvement of the pleura may present grossly as pleural thickening (Vorster et al. 2015), encystment, and extensive parietal pleural plaques (Clarke et al. 2006).

4.2.2 Microscopic Pathology

Pleural TB manifests histologically as multiple granulomas accompanied by variable degrees of chronic inflammation. Granulomas often show caseous necrosis, but necrosis may also be absent (Fig. 18). Other non-specific forms of pleural TB may be seen, including acute fibrinous pleuritis and fibrosis (Allen and Suster 2018). In severe forms, the serosal surface may be destroyed. Fibrothorax may be seen as an accumulation of fibrous tissue in the pleural cavity. Massive calcification may occur (Tomashefski et al. 2008). Typically, tuberculous pleural effusion has a predominant lymphocytic composition with few mesothelial cells (Bibbo and Wilbur 2014). Lymphocytes are occasionally atypical, leading to a misdiagnosis of lymphomatous pleural effusion. In the early stages of infection, some neutrophils and meso-

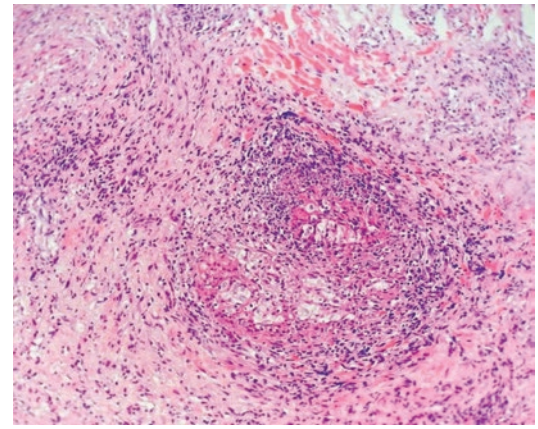

Fig. 18 Pleural tuberculosis. Photomicrograph shows an epithelioid granuloma with fibrotic change in the pleural tissue. Hematoxylin and eosin stain magnification 200×

thelial cells may be seen. The presence of numerous mesothelial cells in the pleural effusion eliminates TB infection. Langhans giant cells and epithelioid cells are rarely seen in tuberculous pleural effusion (Tomashefski et al. 2008).

4.2.3 Differential Diagnosis

The diagnosis of pleural TB may be challenging with many other granulomatous diseases being usually accompanied by underlying pulmonary granulomatous diseases, e.g., sarcoidosis, hypersensitivity pneumonitis, fungal infections, nontuberculous mycobacteria infection, Wegener granulomatosis, and rheumatoid disease (Philip et al. 2018).

4.3 Lymph Node Tuberculosis

4.3.1 Gross Pathology

The most common presentation of tuberculous lymphadenitis is an enlarged unilateral cervical lymph node. Other lymphatic regions (axillary, inguinal, supraclavicular, mesenteric, retroperitoneal) are less frequently affected. Multiple and bilateral lymph nodes may be matted to form a large conglomerate mass. Grossly, tuberculous lymph nodes have multiple foci of cheesy necrotic material that are highly suggestive of TB (Eshete et al. 2011) (Fig. 19). In some cases, the necrosis is yellow and liquid, with a suppurative appearance. Caseation may not be seen grossly. Calcification is rare, being mostly observed in treated cases. Lymph nodes may be totally replaced by caseum, and inflammation may extend to adjacent extranodal tissues. Fistula formation may occur, with discharge of caseous material forming a scrofula. In patients with gross features suggestive of TB, unfixed tissues must be sent for microbiological examination for ZN stain and culture.

4.3.2 Microscopic Pathology

In the early phase of tuberculous lymphadenitis, the lymph node shows non-specific lymphadenitis. Inflammatory cells gradually infiltrate the lymph node parenchyma and peri-adenitis appears over time. Initially, abscesses are formed in the lymph node. Gradually, abscesses change to caseous necrosis (Hegde et al. 2014). Tuberculous lymphadenitis frequently exhibits necrotizing granulomas (Fig. 20). The necrosis is often confluent and can be abundant, leading to lymph node destruction (Fig. 21). At the beginning, necrosis is rich in nuclear debris. Caseous necrosis may include cholesterol crystals and become rich in neutrophils, preceding fistula formation. Gradually, fibrosis develops and replaces epithelioid cells (Fig. 22). Nonnecrotizing granulomatous forms of tuberculous lymphadenitis

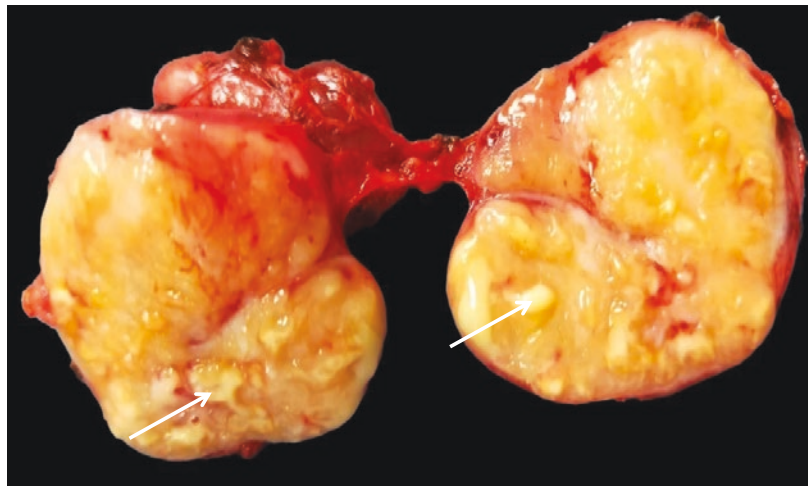

Fig. 19 Specimen photograph of the cut section of a tuberculous lymph node shows multiple, white cheesy, caseous necrotic foci (arrows)

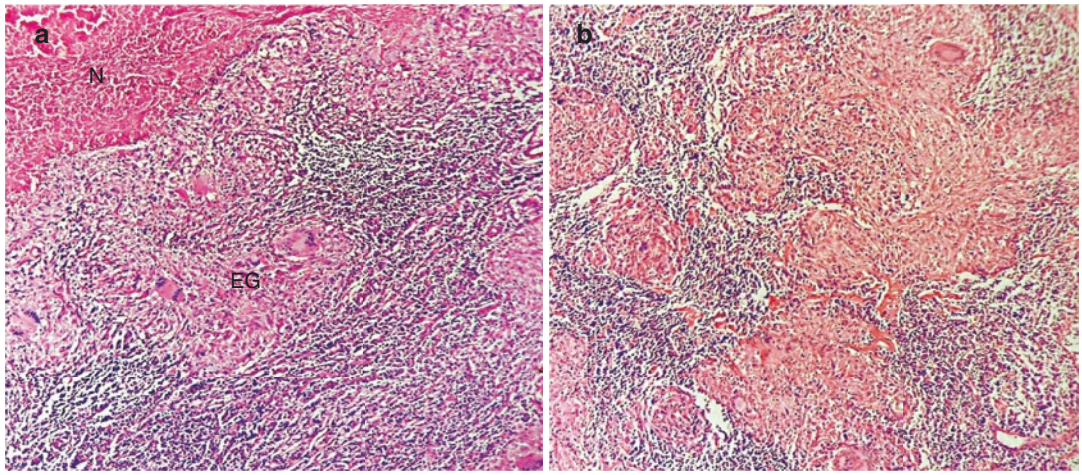

Fig. 20 Lymph node tuberculosis. Photomicrographs show (**a**) areas of eosinophilic, acellular, and granular caseous necrosis (N) with epithelioid granulomas (EG) and (**b**) noncaseating epithelioid granulomas with giant cells. Hematoxylin and eosin stain magnification 200×

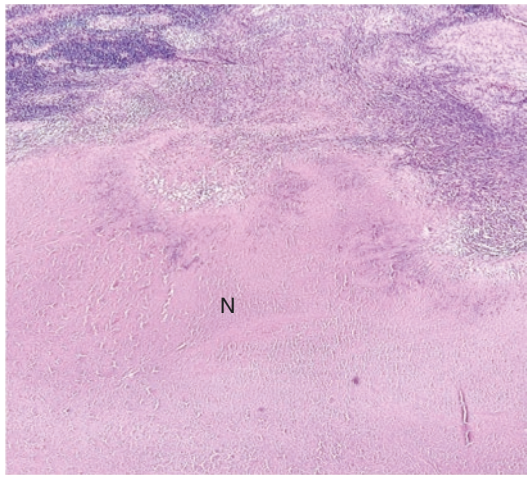

Fig. 21 Lymph node tuberculosis. Photomicrograph shows massive destruction of lymph node parenchyma by caseous necrosis (N). Hematoxylin and eosin stain magnification 100×

are rare and closely mimic sarcoidosis. Based on histology, distinguishing between the two diseases is difficult, if not impossible. Furthermore, AFB are rarely isolated in nonnecrotizing granulomas. Nongranulomatous lymph node parenchyma may show follicular hyperplasia with interfollicular plasmacytosis (Fig. 23).

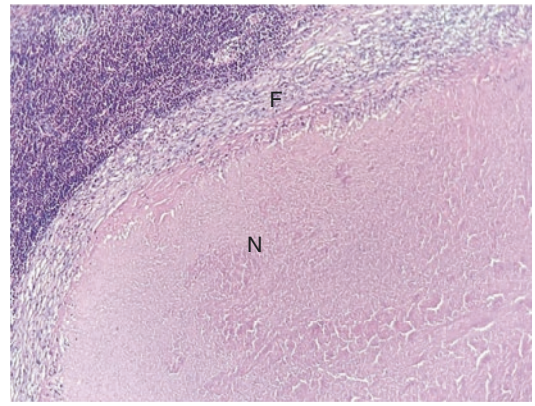

Fig. 22 Lymph node tuberculosis. Photomicrograph shows caseous necrosis (N) surrounded by a fibrous capsule (F). Hematoxylin and eosin stain magnification 200×

4.3.3 Fine-Needle Aspiration Cytology

FNAC is preferred to open biopsy for the diagnosis of lymph node TB (Hemalatha et al. 2014). It is the first-line method for the diagnosis of TB in this location, especially in endemic areas. FNAC is a reliable tool but it is operator-dependent; requiring an experienced cytopathologist, sufficient material, good sampling method, and good coordination between the cytopathologist and the clinician (Rammeh et al. 2019a, b). The aspirated

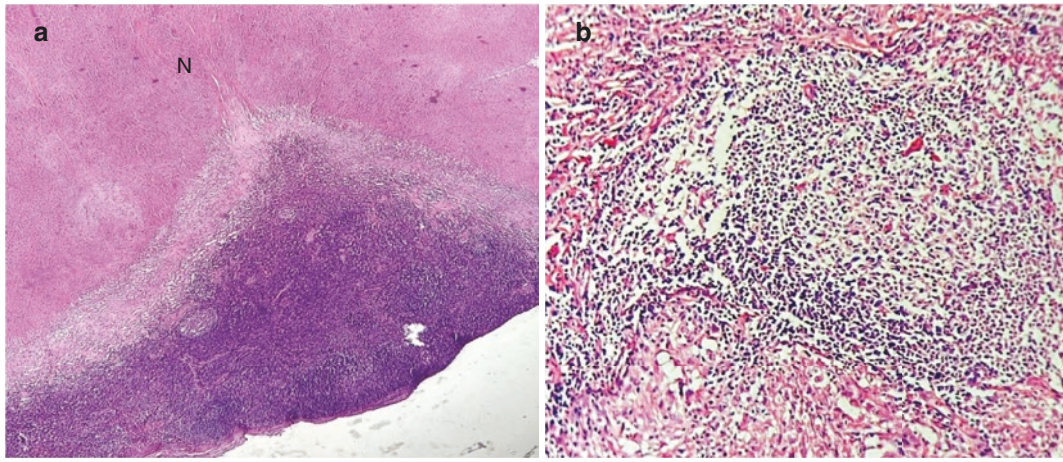

Fig. 23 Lymph node tuberculosis. Photomicrographs show follicular lymphoid hyperplasia with caseous necrosis (N) (**a**) in the residual lymph node parenchyma. Hematoxylin and eosin stain magnification: (**a**) 100× and (**b**) 400×

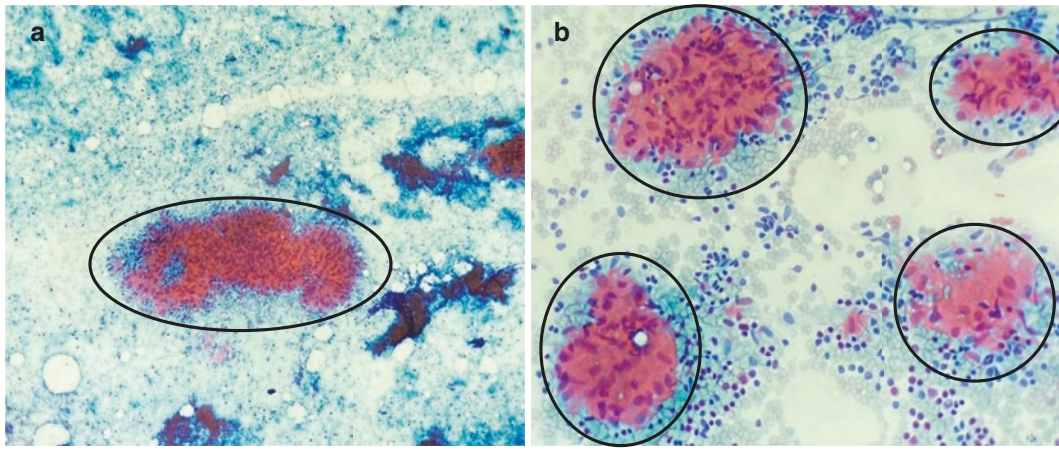

Fig. 24 Fine-needle aspiration cytology of a tuberculous lymph node. Papanicolaou stains show (**a**) epithelioid granuloma (circle) in a granular necrotic background, and (**b**) epithelioid granulomas (circles) with lymphoid background. Papanicolaou stain magnification: (**a**) 100× and (**b**) 400×

material is also used for microbiology and for molecular testing (Akhtar and Al Mana 2004). Grossly, aspirated material is typically sparse, and cheesy-white with a caseous appearance. Not infrequently, aspirated material from a tuberculous lymph node is purulent with a creamy yellow appearance, mimicking suppurative lymphadenitis.

Microscopically, FNAC shows epithelioid groups of cells, forming epithelioid granulomas in an eosinophilic homogeneous granular background with giant cells (Fig. 24). These associated features are highly suggestive of tuberculous etiology, especially in endemic countries (Rammeh et al. 2018). Granulomas with necrosis are found in 69–83% of FNAC of tuberculous lymphadenitis (Majeed and Bukhari 2011; Rammeh et al. 2018). The sensitivity and the specificity of FNAC in the diagnosis of tuberculous lymphadenitis range from 88% to 98% and 48.8% to 100%, respectively (Handa et al. 2012; Rammeh et al. 2018).

4.3.4 Differential Diagnosis

Tuberculous lymphadenitis must be distinguished from tularemia lymphadenitis, cat

scratch lymphadenitis, Yersinia lymphadenitis, lymphogranuloma venereum, atypical mycobacterial infection, Bacillus Calmette–Guérin (BCG) lymphadenitis, toxoplasma lymphadenitis, brucellosis and fungal infections (e.g. Cryptococcus, Histoplasma, Coccidioidomycosis, Pneumocystis) (Zumla and James 1996; Asano 2012; Deveci et al. 2016). BCG lymphadenitis is usually smaller than tuberculous lymphadenitis. It is observed in immunocompromised patients, and characterized histologically by suppurative necrosis surrounded by a rim of histiocytes, and contains numerous bacilli. Necrotizing granulomas and giant cells are rarely observed. Other non-infectious diseases that may mimic tuberculous lymphadenitis include: sarcoidosis, Hodgkin lymphoma, and autoimmune disorders such as systemic lupus erythematosus, autoinflammatory diseases, and Kikuchi disease (Asano 2012).

4.4 Abdominal Tuberculosis

The main forms of abdominal TB are gastrointestinal and peritoneal TB.

4.4.1 Gross Pathology

Infection of the small intestine by TB is referred to as tuberculous enteritis. The ileocecal region is the most commonly-affected site in gastrointestinal TB (Malikowski et al. 2018). Grossly, tuberculous enteritis appears in three forms, namely ulcerative, hypertrophic, and ulcero-hypertrophic. The ulcerative form occurs mostly in the ileum and jejunum. Grossly, it is characterized by one or more transverse ulcers, thickening and stricturing of the bowel wall, stenosis formation, and perforation (Dasgupta et al. 2009). Tubercles may be present in the serosal surfaces. Enlarged mesenteric lymph nodes are frequently present in the ulcerative form. When ulcers heal, reactive fibrosis may cause a "napkin ring" stricture of the bowel lumen (Strayer 2015). The hypertrophic and ulcero-hypertrophic forms commonly affect the ileocecal region, mimicking Crohn disease, and can present as a mass that may cause intestinal obstruction (Malikowski et al. 2018). Colonic and rectal TB present as localized mucosal ulcerations in the acute phase, with massive necrosis and fibrosis in the chronic phase (Akhtar and Al Mana 2004) (Fig. 25).

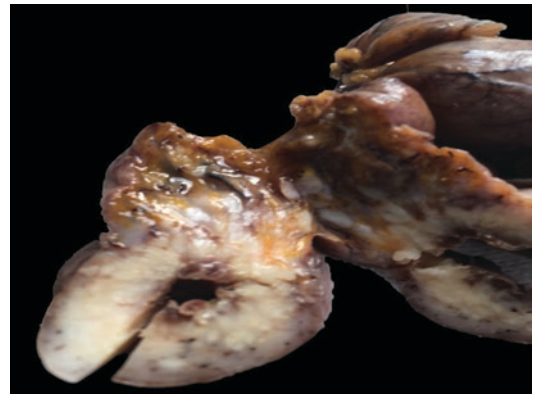

Fig. 25 Photograph of the cut surface of colonic tuberculosis specimen shows necrosis and fibrosis of the colonic wall and omentum

Peritoneal TB has three forms, namely wet type with ascites, dry type with adhesions, and fibrotic type with omental thickening and loculated ascites. Grossly, ascitic effusion is typically straw-colored. Peritoneal TB presents as multiple whitish small nodules of few millimeters size that look like "seedlings" on the parietal and visceral surfaces of the peritoneum. Sometimes, nodules are large, mimicking carcinosis. Inflammation and exudation lead to straw-colored ascites. Thickening of the omentum, intestinal walls, and formation of caseous masses lead to plastic peritonitis (Weledji and Pokam 2017).

4.4.2 Microscopic Pathology

In intestinal TB, the mucosa is ulcerated. The submucosal and serosal layers show large and confluent granulomas (Fig. 26), with central caseous necrosis surrounded by fibrosis. Granulomas display marked variations in size and contain a mixture of lymphocytes, plasma cells, and giant cells at the periphery (Dasgupta et al. 2009). Mesenteric vasculitis may be seen in intestinal TB (Fig. 27). Lesions occur in large, medium, and small mesenteric vessels, leading to intestinal ischemia, which contributes to the development of ulcers, perforation, fibrosis, and

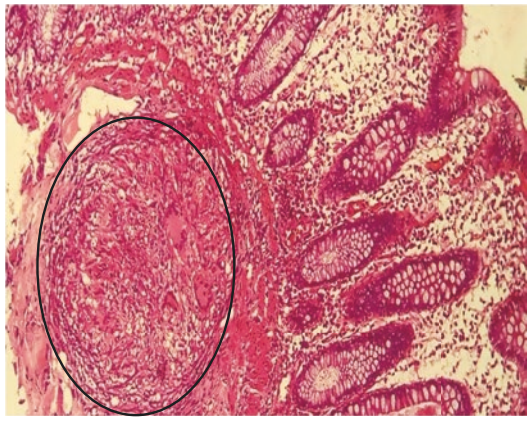

Fig. 26 Photomicrograph shows an epithelioid granuloma (circle) with giant cells in intestinal submucosa. Hematoxylin and eosin stain magnification 400×

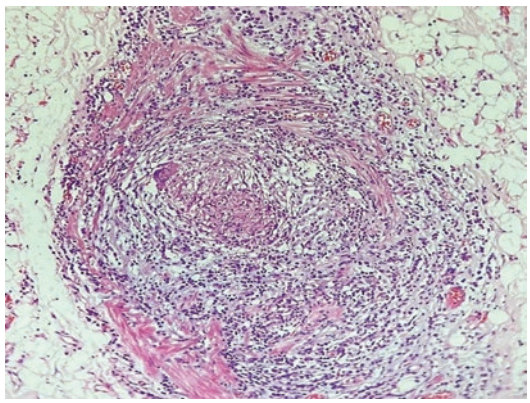

Fig. 27 Granulomatous vasculitis secondary to colonic tuberculosis. Photomicrograph shows an epithelioid granuloma infiltrating the wall of a mesenteric vessel. Hematoxylin and eosin stain magnification 400×

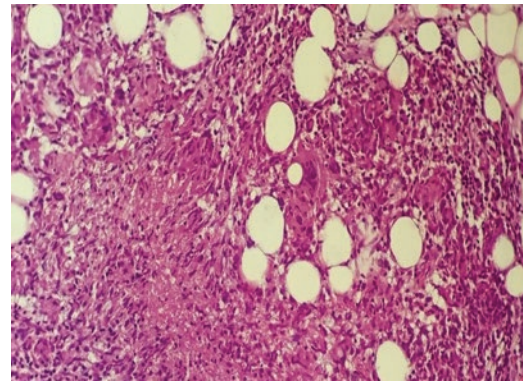

Fig. 28 Peritoneal tuberculosis. Photomicrograph shows epithelioid granulomas with giant cells infiltrating the omentum. Hematoxylin and eosin stain magnification 400×

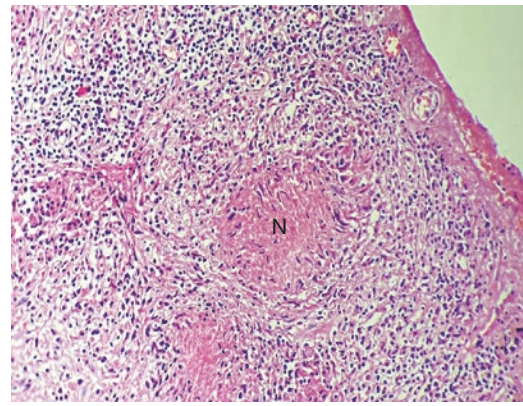

Fig. 29 Peritoneal tuberculosis. Photomicrograph shows epithelioid granulomas with caseous necrosis (N) in peritoneal subserosa. Hematoxylin and eosin stain magnification 400×

strictures (Sharma and Bhatia 2004). Peritoneal TB presents as numerous, large, and confluent epithelioid granulomas, with a peripheral zone of lymphocytes and Langhans giant cells surrounded by fibrosis (Fig. 28). In the center of granulomas, caseous necrosis may be seen (Fig. 29). Peritoneal TB can be diagnosed based on aspirated ascitic fluid. Cytological examination of the ascitic fluid shows an exudate rich in inflammatory cells, predominantly lymphocytes, monocytes, and a few polymorphonuclear cells (Bolognesi and Bolognesi 2013). Epithelioid cells and giant cells are rarely observed.

4.4.3 Differential Diagnosis

The differential diagnosis of intestinal TB includes infectious enteritides such as actinomycosis, histoplasmosis, amebiasis, yersiniosis, and typhlitis (Park 2015), and non-infectious diseases, mainly Crohn disease. Distinguishing intestinal TB from Crohn disease may be problematic in small biopsy samples. In intestinal TB, granulomas are large, confluent, and well-defined, with caseous necrosis, while the granulomas of Crohn disease are small, ill-defined, and sparse. Microbiological and molecular studies are mandatory for the differential diagnosis (Kedia et al. 2019). Peritoneal TB must be dif-

ferentiated from other bacterial peritonitis and talc peritonitis (Weledji and Pokam 2017). Non-infectious diseases, including peritoneal carcinomatosis and malignant mesothelioma, are easily excluded microscopically.

4.5 Central Nervous System Tuberculosis

In the central nervous system, lesions begin with the development of small tuberculous granulomas (called Rich foci) in the brain, spinal cord, or meninges (Malhotra and Kulshreshtha 2017). These foci occur either during the primary tuberculous infection or shortly afterwards, and may remain quiescent for years after the primary infection. The rupture or growth of one or more tuberculous foci induces the development of various types of central nervous system TB (Garg 1999). The specific causes of rupture or growth of Rich foci remain known, but immunological mechanisms may play an important role (Garg 1999). The forms of central nervous system TB include tuberculous meningitis, tuberculous encephalitis, intracranial tuberculoma, tuberculous brain abscess, radiculomyelitis, epiduritis, and intramedullary tuberculoma (Rock et al. 2008; Malhotra and Kulshreshtha 2017).

Biopsies from parenchymal brain lesions are rarely performed. The diagnosis of central nervous system TB is usually based on radiological investigation in association with evidence of TB at other sites (Muzumdar et al. 2018). Indirect diagnosis of TB in the central nervous system can be made by aspirated material from paraspinal abscess, enlarged peripheral lymph node or a mass in the lung (Malhotra and Kulshreshtha 2017). The diagnosis of tuberculous meningitis can be confirmed by a combination of tests (cytology, microbiology, and molecular tests) performed on cerebrospinal fluid (Malhotra and Kulshreshtha 2017; de Almeida et al. 2019).

4.5.1 Gross Pathology

Tuberculous meningitis is the most common form of central nervous system TB. In the majority of cases, it is due to Rich foci rupture into the subarachnoid space or into the ventricular system. Gross appearances of tuberculous meningitis are white tubercles, 3–5 mm in diameter, scattered over the leptomeninges (Malhotra and Kulshreshtha 2017), with cerebral edema and increased brain weight. There is gelatinous or fibrinous exudate around the sylvian fissures, basal cisterns, brainstem, and cerebellum, which may extend into the spinal canal (Davis et al. 2019). The basal exudates of TB are usually more severe in the vicinity of the circle of Willis (Garg 1999).

Central nervous system tuberculomas appear deep in the brain parenchyma. They are unique or multiple well-limited masses, surrounded by normal brain tissue which is compressed around the lesion with perilesional edema. Tuberculoma size varies from 2 to 80 mm (Garg 1999) and can reach 12 cm (Malhotra and Kulshreshtha 2017). The inside of these masses may contain cheesy necrotic areas composed of caseous material. *En plaque* tuberculoma is a rare form of central nervous system tuberculoma which affects the meningeal covering, mimicking meningioma on imaging. It is reported more frequently in the fronto-parietal region (Aggarwal et al. 2016).

Tuberculous brain abscess is a rare form of central nervous system TB. It is usually solitary, larger, and progresses much more rapidly than tuberculomas. Tuberculous brain abscess is frequently multiloculated, with marked surrounding edema, and has a liquid suppurative center (Garg 1999; Chakraborti et al. 2009). Radiculomyelitis is a common manifestation of spinal TB and a complication of tuberculous meningitis characterized by thick gelatinous exudates that occupy the subarachnoid spaces and leptomeninges (Malhotra and Kulshreshtha 2017).

4.5.2 Microscopic Pathology

The initial histological features of tuberculous meningitis are sero-fibrinous exudate with extensive caseous necrosis in the leptomeninges (Gupta et al. 2011). After a few days of infection, the infiltrate contains lymphocytes, plasma cells, epithelioid histiocytes, and giant cells. Epithelioid granulomas are usually few and ill-defined in tuberculous meningitis (Malhotra and

Kulshreshtha 2017). Cytological examination of the cerebrospinal fluid in tuberculous meningitis shows a predominance of lymphocytic pleocytosis. Neutrophil predominance may be seen in early infection (Malhotra and Kulshreshtha 2017). Aggregates of epithelioid cells and giant cells are rarely seen in the cerebrospinal fluid (Jeren and Beus 1982). In immunocompromised patients, the cellular response may be weak and the cerebrospinal fluid may be paucicellular (Bhigjee et al. 2007). The brain parenchyma is edematous with glial reaction.

In severe forms, glial reaction and edema are very important. Ischemic, toxic, and immunoallergic mechanisms are advocated for these lesions (Dastur and Lalitha 1973). Vascular lesions are frequently observed, including phlebitis, mural necrosis, and transmural lymphocytic inflammation (Gupta et al. 2011). These vascular lesions can cause thrombosis. Brain infarctions occur during the acute phase of the disease and also during treatment. The most commonly-affected vessels are those at the base of the brain, including the internal carotid artery, proximal middle cerebral artery, and perforating vessels of the basal ganglia. Hemorrhagic transformation of infarcted tissue is not unusual (Garg 1999).

Tuberculoma is microscopically characterized by clusters of granulomas which join to form nonnecrotizing granulomas. The evolution of these lesions leads to the production of caseous necrosis within the center of granulomas, which is surrounded by epithelioid cells, lymphocytes, and Langhans giant cells (Figs. 30 and 31). Liquefaction of the center core is seen in active cases. Calcification of the necrosis is observed in inactive forms. AFB are rare in tuberculomas found in areas of caseous necrosis (Malhotra and Kulshreshtha 2017). The perilesional brain parenchyma shows edema with some proliferation of astrocytes and glial cells.

Tuberculous brain abscess is a localized collection of pus mixed with bacilli in an abscess cavity (Menon et al. 2011). Histological features of tuberculous brain abscess resemble those of pyogenic abscess and do not show typical necrotizing epithelioid granulomas (Prakash et al. 1989). Palisades of histiocytes around the suppurated center may be observed. The absence of a peripheral granulomatous reaction is possibly explained by the failure of the host's immune mechanisms. Unlike tuberculoma, tuberculous brain abscess is classically rich in bacilli. In radiculomyelitis, the spinal cord and nerve roots are partially affected. Within the inflammatory exudates, there is a granulomatous reaction of leptomeninges. Meningitis can be associated with ischemic lesions in the spinal cord. These lesions are observed mostly in the lumbosacral region but damage in dorsal and cervical regions has been reported (Bazin 2004).

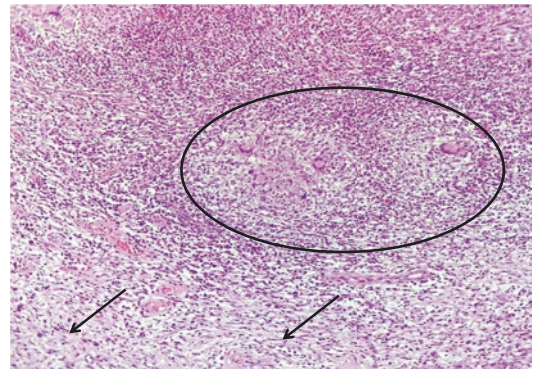

Fig. 30 Cerebral tuberculosis: Photomicrograph shows epithelioid granulomas (circle) surrounded by reactive brain tissue (arrows). Hematoxylin and eosin stain magnification 200×. (Courtesy of Dr. Slim Haouet)

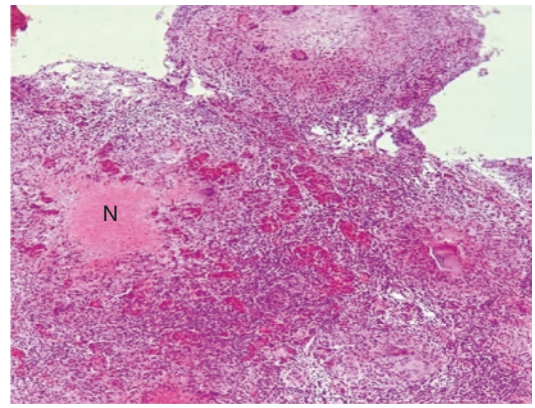

Fig. 31 Pituitary tuberculosis. Photomicrograph shows epithelioid granulomas with caseous necrosis (N) in the pituitary parenchyma. Hematoxylin and eosin stain magnification 200×. (Courtesy of Dr. Slim Haouet)

4.5.3 Differential Diagnosis

In the acute inflammatory stage, tuberculous meningitis can be misdiagnosed as pyogenic meningitis, particularly in people living with HIV (Malhotra and Kulshreshtha 2017). In the chronic inflammatory stage, necrotizing granulomas are highly suggestive of TB. However, a variety of lesions may mimic tuberculoma, such as fungal infection (cryptococcosis, aspergillosis, histoplasmosis, coccidioidomycosis, blastomycosis), and sarcoidosis. Special stains (ZN, periodic acid–Schiff, Gomori methenamine silver) and molecular diagnoses are recommended to aid the differential diagnosis (Malhotra and Kulshreshtha 2017).

4.6 Urogenital Tuberculosis

4.6.1 Gross Pathology

Urogenital TB involves infection of the urinary and/or genital tracts. Grossly, renal TB is seen as enlargement or reduction of the kidney size, with irregular scarring on the surface and multiple cavities containing friable necrotic material (Akhtar and Al Mana 2004) (Fig. 32a). At the end-stage of renal TB, extensive necrosis may destroy the renal parenchyma (Muneer et al. 2019), calcify and become surrounded by fibrous tissue leading to the so-called cement, putty, or chalk kidney. The kidney is frequently involved in miliary TB. Lesions display tiny pale or white tubercles measuring up to 3 mm (Eastwood et al. 2001) (Fig. 32b). In TB infection, the ureter develops multiple strictures. The shrinking and fibrous contraction of the ureter leads to the formation of a "golf hole" orifice in the bladder (Das et al. 2008). Bladder TB usually occurs secondary to renal TB. In the advanced stage, the bladder becomes small, irregular, contracted, and calcified.

In male genital tract TB, the testis and epididymis are enlarged and fibrotic, with caseous necrosis and discharging sinuses (Akhtar and Al Mana 2004). In the prostate, early lesions are rarely detected on palpation. When the disease is advanced, lesions are usually bilateral, and the prostate is enlarged with signs of inflammation and caseous necrosis (Das et al. 2008). Enlarged masses occur in the prostate, containing multiples cavities that can perforate into the urethra and extend to the urinary bladder. In the late stage, the prostate becomes shrunken and fibrotic, mimicking carcinoma (Goldblum et al. 2017).

The fallopian tubes are the most common site involved in female genital tract TB. The fallopian tubes are enlarged, displaying gray to yellow nodules on the surface. Tubal stricture and obstruction, tubo-ovarian masses, and hydrosalpinx may occur in fallopian tube TB (Sharma et al. 2018). Tuberculous manifestations in the

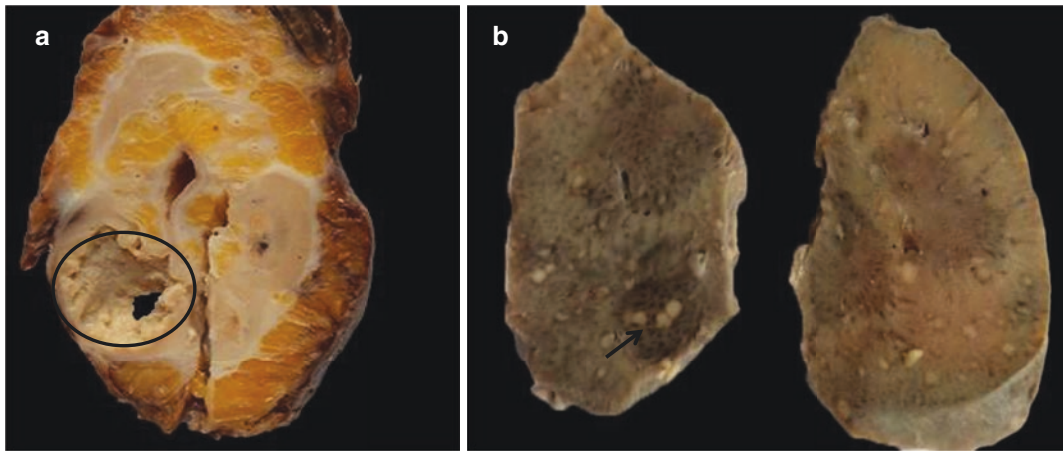

Fig. 32 (**a**) Photograph of the cut surface of nephrectomy specimen shows a dilated calyx lined by caseous material (circle). (**b**) Miliary tuberculosis. Specimen photograph shows multiple tiny tubercles (arrow) in the renal parenchyma of a patient infected by human immunodeficiency virus

ovaries include cyst or mass formation, and even ovary destruction. Gross caseous necrosis is uncommon in the ovaries. In the uterus, TB involves mostly the endometrium which displays ulcers, necrosis, and hemorrhage. Extensive destruction of the endometrium may occur (Sharma et al. 2008).

4.6.2 Microscopic Pathology

In renal TB, multiple and small epithelioid granulomas with caseous necrosis are seen, with neutrophils, plasma cells, and mononuclear cell infiltration (Figs. 33 and 34). In the chronic phases, renal TB displays extensive fibrosis and calcifications (Das et al. 2008). In advanced disease, keratinizing squamous metaplasia may occur in the renal pelvis and may persist even after treatment (Jennette et al. 2014). In immunocompromised patients, granulomas are absent or poorly structured with caseous necrosis (Eastwood et al. 2001) (Fig. 35). In bladder TB (Fig. 36), early lesions are superficial, small, and characterized by the presence of soft caseous material and a peripheral hyperemic zone (Goldblum et al. 2017). When the disease

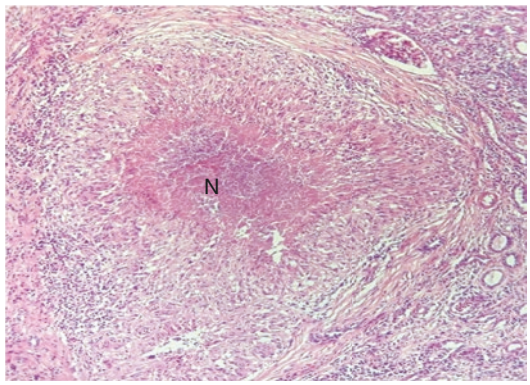

Fig. 33 Renal tuberculosis. Photomicrograph shows an epithelioid granuloma with caseous necrosis (N) in the renal parenchyma. Hematoxylin and eosin stain magnification 200×

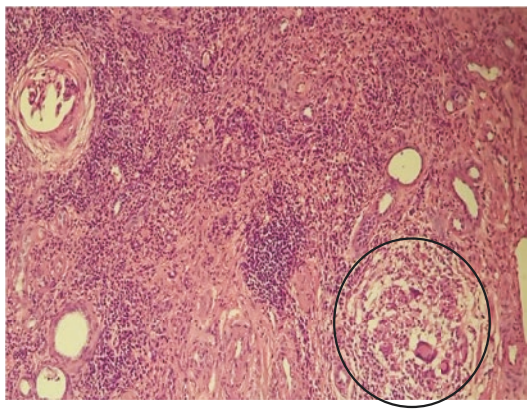

Fig. 34 Renal tuberculosis. Photomicrograph shows an epithelioid granuloma (circle) with lymphocytic inflammation of renal parenchyma. Hematoxylin and eosin stain magnification 200×

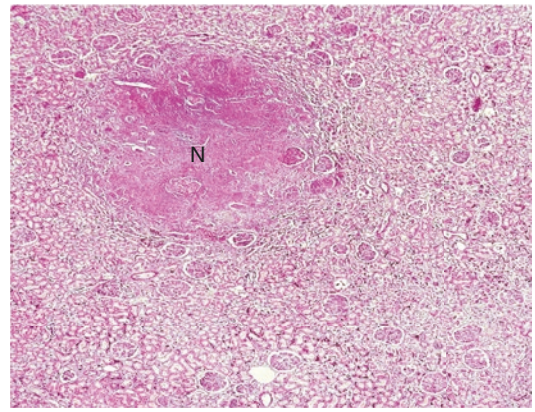

Fig. 35 Renal tuberculosis. Photomicrograph shows caseous necrosis (N) without granulomas in the renal parenchyma of a patient infected by human immunodeficiency virus. Hematoxylin and eosin stain magnification 100×

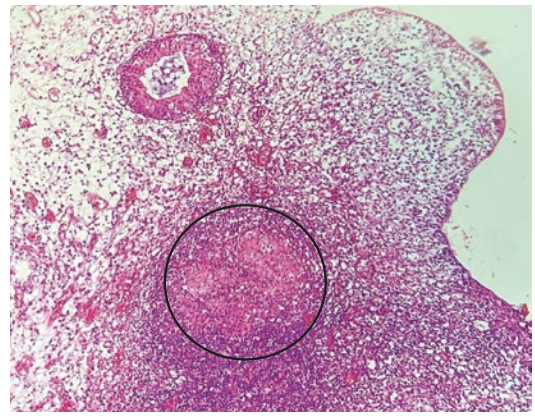

Fig. 36 Bladder tuberculosis. Photomicrograph shows epithelioid granulomas (circle) in the bladder mucosa. Hematoxylin and eosin stain magnification 200×

progresses, multiple ulcers coalesce and may undergo fibrosis. In renal and bladder TB, epithelioid granulomas are rarely observed in urine cytology. When present, epithelioid granulomas are ill-defined and contain giant cells with a necrotic background. Urothelial cell hyperplasia and benign squamous cells may be seen (Arora et al. 2010).

Tuberculous endometritis typically have noncaseating granulomas, composed of epithelial cells, Langhans giant cells, and lymphocytes (Fig. 37). Gradually, the endometrial glands are destroyed. Metaplasia of the endometrial lining and glands is often seen in tuberculous endometritis (Das et al. 2008). In cases where granulomatous inflammation is absent, the endometrium is infiltrated by plasma cells and lymphocytes (Kurman et al. 2019). In the uterine cervix, cytological examination may be useful in the diagnosis of cervical TB. Cytological smears display squamous cells in a background of neutrophils. Macrophages, aggregates of epithelioid cells, and few Langhans giant cells may be seen (Kalyani et al. 2012).

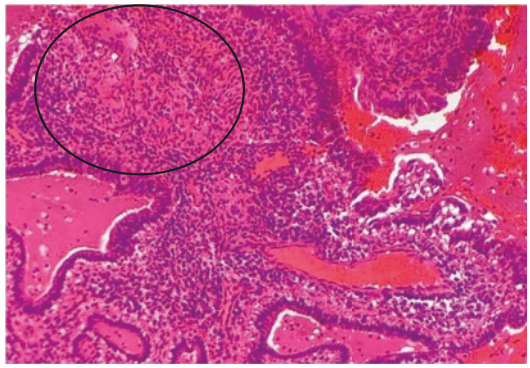

Fig. 37 Tuberculous endometritis. Photomicrograph shows a nonnecrotizing epithelioid granuloma (circle) in the endometrial mucosa. Hematoxylin and eosin stain magnification 200×

In the prostate, lesions begin in the stroma and then spread to the acini (Fig. 38). Necrosis is usually extensive with incomplete fibrous encapsulation. The scrotum shows a variable degree of fibrosis and epithelioid granulomas (Fig. 39), with focal microabscesses (Das et al. 2008). The development of abscesses leads to the formation of a "watermelon" scrotum. In the scrotum, lesions occur mostly in the epididymis (Fig. 40) and can be bilateral, displaying typical granulomatous inflammation (Kulchavenya and Khomyakov 2006).

4.6.3 Differential Diagnosis

Renal and bladder TB may be misdiagnosed as other infectious granulomatous diseases such as

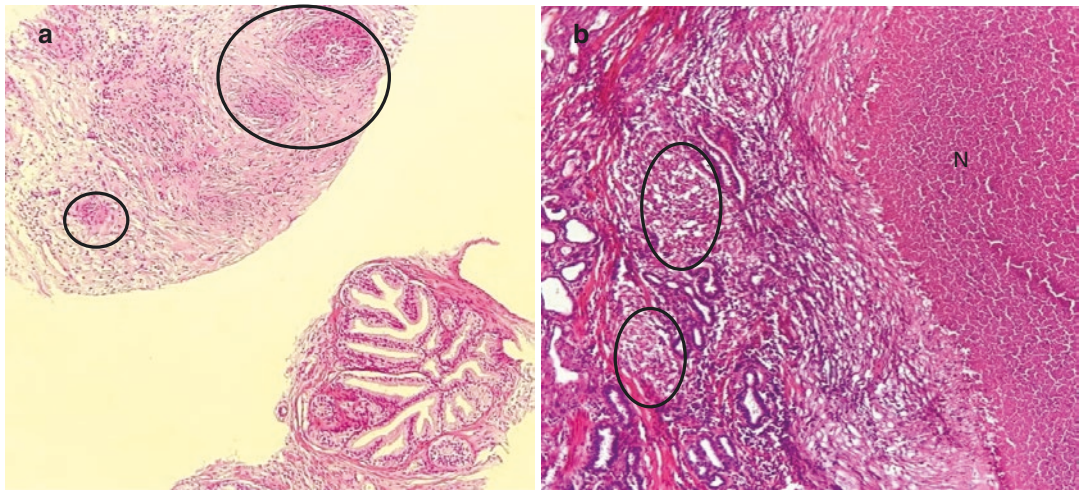

Fig. 38 Prostatic tuberculosis. Photomicrographs show (**a**) epithelioid granulomas (circles) without caseous necrosis and (**b**) epithelioid granulomas (circles) with abundant caseous necrosis (N). Hematoxylin and eosin stain magnification 200×

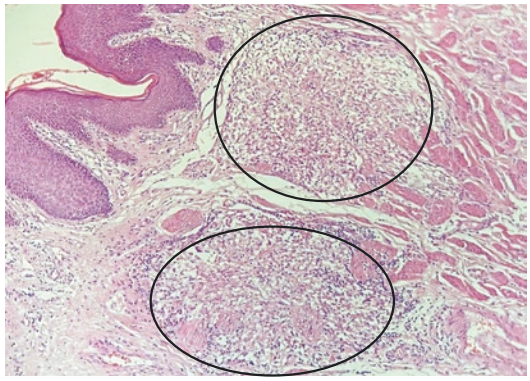

Fig. 39 Scrotal tuberculosis. Photomicrograph shows large epithelioid granulomas (circles) in the dermis of the scrotal skin. Hematoxylin and eosin stain magnification 200×

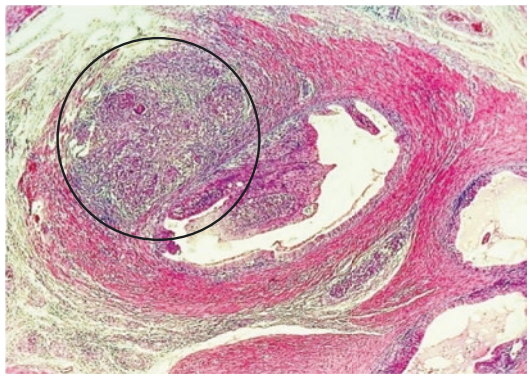

Fig. 40 Epididymal tuberculosis. Photomicrograph shows epithelioid granulomas (circles) in the epididymis wall. Hematoxylin and eosin stain magnification 100×

nontuberculous mycobacteria, other infections (due to *Brucella spp*, *Treponema spp*, *Blastomyces spp)*, and non-infectious granulomatous disorders such as sarcoidosis and idiopathic vasculitides (Muneer et al. 2019). The administration of intravesical BCG to patients treated for bladder carcinoma induces a granulomatous inflammation in the bladder. Lesions may extend to the prostate and to the lung (Goldblum et al. 2017). Granulomatous lesions of female and male genital tract may be misdiagnosed as syphilis, actinomycosis, granuloma inguinale, lymphogranuloma venereum, Crohn disease, schistosomiasis, brucellosis, or histoplasmosis (Sharma 2015).

4.7 Musculoskeletal Tuberculosis

Musculoskeletal TB refers to the involvement of bone and/or joint by TB. Vertebral involvement is the most common type of musculoskeletal TB (Leonard and Blumberg 2017).

4.7.1 Gross Pathology

In tuberculous spondylodiscitis, the lesion begins in the vertebral bodies, usually sparing the lamina, spinous process, and the adjacent vertebrae. The thoracic spine is the part of the spine mostly affected by TB. Extensive necrosis may be seen and destroys the spine, leading to spinal cord compression. It may also extend into the soft tissues, forming cold abscesses (Strayer 2015). In several situations, the vertebral body and disc can be completely replaced by tuberculous tissue, leading to vertebral fusion. In tuberculous arthritis, lesions begin in the bone or in the synovium. When it starts as tuberculous synovitis, the synovium become swollen, hypertrophic and may fill the entire joint space. Multiple rice bodies are commonly detected in the synovial space, which grossly resembles polished grains of rice (Bayram et al. 2016) (Fig. 41). Tissue granulation extends from the synovium to the bone, producing massive destruction of articular cartilage (Tuli 2002). The loss of articular cartilage may lead to bony ankylosis.

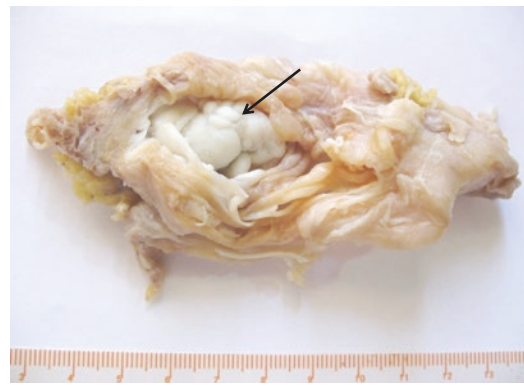

Fig. 41 Synovial tuberculosis. Specimen photograph shows numerous rice bodies in the synovial tissue (arrow). (Courtesy of Dr. Habib Jaafoura)

4.7.2 Microscopic Pathology

In tuberculous spondylodiscitis, necrotizing granulomas are seen in 59–76% of spine biopsies (Cottle and Riordan 2008). Initially, granulomas produce necrosis of the bone marrow (Fig. 42), and then the lesions extend to other sites. The center of the granuloma is filled with eosinophilic, granular, and amorphous material, with a mixture of debris and dead bacilli (Romdhane et al. 2020a, b). Suppurative necrosis without epithelioid granulomas is a rare form of tuberculous spondylodiscitis that is frequently misdiagnosed as pyogenic infection (Rammeh et al. 2019a, b). Bone sequestra are very suggestive of TB, but is not pathognomonic, as brucellar and pyogenic spondylodiscitis may also have bone sequestra. New bone formation can occur in the early phase of chronic tuberculous infection, and may or may not be accompanied by bone sequestra (Li et al. 2016).

In countries that are highly endemic for TB, cytopathological examination is an alternative to histology. However, it is operator-dependent, requiring a well-trained radiologist, sufficient material, good sampling method, and good coordination between the cytopathologist and the radiologist. FNAC is highly recommended for paravertebral abscesses and lytic lesions of the spine (Gupta et al. 1999). In cytology, epithelioid granulomas, giant cells, and caseous necrosis are observed in 50–68% of cases. In case of discordance between cytological and clinical findings, or if the cytological examination is negative, percutaneous biopsy is required to confirm the diagnosis of musculoskeletal TB (Francis et al. 1999; Jorda et al. 2000).

The histological features of tuberculous arthritis are similar to those of tuberculous spondylodiscitis. Tuberculous arthritis is characterized by necrotizing epithelioid granulomas (Fig. 43). Lesions cross the joint to infect the bone on the other side of the joint. In immunocompromised patients, lesions are often composed of histiocytes with numerous bacilli but without epithelioid granulomas (Pigrau-Serrallach and Rodríguez-Pardo 2013). Joint aspiration and synovial fluid aspiration are valuable procedures for the diagnosis of tuberculous arthritis. Caseous necrosis and epithelioid granulomas are uncommon in these specimens. When they are present, a definitive diagnosis of TB can be made easily (Siddaraju and Bundele 2007).

4.7.3 Differential Diagnosis

Musculoskeletal TB may be misdiagnosed as other granulomatous diseases, such as brucellosis, fungal infection, and sarcoidosis (Rammeh et al. 2019a, b). Suppurative forms of

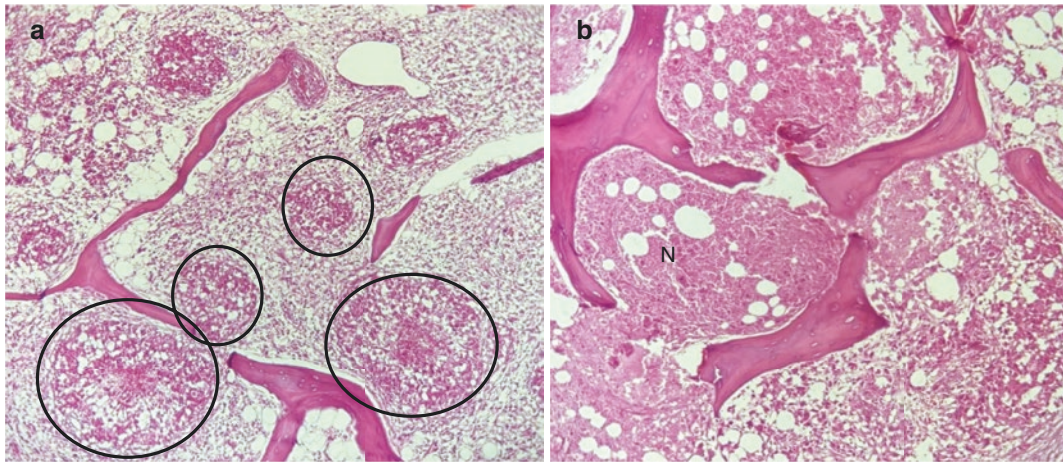

Fig. 42 Tuberculous spondylodiscitis. Photomicrographs show (**a**) numerous epithelioid granulomas (circles) and (**b**) necrotic material (N) in the medullary spaces. Hematoxylin and eosin stain magnification: (**a**)100× and (**b**) 200×

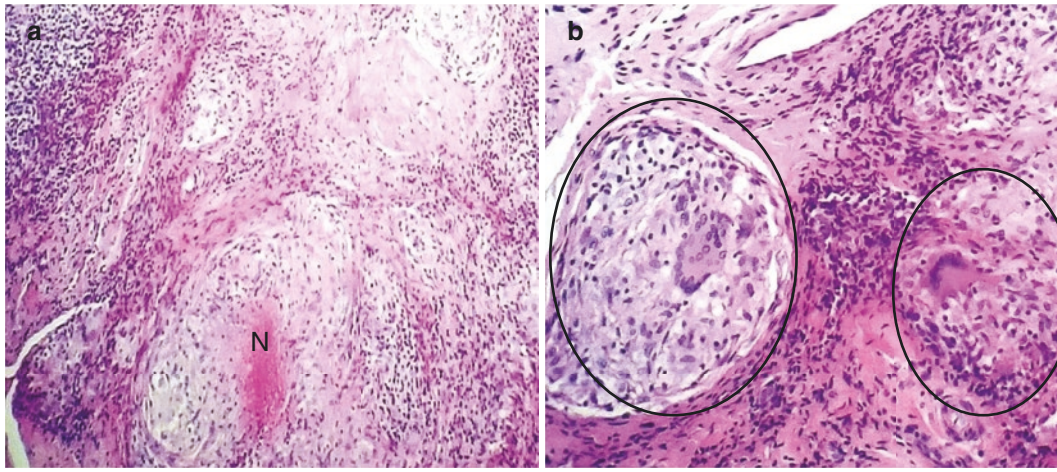

Fig. 43 Synovial tuberculosis. Photomicrographs show (**a**) epithelioid granuloma with caseous necrosis (N) and (**b**) epithelioid granulomas with giant cells (circles) in synovial tissue. Hematoxylin and eosin stain magnification: (**a**) 200× and **(b)** 400×

musculoskeletal TB closely mimic pyogenic infection. Special stains for AFB and fungi on FFPET can be helpful to establish a specific causative infection (Romdhane et al. 2020a, b).

5 Conclusion

Unlike pulmonary TB, extrapulmonary forms of TB are frequently biopsied, as their diagnoses often require invasive procedures to obtain tissues for microbiological and histological examinations. Histopathology provides a rapid diagnosis of extrapulmonary TB, especially in endemic areas with limited resources, where molecular techniques are unavailable. Tuberculous lesions are microscopically heterogeneous, and vary depending on the disease stage, host immunity response and phenotypic characteristics of the tuberculous bacillus. In immunocompetent individuals, a mixture of concomitant lesions is usually observed, consisting of necrotizing and nonnecrotizing granulomas, fibrotic necrotizing granulomas, and liquefactive and suppurative granulomas. Unlike nonnecrotizing granulomas, suppurative granulomas are rich in MTB. In immunocompromised persons, TB may not elicit a granulomatous inflammation. In this situation, granulomas are large and disorganized, containing a large number of bacilli, plasma cells, and few lymphocytes, with large areas of necrosis.

References

Aggarwal A, Patra DP, Gupta K, Sodhi HB (2016) Dural tuberculoma mimicking meningioma: a clinicoradiologic review of dural en-plaque lesions. World Neurosurg 88:686.e1–686.e7

Akhtar M, Al Mana H (2004) Pathology of tuberculosis. In: Madkour MM (ed) Tuberculosis. Springer, Berlin, pp 153–161

Allen TG, Suster S (eds) (2018) Pathology of the pleura and mediastinum. Springer International, Switzerland, pp 139–152

Ansari AW, Kamarulzaman A, Schmidt RE (2013) Multifaceted impact of host C-C chemokine CCL2 in the immuno-pathogenesis of HIV-1/M tuberculosis co-infection. Front Immunol 4:312

Arora D, Dhanashree B (2020) Utility of smear microscopy and GeneXpert for the detection of Mycobacterium tuberculosis in clinical samples. Germs 10:81–87

Arora SK, Gupta N, Nijhawan R, Mandal AK (2010) Epithelioid cell granulomas in urine cytology smears: same cause, different implications. Diagn Cytopathol 38:765–767

Asano S (2012) Granulomatous lymphadenitis. J Clin Exp Hematop 52:1–16

Bayram S, Erşen A, Altan M, Durmaz H (2016) Tuberculosis tenosynovitis with multiple rice bodies of the flexor tendons in the wrist: a case report. Int J Surg Case Rep 27:129–132

Bazin C (2004) Tuberculose du système nerveux central. EMC-Neurologie 1:169–192
Bhigjee AI, Padayachee R, Paruk H et al (2007) Diagnosis of tuberculous meningitis: clinical and laboratory parameters. Int J Infect Dis 11:348–354
Bibbo M, Wilbur D (2014) Comprehensive cytopathology, 4th edn. Saunders Elsevier
Bolognesi M, Bolognesi D (2013) Complicated and delayed diagnosis of tuberculous peritonitis. Am J Case Rep 14:109–112
Budvytiene I, Banaei N (2020) Simple processing of formalin-fixed paraffin-embedded tissue for accurate testing with the Xpert MTB/RIF assay. J Clin Microbiol 58:e01905–e01919
Cao Z, Wu W, Wei H et al (2020) Using droplet digital PCR in the detection of Mycobacterium tuberculosis DNA in FFPE samples. Int J Infect Dis 99:77–83
Cardona PJ (2018) Pathogenesis of tuberculosis and other mycobacteriosis. Enferm Infecc Microbiol Clin (Engl Ed) 36:38–46
Carrisoza-Urbina J, Morales-Salinas E, Bedolla-Alva MA, Hernández-Pando R, Gutiérrez-Pabello JA (2019) Atypical granuloma formation in Mycobacterium bovis-infected calves. PLoS One 14:e0218547
Chakraborti S, Mahadevan A, Govindan A et al (2009) Clinicopathological study of tuberculous brain abscess. Pathol Res Pract 205:815–822
Chakravorty S, Sen MK, Tyagi JS (2005) Diagnosis of extrapulmonary tuberculosis by smear, culture, and PCR using universal sample processing technology. J Clin Microbiol 43:4357–4362
Chatterjee D, Dey P (2014) Tuberculosis revisited: cytological perspective. Diagn Cytopathol 42: 993–1001
Clarke CC, Mowat FS, Kelsh MA, Roberts MA (2006) Pleural plaques: a review of diagnostic issues and possible nonasbestos factors. Arch Environ Occup Health 61:183–192
Cottle L, Riordan T (2008) Infectious spondylodiscitis. J Infect 56:401–412
Das P, Ahuja A, Gupta SD (2008) Incidence, etiopathogenesis and pathological aspects of genitourinary tuberculosis in India: a journey revisited. Indian J Urol 24:356–361
Dasgupta A, Singh N, Bhatia A (2009) Abdominal tuberculosis: a histopathological study with special reference to intestinal perforation and mesenteric vasculopathy. J Lab Physicians 1:56–61
Dastur DK, Lalitha VS (1973) The many facets of neurotuberculosis: an epitome of neuropathology. In: Zimmerman HM (ed) Progress in neuropathology. Grune Stratton, New York, pp 351–408
Davis AG, Rohlwink UK, Proust A, Figaji AA, Wilkinson RJ (2019) The pathogenesis of tuberculous meningitis. J Leukoc Biol 105:267–280
De Almeida SM, Dalla Costa LM, Siebra C, Arend L, Nogueira KDS (2019) Validation of multiplex PCR for the diagnosis of acute bacterial meningitis in culture negative cerebrospinal fluid. Arq Neuropsiquiatr 77:224–231
Deveci HS, Kule M, Kule ZA, Habesoglu TE (2016) Diagnostic challenges in cervical tuberculous lymphadenitis: a review. North Clin Istanb 3:150–155
Dietrich D, Uhl B, Sailer V et al (2013) Improved PCR performance using template DNA from formalin-fixed and paraffin-embedded tissues by overcoming PCR inhibition. PLoS One 8:e77771
Eastwood JB, Corbishley CM, Grange JM (2001) Tuberculosis and the kidney. J Am Soc Nephrol 12:1307–1314
Eshete A, Zeyinudin A, Ali S, Abera S, Mohammed M (2011) M. tuberculosis in lymph node biopsy paraffin-embedded sections. Tuberc Res Treat 2011:127817
Francis IM, Das DK, Luthra UK et al (1999) Value of radiologically guided fine needle aspiration cytology (FNAC) in the diagnosis of spinal tuberculosis: a study of 29 cases. Cytopathology 10:390–401
Fukunaga H, Murakami T, Gondo T, Sugi K, Ishihara T (2002) Sensitivity of acid-fast staining for *Mycobacterium tuberculosis* in formalin-fixed tissue. Am J Respir Crit Care Med 166:994–997
Garg RK (1999) Tuberculosis of the central nervous system. Postgrad Med J 75:133–140
Gaur M, Singh A, Sharma V et al (2020) Diagnostic performance of non-invasive, stool-based molecular assays in patients with paucibacillary tuberculosis. Sci Rep 10:7102
Goldblum J, Lamps L, McKenney J, Myers J (2017) Rosai and Ackerman's surgical pathology, 11th edn. Elsevier
Gous N, Scott LE, Wong E, Omar T, Venter WD, Stevens W (2012) Performance of the Roche LightCycler real-time PCR assay for diagnosing extrapulmonary tuberculosis. J Clin Microbiol 50:2100–2103
Gupta M, Lobo FD, Adiga DS, Gupta A (2016) A histomorphological pattern analysis of pulmonary tuberculosis in lung autopsy and surgically resected specimens. Pathol Res Int 2016:8132741
Gupta P, Guleria S, Agarwal S (2011) Role of endoscopic ultrasound guided FNAC in diagnosis of pancreatic TB presenting as mass lesion: a case report and review of literature. Indian J Tuberc 58:120–124
Gupta RK, Kumar S (2011) Central nervous system tuberculosis. Neuroimaging Clin North Am 21:795–814
Gupta S, Takhtani D, Gulati M et al (1999) Sonographically guided fine-needle aspiration biopsy of lytic lesions of the spine: technique and indications. J Clin Ultrasound 27:123–129
Handa U, Bal A, Mohan H, Bhardwaj S (2005) Fine needle aspiration cytology in the diagnosis of bone lesions. Cytopathology 16:59–64
Handa U, Mundi I, Mohan S (2012) Nodal tuberculosis revisited: a review. J Infect Dev Ctries 6:6–12
Hegde S, Rithesh KB, Baroudi K, Umar D (2014) Tuberculous lymphadenitis: early diagnosis and intervention. J Int Oral Health 6:96–98
Hemalatha A, Shruti P, Kumar MU, Bhaskaran A (2014) Cytomorphological patterns of tubercular lymphadenitis revisited. Ann Med Health Sci Res 4:393–396
Hoel IM, Sviland L, Syre H et al (2020) Diagnosis of extrapulmonary tuberculosis using the MPT64 anti-

gen detection test in a high-income low tuberculosis prevalence setting. BMC Infect Dis 20:130
Hunter R, Actor J (2019) The pathogenesis of post-primary tuberculosis. A game changer for vaccine development. Tuberculosis (Edinb) 116S:S114–s117
Hunter RL (2011) Pathology of post primary tuberculosis of the lung: an illustrated critical review. Tuberculosis (Edinb) 91:497–509
Hunter RL (2016) Tuberculosis as a three-act play: a new paradigm for the pathogenesis of pulmonary tuberculosis. Tuberculosis (Edinb) 97:8–17
Hunter RL (2020) The pathogenesis of tuberculosis—the Koch phenomenon reinstated. Pathogens 9:813
Hunter RL, Actor JK, Hwang SA, Karev V, Jagannath C (2014) Pathogenesis of post primary tuberculosis: immunity and hypersensitivity in the development of cavities. Ann Clin Lab Sci 44:365–387
Hunter RL, Jagannath C, Actor JK (2007) Pathology of postprimary tuberculosis in humans and mice: contradiction of long-held beliefs. Tuberculosis (Edinb) 87:267–278
Jain D, Ghosh S, Teixeira L, Mukhopadhyay S (2017) Pathology of pulmonary tuberculosis and non-tuberculous mycobacterial lung disease: facts, misconceptions, and practical tips for pathologists. Semin Diagn Pathol 34:518–529
Jennette JC, D'agati VD, Olson JL, Silva FG (2014) Heptinstall's pathology of the kidney, 7th edn. Lippincott Williams & Wilkins, Philadelphia
Jeren T, Beus I (1982) Characteristics of cerebrospinal fluid in tuberculous meningitis. Acta Cytol 26:678–680
Johansen IS, Thomsen V, Forsgren A, Hansen BF, Lundgren B (2004) Detection of Mycobacterium tuberculosis complex in formalin-fixed, paraffin-embedded tissue specimens with necrotizing granulomatous inflammation by strand displacement amplification. J Mol Diagn 6:231–236
Jorda M, Rey L, Hanly A, Ganjei-Azar P (2000) Fine-needle aspiration cytology of bone: accuracy and pitfalls of cytodiagnosis. Cancer 90:47–54
Kalyani R, Sheela S, Rajini M (2012) Cytological diagnosis of tuberculous cervicitis: a case report with review of literature. J Cytol 29:86–88
Karimi S, Shamaei M, Pourabdollah M et al (2014) Histopathological findings in immunohistological staining of the granulomatous tissue reaction associated with tuberculosis. Tuberc Res Treat 2014:858396
Kedia S, Das P, Madhusudhan KS et al (2019) Differentiating Crohn's disease from intestinal tuberculosis. World J Gastroenterol 25:418–432
Kim MJ, Wainwright HC, Locketz M et al (2010) Caseation of human tuberculosis granulomas correlates with elevated host lipid metabolism. EMBO Mol Med 2:258–274
Kohli R, Punia RS, Kaushik R, Kundu R, Mohan H (2014) Relative value of immunohistochemistry in detection of mycobacterial antigen in suspected cases of tuberculosis in tissue sections. Indian J Pathol Microbiol 57:574–578
Kulchavenya E, Khomyakov V (2006) Male genital tuberculosis in Siberians. World J Urol 24:74–78
Kurman RJ, Hedrick Ellenson L, Ronnett BM (eds) (2019) Blaustein's pathology of the female genital tract, 7th edn. Springer International, Switzerland
Lee HS, Park KU, Park JO et al (2011) Rapid, sensitive, and specific detection of Mycobacterium tuberculosis complex by real-time PCR on paraffin-embedded human tissues. J Mol Diagn 13:390–394
Leonard MK, Blumberg HM (2017) Musculoskeletal tuberculosis. Microbiol Spectr 5(2). https://doi.org/10.1128/microbiolspec.TNMI7-0046-2017
Leong FJ, Dartois V, Dick T (eds) (2016) A color atlas of comparative pathology of pulmonary tuberculosis. CRC Press, New York
Lewinsohn DM, Leonard MK, Lobue PA et al (2017) Official American Thoracic Society/Infectious Diseases Society of America/Centers for Disease Control and Prevention Clinical Practice Guidelines: diagnosis of tuberculosis in adults and children. Clin Infect Dis 64:111–115
Li T, Liu T, Jiang Z, Cui X, Sun J (2016) Diagnosing pyogenic, brucella and tuberculous spondylitis using histopathology and MRI: a retrospective study. Exp Ther Med 12:2069–2077
Madkour MM (2004) Primary tuberculosis in adults. In: Madkour MM (ed) Tuberculosis. Springer, Berlin, pp 265–272
Majeed MM, Bukhari MH (2011) Evaluation for granulomatous inflammation on fine needle aspiration cytology using special stains. Pathol Res Int 2011:851524
Malhotra KP, Kulshreshtha D (2017) Pathology of tuberculosis of the nervous system (tuberculous meningitis, tuberculoma, tuberculous abscess). In: Turgut M, Akhaddar A, Turgut AT, Garg RK (eds) Tuberculosis of the central nervous system. Springer, pp 33–53
Malikowski T, Mahmood M, Smyrk T, Raffals L, Nehra V (2018) Tuberculosis of the gastrointestinal tract and associated viscera. J Clin Tuberc Other Mycobact Dis 12:1–8
Marouane C, Smaoui S, Kammoun S, Slim L, Messadi-Akrout F (2016) Evaluation of molecular detection of extrapulmonary tuberculosis and resistance to rifampicin with GeneXpert® MTB/RIF. Med Mal Infect 46:20–24
Mattila JT, Ojo OO, Kepka-Lenhart D et al (2013) Microenvironments in tuberculous granulomas are delineated by distinct populations of macrophage subsets and expression of nitric oxide synthase and arginase isoforms. J Immunol 191:773–784
Mechal Y, Benaissa E, El Mrimar N et al (2019) Evaluation of GeneXpert MTB/RIF system performances in the diagnosis of extrapulmonary tuberculosis. BMC Infect Dis 19:1069
Menon S, Bharadwaj R, Chowdhary A, Kaundinya D, Palande D (2011) Tuberculous brain abscesses: case series and review of literature. J Neurosci Rural Pract 2:153–157
Milburn HJ (2001) Primary tuberculosis. Curr Opin Pulm Med 7:133–141

Morel F, Jaffré J, Sougakoff W, Aubry A, Véziris N (2020) Molecular diagnosis of tuberculosis. Rev Mal Respir 37:412–416

Moure Z, Castellví J, Sánchez-Montalvá A, Pumarola T, Tórtola MT (2019) The role of molecular techniques for the detection of *Mycobacterium tuberculosis* complex in paraffin-embedded biopsies. Appl Immunohistochem Mol Morphol 27:77–80

Mukhopadhyay S, Gal AA (2010) Granulomatous lung disease: an approach to the differential diagnosis. Arch Pathol Lab Med 134:667–690

Muneer A, Macrae B, Krishnamoorthy S, Zumla A (2019) Urogenital tuberculosis—epidemiology, pathogenesis and clinical features. Nat Rev Urol 16:573–598

Mustafa T, Wiker HG, Mfinanga SG, Mørkve O, Sviland L (2006) Immunohistochemistry using a *Mycobacterium tuberculosis* complex specific antibody for improved diagnosis of tuberculous lymphadenitis. Mod Pathol 19:1606–1614

Mustafa T, Wergeland I, Baba K, Pathak S, Hoosen AA, Dyrhol-Riise AM (2020) Mycobacterial antigens in pleural fluid mononuclear cells to diagnose pleural tuberculosis in HIV co-infected patients. BMC Infect Dis 20:459

Muzumdar D, Vedantam R, Chandrashekhar D (2018) Tuberculosis of the central nervous system in children. Childs Nerv Syst 34:1925–1935

Nassaji M, Azarhoush R, Ghorbani R, Kavian F (2014) Acid fast staining in formalin-fixed tissue specimen of patients with extrapulmonary tuberculosis. Int J Sci Res Publ 4:1–5

O'Garra A, Redford PS, Mcnab FW, Bloom CI, Wilkinson RJ, Berry MP (2013) The immune response in tuberculosis. Annu Rev Immunol 31:475–527

Opota O, Mazza-Stalder J, Greub G, Jaton K (2019) The rapid molecular test Xpert MTB/RIF ultra: towards improved tuberculosis diagnosis and rifampicin resistance detection. Clin Microbiol Infect 25: 1370–1376

Pagnoux C, Bienvenu B, Guillevin LJIJOCR (2006) The spectrum of granulomatous vasculitides. Future Rheumatol 1:729–750

Pai M, Behr MA, Dowdy D et al (2016) Tuberculosis. Nat Rev Dis Primers 2:16076

Park DY, Kim JY, Choi KU et al (2003) Comparison of polymerase chain reaction with histopathologic features for diagnosis of tuberculosis in formalin-fixed, paraffin-embedded histologic specimens. Arch Pathol Lab Med 127:326–330

Park JJ (2015) Differential diagnosis: intestinal tuberculosis. In: Park JJ, Cheon JH (eds) Atlas of inflammatory bowel diseases. Springer, Berlin, pp 71–85

Philip KEJ, Kon OM, Roddie M, Ross C (2018) Pleural tuberculosis: a key differential diagnosis for pleural thickening, even without obvious risk factors for tuberculosis in a low incidence setting. BMJ Case Rep 2018:bcr2018224992

Pigrau-Serrallach C, Rodríguez-Pardo D (2013) Bone and joint tuberculosis. Eur Spine J 22(Suppl 4): 556–566

Polepole P, Kabwe M, Kasonde M et al (2017) Performance of the Xpert MTB/RIF assay in the diagnosis of tuberculosis in formalin-fixed, paraffin-embedded tissues. Int J Mycobacteriol 6:87–93

Prakash B, Mehta G, Gondal R, Kumar S, Malhotra V (1989) Tuberculous abscess of the brain stem. Surg Neurol 32:445–448

Purohit MR, Mustafa T, Wiker HG, Mørkve O, Sviland L (2007) Immunohistochemical diagnosis of abdominal and lymph node tuberculosis by detecting Mycobacterium tuberculosis complex specific antigen MPT64. Diagn Pathol 2:36. https://doi.org/10.1186/1746-1596-2-36

Purohit MR, Sviland L, Wiker H, Mustafa T (2017) Rapid and specific diagnosis of extrapulmonary tuberculosis by immunostaining of tissues and aspirates with anti-MPT64. Appl Immunohistochem Mol Morphol 25:282–288

Rammeh S, Romdhane E, Arfaoui Toumi A et al (2018) Efficacy of fine-needle aspiration cytology in the diagnosis of tuberculous cervical lymphadenitis. Acta Cytol 62:99–103

Rammeh S, Romdhane E, Riahi H, Chebbi Y, Bouaziz MC, Achour W, Saidi LS, Benaissa HT, Ladeb MF (2019a) Granulomatous spondylodiscitis: a case series with focus on histopathological features. J Spinal Cord Med:1–6

Rammeh S, Romdhane E, Sassi A et al (2019b) Accuracy of fine-needle aspiration cytology of head and neck masses. Diagn Cytopathol 47:394–399

Raveendran R, Wattal C (2016) Utility of multiplex real-time PCR in the diagnosis of extrapulmonary tuberculosis. Braz J Infect Dis 20:235–241

Reddy RAN, Narayana SM, Shariff S (2013) Role of fine-needle aspiration cytology and fluid cytology in extra-pulmonary tuberculosis. Diagn Cytopathol 41:392–398

Rindi L, Alì G, Fabiani B, Fontanini G, Garzelli C (2017) Detection of Mycobacterium tuberculosis from paraffin-embedded tissues by GeneXpert MTB/RIF. Tuberculosis (Edinb) 106:53–55

Rock RB, Olin M, Baker CA, Molitor TW, Peterson PK (2008) Central nervous system tuberculosis: pathogenesis and clinical aspects. Clinical Microbiol Rev 21:243–261

Romdhane E, Arfaoui A, Benabdessalem C, Ksentini M, Ferjani A, Dekhil N, Lahiani R, Bchiri S, Mardassi H, Barbouche MR, Boutiba Ben Boubake I, Ben Salah M, Rammeh S (2020a) Performance of GeneXpert ultra in the diagnosis of Tuberculous cervical lymphadenitis in formalin fixed paraffin embedded tissues. Tuberculosis (Edinb) 125:102012

Romdhane E, Rammeh S, Riahi H, Chebbi Y, Mouna CB, Achour W, Slim-Saidi L, Benaissa HT, Ladeb MF (2020b) The value of histology in the diagnosis of tuberculous spondylodiscitis. J Clin Rheumatol 26:63–66

Romdhane E, Rammeh S, Bouaziz CM, Riahi H, Ben MR, Ksentini M, Chebbi Y, Achour W, Ferjani A, Boutiba BBI, Slim-Saidi L, Ladeb MF (2021) Performances

of single tube nested polymerase chain reaction and GeneXpert ultra on formalin fixed paraffin embedded tissues in the diagnosis of tuberculous spondylodiscitis. Clin Rheumatol. https://doi.org/10.1007/s10067-021-05782-9. Online ahead of print.

Russell DG (2007) Who puts the tubercle in tuberculosis? Nat Rev Microbiol 5:39–47

Sasindran SJ, Torrelles JB (2011) Mycobacterium tuberculosis infection and inflammation: what is beneficial for the host and for the bacterium? Front Microbiol 2:2. https://doi.org/10.3389/fmicb.2011.00002

Schaumburg F, Peters G, Wardelmann E, Becker K, Sperveslage J (2017) Evaluation of GenoType MTBDRplus by use of extracted DNA from formalin-fixed paraffin-embedded specimens. J Clin Microbiol 55:3300–3302

Schewe C, Goldmann T, Grosser M et al (2005) Inter-laboratory validation of PCR-based detection of Mycobacterium tuberculosis in formalin-fixed, paraffin-embedded tissues. Virchows Arch 447:573–585

Sener A, Erdem H (eds) (2019) Extrapulmonary tuberculosis. Springer International

Seo AN, Park HJ, Lee HS et al (2014) Performance characteristics of nested polymerase chain reaction vs real-time polymerase chain reaction methods for detecting Mycobacterium tuberculosis complex in paraffin-embedded human tissues. Am J Clin Pathol 142:384–390

Sharma JB, Roy KK, Pushparaj M et al (2008) Genital tuberculosis: an important cause of Asherman's syndrome in India. Arch Gynecol Obstet 277:37–41

Sharma JB (2015) Current diagnosis and management of female genital tuberculosis. J Obstet Gynaecol India 65:362–371

Sharma JB, Sharma E, Sharma S, Dharmendra S (2018) Female genital tuberculosis: revisited. Indian J Med Res 148:S71–S83

Sharma MP, Bhatia V (2004) Abdominal tuberculosis. Indian J Med Res 120:305–315

Sharma SK, Mohan A (2017) Miliary tuberculosis. Microbiol Spectr 5(2). https://doi.org/10.1128/microbiolspec.TNMI7-0013-2016

Shim D, Kim H, Shin SJ (2020) Mycobacterium tuberculosis infection-driven foamy macrophages and their implications in tuberculosis control as targets for host-directed therapy. Front Immunol 11:910. https://doi.org/10.3389/fimmu.2020.00910

Siddaraju N, Bundele MM (2007) Caseous, necrotic material and epithelioid cell granulomas in synovial fluid from a patient with tuberculous infection: a case report. Acta Cytol 51:597–598

Stephenson L, Byard RW (2020) An atlas overview of characteristic features of tuberculosis that may be encountered at autopsy. Forensic Sci Med Pathol 16:143–151

Strayer DS (ed) (2015) Rubin's pathology: clinicopathologic foundations of medicine, 7th edn. Wolters Kluwer, Philadelphia

Subbian S, Tsenova L, Kim MJ et al (2015) Lesion-specific immune response in granulomas of patients with pulmonary tuberculosis: a pilot study. PLoS One 10:e0132249

Sumi S, Radhakrishnan VV (2009) Evaluation of immunohistochemistry with a panel of antibodies against recombinant mycobacterial antigens for the diagnosis of tuberculous lymphadenitis. Int J Med Med Sci 1:215–219

Tadele A, Beyene D, Hussein J et al (2014) Immunocytochemical detection of Mycobacterium tuberculosis complex specific antigen, MPT64, improves diagnosis of tuberculous lymphadenitis and tuberculous pleuritis. BMC Infect Dis 14:585

Tomashefski J Jr, Cagle PT, Farver CF, Fraire AE (eds) (2008) Dail and Hammar's pulmonary pathology, 3rd edn. Springer

Tuli SM (2002) General principles of osteoarticular tuberculosis. Clin Orthop Relat Res 398:11–19

Vilchèze C, Kremer L (2017) Acid-fast positive and acid-fast negative *Mycobacterium tuberculosis*: the Koch paradox. Microbiol Spectr 5(2). https://doi.org/10.1128/microbiolspec.TBTB2-0003-2015

Vohra S, Dhaliwal HS (2021) Miliary tuberculosis. [Updated 2021 Apr 7]. In: StatPearls [Internet]. StatPearls Publishing, Treasure Island (FL). Available from: https://www.ncbi.nlm.nih.gov/books/NBK562300/

Vorster MJ, Allwood BW, Diacon AH, Koegelenberg CF (2015) Tuberculous pleural effusions: advances and controversies. J Thorac Dis 7:981–991

Weledji EP, Pokam BT (2017) Abdominal tuberculosis: is there a role for surgery? World J Gastrointest Surg 9:174–181

Wöckel W (1995) Auramine fluorescence for acid-fast bacilli in formalin-fixed, paraffin-embedded tissues. Am J Clin Pathol 103:667–668

Zerbi P, Schønau A, Bonetto S et al (2001) Amplified in situ hybridization with peptide nucleic acid probes for differentiation of Mycobacterium tuberculosis complex and nontuberculous Mycobacterium species on formalin-fixed, paraffin-embedded archival biopsy and autopsy samples. Am J Clin Pathol 116:770–775

Zumla A, James DG (1996) Granulomatous infections: etiology and classification. Clin Infect Dis 23:146–158

Imaging Techniques for Tuberculosis

Tiffanie S. F. Teo, Anbalagan Kannivelu, Sivasubramanian Srinivasan, and Wilfred C. G. Peh

Contents

Abstract

Imaging has an important complementary role in the diagnosis of pulmonary and extrapulmonary tuberculosis, particularly in patients with non-specific symptoms. It helps to detect lesions and confirm the diagnosis, evaluate the extent of disease and its complications, monitor its progress and response to treatment, as well as demonstrate residual or recurring disease after completion of therapy. Radiographs are an excellent screening tool and typically the initial radiological investigation, particularly for pulmonary and musculoskeletal tuberculosis. Computed tomography is utilized to further evaluate pulmonary, abdominal, urinary tract, and head and neck tuberculosis. Magnetic resonance imaging is the modality of choice for assessing tuberculosis in the brain, spine, and musculoskeletal system. Imaging modalities such as contrast fluoroscopy studies, ultrasound imaging, and nuclear medicine imaging, particularly positron-emission tomography, may also be of benefit in the management of selected patients suspected to have tuberculosis. Imaging techniques, such as ultrasound and computed tomography, are also used to guide diagnostic and therapeutic aspirations and drainages, as well as biopsies for histopathological confirmation of tuberculosis. As each of these modalities have their own advantages,

T. S. F. Teo (✉) · A. Kannivelu · S. Srinivasan
W. C. G. Peh
Department of Diagnostic Radiology,
Khoo Teck Puat Hospital, 90 Yishun Central,
Singapore, Republic of Singapore
e-mail: teo.tiffanie.sf@ktph.com.sg;
kannivelu.anbalagan@ktph.com.sg;
sivasu2@gmail.com; wilfred.peh@gmail.com

© The Author(s), under exclusive license to Springer Nature Switzerland AG 2022

M. F. Ladeb, W. C. G. Peh (eds.), *Imaging of Tuberculosis*, Medical Radiology Diagnostic Imaging,
https://doi.org/10.1007/978-3-031-07040-2_4

disadvantages, and limitations, the modality of choice therefore varies, depending on the clinical indications, and should be tailored to each individual patient.

Abbreviations

CT	Computed tomography
IVU	Intravenous urography
MRI	Magnetic resonance imaging
PET	Positron-emission tomography
TB	Tuberculosis
US	Ultrasound

1 Introduction

Tuberculosis (TB) may infect virtually all organ systems, with the lung being the most common organ affected. Extrapulmonary TB comprises up to 15% of all tuberculous infections (Peto et al. 2009). The definitive diagnosis of TB is made by isolation of *Mycobacterium tuberculosis* from a bodily sample (Pai et al. 2016). However, as a laboratory diagnosis cannot be achieved in approximately 15–20% of individuals (Taylor et al. 2000), treatment can be instituted based on a presumptive diagnosis ("clinically diagnosed TB") (World Health Organization 2020), particularly in the presence of risk factors (see the first Chapter on Epidemiology of Tuberculosis and the last Chapter on Diagnostic Algorithm of Tuberculosis).

Patients with TB may present with a range of diverse clinical manifestations, which can be broadly classified into three groups, namely: (1) signs and symptoms of pulmonary TB, (2) signs and symptoms of extrapulmonary TB, and (3) asymptomatic patients suspected to have latent TB. Patients with extrapulmonary TB typically have either non-specific constitutional symptoms or clinical features relating to a specific organ, which mimic some other pathology and are hence particularly challenging to diagnose clinically. The roles of imaging are to detect lesions, suggest the diagnosis, evaluate the extent of the disease, look for complications, follow its response to treatment, as well as demonstrate residual or recurring disease upon completion of therapy (Bomanji et al. 2015).

2 Imaging Techniques

Conventional radiographs are the initial radiological investigation for pulmonary and musculoskeletal TB in most instances. Further cross-sectional evaluation using ultrasound (US) imaging, computed tomography (CT), and/or magnetic resonance imaging (MRI) is commonly the subsequent step in the line of investigations. The use of other imaging modalities, such as intravenous urography (IVU), barium studies, as well as a whole host of different radiological techniques, may also be beneficial in the management of patients suspected to have TB. In patients in whom TB is not suspected at presentation, imaging findings may raise the first concern for a tuberculous etiology. Imaging modalities such as US imaging and CT have an additional role in aiding aspiration and biopsy for confirmation of the diagnosis, as well as guiding therapeutic interventional procedures, such as drainage of abscesses and fluid collections. This chapter provides an overview of the major imaging techniques employed in investigating patients with TB. Some specific techniques will be covered in more detail in the following chapters dealing with imaging of TB affecting various organ systems.

2.1 Radiography

Radiographs are often the first-line imaging examination requested for detection of disease and sometimes provide a diagnosis. Radiographs complement the referring physician's clinical suspicion based on the patient's history and physical examination, together with laboratory findings. This assessment should ideally be made in conjunction with the knowledge of established risk factors, i.e., host and environmental factors

(see the first Chapter on Epidemiology of Tuberculosis and the last Chapter on Diagnostic Algorithm of Tuberculosis).

2.1.1 Advantages of Radiography

Radiography has several advantages, namely:

1. It is readily available, often being the primary and/or sole imaging modality in small hospitals and clinics with limited resources, particularly in developing countries.
2. It is relatively simple to perform. All radiographers who have finished their basic training should be competent.
3. It is cost efficient, being far less expensive compared to all other imaging modalities.
4. It provides a quick overall imaging assessment of a relatively large area of interest, with less radiation exposure compared to many other imaging modalities, e.g., CT.
5. Its identification and localization of lesion(s) serve as a guide for further imaging such as CT or MRI.
6. It is a simple imaging tool for follow-up of treated lesions and for detection of complications or disease recurrence.
7. Being potentially portable, it is quickly available, even to the sickest patients at the emergency department, ward, or intensive care unit (ICU).

2.1.2 Computed Radiography, Digital Radiography, and PACS

Although still utilized in many developing countries and in facilities with limited resources, the time-honored traditional film-screen system has been superseded by computed radiography (CR) and digital radiography (DR). Being digital imaging systems, both CR and DR allow digital display of the acquired images. These digital images can be uploaded into the picture archiving and communication system (PACS).

CR is a cassette-based digital imaging method, as the image is obtained using a cassette, before the data is converted into a digital image in a CR reader. In CR, photostimulable phosphor plates are used in cassettes that are similar in appearance and dimensions to those used in traditional film-screen radiography. This is in contradistinction to the film-screen system, where a film has to be inserted in a dark room prior to its use. As both systems employ cassettes, the same X-ray machines used in the traditional film-screen cassette system may be retained, making the transition from traditional analogue to digital imaging seamless.

In DR, a built-in detector unit allows the X-ray photons to be converted directly into electrical signals that can be read directly as digital images. There are two types of detectors: one which uses indirect conversion, and the other which uses direct conversion with amorphous selenium. In the former, phosphor is used to convert the X-ray photons into light, which is then detected by photodiodes in an amorphous silicon thin-film transistor (TFT) array. The photodiode, each representing a single pixel, then produces an electrical charge that is sent to the image processor. In the latter, amorphous selenium is used as a photoconductor that will pass on electrical charges to charge collectors in the TFT array upon irradiation (Allisy-Roberts and Williams 2008).

The PACS enables the rapid transmission of digital images from the site of image acquisition to multiple different locations within a hospital, and even across the globe. PACS allows remote viewing and storage of these images while retaining their original quality. In PACS, a more economical, filmless, and efficient workflow is set up, whereby the digital images acquired can be viewed almost in real time, by both radiologists and clinical teams simultaneously. It also allows convenient access across multiple modalities, allowing prior studies from the same patient to be referenced and compared immediately.

Both CR and DR offer several advantages over conventional film-screen radiography:

1. The wide dynamic range of the photostimulable phosphor plate and DR detector reduces exposure errors and the need for repeat examinations.

2. They allow immediate manual optimization of the display features desired for the particular anatomical part to be imaged.
3. When integrated into the PACS, there is an efficient and almost live transmission of the acquired images. The system also stores and archives the digital images for convenient and fast retrieval in the future, without compromising image quality.
4. Viewing of digital films has various added benefits of windowing, enhancing contrast, magnification, and a host of other methods to improve lesion detection, which traditional film-screen radiography would not be able to offer.

2.1.3 Disadvantages and Limitations of Radiography

Despite the improvements brought about by the usage of CR and DR, radiography has some inherent disadvantages and limitations. These include the following:

1. Intrinsically poor soft tissue contrast: For example, it is good for detecting a tuberculous lesion within the lung because of wide contrast between soft tissue of the lesion and air within alveoli, but poor for detecting a tuberculous lesion within the renal parenchyma because of lack of contrast with adjacent normal tissue.
2. It is relatively insensitive for the detection of small or early bone lesions, particularly in structures with a complex anatomy, for example, early tuberculous osteomyelitis in the scapula.
3. Ionizing radiation hazards, albeit small, exist. Standard clinical indications and the ALARA (as low as reasonably achievable) principle should always be followed.

2.1.4 Chest Radiographs

Radiographs remain the mainstay for mass screening and the initial imaging modality for investigating pulmonary TB. The combination of chest radiographs and clinical correlation has been reported to have a 100% sensitivity and negative predictive value for excluding TB (World Health Organization 2018). In addition to being the first-line investigation in suspected cases of TB, chest radiographs are also useful in the follow-up of patients during treatment and are obtained in all patients at the end of anti-TB drug therapy. Documenting the new baseline chest radiographs for these patients, which may show findings such as residual fibrosis and nodular opacities, allows easy detection of new findings upon future comparison (Nachiappan et al. 2017).

The frontal chest radiograph may be obtained as a posterior-anterior (PA) or anterior-posterior (AP) radiograph, with the former being the preferred standard technique. The PA radiograph is usually taken in a relatively well patient who is able to stand, facing the cassette in full inspiration, with the X-ray beam passing through the patient in a posterior-to-anterior direction (Fig. 1a). The lateral chest radiograph is useful for assessing the retrosternal and retrocardiac airspaces, as well as posterior costophrenic recesses for small effusions. The apical view radiograph is particularly useful in the context of pulmonary TB, where the lung apices are often involved by disease. In this view, there is good demonstration of the lung apices, which would otherwise be obscured by the overlying soft tissues, ribs, calcified costal cartilage, and clavicles (Fig. 1b).

2.1.5 Other Radiographs

Radiographs may not yield much information in many patients with abdominal and/or urogenital TB. However, abdominal radiographs may still be useful in demonstrating focal globular calcifications associated with a granulomatous mass, hepatic or splenic calcifications, and calcified lymph nodes in abdominal TB. In urinary tract TB, a radiograph of the kidneys, ureters, and bladder (KUB) may show triangular ring-like calcifications within the collecting system (Gibson et al. 2004), characteristic renal parenchymal calcifications in a lobar distribution, a calcified "putty kidney," and/or calcified bladder, particularly in end-stage disease (Engin et al. 2000). When there is involvement of bowel in gastrointestinal TB, ileocecal involvement is

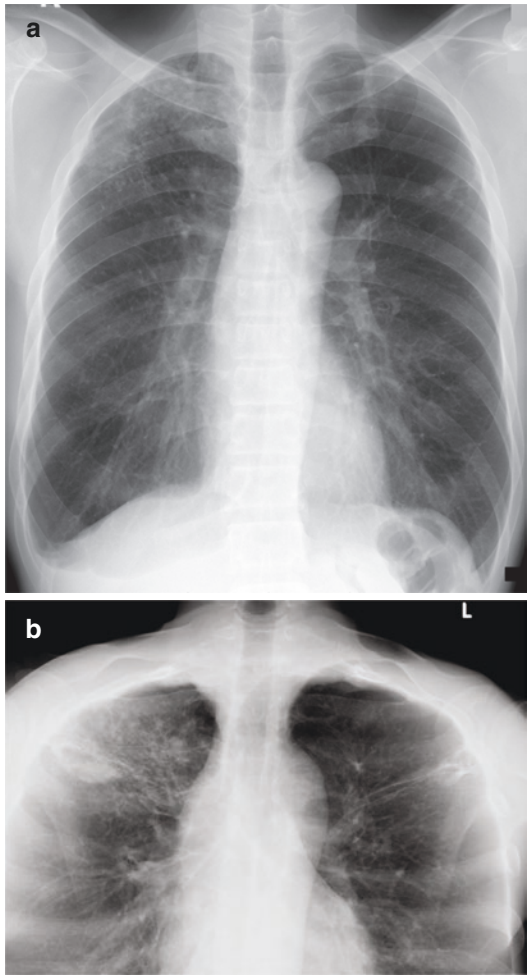

Fig. 1 Pulmonary tuberculosis. (**a**) PA chest radiograph shows patchy opacities mainly in the right upper zone. Fibronodular scarring is also present in the periphery of the left mid zone. (**b**) Apical view radiograph in the same patient. In this projection, the opacities in the right upper lobe, as well as the left-sided scarring, are much better demonstrated, without the overlying clavicle and ribs

common, and may result in small bowel obstruction. The role of the abdominal radiograph is to detect dilated bowel loops and pneumoperitoneum. The erect abdominal radiograph is useful for demonstrating air–fluid levels in obstruction and free air from perforation.

Similar to pulmonary TB and contrary to urogenital and gastrointestinal TB, radiographs still have an important role in assessing musculoskeletal TB. In musculoskeletal TB, radiographs of the spine and extremities are ideally performed in two orthogonal views, i.e., AP and lateral projections. If orthogonal views are not possible, e.g., to evaluate the metatarsals of the foot, then alternatives such as AP and oblique projections are obtained. Special radiographic views may be required for specific bones with complex anatomy, e.g., scaphoid views or open-mouth view for the cervical spine odontoid process. Patients with spinal TB usually have a radiograph of the spine obtained at their initial presentation. Similarly, dedicated radiographs of the affected joint or part are also normally first obtained in patients subsequently known to have tuberculous involvement of large joints, long bones, and small bones of the hands and feet.

However, in early TB, these radiographs may be normal or show non-specific findings. For example, in the early stages of spondylodiscitis, while the initial spine radiograph may be normal, subsequent radiographs may reveal findings such as vertebral body destruction, progressive vertebral collapse, anterior wedging, and gibbus formation, as the disease progresses. In the affected extremity, be it joint, long, or short bones, the initial radiographs may depict non-specific findings of osteopenia, osteolytic foci with poorly defined edges, varying amounts of sclerosis, abnormal periosteal reaction, and/or soft tissue swelling (Engin et al. 2000) (Fig. 2a, b). These patients usually go on to have an MRI, which aims at evaluating the full lesion extent or revealing lesions not well seen on radiographs (Fig. 2c, d).

2.2 Intravenous Urography

Intravenous urography (IVU) provides a general overview of the whole urinary tract. Prior to imaging, patient bowel preparation, usually starting from one day before, is required and is an important part of the IVU technique. IVU consists of a series of radiographs, starting with a control radiograph obtained to look for any calcifications in the urinary tract (Fig. 3a). A nonionic iodinated contrast agent is then administered

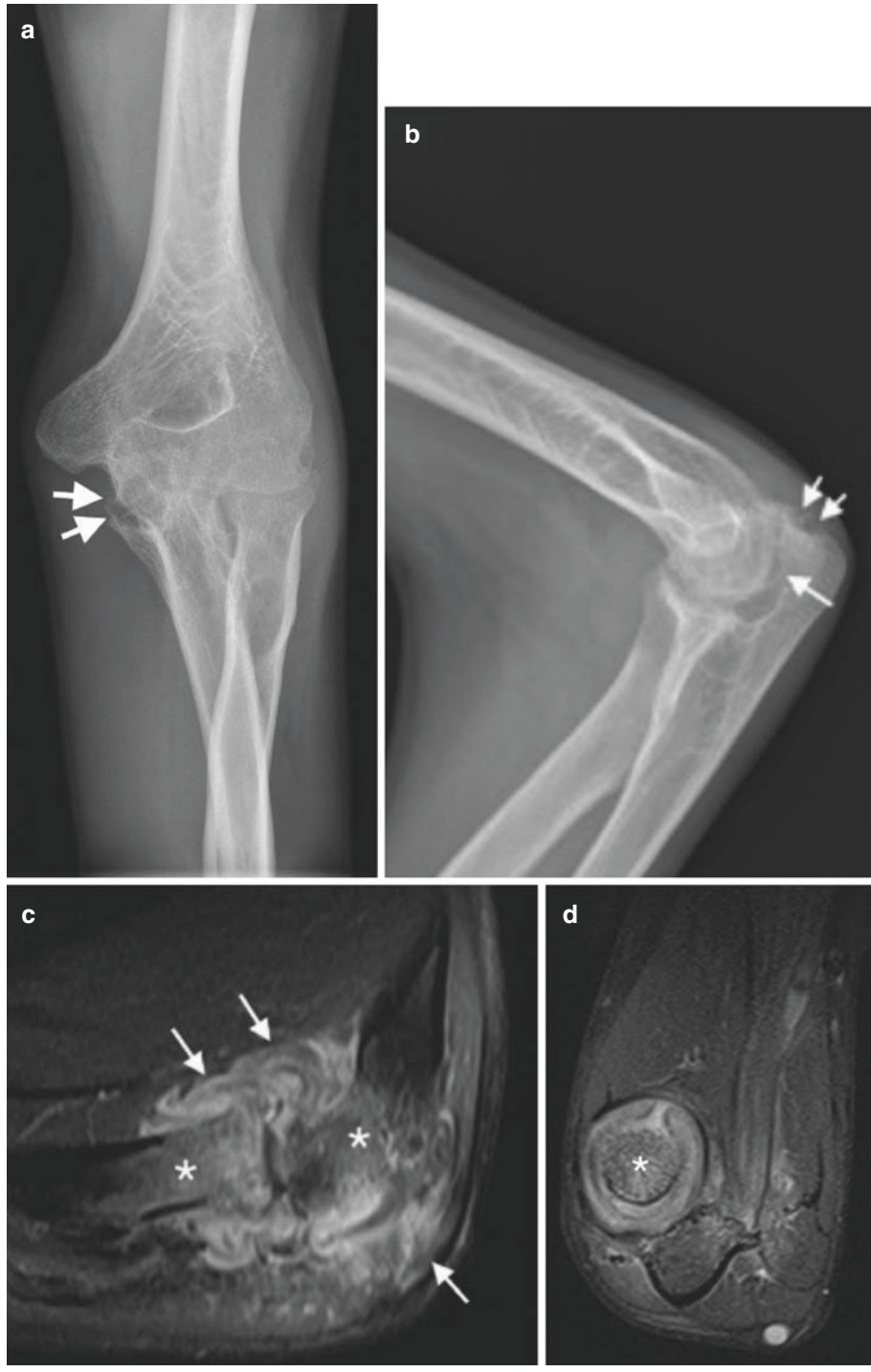

Fig. 2 Tuberculous arthropathy of the elbow joint. (**a**) AP and (**b**) lateral radiographs of the elbow show the small erosions in the proximal ulna (white arrows) and an associated joint effusion. (**c**) Sagittal and (**d**) axial fat-suppressed contrast-enhanced T1-W MR images of the elbow show diffuse synovial proliferation and enhancement at both the ventral and dorsal aspects of the elbow joint (white arrows). There is also marrow enhancement in the proximal radius and lateral humeral condyle (asterisks). The extent of these soft tissue changes is not appreciated on the radiographs

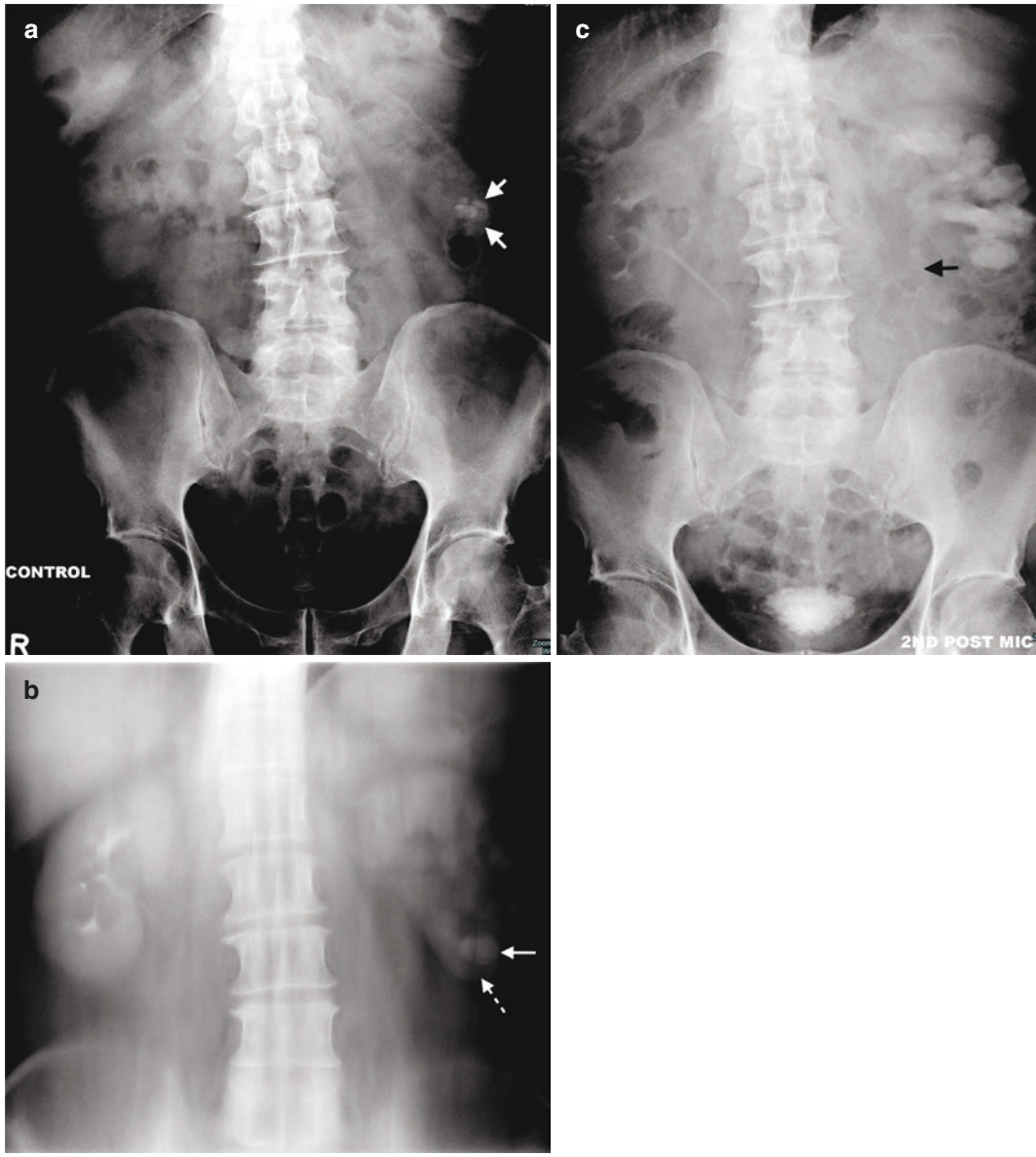

Fig. 3 Left renal and ureteric tuberculosis. (**a**) IVU control radiograph shows a cluster of calcifications projected over the lower pole of the left kidney (arrows). (**b**) Coned renal tomogram, obtained after intravenous contrast administration, shows contrast opacification of the right pelvicalyceal system with none seen in the left pelvicalyceal system. The left lower renal parenchyma is thinned (dotted arrow), and the calculi (solid arrow) seen on the control radiograph are located in the lower pole calyces. The left renal nephrogram is slightly dense with subsequent delayed contrast excretion into the left pelvicalyceal system. (**c**) Postmicturition full-length radiograph shows a stricture (arrow) at the left proximal ureter, with upstream hydroureteronephrosis. The left renal pelvis is contracted, relative to the dilated proximal ureter and calyces. Most of the calyces, particularly in the upper and mid-poles, are distorted and irregular, consistent with papillary destruction

intravenously, and radiographs are obtained in the nephrogenic and excretory phases at different timings to comprehensively show the components of the urinary tract. The dose of contrast agent administered varies according to the weight of the patient, usually up to 1.5 ml/kg body

weight. A typical series will comprise 1-min coned renal radiograph, 5-min coned renal radiograph with compression, 15-min full-length release radiograph, 30-min coned bladder radiograph, and postmicturition full-length radiograph (Fig. 3b, c). Modifications include addition of oblique radiographs and tomograms.

IVU is relatively sensitive for the detection of renal TB, being normal in only 10–15% of patients known to be affected (Kenney 1990). In TB of the urinary tract, contrast material within the pelvicalyceal system, ureters, and bladder allows filling defects and areas of mucosal irregularity to be demonstrated. It is also able to depict segments of strictures and focal caliectasis, as well as ureteric angulation from scarring. However, while IVU provides a good assessment of the pelvicalyceal system, it yields relatively little direct information about the renal parenchyma, compared to CT urography. IVU also does not have the added benefit of a broader cross-sectional assessment, which enables a simultaneous search for extrarenal features of TB in the rest of the abdomen and spine, which is a great benefit of CT urography. For these reasons, in modern practice, IVU has largely been replaced by cross-sectional imaging techniques, particularly CT urography.

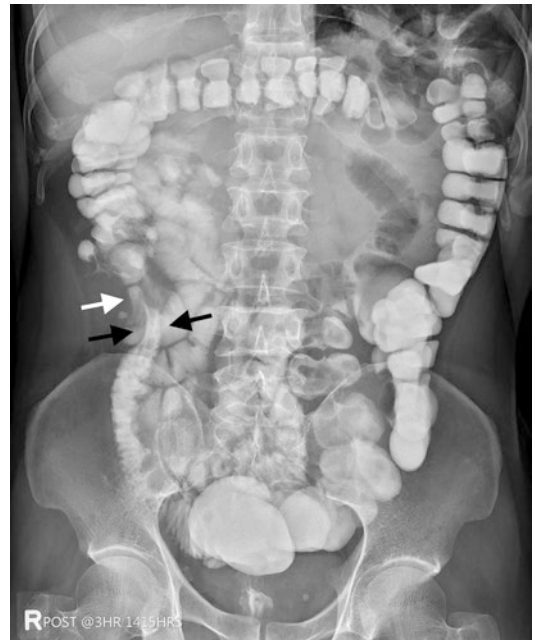

Fig. 4 Ileocecal tuberculosis. Small bowel series. Abdominal radiograph taken 3 h after the start of the study shows a short segment of luminal narrowing in the terminal ileum (black arrows), as well as mild deformity of a contracted cecum (white arrow). This patient had subsequent histological confirmation of terminal ileal tuberculosis

2.3 Contrast Fluoroscopy Studies

These are imaging studies used to evaluate various structures, particularly the gastrointestinal tract, typically in double contrast utilizing air and barium, under real-time fluoroscopic imaging. In a barium swallow and meal, the patient drinks a barium suspension and swallows fluid or tablets that produces effervescent gas. The aim is to coat the esophagus, stomach, and duodenum, as well as distend these structures, in the evaluation of the upper gastrointestinal tract. In a small bowel series, the small bowel may also be subsequently imaged with both real-time fluoroscopy and serial radiographs after ingestion of diluted barium suspension (Fig. 4). This is sometimes also known as a barium meal and follow-through study (BMFT). Barium enteroclysis, in which a nasogastric tube is used to intubate the proximal jejunum, enables better small bowel distention and detection of mucosal abnormalities, compared to BMFT. When evaluating the large bowel, there is a need for prior bowel preparation, and the patient should be able to tolerate air insufflation and barium introduced into the large bowel via a rectal tube. Furthermore, these studies require the patient to have a certain level of mobility, as they have to be able to turn and adopt various positions on the fluoroscopic table, in order to thoroughly coat the colonic mucosa with barium and to obtain images of different segments of the colon in various projections.

These double-contrast barium studies are able to identify ulcers, mucosal irregularity, strictures, as well as fistulas and have been extensively used in the past for the evaluation of gastrointestinal TB, particularly in the region of the ileocecal junction, which is the commonest site for

tuberculous involvement of the bowel (Nakano et al. 1992; Leder and Low 1995). These studies are being increasingly replaced by CT, which does not require as much patient cooperation compared to barium studies and has the added benefit of evaluating bowel wall abnormalities and extraintestinal pathology. Regardless of the type of study the patient undergoes, these patients would usually be further evaluated with gastro- or colonoscopy, to complement the radiological findings and also obtain tissue for histopathological confirmation.

A water-soluble contrast agent (usually a nonionic iodinated contrast agent) may also be used in the assessment of the gastrointestinal tract; however, it is usually only used when barium is contraindicated, e.g., in suspected cases of perforation, and in the post-operative patient to look for anastomotic leaks. In these cases, the leakage of barium into the peritoneum may be complicated by barium peritonitis, acutely resulting in large-volume exudative ascites and hypovolemic shock. In the later stages, granulomas, fibrosis, and adhesions may develop, leading to small bowel obstruction. Water-soluble contrast follow-through series of the small bowel is also often performed in cases of small bowel obstruction to determine the transit time of contrast material into the large bowel, which would help surgeons to predict which patients may be managed conservatively. Thus, water-soluble contrast studies of the gastrointestinal tract have a limited but useful role in the diagnosis of gastrointestinal TB. Water-soluble contrast agents may also be used in sinography/fistulography, where the contrast agent is injected via a cannula into a cutaneous opening, prior to imaging with fluoroscopy or CT, to demonstrate possible communication with bowel and other deep structures, e.g., abscess, which will opacify with contrast material if there is a fistulous communication.

2.4 Ultrasound Imaging

Ultrasound (US) imaging is an excellent modality for targeted assessment of a superficial body part or organ in patients with extrapulmonary TB. In US imaging of enlarged cervical lymph nodes, features such as hypoechoic cortical thickening, decreased hilar fat, decreased internal vascularity, and necrosis may be detected. US imaging may also be used to assess the kidney in renal TB. However, it is less sensitive in identifying isoechoic masses, small calcifications, and cavities that communicate with the pelvicalyceal system (Gambhir et al. 2017). US imaging also allows assessment of the prostate gland, testes, and epididymis in urogenital TB, although findings may be non-specific. In musculoskeletal TB, it is particularly helpful in the evaluation of superficial soft tissue masses, tendons, synovium, and bursal spaces, as well as to look for abscesses and joint effusions (Fig. 5). It also allows quick comparison with the contralateral side or extremity, which is not possible with other imaging modalities, e.g., MRI, where only the affected side is imaged. There are several other specialized US imaging techniques, e.g., endoluminal US imaging to enable clearer visualization of bowel wall abnormalities, transrectal ultrasound imaging to evaluate prostate TB, and contrast-enhanced US imaging.

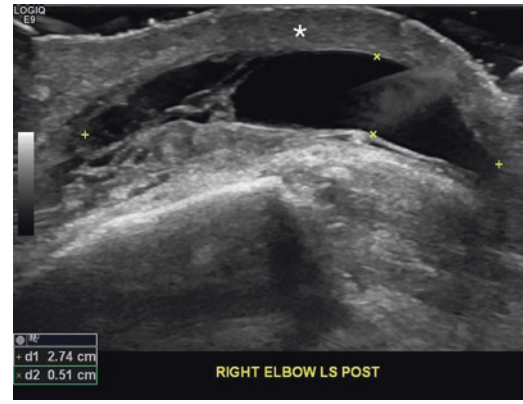

Fig. 5 Tuberculous abscess of the elbow. Longitudinal US image shows a predominantly anechoic fluid collection (between small yellow cursors), with few thick internal septations, in the subcutaneous plane on the posterior aspect of the elbow, with overlying skin thickening (asterisk). This fluid collection was subsequently aspirated and the diagnosis of a tuberculous abscess made

2.4.1 Advantages of US Imaging

1. There is no ionizing radiation hazard, as it utilizes sound waves, making US an eminently suitable imaging technique for young and pregnant patients.
2. It is portable and is readily available at the bedside for ill patients in the emergency department and ICU. US imaging is also useful in outpatient clinics.
3. It provides images in real time and can therefore be used in various interventional procedures. These include guiding biopsy needles in obtaining tissue for the histopathological confirmation of TB, fine-needle aspiration cytology (FNAC) of superficial tuberculous masses and lesions, as well as drainage of pleural effusions and abscesses in patients with TB.

2.4.2 Disadvantages and Limitations of US Imaging

1. Its range of anatomical assessment is limited as US does not cross tissue–bone and tissue–gas boundaries, thus preventing the evaluation of deeper structures beyond these barriers. Therefore, US imaging is not generally used as a modality in the investigation of pulmonary TB, except when looking for pleural effusion. In the abdomen, the presence of air in the stomach may obscure deep structures such as the pancreas. Abnormalities in areas surrounded by or deep to bony structures, e.g., hip joint, will be difficult to image.
2. It may be technically challenging in patients with an abnormally large body habitus, which limits the extent of examination.
3. US imaging is operator-dependent, i.e., much depends on the experience and expertise of the ultrasonologist, particularly for the musculoskeletal system. The quality of the equipment, e.g., use of high-resolution probes, is also important.

2.5 Computed Tomography

CT is the modality of choice for comprehensive assessment of the thorax, abdomen, pelvis, and head and neck and is also useful for the brain and musculoskeletal system. CT is rapid to perform and well tolerated by most patients, including those who are ill or less cooperative. There are many techniques to optimize image quality, such as choice of imaging parameters, multiplanar reconstructions, administration of contrast agents, and postprocessing techniques.

2.5.1 Image Optimization

Patient positioning is important in order to avoid beam hardening artifacts from the upper limbs, which may limit assessment in the region of concern. When imaging the head, neck, and cervical spine, the patient's arms should be kept down at the side of the body. For the same reason, the arms are raised for imaging of the thorax, abdomen, pelvis, and thoracolumbar spine. A scanogram is initially obtained in order to plan the anatomical length and field of view (FOV) to be examined. This is important as decreasing the FOV to fit the region of interest helps to improve spatial resolution. Optimal kilovoltage peak is dependent on the indication for the scan and size of the patient, while tube current is modulated automatically in current machines. High-resolution filters are used for imaging of the lung and bones, while standard filters usually suffice for all other parts. The scan direction is usually craniocaudal.

Administration of an intravenous nonionic iodinated contrast agent is an important means for image optimization. It allows the delineation of abnormal from normal structures by improving the differential contrast enhancement of the various tissues, e.g., structures in the thorax, abdomen, and pelvis. An 18–20G intravenous cannula is set, ideally in the antecubital vein, in order to withstand the consistent high flow rate of 3–5 ml/s produced by a mechanical contrast injector. A test dose of saline is introduced to check if the cannula is properly set within the vein, as well as to test its patency, prior to contrast administration. This is to prevent contrast extravasation into the arm. Following intravenous contrast administration, a saline chaser is used to flush the contrast material along the arm veins, thus fully utilizing the injected contrast material.

It is worth mentioning that overt hyperthyroidism is an absolute contraindication to the intravenous administration of iodinated contrast material. Additionally, it should also not be administered in patients with known severe contrast allergy, severe asthma, or end-stage renal disease who are not on hemodialysis. Patients with known minor allergic reactions to contrast agents and asthma should be given corticosteroids prior to intravenous contrast administration. Patients with renal dysfunction should be hydrated prior to and/or after the study and have their renal function monitored. Patients with renal dysfunction and on metformin are at risk of developing lactic acidosis and should have the medication withheld for a total of 48 h after the study. As the exact protocol for patient preparation differs among institutions, it is prudent to check the local departmental guidelines.

2.5.2 Roles and Advantages of CT

1. CT is the modality of choice for the cross-sectional evaluation of patients with TB, particularly involving the thorax, abdomen, pelvis, and head and neck.
2. It has the benefits of multiplanar reconstruction in the coronal and sagittal planes and volume-rendering/three-dimensional (3D) reconstruction and allows the images to be viewed in the lung, soft tissue, and bone windows.
3. CT has a much faster scan time compared to MRI, and is better tolerated, cheaper, and more accessible.
4. CT is the preferred imaging-guided technique in percutaneous biopsies of deeper structures when a histological diagnosis of TB is necessary; these sites include the mediastinum, abdomen, and spine.

2.5.3 Pulmonary TB

CT has an important role in the diagnosis of pulmonary TB, when the initial chest radiograph is normal or inconclusive. Viewing the lung window allows assessment of the lungs and airways for changes indicative of TB (Fig. 6a, b). Added assessment of the soft tissue structures is possible using the soft tissue window, which reveals characteristic tuberculous lymphadenopathy (Fig. 7a), if present. With CT, the diagnosis of pulmonary TB is correctly made in 91% of cases and correctly excluded in 76% of patients (Lee et al. 1996). It also aids in determining disease activity, being able to characterize 80% of patients with active disease and 89% of those with inactive disease (Lee et al. 1996).

In our institution, besides covering the entire thoracic cage, the coverage of CT of the thorax is usually extended further caudally to include the liver and adrenal glands. Images are obtained at 40–60 s after the intravenous administration of 70–80 ml of nonionic iodinated contrast agent at a rate of 2 ml/s, with typical parameters of 110 kVp, pitch value of 1.2, and slice thickness of 3 mm. High-resolution CT (HRCT) is a CT technique which uses a high spatial frequency reconstruction algorithm to postprocess thin-slice images of the thorax obtained, providing exquisite lung detail. HRCT of the thorax is valuable in the detailed assessment of various manifestations of pulmonary TB, such as interstitial lung involvement, bronchiectasis, and cystic lung lesions. CT aortography is useful for the detection of Rasmussen aneurysm and for preembolization mapping of bronchial and nonbronchial arteries.

2.5.4 Urogenital TB

CT urography is a dedicated technique that is preferred over CT of the abdomen and pelvis for imaging of urinary tract involvement in TB, as it best demonstrates all manifestations of renal TB (Gambhir et al. 2017). It has the additional benefit of having an initial unenhanced scan, which allows better detection of calcifications, as well as a delayed excretory phase. With contrast opacification of the pelvicalyceal system and ureters in the excretory phase, it is akin to an IVU, but with the added advantage of cross-sectional images (Fig. 8). CT urography comprises an unenhanced study, as well as a portovenous phase at 80 s and an excretory phase at 10 min, after intravenous injection of 80 ml of nonionic iodinated contrast agent at a rate of 4 ml/s. Its scan coverage extends from the diaphragm through to the level of the pubic symphysis, with typical

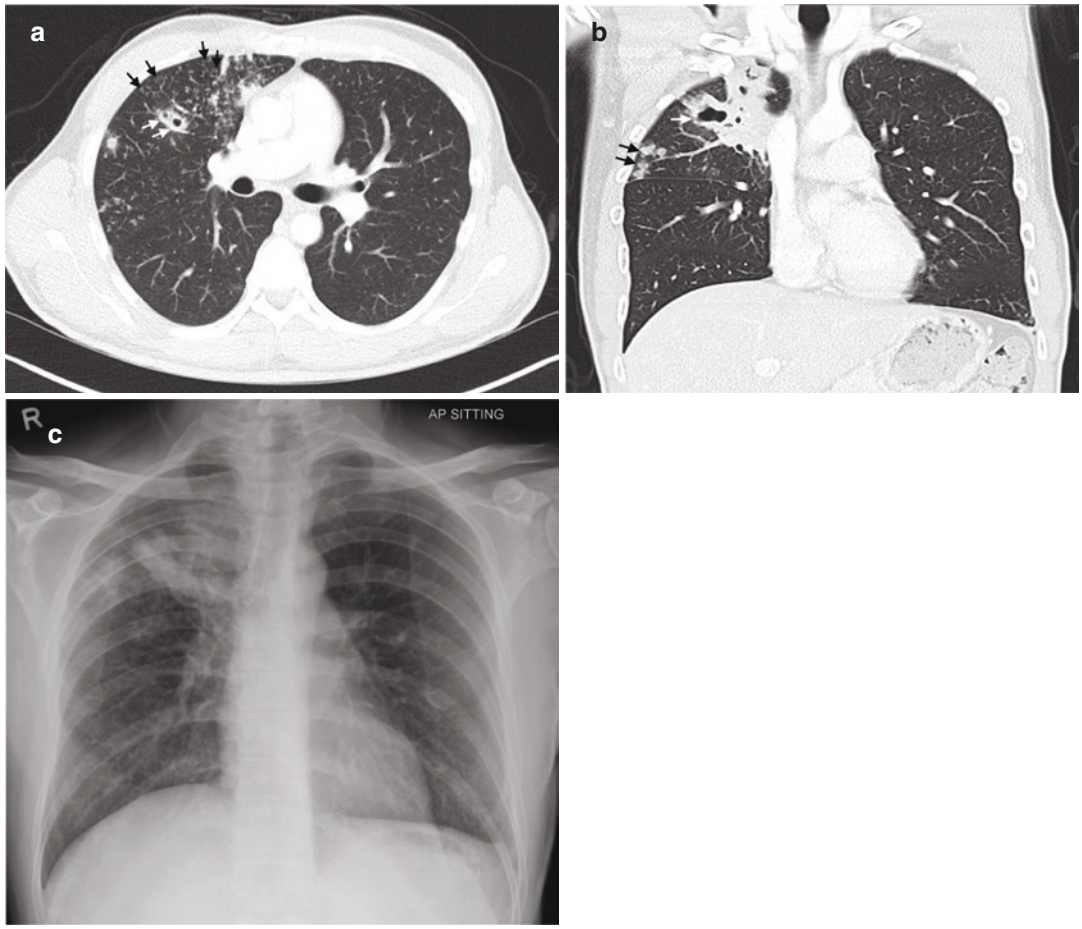

Fig. 6 Pulmonary tuberculosis. (**a**) Axial and (**b**) coronal CT images taken in the lung window setting. In the right upper lobe, there are areas of consolidation with internal cavitation (white arrows), as well as centrilobular tree-in-bud opacities (black arrows). Sputum cultures confirmed tuberculosis. (**c**) AP chest radiograph shows consolidation in the right upper and mid zones. However, neither the internal cavitation nor the tree-in-bud opacities could be appreciated, being only depicted with CT

parameters of 120 kVp, pitch value of 0.6, and slice thickness of 3 mm.

2.5.5 Abdominal TB

CT is the mainstay of investigation of patients with abdominal TB, the findings of which are generally not evident on radiographs. It demonstrates tuberculous lymphadenopathy, which is the commonest manifestation of abdominal TB (Engin et al. 2000) (Fig. 9). It also comprehensively depicts the features of tuberculous infection of various organs such as the liver, spleen, adrenal glands, gastrointestinal tract, and peritoneum (Fig. 10). A routine CT of the abdomen and pelvis is obtained typically at 120 kVp, with a pitch value of 0.6 and slice thickness of 3 mm, scanned in the portovenous phase at 60 s, utilizing 60–70 ml of intravenous nonionic iodinated contrast agent in the average-sized patient, injected at a rate of 2 ml/s. Care should be taken to ensure that the cranial extent of the scan covers the hepatic dome, with the caudal landmark being the pubic symphysis.

CT enterography is an improved technique for the evaluation of the small bowel. It involves ingestion of 1.5–2 L of neutral or low-density

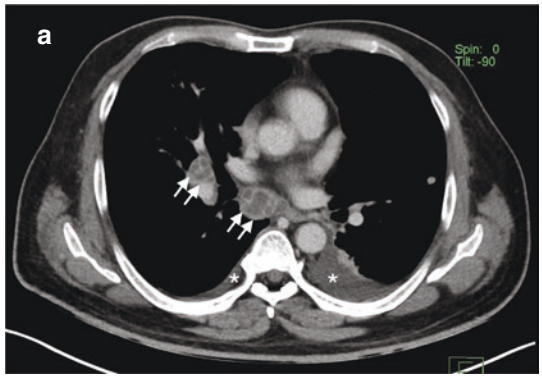

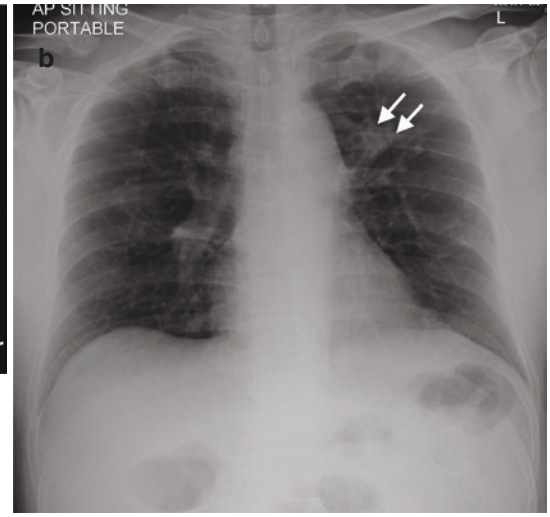

Fig. 7 Pulmonary tuberculosis. (**a**) Axial CT image taken in the soft tissue window setting shows necrotic right hilar and mediastinal lymph nodes with a hypoattenuating center and rim enhancement (arrows), due to active tuberculosis. Small pleural effusions are also present bilaterally (asterisks). (**b**) AP chest radiograph of the patient shows a small area of consolidation in the left mid zone, with internal lucencies suggestive of cavitation (arrows). The hilar and mediastinal lymphadenopathy are not visible

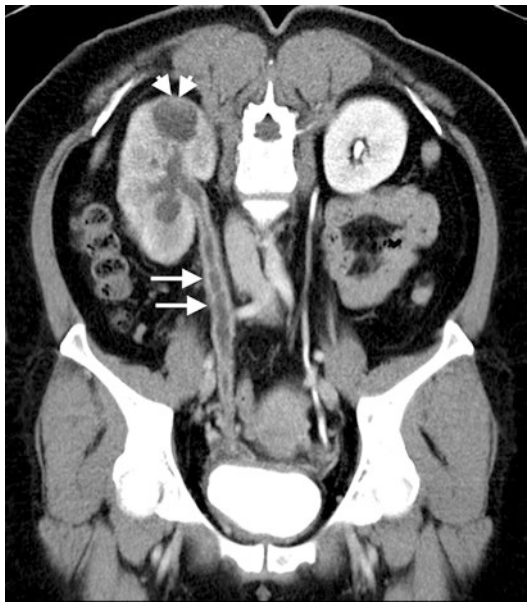

Fig. 8 Right renal and ureteric tuberculosis. Oblique coronal CT urography image reconstructed to display the whole length of the ureters shows a long segment of dilated right ureter with irregular wall thickening (long arrows). There is also right hydronephrosis and a large cavity (short arrows) in the right upper pole renal parenchyma. There is no normal contrast excretion into the right pelvicalyceal system. The left kidney, left ureter, and bladder are normal, with normal pelvicalyceal system opacification

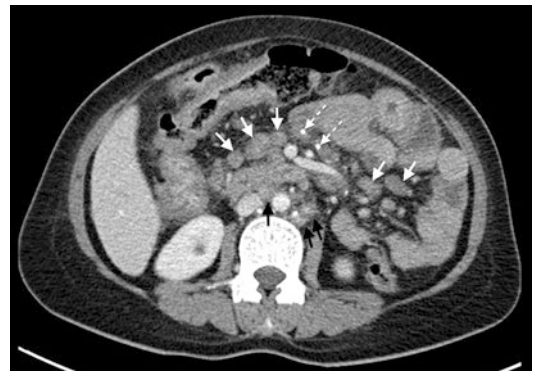

Fig. 9 Tuberculous lymphadenopathy. Axial contrast-enhanced CT image shows a cluster of enlarged, low-density aorto-caval (black arrow), left para-aortic (paired black arrows), and mesenteric lymph nodes (white solid arrows). In this background, there are also a few calcified nodes (white dotted arrows) resulting from previously treated tuberculosis

contrast material (e.g., water–methylcellulose solution, polyethylene glycol, and low-density barium) over 45–60 min, enabling good distension of small bowel and better visualization of wall and intraluminal abnormalities. Virtual CT enteroscopy is a recent technique in which the small bowel is cannulated with a nasogastric

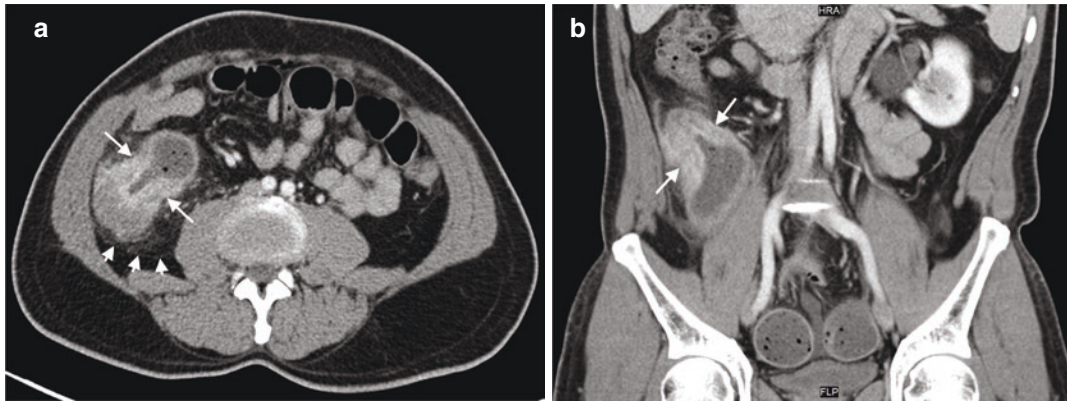

Fig. 10 Ileocecal tuberculosis. (**a**) Axial and (**b**) coronal contrast-enhanced CT images show mural thickening at the ileocecal junction (long arrows) with adjacent inflammatory stranding (short arrows) and free fluid. This patient subsequently underwent colonoscopy, with histopathological confirmation of tuberculosis

tube and distended using carbon dioxide, following which CT images are obtained and reconstructed to produce endoluminal images of the small bowel. This technique produces superior images of mucosal wall and intraluminal abnormalities.

2.5.6 Cranial TB

CT may be helpful in detecting tuberculous pachymeningitis, cranial tuberculomas, and cerebral tuberculous abscesses. However, it is not the preferred modality in the assessment of central nervous system (CNS) TB, if MRI is available. The initial scanogram obtained should extend from the vertex of the skull to the level of C1 vertebra caudally. Typical parameters are 120 kVp, pitch value of 0.55, and slice thickness of 5 mm. For the average patient, 60 ml of intravenous nonionic iodinated contrast agent is administered at a rate of 2 ml/s, and the scan is obtained 1 min later. A CT venogram may also be performed to assess for complications of venous thrombosis in intracranial TB; this technique has some differences in the scanning protocol for a routine cranial CT. Firstly, the coverage for a CT venogram extends further caudally to the level of C3 vertebra to include a longer segment of the internal jugular veins. Scanning is also done earlier, at 40 s and at a faster rate of 3–5 ml/s, utilizing 70 ml of intravenous nonionic iodinated contrast agent.

2.5.7 Head and Neck TB

In the neck, CT may help in the assessment of pharyngeal and laryngeal TB and is ideal for demonstrating cervical lymphadenitis. As it is a better modality compared to MRI for showing calcifications, CT allows better appreciation of fibrocalcified nodes that may be found in patients treated for TB. The scan coverage for a neck CT includes the frontal sinus and extends caudally to the level of the tracheal carina. The images are obtained 40 s after the administration of 50–60 ml of nonionic intravenous contrast agent, at a rate of 2 ml/s, with typical parameters of 120 kVp, pitch value of 0.8, and slice thickness of 3 mm.

CT is also used for the evaluation of sinonasal disease, although findings are non-specific and are often similar to those of the more common infections. CT coverage for the sinuses extends from the vertex of the skull to the mandible and includes the ears and tip of the nose. Unenhanced images using a bone algorithm, as well as contrast-enhanced scans in soft tissue window settings, are obtained, following intravenous administration of 50 ml of nonionic iodinated contrast agent, delivered at a rate of 2 ml/s. Typical CT imaging parameters are 100 kVp, pitch value of 0.55, and a slice thickness of 3 mm.

CT of the temporal bone is essential in the diagnosis of tuberculous otomastoiditis. It allows assessment of the ossicles, walls of the tympanic membrane, and inner ear structures and reveals

the presence of retroauricular abscesses. Images are acquired using a bone algorithm, with a slice thickness of 0.4 mm, at 120 kVp, and a pitch value of 0.55, which includes the frontal sinus to the level of the upper palate, with care taken to include both ears in the lateral extents.

2.5.8 Musculoskeletal TB

When viewed in bone window settings, CT is able to depict the degree and extent of cortical erosions, osseous destruction, and small calcifications in far greater detail compared to radiographs and MRI. However, assessment of soft tissue structures, intervertebral discs, and bone marrow is limited and inferior to MRI. CT has a useful and selected complementary role to radiographs and MRI in the diagnosis of tuberculous spondylitis, tuberculous arthritis, and tuberculous osteomyelitis. When imaging the upper or lower extremities, the entire region of interest should be included and scanned with typical parameters of 120 kVp, pitch value of 0.8, and slice thickness of 3 mm.

2.5.9 Dual-Energy CT

In dual-energy CT (DECT), two sets of X-ray sources and detectors are used to simultaneously acquire CT attenuation data at two different energy levels, namely 80 or 100 kVp and 140 kVp. This technique allows interrogation of different tissues in the body and how they behave at these different radiation energy levels. Initially, DECT was used in the detection of uric acid stones in the urinary tract. Its use, however, has been gradually extended to musculoskeletal imaging, starting with identifying uric acid deposition within various soft tissues in gout, and subsequently evolving into the detection of bone marrow edema. This technique allows calcium to be subtracted from cancellous bone, creating a virtual noncalcium image from an unenhanced image, thus depicting marrow edema in trauma (Pache et al. 2010).

Additionally, visual detection of attenuation changes in the bone marrow could be improved with the use of color-coded maps of the virtual noncalcium subtracted images (Pache et al. 2010). Extrapolating this, the use of DECT in the detection of marrow edema in trauma may be extended to the detection of marrow edema in tuberculous spondylitis, particularly in patients who are unable to undergo MRI. However, this does not replace MRI, which remains the gold standard for identifying marrow edema. Furthermore, there remains the inability of DECT to depict marrow alterations directly subjacent to cortical bone as a result of masking of the cortex and spatial averaging (Pache et al. 2010).

2.5.10 Disadvantages and Pitfalls of CT

1. Artifacts can occur, in particular, movement, beam hardening, and streak artifacts (Fig. 11) due to very high attenuation materials, and may cause problems for image interpretation. Movement artifacts can occur with swallowing in neck CT, breathing in CT of the thorax and abdomen, and movement of the patient in general. Thus, clear instructions to the patient are important. They need to be informed that they need to stay still during the duration of the scan and to carefully follow the instructions given. Shorter CT scan times also aid in reducing/removing movement artifacts, and this is generally achieved with new-generation CT scanners. Beam hardening artifacts occur when the X-ray beam "hardens" and mean energy increases, producing a dark area which obscures an area of interest. This occurs when the lower energy photons are absorbed more rapidly and the higher energy photons pass through a very dense area; for example, the posterior fossa in cerebral CT due to the close presence of dense petrous bones in the base of skull is a common site (Fig. 12). Manufacturers utilize filtration, calibration correction, and beam hardening correction software to overcome this artifact (Barrett and Keat 2014).
2. High radiation doses and radiation protection should be considered. It is advisable to tailor the imaging parameters in order to adhere to the ALARA principle. For example, using a high pitch, low kVp, and mAs, and limiting the region of interest, should be considered, especially in children. Increasing pitch

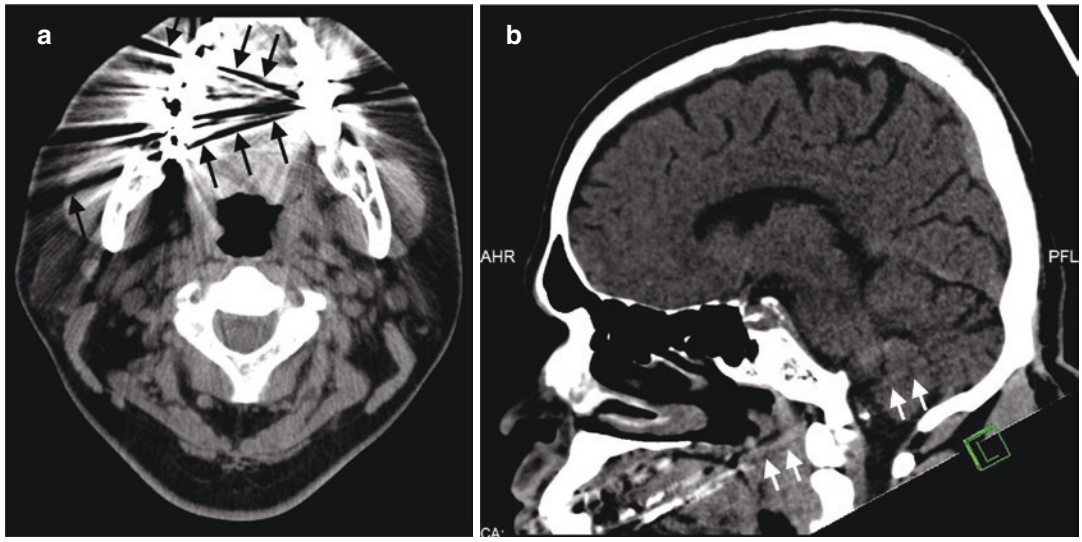

Fig. 11 Streak artifacts in two different patients. (**a**) Axial CT image shows prominent streak artifacts (black arrows) from dental amalgam, which limits assessment of the adjacent structures in the mandible. (**b**) Sagittal CT image in another patient shows streak artifacts (white arrows) from dental amalgam, which extends posteriorly to the cerebellum

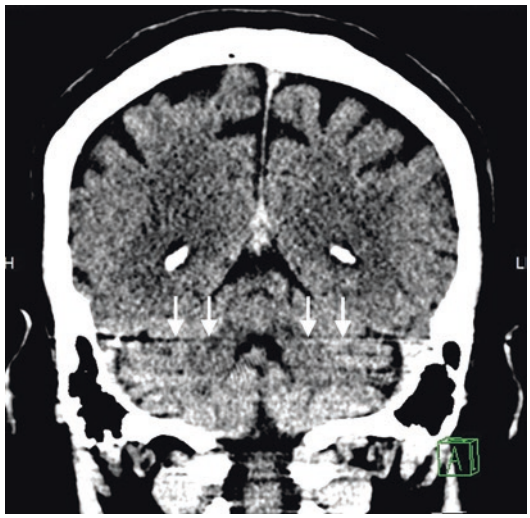

Fig. 12 Beam hardening artifacts. Coronal CT image shows beam hardening artifacts across the cerebellum (arrows), caused by dense petrous bone at the skull base

decreases radiation dose proportionally. Similarly, there is a proportional increase in radiation dose with increase in tube current; doubling the tube current time product doubles the exposure to the patient. Tube current modulation is an essential imaging tool, which allows higher values of tube current in higher attenuation regions; the converse holds true for lower attenuation regions, potentially reducing the radiation dose. Modulation of tube current is also done along the length of the patient. Hence, the CT scanogram helps to appropriately lower the estimate of tube current modulation in relation to differing patient sizes without compromising imaging quality. Modulation of tube current has been known to reduce radiation dose by up to 40% per examination, providing appropriate settings catered to individual patient size and examination type, while maintaining consistency in image quality (Mayo-Smith et al. 2014). Likewise, a decrease in tube voltage will reduce radiation dose; for example, reducing tube voltage from 140 kV to 120 kV will reduce patient exposure and radiation dose by up to 35% (Huda and Mettler 2011). In recent times, automated tube voltage-assisted technology and selection software have been aiding automation of tube voltage based on different CT examination types, as well as each individual patient's attenuation profile gathered from

the initial CT scanogram, while providing diagnostically acceptable image quality (Mayo-Smith et al. 2014).

3. CT does not allow full assessment of the pathological changes in the brain, spinal cord, intervertebral disc, and bone marrow. It is also less sensitive than MRI in the depiction of meningeal abnormalities (Chaudhary et al. 2017). MRI has a much greater range of soft tissue contrast and better shows anatomical details in the brain and cord, thus providing greater appreciation of abnormalities within and distinct from normal structures. Similarly, MRI remains the gold standard in detecting discal and marrow edema, as well as assessment of the spine and paraspinal structures and is the modality of choice in spinal infections (Leone et al. 2012).

2.6 Magnetic Resonance Imaging

MRI is a non-invasive imaging technology, which produces high-quality anatomical images in different orthogonal planes. A powerful magnet magnetizes hydrogen protons found in water that make up living tissues in the patient's body, such that they align with the main magnetic field. Radiofrequency (RF) pulses are employed to stimulate and detect the responses of these protons, enabling MRI sensors to create images that show the differences among various types of tissues, normal or abnormal, based on these magnetic properties. It is often used for detection, diagnosis, and treatment monitoring of various diseases, including TB.

2.6.1 Advantages of MRI

1. There is no ionizing radiation hazard. For pregnant and young patients where comprehensive cross-sectional imaging of a body region or organ is required and in which ionizing radiation should be avoided, MRI is preferable to CT.
2. MRI allows direct acquisition of images in different planes without having to reposition the patient.
3. The superior soft tissue contrast of MRI makes it the imaging modality of choice for providing exquisite anatomical and pathological detail and is excellent for imaging of the brain, meninges, spinal cord, and spine, as well as joints and extremities, in CNS and musculoskeletal TB, respectively. It is the gold standard for imaging of tuberculous spondylodiscitis, demonstrating well the local extent of disease and any complications (Gambhir et al. 2017) (Fig. 13). MRI is also considered superior to CT and is the modality of choice in the detection and assessment of CNS TB (Trivedi et al. 2009; Skoura et al. 2015) (Fig. 14). In particular, it is more sensitive than CT in depicting abnormalities in meningeal TB (Chaudhary et al. 2017) (Fig. 15).

2.6.2 Pulse Sequences

Spin-echo (SE) T1-weighted images are acquired using a short time-to-repetition (TR) of <800 milliseconds (ms) and short time-to-echo (TE) of <30 ms. It is the favored sequence for the detailed depiction of anatomical structures. It is also the sequence used for imaging after intravenous administration of gadolinium (Gd)-based contrast agents, improving detection of enhancing tuberculous lesions, and allows assessment of its enhancement characteristics and extent of infection. Although Gd-based contrast agents may be administered by other means, e.g., intra-articularly in MR arthrography, these techniques have very limited applications in the context of patients with TB.

SE T2-weighted images are obtained using a long TR of >2000 ms and long TE of >60 ms. This sequence is sensitive to the presence of fluid, making it particularly useful in the detection of edema and pathological lesions, which typically have hyperintense T2 signal. Hence, this sequence is ideal for the detection of diseases such as tuberculous infection. Being time-saving, fast or turbo SE (TSE) sequences are currently often used in routine MRI in place of SE T2-weighted sequences. As fat appears hyperintense on TSE T2-weighted images, fat suppression is usually applied to differentiate the abnormal signal from

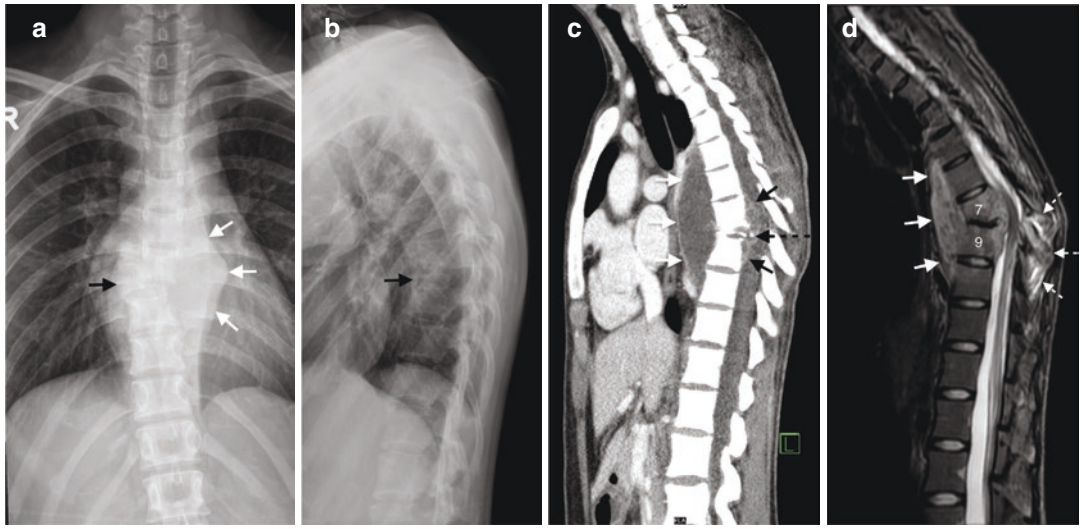

Fig. 13 Tuberculous spondylodiscitis. (**a**) AP and (**b**) lateral radiographs of the thoracic spine show the right lateral remnant of a severely compressed and largely destroyed T8 vertebral body (black arrow), loss of the normal intervening T7/8 and T8/9 disc spaces, as well as a large associated paravertebral mass (white arrows). (**c**) Sagittal contrast-enhanced CT image better shows the severely compressed T8 vertebral body with small retropulsed bony fragments (black dotted arrow). Large anterior prevertebral abscess (white solid arrows) and epidural extension (black solid arrows) are seen. (**d**) Corresponding sagittal STIR MR image shows hyperintense T7 and T9 vertebral bodies, with the severely compressed T8 vertebral body being barely visible. The T8 vertebral posterior elements and adjacent soft tissues show hyperintense signal (dotted arrows), indicating the full extent of infection. The anterior subligamentous spread of the paravertebral abscess (arrows) and epidural phlegmon causing cord compression are well shown

the background fat, particularly in areas where the suspected lesion is in close proximity to fat, e.g., TB of the spine and musculoskeletal system.

The proton density (PD) sequence reflects the density of protons rather than the magnetic characteristics of hydrogen nuclei and is an intermediate sequence sharing features of both T1- and T2-weighted images. It has a long TR of >2000 ms and short TE of 20 ms, minimizing T1 and T2 differences, respectively. This sequence is used in musculoskeletal imaging as it is ideal for the assessment of the joints by providing excellent signal distinction between fluid, hyaline cartilage, and fibrocartilage.

The short tau inversion recovery (STIR) sequence has a TR >2000 ms, TE >30 ms, and inversion time (TI) of 120–150 ms. As fat has a relatively shorter T1 compared to other tissues in the body, its signal may be selectively nulled with this fat suppression sequence, which aims to increase the signal intensity difference between abnormal fluid and adjacent fat. While the imaging quality is usually not as good as that of conventional fat-suppressed T2-weighted images, it is less susceptible to magnetic field inhomogeneity and is favored in certain indications, e.g., where the patient has metallic implants close to the location of the tuberculous lesion. It is also important to note that the signal suppression in STIR is not specific to fat and may also nullify signal from any material with a short T1, e.g., melanin, methemoglobin, proteinaceous fluid, and more importantly gadolinium. Therefore, the STIR sequence cannot be used to demonstrate post-Gd-based contrast enhancement, and it is its most noteworthy limitation.

The fluid-attenuated inversion recovery (FLAIR) sequence is a special inversion recovery sequence with a long TI. Its typical acquisition parameters are TR >3000 ms, TE >80 ms, and TI

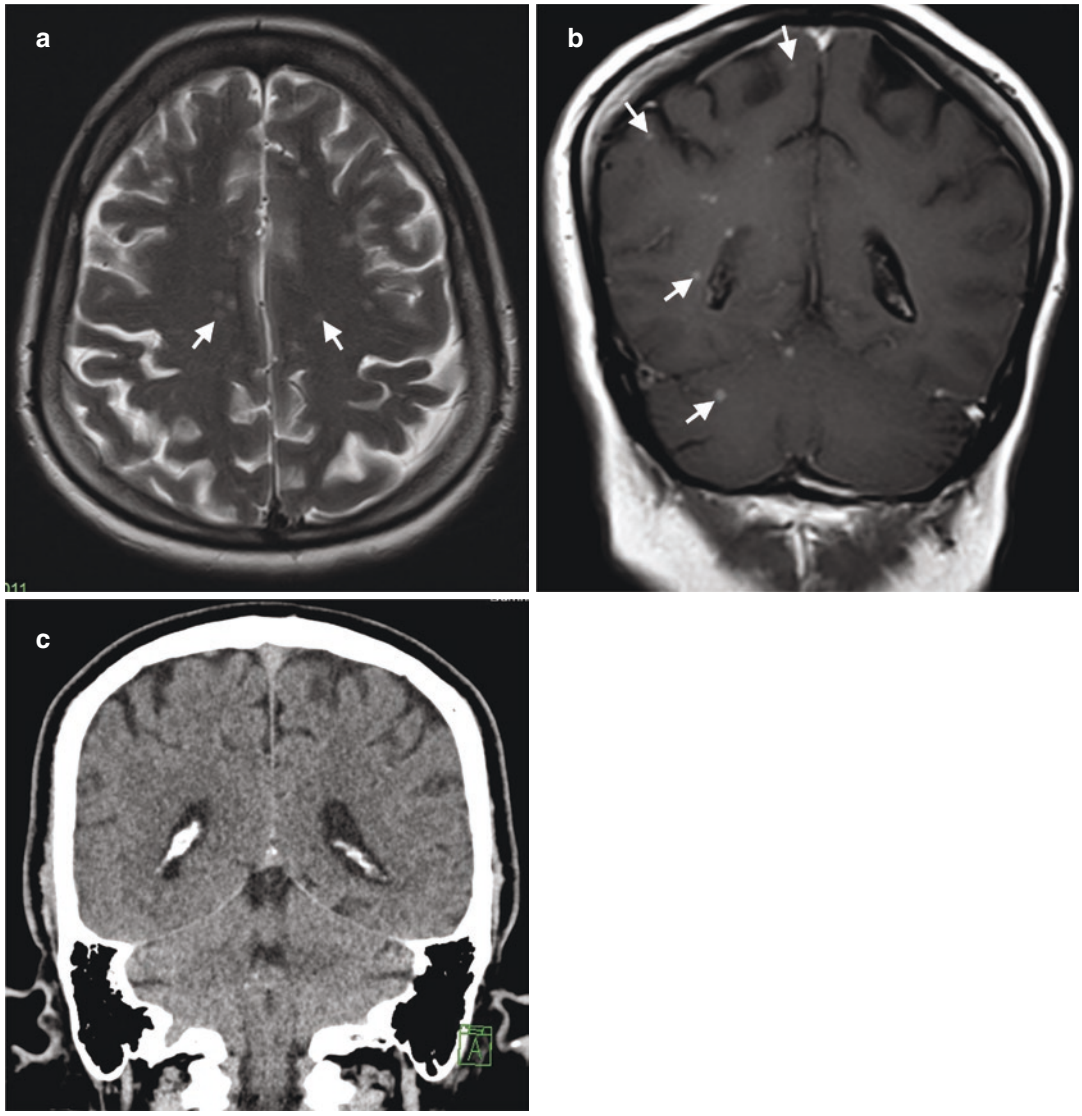

Fig. 14 Cerebral tuberculosis. (**a**) Axial T2-W MR image of the brain shows numerous tiny subcentimeter hyperintense foci in the centrum semiovale bilaterally (arrows). (**b**) Coronal contrast-enhanced FLAIR MR image shows multifocal enhancing foci scattered in the cerebrum and cerebellum (arrows). These lesions are better demonstrated following intravenous Gd-based contrast agent administration. (**c**) Coronal unenhanced CT of the same patient. These tiny subcentimeter foci seen on MRI are hard to identify in the corresponding CT image, particularly without intravenous contrast administration

of 1700–2200 ms. It is essential in imaging the CNS in TB, being able to suppress fluid signal from cerebrospinal fluid (CSF), thus accentuating parenchymal edema, and is helpful in distinguishing periventricular subependymal edema from obstructing hydrocephalus. For the same reason, it also better demonstrates exudates and meningeal enhancement, following Gd-based contrast administration (Fig. 15d).

Diffusion-weighted imaging (DWI) is an MRI technique that detects changes in the Brownian motion of water molecules within tissues (Brant 2012). In routine clinical practice, DWI *b*-values between 0 and 1000 are typically used; for

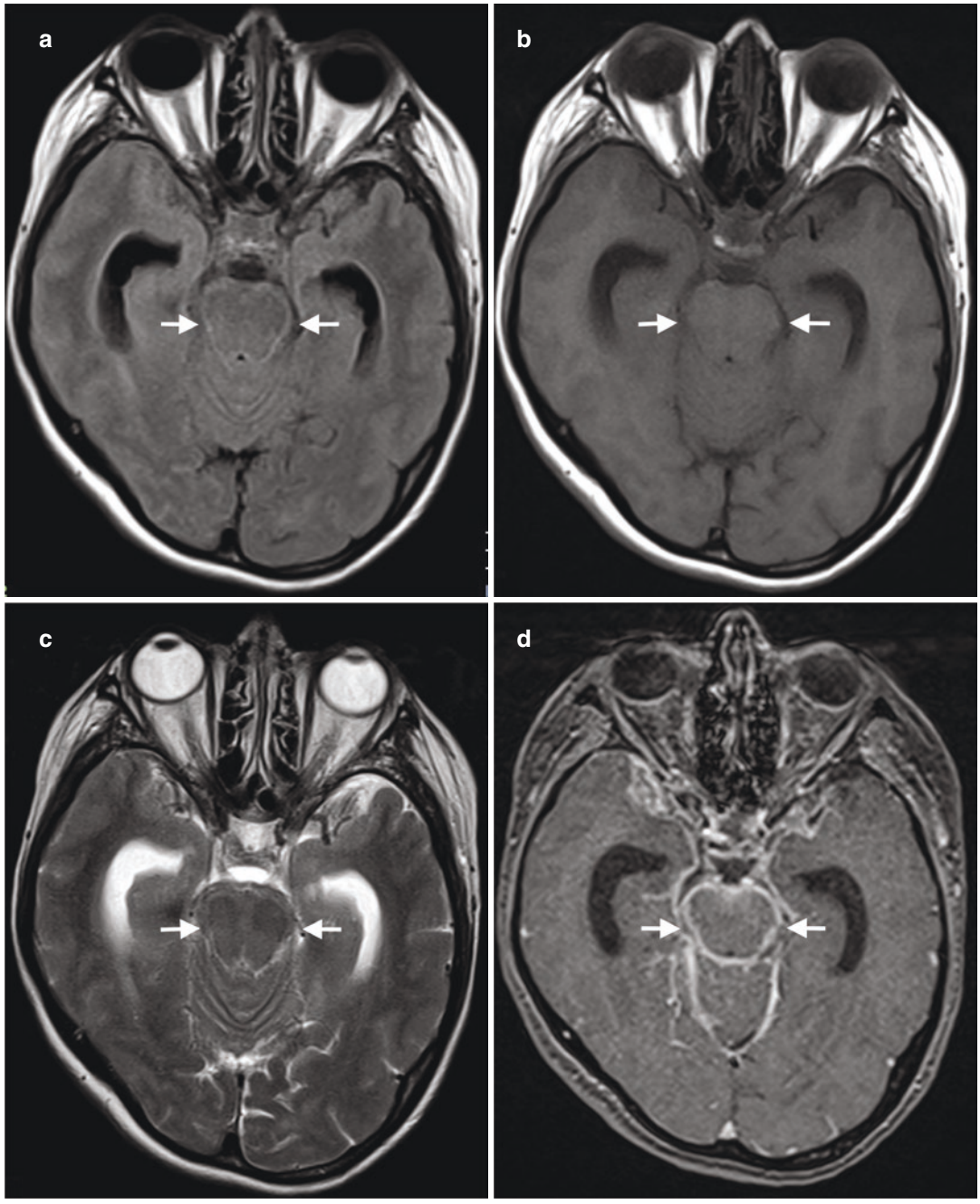

Fig. 15 Leptomeningeal tuberculosis. (**a**) Axial FLAIR MR image shows abnormal hyperintense signal outlining the pons (arrows). Suppression of CSF signal in FLAIR sequences accentuates this area of leptomeningeal abnormality, which would otherwise be difficult to detect on corresponding axial (**b**) T1-W and (**c**) T2-W images. (**d**) Corresponding axial contrast-enhanced FLAIR MR image shows leptomeningeal enhancement. The use of intravenous Gd-based contrast agents better depicts leptomeningeal involvement

example, a *b*-value of 1500 is used in MRI of the prostate. The *b*-value is a factor that reflects the timing and strength of gradients used to generate these images; the higher the *b*-value, the stronger the diffusion effects depicted. DWI is used to identify hypercellular tissue, which demonstrates restricted diffusion.

Apparent diffusion coefficient (ADC) measures the magnitude of diffusion of water molecules within tissues and is clinically calculated using MRI with DWI (Sener 2001). Higher ADC values indicate more mobile water molecules, while low ADC values indicate restricted movement of water molecules in tissues (Mukherjee et al. 2008). In neuroimaging of TB, the DWI sequence allows detection of cerebral infarction (Rodriguez-Takeuchi et al. 2019). This sequence may also help differentiate pyonephrosis from hydronephrosis in renal TB and spondylodiscitis from disc degeneration in spinal TB. Generally, in tissues infected by TB, restricted diffusion may be demonstrated; this may make it a useful sequence in identifying other sites of involvement, rather than just differentiating TB from other disease processes (Dunn et al. 2015).

Gradient-recalled echo (GRE) sequences are used to acquire fast images and are therefore useful in minimizing motion artifacts from breathing, heartbeat, and vessel pulsation, as well as peristalsis. Magnetization decay time in GRE is termed T2* and is much shorter than the T2 decay times in SE imaging. On GRE images, signal intensity arising from T2 relaxation characteristics of tissue is strongly affected by imperfections in the magnetic field. By utilizing GRE T2*-weighted MRI sequences, in addition to relatively long TE values, local magnetic field homogeneity effects are accentuated which is useful to detect blood products, iron, or calcifications (Brant 2012).

Susceptibility-weighted imaging (SWI) is a high-spatial-resolution 3D GRE MRI technique, which has increased sensitivity in the identification of blood products and/or calcium, which may not be as apparent on T2*-GRE imaging; but there are potentially more false positives in SWI. Additionally, SWI has the ability to distinguish paramagnetic (e.g., hemorrhage or iron) from diamagnetic (e.g., calcification) substances using filtered phase postprocessing images, where they demonstrate opposed signal intensity (Tong et al. 2008).

Chemical shift imaging, also known as opposed-phase or in- and out-of-phase imaging, is used to detect the presence of intracellular or microscopic fat, by taking advantage of the differences in precessional frequencies between fat and water. It is acquired simultaneously using two different TEs; the echoes are timed to coincide with out-of-phase and in-phase timings of the relevant spins, and the data is subsequently divided into two different image sets covering the same anatomical region (Roth and Deshmukh 2017). The presence of intracellular or microscopic fat is then identified when there is significant reduction in signal intensity on out-of-phase images.

The Dixon method is a fat suppression sequence, which is based on chemical shift imaging. This technique uses a nonspectrally selective pulse with TEs, which capture phase differences between fat and water protons, which, over time, alternate between being in-phase and opposed-phase. Acquiring both in-phase and opposed-phase images simultaneously allows the images to be either added or subtracted to produce water-only (fat-suppressed) or fat-only (water-suppressed) images, respectively. The Dixon method has the advantage of uniform fat suppression and ability to quantify fat.

All the different MRI manufacturers have developed their own special sequences; most of them are named with easy-to-remember and/or catchy acronyms. For example, Siemens' fast low angle shot (FLASH) and volumetric interpolated breath-hold examination (VIBE) are spoiled GRE sequences, which utilize RF spoiling to eliminate transverse magnetization prior to each RF pulse. With FLASH, both T2*- and T1-weighted imaging may be obtained, and with

its short repetition time enabling images to be acquired within a single breath hold, it is commonly used in abdominal imaging. VIBE is a modified form of FLASH, which allows high-resolution dynamic images to be acquired. Using fast 3D GRE sequences to produce T1 images, it is a form of volumetric imaging used in abdominal imaging to acquire dynamic contrast-enhanced images using short breath-hold-length acquisition times.

The double-echo steady state (DESS) is a 3D GRE sequence by Siemens, which produces higher T2*-weighted imaging. It is mainly used in musculoskeletal imaging, providing high-resolution cartilage imaging, as well as synovial fluid imaging. Half-Fourier acquisition with single-shot turbo spin echo (HASTE) is a product by Siemens, which uses a single-shot technique to acquire only slightly more than half of the required data within a single TR for an entire T2-weighted image. This is made possible by half-Fourier transformation, which enables computer reconstruction of the remaining data that was not acquired, thus reducing scan times, allowing for fast breath-hold imaging (Regan et al. 1998). Sampling perfection with application-optimized contrasts using different flip angle evolution (SPACE) is an isotropic 3D FSE acquisition sequence by Siemens. It enables acquisition of T1-, T2-, FLAIR-, and PD-weighted imaging in high-resolution 3D datasets.

MR spectroscopy (MRS), on the basis of the chemical shift phenomena, provides information about the presence and concentration of metabolites in tissue (Brant 2012). The more common metabolite peaks measured are lactate, N-acetylaspartate (NAA), citrate, creatine, and choline, and these change with different pathologies. For example, MRS helps to differentiate tuberculoma from pyogenic abscesses and neoplasms (Gupta et al. 1995).

Magnetization transfer (MT) imaging manipulates differences in relaxation of freely mobile unbound water protons, immobile protons with restricted motion (macromolecular pool), and protons at the boundary, where exchange of magnetization transfer occurs (Yousem and Grossman 2010). When MT pulses are applied to the macromolecular pool, some of this energy is transferred to the free water pool, which would partially saturate, resulting in reduced signal due to the MT effect. The MT effect can be quantified by obtaining two sets of images, one before the MT pulse (x) and the other with the MT pulse (y), and subsequently subtracting them digitally ($x - y$). The magnetization transfer ratio (MTR) for a given voxel is then taken to be $(x - y)/x$. MT imaging is used most frequently in time-of-flight (TOF) magnetic resonance angiography (MRA) to suppress the signal intensity of the background brain, thus improving visualization of the vessels. In combination with contrast-enhanced MRI, it also improves conspicuity of white matter-enhancing lesions with its greater suppression of white matter signal compared to gray matter (Yousem and Grossman 2010).

TOF MRA or MRV is an MRI technique used to visualize flow within arteries and veins, respectively, using a GRE sequence, without the need for intravenous contrast administration. In TOF imaging, unsaturated spins moving into the image slice have high signal, while the saturated stationary ones have low signal; this effect is thus termed flow-related enhancement. The source images are then postprocessed using different algorithms to depict only flowing blood, seen as the brightest pixels, and projected in any plane to better demonstrate the vascular anatomy in multiple views (Yousem and Grossman 2010).

When dynamic contrast-enhanced GRE T1-weighted sequences are performed to acquire contrast-enhanced MRA/MRV images, sequential images in different phases are obtained; the "first-pass" images are acquired in the arterial phase in the vessel of interest, and subsequent images acquired have varying degrees of mixed arterial and venous enhancement. From these, arterial as well as selective venous phase studies in the vein of interest may be obtained by subtracting the arterial phase study from the mixed arterial and venous phase study. The use of Gd-based contrast agent results in blood appearing bright.

2.6.3 Patient Positioning and Coils

It is imperative that the patient is in a comfortable position for the relatively long duration of the MRI scan. Typically, patients lie supine, "head in" first into the scanner gantry. The "feet in" first position is used when imaging the lower extremity and may be attempted in patients who are claustrophobic when imaging the spine and abdomen. Other positions may be adopted according to clinical circumstances, e.g., decubitus position for a patient with kyphosis. Pads, sponges, straps, and other mobilizing devices may be used to help the patient to keep still and maintain their position on the MRI couch.

Once within the bore of the magnet, the patient is surrounded by a series of coils, each with its own function. Working from outwards to inwards, the outermost coils are shim coils, which are fine-tuned to improve magnet field homogeneity and maintain as uniform a main magnetic field as possible throughout the imaging process. The role of gradient coils is primarily to allow spatial encoding of the MRI signal. Lastly, the RF coil can be used as a transmitter, generating RF magnetic field pulses perpendicular to the static main magnetic field, and/or used as a receiver for detecting the MRI signal emitted by the excited hydrogen protons within the tissues in the body part under examination. RF coils may also be grouped into volume and surface coils.

There are several types of RF coils including the following:

1. Volume coils: These are designed to provide homogeneous RF excitation across a large volume, thus providing a better magnetic field homogeneity compared to surface coils. The largest volume coil is the standard body coil, which is both a transmit and receive coil, incorporated as part of the scanner and used in imaging large parts of the body, such as the abdomen, pelvis, and chest. The smaller volume coils, for example, the head coil, also both a transmit and receive coil, are used in imaging of the brain. Small-volume coils are also used in imaging of the neck, cervical spine, and extremities, e.g., in the knee and wrist.
2. Surface coils are receiver coils placed as close as possible to the region of concern to be imaged, e.g., the orbits, in order to maximize the signal and obtain a high signal-to-noise ratio (SNR) and resolution. The drawback to this coil is its small FOV, which has been overcome by the advent of phased array coils.
3. Phased array coils are receive-only RF coils made up of a collection of four or more receiver coils, which together form a larger array. The individually received signals are combined to increase the SNR with a larger FOV, with all data acquired in a single sequence. An example of such usage will be MRI of multiple segments of the spine (Asher et al. 2010).

2.6.4 MRI Protocols

As a general principle, MRI protocols are designed with the aim of providing answers to the clinical problem by comprehensively evaluating the area of interest, yet in a timely and cost-effective manner. Besides coil selection to cover the specified region of interest and using the correct sequences, several other parameters have to be applied to achieve the best possible images, including the ideal imaging planes, FOV size, slice thickness, and interslice gap. It is worthwhile to emphasize the importance of having the radiologist available to review the images on completion of the scans, with the view of protocol modification, e.g., adding extra or special sequences, extending the scan region of interest, and assessing the need for contrast enhancement.

Routine MRI protocols will differ among institutions and the requirements of individual clinical practices. These differences will not be marked if MRI principles are followed. Even in a single institution, the MRI protocols will not be exactly the same. For example, in our department, we have MRI scanners from different manufacturers and magnets of 1.5 T and 3.0 T field strengths. In the following paragraphs, we have provided sample MRI protocols for the Siemens Avanto 1.5 T scanner in our institution that are used for imaging of suspected infection in various parts of the body. Note that the turbo inversion recovery magnitude (TIRM) sequence is the Siemens equivalent to the STIR sequence.

In imaging the spine in a patient with suspected tuberculous infection, we use a phased array coil system for spine imaging that is built into the table of the MRI machine, allowing imaging of multiple segments of the spine. For the cervical spine, there is an option to add an additional neck matrix coil, with multisegment attachment, that integrates with the spine coil and will produce better quality images (Leow et al. 2021). The scan coverage should cover the entire spinal area of interest, i.e., from above the craniocervical junction to T4 vertebral level in the cervical spine; C6–L1 vertebral levels in the thoracic spine; and T10–S4 levels in the lumbar spine. A sagittal localizer image of the entire spine is first obtained in order to correctly identify the vertebral levels and the presence of a transitional lumbosacral vertebral segment (Peh et al. 1999). MRI protocols for the cervical, thoracic, and lumbar spine are listed in Tables 1–3.

Patients undergoing MRI of the brain and/or neck for suspected intracranial and head and neck TB are imaged using a combined head/neck coil, or a head coil for the brain and a neck coil for the neck, depending on the MRI machine used. These coils are volume coils that both transmit and receive RF signals. For the brain, the scan coverage should extend at least 1 cm above the vertex of the skull and through the skull base, in its craniocaudal extent, and cover both ears from side to side. For the head and neck, the scan coverage is from the frontal sinus to the distal sternoclavicular joint. MRI protocols for patients in whom brain and head and neck TB is suspected are listed in Tables 4 and 5.

Generally, when assessing for abdominal, gastrointestinal, and urogenital TB, as well as tuberculous lymphadenopathy, CT is the preferred imaging modality. MRI of the abdomen is reserved for patients in whom CT is contraindicated. In our institution, MRI of the liver, pancreas, or kidneys is usually reserved for troubleshooting and further characterization of a known lesion that has already been detected with US imaging or CT. A body coil is used when acquiring an MRI of the abdomen or MR urography. The coverage for MRI of the abdomen should include the liver and extend through the lower abdomen, clearing the inferior poles of the kidneys. MR urography covers the entire urinary tract, extending from the superior poles of the kidneys to the urinary bladder. Dynamic contrast-enhanced images of the kidneys are acquired, in addition to delayed imaging in the excretory phase with contrast opacification of the ureters and urinary bladder. Protocols of an MRI of the abdomen and MR urography are listed in Tables 6 and 7.

MRI is the imaging modality of choice for imaging musculoskeletal TB. A large selection of coils may be used, tailored to the area of interest. This may range from using a whole-body coil to image extensive necrotizing fasciitis of the thigh to a dedicated wrist coil for tuberculous arthritis of the radiocarpal joint. As a principle, images are acquired in two orthogonal planes (usually axial plus either sagittal or coronal) as a minimum for lesions in or around long bones and three orthogonal planes for complex joints (e.g., ankle and knee). In our practice, intravenous Gd-based contrast agent is administered routinely as we have found that the additional information it provides enhances diagnostic confidence. Sample protocols for MRI of the upper limb long bones are listed in Tables 8 and 9.

2.6.5 Disadvantages and Pitfalls of MRI

MRI is generally less accessible, usually has longer waiting times, and is costlier compared to CT. The long acquisition times of MRI require the patient to lie still in the magnet for a relatively long time, and it is hence not ideal for patients with claustrophobia. It may also be difficult to image young children or patients with altered mental status, without first giving sedation. Motion blurring occurs and degrades the MR images, should the patient find it difficult to stay still throughout the duration of the study or hold their breath at the appropriate times. This is particularly important in imaging of the abdomen when breathing motion artifacts limit assessment of the solid organs, peritoneum, and lymph nodes.

It may also not be possible for patients with certain MRI-incompatible implants and foreign

Table 1 MRI of the cervical spine protocol

Plane	Sequence type		Fat suppression	Slice thickness (mm)	Interslice gap (mm)	FOV (mm)	Matrix	TR (ms)	TE (ms)	ETL	Flip angle	Bandwidth (Hz/pixel)	NEX
SAG	T1	TSE	–	3	0.3	240	270 × 384	531	9.7	3	150	181	3
SAG	T2	TSE	–	3	0.3	240	270 × 384	1600	98	19	150	191	2
SAG	T2	TIRM	–	3	0.3	240	224 × 320	4120	80	14	150	150	2
AX	T2*	GRE	–	3	0.6	180	224 × 320	950	16	–	28	150	2
AX	T2	TSE	YES	3	0.6	180	204 × 256	3160	78	13	150	150	2
AX	T1	TSE	–	3	0.6	180	204 × 256	418	11	3	150	150	3
Post IV contrast administration													
SAG	T1	TSE	YES	3	0.3	240	256 × 320	531	9.7	3	150	181	3
AX	T1	TSE	YES	3	0.6	180	204 × 256	418	11	3	150	150	3
COR	T1	TSE	YES	3	0.3	240	256 × 320	531	9.7	3	150	181	3

SAG sagittal, *AX* axial, *COR* coronal, *TSE* turbo spin echo, *TIRM* turbo inversion recovery magnitude, *GRE* gradient-recalled echo, *FOV* field of view, *TR* time to repetition, *TE* time to echo, *ETL* echo train length, *NEX* number of acquisitions, *IV* intravenous

Table 2 MRI of the thoracic spine protocol

Plane	Sequence type		Fat suppression	Slice thickness (mm)	Interslice gap (mm)	FOV (mm)	Matrix	TR (ms)	TE (ms)	ETL	Flip angle	Bandwidth (Hz/pixel)	NEX
SAG	T1	TSE	–	4	0.4	350	310 × 448	684	11	3	150	170	1
SAG	T2	TSE	–	4	0.4	350	270 × 384	4730	76	16	150	161	2
AX	T1	TSE	–	5	0.5	200	224 × 320	462	8.7	3	150	180	2
AX	T2	TSE	YES	5	0.5	200	224 × 320	2320	76	13	160	161	2
Post IV contrast administration													
SAG	T1	TSE	YES	4	0.4	350	270 × 384	684	11	3	150	170	1
AX	T1	TSE	YES	5	0.5	200	204 × 256	462	8.7	3	150	180	2

SAG sagittal, *AX* axial, *COR* coronal, *TSE* turbo spin echo, *TIRM* turbo inversion recovery magnitude, *FOV* field of view, *TR* time to repetition, *TE* time to echo, *ETL* echo train length, *NEX* number of acquisitions, *IV* intravenous

Table 3 MRI of the lumbosacral spine protocol

Plane	Sequence type		Fat suppression	Slice thickness (mm)	Interslice gap (mm)	FOV (mm)	Matrix	TR (ms)	TE (ms)	ETL	Flip angle	Bandwidth (Hz/pixel)	NEX
SAG	T1	TSE	–	4	0.4	330	310 × 448	624	9.9	3	150	180	2
SAG	T2	TSE	YES	4	0.4	330	310 × 448	3080	96	14	150	90	1
AX	T1	TSE	–	5	0.5	200	224 × 320	462	8.7	3	150	180	2
AX	T2	TSE	YES	5	0.5	200	224 × 320	2320	76	13	160	161	2
Post IV contrast administration													
SAG	T1	TSE	YES	4	0.4	330	270 × 384	624	9.9	3	150	180	2
AX	T1	TSE	YES	5	0.5	200	204 × 256	462	8.7	3	150	180	2
COR	T1	TSE	YES	4	0.4	330	270 × 384	624	9.9	3	150	180	2

SAG sagittal, *AX* axial, *COR* coronal, *TSE* turbo spin echo, *TIRM* turbo inversion recovery magnitude, *FOV* field of view, *TR* time to repetition, *TE* time to echo, *ETL* echo train length, *NEX* number of acquisitions, *IV* intravenous

Table 4 MRI of the brain protocol

Plane	Sequence type		Fat suppression	Slice thickness (mm)	Interslice gap (mm)	FOV (mm)	Matrix	TR (ms)	TE (ms)	ETL	Flip angle	Bandwidth (Hz/pixel)	NEX
SAG	T1	SE	–	5	2	230	224 × 320	427	10	–	90	90	1
AX	T2	TSE	–	5	1.5	230	310 × 384	4550	92	14	180	130	1
AX	T2	FLAIR	–	5	1.5	230	204 × 256	9000	92	17	150	200	1
AX	T2	DWI	YES	5	1.5	230	192 × 192	3700	91	–	–	–	4
AX	T2*	SWI	–	2	1	230	200 × 256 × 192	49	40	–	15	80	1
AX	T1	SE	–	5	1.5	230	256 × 320	470	10	–	90	130	1
Post IV contrast administration													
AX	T1	SE	–	5	1.5	230	256 × 320	400	17	–	90	130	1
SAG	T1	SE	–	5	2	230	224 × 320	552	17	–	90	130	1
COR	T1	SE	–	5	1.5	230	224 × 320	608	17	–	90	130	1
AX	T1	VIBE	YES	1	0.2	250	240 × 256 × 240	9.78	4.64	–	10	130	1
AX	T2	FLAIR	YES	5	1.5	230	204 × 256	9000	92	17	150	200	1

SAG sagittal, *AX* axial, *COR* coronal, *SE* spin echo, *TSE* turbo spin echo, *FLAIR* fluid-attenuated inversion recovery, *DWI* diffusion-weighted imaging, *SWI* susceptibility-weighted imaging, *VIBE* volumetric interpolated breath-hold examination, *FOV* field of view, *TR* time to repetition, *TE* time to echo, *ETL* echo train length, *NEX* number of acquisitions, *IV* intravenous

Table 5 MRI of the neck protocol

Plane	Sequence type		Fat suppression	Slice thickness (mm)	Interslice gap (mm)	FOV (mm)	Matrix	TR (ms)	TE (ms)	ETL	Flip angle	Bandwidth (Hz/pixel)	NEX
SAG	T1	TSE	–	4	0.8	260	270 × 384	486	10	3	150	180	1
COR	T1	TSE	–	4	0.8	260	310 × 384	429	9	3	150	180	1
COR	T2	TIRM	–	4	0.8	260	310 × 384	3560	78	10	150	180	1
AX	T1	TSE	–	5	1	180	256 × 320	689	11	3	150	180	1
AX	T2	DIXON	YES	5	1	180	256 × 320	4700	82	11	160	140	1
AX	T2	DWI	YES	5	1	240	162 × 162	8100	83	–	–	1144	4
Post IV contrast administration													
SAG	T1	TSE	YES	4	0.8	260	256 × 320	560	11	3	150	120	1
COR	T1	DIXON	YES	4	0.8	260	256 × 320	460	14	3	160	180	1
AX	T1	DIXON	YES	5	1	180	204 × 256	645	14	3	150	120	1

SAG sagittal, *AX* axial, *COR* coronal, *TSE* turbo spin echo, *TIRM* turbo inversion recovery magnitude, *DWI* diffusion-weighted imaging, *FOV* field of view, *TR* time to repetition, *TE* time to echo, *ETL* echo train length, *NEX* number of acquisitions, *IV* intravenous

Table 6 MRI of the abdomen protocol

Plane	Sequence type		Fat suppression	Slice thickness (mm)	Interslice gap (mm)	FOV (mm)	Matrix	TR (ms)	TE (ms)	ETL	Flip angle	Bandwidth (Hz/pixel)	NEX
COR	T2	HASTE	–	6	1.8	330	272 × 320	1200	79	272	150	411	1
AX	T2	HASTE	–	5	1.5	330	240 × 256	1200	82	243	150	407	1
AX	T1	DIXON FLASH	–	5	1.5	330	180 × 256	91	2.38/4.78	–	70	450	1
AX	T2	HASTE	YES	4	0.4	330	180 × 256	1200	81	179	150	407	1
COR	T2	HASTE	YES	4	0.4	330	180 × 256	1200	81	179	150	407	1
AX	T2	DWI	YES	5	1.5	360	162 × 180	4600	78	–	–	1634	3
AX	T1	VIBE	YES	2.5	0.5	330	180 × 256 × 150	4.29	1.91	–	10	410	1
Post IV contrast administration													
AX	T1	VIBE (Dynamic arterial, arterial/venous, delay)	YES	2.5	0.5	330	180 × 256 × 150	4.29	1.91	–	10	410	1
COR	T1	VIBE	YES	2.5	0.5	350	200 × 256 × 180	2.98	1.1	–	10	590	1
AX	T1	VIBE (Delayed 5 min)	YES	2.5	0.2	330	180 × 256 × 150	4.29	1.91	–	10	410	1

AX axial, *COR* coronal, *HASTE* half-Fourier acquisition single-shot turbo spin echo, *FLASH* fast low-angle shot, *SPACE* sampling perfection with application-optimized contrasts using different flip angle evolution, *DWI* diffusion-weighted imaging, *VIBE* volumetric interpolated breath-hold examination, *FOV* field of view, *TR* time to repetition, *TE* time to echo, *ETL* echo train length, *NEX* number of acquisitions, *IV* intravenous

Table 7 MR urography protocol

Plane	Sequence type		Fat suppression	Slice thickness (mm)	Interslice gap (mm)	FOV (mm)	Matrix	TR (ms)	TE (ms)	ETL	Flip angle	Bandwidth (Hz/pixel)	NEX
COR	T2	HASTE	–	6	1.8	380	270 × 384	1200	79	269	150	407	1
AX	T2	HASTE	–	5	1.5	330	240 × 256	1200	82	194	150	407	1
AX	T1	VIBE	–	3	0.6	350	200 × 288 × 200	7.12	4.78	–	10	400	1
AX	T1	VIBE (DIXON)	–	2.5	0.5	350	200 × 288 × 200	6.68	2.39/4.78	–	10	600	1
AX	T1	VIBE	YES	2.5	0.5	350	180 × 256 × 254	3.72	1.67	–	10	500	1
AX	T2	DWI	YES	5	0.5	360	162 × 180	4800	78	–	–	1634	3
COR	T2	SPACE (3D)	–	1.2	–	380	384 × 384 × 230	2400	706	281	140	372	1.4
Post IV contrast administration													
AX	T1	VIBE (Upper kidneys – Dynamic 3 phases)	YES	2.5	0.5	350	180 × 256 × 254	3.72	1.67	–	10	500	1
AX	T1	VIBE (Lower pelvis – 1 min)	YES	2.5	0.5	350	180 × 256 × 254	3.72	1.67	–	10	500	1
AX	T1	VIBE (Upper kidneys – 3 min)	YES	2.5	0.5	350	180 × 256 × 254	3.72	1.67	–	10	500	1
AX	T1	VIBE (Lower pelvis – 3 min)	YES	2.5	0.5	350	180 × 256 × 254	3.72	1.67	–	10	500	1
COR	T1	VIBE (5 min)	YES	2.5	0.5	350	200 × 256 × 180	2.82	1.03	–	10	650	1
AX	T1	VIBE (Upper kidneys – 8 min)	YES	2.5	0.5	350	180 × 256 × 254	3.72	1.67	–	10	500	1
AX	T1	VIBE (Lower pelvis – 8 min)	YES	2.5	0.5	350	180 × 256 × 254	3.72	1.67	–	10	500	1

X axial, *COR* coronal, *HASTE* half-Fourier acquisition single-shot turbo spin echo, *DWI* diffusion-weighted imaging, *VIBE* volumetric interpolated breath-hold examination, *SPACE* sampling perfection with application-optimized contrasts using different flip angle evolution, *FOV* field of view, *TR* time to repetition, *TE* time to echo, *ETL* echo train length, *NEX* number of acquisitions, *IV* intravenous

Table 8 MRI of the humerus protocol

Plane	Sequence type		Fat suppression	Slice thickness (mm)	Interslice gap (mm)	FOV (mm)	Matrix	TR (ms)	TE (ms)	ETL	Flip Angle	Bandwidth (Hz/pixel)	NEX
COR	T1	TSE	–	4	0.4	380	270 × 384	590	8	3	150	200	1
COR	T2	TIRM	–	4	0.4	380	256 × 320	4390	67	10	150	200	1
SAG	T1	TSE	–	4	0.4	380	270 × 384	590	8	3	150	200	1
SAG	T2	TIRM	–	4	0.4	380	256 × 320	4000	66	10	150	250	1
AX	T1	TSE	–	5	1.0	160	224 × 320	490	10	3	180	160	2
AX	T2	TSE	YES	5	1.0	160	204 × 256	3600	73	10	180	160	2
Post IV contrast administration													
COR	T1	TSE	YES	4	0.4	380	256 × 320	640	8	3	150	200	1
SAG	T1	TSE	YES	4	0.4	380	256 × 320	610	8	3	150	200	1
AX	T1	TSE	YES	5	1.0	160	204 × 256	520	10	3	180	160	2

SAG sagittal, *AX* axial, *COR* coronal, *TSE* turbo spin echo, *TIRM* turbo inversion recovery magnitude, *FOV* field of view, *TR* time to repetition, *TE* time to echo, *ETL* echo train length, *NEX* number of acquisitions, *IV* intravenous

Table 9 MRI of the forearm (radius/ulna) protocol

Plane	Sequence type		Fat suppression	Slice thickness (mm)	Interslice gap (mm)	FOV (mm)	Matrix	TR (ms)	TE (ms)	ETL	Flip Angle	Bandwidth (Hz/pixel)	NEX
COR	T1	TSE	–	3	0.6	350	270 × 384	400	9	–	90	150	1
COR	T2	TIRM	–	3	0.6	350	256 × 320	2750	67	13	150	150	3
SAG	T1	TSE	–	3	0.6	350	270 × 384	400	9	–	90	150	1
SAG	T2	TIRM	–	3	0.6	350	256 × 320	2750	67	13	150	150	3
AX	T1	TSE	–	3.5	0.7	140	256 × 320	614	9	–	90	150	1
AX	T2	TSE	YES	3.5	0,7	140	204 × 256	4820	71	13	150	150	3
Post IV contrast administration													
COR	T1	TSE	YES	3	0.6	350	256 × 320	650	9	–	90	150	1
SAG	T1	TSE	YES	3	0.6	350	256 × 320	650	9	–	90	150	1
AX	T1	TSE	YES	3.5	0.7	140	204 × 256	540	9	–	90	150	1

SAG sagittal, *AX* axial, *COR* coronal, *TSE* turbo spin echo, *TIRM* turbo inversion recovery magnitude, *FOV* field of view, *TR* time to repetition, *TE* time to echo, *ETL* echo train length, *NEX* number of acquisitions, *IV* intravenous

bodies to obtain an MRI. Some of these include the following:

1. Temporary transvenous pacing wires and abandoned intracardiac pacing wires are absolute contraindications, as current induced by RF pulses could result in thermal injuries.
2. Insulin pumps, as well as other drug infusion pumps for chemotherapy and analgesic agents, must also be removed prior to MRI as they may malfunction.
3. Certain catheters come with known metallic components, e.g., Swan-Ganz catheter.
4. Implantable neurostimulation systems, e.g., deep brain stimulators: There is the risk of possible thermal injury along wires and malfunction of the device.
5. Known metallic foreign bodies in the eye could heat up, move, or be displaced during MRI, resulting in injury to the eye and adjacent structures. When in doubt, a radiograph of the orbits should be obtained to search for these metallic objects. This search should also be applied to known metallic fragments elsewhere in the body, e.g., bullets, pellets, and metal shrapnel.
6. Smart contact lenses, which are used to record continuous intraocular pressures to guide glaucoma treatment, may result in thermal injury to the eye and must be removed.

This list is not exhaustive, and certain cardiac pacemakers, implantable cardioverter defibrillators, and cardiac monitors, as well as aneurysm clips, intraocular lenses, and cochlear implants, are deemed unsafe. The exact model of all known implants, prostheses, and devices should be cross-checked for MR compatibility prior to MRI.

As the more recent implants and prostheses are usually MR compatible, MRI is now possible for many patients with implants. Despite this, interpretation of MR images may still be challenging, due to image distortion or artifacts relating to or surrounding the implant or prostheses. This is particularly important when assessing a joint, extremity, or spine in the context of musculoskeletal TB. Many of these artifacts (e.g., magnetic susceptibility (Fig. 16), motion (Fig. 17), CSF flow, truncation) can be identified, reduced, or corrected by various measures and techniques (Peh and Chan 2001; Shikhare et al. 2014).

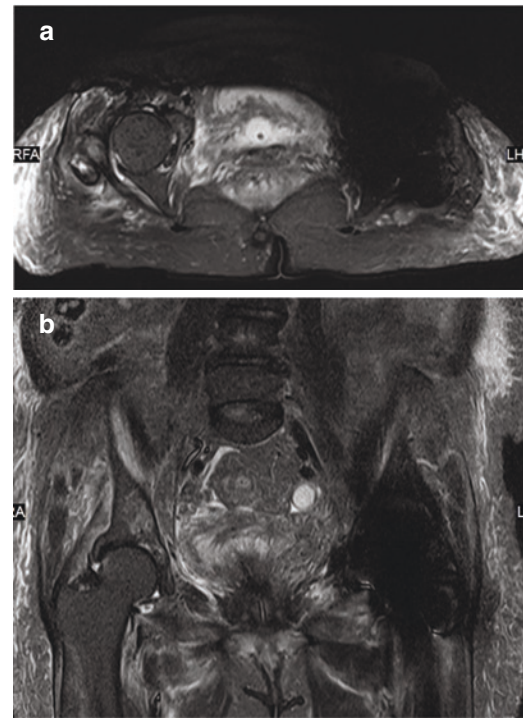

Fig. 16 Susceptibility artifacts. (**a**) Axial and (**b**) coronal MR images of the pelvis show susceptibility artifacts due to a left hip prosthesis. The large area of signal void produced by the susceptibility artifact prevents assessment of the affected region

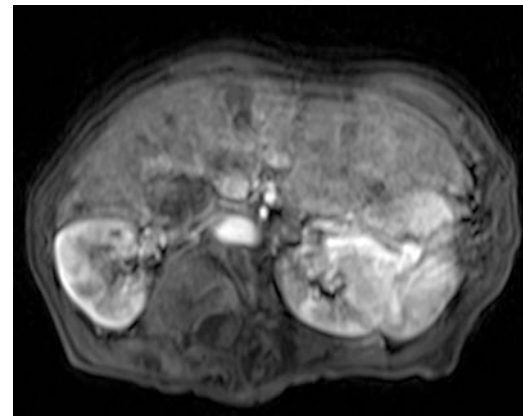

Fig. 17 Motion artifacts. Axial MR image of the liver shows severe motion blurring, making detection of any abnormality difficult. The patient was unable to breath hold

It is important to note that some Gd-based contrast agents have been linked to a very small inci-

dence of nephrogenic systemic fibrosis, a rare debilitating systemic fibrotic condition seen in patients with renal dysfunction (Kaewlai and Abujuneh 2012). Recognizing this disease is very important as it is progressive, potentially fatal and may affect multiple organs. In patients with renal impairment, the prolonged excretory half-life of these agents increases the likelihood of deposition of Gd ions in the skin, bone, liver, and brain. This results in hardening of the skin, contractures, and involvement of the skeletal muscles, including the diaphragm, causing respiratory failure.

In patients with a normal renal function, Gd is excreted by the kidneys with a half-life of 90 min. Current practice requires determining the necessity of intravenous Gd-based contrast administration in answering the clinical question. Assessment of the renal function is recommended in patients not undergoing dialysis and not having acute kidney injury, and according to which type of Gd-based contrast agent is used (Mathur et al. 2020). According to the consensus statement by the American College of Radiology and National Kidney Foundation, since the risk of nephrogenic systemic fibrosis is so low with Gd-based contrast media, the potential harms of delaying or withholding contrast administration for MRI in a patient with acute kidney injury or estimated glomerular filtration rate less than 30 ml/min per $1.73m^2$ are likely to outweigh the risk in most clinical situations (Weinreb et al. 2021).

2.7 Nuclear Medicine Imaging

Nuclear medicine imaging is based on the use of radiopharmaceuticals, which are chemical compounds labeled with single-photon-emitting radioisotopes such as technetium-99m (^{99m}Tc) or positron-emitting isotopes such as [fluorine-18]-fluoro-2-deoxy-D-glucose (^{18}F-FDG). In general, nuclear imaging is rarely used to diagnose active TB, and its impact on the clinical care of patients with TB is limited. However, ^{18}F-FDG positron-emission tomography (PET)/CT is an important non-invasive method for assessing disease activity, detecting extrapulmonary TB, and determining the treatment response (Sathekge et al. 2012).

2.7.1 Conventional Nuclear Medicine Imaging Techniques

The most commonly used and studied single-photon-emitting tracers for the diagnosis and management of TB are thallium-201 chloride (^{201}Tl-chloride), gallium-67 citrate (^{67}Ga-citrate), ^{99m}Tc-sestamibi, and ^{99m}Tc-tetrofosmin. ^{99m}Tc-methylene diphosphonate (^{99m}Tc-MDP) bone scintigraphy is used to evaluate spinal TB, even though it is non-specific.

2.7.1.1 Thallium-201 Scintigraphy

^{201}Tl-chloride scintigraphy is usually done in dual phases, with the early phase around 15 min and delayed phase around 3 h after injection. It has the potential to differentiate benign from malignant pulmonary lesions. Ratios of uptake are calculated from the early and delayed tracer uptake, compared to the normal contralateral lung in both phases. The retention index of the lesion, derived from the formula (delayed ratio – early ratio)/(early ratio) × 100%, is significantly different for benign lesions and malignant lesions. The retention index of benign lesions, including tuberculomas, has been found to be significantly low, compared to that of malignant lesions (Suga et al. 1993; Yu et al. 2004). The combination of HRCT and thallium-201 scintigraphy is more useful and relevant clinically, with improvement of sensitivity and specificity to near 100% (Kashimada 1998).

2.7.1.2 ^{67}Ga-Citrate and ^{99m}Tc-MDP Scintigraphy

^{67}Ga-citrate scintigraphy has a high sensitivity to diagnose suspected active pulmonary TB but has limited specificity. The degree of tracer uptake is proportionally related to the bacterial load in the sputum. This technique is better than chest radiographs and fairly similar to HRCT and ^{201}Tl-chloride scintigraphy in detecting parenchymal lesions. They are especially useful in the subgroups of patients with TB who are sputum negative and have disseminated, military, or diffuse pulmonary involvement. ^{67}Ga-citrate scintigraphy can also correctly predict the involvement of extrapulmonary sites of TB, such as the spine, peritoneum, and lymph nodes, efficiently (Sathekge et al. 2012). ^{99m}Tc-MDP and/or

^{67}Ga-citrate are the most commonly used tracers in spinal TB.

These methods are sensitive and permit whole-body evaluation, but are less specific and have poor spatial resolution. Their limitations can be overcome and improved by single-photon emission computed tomography (SPECT)/CT which provide better resolution and anatomical localization. The three-phase bone scan can evaluate the inflammatory process associated with intense infections of early stage and identify bone remodeling associated with late-stage spondylitis. Combination of ^{67}Ga-citrate scintigraphy with bone scan efficiently diagnoses both osseous and soft tissue infections, monitors therapeutic response, and detects reactivation (Rivas-Garcia et al. 2013).

2.7.1.3 Other Single-Photon-Emitting Radiopharmaceuticals

^{99m}Tc-sestamibi and ^{99m}Tc-tetrofosmin have been studied extensively for the evaluation of pulmonary TB and have been found to show increased uptake in active lesions, proportional to the disease activity. Hence, they can be used for differentiation between active and inactive disease and to monitor the therapeutic response with good negative predictive value (Ahmadihosseini et al. 2008). Multiple radioisotopes, such as N-isopropyl-p-[1^{23}I] iodoamphetamine (^{123}I-IMP), ^{99m}Tc-dimercapto succinic acid (^{99m}Tc-DMSA), ^{99m}Tc-glucoheptonate, indium-111 octreotide (^{111}In-octreotide), ^{99m}Tc-hexamethylpropyleneamine oxime-white blood cell (^{99m}Tc-HMPAO-WBC), ^{99m}Tc-ciprofloxacin, and ^{99m}Tc-ethyl cysteinate dimer (^{99m}Tc-ECD), have been studied for the evaluation of pulmonary and extrapulmonary TB, with variable results produced with nominal clinical impact (Sathekge et al. 2012).

Recently, ^{99m}Tc-ethambutol has been evaluated for its diagnostic value in TB, as it specifically binds to mycolic acid in the cell wall of the *M. tuberculosis* bacteria. Early results have been promising with good sensitivity, specificity, and diagnostic accuracy. ^{99m}Tc-ethambutol scintigraphy can detect and localize both pulmonary and extrapulmonary TB. This procedure has no side effects and can be performed safely, even in pediatric patients (Kartamihardja et al. 2018).

2.7.2 Positron-Emission Tomography/CT

2.7.2.1 ^{18}F-FDG PET/CT

^{18}F-FDG is used in the diagnosis of TB, based on its ability to detect increased glucose metabolism occurring in the disease process, due to increased macrophage and neutrophil activity. ^{18}F-FDG PET/CT is sensitive for detecting diseases such as TB, which can cause both acute and chronic infections and relative uptake quantification. Standard uptake value (SUV) measurement can be used to distinguish between residual active and inactive lesions. Although morphological imaging is the current cornerstone for diagnosing and staging TB, ^{18}F-FDG PET/CT has been evaluated and proven to be a valuable adjunct for differentiation of active and nonactive lesions, monitoring the treatment response and follow-up (Sathekge et al. 2012; Vorster et al. 2014).

2.7.2.2 Evaluation of Active and Inactive Disease

There are two different patterns of ^{18}F-FDG PET activity in TB, namely the pulmonary pattern and the lymphatic pattern. In the pulmonary pattern, ^{18}F-FDG uptake is primarily seen in cavitary and noncavitary consolidation and adjacent micronodules, with mild-to-moderate uptake in mediastinal and hilar lymph nodes. In the lymphatic pattern, increased ^{18}F-FDG uptake is seen in the enlarged mediastinal and hilar lymph nodes and at extrapulmonary sites of involvement (Fig. 18) (Soussan et al. 2012).

Active pulmonary tuberculomas usually have significant ^{18}F-FDG uptake with SUVmax greater than 4. Double-phase acquisition of ^{18}F-FDG PET/CT acquired at 60 and 120 min postinjection can better differentiate active from inactive lesions, with analysis of multiple-point SUV ($SUVmax_E$ – early phase, $SUVmax_D$ – delayed phase, %DeltaSUVmax – difference). With $SUVmax_E$ of 1.05, $SUVmax_D$ of 0.97, and %DeltaSUVmax of 6.59 as cutoff values, active

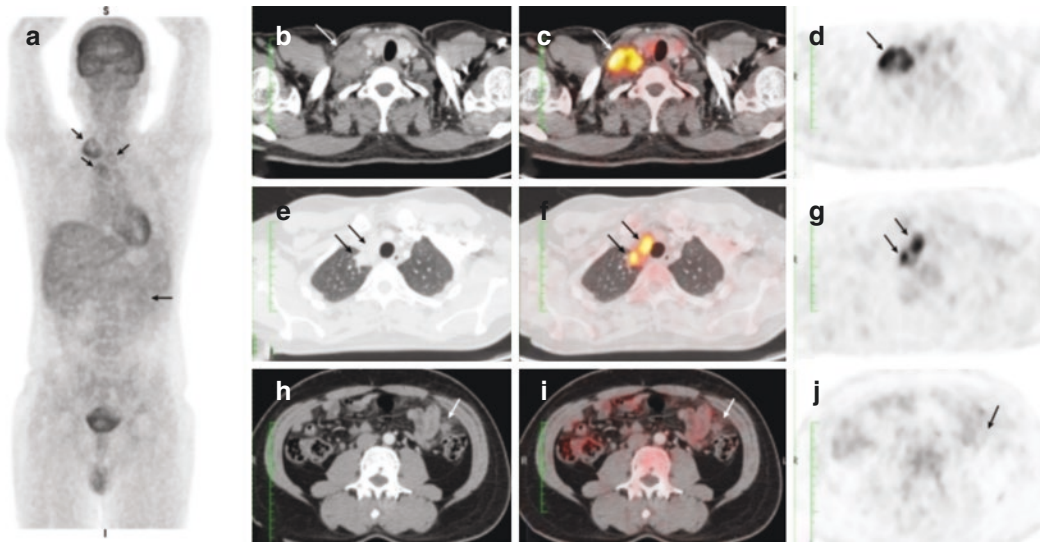

Fig. 18 Disseminated tuberculosis. (**a**) Whole-body PET MIP image shows increased ^{18}F-FDG uptake in the right cervicothoracic region and superior mediastinum. Faintly increased ^{18}F-FDG uptake is seen in left hypochondrium. Corresponding (**b–j**) axial CT, fusion PET/CT, and axial PET images show increased tracer uptake in the conglomerate right supraclavicular lymphadenopathy (**b–d**), right paratracheal lymph node and consolidation in the medial right upper lobe medially (**e–g**), and omental nodule in left hypochondrium (**h–j**). These lesions in pulmonary and extrapulmonary locations of disseminated tuberculosis are arrowed (courtesy of Dr. Godwin Jeeva, Gemini Scans, Chennai, India)

and inactive lesions can be differentiated with a specificity of 100% (Goo et al. 2000; Kim et al. 2008). Similarly, dual-phase ^{18}F-FDG PET/CT is also helpful in identifying extrapulmonary sites of TB with more diagnostic accuracy. In a study conducted on 16 patients with TB, ^{18}F-FDG PET/CT identified sites of lymph node, bone, and joint involvement, which were initially missed on CT (Sathekge et al. 2010a).

2.7.2.3 Differentiation of Malignant Lesions and Tuberculoma

Increased ^{18}F-FDG uptake is non-specific for tumors, as well as infectious and inflammatory conditions. ^{18}F-FDG-avid lesions in the TB-endemic regions are always a diagnostic challenge for differentiating between neoplasm and tuberculoma. Unfortunately, there is no significant difference between the SUVmax values of tuberculomas and malignant nodules, and ^{18}F-FDG PET/CT cannot confidentially differentiate them. The SUV values of involved lymph nodes in TB and malignancy are also not statistically different. Sathegke et al. (2010b) found the SUVmean values of involved lymph node basins to be 6.5 (3.4–9.2 range) in TB and 8.0 (2.5–20.1 range) for malignancy, with significant overlap. These findings are in agreement with the data derived from other studies conducted for the same purpose. Hence, we can safely conclude that ^{18}F-FDG PET/CT is not indicated for differentiating malignancy from TB (Fig. 19) (Chen et al. 2008; Sathekge et al. 2010b).

2.7.2.4 Monitoring Treatment Response and Follow-Up

This is the most accepted and important clinical application of ^{18}F-FDG PET/CT in patients with TB. After completion of treatment, morphological changes of response such as reduction in size and decrease in enhancement often take a longer time to manifest. In endemic areas where multidrug-resistant TB is common, assessment of the treatment response at an early stage is needed, so as to facilitate change or modification of treatment in nonresponders. As there is correlation between decrease in ^{18}F-FDG uptake and successful treatment, quantita-

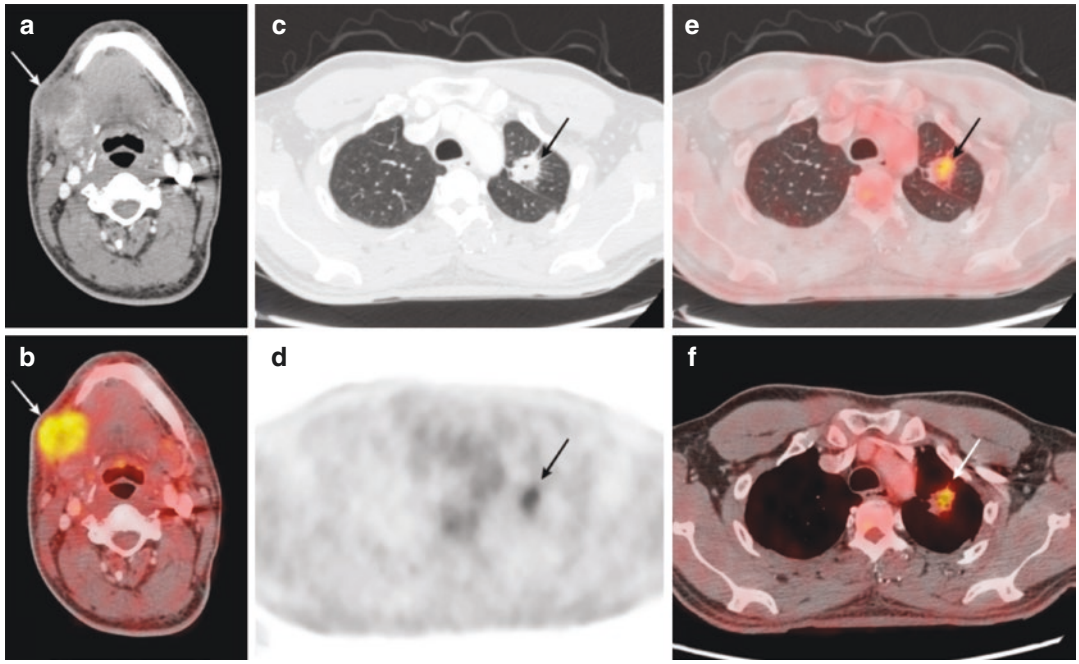

Fig. 19 Patient with known right buccal carcinoma and concomitant pulmonary tuberculosis. Axial (**a**) CT and (**b**) fusion PET/CT images show increased ^{18}F-FDG uptake at the site of the primary malignancy (arrow). Staging axial (**c**) CT, (**d**) PET, and (**e** and **f**) fusion PET/CT images taken in (**e**) lung and (**f**) soft tissue window settings show increased ^{18}F-FDG uptake within an irregular spiculated nodule with small cavitation in the left upper lobe. This was indeterminate for metastases and active tuberculosis. Subsequent histological examination revealed the left lung nodule to be due to tuberculous infection (courtesy of Dr. Godwin Jeeva, Gemini Scans, Chennai, India)

tive PET assessment is helpful to evaluate the treatment response. Some lesions may even increase in size, instead of decreasing in size, with good treatment response. In those patients, decreased ^{18}F-FDG activity in those lesions likely suggests that the tuberculoma is responsive to anti-TB treatment and current treatment should be continued. Similarly, the SUVmax of the involved lymph node basins is significantly higher in pre-treatment scans and interim scans in nonresponders. The metabolic response may indicate clinical response and guide the duration of the antimicrobial therapy (Park et al. 2008; Sathekge et al. 2013; Vorster et al. 2014).

2.7.2.5 Other Positron-Emitting Tracers

Various other positron-emitting tracers, including ^{11}C-choline, ^{18}F-fluorothymidine (^{18}F-FLT), and gallium-68 (^{68}Ga), have been investigated for diagnosis of TB. Among them, early results of ^{11}C-choline have been encouraging. Hara et al. (2003) concluded that combined use of ^{18}F-FDG PET/CT and ^{11}C-choline PET/CT can differentiate lung cancers, TB, and atypical mycobacterial infections.

2.8 Interventional Radiology

Interventional radiology has a role, not only in establishing the diagnosis, but also in the management of TB (Nachiappan et al. 2017).

2.8.1 Percutaneous Biopsy

Tissue diagnosis is needed when the imaging features are not classical of TB or mimic other infections or neoplasms. Specimens should be sent for histology, acid-fast bacilli (AFB) staining, and culture. If there is a lack of AFB, differentiating TB from other granulomatous lymphadenitis could be challenging. Polymerase chain reaction (PCR) testing of lymph node tissue for

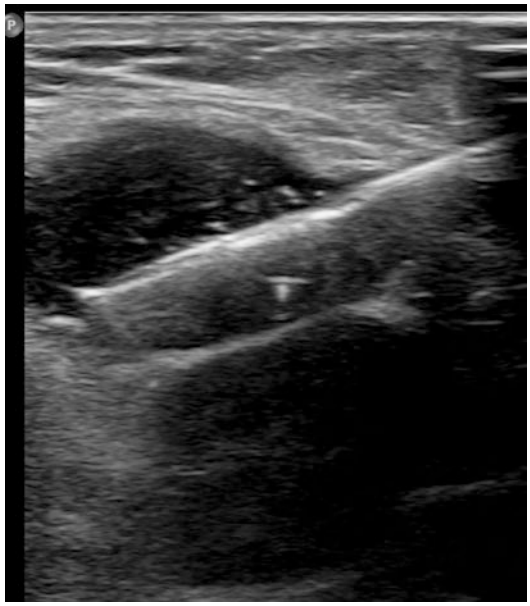

Fig. 20 High-resolution US image shows an enlarged cervical lymph node with biopsy needle in situ

M. tuberculosis may help in the final diagnosis. Biopsy or aspiration can be performed under imaging guidance, depending upon the region. For superficially located lesions such as lymph nodes in the head and neck region, US imaging is the modality of choice (Fig. 20). However, for deep-seated lesions such as mediastinal lymphadenopathy or retroperitoneal lymphadenopathy, CT guidance is necessary. CT is usually also needed when a biopsy is required in the musculoskeletal system.

2.8.1.1 General Principles

Informed consent should be obtained from the patient. The procedure can be performed under local anesthesia, with or without moderate sedation. Care should be taken with the dosage of these medications in elderly patients. The laboratory test values, especially full blood counts and clotting profile, should be carefully noted, and they should be within the acceptable range. Relative contraindications include significant coagulopathy, low platelet count (less than 50,000/mm^3), severely compromised cardiopulmonary function, inaccessible sites or lack of safe pathway, and patient's inability to cooperate during the procedure.

2.8.1.2 Imaging Guidance

The biopsy can be performed by US imaging guidance in superficial lesions such as enlarged lymph nodes in the neck (Fig. 20). US imaging is preferred for superficial lesions because of multiple advantages such as real-time imaging, low cost, absence of ionizing radiation hazard, and dynamic imaging capabilities. Color Doppler US imaging aids in assessing the vascularity of the lesion and location of vessels along the needle trajectory or that lie close to the lesion.

CT guidance is preferred for deep-seated lesions such as enlarged lymph nodes in the mediastinum or abdomen or focal lesions in the lungs. Fluoroscopy or CT can be used for biopsy in the musculoskeletal system, such as spine lesions. However, CT is the imaging modality of choice as it enables precise localization and is safer compared to fluoroscopy, especially to avoid vital structures such as nerves and blood vessels. The technique of CT fluoroscopy uses less radiation dose and tracks the needle almost close to real time. Up to six frames per second can be reconstructed while performing CT fluoroscopy. A viewing monitor is usually set up within the CT suite. The CT couch can be moved using the console or operated manually, and image acquisition is usually done with a foot switch. The needle tip can be tracked by looking for low-attenuation beam hardening artifacts. Most often, the needle is inserted perpendicularly in the axial plane. Rarely, the angulated approach may be necessary to reach the target.

2.8.1.3 Tools and Techniques for Percutaneous Biopsy

Fine-needle aspiration samples are often too small, and usually core biopsy is preferred. For FNAC, needles of sizes 20–22G are preferred. Core needle biopsies are often performed with needles of sizes 16–20G, with larger caliber outer coaxial needles. The length of the "throw" or distance advanced by the needle after firing is indicated on the needle package and should be selected carefully. For example, if the lesion is 1.5 cm in diameter, a 1 cm throw needle can be safely used. The coaxial needle is usually introduced first, and the

spring-loaded cutting needle is then advanced through the coaxial needle. This avoids multiple punctures. If there is excessive bleeding from the outer coaxial needle after biopsy, the track can be sealed with a Gelfoam plug. If pneumothorax occurs during a lung biopsy, a wire can be inserted through the coaxial needle and a drainage catheter inserted over the wire.

For bone lesions with shell of overlying bone, the cortex is penetrated with a trephine needle (14.5 or 15G), and then a cutting needle can be inserted using a coaxial technique to obtain the tissue sample. If the lesion is completely sclerotic or is an osteolytic lesion with a predominant bone component, then the lesion is sampled with a trephine needle. The cortex is penetrated by a

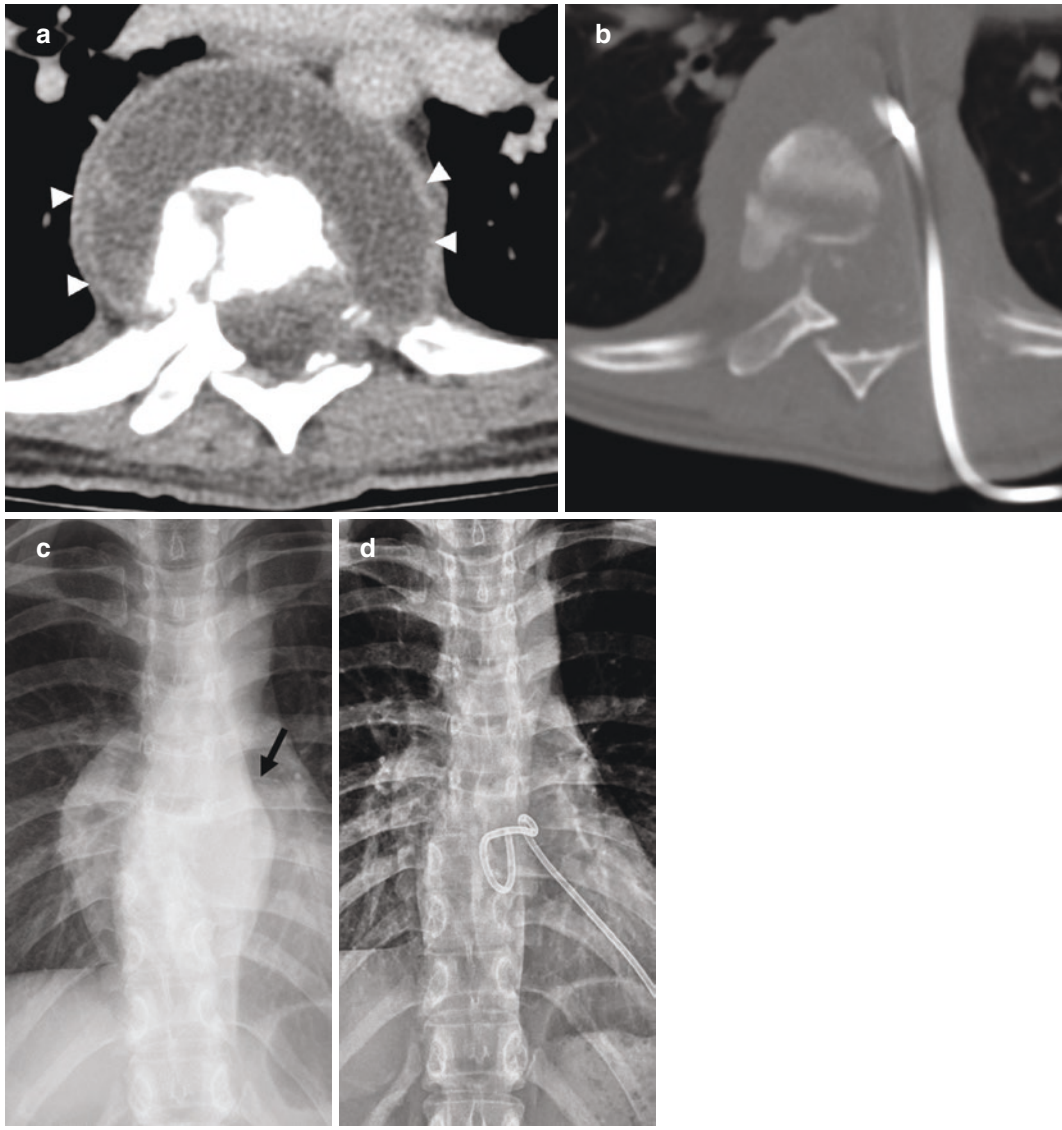

Fig. 21 Tuberculous spondylodiscitis of the thoracic spine. (**a**) Axial contrast-enhanced CT image shows a large paraspinal abscess (arrowheads). (**b**) Axial unenhanced CT image obtained postdrainage of the abscess shows a drainage catheter in the abscess cavity. Frontal radiographs obtained (**c**) before and (**d**) after drainage of the paraspinal collection (black arrow)

corkscrew rotational motion of the trephine needle with a diamond-tip stylet. After penetration of the cortex, when the margin of the bone lesion is reached, the stylet is removed and a syringe is attached. The plunger is withdrawn to create a vacuum. A jiggling motion is applied to dislodge the tissue when the vacuum is being applied. The plunger is then released, and the needle is removed. The tissue sample, which is usually present within the needle, is removed with the help of a blunt stylet. Intermittent CT fluoroscopic screening should be performed when the needle is advanced. Multiple passes should be obtained with needle directed in different directions to obtain samples in different parts of the lesion.

2.8.2 Drainage and Aspiration of Collections

Drainage of collections can be performed under US imaging or CT guidance (Yin et al. 2015). When US imaging guidance is used, fluoroscopy can be utilized to position the catheter in the desired location. For large uncomplicated pleural collections, direct trocar puncture technique can be used under US imaging guidance. However, for deep-seated or complex collections, drainage catheters can be inserted by the Seldinger technique. Initially, the collection is accessed under US imaging or CT guidance by a 18G or 21G needle, and the track is dilated to accommodate an 8Fr or 10Fr pigtail drain. For deep-seated abdominal, paraspinal, or mediastinal collections, CT guidance is preferred (Fig. 21).

2.8.3 Embolization for Hemoptysis

Embolization is the initial treatment of choice in patients with pulmonary TB presenting with massive hemoptysis (approximately 200–1000 ml over a 24-h period). Massive hemoptysis results from a hypertrophied bronchial artery or nonbronchial systemic collaterals supplying the diseased lung (Fig. 22). Rarely, aneurysms from the pulmonary artery (Rasmussen aneurysm) can be the cause of bleeding (Seedat and Seedat 2018) (Fig. 23). Contrast-enhanced CT obtained in the arterial phase is helpful to identify the source of hemoptysis. CT helps assess the degree of lung damage and shows the anatomy and course of hypertrophied bronchial arteries. If CT

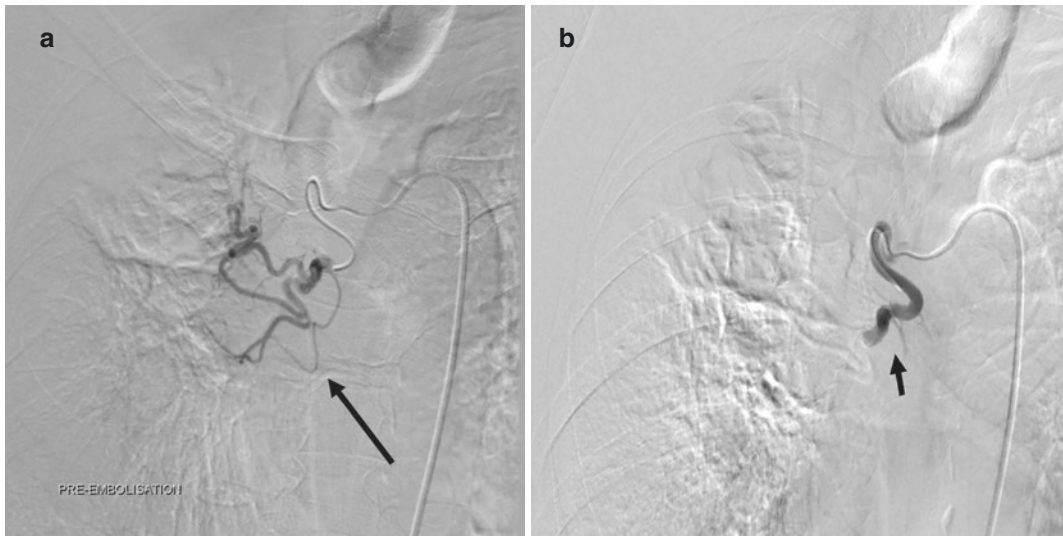

Fig. 22 Post-primary pulmonary tuberculosis involving the upper lobe of the right lung in a 68-year-old woman who presented with massive hemoptysis. (**a**) Selective bronchial angiogram shows a hypertrophied and tortuous right bronchial artery supplying the right lung (long arrow). (**b**) Postembolization angiogram of the right bronchial artery (short arrow) shows absent flow distally. Patient did not have further episodes of hemoptysis after embolization

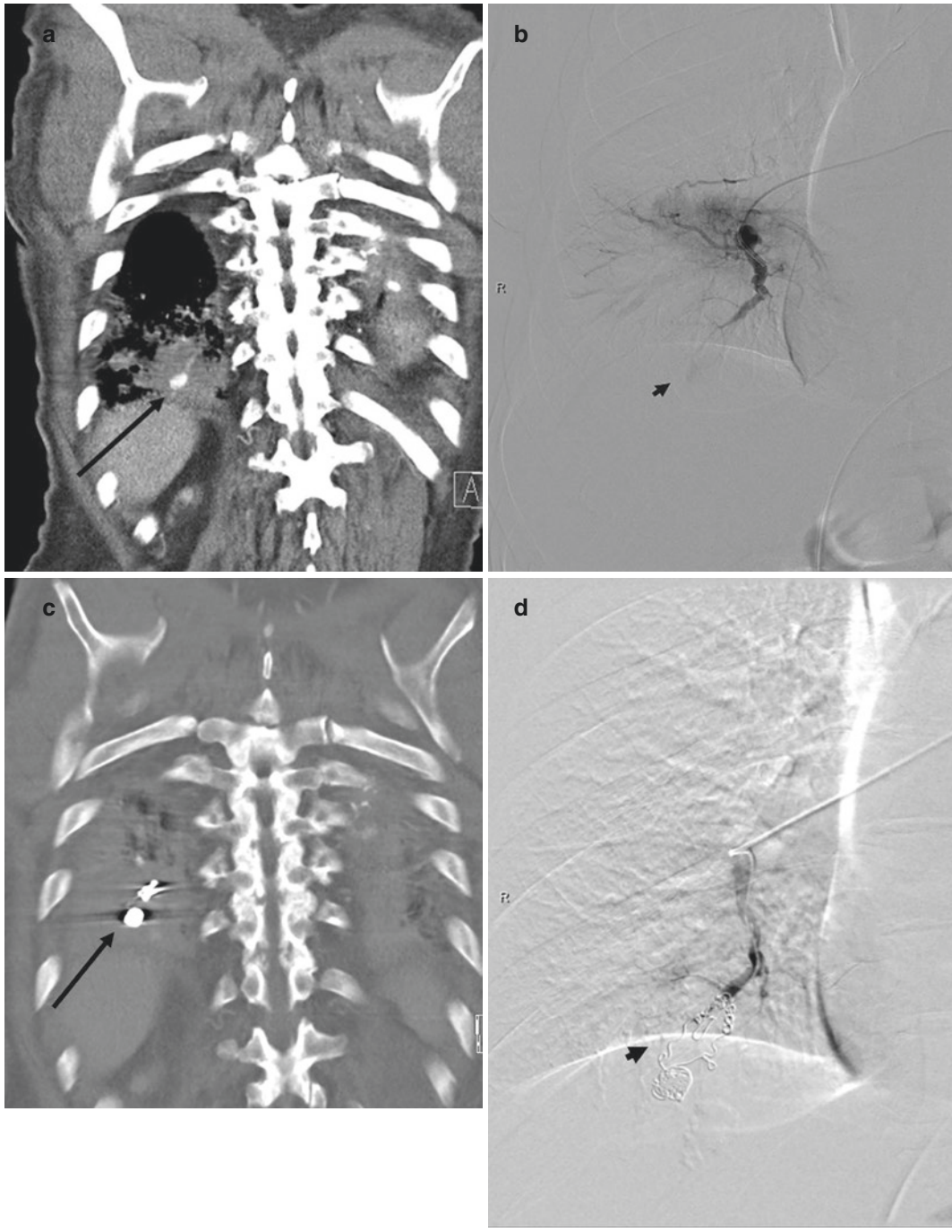

Fig. 23 Rasmussen aneurysm in a 34-year-old man with post-primary pulmonary tuberculosis who presented with massive hemoptysis. (**a**) Coronal contrast-enhanced CT and (**b**) selective right pulmonary angiogram images show a small Rasmussen aneurysm arising from the distal right lower lobe pulmonary artery, along the margin of a cavitary lesion (arrow). Corresponding (**c**) coronal contrast-enhanced CT and (**d**) selective right pulmonary angiogram images show successful embolization (arrow). Patient had resolution of hemoptysis after coil embolization

is not performed, an aortic angiogram using a pigtail catheter may be performed to identify the bronchial arteries. Endovascular stenting with stent-grafts together with anti-TB drug therapy has been reported to be an alternative to traditional open surgery in patients with mycotic aneurysms of major arteries caused by TB (Zhao et al. 2019). Deployment of such stent-grafts is usually done in the angiography suite under fluoroscopic guidance.

3 Conclusion

The role of imaging in the diagnosis of TB complements the clinical and laboratory findings. Its vast role also extends to assessment of the extent of disease and its complications, monitoring the disease response to treatment and detecting residual disease at the end of therapy, as well as guiding biopsies and therapeutic drainage. Conventional radiographs are important as an initial tool for screening, while CT and/or MRI are necessary for further cross-sectional assessment. Each of these modalities has its own advantages, disadvantages, and limitations; thus, the modality of choice varies based on clinical indications and should be catered to each individual patient. In the absence of known contraindications, CT remains the modality of choice in detailed evaluation of pulmonary, abdominal, urinary tract, and head and neck TB, while MRI is the preferred choice in the assessment of intracranial, spinal, and musculoskeletal TB. Other imaging modalities, such as US imaging and ^{18}F-FDG PET/CT, may be selectively employed in the management of patients with TB.

References

Ahmadihosseini H, Sadeghi R, Zakavi R et al (2008) Application of technetium-99m-sestamibi in differentiation of active from inactive pulmonary tuberculosis using a single photon emission computed tomography method. Nucl Med Commun 29:690–694

Allisy-Roberts P, Williams J (2008) Imaging with x-rays, digital radiography, and magnetic resonance imaging. In: Allisy-Roberts P, Williams J (eds) Farr's physics for medical imaging, 2nd edn. Saunders Elsevier, Philadelphia, pp 49–64. 79–90, 169–195

Asher KA, Bangerter NK, Watkins RD et al (2010) Radiofrequency coils for musculoskeletal magnetic resonance imaging. Top Magn Reson Imaging 21:315–323

Barrett J, Keat N (2014) Artifacts in CT: recognition and avoidance. Radiographics 24:1679–1691

Bomanji JB, Gupta N, Gulati P, Das CJ (2015) Imaging in tuberculosis. Cold Spring Harb Perspect Med 5:a017814

Brant W (2012) Diagnostic imaging methods. In: Brant W, Helms C (eds) Fundamentals of diagnostic radiology, 4th edn. Lippincott Williams and Wilkins, Philadelphia, pp 1–25

Chaudhary V, Bano S, Garga UC (2017) Central nervous system tuberculosis: an imaging perspective. Can Assoc Radiol J 68:161–170

Chen CJ, Lee BF, Yao WJ et al (2008) Dual-phase 18F-FDG PET in the diagnosis of pulmonary nodules with an initial standard uptake value less than 2.5. AJR Am J Roentgenol 191:475–479

Dunn DP, Lee KS, Smith MP, Mortele KJ (2015) Non-oncologic applications of diffusion-weighted imaging in the gastrointestinal system. AJR Am J Roentgenol 204:758–767

Engin G, Acunas B, Acunas G, Tunaci M (2000) Imaging of extrapulmonary tuberculosis. Radiographics 20:471–488

Gambhir S, Ravina M, Rangan K (2017) Imaging in extrapulmonary tuberculosis. Int J Infect Dis 56:237–247

Gibson MS, Puckett ML, Shelly ME (2004) Renal tuberculosis. Radiographics 24:251–256

Goo JM, Im JG, Do KH et al (2000) Pulmonary tuberculoma evaluated by means of FDG PET: findings in 10 cases. Radiology 216:117–121

Gupta RK, Poptani H, Kohli A et al (1995) In vivo localized proton magnetic resonance spectroscopy of intracranial tuberculomas. Indian J Med Res 101:19–24

Hara T, Kosaka N, Suzuki T, Kudo K, Niino H (2003) Uptake rates of 18F-fluorodeoxyglucose and ^{11}C-choline in lung cancer and pulmonary tuberculosis: a positron emission tomography study. Chest 124:893–901

Huda W, Mettler FA (2011) Volume CT dose index and dose-length product displayed during CT: what good are they? Radiology 258:236–242

Kaewlai R, Abujuneh H (2012) Nephrogenic systemic fibrosis. AJR Am J Roentgenol 199:W17–W23

Kartamihardja AHS, Kurniawati Y, Gunawan R (2018) Diagnostic value of 99mTc-ethambutol scintigraphy in tuberculosis: compared to microbiological and histopathological tests. Ann Nucl Med 32:60–68

Kashimada A (1998) Diagnostic abilities of high-resolution CT, dynamic CT, and 201T1 SPECT in evaluating pulmonary masses. Nihon Igaku Hoshasen Gakkai Zasshi 58:407–419

Kenney PJ (1990) Imaging of chronic renal infections. AJR Am J Roentgenol 155:485–494

Kim IJ, Lee JS, Kim SJ et al (2008) Double-phase 18F-FDG PET-CT for determination of pulmonary tuberculoma activity. Eur J Nucl Med Mol Imaging 35:808–814
Leder RA, Low VH (1995) Tuberculosis of the abdomen. Radiol Clin North Am 33:691–705
Lee KS, Hwang JW, Chung MP, Kwon OJ (1996) Utility of CT in the evaluation of pulmonary tuberculosis in patients without AIDS. Chest 110:977–984
Leone A, Dell'Atti C, Magarelli N et al (2012) Imaging of spondylodiscitis. Eur Rev Med Pharmacol Sci 2:8–19
Leow KS, Low KTA, Peh WCG (2021) Magnetic resonance imaging of spinal infection. In: Ladeb MF, Peh WCG (eds) Imaging of spinal infection. Springer Nature, Switzerland AG, pp 52–69
Mathur M, Jones JR, Weinreb JC (2020) Gadolinium deposition and nephrogenic systemic fibrosis: a radiologist's primer. Radiographics 40:153–162
Mayo-Smith WW, Hara AK, Mahesh M, Sahani DV, Pavlicek W (2014) How I do it: managing radiation dose in CT. Radiology 273:657–672
Mukherjee P, Berman JI, Chung SW et al (2008) Diffusion tensor MR imaging and fiber tractography: theoretic underpinnings. AJNR Am J Neuroradiol 29: 632–641
Nachiappan AC, Rahbar K, Shi X et al (2017) Pulmonary tuberculosis: role of radiology in diagnosis and management. Radiographics 37:52–72
Nakano H, Jaramillo E, Watanabe M et al (1992) Intestinal tuberculosis: findings on double-contrast barium enema. Gastrointest Radiol 17:108–114
Pache G, Krauss B, Strohm P et al (2010) Dual-energy CT virtual noncalcium technique: detecting post traumatic bone marrow lesions—feasibility study. Radiology 256:617–624
Pai M, Nicol MP, Boehme CC (2016) Tuberculosis diagnostics: state of the art and future directions. Microbiol Spectr 4(5). https://doi.org/10.1128/microbiolspec.TBTB2-0019-2016
Park IN, Ryu JS, Shim TS (2008) Evaluation of therapeutic response of tuberculoma using F-18 FDG positron emission tomography. Clin Nucl Med 33:1–3
Peh WCG, Chan JHM (2001) MR artifacts in musculoskeletal imaging—identification and correction. Skeletal Radiol 30:179–191
Peh WCG, Siu TH, Chan JHM (1999) Determining the lumbar vertebral segments on magnetic resonance imaging. Spine 24:1852–1855
Peto HM, Pratt RH, Harrington TA et al (2009) Epidemiology of extrapulmonary tuberculosis in the United States, 1993–2006. Clin Infect Dis 49:1350–1357
Regan F, Cavaluzzi J, Nguyen B (1998) Fast MR abdominal imaging using the HASTE sequence. AJR Am J Roentgenol 170:1471–1476
Rivas-Garcia A, Sarria-Estrada S, Torrents-Odin C, Casas-Gomila L, Franquet E (2013) Imaging findings of Pott's disease. Eur Spine J 22:567–578
Rodriguez-Takeuchi SY, Renjifo ME, Medina FJ (2019) Extrapulmonary tuberculosis: pathophysiology and imaging findings. Radiographics 39: 2023–2037
Roth CG, Deshmukh S (2017) Introduction and physics of body MRI. In: Fundamentals of body MRI. 2nd ed. Elsevier, Philadelphia, pp1-44
Sathekge M, Maes A, Kgomo M et al (2010a) Impact of FDG PET on the management of TB treatment. Nuklearmedizin 49:35–40
Sathekge M, Maes A, Kgomo M et al (2010b) FDG uptake in lymph-nodes of HIV+ and tuberculosis patients: implications for cancer staging. Q J Nucl Med Mol Imaging 54:698–703
Sathekge M, Maes A, D'Asseler Y, Vorster M, Van De Wiele C (2012) Nuclear medicine imaging in tuberculosis using commercially available radiopharmaceuticals. Nucl Med Commun 33:581–590
Sathekge M, Maes A, Van De WC (2013) FDG-PET imaging in HIV infection and tuberculosis. Semin Nucl Med 43:349–366
Seedat UF, Seedat F (2018) Post-primary pulmonary TB haemoptysis—when there is more than meets the eye. Respir Med Case Rep 25:96–99
Sener RN (2001) Diffusion MRI: apparent diffusion coefficient (ADC) values in the normal brain and a classification of brain disorders based on ADC values. Comput Med Imaging Graph 25:299–326
Shikhare SN, Singh DS, Peh WCG (2014) Variants and pitfalls in MR imaging of the spine. Semin Musculoskelet Radiol 18:23–35
Skoura E, Zumla A, Bomanji J (2015) Imaging in tuberculosis. Int J Infect Dis 32:87–93
Soussan M, Brillet PY, Mekinian A et al (2012) Patterns of pulmonary tuberculosis on FDG-PET/CT. Eur J Radiol 81:2872–2876
Suga K, Kume N, Orihashi N et al (1993) Difference in 201Tl accumulation on single photon emission computed tomography in benign and malignant thoracic lesions. Nucl Med Commun 14:1071–1078
Taylor Z, Marks SM, Rios Burrows NM et al (2000) Causes and costs of hospitalization of tuberculosis patients in the United States. Int J Tuberc Lung Dis 4:931–939
Tong KA, Ashwal S, Obenaus A et al (2008) Susceptibility-weighted MR imaging: a review of clinical applications in children. AJNR Am J Neuroradiol 29:9–17
Trivedi R, Saksena S, Gupta RK (2009) Magnetic resonance imaging in central nervous system tuberculosis. Indian J Radiol Imaging 19:256–265
Vorster M, Sathekge M, Bomanji J (2014) Advances in imaging of tuberculosis. Curr Opin Pulm Med 20:287–293
Weinreb JC, Rodby RA, Yee J et al (2021) Use of intravenous Gadolinium-based contrast media in patients with kidney disease: consensus statements from the American College of Radiology and the National Kidney Foundation. Radiology 298: 28–35
World Health Organization (WHO) (2018) Latent TB infection: updated and consolidated

guidelines for programmatic management. World Health Organization, Geneva, pp 1–64. https://www.who.int/tb/publications/2018/latent-tuberculosis-infection/en/

World Health Organization (WHO) (2020) Definitions and reporting framework for tuberculosis—2013 revision. Updated December 2014 and January 2020. World Health Organization, Geneva, pp. 3 https://apps.who.int/iris/bitstream/handle/10665/79199/9789241505345_eng.pdf?sequence=1

Yin XH, Zhang HQ, Hu XK et al (2015) Treatment of pediatric spinal tuberculosis abscess with percutaneous drainage and low-dose local antituberculous therapy: a preliminary report. Childs Nerv Syst 31:1149–1155

Yousem DM, Grossman RI (2010) Techniques in neuroimaging. In: Yousem DM, Grossman RI (eds) Neuroradiology: the requisites, 3rd edn. Mosby Elsevier, Philadelphia, pp 1–22

Yu YH, Hsu WH, Hsu N et al (2004) The use of dual phase 201Tl SPECT for differentiating pulmonary malignancies from benign lesions. Jpn J Clin Oncol 34:445–451

Zhao S, Wang Z, Li Y, Wang H, Zhao Y (2019) Endovascular treatment of multiple tuberculous mycotic aneurysm. Medicine (Baltimore) 98:e15268

Imaging of Central Nervous System Tuberculosis

Nadia Hammami, Skander Sammoud, Siwar Sbaihi, Fatma Nabli, Cyrine Drissi, Lamia Ammari, Aida Berriche, and Mohamed Chakroun

Contents

N. Hammami (✉) · S. Sammoud · S. Sbaihi
C. Drissi
Department of Neuroradiology, National Institute of Neurology Mongi Ben Hamida, Tunis, Tunisia
e-mail: nadiahamaied@hotmail.com; skander119767@gmail.com; siwar_sb@hotmail.com; drissi.cyrine@gmail.com

F. Nabli
Department of Neurology, National Institute of Neurology Mongi Ben Hamida, Tunis, Tunisia
e-mail: fatmafatnassi@yahoo.fr

L. Ammari · A. Berriche
Department of Infectious Diseases, La Rabta Hospital, Tunis, Tunisia
e-mail: lamia_ammarib@yahoo.fr; aida.berricheg@gmail.com

M. Chakroun
Department of Infectious Diseases, Fattouma Bourguiba Hospital, Monastir, Tunisia

Faculty of Medicine of Monastir, University of Monastir, Monastir, Tunisia
e-mail: chakrounme@gmail.com

Abstract

Central nervous system tuberculosis is a serious infection, comprising approximately 10% of all cases of tuberculosis. It is a potentially curable disease, provided that the diagnosis is timely. Its clinical and radiological manifestations may mimic other infectious and non-infectious neurological conditions. Hence, familiarity with the imaging presentations of the various forms of central nervous system tuberculosis is essential to achieve an early diagnosis, thereby reducing the disease morbidity and mortality. This chapter reviews the imaging characteristics of the different forms of central nervous system tuberculosis involving the brain and the intradural component of the spine.

© The Author(s), under exclusive license to Springer Nature Switzerland AG 2022

M. F. Ladeb, W. C. G. Peh (eds.), *Imaging of Tuberculosis*, Medical Radiology Diagnostic Imaging,
https://doi.org/10.1007/978-3-031-07040-2_5

Abbreviations

AFB	Acid-fast bacilli
CNS	Central nervous system
CSF	Cerebrospinal fluid
CT	Computed tomography
DWI	Diffusion-weighted imaging
FLAIR	Fluid-attenuated inversion recovery
MRI	Magnetic resonance imaging
TB	Tuberculosis
TBA	Tuberculous brain abscess
TBM	Tuberculous meningitis

1 Introduction

Central nervous system (CNS) tuberculosis (TB) has a worse outcome than pulmonary TB, especially with delayed treatment (Verdon et al. 1996; Wilkinson et al. 2017). 5–10% of all patients with TB and up to 20% of patients with acquired immunodeficiency syndrome (AIDS)-related TB have CNS involvement (Taheri et al. 2015). The clinical and radiological manifestations of CNS TB may mimic other infectious and non-infectious neurological conditions, such as brain tumors. Therefore, comprehensive knowledge of the imaging presentations of CNS TB is essential for prompt and accurate diagnosis of this entity. This chapter describes the different forms of CNS TB, including meningitis and parenchymal TB, and addresses spinal intradural TB. Spinal extradural tuberculous infections will be covered in the Chapter on Spinal Tuberculosis.

2 Epidemiology

Mycobacterium tuberculosis is a very important human pathogen and most often affects the lungs. *M. africanum* causes up to half of human TB in West Africa (De Jong et al. 2010). People infected with *M. tuberculosis* have a 5–15% lifetime risk of falling ill with TB. However, immunocompromised individuals such as people living with human immunodeficiency virus (HIV), who have malnutrition or diabetes mellitus, or who use tobacco have a much higher risk of falling ill with TB. The global incidence of TB peaked around 2003 and appeared to be declining slowly (World Health Organization 2019). According to the World Health Organization (WHO), an estimated ten million people fell ill with TB in 2019 globally; among them, 7.1 million people were reported to be newly diagnosed and notified (new and relapsed) cases (World Health Organization 2020). TB usually affects the lungs, but it can also affect other body parts, such as the lymph nodes, spine, bone and joints, brain, and kidneys. Extrapulmonary TB occurred in 16% of the 7.1 million incident cases that were notified in 2019, ranging from 8% in the Western Pacific Region to 24% in the Eastern Mediterranean Region (World Health Organization 2020). Spondylodiscitis and meningitis represented approximately 2% and 3%, respectively, of cases (Robertson et al. 2019).

3 Pathophysiology of Central Nervous System Tuberculosis

The initial point of TB infection is the entry of bacilli into the lungs via inhalation of infectious droplets. The bacteria then colonize macrophages within the alveoli. During the progression of active pulmonary disease, bacteria may disseminate to local lymph nodes and the bloodstream, which results in the spread of bacilli throughout the systemic circulatory system (Be et al. 2009). In 1933, Arnold Rich and Howard McCordock postulated that *M. tuberculosis* gets deposited in the brain parenchyma and meninges during hematogenous dissemination following primary infection. They demonstrated that tuberculomas or "Rich foci" develop around the deposited mycobacteria. Later, the rupture of these foci allows the dissemination of mycobacteria into the cerebrospinal fluid (CSF), causing diffuse inflammatory meningitis (Be et al. 2009; Davis et al. 2019) (Fig. 1). The location of these foci and the capacity to control them determine which form of CNS TB occurs. CNS TB manifests primarily as tuberculous meningitis (TBM) and less

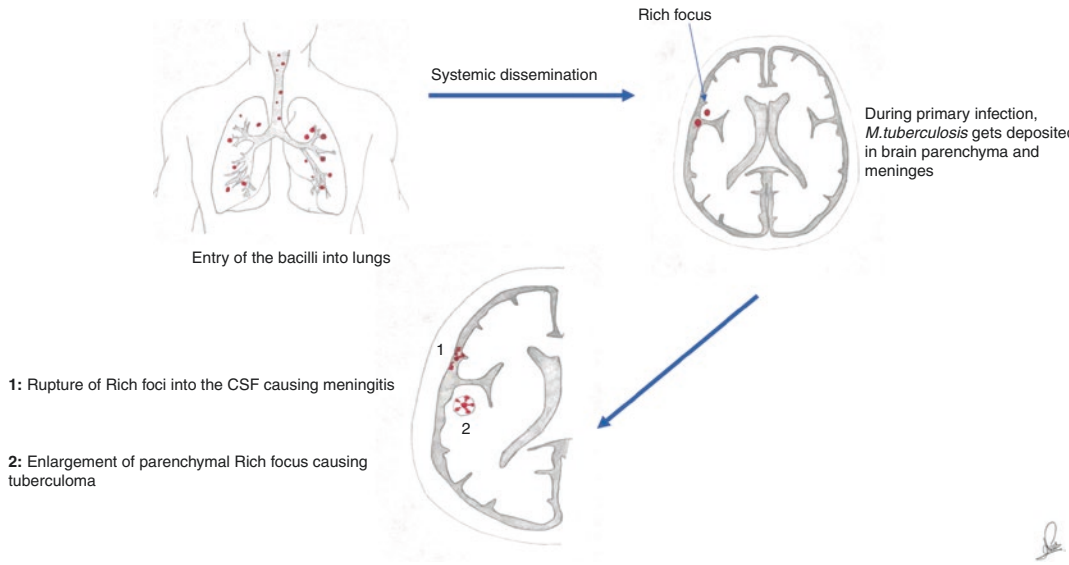

Fig. 1 Diagram shows the pathogenesis of CNS tuberculosis

commonly as tuberculous encephalitis, intracranial tuberculoma, or tuberculous brain abscess (TBA) (Rock et al. 2008).

3.1 Tuberculous Meningitis

A dense gelatinous exudate forms after the release of tuberculous bacilli from granulomatous lesions into the subarachnoid space. It is often located anteriorly in the interpeduncular fossa and suprasellar region and may extend throughout the prepontine cistern and surround the spinal cord. This exudate envelops arteries and cranial nerves, creating a bottleneck in the flow of CSF at the level of the tentorial opening, which leads to hydrocephalus. Tuberculous foci are not preferentially distributed to the basilar areas of the brain where the exudate is typically located. The localization of tuberculous exudate to the basilar region is hypothesized to be simply a result of the regular flow pattern of CSF (Rich and McCordock 1933). However, the most severe consequence of TBM is the development of vasculitis in vessels of the circle of Willis, the vertebrobasilar system, and perforating branches of the middle cerebral artery, resulting in infarctions in the distribution of these vessels (Rock et al. 2008).

3.2 Brain Tuberculoma

Tuberculomas are thought to arise when tuberculous granulomas in the brain parenchyma enlarge without rupturing into the subarachnoid space. Solitary lesions are the most frequent presentation, but multiple tuberculomas may be seen (Rock et al. 2008).

3.3 Tuberculous Brain Abscess

Brain abscess formation is a rare manifestation of CNS TB. TBA develops either from tuberculous parenchymal granulomas or via the spread of tuberculous foci from the meninges. It is characterized by an encapsulated collection of pus containing viable bacilli without evidence of the classic tuberculous granuloma and must be distinguished from granuloma with central caseation and liquefaction mimicking pus (Kumar et al. 2002; Rock et al. 2008).

3.4 Spinal Intradural Tuberculosis

Spinal TB can be extradural (64%), intramedullary (8%), or intradural extramedullary (1%) in location (Chaudhary et al. 2017). Spinal

intradural TB may take various forms, including tuberculous radiculomyelitis, myelitic tuberculoma, and spinal meningitis. The pathophysiology of spinal meningitis is the same as described earlier in tuberculous meningitis. During primary infection, a submeningeal tubercle forms and then ruptures into the subarachnoid space. This causes inflammation, areas of caseation and tubercles, and fibrous tissue development in chronic or treated cases (Gupta and Kumar 2011). The pathogenesis of tuberculous radiculomyelitis can be explained in three ways: (1) primary lesion from hematogenous spread of a tuberculous infection outside the CNS, (2) secondary extension of cranial tuberculous meningoencephalitis, and (3) secondary intraspinal extension from tuberculous spondylitis. Myelitic tuberculomas are very rare and arise from hematogenous dissemination (Bernaerts et al. 2003).

4 Spectrum of Lesions in Central Nervous System Tuberculosis

CNS TB can be broadly divided into (1) intracranial and intradural spinal lesions and (2) parenchymal and nonparenchymal (meningeal) patterns of involvement (Table 1). Any combination of these patterns can also occur.

5 Clinical Manifestations

The CNS manifestations of TB have the most severe complications, resulting in high morbidity and mortality rates, despite the availability of effective forms of treatment (Phypers et al. 2006). CNS TB is an insidious disease and can have an atypical clinical picture.

5.1 Intracranial Nonparenchymal (Meningeal) Tuberculosis

TBM is the most common manifestation of CNS TB overall, with the most frequent and the highest likelihood of an adverse outcome. Approximately 50% of patients with TBM either die or become disabled (Garg et al. 2016). In most patients, prodromal stage one, typically lasting 2–3 weeks, is characterized by the insidious onset of malaise, with a history of vague ill health and non-specific prodromal symptoms such as loss of appetite, fever, and headache. The second stage of disease (or meningitic phase) follows meningismus, protracted headache, lethargy, cranial nerve findings, and pyramidal signs. In the third stage, stupor, coma, and seizures develop (Cherian and Thomas 2011). In infants, the prodromal phase is often shorter and includes irritability, drowsiness, poor feeding, abdominal pain, and bulging fontanelles.

Cranial nerve palsies occur in up to 50% of patients with TBM (Thakur et al. 2018). The sixth cranial nerve is most commonly affected. Hemiplegia may occur at the onset of the disease or at a later stage. Movement disorders and ataxia have been observed, more commonly in children than in adults. Seizures may occur during acute illness or months after treatment. For both survival and sequelae, the most critical determinant of outcome is the stage of TBM at which treatment has been started. About 20–30% of survi-

Table 1 Spectrum of lesions in CNS tuberculosis

	Parenchymal	Nonparenchymal
Intracranial	Tuberculoma Miliary Abscess Encephalopathy	Meningitis: – Leptomeningitis – Pachymeningitis Meningitis complications: – Hydrocephalus – Ventriculitis – Vasculopathy – Cranial nerve involvement
Spinal intradural	Intramedullary tuberculoma	Spinal meningitis

vors manifest various neurological sequelae, with the most important ones being mental retardation, psychiatric disorders, seizures, blindness, deafness, ophthalmoplegia, and hemiparesis. Intracranial calcifications develop in 20–48% of patients with TBM, usually becoming detectable 2–3 years after the disease onset.

Examination of CSF greatly aids early diagnosis of TBM. Pleocytosis with lymphocytic predominance reaction (60–400 white cells per ml) with high protein levels (0.8–4 g/L) and low glucose levels, usually less than 50% of serum glucose concentration, are the hallmark findings in the CSF of patients with TBM. The definitive diagnosis of TBM depends upon the detection of tuberculous bacilli in the CSF. Rates of positivity for clinically diagnosed cases range from 25% to 70%. Culture is necessary to identify *M. tuberculosis* and test its sensitivity to anti-TB drugs (Momjian and George 2014). The polymerase chain reaction (PCR) test is the best method for diagnosing mycobacterial infection, in which cDNA probes are used to identify mycobacterial RNA or DNA sequences in CSF. This test is highly sensitive and specific. The intradermal tuberculin skin test is helpful when positive. Quantiferon-TB Gold is a simple blood test that aids in detecting *M. tuberculosis* with high sensitivity of greater than 95% and high specificity, using innovative CD8+ T cell technology.

A variety of sequelae and complications may result from TB. Hydrocephalus is the most common complication of CNS TB and can be either communicating or noncommunicating. Hydrocephalus frequently develops in children and is associated with a poor prognosis. Communicating hydrocephalus is much more frequent. Cerebrovascular complications are detected in approximately 20–41% of patients (Chatterjee et al. 2015). Tuberculous infection shows a predilection to involve small and medium-sized vessels, primarily in the territories of the middle cerebral artery perforating vessels. There is some evidence that vasospasm may mediate strokes early in the course of the disease (Lammie et al. 2009). Hemorrhagic transformation of infarcted tissue is not unusual (Changal and Raina 2014). TBM can also lead to dural venous sinus thrombosis and subsequent venous infarcts.

Tuberculous arachnoiditis is a relatively common cause of myeloradiculopathy in countries where TB is endemic. This involvement can develop early in the course of TBM or after a long duration. Frequently, there is clinical evidence of multifocal radiculomyelopathy. The CSF changes are those of chronic meningitis. Frequently, the CSF glucose concentration is normal. The onset is often gradual over one or two months, marked by slowly progressive paraparesis. Radicular pain, muscle weakness, paresthesia, and sphincter disorders can precede paralysis, which usually develops within a few days.

5.2 Intracranial Parenchymal Tuberculosis

Parenchymal tuberculomas are the most common form of intracranial parenchymal TB. They can occur at any age. Characteristic clinical features of supratentorial tuberculomas are low-grade fever, headache, vomiting, seizures, focal neurological deficit, and papilledema. Infratentorial tuberculomas are more common among children. Brain abscesses have been reported in 4–7.5% of patients with CNS TB in developing countries (Changal and Raina 2014). It is more common in immunocompromised patients and patients at extremes of age. Clinical features include focal seizures and raised intracranial tension. Surgical exploration and drainage of pus from TBA may produce excellent long-term results, better than with tuberculomas (Be et al. 2009). Tuberculous encephalopathy occurs especially in infants and children. The characteristic features of this entity are development of a diffuse cerebral disorder in the form of convulsions, stupor, and coma, often without signs of meningeal irritation or focal neurological deficit associated with the disseminated intravascular coagulation. The CSF is usually normal or may show a slight increase in proteins and cells.

5.3 Spinal Intradural Tuberculosis

The manifestations of spinal intradural TB are mainly meningeal and radicular involvement, myelitis, intramedullary spinal tuberculoma, and syringomyelia (Schaller et al. 2019). When CNS TB involves the spinal cord, the progression can be acute. Symptom duration at diagnosis may vary from a few days to many months, depending on the spinal pattern, with a median duration of about five months. Approximately 27–47% of patients with tuberculous spinal disease coexhibit paraparesis. Common presenting features are backache (62%), bladder–bowel involvement (58%), paresthesia (18%), and fever (22%), associated with weakness of either or both lower limbs (91%) or all four limbs (9%) (Vaishnav et al. 2019). Multiple sites in the spinal cord may also be affected. Spinal intramedullary tuberculoma is a rare disease, occurring more frequently in younger male patients. The prevalence of this presentation has been reported to be 1–2/100,000 in patients with TB (Wang and Wu 2017). The clinical presentation remains largely non-specific, and the most common symptoms observed are those suggestive of subacute spinal cord compression. The thoracic spine is implicated in most cases of intramedullary tuberculomas (Knobbe and Gaines 2020).

6 Imaging Features

The contribution of imaging to the diagnosis of CNS TB is well established. MRI has a higher sensitivity than CT for detecting abnormalities such as meningeal enhancement, infarcts, and tuberculomas, especially brainstem lesions. The MRI protocol for CNS TB should include T1-weighted, T2-weighted, and fluid-attenuated inversion recovery (FLAIR) sequences, as well as magnetization transfer imaging (MTI), susceptibility-weighted imaging (SWI), diffusion-weighted imaging (DWI), and contrast-enhanced T1-weighted images. In addition, the inclusion of MR spectroscopy for lesions more than 2 cm in size is recommended (Gupta and Kumar 2011). Magnetic resonance angiography (MRA) is routinely performed, and magnetic resonance venography (MRV) may be used in cases with suspected venous complications (Khatri et al. 2018). Neuroimaging procedures should include both the brain and spine, as concomitant intracranial and intraspinal involvement is common.

6.1 Intracranial Tuberculosis

6.1.1 Tuberculous Meningitis

TBM is the most common manifestation of CNS TB, being frequently seen in children and adolescents (Raza et al. 2004; Chaudhary et al. 2017). It is one of the most devastating presentations of TB, constituting about 10% of all TB cases, and is responsible for about 40% of deaths from TB in developing countries (Zhang et al. 2019). Approximately 70–80% of all patients with CNS TB have TBM (Gupta and Kumar 2011).

6.1.1.1 Tuberculous Leptomeningitis

Exudates in the basal cisterns are the most specific manifestation of leptomeningeal TB. They are commonly present in the interpeduncular fossa and suprasellar, perimesencephalic, and pontine cisterns. They frequently extend along the inferomedial surface of the frontal lobes, the anteromedial surface of the temporal lobes, the floor of the third ventricle, and along the Sylvian fissure (Khatri et al. 2018). Exudates appear iso- or hyperdense on unenhanced CT and show dense enhancement on contrast-enhanced CT. Inflamed meninges in the basal cisterns also show intense enhancement (Bernaerts et al. 2003; Chaudhary et al. 2017). In severe TBM, leptomeningeal changes advance over the cerebral convexities, and there is ependymitis in the ventricular walls (Bernaerts et al. 2003).

MRI is more sensitive than CT in depicting these abnormalities. Exudates are best appreciated on FLAIR images. Meningeal enhancement is present on contrast-enhanced MRI (Chaudhary et al. 2017) (Fig. 2). This appearance is non-specific and has a broad differential diagnosis that includes meningitis from other infective agents, inflammatory diseases such as rheumatoid arthritis and sarcoidosis, and meningeal carcinomatosis (Bernaerts et al. 2003). It has been

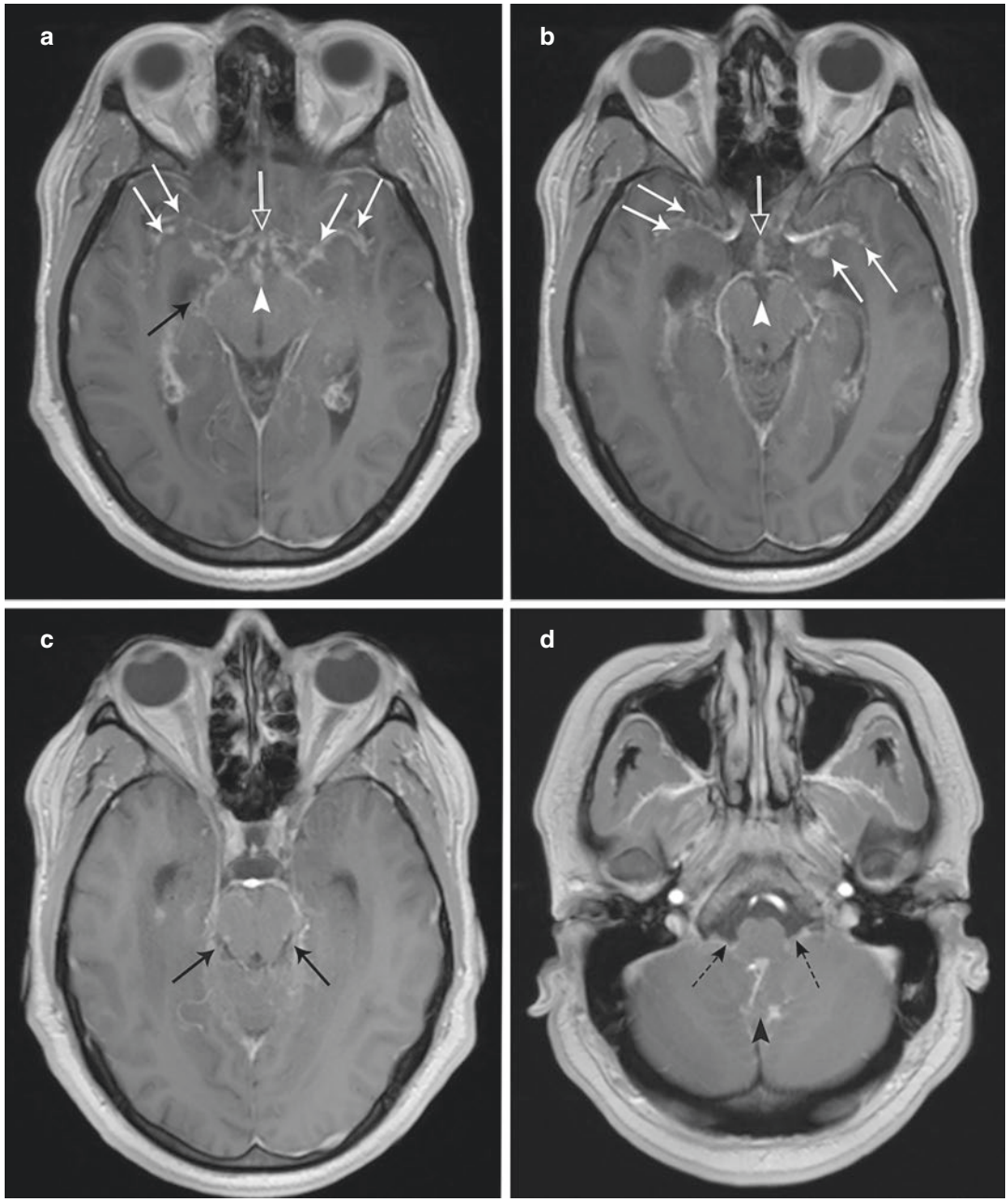

Fig. 2 Intracranial tuberculous leptomeningitis. (**a–d**) Axial contrast-enhanced T1-W MR images show multiple enhancing nodules in the interpeduncular fossa (white arrowheads), suprasellar cistern (white open arrows), ambient cistern (black solid arrows), cerebellomedullary cisterns (black dashed arrows), floor of the fourth ventricle (black arrowhead), and along the Sylvian fissure (white arrows)

demonstrated that MTI is helpful, particularly in cases of mild meningitis, and MT ratio (MTR) quantification helps differentiate TBM from nontuberculous meningeal inflammation. A low MTR is specific for TBM (Ahluwalia et al. 2013; Khatri et al. 2018). Contrast-enhanced FLAIR images have been reported to have a higher specificity compared to contrast-enhanced T1-weighted images in the detection of leptomeningeal enhancement (Parmar et al. 2006;

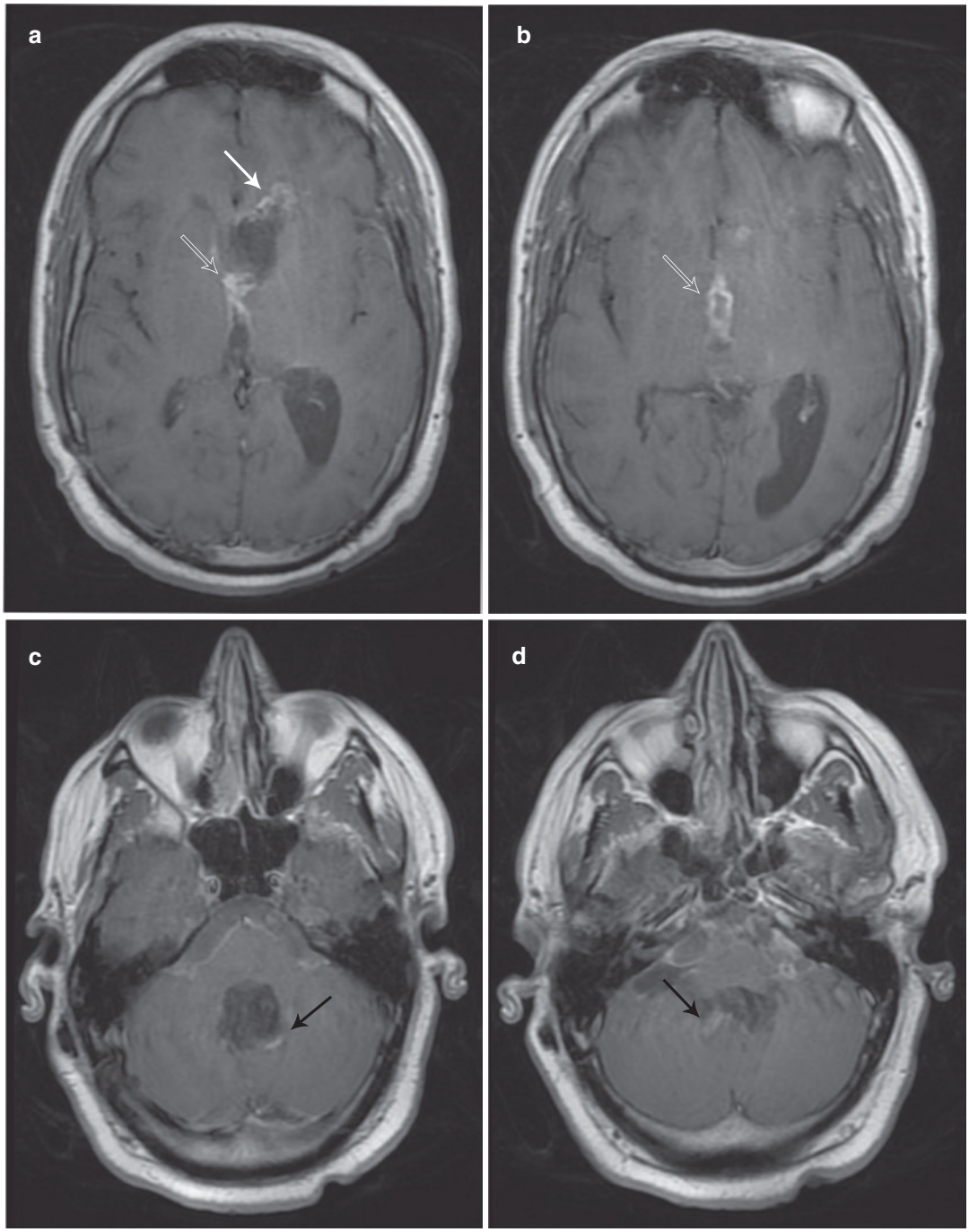

Fig. 3 Intracranial tuberculous ependymitis. (**a–d**) Axial contrast-enhanced T1-W MR images show thick nodular enhancement of the ependymal surfaces of the lateral ventricles (white solid arrow), third (white open arrows) and fourth (black arrows) ventricles

Taheri et al. 2015). Extension of the inflammatory response to the ventricular system through CSF pathways, resulting in ependymitis or choroid plexitis, can cause ependymal or choroid plexus enhancement (Chaudhary et al. 2017) (Fig. 3). Other radiological manifestations of

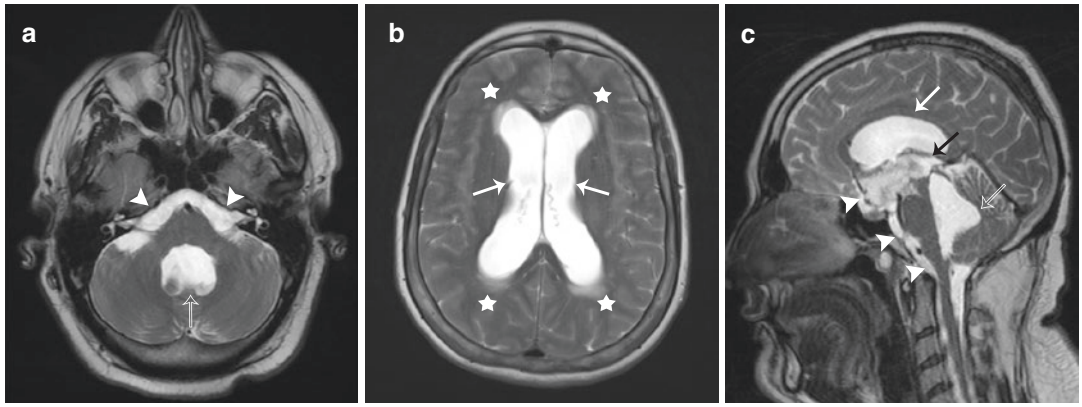

Fig. 4 Communicating hydrocephalus due to inflammatory exudates in the basal subarachnoid cisterns. (**a** and **b**) Axial and (**c**) sagittal T2-W MR images show dilatation of the lateral ventricles (white arrows), third ventricle (black solid arrow), and fourth ventricle (white open arrows), alongside transependymal edema (adjacent to white stars). There are also inflammatory exudates in the basal subarachnoid cisterns (white arrowheads)

TBM are related to its possible complications, including progressive hydrocephalus, vasculitis, infarction, and cranial neuropathies.

Hydrocephalus is the most frequent complication of TBM and is generally of the communicating type, due to blockage of CSF resorption by inflammatory exudates in the basal subarachnoidal cisterns (Fig. 4). Occasionally, hydrocephalus is of the obstructive type, occurring secondary to narrowing of the aqueduct or a ventricle by a focal parenchymal lesion such as tuberculoma or abscess, with mass effect due to entrapment of a ventricle by granulomatous ependymitis (Bernaerts et al. 2003; Taheri et al. 2015; Chaudhary et al. 2017) (Fig. 5). In addition to dilatation of the lateral ventricles, increased periventricular signal may be seen on T2-weighted images as a sign of interstitial edema due to increased intraventricular pressure. Hydrocephalus may also be a complication of bacterial meningitis, but is often transient compared with TBM-associated hydrocephalus where it is progressive. The persistence of hydrocephalus should therefore alert the radiologist to the possibility of a tuberculous etiology (Bernaerts et al. 2003). Ventriculitis may result from spread of infection through the communicating foramina in the late stages of tuberculous leptomeningitis or from rupture of a subependymal focus of infection. It is visualized on MRI as heterogeneous signal hyperintensity of the CSF on T1-weighted images compared to normal CSF, with thickening and contrast enhancement of the ependymal lining. It is often associated with hydrocephalus (Khatri et al. 2018).

The incidence of stroke is about 13–57% in patients with TBM. The mortality rate is about three times higher in patients with TBM and stroke, compared to stroke-free patients (Zhang et al. 2019). The infarction usually involves the basal ganglia and internal capsule and may be due to vasculitis, vascular compression, or occlusion of small perforating vessels, particularly the lenticulostriate and thalamoperforating arteries (Fig. 6). DWI helps in the early detection of infarcts. MR angiography may show vascular occlusion or narrowing (Fig. 7). TBM may also cause dural venous sinus thrombosis with resultant hemorrhagic infarction (Bernaerts et al. 2003; Ahluwalia et al. 2013; Chaudhary et al. 2017). Cranial nerve involvement occurs due to vascular compromise, ischemia, or nerve entrapment in the basal exudates in 17–40% of cases, most commonly affecting the second, third, fourth, and seventh cranial nerves. The affected cranial nerves are best evaluated by MRI, where they may appear thickened, especially in their proximal segments, with T2-hyperintensity and marked enhancement (Taheri et al. 2015; Chaudhary et al. 2017) (Fig. 8).

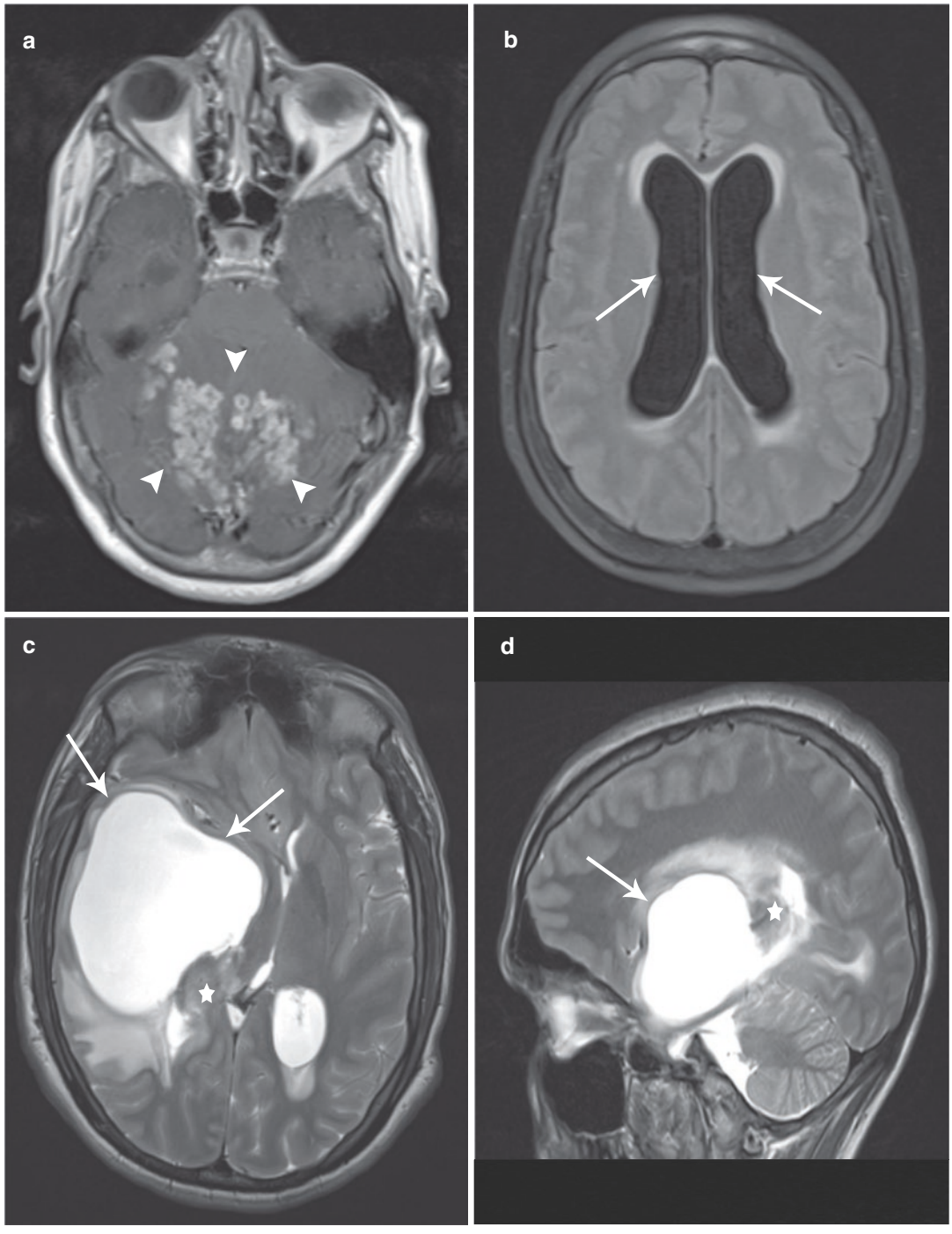

Fig. 5 Obstructive hydrocephalus due to tuberculoma. Axial (**a**) contrast-enhanced T1-W and (**b**) FLAIR MR images show a cluster of tuberculomas in the posterior fossa (white arrowheads) exerting a mass effect on the fourth ventricle with subsequent obstructive hydrocephalus (white arrows). (**c**) Axial and (**d**) sagittal T2-W MR images show a tuberculoma in the right ventricular atrium (white star) and marked dilatation of the ipsilateral temporal horn (white arrows)

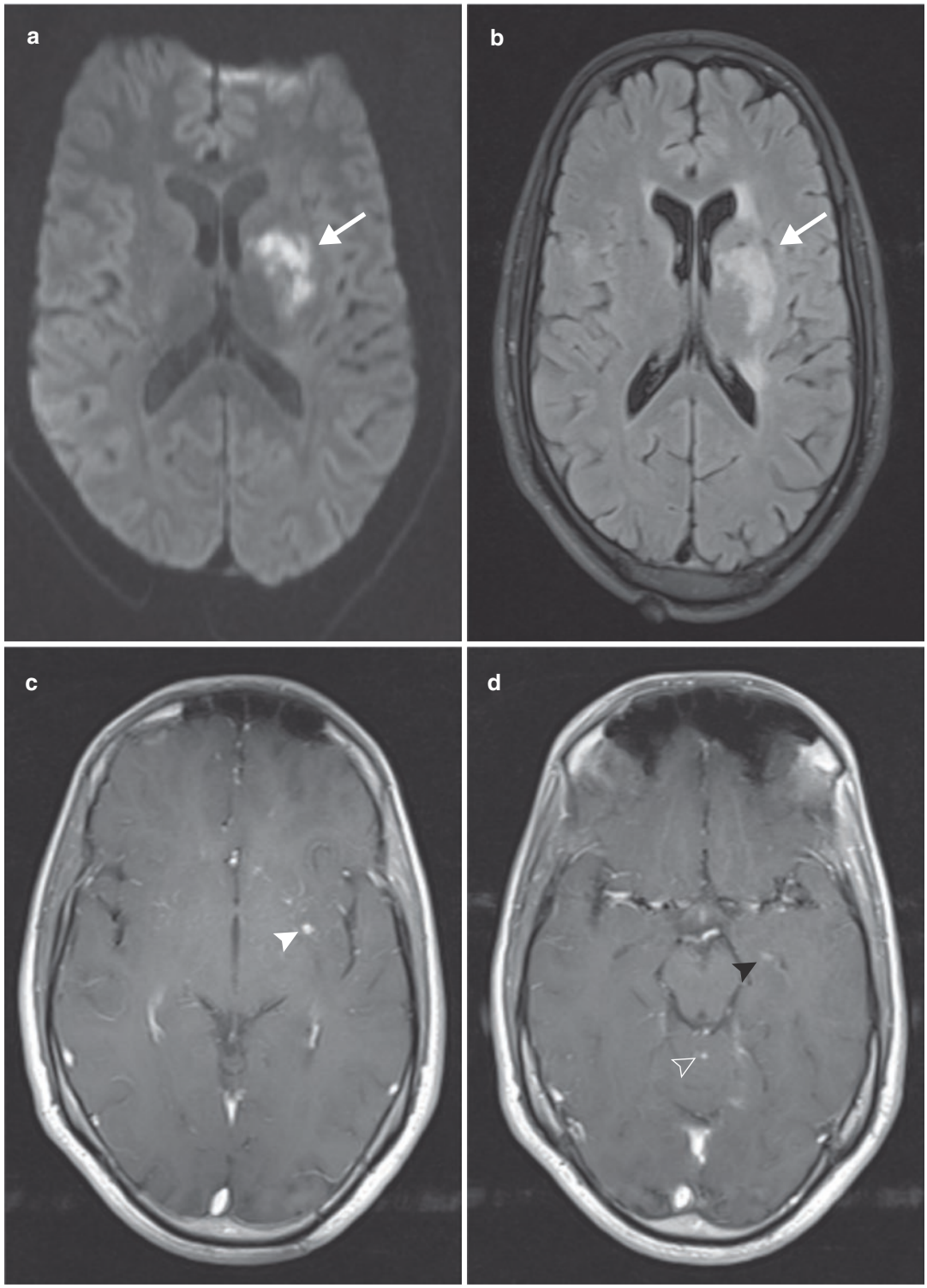

Fig. 6 Tuberculous basal ganglia infarction. Axial (**a**) diffusion-weighted and (**b**) axial FLAIR MR images show restricted diffusion with FLAIR hyperintensity in the left basal ganglia, consistent with a recent infarct (white arrows). (**c** and **d**) Axial contrast-enhanced T1-W MR images of the same patient show nodular enhancement of the left basal ganglia (white solid arrowhead), left temporal lobe (black solid arrowhead), and posterior fossa (white open arrowhead), consistent with tuberculomas

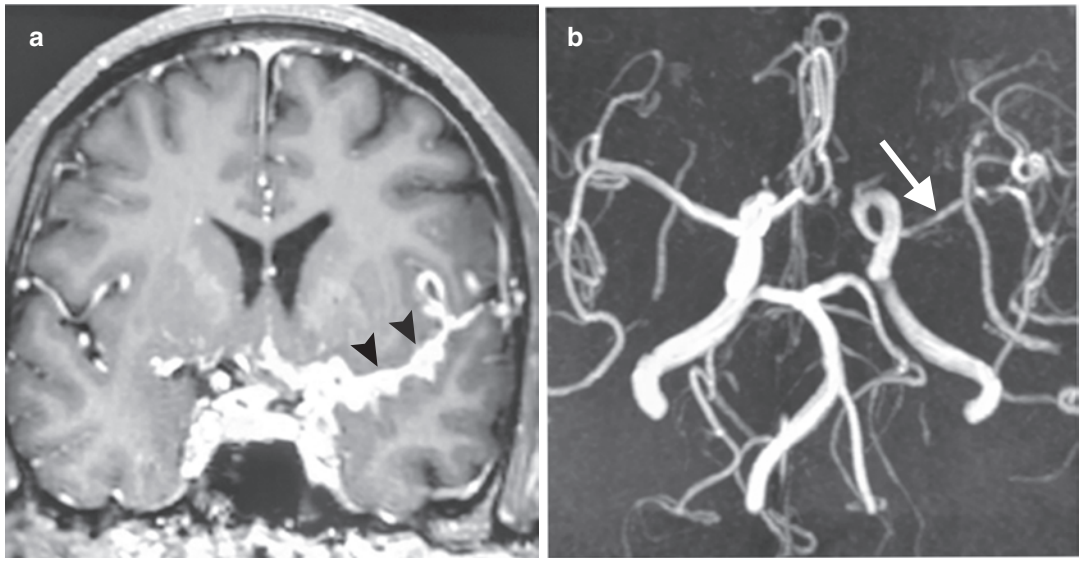

Fig. 7 Middle cerebral artery vasculitis. (**a**) Coronal contrast-enhanced T1-W and (**b**) 3D time-of-flight MR images show nodular meningeal thickening along the left Sylvian fissure (black arrowheads), resulting in narrowing of the left middle cerebral artery (white arrow)

6.1.1.2 Tuberculous Pachymeningitis

Tuberculous pachymeningitis is a relatively uncommon entity, compared to tuberculous leptomeningitis. The majority of cases of pachymeningitis are secondary to acute or chronic tuberculous leptomeningitis. However, a few cases of direct seeding of the dura with bacteria by hematogenous spread, resulting in isolated pachymeningitis, have also been reported (Goyal et al. 1997; Khatri et al. 2018). Pachymeningitis may present as focal or diffuse involvement of the dura mater (Gupta and Kumar 2011). In the literature, the term *en plaque* tuberculoma has been used to describe focal involvement of the pachymeninges (Bernaerts et al. 2003; Aggarwal et al. 2016). Lesions appear hyperdense on CT, isointense to brain parenchyma on T1-weighted MR images, and iso- to hypointense on T2-weighted MR images. Most focal lesions were seen as *en plaque*, homogeneously uniformly - enhancing dural - based masses (Goyal et al. 1997) (Fig. 9). The differential diagnosis includes meningioma for focal pachymeningitis, in which there is associated hyperostosis in the adjacent bone (Bernaerts et al. 2003). Focal and diffuse pachymeningitis can also be seen in a large number of inflammatory and noninflammatory conditions (Gupta and Kumar 2011).

6.1.2 Parenchymal Tuberculosis

Parenchymal infection may be either isolated or accompanied by tuberculous meningitis. The parenchymal disease often presents as tuberculoma and less commonly as cerebritis, brain abscess, miliary TB, or tuberculous encephalopathy.

6.1.2.1 Tuberculoma

Tuberculomas may be solitary or multiple. They are preferentially located at the cortico-subcortical junction and the periventricular region due to hematogenous dissemination (Gupta et al. 2001; Chaudhary et al. 2017). On unenhanced CT, tuberculomas present with variable densities, ranging from hypodense to hyperdense. Contrast-enhanced CT may show peripheral rim enhancement or less frequently nodular or irregular nonhomogeneous

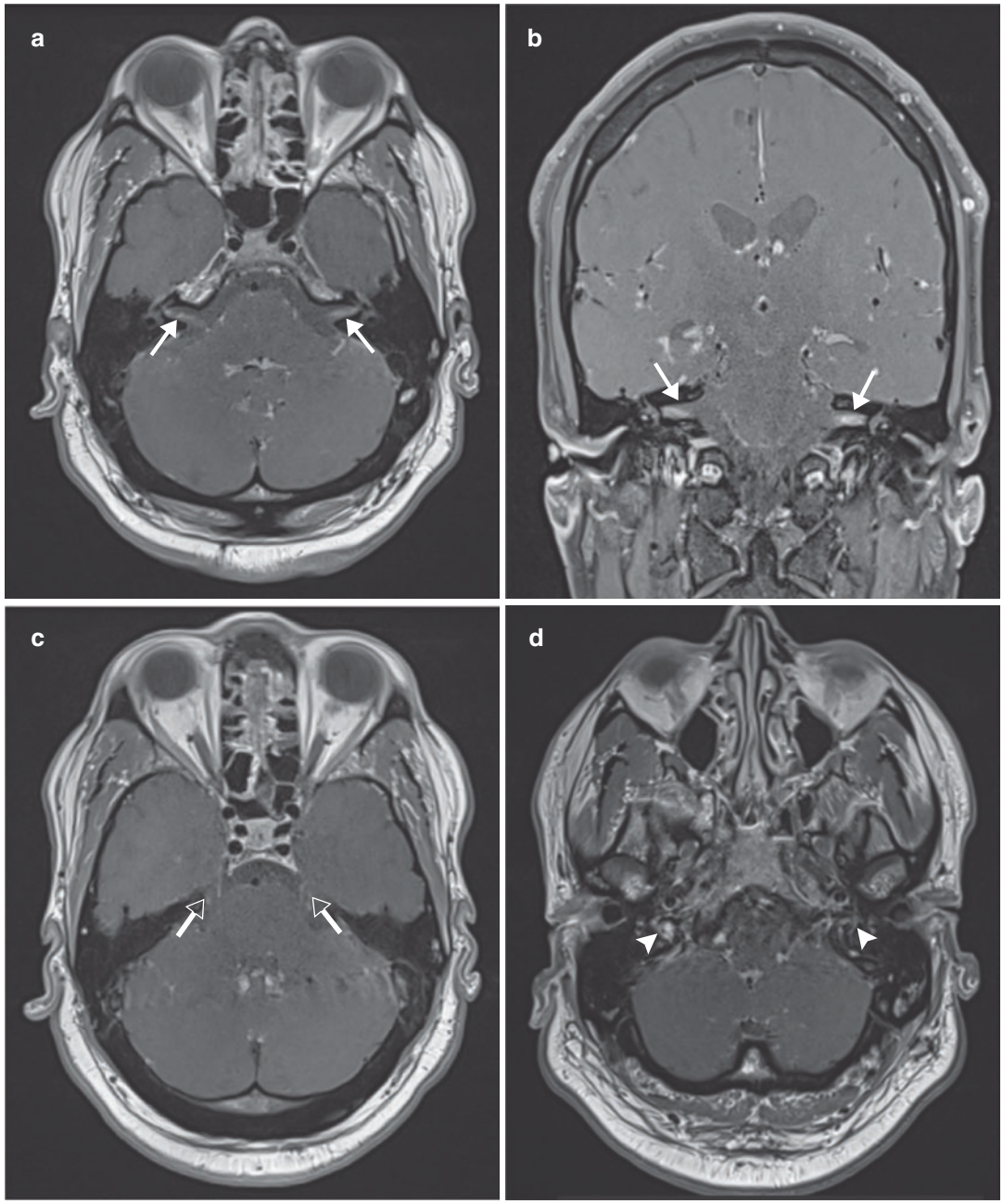

Fig. 8 Cranial nerve involvement in tuberculosis. (**a**) Axial and (**b**) coronal contrast-enhanced T1-W MR images show bilateral nodular thickening of the seventh cranial nerves (white solid arrows). (**c** and **d**) Coronal contrast-enhanced T1-W MR images of the same patient show bilateral nodular thickening along the fifth cranial nerves (white open arrows) and the pars nervosa of the jugular foramina (white arrowheads)

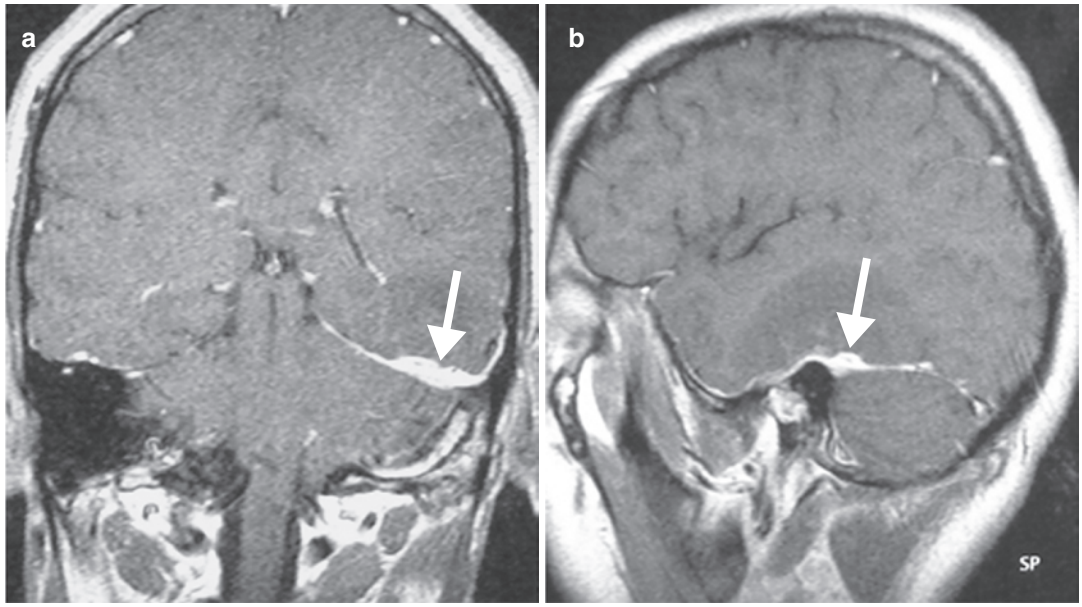

Fig. 9 Tuberculous pachymeningitis. (**a**) Coronal and (**b**) sagittal contrast-enhanced T1-W MR images show left focal pachymeningeal enhancement along the cerebellar tentorium (arrows)

Table 2 MRI features of the different types of tuberculoma

Type of tuberculoma	T1-W	T2-W	FLAIR	DWI	Contrast-enhanced T1-W
Noncaseating granuloma	Hypo- to isointense	Hyperintense	No suppression	No restriction	Nodular enhancement
Caseating granuloma	Hypo- to isointense	Hypointense	No suppression	No restriction	Rim enhancement
Caseating granuloma with central liquefaction	Hypo- to isointense	Hyperintense with a peripheral hypointense rim	Partial suppression	May display restricted diffusion	Rim enhancement

enhancement. A central calcification alongside rim enhancement, reported as the target sign, is highly suggestive of the diagnosis (Whiteman 1997). Occasionally, healed tuberculomas appear as calcified foci on unenhanced CT (Udani 1970).

Tuberculomas have a variable appearance on MRI, depending on the caseation stage (Table 2). They usually have hypointense to intermediate signal on T1-weighted images. Noncaseating granulomas are hyperintense on T2-weighted images, showing nodular homogeneous enhancement (Fig. 10). There is no signal suppression on FLAIR images. Solid caseating granulomas have a markedly hypointense signal on T2-weighted images, with rim enhancement. The T2-hypointense signal is attributed to the high cellularity of caseum (Fig. 11). FLAIR images show no signal suppression. On DWI, solid caseating granulomas have unrestricted diffusion and are easily differentiated from lymphoma, as both are hypointense on T2-weighted images. Caseating granulomas with central liquefaction appear hyperintense on T2-weighted images, with a peripheral hypointense rim representing a collagenous capsule. FLAIR images may show partial signal suppression. Centrally liquefied caseating granulomas have rim enhancement (Fig. 12). They may display restricted diffusion and are thus indiscernible from pyogenic abscesses. There may be an associated vasogenic edema of variable extent (Shah 2000; Bernaerts et al. 2003; Chaudhary et al. 2017).

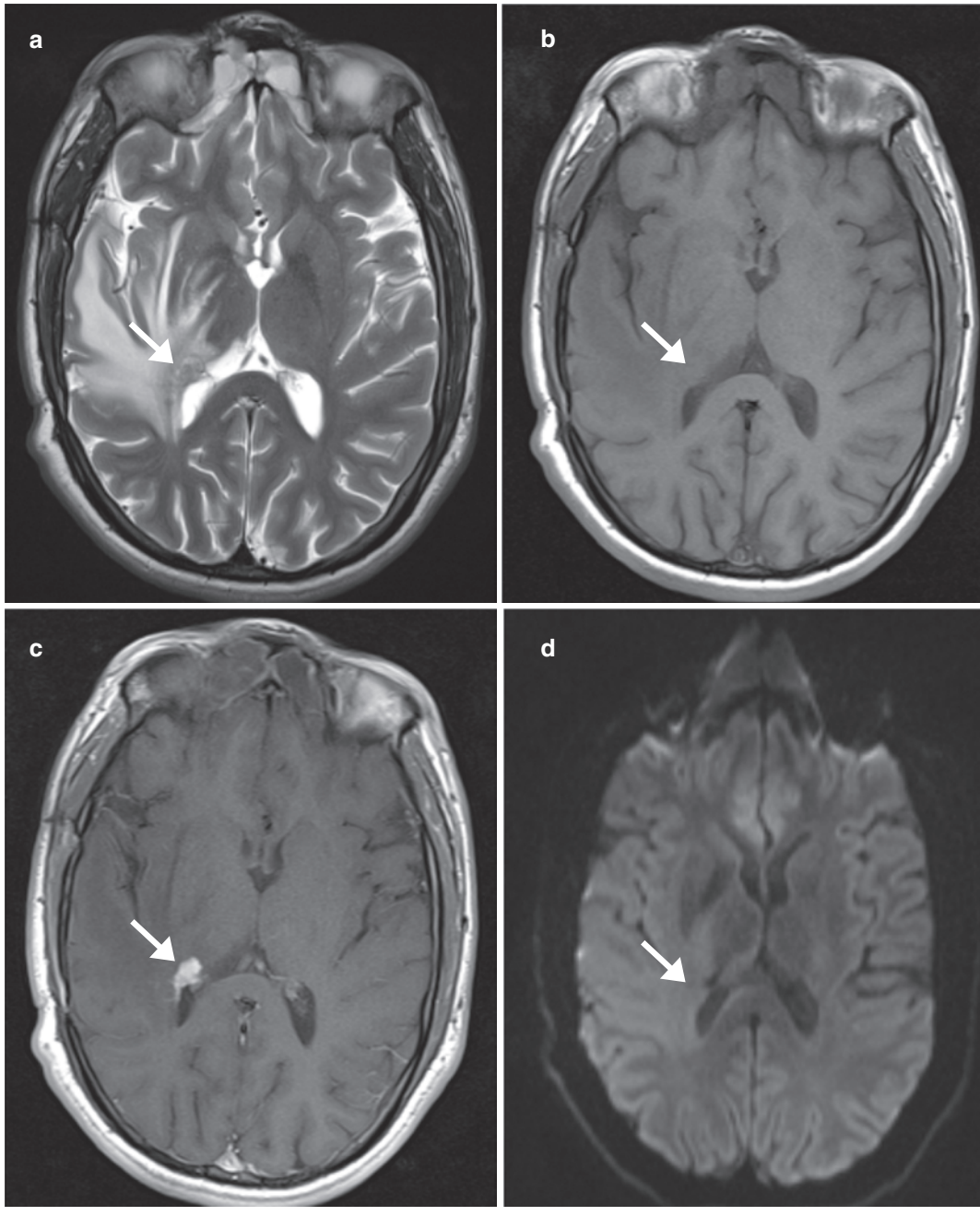

Fig. 10 Cerebral parenchymal noncaseating tuberculoma. Axial (**a**) T2-W, (**b**) T1-W, (**c**) contrast-enhanced T1-W, and (**d**) diffusion-weighted MR images show a right periventricular nodule (arrows) that is T1-isointense and T2-hyperintense. It shows nodular enhancement and no associated restricted diffusion. It is surrounded by marked vasogenic edema

A wide variety of differential diagnoses can be considered for ring-enhancing lesions of tuberculomas. The important ones include neurocysticercosis, metastasis, CNS lymphoma (in immunocompromised patients), toxoplasmosis, tumor (glioblastoma), and pyogenic abscess. Proton MR spectroscopy helps to differentiate tuberculoma from pyogenic abscesses and

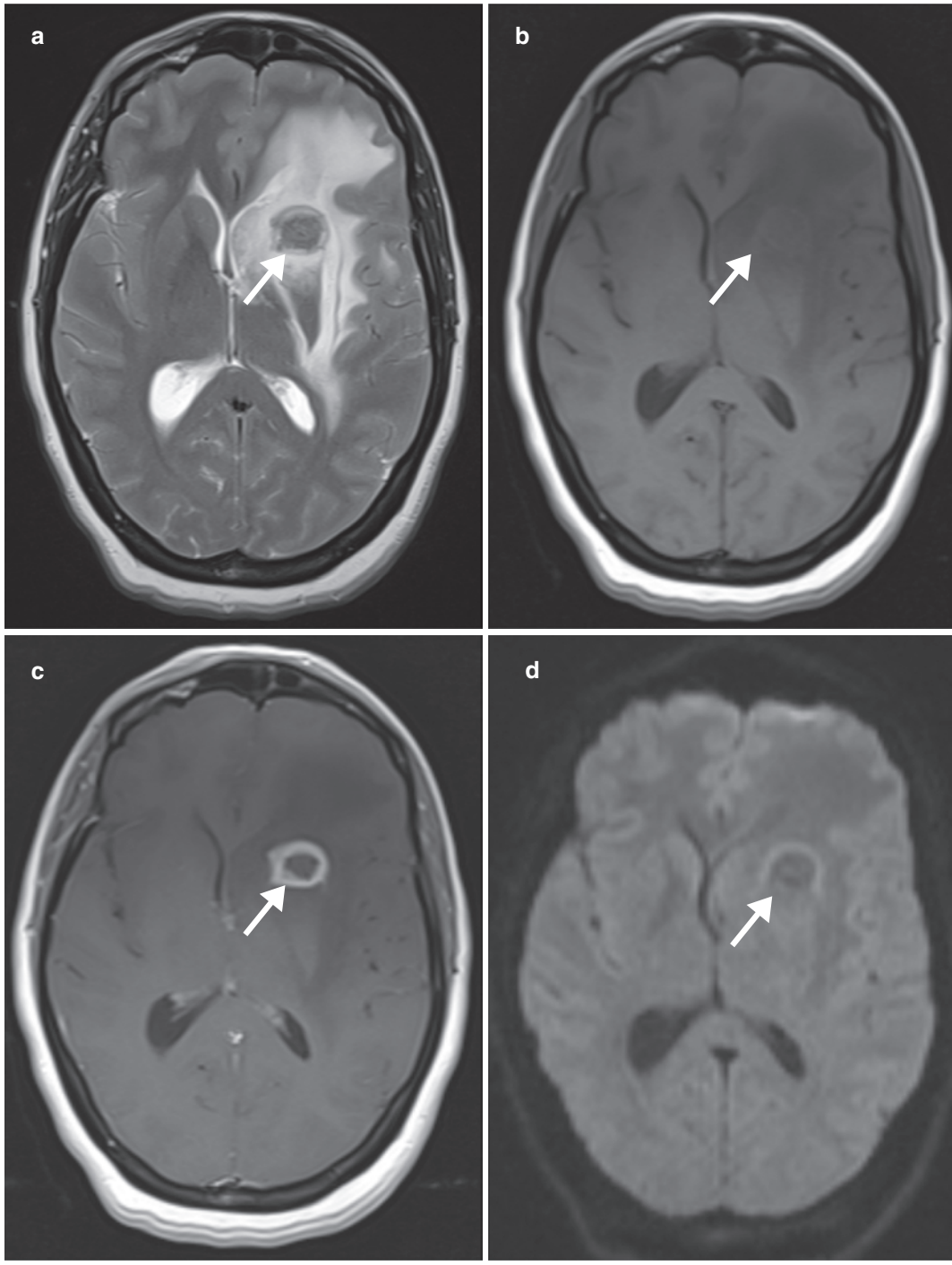

Fig. 11 Cerebral parenchymal solid caseating tuberculoma. Axial (**a**) T2-W, (**b**) T1-W, (**c**) contrast-enhanced T1-W, and (**d**) diffusion-weighted MR images show a left capsulo-lenticular nodule (arrows) that is T1-isointense and T2-hypointense. It shows rim enhancement and no associated restricted diffusion

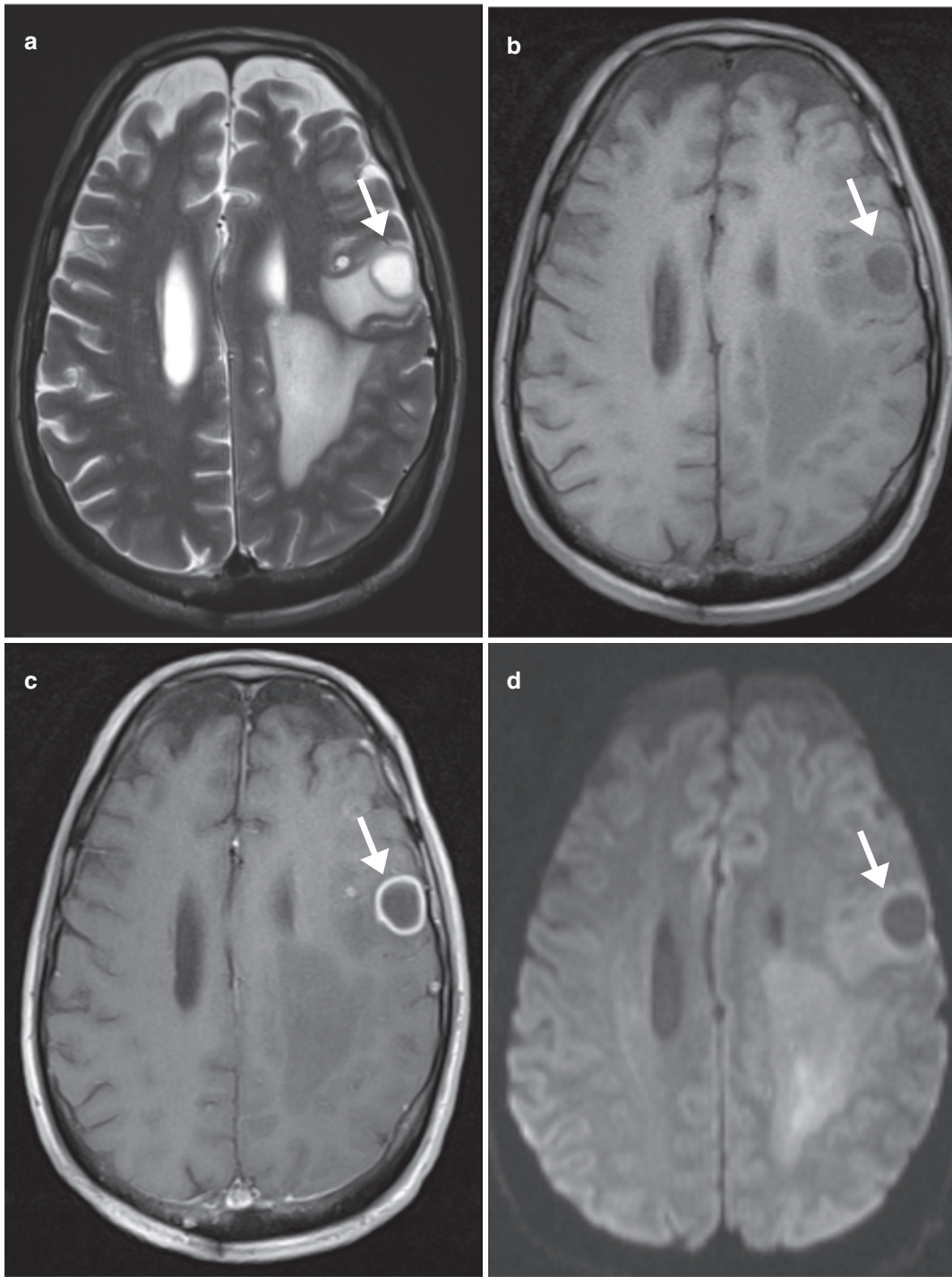

Fig. 12 Cerebral parenchymal liquefied caseating tuberculoma. Axial (**a**) T2-W, (**b**) T1-W, (**c**) contrast-enhanced T1-W, and (**d**) diffusion-weighted MR images show a left frontal nodule (arrows) that is T2-hyperintense with a peripheral hypointense rim representing a collagenous capsule, which is T1-isointense. It shows rim enhancement and no associated restricted diffusion. Marked vasogenic edema is also present

neoplasms. T2-hypointense solid caseating tuberculomas show an isolated lipid peak (which is highly specific for tuberculoma) at 0.9 and 1.3 ppm (Fig. 13). T2-hyperintense liquefied tuberculomas have a choline peak at 3.22 ppm, in addition to a large lipid peak. Pyogenic brain abscesses show an amino acid peak (e.g., valine, leucine, isoleucine) at 0.9 ppm along with a lipid-

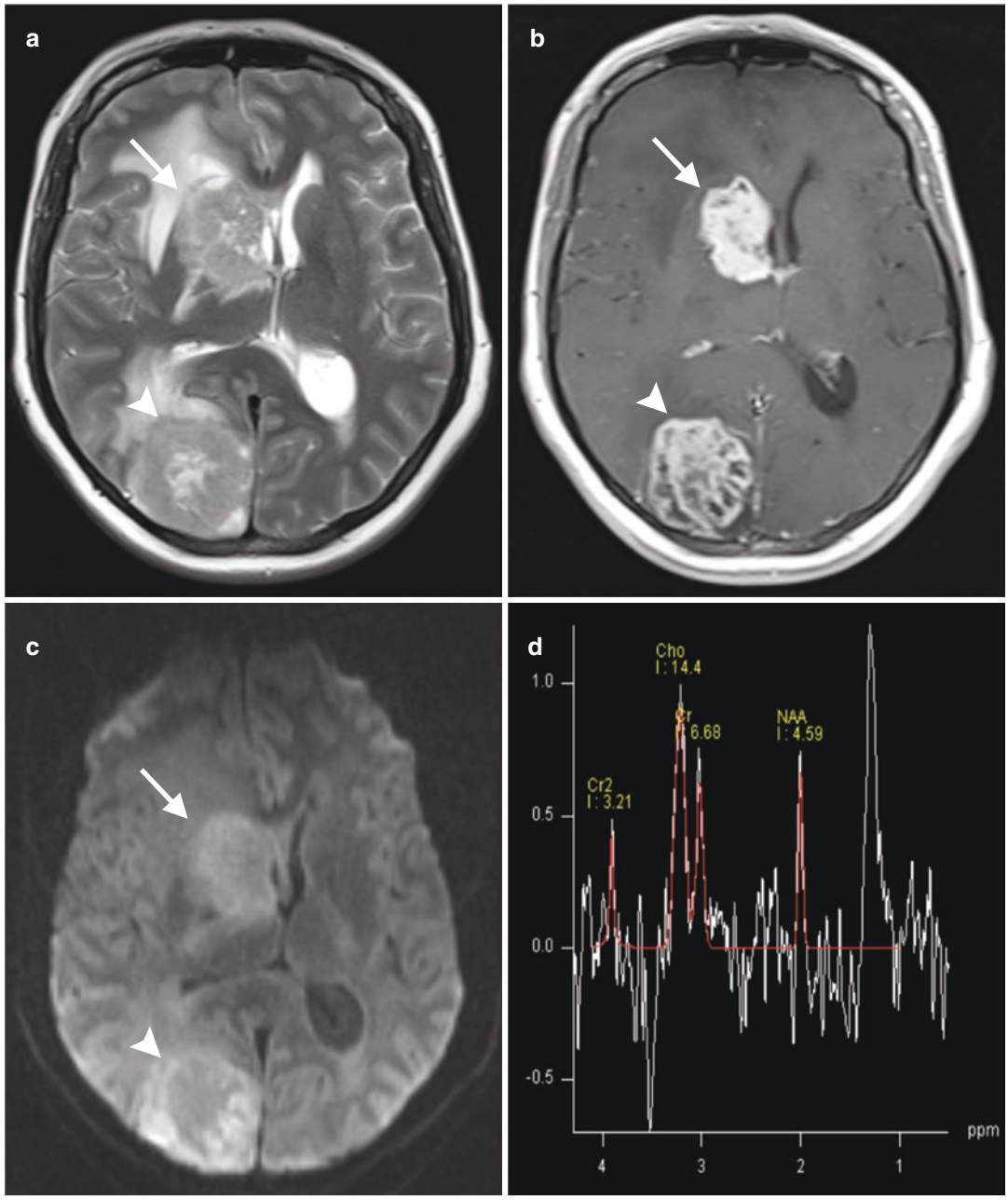

Fig. 13 Pseudotumoral cerebral tuberculosis and the usefulness of spectroscopy. Axial (**a**) T2-W, (**b**) contrast-enhanced T1-W, and (**c**) diffusion-weighted MR images show a right capsulo-lenticulo-caudate mass (arrows) and a second ipsilateral parietal mass (arrowheads), appearing T2-isointense with marked heterogeneous enhancement and slightly restricted diffusion. (**d**) MR spectroscopy shows lipid peaks at 0.9 and 1.3 ppm alongside a decreased NAA peak

lactate peak at 1.3 ppm. Tumors such as metastases and high-grade gliomas have a lipid peak, in addition to significantly elevated choline and reduced N-acetylaspartate (NAA) and creatine peaks (Gupta et al. 1995). It has been demonstrated that abnormal SWI foci are present in most patients with neurotoxoplasmosis, presumably attributable to hemorrhage (Benson et al. 2018). Follow-up CT or MRI has a crucial role in monitoring the response to medical treatment. Occasionally, a paradoxical increase in the size of a pre-existing tuberculoma, or the occurrence of a new CNS tuberculoma in patients receiving adequate treatment, may be seen. Hence, anti-TB therapy should be continued, eventually leading to the resolution of the disease (Afghani 1994; Ku 2009).

6.1.2.2 Miliary Tuberculosis

Miliary TB is seen mainly in severely immunocompromised patients and is usually associated with meningeal involvement. It results from hematogenous spread of infection in which multiple small miliary tubercles of less than 2 mm size are present at the gray-white matter junction. Depending on their caseous components, these lesions may have either hypo- or hyperintense signal on T2-weighted images and show intense nodular enhancement (Khatri et al. 2018; Gupta and Kumar 2011; Taheri et al. 2015; Chaudhary et al. 2017) (Fig. 14). The differential diagnosis for miliary tuberculomas includes Lyme disease, neurosarcoidosis, metastases, lymphoid granulomatosis, and histoplasmosis (Khatri et al. 2018). Brain metastasis is associated with a greater amount of edema. Neurosarcoidosis usually combines parenchymal nodular lesions with dural and leptomeningeal lesions. Hemorrhagic foci on T2*-weighted sequences are generally seen in *CNS* fungal infections. The identification of a scolex is a helpful feature in neurocysticercosis.

6.1.2.3 Tuberculous Brain Abscess

TBA occurs in less than 10% of patients with CNS TB. There are two theories for the formation of a tuberculous abscess. One hypothesizes the progression of tuberculous cerebritis and the other the liquefaction of tuberculomas. Pathologically, TBA consists of a walled-off collection of pus containing viable and dead bacteria, cellular debris, and caseous material (Khatri et al. 2018). On imaging, an abscess appears as a large (usually >3 cm), well-defined, localized lesion with perilesional edema and mass effect. It is frequently multiloculated. The abscess wall

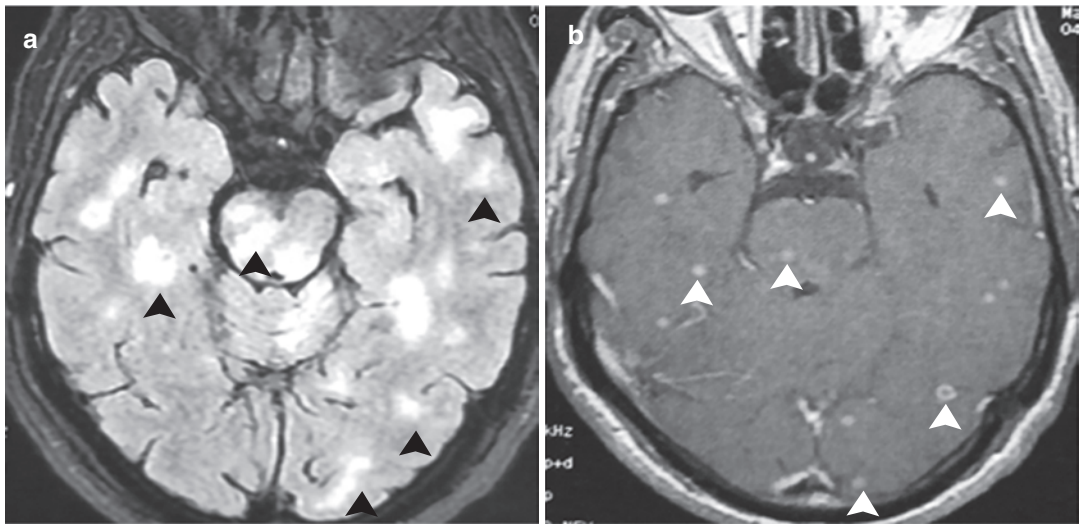

Fig. 14 Cerebral parenchymal miliary tuberculosis. Axial (**a**) FLAIR and (**b**) contrast-enhanced T1-W MR images show numerous miliary nodules that are hyperintense in the FLAIR image (black arrowheads) with nodular and rim enhancement (white arrowheads)

usually appears thin and smooth. The contents of abscesses are usually T1-hypointense and T2-hyperintense or heterogeneous, with variable degrees of suppression on FLAIR images. DWI usually shows restricted diffusion with low apparent diffusion coefficient (ADC) values. The abscess wall is usually T1-isointense and T2-hypointense (Khatri et al. 2018) (Fig. 15).

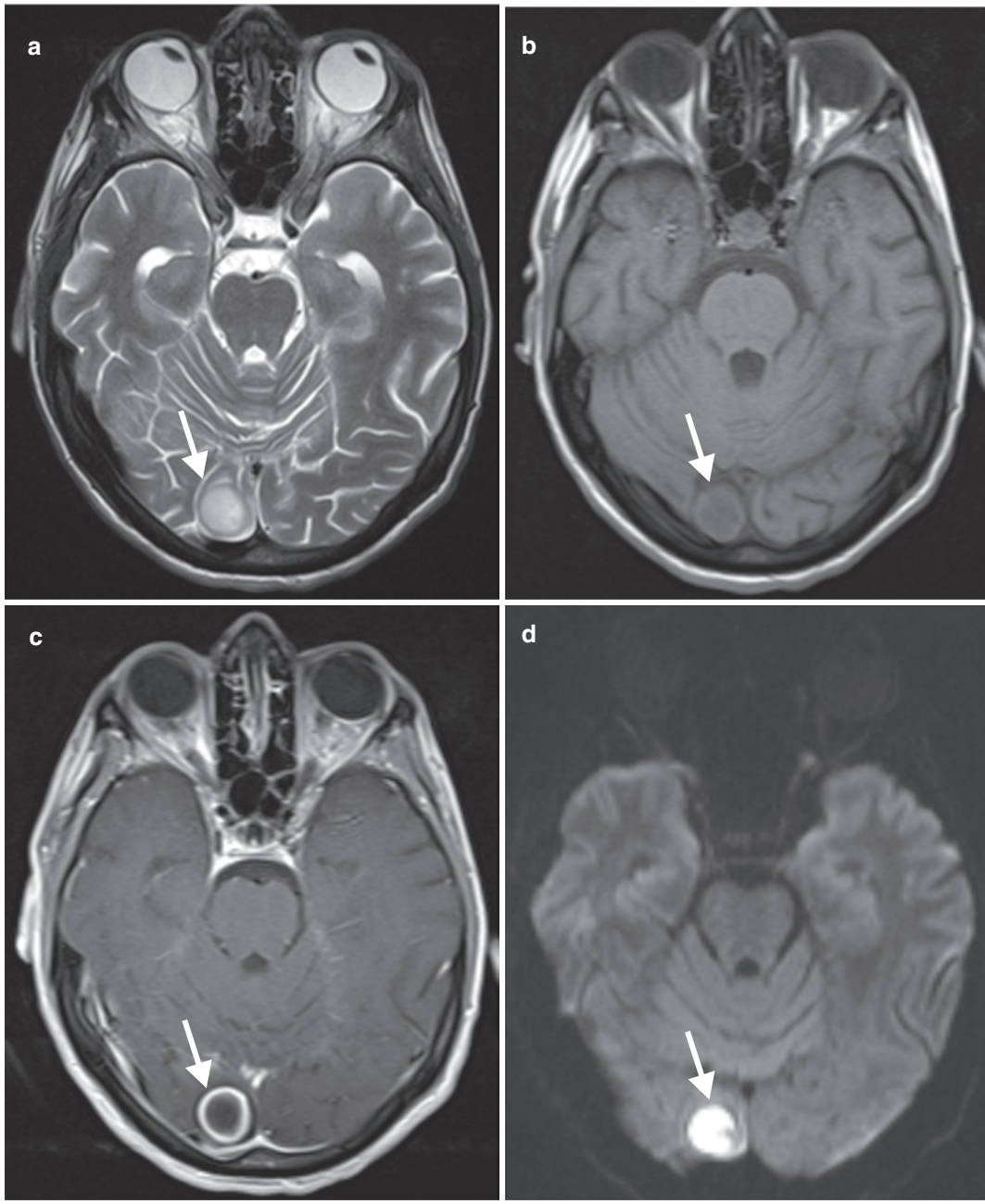

Fig. 15 Tuberculous brain abscess. Axial (**a**) T2-W, (**b**) T1-W, (**c**) contrast-enhanced T1-W, and (**d**) diffusion-weighted MR images show a right occipital mass (arrows) that is T2-hyperintense with a peripheral hypointense rim and T1-isointense with hyperintense rim. It shows rim enhancement with associated restricted diffusion

TBAs may sometimes be difficult to differentiate from caseating tuberculomas with liquefaction. However, this differentiation is very important because the management of tuberculoma involves medical therapy with anti-TB drugs, while the management of TBA involves surgical drainage of the pus. Imaging plays a major role in this differentiation. Size >3 cm, the presence of restricted diffusion, a thin smooth wall, and multiloculation usually favor TBA over tuberculoma (Bernaerts et al. 2003; Khatri et al. 2018; Zunt 2018). On conventional imaging, TBA may also be indistinguishable from pyogenic abscess. However, MR spectroscopy and MTI may help in differentiating between these two lesions. Pyogenic abscess demonstrates an amino acid peak at 0.9 ppm, which is absent in TBA (Menon et al. 2011). TBA shows a significantly lower MTR value, compared to pyogenic abscess (Gupta and Kumar 2011; Chaudhary et al. 2017).

6.1.2.4 Tuberculous Encephalopathy

Tuberculous encephalopathy is another rare outcome of CNS TB. Infants and young children with pulmonary TB are commonly affected. It is thought to be due to a delayed-type hypersensitivity (type IV hypersensitivity) reaction to tuberculous proteins (Bernaerts et al. 2003; Patkar et al. 2012; Khatri et al. 2018). Pathologically, extensive white matter injury and perivascular demyelination are present in the brain parenchyma. On MRI, extensive cerebral edema is found, with unilateral or bilateral extensive T2 and FLAIR hyperintensity. Diffuse contrast enhancement of the involved white matter may be seen. It has a poor prognosis, with death usually occurring within one to two months of onset. Acute disseminated encephalomyelitis (ADEM) is an important differential diagnosis in many cases (Khatri et al. 2018).

6.2 Spinal Intradural Tuberculosis

6.2.1 Spinal Intramedullary Tuberculosis

Spinal intramedullary TB is a rare disease entity. It is caused by active tuberculous lesions spreading via blood or CSF. It can also be rarely caused by direct spread of local spinal TB (Liu et al. 2016; Varghese et al. 2017). Spinal intramedullary TB presents as various types of lesions, depending on the virulence of the bacteria and the host's immune resistance (Varghese et al. 2017). MRI is the imaging modality of choice to detect early infection and to thoroughly evaluate the extent of disease affecting the spinal cord (Balériaux and Neugroschl 2004). Spinal intramedullary tuberculoma is a rare form of TB infecting the CNS (Liu et al. 2016; Sharma et al. 2002). It represents only 2 per 100,000 cases of TB and 2 per 1000 cases of CNS TB (Lu 2010; Sardana and Shringi 2020). This type of tuberculous lesion is more often observed in people aged 18–45 years, with the youngest patient reported being only nine months old (Liu et al. 2016). The thoracic spine is the most common site for intramedullary tuberculoma, described in about 70% of cases (Yusuf et al. 2015; Sardana and Shringi 2020). The reason could be because this region receives about 45% of the entire blood supply to the spinal cord, and it is known that *M. tuberculosis* thrives best in an area where the partial pressure of oxygen is high (Yusuf et al. 2015).

MRI features vary during the different phases of tuberculomas (Lu 2010) (Fig. 16). In the early stage, tuberculomas are characterized by insufficient formation of caseous necrosis and severe edema around the lesion (Lu 2010; Sardana and Shringi 2020). At this stage, tuberculomas are both T1- and T2-isointense and enhance homogeneously. As caseous necrosis in tuberculomas increases, the peripheral edema decreases or may disappear. There is T1-isointensity and T2-iso- or hypointensity. On contrast-enhanced images, there is rim enhancement with hypointense signal in the central region. With the development of caseation, a typical "target sign" is seen on T2-weighted images. The caseous substance forms the target center, whereas the peripheral infective granulation tissues form the hyperintense rim (Lu 2010; Sardana and Shringi 2020). Intramedullary tuberculomas can be associated with arachnoiditis, cord edema, or syrinx (Chaudhary et al. 2017). Intradural extramedullary tuberculomas may mimic *en plaque* meningioma and usually present

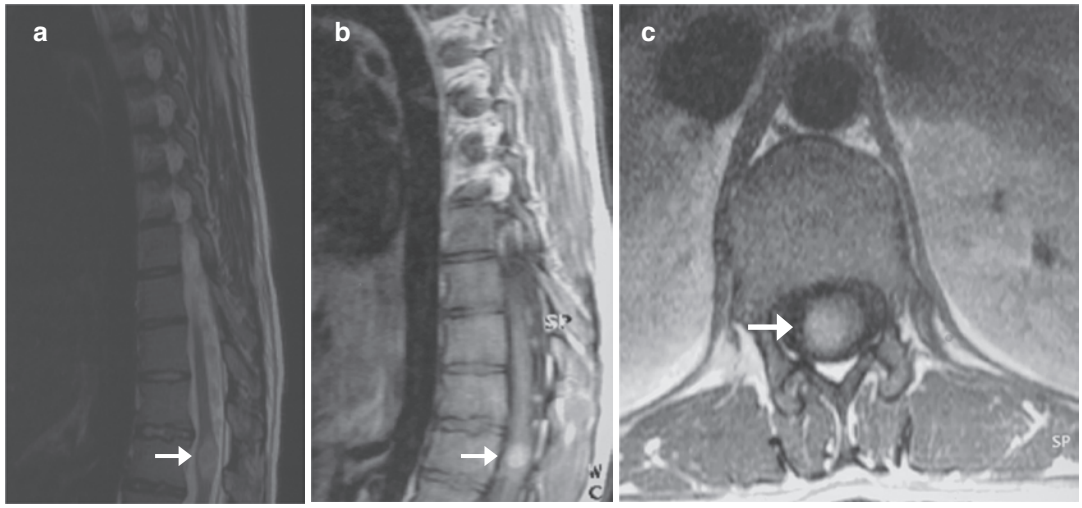

Fig. 16 Spinal intramedullary tuberculoma. (**a**) Sagittal T2-W and (**b**) sagittal and (**c**) axial contrast-enhanced T1-W MR images show an intramedullary nodule (arrows) enlarging the lower thoracic spinal cord and appearing T2-hyperintense with slight nodular enhancement

as a single dural-based ring-enhancing lesion (Chaudhary et al. 2017). The differential diagnosis includes tumors such as astrocytoma, ependymoma, hemangioblastoma, lymphoma and metastatic tumors, demyelinating diseases (multiple sclerosis), and granulomatous diseases such as syphilis, abscess, and fungus (Liu et al. 2016; Parmar et al. 2000).

6.2.2 Tuberculous Myelitis

In most cases, tuberculous myelitis appears in individuals younger than 30 years of age (Almeida 2005). It occurs more frequently as a secondary lesion to osteomyelitis (Almeida 2005). The cervical segment of the spinal cord is the most common location of tuberculous myelitis (Chaudhary et al. 2017). MRI shows diffuse cord swelling and slightly hyperintense T1 and T2 signal without enhancement (Fig. 17) or with slight enhancement that may persist for several months (Chaudhary et al. 2017; Liu et al. 2019). Even after treatment, adjacent meningeal enhancement may remain for months or years (Salvador et al. 2021). Intramedullary abscess, cavitation, cord atrophy, and syringomyelia may be associated with a poor outcome (Chaudhary et al. 2017). The differential diagnosis includes cord contusion, cord infarction due to vasculitis, acute transverse myelitis, and demyelinating diseases (Chaudhary et al. 2017).

6.2.3 Spinal Meningitis

The MRI features of spinal tuberculous arachnoiditis include inflammatory exudates causing obliteration of spinal subarachnoid space, CSF collection, loss of outline of the spinal cord, and matting of cauda equina nerve roots (Chaudhary et al. 2017; Ogul et al. 2017). It also shows nodular or linear enhancement of the spinal cord surface or nerve roots and plaque-like dural thickening (Chaudhary et al. 2017; Liu et al. 2019) (Fig. 18). The main complications of spinal meningitis are radiculitis, vasculitis, spinal infarcts, and disturbance of CSF flow due to adhesion of arachnoid layers, which causes syringomyelia (Schaller et al. 2019). Therefore, anti-TB treatment should be given immediately to avoid irreversible spinal cord injury (Liu et al. 2019). The most important differential diagnosis of tuberculous arachnoiditis is meningeal carcinomatosis (Garg et al. 2015).

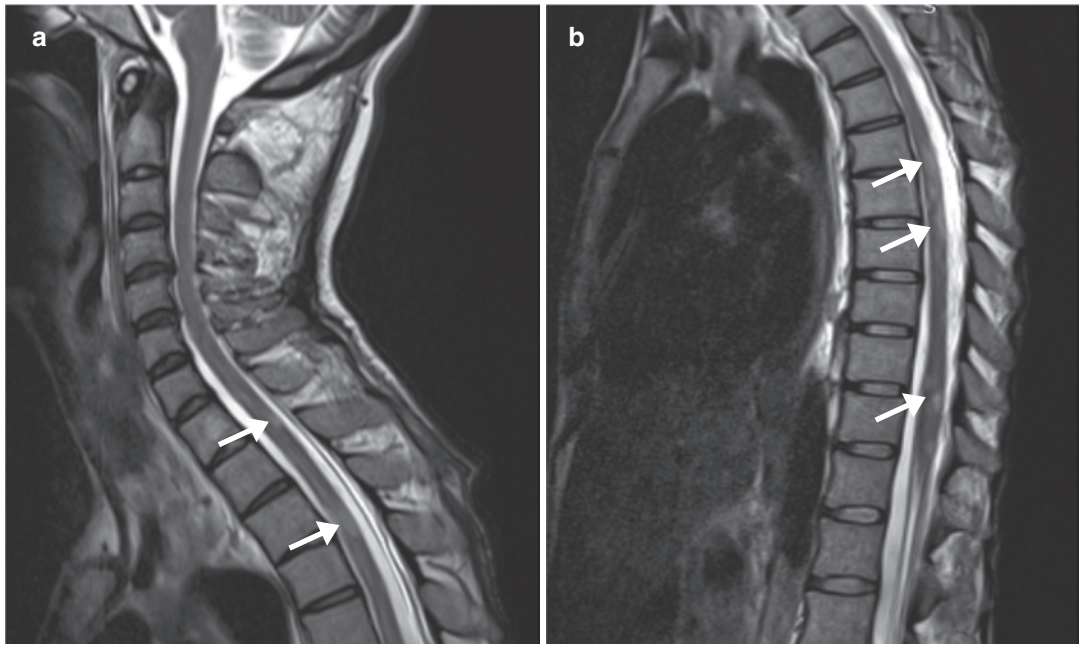

Fig. 17 Spinal tuberculous myelitis. (**a** and **b**) Sagittal T2-W MR images show a slight diffuse spinal cord swelling containing multiple focal demyelinating lesions (arrows) that appear T2-hyperintense in a patient with cerebral tuberculomas

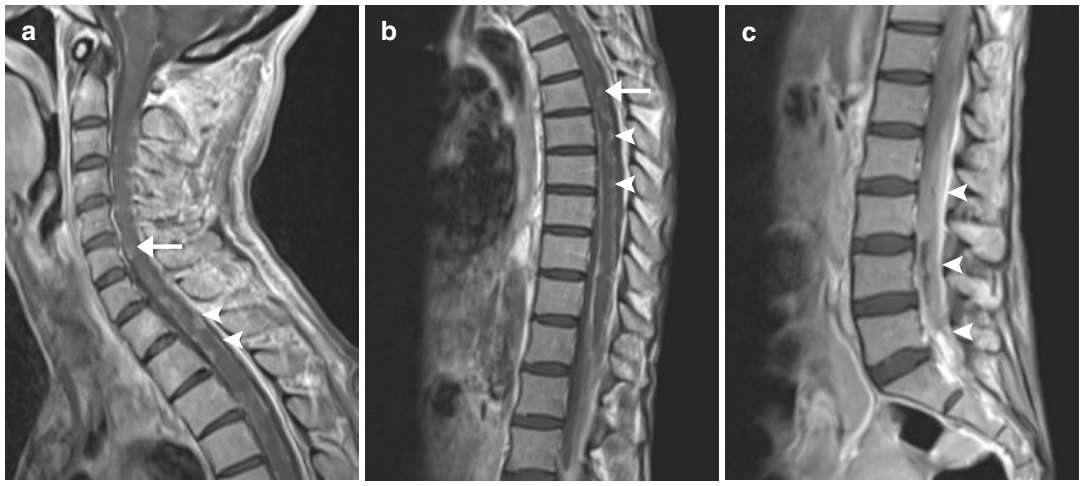

Fig. 18 Extensive spinal tuberculous leptomeningitis. (**a–c**) Sagittal contrast-enhanced T1-W MR images show nodular and linear enhancement along the spinal cord surface (arrows) and nerve roots alongside plaque-like dural thickening (arrowheads)

7 CNS Tuberculosis with HIV Co-infection

TB has seen a resurgence in the past two decades because of the increasing numbers of patients with AIDS. 5–9% of patients with AIDS develop TB, and of these, 2–18% have CNS involvement (Gupta and Kumar 2011). HIV infection is now recognized as the most common risk factor associated with extrapulmonary TB. Severe immunosuppression in advanced HIV infection increases the odds of extrapulmonary TB versus pulmonary TB alone (Leeds et al. 2012). The risk of TBM is more significant in HIV-infected patients with declining CD4 counts. Imaging characteristics of CNS TB in patients with HIV are the same as in those without HIV (Nelson and Zunt 2011).

8 Criteria for Diagnosis

A consensus case definition written by a committee of experts following an international TBM workshop convened in South Africa in May 2009 classifies TBM as definite, possible, probable, and not TBM (Marais et al. 2010; Chin and Mateen 2013). This consensus is based on a scoring system made up of four parts (Table 3), namely clinical criteria (maximum score 6), CSF criteria (maximum score 4), cerebral imaging criteria (maximum score 4), and evidence of TB elsewhere (maximum score 4). Definite TBM is defined by microbiological identification or evidence from commercial nuclei acid amplification tests of CNS *M. tuberculosis* infection. Probable TBM is defined as a score of 10 or more (when cerebral imaging is not available) or 12 or more

Table 3 Diagnostic criteria for the classification of definite, probable, possible, and not tuberculous meningitis [adapted from Marais et al. (2010)]

Criteria	Scoring
Clinical	Maximum = 6
* Evolution for more than 5 days	4
* Long-standing (more than 15 days) systemic symptoms (weight loss, fever, night sweats, persistent cough)	2 2
* History of close contact with patient suffering from pulmonary tuberculosis	1
* Focal neurological deficit (excluding cranial nerve involvement)	1
* Cranial nerve palsy	1
Biological (CSF analysis)	Maximum = 4
* Clear appearance	1
* Pleocytosis 10–500 leucocytes/μl	1
* Lymphocytic predominance (>50%)	1
* Hyperproteinorrhachia (>1 g/l)	1
* Hypoglycorrhachia (<2.2 mmol/l) or CSF-to-plasma ratio (<50%)	1
Imaging	Maximum = 6
* Hydrocephalus	1
* Basal leptomeningitis	2
* Tuberculoma	2
* Infarction	1
* Basal hyperattenuation (precontrast)	1
Manifestations of extraneurological tuberculosis	Maximum = 4
* Chest radiographs suggestive of pulmonary tuberculosis =2, miliary = 4	2/4
* CT/MRI/ultrasound imaging evidence of extraneurological tuberculosis	2
* Acid-fast bacilli or *Mycobacterium tuberculosis* cultured from biological fluids: sputum, urine, gastric washing, urine, blood culture, lymphadenopathy	4
* Positive nucleic acid amplification test from extraneurological sampling	4
No alternative diagnosis * Confirmed by microbiology, serology, or histopathology * Include pyogenic bacterial meningitis, bacterial brain abscess, cerebral toxoplasmosis, and malignancy	

(when cerebral imaging is available). Possible TBM is defined as a score of 6–9 (when cerebral imaging is not available) or 6–11 (when cerebral imaging is available). The diagnosis of not TBM is maintained if an alternative cause is identified and confirmed microbiologically.

The diagnosis of tuberculoma is difficult. Clinical features supported by indirect evidence, such as CSF examination and imaging studies of the head and spine, are used for early diagnosis. Surgical intervention is considered mandatory in patients with clinically diagnosed tuberculoma and worsening clinical or radiological features (Raza et al. 2004). A biopsy may be necessary to differentiate tuberculoma from other intracranial brain lesions, including glioma, lymphoma, metastases, and other infectious processes (Chin and Mateen 2013).

9 Treatment

The poor prognosis underlines the value of an early diagnosis, which should be established without delay, and appropriate treatment in the event of strong suspicion. Pharmacological therapy includes combination anti-TB drug regimens and adjunctive corticosteroids, which improves survival rates and neurological outcome in patients with TBM, possibly reducing hydrocephalus and preventing infarction (Schaller et al. 2019). Both the WHO and the American Thoracic Society recommend an 8-week intensive phase of treatment, during which patients receive isoniazid, rifampin, and pyrazinamide, followed by a continuation phase during which isoniazid and rifampicin are given for 6–10 months. Current recommendations include using azithromycin and clarithromycin combined with ethambutol or clofazimine, especially if the response is not satisfactory. The composition and dosing of the regimen are the same as for pulmonary TB, but for TBM, treatment duration is extended from 6–9 to 12 months (Thakur et al. 2018).

A significant increase in the frequency of adverse reactions to anti-TB therapy has been observed in patients with HIV infection. Intracranial tuberculomas that are single space-occupying lesions with midline shift and increased intracranial pressure, and which fail to respond to chemotherapy, should be surgically removed. The list of differential diagnoses is vast, and symptoms of CNS TB often present non-specifically in the early stages. Early recognition and timely treatment of the disease are critical, if the considerable mortality and morbidity associated with this condition are to be prevented.

After treatment, meningeal enhancement may persist in some cases of TBM. Potential sequelae of TBM include meningeal or ependymal calcifications, focal areas of atrophy secondary to infarcts, hydrocephaly, encephalomalacia in the areas of cerebral infarction, and occasionally syringomyelia or syringobulbia (Jinkins et al. 1995; Patkar et al. 2012). However, many lesions leave no radiological traces following successful medical treatment. The activity of a tuberculoma may be evaluated by the degree of contrast enhancement on follow-up CT or MRI (McGuinness 2000).

Occasionally, newly developing or enlarging intracranial tuberculomas may be observed, despite appropriate anti-TB therapy. This is called paradoxical reaction, which occurs in approximately one-third of patients with TBM. Paradoxical reactions in these patients result from an excessive inflammatory response against mycobacterial antigens (Bernaerts et al. 2003; Singh et al. 2016). It has been demonstrated that female gender, concomitant HIV infection, and a shorter duration of the illness are significant predictors of paradoxical reactions in patients with TBM, and the development of paradoxical reactions does not adversely affect the outcome of TBM (Singh et al. 2016).

10 Conclusion

CNS TB is one of the more severe forms of extrapulmonary TB. Early recognition and timely treatment of CNS TB are crucial in reducing the mortality and morbidity associated with this disease. Familiarity with the various imaging

presentations of CNS TB is the key to a timely diagnosis. Advanced MRI techniques help in better characterization of tuberculous lesions.

References

Afghani B (1994) Paradoxical enlargement or development of intracranial tuberculomas during therapy: case report and review. Clin Infect Dis 19:1092–1099

Aggarwal A, Patra DP, Gupta K et al (2016) Dural tuberculoma mimicking meningioma: a clinicoradiologic review of dural en plaque lesions. World Neurosurg 88:686.e1

Ahluwalia VV, Dayananda Sagar G, Singh TP et al (2013) MRI spectrum of CNS tuberculosis. J Indian Acad Clin Med 14:83–90

Almeida A (2005) Tuberculosis of the spine and spinal cord. Eur J Radiol 55:193–201

Balériaux DL, Neugroschl C (2004) Spinal and spinal cord infection. Eur Radiol 14(Suppl. 3):E72–E83

Be NA, Kim KS, Bishai WR et al (2009) Pathogenesis of central nervous system tuberculosis. Curr Mol Med 9:94–99

Benson JC, Cervantes G, Baron TR et al (2018) Imaging features of neurotoxoplasmosis: a multiparametric approach, with emphasis on susceptibility-weighted imaging. Eur J Radiol Open 5:45–51

Bernaerts A, Vanhoenacker FM, Parizel PM et al (2003) Tuberculosis of the central nervous system: overview of neuroradiological findings. Eur Radiol 13:1876–1890

Changal K, Raina AH (2014) Central nervous system manifestations of tuberculosis: a review article. J Mycobac Dis 4:2. https://doi.org/10.4172/2161-1068.1000146

Chatterjee D, Radotra BD, Vasishta RK, Sharma K (2015) Vascular complications of tuberculous meningitis: an autopsy study. Neurol India 63:926–932

Chaudhary V, Bano S, Garga UC (2017) Central nervous system tuberculosis: an imaging perspective. Can Assoc Radiol J 68:1–10

Cherian A, Thomas SV (2011) Central nervous system tuberculosis. Afr Health Sci 11:116–127

Chin JH, Mateen FJ (2013) Central nervous system tuberculosis: challenges and advances in diagnosis and treatment. Curr Infect Dis Rep 15:631–635

Davis AG, Rohlwink UK, Proust A et al (2019) The pathogenesis of tuberculous meningitis. J Leukoc Biol 105:267–280

De Jong BC, Antonio M, Gagneux S (2010) Mycobacterium africanum—review of an important cause of human tuberculosis in West Africa. PLoS Negl Trop Dis 4:e744

Garg RK, Malhotra HS, Gupta R (2015) Spinal cord involvement in tuberculous meningitis. Spinal Cord 53:649–657

Garg RK, Malhotra HS, Jain A (2016) Neuroimaging in tuberculous meningitis. Neurol India 64:219–227

Goyal M, Sharma A, Mishra NK et al (1997) Imaging of pachymeningeal tuberculosis. AJR Am J Roentgenol 169:1421–1424

Gupta RK, Kumar S (2011) Central nervous system tuberculosis. Neuroimag Clin North Am 21:795–814

Gupta RK, Poptani H, Kohli A et al (1995) In vivo localized proton magnetic resonance spectroscopy of intracranial tuberculomas. Indian J Med Res 101:19–24

Gupta RK, Husain N, Kathuria MK et al (2001) Magnetization transfer MR imaging correlation with histopathology in intracranial tuberculomas. Clin Radiol 56:656–663

Jinkins JR, Gupta R, Chang KH (1995) MR imaging of central nervous system tuberculosis. Radiol Clin North Am 33:771–786

Khatri GD, Krishnan V, Antil N et al (2018) Magnetic resonance imaging spectrum of intracranial tubercular lesions: one disease, many faces. Pol J Radiol 83:524–535

Knobbe K, Gaines M (2020) Intramedullary tuberculoma of the spinal cord. Kans J Med 13:300–303

Ku BD (2009) Extensive meningeal and parenchymal calcified tuberculoma as long-term residual sequelae of tuberculous meningitis. Neurol India 57:521

Kumar R, Pandey CK, Bose N (2002) Tuberculous brain abscess: clinical presentation, pathophysiology and treatment (in children). Childs Nerv Syst 18:118–123

Lammie GA, Hewlett RH, Schoeman JF et al (2009) Tuberculous cerebrovascular disease: a review. J Infect 59:156–166

Leeds IL, Magee MJ, Kurbatova EV et al (2012) Site of extrapulmonary tuberculosis is associated with HIV infection. Clin Infect Dis 55:75–81

Liu J, Zhang H, He B et al (2016) Intramedullary tuberculoma combined with abscess: case report and literature review. World Neurosurg 89:726.e1–726.e4

Liu X, Rui M, Lyu L (2019) Tuberculous meningomyelitis in magnetic resonance imaging: a Chinese case report. Eur J Radiol Open 6:284–286

Lu M (2010) Imaging diagnosis of spinal intramedullary tuberculoma: case reports and literature review. J Spinal Cord Med 33:159–162

Marais S, Thwaites G, Johan F et al (2010) Tuberculous meningitis: a uniform case definition for use in clinical research. Lancet Infect Dis 10:803–812

McGuinness FE (2000) Intracranial tuberculosis. In: Clinical imaging in non-pulmonary tuberculosis. Springer, Berlin Heidelberg, New York, pp 5–25

Menon S, Bharadwaj R, Chowdhary AS et al (2011) Tuberculous brain abscesses: case series and review of literature. J Neurosci Rural Pract 2:153–157

Momjian R, George M (2014) Atypical imaging features of tuberculous spondylitis: case report with literature review. J Radiol Case Rep 8(11):1–14

Nelson CA, Zunt JR (2011) Tuberculosis of the central nervous system in immunocompromised patients:

HIV infection and solid organ transplant recipients. Clin Infect Dis 53:915–926
Ogul H, Ozkurt Z, Polat G (2017) Cerebral and spinal tuberculous leptomeningitis: advanced magnetic resonance imaging findings. J Craniofac Surg 28:477–478
Parmar H, Shah J, Patkar D et al (2000) Intramedullary tuberculomas. MR findings in seven patients. Acta Radiol 41:572–577
Parmar H, Sitoh Y, Anand P et al (2006) Contrast-enhanced flair imaging in the evaluation of infectious leptomeningeal diseases. Eur J Radiol 58:89–95
Patkar D, Narang J, Yanamandala R et al (2012) Central nervous system tuberculosis pathophysiology and imaging findings. Neuroimaging Clin North Am 22:677–705
Phypers M, Harris T, Power C (2006) CNS tuberculosis: a longitudinal analysis of epidemiological and clinical features. Int J Tuberc Lung Dis 10:99–103
Raza S, Sadaf A, Fecto F et al (2004) Patterns of tuberculosis in the central nervous system. Infect Dis J Pak 13:99–104
Rich AR, McCordock HA (1933) The pathogenesis of tuberculous meningitis. Bull Johns Hopkins Hosp 52:5–37
Robertson FC, Lepard JR, Mekary RA et al (2019) Epidemiology of central nervous system infectious diseases: a meta-analysis and systematic review with implications for neurosurgeons worldwide. J Neurosurg 130:1107–1126
Rock RB, Olin M, Baker CA et al (2008) Central nervous system tuberculosis: pathogenesis and clinical aspects. Clin Microbiol Rev 21:243–261
Salvador GLO, Basso ACN, Barbieri PP et al (2021) Central nervous system and spinal cord tuberculosis: revisiting an important disease. Clin Imaging 69:158–168
Sardana V, Shringi P (2020) Intramedullary tuberculoma of the spinal cord, clinical features and imaging: possibility of early diagnosis with imaging? Indian J Tuberc 67:346–348
Schaller MA, Wicke F, Foerch C et al (2019) Central nervous system tuberculosis: etiology, clinical manifestations and neuroradiological features. Clin Neuroradiol 29:3–18
Shah GV (2000) Central nervous system tuberculosis: imaging manifestations. Neuroimaging Clin North Am 10:355–374
Sharma MC, Arora R, Deol PS (2002) Intramedullary tuberculoma of the spinal cord: a series of 10 cases. Clin Neurol Neurosurg 104:279–284
Singh AK, Malhotra HS, Garg RK et al (2016) Paradoxical reaction in tuberculous meningitis: presentation, predictors and impact on prognosis. BMC Infect Dis 16:306
Taheri MS, Karimi MA, Haghighatkhah H (2015) Central nervous system tuberculosis: an imaging-focused review of a reemerging disease. Radiol Res Pract 2015:1–8
Thakur K, Das M, Dooley KE (2018) The global neurological burden of tuberculosis. Semin Neurol 38:226–237
Udani PM (1970) Tuberculous encephalopathy with and without meningitis clinical features and pathological correlations. J Neurol Sci 10:541–561
Vaishnav B, Suthar N, Shaikh S et al (2019) Clinical study of spinal tuberculosis presenting with neuro-deficits in Western India. Indian J Tuberc 66:81–86
Varghese P, Abdul Jalal M, Kandathil J (2017) Spinal intramedullary tuberculosis. Surg J (NY) 3:e53–e57
Verdon R, Chevret S, Laissy JP (1996) Tuberculous meningitis in adults: review of 48 cases. Clin Infect Dis 22:982–988
Wang GC, Wu SW (2017) Spinal intramedullary tuberculoma following pulmonary tuberculosis: a case report and literature review. Medicine 96:49
Whiteman ML (1997) Neuroimaging of central nervous system tuberculosis in HIV-infected patients. Neuroimaging Clin North Am 7:199–214
Wilkinson RJ, Rohlwink U, Misra UK et al (2017) Tuberculous meningitis. Nat Rev Neurol 13:581–598
World Health Organization (2019) Global tuberculosis report 2019. World Health Organization, Geneva. Available at: https://www.who.int/teams/global-tuberculosis-programme/tb-reports/global-report-2019
World Health Organization (WHO) (2020) Global tuberculosis report 2020. World Health Organization, Geneva. Available at: https://apps.who.int/iris/bitstream/handle/10665/336069/9789240013131-eng.pdf
Yusuf A, Adeleke N, Babalola O et al (2015) Intramedullary tuberculoma of thoracic spinal cord in an apparently healthy Nigerian: case report. J West Afr Coll Surg 5:90–97
Zhang L, Zhang X, Li H et al (2019) Acute ischemic stroke in young adults with tuberculous meningitis. BMC Infect Dis 19:362
Zunt JR (2018) Tuberculosis of the central nervous system. Continuum (Minneap Minn) 24(5 Neuroinfectious Disease):1422–1438

Imaging of Head and Neck Tuberculosis: Lymph Nodes, Deep Neck Spaces, and Salivary Glands

Pailin Kongmebhol
and Jose Florencio Lapeña Jr

Contents

Abstract

Tuberculosis of the head and neck accounts for approximately one-third of extrapulmonary tuberculosis. From the surgical perspective, cervical lymph nodes, deep neck spaces, and salivary glands may be covered by head and neck surgery, while the ear, nose, and throat are traditionally classified under otorhinolaryngology. In this chapter, we discuss the pathophysiology, clinical features, course and complications, imaging features, imaging differential diagnosis, diagnosis confirmation, and treatment of cervical lymph nodes, deep spaces of the neck, and salivary glands. Although the imaging of tuberculosis in the head and neck is non-specific, there are some imaging clues that may help suggest the diagnosis. Imaging of important diseases that must be differentiated from tuberculosis is also covered in this chapter.

P. Kongmebhol (✉)
Department of Radiology, Faculty of Medicine, Chiang Mai University, Chiang Mai, Thailand
e-mail: mailtoann@gmail.com, pailin.k@cmu.ac.th

J. F. Lapeña Jr
Department of Otolaryngology—Head and Neck Surgery, College of Medicine—Philippine General Hospital, University of the Philippines Manila, Ermita, Manila, The Philippines
e-mail: lapenajf@upm.edu.ph, jflapena@up.edu.ph

© The Author(s), under exclusive license to Springer Nature Switzerland AG 2022

M. F. Ladeb, W. C. G. Peh (eds.), *Imaging of Tuberculosis*, Medical Radiology Diagnostic Imaging,
https://doi.org/10.1007/978-3-031-07040-2_6

Abbreviations

CT	Computed tomography
MRI	Magnetic resonance imaging
TB	Tuberculosis
US	Ultrasound

1 Introduction

Tuberculosis (TB) of the head and neck accounts for approximately one-third of extrapulmonary TB (Vaid et al. 2010). Cervical lymph nodes are the most common organs involved by TB in the head and neck region, while most neck abscesses result from ruptured tuberculous lymphadenitis or originate from nearby foci (including the salivary glands). Both conditions commonly present with a neck mass or abscess. Salivary gland TB is rare, and the clinical presentation may mimic infection or tumor. Imaging can confirm the organ or area of involvement and evaluate the extension of disease, which can help in treatment planning. There are some imaging clues that may suggest the possibility of TB; these help the clinician arrive at an early diagnosis and initiate proper treatment. Imaging can also be used for follow-up monitoring after treatment.

2 Tuberculous Lymphadenitis

2.1 Introduction

Tuberculous lymphadenitis is the most common form of extrapulmonary TB (Alvarez and McCabe 1984; Lekhbal et al. 2020), with cervical lymphadenopathy being the most common manifestation of tuberculous lymphadenitis (Dandapat et al. 1990; Mekonnen et al. 2019; Qian et al. 2019; Geldmacher et al. 2002). "Scrofula" is the classic term used for tuberculous lymphadenitis in the cervical region. Aristotle (384–322 BCE) first described scrofula on the skin of phthisic pigs, believing phthisis to be contagious (Herzog 1998), although the account of scrofula is basically derived from the classical tradition represented by Cassius Felix (447 CE) (Barlow 1980). It was Wilson (1842) who postulated an intimate relation between scrofula and tubercular consumption and that the same causes would produce one as the other, with scrofula being more of a disease of infancy than phthisis.

This disease entity is a chronic, specific granulomatous inflammation of the cervical lymph nodes with caseation necrosis. *Mycobacterium tuberculosis* is not the only causative agent; the *M. tuberculosis* complex includes *M. bovis* and *M. africanum*. Nontuberculous (previously called atypical) *Mycobacterium* spp. (NTM) that can cause tuberculous lymphadenopathy include *M. avium* and *M. intracellulare of* the *M. avium* complex (MAC), *M. kansasii, M. xenopi, M. malmoense, M. haemophilum, M. genavense, M. marinum, M. szulgai*, and *M. scrofulaceum* (Forbes et al. 2018). Cervical lymphadenitis in adults is almost exclusively caused by the *M. tuberculosis* complex, while most cases in children are caused by (atypical) NTM (Christensen and Koeppe 2010).

2.2 Pathophysiology

Mycobacteria tuberculosis can adapt to a quiescent physiological state and is noted for its complex interaction with the host that produces poorly understood disease states ranging from latent infection to active clinical disease (Gambhir et al. 2017). Tuberculous lymphadenitis may be caused by hematogenous or lymphatic dissemination from a pulmonary or extrapulmonary tuberculous focus, reactivation of latent TB, or primary involvement of such structures as the tonsils, adenoids, and Waldeyer's ring (Alvarez and McCabe 1984; Dandapat et al. 1990; Bray et al. 2015; Purohit and Mustafa 2015). A meta-analysis of 6,746 cases of tuberculous lymphadenitis from 12 African countries revealed that 52% had a history of livestock exposure, 46% had a history of consuming raw milk/meat, and 24% had a history of Bacillus Calmette–Guérin (BCG) vaccination (Mekonnen et al. 2019).

2.3 Clinical Features, Course, and Complications

The disease is indolent, with a mean duration of 3 months (7 days to 12 months) from the onset of presentation to hospitalization (Fontanilla et al. 2011; Qian et al. 2019). It usually presents as a unilateral painless neck mass, most frequently located in the posterior and anterior cervical triangles, but may also occur in the submandibular and supraclavicular lymph nodes (Dandapat et al. 1990; Artenstein et al. 1995; Qian et al. 2019). Dandapat et al. (1990) noted multiple sites of lymph node involvement, and enlarged nodes which were matted in many cases and discrete in some cases, while the rest had either an abscess or a discharging sinus. According to Qian et al. (2019), lymph nodes were generally indolent and enlarged (<3 cm in most cases but reaching diameters of 7 cm). Aside from cervical lymphadenopathy, other signs and symptoms classically associated with TB include malaise, weight loss, fever, night sweats, cough greater than 2 weeks, and cold abscess (Mekonnen et al. 2019), but constitutional symptoms are rare, except in individuals infected with the human immunodeficiency virus (HIV) (Artenstein et al. 1995). Among HIV-infected patients with extrapulmonary TB, fever is nearly universal, and the course is rapidly progressive and often fatal, if not promptly diagnosed and treated (Shafer et al. 1991).

2.4 Imaging Features

2.4.1 Ultrasound Imaging

In the early stage of disease, the lymph node is enlarged with granuloma formation. Ultrasound (US) imaging shows non-specific lymph node enlargement with hypoechoic cortical thickening, decreased hilar fat, and decreased internal vascularity (Fig. 1a). Later, caseating necrosis is formed within the granuloma. On US imaging, the necrotic area is seen as heterogeneous echoes with absent vascular flow. Displacement of vascularity to the periphery of the lymph node can be observed (Park and Kim 2014) (Fig. 1b). When the disease progresses, damage of the lymph node capsule produces peri-adenitis and aggregation of adjacent lymph nodes. US imaging at this stage shows matted lymph nodes with surrounding soft tissue edema. The infected lymph node may be ruptured due to capsular break, resulting in loculated abscess. A sinus tract connecting abscess to the skin may be present.

Chronic granulomatous inflammation may result in calcium deposition. Calcific foci appear as hyperechoic spots with acoustic shadowing

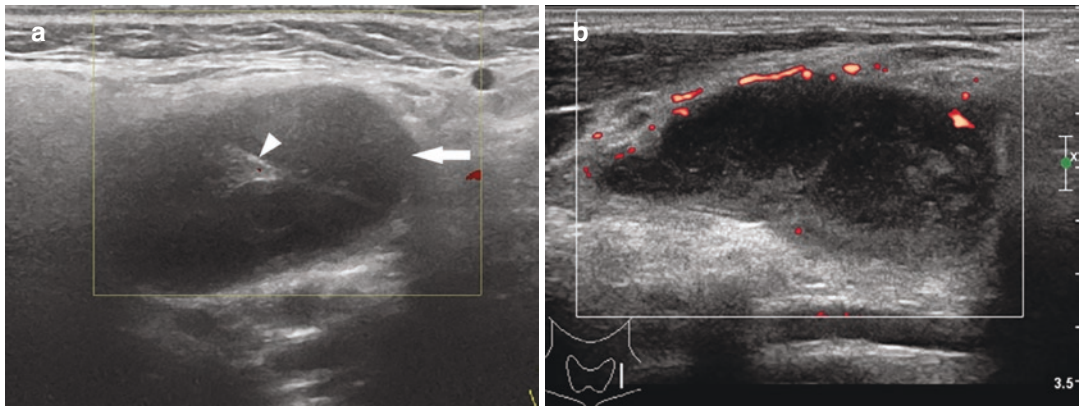

Fig. 1 Color Doppler US imaging of tuberculous lymphadenitis in two different patients. (**a**) Early change in tuberculous lymphadenitis. The lymph node is enlarged with hypoechoic cortex thickening and decreased vascular flow (arrow). The hilar fat is effaced (arrowhead). (**b**) Tuberculous lymphadenitis with internal necrosis. The lymph node shows internal heterogeneous echoes with absent internal vascular flow from caseous necrosis. Vascularity is seen at the periphery of the lymph node cortex

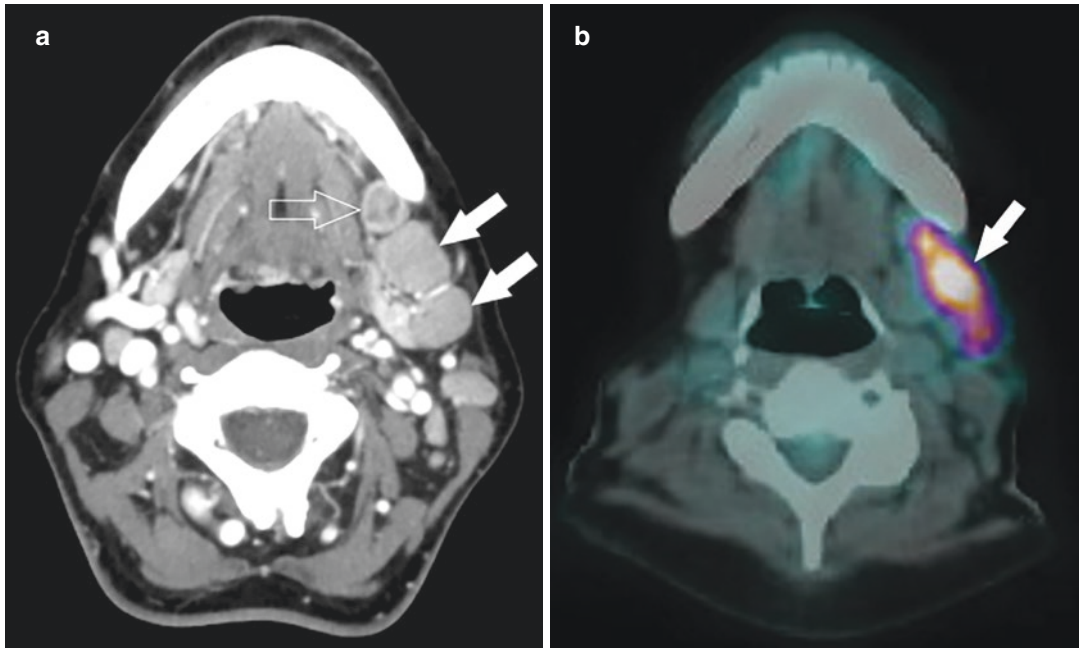

Fig. 2 CT of tuberculous lymphadenitis (granulomatous stage). (**a**) Axial contrast-enhanced CT image shows lymphadenopathy at the left submandibular region, which has homogeneous enhancement (solid arrows). One of the nodes has rim enhancement with internal heterogeneous density suggesting early-forming caseous necrosis (open arrow). (**b**) PET/CT image taken at the same level as (**a**) shows increased FDG uptake within the abnormal lymph nodes (solid arrow)

that may be observed in the lymph node. After treatment, the lymph node transforms to a fibrocalcific stage, resulting from the healing process. The fibrotic lymph node shows absent internal vascularity on color Doppler US imaging.

2.4.2 Computed Tomography

During the granulomatous stage, the enlarged lymph node appears solid with homogeneous enhancement on computed tomography (CT) (Fig. 2a). When caseous necrosis is formed, the lymph node shows internal low density with peripheral rim enhancement. The necrotic area can be uni- or multiloculated with smooth or irregular rims (Fig. 3). Perinodal fat stranding and matted lymphadenopathy can be well demonstrated on CT (Fig. 4).

Calcific foci within the necrotic lymph node are readily demonstrated on CT (Fig. 5a), but they are difficult to detect on magnetic resonance

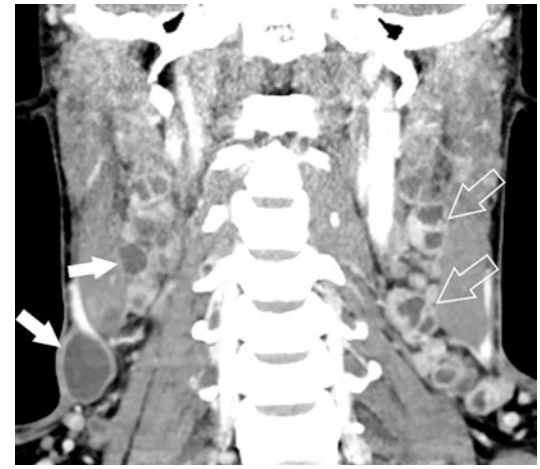

Fig. 3 Necrotic lymph nodes in tuberculous lymphadenitis. Coronal contrast-enhanced CT image shows bilateral cervical lymphadenopathy. Some of the lymph nodes show multiloculated necrosis with irregular, thick rim enhancement (open arrows), while some of them show uniloculated necrosis with smooth, thin rim enhancement (solid arrows)

imaging (MRI). Lymph node calcification can be detected on pre-treatment CT in 0–28.6% of cases (Lee et al. 1994; Je et al. 2005; Onoue et al. 2020). At a fibrocalcific stage, the healed lymph node becomes nonenhanced. Newly formed calcification can be found in 10.7% after treatment (Je et al. 2005) (Fig. 5b, c).

2.4.3 Magnetic Resonance Imaging

On MRI, the necrotic area of the lymph node appears hypointense on T1-weighted images and hyperintense on T2-weighted images and shows no enhancement. The solid granulomatous rim is T1-isointense and T2-hypointense and enhances (Fig. 6).

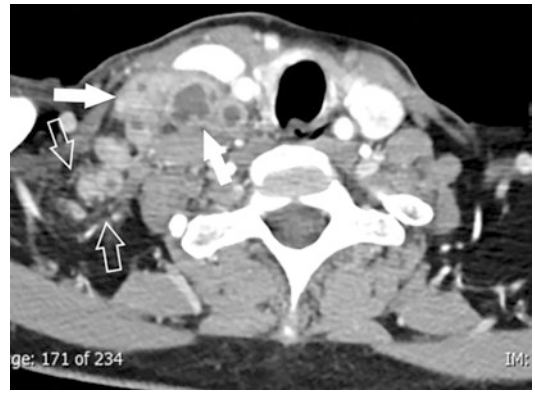

Fig. 4 Matted lymph nodes with peri-adenitis in tuberculous lymphadenitis. Axial contrast-enhanced CT image shows matted necrotic cervical lymphadenopathy (arrows) with perinodal fat stranding (open arrows)

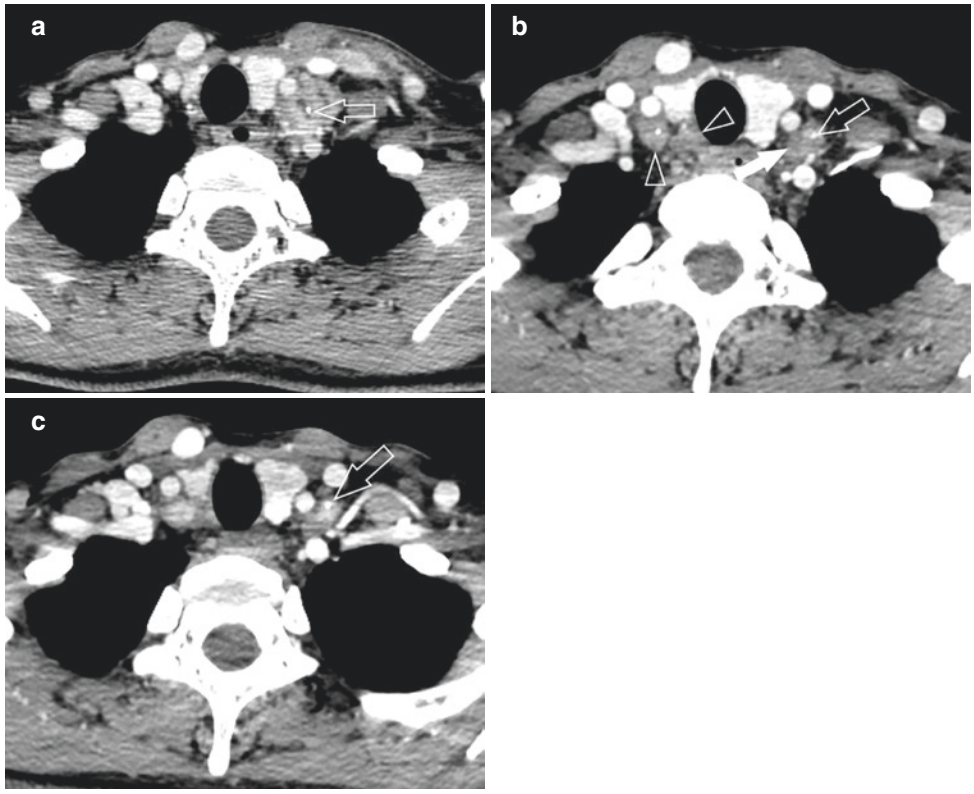

Fig. 5 Calcified lymph nodes in tuberculous lymphadenitis on pre- and post-treatment CT. (**a**) Axial contrast-enhanced CT image before treatment shows inhomogeneously enhancing lymphadenopathy in the left lower internal jugular chain with a small round internal calcification (open arrow). (**b**) Axial contrast-enhanced CT image taken after 6 months of anti-TB drug therapy shows decreased size of the lymph node with low-density change, compatible with fibrotic stage (arrow). The calcification seen on the pre-treatment CT is still present (open arrow). However, the patient has developed new right lower internal jugular and right paratracheal lymphadenopathy (open arrowheads). (**c**) Axial contrast-enhanced CT image at a more caudal level shows a new calcification in the treated lymph node (open arrow)

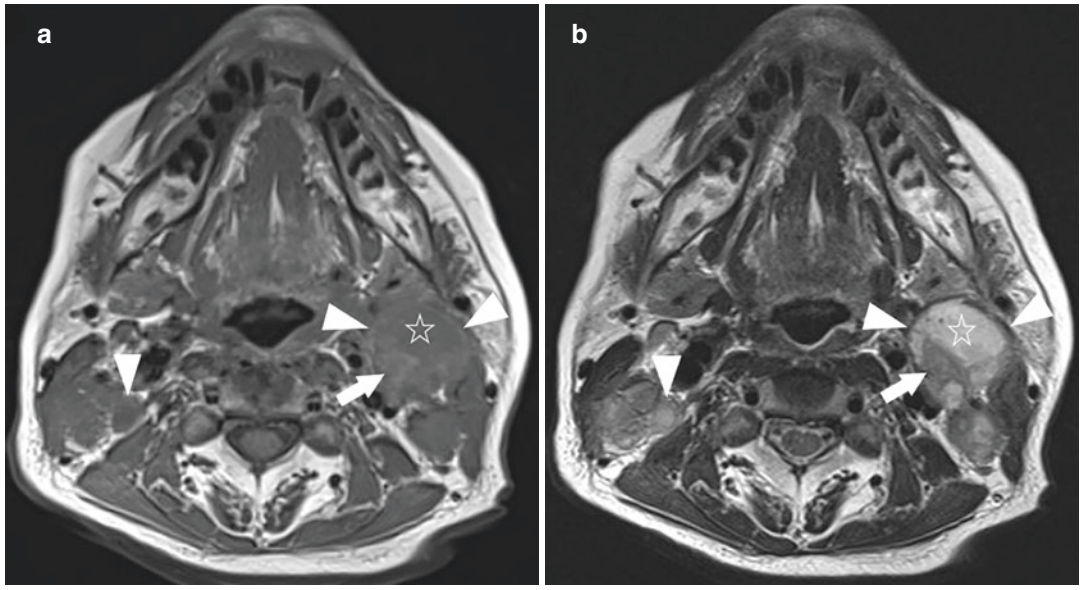

Fig. 6 MRI of tuberculous lymphadenitis. Axial (**a**) T1-W and (**b**) T2-W MR images show bilateral cervical lymphadenopathy. The necrotic area appears T1-hypointense and T2-hyperintense (open star). The solid granulomatous component (arrow) and granulomatous rim (arrowheads) are T1-isointense and T2-hypointense

2.4.4 Positron-Emission Tomography

Tuberculous lymphadenitis shows increased [fluorine-18]-fluoro-2-deoxy-D-glucose (^{18}F-FDG) uptake on positron-emission tomography (PET) (Fig. 2b). ^{18}F-FDG PET/CT demonstrates more sites of lymph node involvement than CT and may be used to predict the response of treatment (Sathekge et al. 2012). However, increased ^{18}F-FDG uptake on PET is not specific for TB, as it can be observed in other granulomatous lesions, inflammation, and malignancies.

2.5 Imaging Differential Diagnosis

The enlarged, homogeneously enhancing lymph nodes during the early granulomatous stage have no specific imaging appearance and should be differentiated from other causes of lymph node enlargement such as reactive hyperplasia, infection, malignancy, or other granulomatous diseases. However, in tuberculous lymphadenitis, multiple stages of lymphadenopathy are usually seen on imaging. Necrotic lymph nodes are usually present at the same time as the solid-appearing ones. It is the necrotic appearance, sometimes with calcifications, that helps alert to the possibility of tuberculous lymphadenitis. The important differential diagnoses of necrotic/cystic appearing lymph nodes are metastasis, pyogenic lymphadenitis, lymphoma, histiocytic necrotizing lymphadenitis (Kikuchi disease), and NTM lymphadenitis.

Squamous cell carcinoma is a major cause of necrotic or cystic appearing metastatic lymph nodes in the head and neck (Fig. 7a). Human papillomavirus (HPV)-related squamous cell carcinoma of the oropharyngeal region has a high association with cystic appearing lymph nodes. The metastatic lymph nodes from squamous cell carcinoma in non-HPV patients are more likely to have thick, irregular walls with complex-fluid content on MRI, while in HPV-positive patients, the lymph nodes are more likely to have thin, well-defined margins with homogeneous fluid content (Huang et al. 2017). Both patterns are also observed in tuberculous lymphadenitis.

Perinodal fat infiltration can be seen in extracapsular spreading of metastatic nodes and in late stages of TB. If the primary cancer cannot be demonstrated on imaging, the differentiation between tuberculous lymphadenitis and necrotic

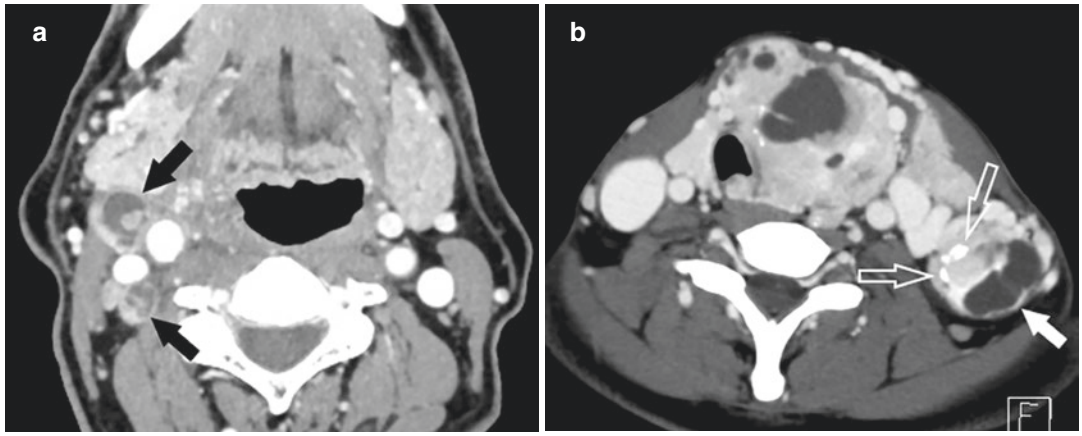

Fig. 7 Necrotic/cystic metastatic cervical lymph nodes in two different patients. (**a**) Axial contrast-enhanced CT image in a patient who has metastatic lymph nodes from supraglottic squamous cell carcinoma shows irregular rim-enhancing lymph nodes with central necrosis at right level II (arrows). (**b**) Axial contrast-enhanced CT image in a patient who has metastatic lymph nodes from papillary thyroid carcinoma shows an enlarged lymph node with a prominent enhancing solid component, cystic component (solid arrow), and coarse calcifications (open arrows). The nodes have a similar appearance to the primary carcinoma in the thyroid gland

or cystic metastatic lymph nodes can be difficult. Diffusion-weighted imaging (DWI) and apparent diffusion coefficient (ADC) values have been studied to differentiate between metastatic necrotic lymph nodes and tuberculous lymph nodes. The ADC value at the necrotic area of a metastatic lymph node is higher than that at the necrotic area of a tuberculous lymph node, and an ADC value of 1.59×10^{-3} mm^2/s has been suggested as a cutoff point for distinguishing between the two conditions (Zhang et al. 2013).

Metastasis from papillary thyroid carcinoma can produce cystic areas and calcifications within the lymph node (Fig. 7b). The enhancing solid component is more prominent, and perinodal fat stranding is not present in metastatic papillary thyroid carcinoma (Onoue et al. 2020).

Pyogenic lymphadenitis can manifest as necrotic appearing lymph nodes similar to tuberculosis, but in pyogenic lymphadenitis, the perinodal fat stranding is more prominent and is almost always present (Lee et al. 1994) (Fig. 8). Associated muscle swelling is common and more severe in pyogenic lymphadenitis.

On occasion, untreated lymphoma can have a necrotic appearance (Fig. 9). The central necrosis in lymphoma tends to be large with smooth inner margins (You et al. 2019). Perinodal fat stranding may occur if there is lymphatic obstruction. The necrotic lymph nodes in TB and lymphoma may be similar in appearance, but the number of necrotic lymph nodes compared to the total

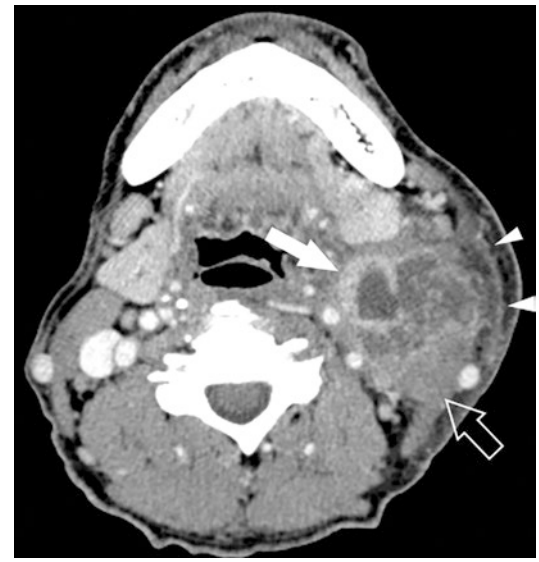

Fig. 8 Pyogenic lymphadenitis from gram-negative bacilli infection. Axial contrast-enhanced CT image shows necrotic cervical lymphadenopathy with rim enhancement (solid arrow). Note the prominent perinodal fat stranding (arrowheads) and swelling of adjacent sternocleidomastoid muscle (open arrow)

affected lymph nodes may help in differentiation. A small proportion of necrotic lymph nodes is observed in lymphoma, while a large proportion (over 50%) of necrotic lymph nodes is found in TB (You et al. 2019).

Histiocytic necrotizing lymphadenitis or Kikuchi disease is a primary lymph node disease that commonly shows internal necrosis. Some CT features in Kikuchi disease may help differentiate it from tuberculous lymphadenitis. Most lymph nodes in Kikuchi disease show multiple necrotic foci that have indistinct margins of the necrotic area (Fig. 10). Perinodal infiltration is seen in more than 90% of cases, and calcification is absent in Kikuchi disease (Lee et al. 2012). In contrast, the margin of the necrotic area in tuberculous lymphadenitis is rather well defined, and calcification may be present.

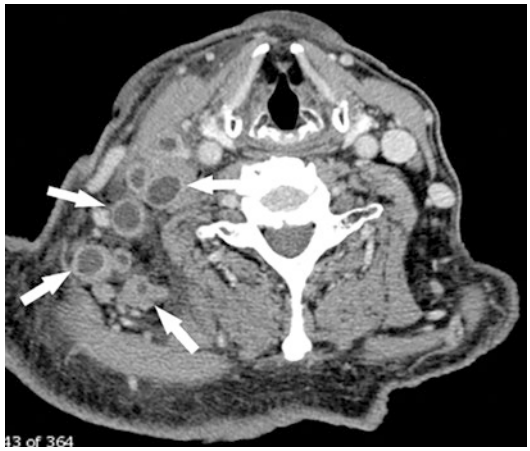

Fig. 9 Necrotic cervical lymph nodes in lymphoma. Axial contrast-enhanced CT image shows rim-enhancing lymph nodes, with large central necrosis, which have smooth inner margins (arrows). Perinodal fat stranding is also present

NTM lymphadenitis is rare. Most cases reported have been in children. The affected lymph nodes have heterogeneous enhancement with an adjacent abscess in the subcutaneous tissue, while some lymph nodes may have ring enhancement with central necrosis (Robson et al. 1999) (Fig. 11). Adjacent fat stranding is usually minimal or absent in children but may be pronounced in adults (Hanck et al. 2004). The findings are indistinguishable from tuberculous lymphadenitis.

2.6 Diagnosis Confirmation

Diagnosis is difficult due to the paucibacillary nature of the disease (Lee 2015; Purohit and

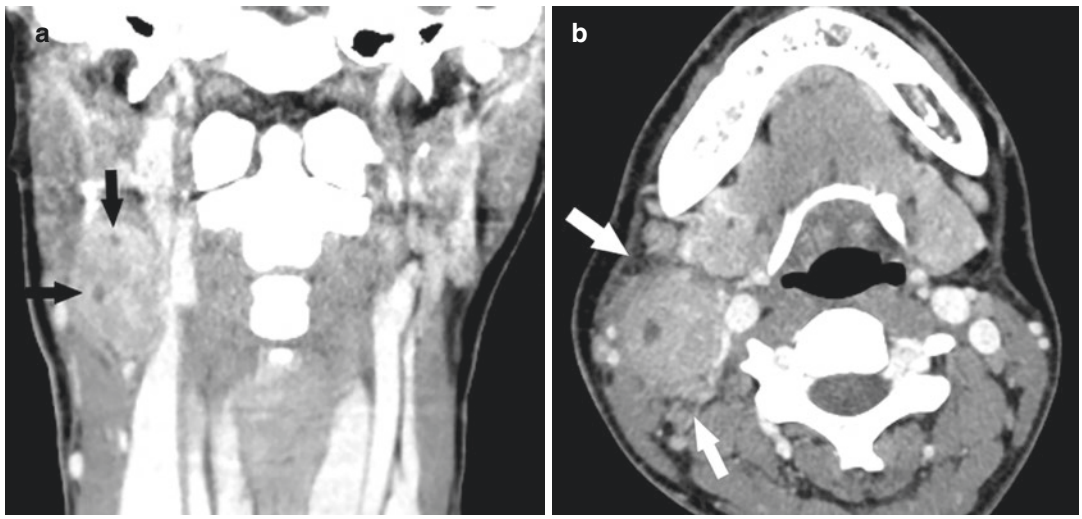

Fig. 10 Necrotic cervical lymph node in Kikuchi disease. (**a**) Coronal contrast-enhanced CT image shows multiple indistinct necrotic foci within an enlarged lymph node (black arrows). (**b**) Axial contrast-enhanced CT image shows prominent perinodal fat infiltration (white arrows) causing ill-defined margins of the lymph node

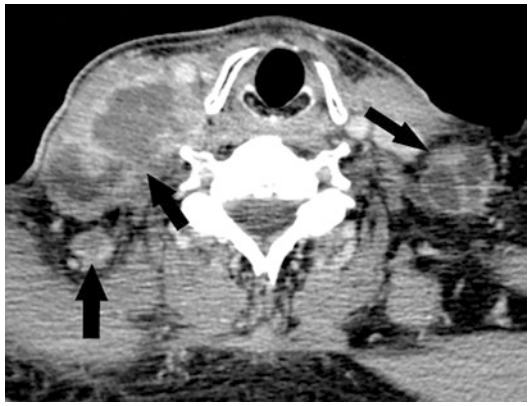

Fig. 11 Necrotic cervical lymph nodes in nontuberculous mycobacterium lymphadenitis. Axial contrast-enhanced CT image shows multiple irregular rim-enhancing lymph nodes with central necrosis (arrows). Mild perinodal fat stranding is seen

Mustafa 2015; Qian et al. 2019), variable clinical presentation, need for invasive procedures to secure appropriate samples, and lack of laboratory facilities in resource-limited settings (Purohit and Mustafa 2015). The diagnosis can be confirmed by a variety of techniques (Alvarez and McCabe 1984), although histology, acid-fast bacilli (AFB) staining, and culture remain the most widely used tests in endemic areas (Purohit and Mustafa 2015).

Excisional biopsy for histopathological and microbiological evaluations provides the highest diagnostic yield, but fine-needle aspiration (FNA) may be useful for HIV-infected individuals and in areas of the world with a high prevalence of disease (Artenstein et al. 1995). Granulomatous inflammation may be seen on histological or cytological analysis of excision or aspiration biopsies, although histological features may be atypical at extrapulmonary sites and in patients with concomitant immunosuppression (Purohit and Mustafa 2015). In a series of 80 cases, fine-needle aspiration cytology (FNAC) gave a positive diagnosis in 66 cases (83%). 52 cases (65%) showed a positive culture for *M. tuberculosis* of human type in Lowenstein-Jensen medium (Dandapat et al. 1990).

Fontanilla et al. (2011) reported that excisional biopsy has the highest sensitivity at 80%, but FNA is less invasive and may be useful, especially in immunocompromised hosts and in resource-limited settings. Geldmacher et al. (2002) found that lymph node excision and FNA were similarly effective in obtaining sufficient material for microscopic and microbiological analysis. Whenever practical, every effort should be made to obtain appropriate specimens for both mycobacteriological and histopathological examinations (Lee 2015). Sputum tests do not have a good performance, and most cases are diagnosed by FNAC and excision biopsies in combination with clinical presentation (Qian et al. 2019). The results of skin testing with purified protein derivative (PPD) are invariably positive (Dandapat et al. 1990; Artenstein et al. 1995; Geldmacher et al. 2002).

The definitive diagnosis is by culture or nucleic amplification (Fontanilla et al. 2011). The measurement of biochemical markers in TB-affected fluids (adenosine deaminase or gamma interferon) and molecular biology techniques such as polymerase chain reaction (PCR) may be useful adjuncts in diagnosis (Lee 2015). More sophisticated techniques are available (Ryu 2015), but are beyond the reach of the majority of patients, physicians, and public health workers in the most endemic areas. In such resource-poor settings, indirect evidence may be the mainstay for the diagnosis (Purohit and Mustafa 2015).

2.7 Treatment

Although the disease usually responds to standard anti-TB drug therapy, the ideal regimen and duration of treatment have not yet been established (Lee 2015), and regimens range from 6 (Artenstein et al. 1995) to 9 months (Dandapat et al. 1990). The response to treatment is slower than with pulmonary TB, and persistent pain and swelling are common (Fontanilla et al. 2011). Despite standard treatment, initial enlargement of the lymph nodes (paradoxical upgrading) frequently occurs during therapy (Geldmacher et al. 2002; Fontanilla et al. 2011; Lee 2015).

Opinions on the role of surgery range from "not required" (Dandapat et al. 1990), through "required mainly to obtain valid diagnostic

specimens and to manage complications" (Lee 2015), to "initial excisional biopsy deserves consideration for both optimal diagnosis and management of the otherwise slow response to therapy" (Fontanilla et al. 2011). Kanjanopas et al. (2014) concluded that surgical treatment for all accessible lymph nodes greater than or equal to 3 cm in diameter in patients with tuberculous cervical lymphadenitis prior to a full course of drug therapy significantly increases the cure rate, compared to medication alone. A retrospective cohort study by Lekhbal et al. (2020) involving 104 patients recommends surgical excision for nodes greater than or equal to 3 cm in diameter, abscesses, fistulas, recurrence, resistance to anti-TB drugs, and paradoxical upgrading reactions.

3 Tuberculous Neck Abscess

3.1 Introduction

The deep neck spaces are potential spaces between the three layers of deep fascial planes of the neck. These are the superficial, middle, and deep layers of deep cervical fascia and include the suprasternal, pretracheal, retropharyngeal, retrovisceral, danger, and prevertebral spaces (Grodinsky and Holyoke 1938; Feigl 2015). The hyoid bone divides the anterior spaces into suprahyoid (peritonsillar, submandibular, parapharyngeal, masticator, buccal, and parotid spaces) and subhyoid (superior visceral space), whereas spaces posterior to the hyoid extend the whole length of the neck (e.g., retropharyngeal, danger, prevertebral, and carotid spaces) and into the mediastinum (Sutcliffe and Lasrado 2020).

Deep neck space infections are rare. A 10-year nationwide population-based survey of the incidence of parapharyngeal and retropharyngeal abscess in Taiwan revealed an annual incidence rate of 2.43–3.17 per 100,000 adults between 2007 and 2016 (Yang et al. 2021). This was higher than the figures of 1.32–1.94 per 100,000 people older than 15 years old in Germany (Windfuhr and Chen 2019), 0.55–2.45 per 100,000 people older than 16 years old from 2012 to 2016 in Scotland (Hurley et al. 2018), and 3–5 per 100,000 including pediatric patients for 1991–2011 in England (Lau et al. 2014). Deep neck space infection of tuberculous origin is even rarer. An 8-year review of 234 patients with deep neck infections identified only six cases of TB (Ridder et al. 2005), although another series of 270 patients identified 28 cases of TB (Gujrathi et al. 2016).

Retropharyngeal tuberculous abscesses have been found to be associated with Pott disease of the cervical spine (Öktem et al. 2006; Mizumura et al. 2010; Alawad and Khalifa 2015; Thomas et al. 2020), TB of the upper cervical spine and sternum (Al Soub 1996), and cervical Pott disease and tuberculous abscess of the chest wall (Hsu and Chen 2019). Retropharyngeal tuberculous abscess has also been reported with no evidence of cervical spine TB (Patil et al. 2011; Christoforidou et al. 2012). Tuberculous retropharyngeal abscess has also been reported along with pulmonary TB, without involvement of the cervical spine (Ekka and Sinha 2015). Even rarer are isolated parapharyngeal tuberculous infections (Rao et al. 2013; Sabri 2015; Gopakumar et al. 2019), with a case of bilateral parapharyngeal space tuberculous abscess reported (Meher et al. 2006).

3.2 Pathophysiology

The fascia and fascial spaces of the head and neck were described in detail by Grodinsky and Holyoke (1938) and revisited and clarified by Feigl (2015). For instance, the danger space number 4 of Grodinsky and Holyoke (1938) extends from the skull base cranially to the posterior mediastinum caudally and is limited ventrally by the alar fascia (the superficial layer of deep cervical fascia or fascia intercarotica of Fiegl (2015)) and dorsally by the deep layer of deep cervical fascia (the fascia prevertebralis of Feigl (2015)).

The more ventral retropharyngeal space extends from the skull base to the upper mediastinum between the pharynx and prevertebral musculature (Hsu and Chen 2019), bounded by fascia anteriorly and posteriorly and the carotid space laterally (Debnam and Guha-Thakurta 2012); but its actual extent and boundaries are disputed by Feigl (2015) as misinterpretations of the very precise and profound descriptions of Grodinsky and Holyoke (1938). Not all the potential spaces are totally empty, or always so; the retropharyngeal lymph nodes of Rouviere (1938) are normal in children but regress in puberty (Costa et al. 2011; Debnam and Guha-Thakurta 2012).

Deep neck infections involve potential spaces and actual fascial planes. For instance, acute retropharyngeal abscesses from infected nodes that drain lymph from the ear, nose, and throat are usually seen in young children below 5 years of age (Christoforidou et al. 2012), while acute retropharyngeal abscesses in adults may result from foreign bodies, penetrating injuries, endotracheal intubation, or endoscopic procedures (Harkani et al. 2011; Patil et al. 2011). On the other hand, chronic retropharyngeal abscesses are commonly seen in adults and are usually of tuberculous etiology (Hsu and Chen 2019). They are usually due to tuberculous involvement of the cervical spine, spreading by direct erosion (Raza and Rahat 2010; Hsu and Chen 2019) or via the lymphatics to a persisting retropharyngeal lymph node (Patil et al. 2011). Tuberculous deep neck space infections or retropharyngeal abscesses may also originate from pulmonary or extrapulmonary TB at other sites. In rare cases, pulmonary TB can spread hematogenously and form an abscess in the retropharyngeal space (Meher et al. 2006).

3.3 Clinical Features, Course, and Complications

The clinical presentation of deep neck space tuberculous infections is related to the space involved and extent of infection. Common presentations of retropharyngeal abscesses include chronic dysphagia (Thomas et al. 1995; Christoforidou et al. 2012), neck pain and dysphagia (Menon and Baruah 2014), neck pain, dysphagia, and odynophagia (Hsu and Chen 2019). Neck pain, dysphagia, and headache can also occur (Kosmidou et al. 2020). Presentations may range from indolent odynophagia and neck pain for 2 months, without any other constitutional symptoms (Ekka and Sinha 2015), to insidious-onset fever, neck pain, dysphagia, and hoarseness of voice (Al Soub 1996) and to more fulminant fever, odynophagia, torticollis, and trismus (Harkani et al. 2011).

In children particularly, retropharyngeal tuberculous abscesses may present as obstructive sleep apnea (OSA) (Zafereo and Pereira 2008; Koçak et al. 2017; Weldetsadik et al. 2019), although new-onset and worsening stertor or snoring, with signs and symptoms of OSA, has been reported in an adult (Patel and Hinni 2013). In other cases, neurological deficits may occur, ranging from retropharyngeal tuberculous abscess with isolated twelfth nerve palsy (Gunawardana et al. 2004) to Horner syndrome (Raza and Rahat 2010) and to a large cervicothoracic spinal tuberculous abscess extending from C5 to T3 vertebrae causing spinal cord compression and presenting with weakness of the right hand and unsteady gait (Manoharan et al. 2013).

Many tuberculous abscesses are "cold," presenting without the usual signs of inflammation such as hyperemia and heat (in contrast to other bacterial infections), and the classic symptoms of TB (night sweats, weight loss, cachexia, fever) may not be present. However, neck rigidity, external neck swelling, and airway obstruction may occur in more severe cases (Christoforidou et al. 2012). Indeed, tuberculous deep neck space abscesses may become fatal by extension into the carotid sheath, cause airway obstruction from direct mass effect or tracheobronchial aspiration from spontaneous rupture, and spread into the mediastinum (causing mediastinitis and empyema thoracis) or even septic shock, with mortality rates as high as 50% (Mizumura et al. 2010; Hsu and Chen 2019).

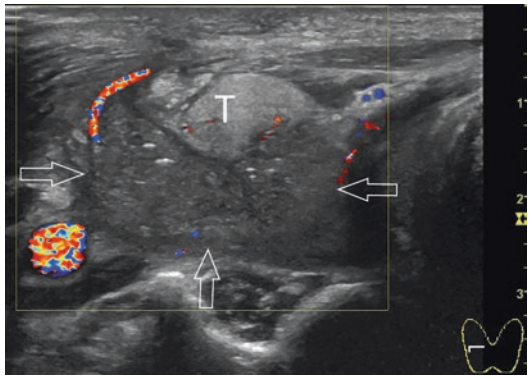

Fig. 12 US imaging of neck tuberculous abscess. Transverse color Doppler US image taken at the level of the thyroid gland in a patient who presented with neck pain and right neck mass shows echogenic fluid collection (open arrows) posterior to the thyroid right lobe (T) causing anterior displacement of the thyroid gland. The fluid collection has peripheral vascular flow at the rim and absent vascular flow in the center

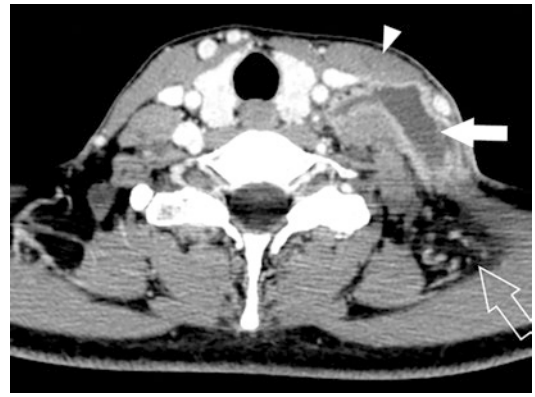

Fig. 13 Tuberculous neck abscess from ruptured tuberculous lymphadenitis. Axial contrast-enhanced CT image shows a loculated rim-enhancing fluid collection in the left posterior cervical space (arrow). The patient had US imaging of the neck 6 weeks before CT, which showed left cervical lymphadenopathy with internal necrosis at the same area as an abscess (see Fig. 1b). Note that the adjacent sternocleidomastoid muscle appears normal (arrowhead). Minimal fat stranding is present in the posterior cervical space (open arrow)

3.4 Imaging Features

3.4.1 Ultrasound Imaging

Abscess collections due to TB have a similar appearance to abscesses elsewhere in the body. An irregular area of echogenic fluid collection in the neck space with absent internal vascular flow on color Doppler US study typical for an abscess can be demonstrated in the superficial neck spaces (Fig. 12). Sometimes, moving internal echogenic content suggestive of fluid can be demonstrated on US images. An abscess in the deep neck space such as in the retropharyngeal space cannot be explored with US imaging and should be evaluated with CT or MRI.

3.4.2 Computed Tomography

CT better demonstrates extension of tuberculous abscesses in the neck, especially in deep locations. The abscess collection shows irregular rim enhancement with central low density (Fig. 13). The abscess may be present in the area of tuberculous lymphadenitis, such as in the retropharyngeal space, posterior cervical space, submandibular space, and submental space. Some abscesses may extend from the adjacent primary organ infection, such as in the peritonsillar region from tonsillitis, or prevertebral space from spinal infection. Adjacent fat stranding and muscle thickening are absent, or mild to moderate in degree (Lee et al. 1994).

3.4.3 Magnetic Resonance Imaging

Tuberculous abscesses have the same MRI characteristics as other causes of abscess formation. Findings of a hyperintense rim with central hypointense content on T1-weighted MR images, or penumbra sign, and hypointense rim with central hyperintense content on T2-weighted MR images, are highly suggestive of an abscess (McGuinness et al. 2007; Chun et al. 2018) (Fig. 14). Peripheral rim enhancement with central nonenhancing contents is a typical finding.

3.5 Imaging Differential Diagnosis

The major differential diagnosis is pyogenic abscess. Compared to tuberculous abscess, a pyogenic abscess shows more severe adjacent

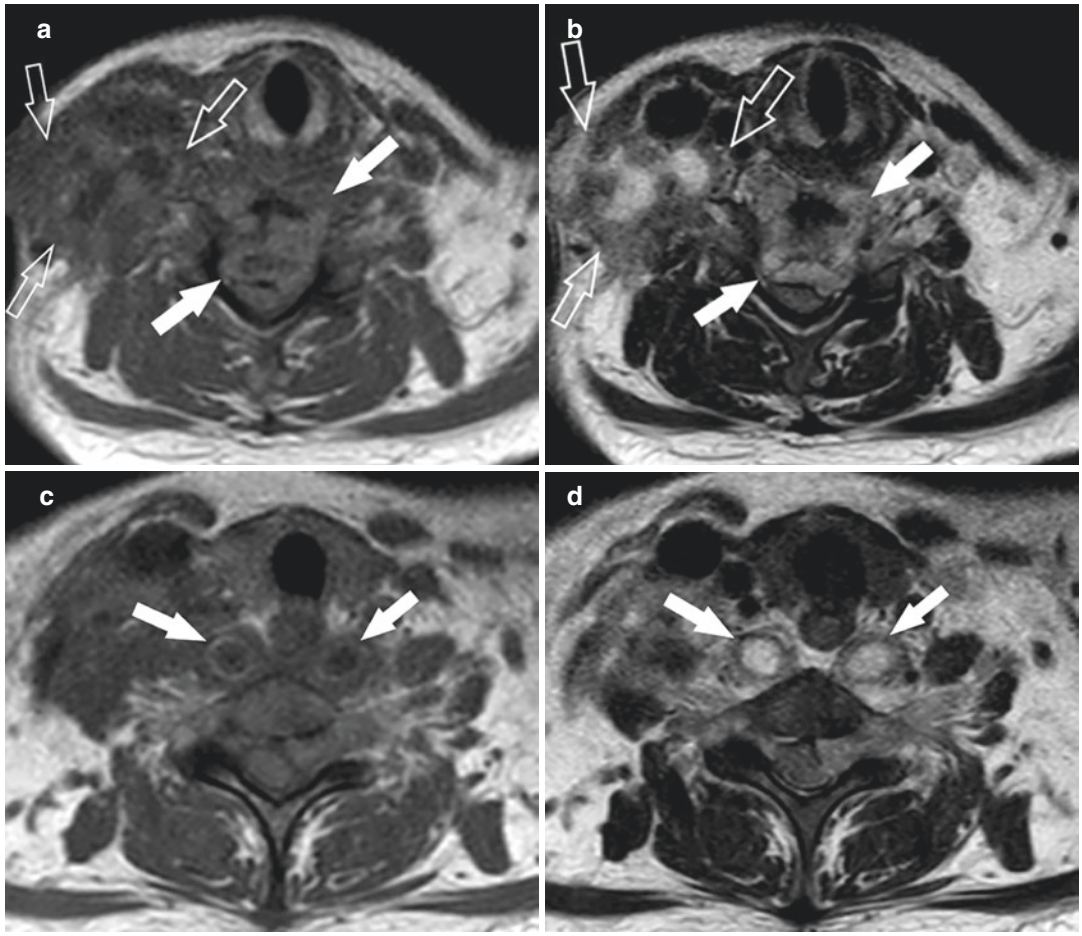

Fig. 14 Tuberculous neck abscesses in a woman who has underlying end-stage renal disease with disseminated TB of the brain, lung, lymph nodes, spine, and adrenal glands. Axial (**a**) T1-W and (**b**) T2-W MR images show a right neck abscess, which is T1-hypointense and T2-hyperintense at the center and has an irregular T1-hyperintense and T2-hypointense rim (open arrows). The patient also has tuberculous spondylodiscitis with a large anterior epidural abscess (solid arrows) at C5–6 vertebrae. Axial (**c**) T1-W and (**d**) T2-W MR images of the lower cervical spine show bilateral prevertebral abscesses (arrows), which have a characteristic T1-hypointense and T2-hyperintense center and a T1-hyperintense and T2-hypointense rim. The abscesses extend from the spondylodiscitis at C5–6 level

soft tissue reaction. The fat infiltration, subcutaneous tissue swelling, and adjacent muscle thickening are more prominent than in tuberculous abscess (Lee et al. 1994) (Fig. 15).

3.6 Diagnosis Confirmation

A high index of clinical suspicion is needed, along with a careful history and physical examination, since many deep neck infections are not evident on palpation or visual inspection (Gujrathi et al. 2016). Early diagnosis is the key to definitive treatment and is based on clinical suspicion particularly in an endemic area, radiological features, bacteriology cultures, histopathology, and PCR test (Christoforidou et al. 2012). Needle aspiration can be both diagnostic and therapeutic and may be performed under ultrasound or CT guidance, avoiding the

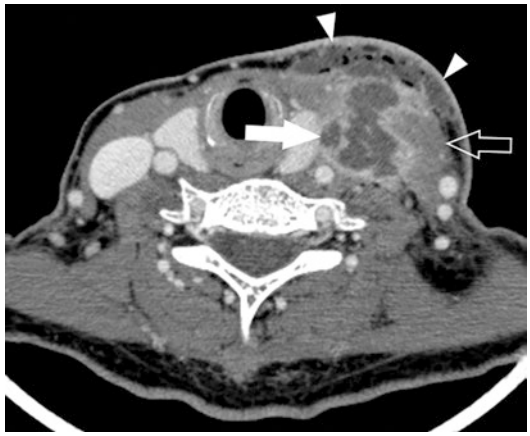

Fig. 15 Pyogenic neck abscess in a patient who has underlying diabetic mellitus. Axial contrast-enhanced CT image shows an irregular rim-enhancing fluid collection in the left carotid space (solid arrow). Note the swelling of adjacent sternocleidomastoid muscle (open arrow), clouding and swelling of the subcutaneous fat, and thickening of the overlying skin (arrowheads). These features are more severe than those of tuberculous abscess. Pus culture showed *Klebsiella pneumoniae*

need for more invasive surgical drainage (Mizumura et al. 2010; Manoharan et al. 2013; Martin et al. 2014; Menon and Baruah 2014; Kosmidou et al. 2020). Aspirates can be submitted for AFB stains and microbiological culture and sensitivity, as well as microscopic examination by PCR gene probe (Menon and Baruah 2014; Kosmidou et al. 2020).

3.7 Treatment

If an abscess is large enough to be clinically detected, surgical drainage is indicated through the best access route (transoral or external cervical) using traditional incision or needle aspiration (Meher et al. 2006; Mizumura et al. 2010), although there may be room for closely monitored conservative treatment alone with anti-TB drugs (Al Soub 1996; Ekka and Sinha 2015). However, it may be more prudent and effective to combine aspiration, which is both diagnostic and therapeutic, with anti-TB therapy (Mizumura et al. 2010; Manoharan et al. 2013; Martin et al. 2014; Menon and Baruah 2014; Kosmidou et al. 2020). In all cases, the decision to choose aspiration and antibiotic therapy over surgical drainage should consider airway protection (Gujrathi et al. 2016). The duration of combination TB therapy for extrapulmonary TB ranges between nine and 12 months (Menon and Baruah 2014; Hsu and Chen 2019).

4 Salivary Gland Tuberculosis

4.1 Introduction

The first recorded case of parotid gland TB in the English literature was reported by De Paoli in 1893 (Chaudhary 1997). Salivary gland TB ranked second to cervical lymphadenopathy among 128 cases of head and neck TB, out of 1,315 cases of TB (Menon et al. 2007). TB of the salivary glands should be included in the differential diagnosis of a possible salivary gland mass, especially when the patient is from a low socioeconomic group with poor hygiene standards, is malnourished, and is from an endemic area (Ataman et al. 1992). Salivary gland TB is also more common in immunosuppressed patients (Tauro et al. 2011), reflected, for example, in the general increase in the proportion of extrapulmonary TB along with the rise of HIV infection (Al-Serhani 2001).

4.2 Pathophysiology

According to Dadwal (2011), primary TB is a common cause of granulomatous disease of the salivary glands, is usually unilateral, and is more common in the parotid gland. Primary salivary gland TB may arise from a preceding tooth or possible tonsil infection, and direct extension to the salivary gland parenchyma by the bacillus may occur through the duct system (Tauro et al. 2011; Gupta et al. 2012). Consumption of unpasteurized raw milk may be a source of contamination by *M. bovis* (Belatik et al. 2019). An unusual

route of infection of intraparotid and periparotid lymph nodes is by lymphatic drainage from the oral cavity. Hematogenous spread from a pulmonary focus has also been identified (Garg et al. 2010). Primary TB of the salivary gland occurs in two forms, namely as an acute inflammatory lesion mimicking acute suppurative sialadenitis or as a chronic tumorous lesion (Ataman et al. 1992; Dadwal 2011). Secondary TB refers to the involvement of the salivary glands by TB in the setting of systemic TB infection, particularly pulmonary TB (Dadwal 2011). Unlike primary TB, secondary TB involves the submandibular and sublingual glands more frequently than the parotid glands (Dadwal 2011).

4.3 Clinical Features, Course, and Complications

Tuberculous disease is very difficult to distinguish clinically from other possible diffuse diseases of the salivary glands. Such nonneoplastic disorders affecting the salivary glands include chronic sialadenitis, sarcoidosis, animal scratch disease, actinomycosis, and Sjogren syndrome (Dadwal 2011). The rate of growth may be a distinguishing factor, as other benign salivary gland neoplasms grow slowly over years, compared to a few months in a tuberculous mass (Tauro et al. 2011). This rate of growth gradually increases painlessly over a period of 2–6 months on average (Belatik et al. 2019). However, clinical symptoms may vary from an acute infectious process to an indolent chronic presentation (Garg et al. 2010). Parotid gland TB mostly presents as a localized and progressive chronic swelling (Garg et al. 2010). The swelling may be firm and hard, sometimes nodular, with varying degrees of fixation resembling a tumor, but fistulization may reveal the tuberculous etiology (Belatik et al. 2019). Constitutional symptoms of TB are usually absent. In addition, there may often be no evidence of active TB in other parts of the body (Ataman et al. 1992).

4.4 Imaging Features

The TB mycobacteria may involve the parenchyma of the salivary gland, intraglandular lymph node, or both. The parotid gland is the only major salivary gland that has lymph nodes embedded within its parenchyma, so the intraglandular lymph node pattern is only observed in the parotid gland.

4.4.1 Ultrasound Imaging

In the parenchymal type of salivary gland TB, US imaging shows diffuse enlargement of the salivary gland with hypoechoic or heterogeneous echoic changes of the parenchyma (Chou et al. 2004). Anechoic or marked hypoechoic areas with absent interval vascular flow from abscess formation may be present. Intraparotid lymphadenopathy is usually multiple, located in the superficial lobe, and 6 mm or larger in size. The enlarged lymph node has marked hypoechoic cortex thickening with decreased or absent hilar fat, which is a non-specific feature. As US imaging has limitations in the evaluation of deep lobe parotid involvement; CT or MRI is better for assessment, particularly if there is extension into the deeper tissues.

4.4.2 Computed Tomography

On contrast-enhanced CT, parenchymal involvement is seen as enlargement of the affected salivary gland with diffusely increased parenchymal enhancement, compared to the unaffected side (Fig. 16a). Intraparotid lymphadenopathy may be homogeneous or show areas of low density from caseous necrosis, together with rim enhancement (Fig. 16b). The enhancing solid rim can be smooth and thin or irregular and thick (Sah et al. 2016). If a dominant lymph node is present, the appearance of a solid mass or a mass with internal cystic/necrotic components may mimic a salivary gland tumor (Fig. 17). On occasion, a rim-enhancing fluid collection typical of abscess may be present within the parenchyma (Fig. 18). There is usually accompanying surrounding

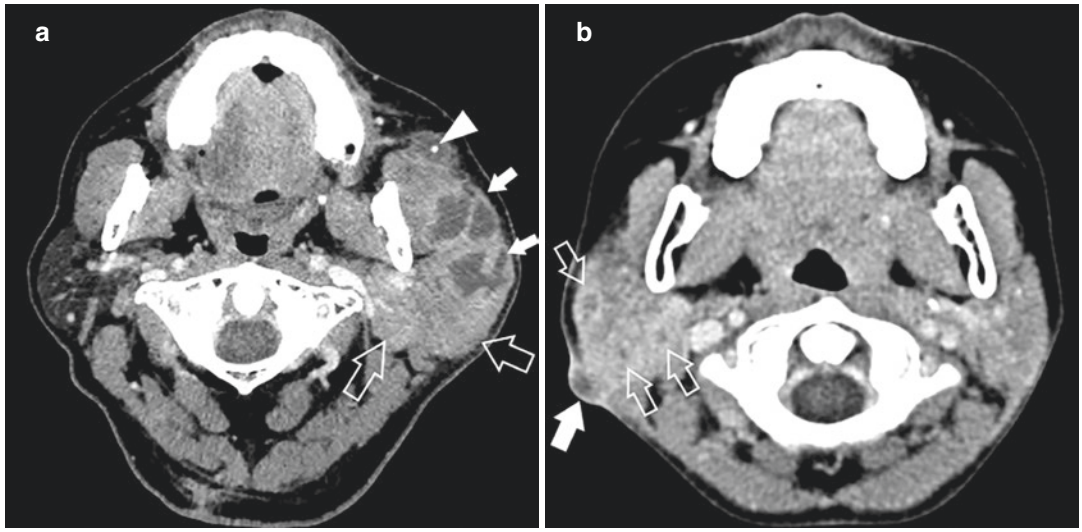

Fig. 16 Parenchymal and lymph node involvement in parotid tuberculosis in two different patients. (**a**) Axial contrast-enhanced CT image shows diffuse enlargement and increased enhancement of the left parotid gland (open arrows) with multiple parotid lymph nodes showing irregular thin rim enhancement with central necrosis (small solid arrows). A small round calcification (arrowhead) is present in a necrotic lymph node within an accessory parotid tissue overlying the left masseter muscle. (**b**) Axial contrast-enhanced CT image in another patient shows multiple low-density intraparotid lymph nodes with rim enhancement in the right parotid gland (small open arrows). The right parotid gland is slightly enlarged with increased parenchymal enhancement. A rim-enhancing periparotid lymph node with central low density is also present (solid arrow)

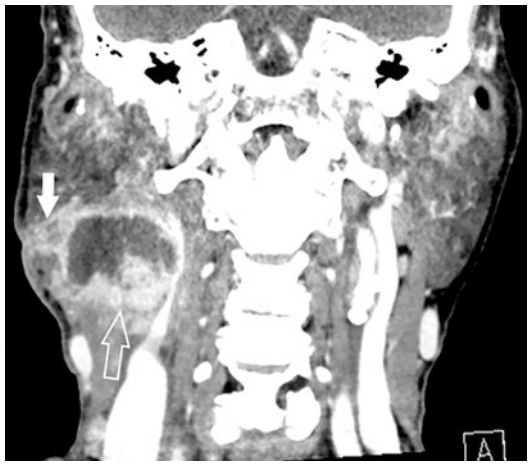

Fig. 17 Parotid tuberculosis presenting as a mass. Coronal contrast-enhanced CT image shows a mass with ill-defined margins in the right parotid tail (open arrow). The mass has internal enhancing solid nodules and a large necrotic component. Note the adjacent parotid parenchymal enhancement (arrow)

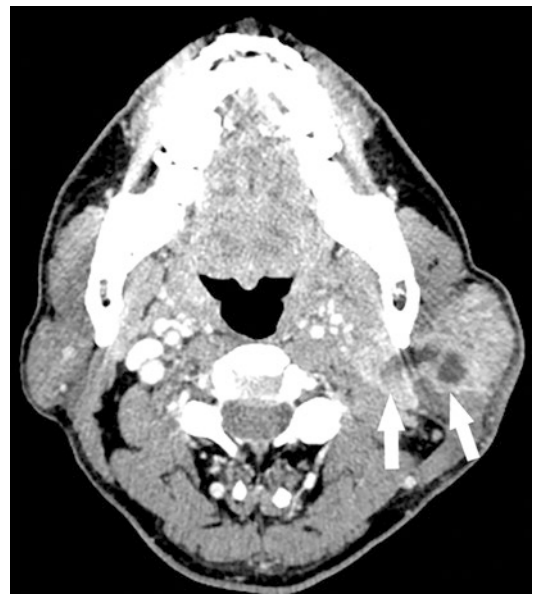

Fig. 18 Abscess formation in parotid tuberculosis. Axial contrast-enhanced CT image shows an irregular rim-enhancing fluid collection typical of an abscess in the superficial lobe of left parotid gland with extension to the deep lobe (arrows). The surrounding left parotid parenchyma shows increased enhancement with enlargement of the gland compared to the normal right side

parenchymal enhancement. Associated fat stranding and overlying fascial thickening are usually seen. Fistulation to the skin may be observed in late stages. Calcifications may be present but do not help in diagnosis, since other conditions may produce intraglandular calcifications, such as sialolithiasis or chronic sialadenitis.

4.4.3 Magnetic Resonance Imaging

On MRI, lymphadenopathy in the salivary gland shows isointense signal on T1-weighted images, hyperintense signal on T2-weighted images, hyperintense signal from restriction on DWI, and hypointense signal on the ADC map (Zhang et al. 2018).

4.5 Imaging Differential Diagnosis

The differential diagnosis of salivary gland TB depends on the pattern of involvement. The parenchymal pattern of salivary gland TB, which is seen as diffuse salivary gland enlargement with increased enhancement, can be observed in sialadenitis from other causes such as bacterial or viral sialadenitis. The multiple intraparotid lymph nodes detected on imaging should be differentiated from lymphoid hyperplasia in autoimmune disease, lymphoma, Warthin tumor, and metastasis. If there is one dominant lymph node mimicking a mass, the disease should be differentiated from benign and malignant tumors such as pleomorphic adenoma, Warthin tumor, mucoepidermoid carcinoma, adenoid cystic carcinoma, and metastasis. Frank abscess formation should be differentiated from acute bacterial suppurative sialadenitis.

In acute bacterial suppurative sialadenitis, the gland enlargement and parenchymal enhancement, as well as abscess formation, are indistinguishable from tuberculous sialadenitis on imaging (Fig. 19). The degree of overlying fascia thickening, fat stranding, and skin thickening are similar to tuberculous infection. Clinical features of acute painful swelling of the affected area may suggest acute bacterial infection rather than TB. However, the diagnosis is based on bacteriological confirmation.

Warthin tumor may present as a single mass or multiple masses within the salivary gland. Warthin tumor usually contains internal cystic components, which lack rim enhancement or may have smooth, very thin rim enhancement (Fig. 20), while the rim enhancement of necrotic lymph nodes in TB tends to be thicker and sometimes irregular. Lymphoma may present as a single mass within the salivary gland or as multiple intraglandular lymph nodes. Occasionally, untreated lymphoma shows areas of tumor necrosis. The necrotic area within the lymphoma usually shows no rim enhancement or faint thin rim enhancement (Fig. 21), different from TB which always shows distinct rim enhancement.

Other tumors such as pleomorphic adenoma, adenoid cystic carcinoma, mucoepidermoid carcinoma, and parotid lymph node metastasis may contain internal cystic or necrotic components, similar to TB. However, in these tumors, the surrounding parotid parenchyma usually shows normal enhancement, while in TB, it is common to see surrounding parenchymal enhancement (Fig. 22).

4.6 Diagnosis Confirmation

A presumptive diagnosis of tuberculous sialadenitis should be considered in patients presenting with a salivary gland mass and if there is evidence of TB elsewhere in the body (Ataman et al. 1992; Bottini et al. 2007). The diagnosis can be made from saliva specimens, but is particularly difficult if glandular secretions from Wharton duct or saliva are negative for AFB (Ataman et al. 1992; Bottini et al. 2007). However, in cases where no lesion is detectable elsewhere, FNAC, tissue culture, or histopathology has been utilized (Tauro et al. 2011). The specimen can be subjected to AFB staining.

The PCR test for *M. tuberculosis* is a reliable diagnostic tool that can be used if available and should always be considered before surgical intervention (Kim et al. 2005). Rapid molecular tests are currently the WHO-recommended initial

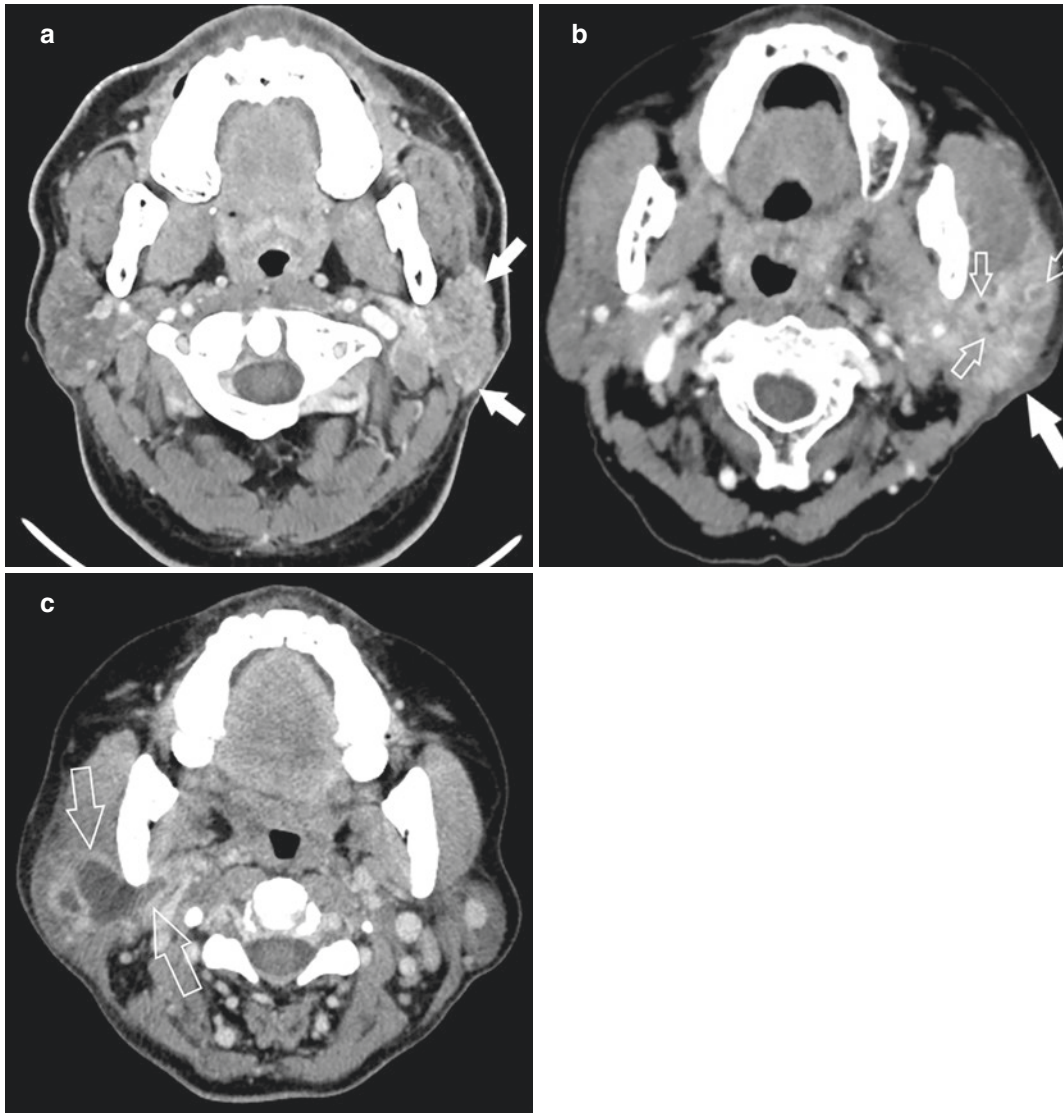

Fig. 19 Acute suppurative bacterial parotitis in three different patients. (**a**) Axial contrast-enhanced CT image shows diffuse increased enhancement with slight heterogeneous enhancement of the left parotid gland (solid arrows). Pus culture from left parotid tissue grew *Streptococcus viridans*. (**b**) Axial contrast-enhanced CT image in a different patient shows diffuse enlargement and increased enhancement of the left parotid gland containing multiple intraparotid lymph nodes with areas of central low density and rim enhancement (small open arrows). Fat stranding and subcutaneous tissue swelling adjacent to the left parotid gland are present (large solid arrow). Pus culture from the left parotid gland grew *Staphylococcus aureus*. (**c**) Axial contrast-enhanced CT image in a different patient shows an irregular rim-enhancing abscess in the superficial and deep lobes of the right parotid gland (large open arrows). Pus culture from the right parotid gland grew *Staphylococcus aureus*

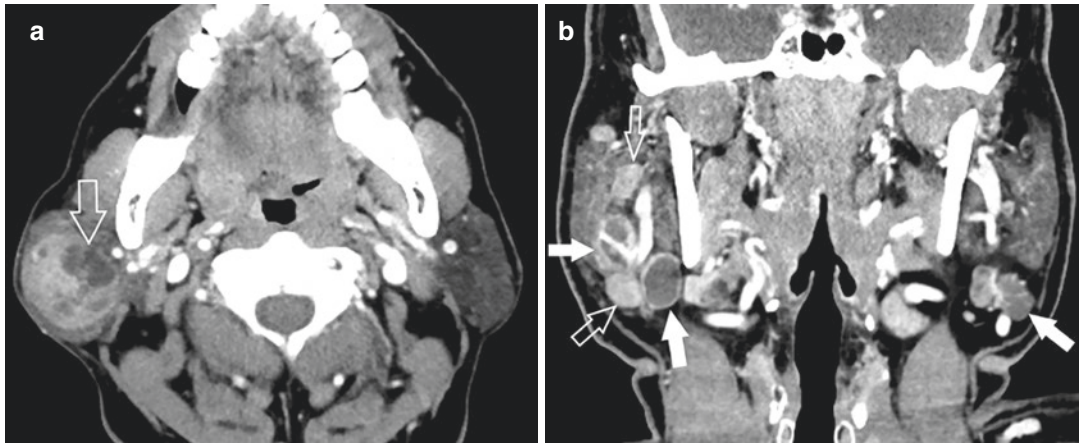

Fig. 20 Warthin tumor in two different patients. (**a**) Axial contrast-enhanced CT image shows a round, circumscribed solid mass with internal cystic component in the right parotid gland. The cystic component has no rim enhancement (open arrow). (**b**) Coronal contrast-enhanced CT image in a different patient shows multiple well-circumscribed masses in both parotid glands mimicking multiple lymphadenopathy. Some of the masses are solid and homogeneously enhanced (small open arrows), while some show internal cystic components, which have thin rim enhancement (small solid arrows). The surrounding parotid parenchyma appears normal

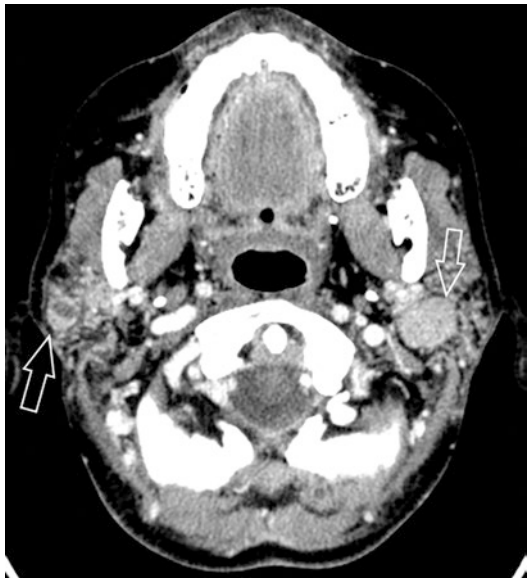

Fig. 21 Lymphoma of the parotid gland in a patient with underlying systemic lupus erythematosus. Axial contrast-enhanced CT image shows multiple circumscribed masses in the parotid glands bilaterally (open arrows). The mass in the right parotid shows an internal necrotic area that has no rim enhancement. Fatty change of the parotid parenchyma is present

diagnostic tool for TB (WHO 2020). Testing should be performed prior to any surgical intervention to identify the differential diagnosis of salivary gland tumor (Tauro et al. 2011). Otherwise, the diagnosis may be a histological surprise after surgical excision (Kim et al. 2005; Belatik et al. 2019). Incision biopsy is generally avoided as it can lead to a chronic fistula (Tauro et al. 2011). If the lesion needs to be surgically exposed, an excisional biopsy should be carried out (Ataman et al. 1992; Bottini et al. 2007).

4.7 Treatment

If treated properly, the prognosis of TB of the salivary glands is good, and surgery is not required in most cases (Kim et al. 2005; Garg et al. 2010). The majority of cases of salivary gland TB resolve after initiation of anti-TB medication, and surgery should be reserved for lesions showing poor or no response to anti-TB medication (Kim et al. 2005; Gupta et al. 2020).

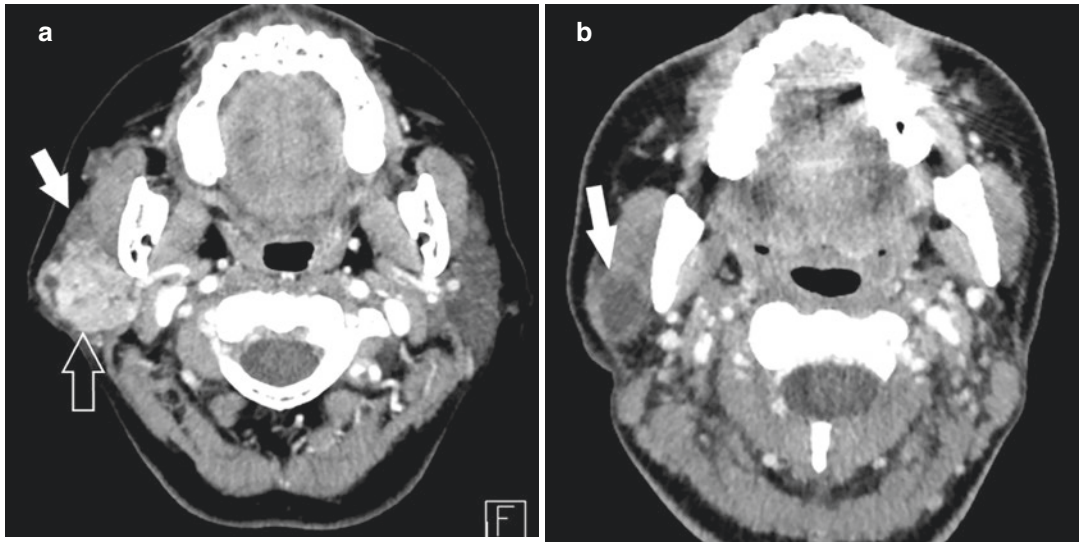

Fig. 22 Malignant parotid tumors in two different patients. (**a**) Mucoepidermoid carcinoma of the right parotid gland. Axial contrast-enhanced CT image shows a lobulated mass containing an internal cystic component (open arrow). The parenchyma adjacent to the mass shows normal enhancement (solid arrow). (**b**) Primary squamous cell carcinoma of the right parotid gland. Axial contrast-enhanced CT image shows a circumscribed mass with central low density and faint rim enhancement in the right parotid tail (large solid arrow). Excision revealed squamous cell carcinoma of the right parotid gland. The patient had no malignancy elsewhere

5 Conclusion

Imaging of TB in the head and neck region is non-specific and has to be differentiated from other infections and malignancy. Some imaging clues may help suggest a diagnosis of TB rather than other diseases. Radiologists should know the spectrum of imaging features of head and neck TB and include TB in the differential diagnosis in the appropriate clinical and imaging settings. Close collaboration with head and neck surgeons is important for optimum patient care.

References

Al Soub H (1996) Retropharyngeal abscess associated with tuberculosis of the cervical spine. Tuber Lung Dis 77:563–565

Alawad AAM, Khalifa AFM (2015) A rare cause of retropharyngeal abscess: cervical Pott's disease. Am J Trop Med Hyg 92:884

Al-Serhani AM (2001) Mycobacterial infection of the head and neck; presentation and diagnosis. Laryngoscope 111:2012–2016

Alvarez S, McCabe WR (1984) Extrapulmonary tuberculosis revisited: a review of experience at Boston city and other hospitals. Medicine (United States) 63:25–55

Artenstein AW, Kim JH, Williams WJ, Chung RCY (1995) Isolated peripheral tuberculous lymphadenitis in adults: current clinical and diagnostic issues. Clin Infect Dis 20:876–882

Ataman M, Sözeri B, Özçelik T, Gedikoglu G (1992) Tuberculosis of the parotid salivary gland. Auris Nasus Larynx 19:271–273

Barlow F (1980) The king's evil. English Historical Rev 95:3–27

Belatik H, Aouinti L, Touiheme N et al (2019) Histological surprise of parotid tuberculosis: about two cases. Pan Afr Med J 32:85

Bottini DJ, Garelli A, Felici M et al (2007) Primary tuberculosis of submandibular gland. J Craniofac Surg 18:218–219

Bray FN, Alsaidan M, Simmons BJ et al (2015) Scrofula and the divine right of royalty: the king's touch. JAMA Dermatol 151:702

Chaudhary S (1997) Tuberculosis of the salivary glands. In: Norman JED, McGurk M (eds) Colour atlas and text of the salivary glands. Mosby-Wolfe, London, pp 337–339

Chou YH, Tiu CM, Liu CY et al (2004) Tuberculosis of the parotid gland: sonographic manifestations and sonographically guided aspiration. J Ultrasound Med 23:1275–1281

Christensen JB, Koeppe J (2010) Mycobacterium avium complex cervical lymphadenitis in an immunocompetent adult. Clin Vaccine Immunol 17:1488–1490

Christoforidou A, Metallidis S, Kollaras P et al (2012) Tuberculous retropharyngeal abscess as a cause of oropharyngeal dysphagia. Am J Otolaryngol Head Neck Med Surg 33:272–274

Chun CW, Jung JY, Baik JS et al (2018) Detection of soft-tissue abscess: comparison of diffusion-weighted imaging to contrast-enhanced MRI. J Magn Reson Imaging 47:60–68

Costa NS, Salisbury SR, Donnelly LF (2011) Retropharyngeal lymph nodes in children: a common imaging finding and potential source of misinterpretation. AJR Am J Roentgenol 196:W433–W437

Dadwal M (2011) Primary submandibular tuberculosis: an unusual cause of submandibular salivary gland enlargement. Indian J Otolaryngol Head Neck Surg 63:298–299

Dandapat MC, Mishra BM, Dash SP, Kar PK (1990) Peripheral lymph node tuberculosis: a review of 80 cases. Br J Surg 77:911–912

Debnam JM, Guha-Thakurta N (2012) Retropharyngeal and prevertebral spaces: anatomic imaging and diagnosis. Otolaryngol Clin North Am 45:1293–1310

Ekka M, Sinha S (2015) Retropharyngeal abscess as a rare presentation of pulmonary tuberculosis. Lung India 32:262–264

Feigl G (2015) Fascia and spaces on the neck: myths and reality. Med Flum 51:430–439

Fontanilla JM, Barnes A, Von Reyn CF (2011) Current diagnosis and management of peripheral tuberculous lymphadenitis. Clin Infect Dis 53:555–562

Forbes BA, Hall GS, Miller MB et al (2018) Practice guidelines for clinical microbiology laboratories: mycobacteria. Clin Microbiol Rev 31:e00038–e00017

Gambhir S, Ravina M, Rangan K et al (2017) Imaging in extrapulmonary tuberculosis. Int J Infect Dis 56:237–247

Garg R, Verma SK, Mehra S, Srivastawa A (2010) Parotid tuberculosis. Lung India 27:253–255

Geldmacher H, Taube C, Kroeger C et al (2002) Assessment of lymph node tuberculosis in northern Germany: a clinical review. Chest 121:1177–1182

Gopakumar KG, Mohan N, Prasanth VR, Ajayakumar MK (2019) Isolated parapharyngeal cold abscess in a 9-year-old boy. Paediatr Int Child Health 39:139–141

Grodinsky M, Holyoke EA (1938) The fasciae and fascial spaces of the head, neck and adjacent regions. Am J Anat 63:367–408

Gujrathi AB, Ambulgekar V, Kathait P (2016) Deep neck space infection—a retrospective study of 270 cases at tertiary care center. World J Otorhinolaryngol Head Neck Surg 2:208–213

Gunawardana SS, Earley AR, Pollard AJ, Bethell D (2004) Twelfth nerve palsy due to a retropharyngeal tuberculous abscess. Arch Dis Child 89:579

Gupta V, Patankar K, Shinde A et al (2012) Tuberculosis of the parotid gland. Case Rep Radiol 2012:278793

Gupta N, Aggarwal A, Tripathi M, Nischal N (2020) Parotid gland tuberculosis. QJM 113:500–501

Hanck C, Fleisch F, Katz G, Robson CD (2004) Imaging appearance of nontuberculous mycobacterial infection of the neck (multiple letters). AJNR Am J Neuroradiol 25:349–350

Harkani A, Hassani R, Ziad T et al (2011) Retropharyngeal abscess in adults: five case reports and review of the literature. Sci World J 11:1623–1629

Herzog H (1998) History of tuberculosis. Respiration 65:5–15

Hsu HE, Chen CY (2019) Tuberculous retropharyngeal abscess with Pott disease and tuberculous abscess of the chest wall: a case report. Medicine (Baltimore) 98:e16280

Huang YH, Yeh CH, Cheng NM et al (2017) Cystic nodal metastasis in patients with oropharyngeal squamous cell carcinoma receiving chemoradiotherapy: relationship with human papillomavirus status and failure patterns. PLoS One 12:e0180779

Hurley R, Douglas CM, Montgomery J, Clark LJ (2018) The hidden cost of deep neck space infections. Ann R Coll Surg Engl 100:129–134

Je BK, Kim MJ, Kim SB et al (2005) Detailed nodal features of cervical tuberculous lymphadenitis on serial neck computed tomography before and after chemotherapy: focus on the relation between clinical outcomes and computed tomography features. J Comput Assist Tomogr 29:889–894

Kanjanopas K, Siripan N, Phoophitphong R (2014) Tuberculous cervical lymphadenopathy and the role of surgical treatment. Southeast Asian J Trop Med Public Health 45:1419–1424

Kim YH, Jeong WJ, Jung KY et al (2005) Diagnosis of major salivary gland tuberculosis: experience of eight cases and review of the literature. Acta Otolaryngol 125:1318–1322

Koçak HE, Kiral MN, Acipayam H et al (2017) Retropharyngeal abscess presenting with sleep apnea syndrome. J Craniofac Surg 28:e368–e369

Kosmidou P, Kosmidou A, Angelis S et al (2020) Atypical retropharyngeal abscess of tuberculosis: diagnostic reasoning, management, and treatment. Cureus 12:e9124

Lau AS, Upile NS, Wilkie MD et al (2014) The rising rate of admissions for tonsillitis and neck space abscesses in England, 1991-2011. Ann R Coll Surg Engl 96:307–310

Lee JY (2015) Diagnosis and treatment of extrapulmonary tuberculosis. Tuberc Respir Dis (Seoul) 78:47–55

Lee Y, Park KS, Chung SY (1994) Cervical tuberculous lymphadenitis: CT findings. J Comput Assist Tomogr 18:370–375

Lee S, Yoo JH, Lee SW (2012) Kikuchi disease: differentiation from tuberculous lymphadenitis based on patterns of nodal necrosis on CT. AJNR Am J Neuroradiol 33:135–140

Lekhbal A, Chaker K, Halily S et al (2020) Treatment of cervical lymph node tuberculosis: when surgery

should be performed? A retrospective cohort study. Ann Med Surg (Lond) 55:159–163
Manoharan SR, Leitao J, Emberton P, Quraishi NA (2013) A large tuberculosis abscess causing spinal cord compression of the cervico-thoracic region in a young child. Eur Spine J 22:1459–1463
Martin CA, Gabrillargues J, Louvrier C et al (2014) Contribution of CT scan and CT-guided aspiration in the management of retropharyngeal abscess in children based on a series of 18 cases. Eur Ann Otorhinolaryngol Head Neck Dis 131:277–282
McGuinness B, Wilson N, Doyle AJ (2007) The "penumbra sign" on T1-weighted MRI for differentiating musculoskeletal infection from tumor. Skeletal Radiol 36:417–421
Meher R, Agarwal S, Singh I (2006) Tuberculous retropharyngeal abscess in an HIV patient. Hong Kong Med J 12:483–485
Mekonnen D, Derbie A, Abeje A et al (2019) Epidemiology of tuberculous lymphadenitis in Africa: a systematic review and meta-analysis. PLoS One 14:e0215647
Menon E, Baruah P (2014) Tuberculous retropharyngeal abscess revisited. BMJ Case Rep 2014:bcr2013202514
Menon K, Bem C, Gouldesbrough D, Strachan DR (2007) A clinical review of 128 cases of head and neck tuberculosis presenting over a 10-year period in Bradford, UK. J Laryngol Otol 121:362–368
Mizumura K, Machino T, Sato Y et al (2010) Tuberculous retropharyngeal abscess associated with spinal tuberculosis well controlled by fine-needle aspiration and anti-tuberculous chemotherapy. Intern Med 49:1155–1158
Öktem F, Güvenç MG, Yilmaz S et al (2006) Asymptomatic retropharyngeal abscess related to cervical Pott's disease. Am J Otolaryngol Head Neck Med Surg 27:278–280
Onoue K, Fujima N, Andreu-Arasa VC et al (2020) Cystic cervical lymph nodes of papillary thyroid carcinoma, tuberculosis and human papillomavirus positive oropharyngeal squamous cell carcinoma: comparative CT analysis for their differentiation. Eur J Radiol 132:109310
Park JH, Kim DW (2014) Sonographic diagnosis of tuberculous lymphadenitis in the neck. J Ultrasound Med 33:1619–1626
Patel AB, Hinni ML (2013) Tuberculous retropharyngeal abscess presenting with symptoms of obstructive sleep apnea. Eur Arch Otorhinolaryngol 270:371–374
Patil C, Kharat R, Deshmukh P et al (2011) Tuberculous retropharyngeal abscess without cervical spine TB. Asian Pac J Trop Med 4:251–252
Purohit M, Mustafa T (2015) Laboratory diagnosis of extrapulmonary tuberculosis (EPTB) in resource-constrained setting: state of the art, challenges and the need. J Clin Diagn Res 9:EE01–EE06
Qian X, Albers AE, Nguyen DTM et al (2019) Head and neck tuberculosis: literature review and meta-analysis. Tuberculosis 116:s78–s88
Rao MJ, Gowda RSN, Umapathy BL, Navaneeth BV (2013) Tuberculosis of the parapharyngeal space: a rare case report. Indian J Pathol Microbiol 56: 480–481
Raza SN, Rahat ZM (2010) Horner's syndrome as a co-presentation of tuberculous retropharyngeal abscess. J Coll Physicians Surg Pak 20:279–281
Ridder GJ, Technau-Ihling K, Sander A, Boedeker CC (2005) Spectrum and management of deep neck space infections: an 8-year experience of 234 cases. Otolaryngol Head Neck Surg 133:709–714
Robson CD, Hazra R, Barnes PD et al (1999) Nontuberculous mycobacterial infection of the head and neck in immunocompetent children: CT and MR findings. AJNR Am J Neuroradiol 20:1829–1835
Rouviere H (1938) Lymphatic system of the head and neck. In: Tobias MJ (ed) Anatomy of the human lymphatic system. Edward Brothers, Ann Arbor, MI, pp 3–28
Ryu YJ (2015) Diagnosis of pulmonary tuberculosis: recent advances and diagnostic algorithms. Tuberc Respir Dis (Seoul) 78:64–71
Sabri AN (2015) Mycobacterium tuberculosis presenting as a cystic parapharyngeal space mass. Ann Otolaryngol Rhinol 2:1077–1080
Sah SK, Zeng C, Li X et al (2016) CT features and analysis for misdiagnosis of parotid tuberculosis. Clin Imaging 40:810–815
Sathekge M, Maes A, D'Asseler Y et al (2012) Tuberculous lymphadenitis: FDG PET and CT findings in responsive and nonresponsive disease. Eur J Nucl Med Mol Imaging 39:1184–1190
Shafer RW, Kim DS, Weiss JP, Quale JM (1991) Extrapulmonary tuberculosis in patients with human immunodeficiency virus infection. Medicine (Baltimore) 70:384–397
Sutcliffe P, Lasrado S (2020) Anatomy, head and neck, deep cervical neck fascia. StatPearls [Internet]. StatPearls Publishing, Treasure Island, FL; 2021 Jan. [cited 2021 May 31]
Tauro LF, George C, Kamath A et al (2011) Primary tuberculosis of submandibular salivary gland. J Glob Infect Dis 3:82–85
Thomas MD, Tierney PA, Samuel D et al (1995) Tuberculosis: an unusual cause of dysphagia. Otolaryngol Head Neck Surg 113:644–650
Thomas K, Gupta M, Gaba S, Gupta M (2020) Tubercular retropharyngeal abscess with Pott's disease in an elderly male patient. Cureus 12:e8256
Vaid S, Lee YYP, Rawat S et al (2010) Tuberculosis in the head and neck- a forgotten differential diagnosis. Clin Radiol 65:73–81
Weldetsadik AY, Bedane A, Riedel F (2019) Retropharyngeal tuberculous abscess: a rare cause of upper airway obstruction and obstructive sleep apnea in children: a case report. J Trop Pediatr 65:642–645
Wilson W (1842) On the principles of treatment of pulmonary consumption. Lancet 38:227–230

Windfuhr JP, Chen YS (2019) Hospital admissions for acute throat and deep neck infections versus tonsillectomy rates in Germany. Eur Arch Otorhinolaryngol 276:2519–2530

World Health Organization (2020) Global Tuberculosis Report 2020. Geneva. Licence: CC BY-NC-SA 3.0 IGO. https://www.who.int/tb/publications/global_report/en/

Yang TH, Xirasagar S, Cheng YF et al (2021) A nationwide population-based study on the incidence of parapharyngeal and retropharyngeal abscess—a 10-year study. Int J Environ Res Public Health 18:1049

You SH, Kim B, Yang KS, Kim BK (2019) Cervical necrotic lymphadenopathy: a diagnostic tree analysis model based on CT and clinical findings. Eur Radiol 29:5635–5645

Zafereo ME, Pereira KD (2008) Chronic retropharyngeal abscess presenting as obstructive sleep apnea. Pediatr Emerg Care 24:382–384

Zhang Y, Chen J, Shen J et al (2013) Apparent diffusion coefficient values of necrotic and solid portion of lymph nodes: differential diagnostic value in cervical lymphadenopathy. Clin Radiol 68:224–231

Zhang D, Li X, Xiong H et al (2018) Tuberculosis of the parotid lymph nodes: clinical and imaging features. Infect Drug Resist 11:1795–1805

Imaging of Ear, Nose, and Throat Tuberculosis: Temporal Bone, Sinonasal Cavities, Pharynx, and Larynx

Pailin Kongmebhol
and Jose Florencio Lapeña Jr

Contents

Abstract

Otorhinolaryngology evolved from the convergence of the disciplines of Otology (from "above") and Laryngology and Bronchoesophagology (from "below") with Rhinopharyngology (in the "middle"). In this chapter, we discuss the pathophysiology, clinical features, course and complications, imaging features, imaging differential diagnosis, diagnosis confirmation, and treatment of tuberculosis of the ear and temporal bone, nose and sinonasal cavities, pharynx, and

P. Kongmebhol
Department of Radiology, Faculty of Medicine, Chiang Mai University, Chiang Mai, Thailand
e-mail: mailtoann@gmail.com, pailin.k@cmu.ac.th

J. F. Lapeña Jr (✉)
Department of Otolaryngology—Head and Neck Surgery, College of Medicine—Philippine General Hospital, University of the Philippines Manila, Ermita, Manila, The Philippines
e-mail: lapenajf@upm.edu.ph, jflapena@up.edu.ph

© The Author(s), under exclusive license to Springer Nature Switzerland AG 2022

M. F. Ladeb, W. C. G. Peh (eds.), *Imaging of Tuberculosis*, Medical Radiology Diagnostic Imaging,
https://doi.org/10.1007/978-3-031-07040-2_7

larynx. Each of these organs or structures has different clinical presentations and imaging characteristics, and important pointers and imaging findings that may suggest tuberculosis are mentioned. Knowing the imaging spectrum of tuberculosis in these organs is important for radiologists because they can help alert clinicians, such as otorhinolaryngologists, initiate proper investigation and early treatment.

Abbreviations

COM	Chronic otitis media
CT	Computed tomography
MRI	Magnetic resonance imaging
TB	Tuberculosis
TBOM	Tuberculous otomastoiditis

1 Introduction

The ear and temporal bone, nose and sinonasal cavities, pharynx and larynx are deep structures in the head and neck which are difficult to assess by routine ear, nose, and throat (ENT) examination alone. Imaging plays an important role in the evaluation of the diseases in these structures. Imaging findings of sinonasal, pharyngeal, and laryngeal tuberculosis (TB) are varied and the differential diagnosis depends on the pattern of involvement. For instance, the imaging features of early tuberculous otomastoiditis may be similar to those of bacterial otomastoiditis, except for the lack of mastoid sclerosis that may help suggest TB.

Although imaging findings of TB in these structures are non-specific and have to be differentiated from other diseases, including other infections, malignancy, and other granulomatous diseases; there are some clinical or imaging characteristics that can help suggest a diagnosis of TB. Imaging can also help in the localization of disease, evaluate extension, and can be used for follow-up after treatment. It may be difficult to make a diagnosis of TB at first presentation, but awareness of the possibility of this disease can help in achieving a diagnosis, and early treatment can prevent serious sequelae.

2 Tuberculous Otomastoiditis

2.1 Introduction

Tuberculous otomastoiditis (TBOM) is one of the many forms of extrapulmonary TB, and one of its rarer manifestations. In the early eighteenth century, the French surgeon Jean Louis Petit (1674–1750) first described tuberculous involvement of the temporal bone (Ormerod 1931). Its apparent rarity may be compounded by its being a commonly missed diagnosis (Bhalla et al. 2001). The post-operative incidence of TBOM in two separate two-year series in India ranged from 4.9% (25 out of 502) to 8.2% (15 out of 181) of cases operated on for chronic suppurative otitis media reported by Kameswaran et al. (2017) and Deenadayal et al. (2016), respectively. Difficulty and delay in its diagnosis are a persistent issue, as it can be mistaken for chronic otitis media (COM) due to its variable presentations (Aremu and Alabi 2010; Abes et al. 2011).

2.2 Pathophysiology

In 1835, Romberg and Geissler associated TBOM with pulmonary TB (Ormerod 1931). The coincidence of TBOM with pulmonary TB ranges from 32% (Yaniv 1987) to 75% (Nishiike et al. 2003); and a history of pulmonary TB has been identified as a predictor of TBOM (Abes et al. 2011). It may be prudent to heed the advice of Aremu and Alabi (2010) that otorrhea in a patient with known or suspected active pulmonary TB should be assumed to be TBOM until proven otherwise.

Prosper Ménière is credited with the description of the tympanic membrane destruction to which he ascribed the severe deafness in TB, before Koch demonstrated the tuberculous bacillus in 1882 (Myerson and Gilbert 1941; Birrell 1973) and Esche found the bacillus in aural discharge in 1883 (Birrell 1973). Three mechanisms are considered in TBOM, namely spread to the middle ear from the Eustachian tube, hematogenous spread from another organ site, and direct implantation in the middle ear via the external auditory canal through a perforated tympanic membrane (Cho et al. 2006).

2.3 Clinical Features, Course, and Complications

The clinical presentation of TBOM can be very similar to the more commonly diagnosed COM. These are otorrhea, hearing loss, tympanic membrane perforations, and (in advanced cases) swelling around the ear and facial palsies (Deenadayal et al. 2016). The now classical picture of painless onset of discharge and appearance of the tympanic membrane was first discussed by Wilde in 1853, while Schwartze noted the cheesy infiltration and tubercles of the middle ear mucosa in 1878 (Birrell 1973). The classic triad for TBOM consists of painless otorrhea, multiple small tympanic membrane perforations, and facial nerve paralysis (Cho et al. 2006).

The main symptom is otorrhea, accompanied by hearing loss in most cases (Cho et al. 2006) although both Windle-Taylor and Bailey (1980) and Yaniv (1987) did not find otorrhea significant in their retrospective series of 22 cases and 31 cases (33 ears) of TBOM, respectively. Otorrhea, hearing loss, and facial palsy have been reported together (Bhalla et al. 2001; Aremu and Alabi 2010), with facial palsy being less frequent (Vital et al. 2002; Cho et al. 2006). Lee and Drysdale (1993) reported two cases of concurrent otorrhea and facial paralysis. Concurrent hearing loss and facial paralysis have also been described (Vital et al. 2002; Kameswaran et al. 2017). Windle-Taylor and Bailey (1980) identified unexpectedly severe hearing loss and facial paralysis as significant features in a series of 22 cases of TBOM. Aside from severe hearing loss and facial paralysis, other complications are labyrinthine fistula, postaural fistula, perichondritis, and extradural abscess (Kameswaran et al. 2017).

Multiple small tympanic membrane perforations are noted less frequently (Vital et al. 2002; Deenadayal et al. 2016), or not at all. In a series of 12 patients (13 ears) with TBOM, Nishiike et al. (2003) observed central or total perforations of the tympanic membrane in most cases, but none had multiple perforations. Yaniv (1987) did not find multiple perforations significant in a series of 31 cases (33 ears) of TBOM, and only a large subtotal perforation was found by Aremu and Alabi (2010). It is conceivable that while they may be present in early TBOM, multiple perforations can eventually merge to form a single larger perforation. In a six-year review of 12 cases (13 ears) of TBOM, the five otoscopic presentations identified were multiple perforations, single perforation with refractory otorrhea and exuberant granulation tissue formation, single perforation with minimal otorrhea and no granulation tissue formation, intact tympanic membrane with middle ear effusion, and intact tympanic membrane with tumor-like tissue in the middle ear (Abes et al. 2011). Abundant pale granulations are frequently found in the middle ear (Windle-Taylor and Bailey 1980; Yaniv 1987; Deenadayal et al. 2016) and external auditory canal (Deenadayal et al. 2016).

The variable presentations of TBOM and their similarity to COM and other chronic ear conditions demand that especially in endemic areas or potentially susceptible populations (or in cases resistant to treatment of other conditions), physicians maintain a high index of suspicion to catch the disease early on, before complications start to manifest (Myerson and Gilbert 1941; Yaniv 1987; Bhalla et al. 2001; Abes et al. 2011).

2.4 Imaging Features

2.4.1 Computed Tomography

Computed tomography (CT) is the imaging modality of choice for evaluating patients presenting with symptoms of COM. CT can demonstrate extension of soft tissue and integrity of the bony structures in the external auditory canal (EAC), middle ear, inner ear, and mastoid which are useful information for surgery. In TBOM, the EAC often shows mucosal thickening or soft tissue occlusion (Fig. 1a). The hallmark CT features of TBOM are total opacification of the middle ear cavity and mastoid air cells in a well-developed mastoid without sclerotic change (Cho et al. 2006; Rho et al. 2007) (Fig. 1b). If sclerosis of mastoid air cells is present in TBOM, it is likely that the patient has pre-existing COM with superimposition of TB.

Bone erosion occurs in late disease of TBOM and can be observed at the mastoid septa, outer cortex of mastoid bone, EAC, ear ossicles, and bony labyrinth (Fig. 2a). More extensive disease may result in skull base destruction (Cho et al. 2006). The scutum is usually intact in TBOM (Rho et al. 2007). TBOM that shows scutum erosion should raise the suspicion of concurrent cholesteatoma. Coexistent cholesteatoma has been found in 14.3–33.3% of cases with TBOM (Wolfowitz 1972; Chaturvedi and Chaturvedi 1986; Yaniv 1987; Maheshwari and Panigrahi 2017). Patients who have concurrent TBOM and cholesteatoma may have imaging appearances of both diseases, causing difficulty in diagnosis (Fig. 2).

2.4.2 Magnetic Resonance Imaging

Magnetic resonance imaging (MRI) shows benefit over CT in demonstration of membranous labyrinth involvement, facial nerve involvement, skull base infiltration, and intracranial complications which are present in severe cases of TBOM. There are limited reports of the MRI findings in TBOM due to rarity of the disease. On MRI, the inflammatory granulomatous tissue appears hypointense on both T1-weighted and T2-weighted images, with diffuse contrast enhancement (Munoz et al. 2009) (Fig. 2e–g).

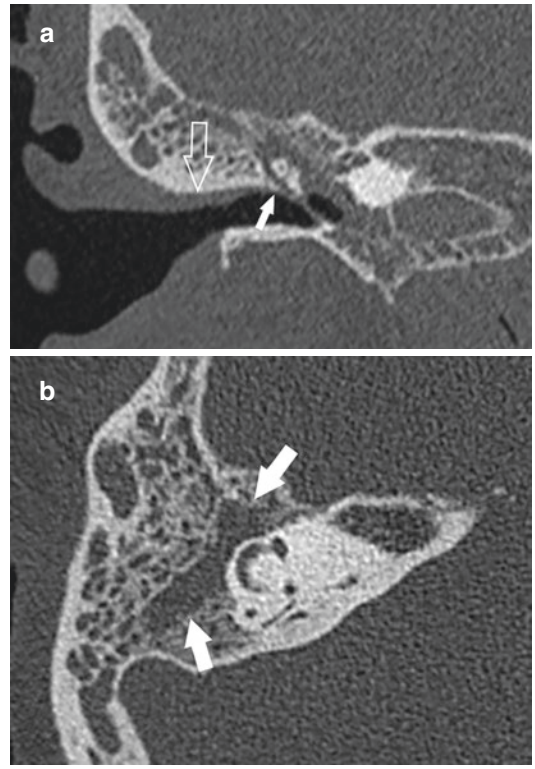

Fig. 1 Tuberculous otomastoiditis. (**a**) Coronal CT image shows mucosal thickening along the roof of external auditory canal (open arrow). The scutum is intact (small solid arrow). (**b**) Axial CT image shows total opacification of the middle ear cavity, aditus ad antrum, mastoid antrum, and mastoid air cells (large solid arrows). Note that the opacified mastoid air cells are well developed and show no sclerosis

2.5 Imaging Differential Diagnosis

The two major diseases that should be differentiated from tuberculous otomastoiditis are COM and cholesteatoma. Middle ear and mastoid opacification in COM are always accompanied by mastoid sclerosis and poor pneumatization (Fig. 3). This is in contrast to TBOM where sclerosis is uncommon and tends to occur in well-developed mastoid air cells. Bone destruction is less common in COM, compared to TBOM (Cho et al. 2006). As cholesteatoma is a complication of COM, mastoid sclerosis is always present. The typical location of bony erosion in cholesteatoma is at the scutum; while in TB, the scutum is spared

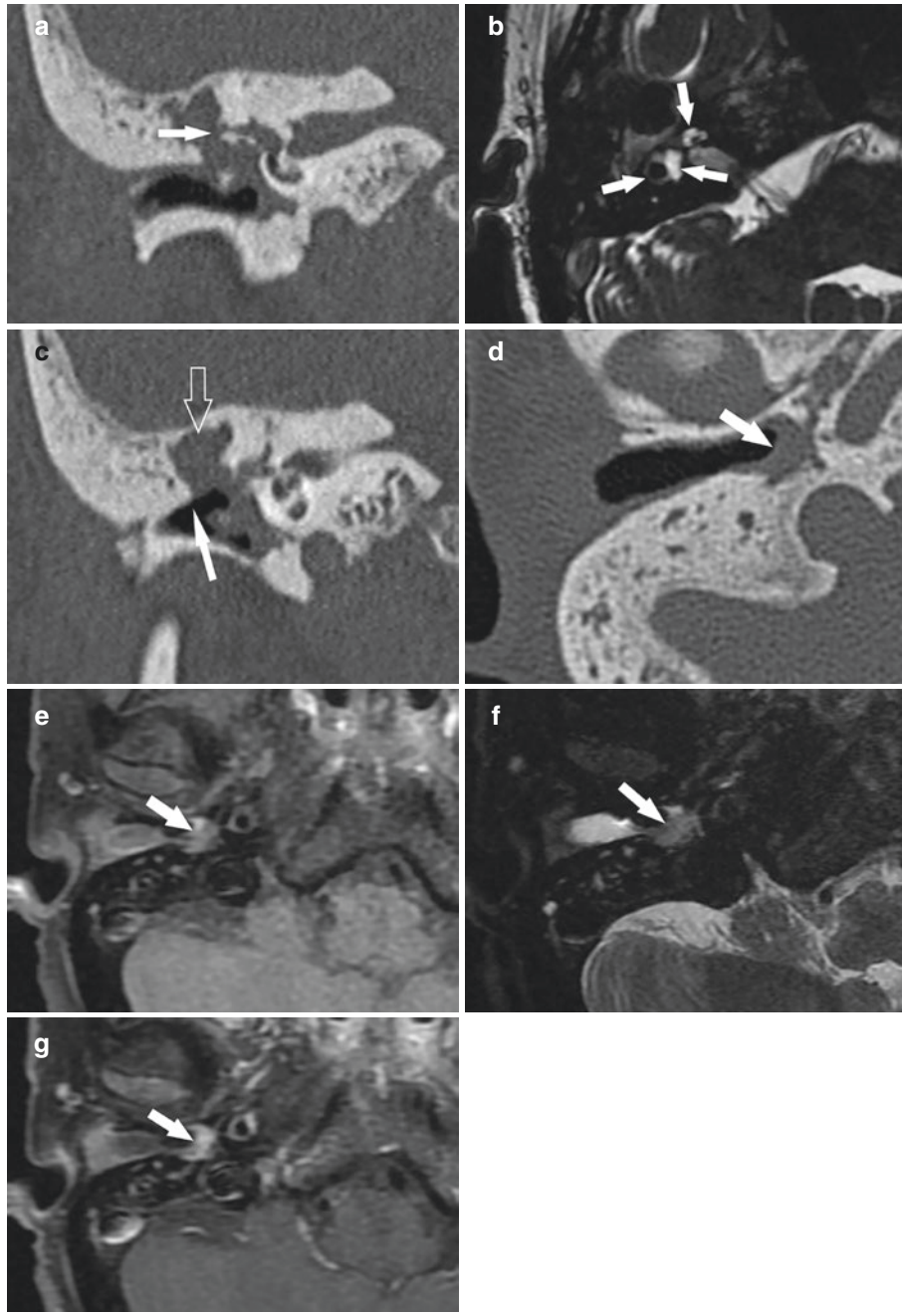

Fig. 2 Tuberculous otomastoiditis with bony labyrinth erosion and cholesteatoma. (**a**) Coronal CT image shows lateral semicircular canal erosion (arrow). (**b**) Axial heavily T2-W (FIESTA) MR image shows hyperintense signal in the cochlea, vestibule, and lateral semicircular canal (arrows) suggesting that the membranous labyrinth is intact. At surgery, granulation tissue was found in the middle ear and on the lateral semicircular canal, resulting in lateral semicircular canal erosion. (**c**) Coronal CT image shows blunting of scutum (solid arrow) with soft tissue opacification in the epitympanum (open arrow), mesotympanum, and hypotympanum. At surgery, cholesteatoma was found in the epitympanum causing scutum erosion. (**d**) Axial CT image taken at level of hypotympanum shows soft tissue opacification in the hypotympanum from granulation tissue (arrow). Note sclerosis and poor pneumatization of the mastoid air cells from chronic mastoiditis. Axial (**e**) fat-suppressed T1-W, (**f**) fat-suppressed T2-W and (**g**) contrast-enhanced fat-suppressed T1-W MR images taken at the same level as (**d**) show hypointense soft tissue with enhancement, suggestive of granulation tissue (arrow)

(Rho et al. 2007) (Fig. 4). However, on MRI, cholesteatoma can be distinguished from granulomatous tissue due to TB by its T2-hyperintensity, lack of contrast enhancement and hyperintense signal on diffusion-weighted imaging (DWI).

2.6 Diagnosis Confirmation

Early diagnosis and prompt treatment of TBOM may prevent devastating otologic sequelae and central nervous system complications. In atypical cases of COM, repeated cultures of ear discharge can be obtained to rule out TBOM (Aremu and Alabi 2010). However, bacteriological cultures of ear discharge may not be reliable, as other organisms (such as *Staphylococcus, Pseudomonas, Klebsiella, Proteus,* and *Streptococcus* spp.) can interfere with the growth of *Mycobacteria tuberculosis* (Windle-Taylor and Bailey 1980). Acid-fast bacilli (AFB) are rarely found because of low mycobacterial counts in extrapulmonary TB; ear discharge smears are positive for AFB in only 0–20% of cases and cultures are positive for *M. tuberculosis* in 5–44% of cases (Yaniv 1987; Aremu and Alabi 2010). Gene amplification techniques such as polymerase chain reaction (PCR) may be used as a rapid and highly sensitive and specific method to isolate *M. tuberculosis* DNA from ear discharge as well as peripheral blood (Taci et al. 2003).

If the cause of suppurative infection of the middle ear is still undiagnosed, surgery (i.e., middle ear exploration and operative biopsy) may be required for diagnosis (Robertson and Kumar 1995; Vital et al. 2002). This may range from a middle ear biopsy under direct visualization with a middle ear lavage (Aremu and Alabi 2010), to microbiological and histopathological examinations and PCR analysis of tissue taken during tympanomastoidectomy (Kameswaran et al. 2017). Windle-Taylor and Bailey (1980) and Yaniv (1987) reported histological and bacteriological examination of operative

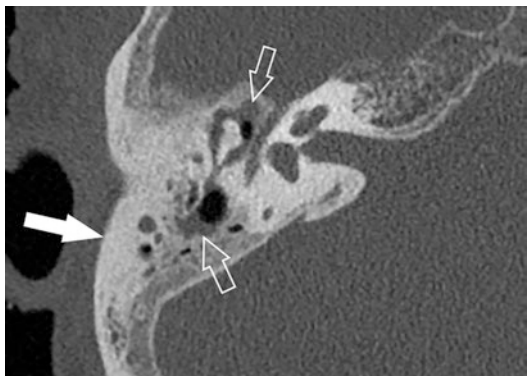

Fig. 3 Chronic otomastoiditis. Axial CT image shows opacification in the middle ear cavity, mastoid antrum and mastoid air cells (open arrows). Poor pneumatization of mastoid air cells with sclerotic changes is noted (solid arrow)

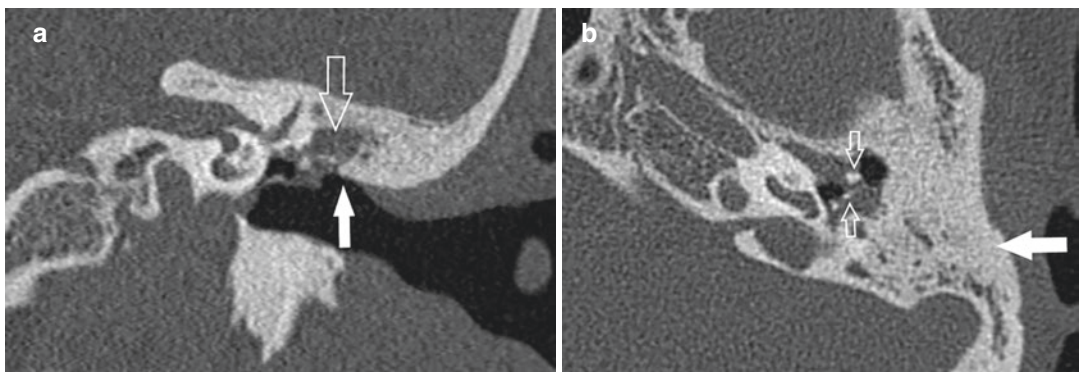

Fig. 4 Cholesteatoma. (**a**) Coronal CT image shows soft tissue opacification in the epitympanum (open arrow). The scutum is blunted (arrow) typical for Prussak space cholesteatoma. (**b**) Axial CT image shows erosions of the ear ossicles (small open arrows). Sclerosis and poor pneumatization of the mastoid air cells are suggestive of chronic mastoiditis (large solid arrow)

material (granulation tissue from the middle ear or mastoid) to be the diagnostic procedure in 20/22 and 31/31 cases, respectively. The diagnosis was based on histology, following middle ear exploration for chronic middle ear disease, in four other cases (Vital et al. 2002). According to Abes et al. (2011), intraoperative granulation with cheesy material is a clinical predictor of disease, along with a positive purified protein derivative (PPD) test and positive chest radiographical findings.

Out of 15 cases diagnosed with TBOM on the basis of exuberant pale granulation tissue obtained during mastoid surgery, direct smear Ziehl–Neelsen staining was positive in four cases, concentration techniques were positive in seven cases, molecular genetic studies were diagnostic in all cases, but none was positive on histopathology (Deenadayal et al. 2016). A combination of tests should be obtained, and the diagnosis made on the basis of any, rather than all, tests. In a series of 52 patients (53 ears) with TBOM by Cho et al. (2006), a diagnosis of TBOM was made if a specimen of the middle ear revealed AFB, grew *M. tuberculosis* on a culture, revealed characteristic histology, and/or was PCR positive for *M. tuberculosis*. When present, the classic histological findings (granulomas, Langhans giant cells, and caseation necrosis) in association with biomolecular PCR positivity represent the cardinal diagnostic elements of TBOM (Bhalla et al. 2001; Cho et al. 2006).

2.7 Treatment

The treatment of choice for TBOM is the same as the standard treatment for extrapulmonary TB. Patients will usually require combination anti-TB drug therapy from at least six months (Emmett et al. 1977; Yaniv 1987; Aremu and Alabi 2010) up to nine months (Kahane and Crane 2009). In most patients, anti-TB drugs are an effective form of treatment (Cho et al. 2006). Patients who were treated early and did not have middle ear surgery showed significantly better clinical, radiological, and audiometric outcomes than those who were diagnosed late and had more complicated surgical procedures (Abes et al. 2011). On the other hand, patients who underwent drug therapy after surgery achieved more rapid healing of the ear and more frequent closure of the tympanic membrane than those who did not undergo surgery (Cho et al. 2006).

For early TBOM, surgery does not appear to provide any advantage over medical treatment, and is reserved for the removal of bony sequestra and to treat or prevent complications (Windle-Taylor and Bailey 1980; Lee and Drysdale 1993; Vital et al. 2002). Such complications for which radical mastoidectomy is recommended include facial paralysis, subperiosteal abscess, and labyrinthitis (Myerson and Gilbert 1941). On the other hand, treatment with anti-TB drugs and surgery gives good results and in selected cases, tympanoplastic surgery may be useful (Windle-Taylor and Bailey 1980). At the very least, a tympanoplasty is necessary after resolution of TBOM, as tympanic membrane perforation does not heal spontaneously.

3 Sinonasal Tuberculosis

3.1 Introduction

Primary sinonasal TB is rare (Sanehi et al. 2008); its rarity is probably due to self-protective functions of the nose such as ciliary movement, bactericidal secretions, and mechanical filtering by vibrissae (Goguen and Karmody 1995). Much rarer is paranasal sinus TB, which usually involves the maxillary sinus and is usually unilateral (Sanehi et al. 2008). Joseph William Gleitsmann (1907) credited Zdzislaw Dmochowski (1864–1924) with first documenting tuberculous bacilli in the maxillary sinus post-mortem in 1895; and Ernst Oppikofer (1874–1951) with positing TB as a preponderant cause of general sinus disease among 25 sinus pathologies out of 51 TB cases. Gleitsmann (1907) himself reported 20 cases of maxillary sinus TB, and Kim et al. (2007) reported eight cases of sinonasal TB, of which only two involved both the nasal cavity and sinus.

3.2 Pathophysiology

Sinonasal TB may occur secondary to pulmonary TB via inhalation of infected particles (Kim et al. 2014) or from traumatic digital inoculation of bacilli into the nasal cavity (Kameswaran et al. 2007). Paranasal sinus TB can be seeded from the bloodstream and lymphatics or by direct extension, although posterior nasal space TB without nasal cavity involvement is extremely rare (Kim et al. 2014). Of the 20 cases of maxillary sinus TB reported by Gleitsmann (1907), 12 were from tuberculous lesions of the nasal bones or upper maxilla, while eight were from carious teeth. Patients with tuberculous osteomyelitis of the maxilla can present with multiple periodontal dental abscesses (Gupta et al. 2014). Many cases of sinonasal TB have been documented in otherwise healthy, immunocompetent individuals (Khan et al. 2017; Dey et al. 2018) who were human immunodeficiency virus (HIV)-seronegative (Kant et al. 2013).

3.3 Clinical Features, Course, and Complications

Primary nasal TB has been described in the columella (Swain and Behera 2020), although it commonly involves the septum and inferior turbinate (Goguen and Karmody 1995; Kim et al. 2014). Common symptoms of nasal TB are chronic nasal obstruction, nasal discharge, crusting, ulcerations at the nasal vestibule and nasal cavity, and epistaxis (Kim et al. 2014; Swain et al. 2017). Left untreated, TB of the nasal cavity may invade the septum, leading to septal perforation and involvement of the contralateral nose. Septal perforation and cleft of the nasal ala may be present (Kim et al. 2007), and progression may result in a saddle nose deformity. Neglected cases of sinonasal TB may also lead to lupus vulgaris of the face and nasal vestibule (Kim et al. 2007). In this form, TB may encroach on the skin of the external nose and the paranasal area. Repeated activation of TB infection in the nasal cavity may also result in chronic fibrosis and contracture of the nasal alar region, leading to atrophic rhinitis and nasal cavity stenosis (Khan et al. 2017; Swain et al. 2017). Involvement of the lateral nasal wall and paranasal sinuses can cause unilateral nasal obstruction and epiphora (Dey et al. 2018).

Paranasal sinus TB mostly involves the maxillary sinus, and other sinuses are less frequently involved. Paranasal sinus TB resembles other granulomatous or neoplastic diseases and remains an underdiagnosed entity (Kant et al. 2013). Maxillary sinus TB may present with a facial abscess (Jha et al. 2002) or as a more chronic condition, such as multiple periodontal dental abscesses (Gupta et al. 2014). Sanehi et al. (2008) reported a case of maxillary and frontal sinus TB that presented as a swelling above the medial canthus, with no eye or nasal complaints, that was initially diagnosed as a frontal mucocele. Sharma and Baruah (2003) reported two cases of isolated sphenoid TB in children. On the other hand, sinus TB can be more destructive, mimicking a neoplasm. Muhammad et al. (2020) reported a left nasal cavity mass with contact bleeding extending to the nasopharynx, involving the nasal septum and filling the entire left maxillary sinus with bony destruction of anterolateral, posterior, and medial walls that manifested with five months of nasal blockade and epistaxis, and was initially diagnosed as a malignancy.

3.4 Imaging Features

3.4.1 Computed Tomography

There is a wide spectrum of CT appearances of sinonasal TB, ranging from diffuse mucosal thickening or opacification of sinus mimicking bacterial sinusitis, to heterogeneously enhancing soft tissue mimicking tumor (Lee et al. 1999; Shah et al. 2010; Kim et al. 2014; Rai et al. 2016; Swain et al. 2017; Upadhya et al. 2017; Dey et al. 2018; Muhammad et al. 2020) (Fig. 5a). The

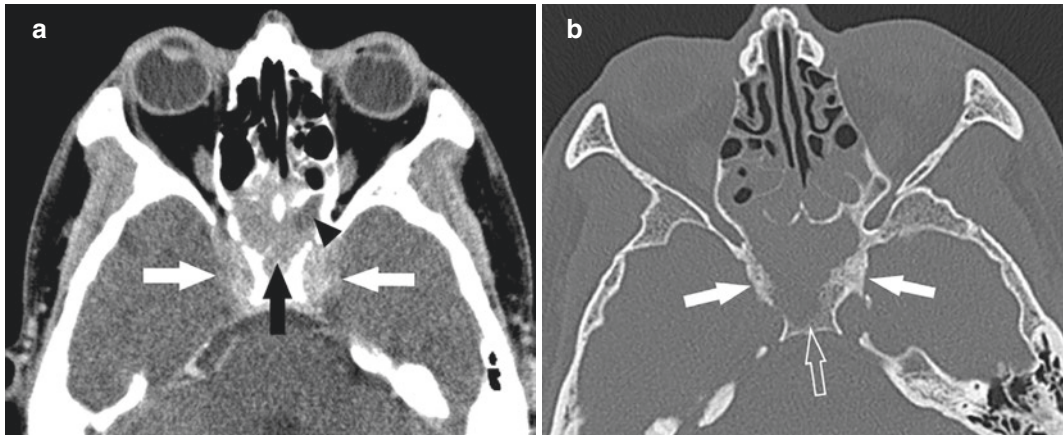

Fig. 5 Sinonasal tuberculosis. (**a**) Axial contrast-enhanced CT image shows an enhancing soft tissue mass in both sphenoid sinuses (black arrow) with hypodense area of necrosis (black arrowhead). The soft tissue extends outside the sphenoid sinus to involve both cavernous sinuses (white arrows). (**b**) Axial CT image taken in bone window setting shows sclerotic changes of the lateral walls of the sphenoid sinus (solid arrows) and destruction of the posterior wall of the sphenoid sinus (open arrow). The intersphenoid septum is also destroyed and cannot be identified

lesion may contain internal calcifications which may be a clue to diagnosis (Moon et al. 1997). The bony wall of the sinus may be intact, sclerotic, eroded, or extensively destroyed. Mixed sclerosis and erosion of the sinus wall can occur (Lee et al. 1999) (Fig. 5b). Obstruction of the sinus from TB may result in mucocele with bony wall erosion (Swain et al. 2017). The soft tissue infection may extend outside the sinonasal cavity to involve the orbit or intracranial structures such as the cavernous sinus, dura, or floor of the anterior cranial fossa.

3.4.2 Magnetic Resonance Imaging

Shah et al. (2010) reported the MRI appearance of a case of sinonasal TB seen as a soft tissue lesion that had isointense T1 signal, iso- to hyperintense T2 signal, and homogeneous contrast enhancement (Shah et al. 2010). In another report of tuberculous pansinusitis with orbital and intracranial extension, the lesion appeared as an infiltrative heterogeneous mass that had central hypointense signal on T2-weighted images and showed peripheral contrast enhancement (Rai et al. 2016).

3.5 Imaging Differential Diagnosis

Early sinonasal TB that shows only mucosal thickening in the sinus or opacification of the sinus, with or without bony wall sclerosis, is indistinguishable from the imaging appearances of acute or chronic bacterial sinusitis. When the disease progresses and appears as enhancing soft tissue, usually with bony destruction, the differential diagnosis may include invasive fungal sinusitis, and malignancy such as lymphoma, primary sinus carcinoma, or metastasis. Malignant tumors of the paranasal sinuses appear as an enhancing mass with bone destruction that is indistinguishable from sinonasal TB (Fig. 6).

On imaging, invasive fungal sinusitis may be seen as enhancing mucosal thickening, infiltrative enhancing soft tissue, bony destruction or extension outside the paranasal, similar to sinonasal TB. One uncommon finding that may help suggest acute invasive fungal sinusitis is nonenhancement of the nasal turbinate on contrast-enhanced MRI or the "black turbinate sign"

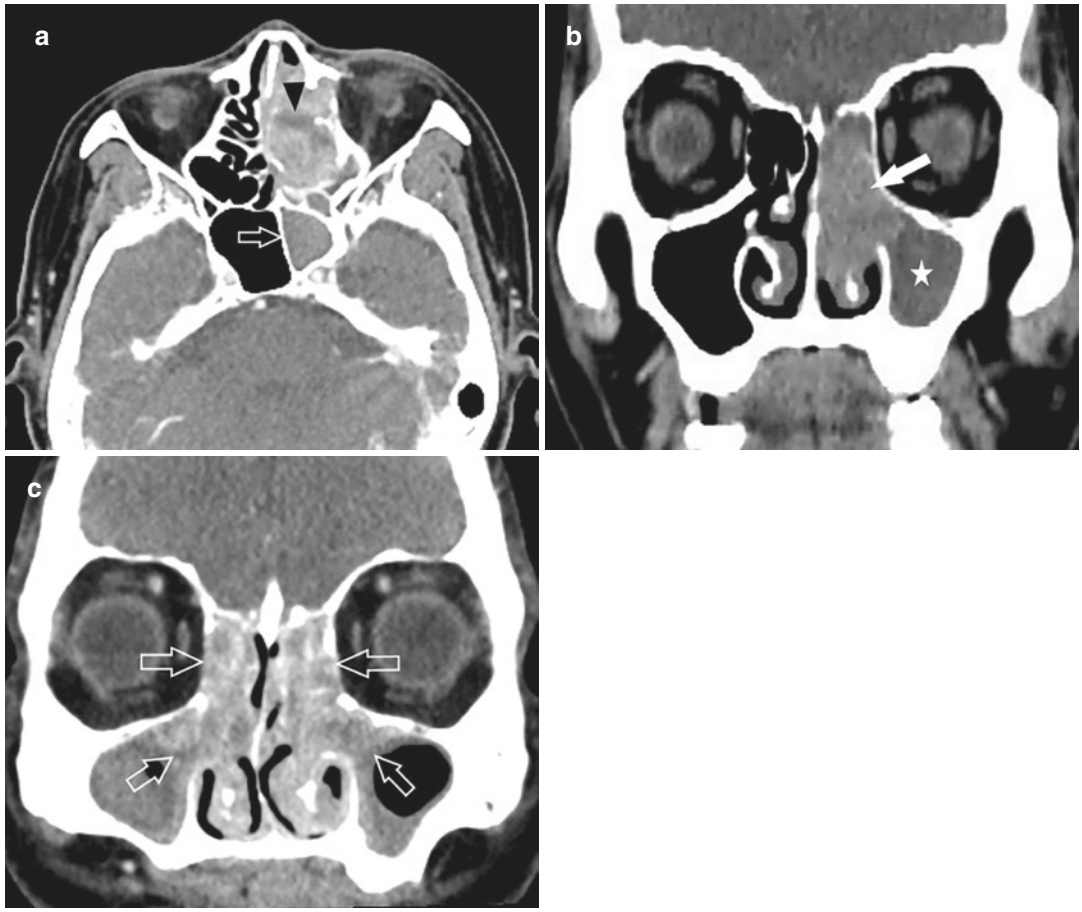

Fig. 6 Malignancies of paranasal sinuses in three different patients. (**a**) Squamous cell carcinoma of the left ethmoid sinus. Axial contrast-enhanced CT image shows an inhomogeneously enhancing mass with ethmoid septa destruction. Note the necrotic area within the mass (black arrowhead). The left sphenoid sinus is opacified due to ostial obstruction (open arrow). (**b**) Diffuse large B cell lymphoma in the left nasal cavity, left ethmoid sinus and ostium of left maxillary sinus. Coronal contrast-enhanced CT image shows inhomogeneously enhancing soft tissue with bony destruction of nasal turbinates, ethmoid septa and uncinate process (arrow). Opacification of the remaining part of the left maxillary sinus from ostium obstruction is present (star). (**c**) Extranodal natural killer (NK)/T cell lymphoma in bilateral nasal cavities, bilateral ethmoid sinuses and bilateral maxillary sinuses. Coronal contrast-enhanced CT image shows inhomogeneously enhancing soft tissue with destruction of the ethmoid walls, turbinates, and uncinate processes (open arrows)

(Safder et al. 2010). This sign may be occasionally observed on CT (Fig. 7a). Chronic invasive fungal sinusitis may present as a soft tissue mass with bony destruction (Fig. 7b, c). The characteristic marked T2-hypointense MRI signal within the lesion can help suggest fungal infection.

3.6 Diagnosis Confirmation

The diagnosis of nasal TB is based on histological identification of granulomatous inflammation, positive testing for acid-alcohol-resistant AFB and positive culture (Masterson et al. 2011). Aside from fine-needle aspiration

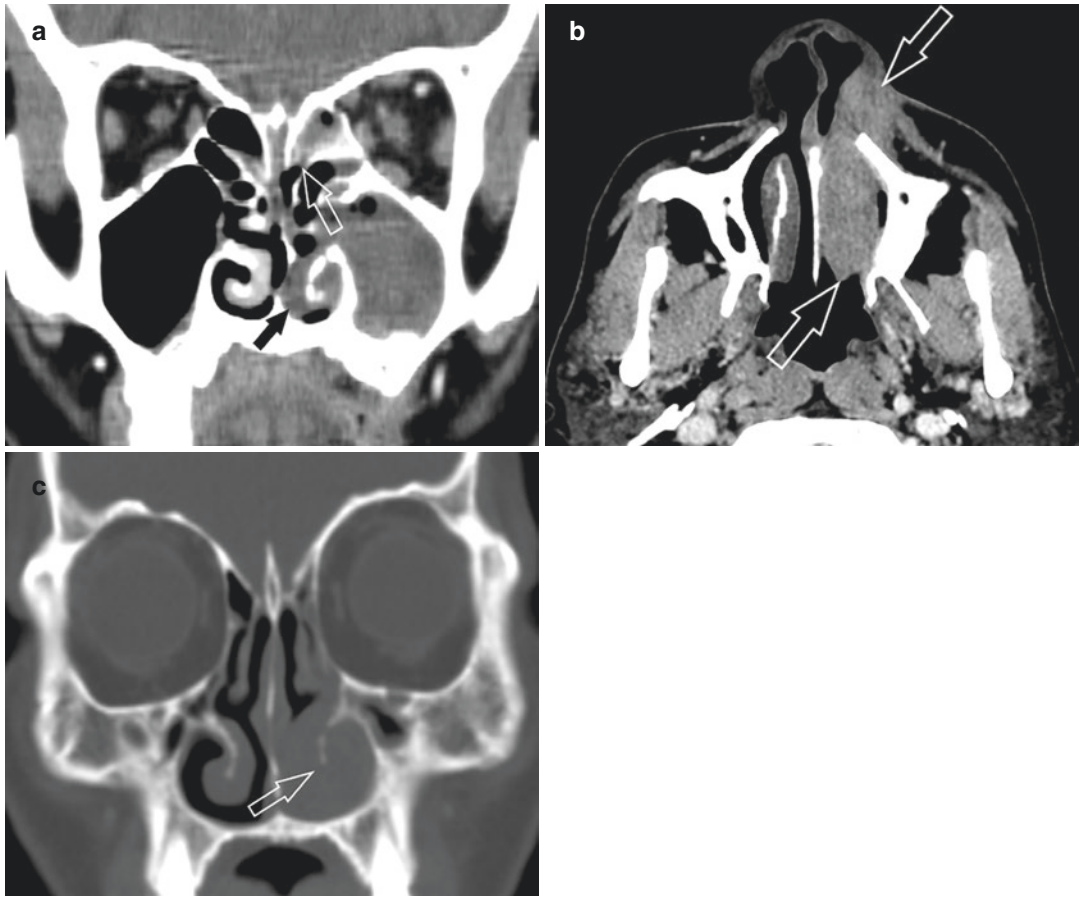

Fig. 7 Invasive fungal sinusitis in two different patients. (**a**) Acute invasive fungal sinusitis from *Rhizopus* species. Coronal contrast-enhanced CT image shows enhancing mucosal thickening in the left nasal cavity and left ethmoid sinus (open arrow) and opacification of the left maxillary sinus. Note nonenhancing mucosal lining of left inferior turbinate (black arrow) from ischemia (compared to the enhancing mucosa on the right side) which help suggest the diagnosis. (**b** and **c**) Chronic invasive fungal sinusitis from entomophthoromycosis. (**b**) Axial contrast-enhanced CT image shows homogeneously enhancing soft tissue infiltration at the left inferior turbinate, left nasal ala and premaxillary soft tissue (open arrows). (**c**) Coronal CT image taken in bone window setting shows erosion of the tip of the left inferior turbinate (open arrow)

cytology (FNAC) and Ziehl–Neelsen stain, Sanehi et al. (2008) also mentioned using the Mantoux tuberculin skin test to establish the diagnosis. However, such diagnosis of primary sinonasal TB is difficult. Nasal secretions and a nasal swab are not used for diagnosis due to low yield, and AFB are difficult to detect in surgical specimens (Kim et al. 2014). Cases are often diagnosed in hindsight by histopathology (Gleitsmann 1907; Sharma and Baruah 2003; Kant et al. 2013; Khan et al. 2017; Dey et al. 2018; Muhammad et al. 2020). Histologically, spherical granulomas with central caseous necrosis imply TB (Kim et al. 2014). Often, neither histological nor bacteriological confirmation is possible, and diagnosis is made based on empirical response to anti-TB medications (Kim et al. 2014).

3.7 Treatment

Multidrug anti-TB therapy is the keystone of management for nasal TB (Khan et al. 2017; Swain et al. 2017). As with other forms of extrapulmonary TB, the duration of treatment may last from six to 12 months, depending on local TB guidelines (Kim et al. 2007). Therapy usually includes initial treatment with three or more bactericidal drugs (active phase), followed by a prolonged maintenance phase with at least two anti-TB drugs (Swain et al. 2017). According to Kim et al. (2014), TB involving the nasal cavity can be treated with anti-TB medications only, while TB involving both the nasal cavity and paranasal sinus as well as those involving the paranasal sinus alone may need additional sinus surgery for sinus drainage and specimen collection. Of the two cases of maxillary sinus TB reported by Kant et al. (2013), one that presented at an early stage could be managed with anti-TB medications alone; the other that presented late required surgical intervention as well. Good responses to anti-TB medications were reported in cases of TB of the maxillary and frontal sinus (Sanehi et al. 2008) and sphenoid sinus (Sharma and Baruah 2003).

4 Pharyngeal Tuberculosis

4.1 Introduction

Primary pharyngeal TB is extremely rare, even in endemic areas (Theisen 1899; Gupta et al. 2005). Before the turn of the century when it was seen more frequently, reports of TB of the pharynx ranged from a high of 1% of all cases of TB of the upper air passages claimed by Lennox Browne, to a more probable low of 0.07%, representing one case out of 1,317 autopsies of cases of TB reported by Willigk (Theisen 1899; Williams 1901; Newcomb 1904). The pharynx is much less affected than the larynx (Goyal et al. 1998). Theisen (1899) cited Bosworth as having seen only five cases, and Levy only finding 17 cases confined to the pharynx compared to 145 cases with laryngeal involvement.

Although it occurs more commonly in association with pulmonary TB (Hajioff et al. 1999; Gupta et al. 2005), secondary TB of the pharynx is also quite rare (Madhuri et al. 2002). According to Newcomb (1904), TB of the pharynx was only found in 14/1226 cases of pulmonary TB. Pharyngeal TB has been described in the oropharynx-soft palate (Haddad et al. 1987), tonsils (Selimoglu et al. 1995; Al-Serhani and Al-Mazrou 2001; Krishnappa 2006; Sellami et al. 2017; Tisekar et al. 2020), and posterior oropharyngeal wall (Hajioff et al. 1999; Madhuri et al. 2002; Gupta et al. 2005). Other reported sites are the nasopharynx (Bath et al. 1992; Chopra et al. 1994; Percodani et al. 1999; Al-Serhani and Al-Mazrou 2001; Cai et al. 2013; Mishra et al. 2015; Srivanitchapoom and Sittitrai 2016) including the adenoids (Mahindra et al. 1981; Patil et al. 2013), and hypopharynx (Al-Serhani and Al-Mazrou 2001)—vallecula and pyriform sinus (Goyal et al. 1998; Iravani et al. 2015).

4.2 Pathophysiology

Pharyngeal TB may be uncommon due to the protective mechanisms of the upper respiratory tract. These may include the cleansing mechanism of saliva containing saprophytes with phagocytic properties, thick epithelium cover (Goyal et al. 1998), and antagonistic property of striated musculature to bacillus invasion (Gupta et al. 2005). Other protective characteristics of the pharynx are its local pH (Pande et al. 1995). Although the usual lymphatic and hematogenous routes may be involved in secondary pharyngeal tuberculous infection, nonpulmonary primary infection, contiguous spread from another organ and epithelial implantation are still possible mechanisms of infection (Srivanitchapoom and Sittitrai 2016).

The main predisposing factor for direct inoculation is a breach or break in the mucosa which

then allows admission of TB bacilli (Madhuri et al. 2002). This may be secondary to chronic irritation or inflammation. According to Lugton (1999), another mechanism by which pathogenic mycobacteria cross mucosal barriers is by endocytosis within mucosal lymphoepithelial sites (e.g., tonsils, adenoids, Peyer's patches): bacilli discharged at basolateral surfaces of engulfing epithelial M cells are taken up by antigen-presenting cells associated with parafollicular T lymphocytes. Dendritic cells and macrophages in these sites allow mycobacterial replication, due to the permissive immunological environment in lymphoepithelial tissues. Abrogation of local delayed-type hypersensitivity reactions generally ensures continuing integrity and function of these tissues. Phagocytes containing intracellular mycobacteria disseminate infection to other parts of the body and also probably migrate back onto the mucosal surface to shed bacilli. Other predisposing factors for infection are poor dental hygiene, leukoplakia, and dental extraction (Gupta et al. 2005).

4.3 Clinical Features, Course, and Complications

Pharyngeal TB should be considered in patients presenting with sore throat, odynophagia, dysphagia, and neck swelling (Gupta et al. 2005). According to Al-Serhani and Al-Mazrou (2001), the main presenting symptom in nasopharyngeal TB is a neck mass, whereas tonsillar TB presents with sore throat or discomfort, and hypopharyngeal TB manifests with dysphagia. There may be fever and malaise (Hajioff et al. 1999). Both tonsils may be symmetrically enlarged, but unilateral enlargement, with or without ulcers, may be seen on the tonsil or oropharyngeal wall (Al-Serhani and Al-Mazrou 2001). Ulcero-granulomatous lesions of the tonsil may be tender, bleed when touched (Krishnappa 2006), and may mimic a malignancy (Sellami et al. 2017).

Ulcerative oropharyngeal lesions can also be red, granular, and bleed on touch (Madhuri et al. 2002; Gupta et al. 2005), and can be confined to the posterior oropharyngeal wall (Gupta et al. 2005) or extend to the nasopharynx and laryngopharynx (Madhuri et al. 2002). Such lesions can masquerade as a malignancy (Goyal et al. 1998). Nasopharyngeal TB may present similarly to nasopharyngeal carcinoma, with neck masses or cervical lymphadenopathy, nasal obstruction, rhinorrhea, epistaxis, otalgia, and hearing loss; along with such constitutional symptoms as fever, weight loss, and night sweats (Al-Serhani and Al-Mazrou 2001; Mishra et al. 2015). Concomitant otalgia and otorrhea in a case of nasopharyngeal TB have been reported (Bath et al. 1992). Cai et al. (2013) recorded a case of diplopia in nasopharyngeal TB without signs of involvement of the orbits, orbital fissures, or orbital apex. Nasal endoscopy may exhibit a normal nasopharynx, diffuse inflammation and ulceration of respiratory mucosa (Cai et al. 2013), polypoidal mass lesion arising from the adenoids (Mishra et al. 2015), or granulomas (Al-Serhani and Al-Mazrou 2001).

4.4 Imaging Features

4.4.1 Computed Tomography

There are two CT patterns of TB in the nasopharynx, namely polypoid mass and diffuse mucosal thickening. The polypoid mass is more common and almost always involves the roof of the nasopharynx where adenoid tissue is located (King et al. 2003a; Cai et al. 2013). The mass may appear homogeneous on CT or heterogeneous from internal necrosis (Fig. 8). The polypoid mass arising from TB is small, being generally smaller than 2 cm in size (Cai et al. 2013). A small mass at the roof of the nasopharynx with internal necrosis is unlikely to be malignant and if present, may help suggest TB (Cai et al. 2013). The diffuse mucosal thickening type may be unilateral (Fig. 9) or bilateral but asymmetrical. Both polypoid mass and

diffuse mucosal thickening types are usually confined within the nasopharynx (King et al. 2003a; Cai et al. 2013).

Extension outside the nasopharynx is extremely rare and only one case with mild involvement of the longus capitis muscle has been reported (Percodani et al. 1999). Calcification was not observed in a large series of nasopharyngeal TB by Cai et al. (2013). Necrotic cervical lymphadenopathy is common in nasopharyngeal TB and the most commonly involved site is the retropharyngeal region. Oropharyngeal and hypopharyngeal TB is rarely investigated by imaging except when it presents with a mass. A heterogeneously enhancing mass with internal calcifications from oropharyngeal TB has been reported in one study, in which the mass showed a large necrotic area suggesting abscess formation on the follow-up imaging (Bharatha et al. 2010).

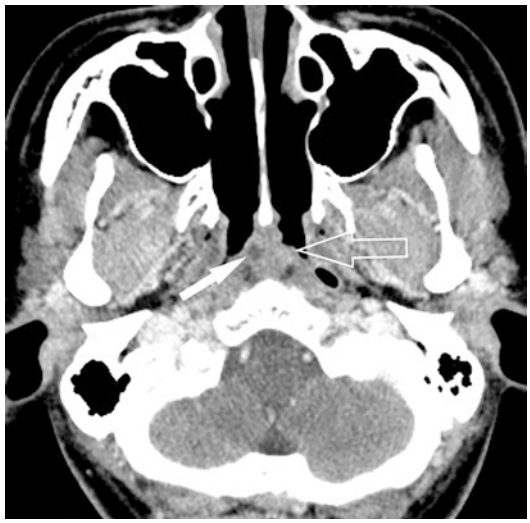

Fig. 8 Nasopharyngeal tuberculosis (polypoid mass type). Axial contrast-enhanced CT image shows a polypoid mass at the nasopharyngeal roof (open arrow) with internal hypodense area of necrosis (solid arrow)

4.4.2 Magnetic Resonance Imaging

Nasopharyngeal TB appears as having iso- or slightly hyperintense signal on T1-weighted images and slightly hyperintense signal on T2-weighted images (Cai et al. 2013) (Fig. 10). The area of internal necrosis shows T1-hypointense and T2-hyperintense signals. The adenoid involvement may show destruction of the normal vertical stripe from destruction of the internal architecture of lymphoid tissue (King et al. 2003a).

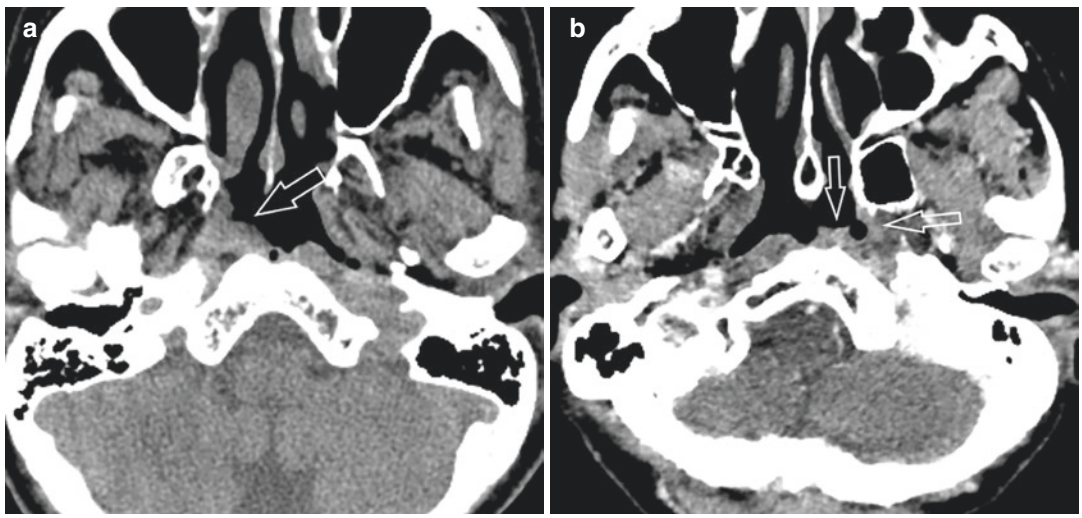

Fig. 9 Nasopharyngeal tuberculosis (diffuse mucosal thickening type) in two different patients. (**a**) Axial unenhanced CT image shows mucosal thickening at right posterior and lateral wall of nasopharynx (open arrow). (**b**) Axial contrast-enhanced CT image in a different patient shows enhancing mucosal thickening at left posterior and lateral wall of nasopharynx (open arrows). No extension outside the nasopharynx is observed

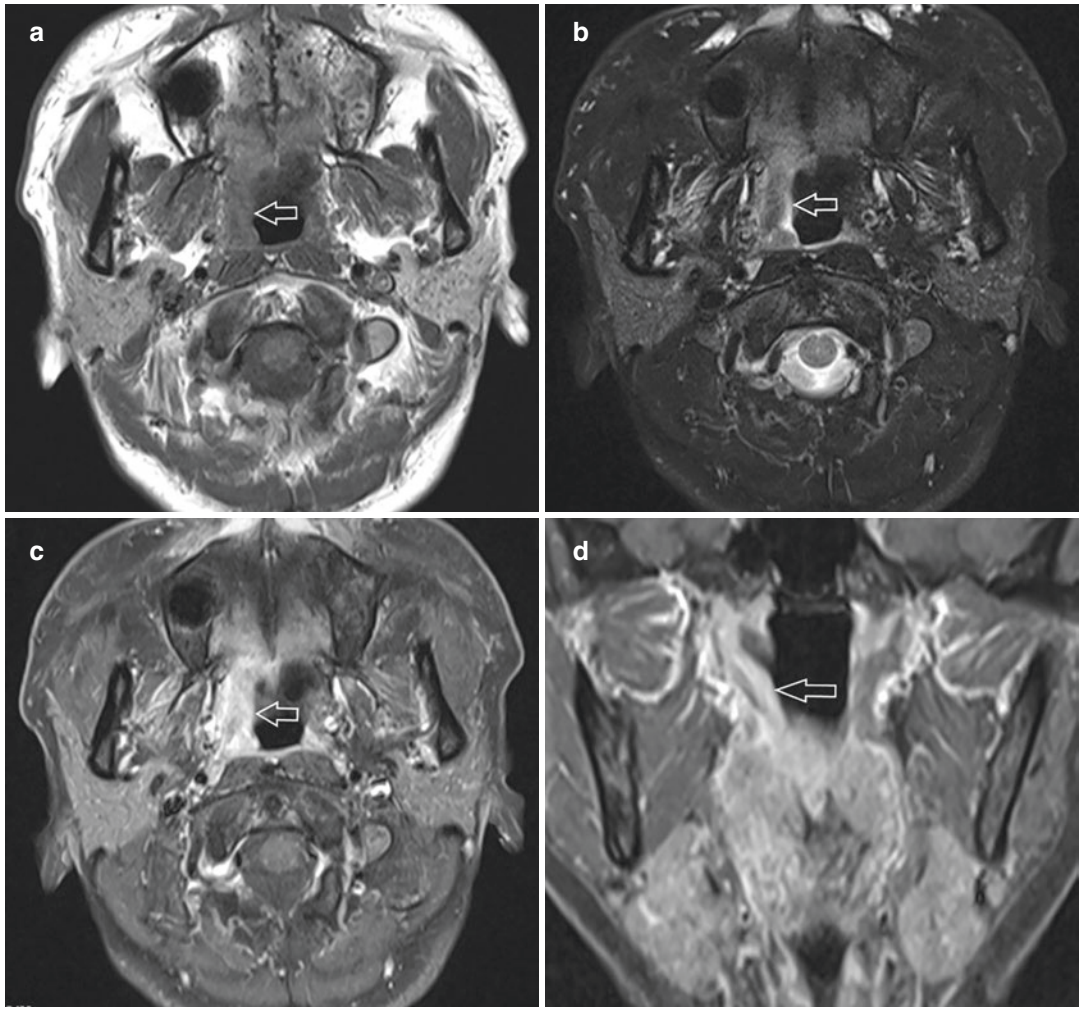

Fig. 10 MRI of nasopharyngeal tuberculosis in a 43-year-old man who presented with right otitis media and right-sided hearing loss. Axial (**a**) T1-W and (**b**) fat-suppressed T2-W MR images show mucosal thickening at right lateral wall of nasopharynx which show isointense signal on T1-W and slightly hyperintense signal on T2-W images (open arrows). Axial (**c**) and coronal (**d**) contrast-enhanced fat-suppressed T1-W MR images show enhancement of the mucosal thickening at the right lateral wall of nasopharynx (open arrows). [Courtesy of Dr. Geoiphy Pulickal, Khoo Teck Puat Hospital, Singapore]

4.5 Imaging Differential Diagnosis

Adenoid hypertrophy may be present in some adults and sometimes be confused with nasopharyngeal pathology such as malignancy or inflammatory disease. Since the adenoids are the primary site of tuberculous involvement in the nasopharynx, adenoid enlargement from TB may be confused with adenoid hypertrophy. Almost half of normal adenoids typically show vertical, alternating dark and bright stripes on contrast-enhanced MRI (Bhatia et al. 2012) (Fig. 11). In TB, the stripe changes may be undefined, curved, and thick, compared to normal adenoids (Cai et al. 2013).

Nasopharyngeal carcinoma may present as a mass or infiltrative lesion along the nasopharyngeal wall. The common location of early cancer is at the fossa of Rosenmuller, while TB usually occurs at the nasopharyngeal roof. Nasopharyngeal carcinoma rarely shows

internal necrosis, especially when it is small, while nasopharyngeal TB does. More advanced nasopharyngeal carcinoma can be large and extends outside the nasopharynx (Fig. 12), while TB is usually small and confined within the nasopharynx. Nasopharyngeal lymphoma can present as a mass or infiltrative lesion in the nasopharynx. Lymphoma tends to be large, homogeneously enhanced without necrosis, and extends outside the nasopharynx at presentation (Fig. 13), in contrast to TB (King et al. 2003b).

Other infiltrative diseases in the nasopharynx may have the same appearance as TB on imaging. Nasopharyngeal amyloidosis may present as diffuse mucosal thickening with heterogeneous enhancement, mimicking tumor and TB (Fig. 14). Associated calcifications within the mass on CT may help suggest the diagnosis of amyloidosis rather than TB (Gean-Marton et al. 1991). On MRI, T2-hypointense signal has been suggested to be characteristic of amyloidosis (Gean-Marton et al. 1991). However, amyloidosis showing T2-hyperintense signal has also been reported (Hegarty and Rao 1993; Chen et al. 2010).

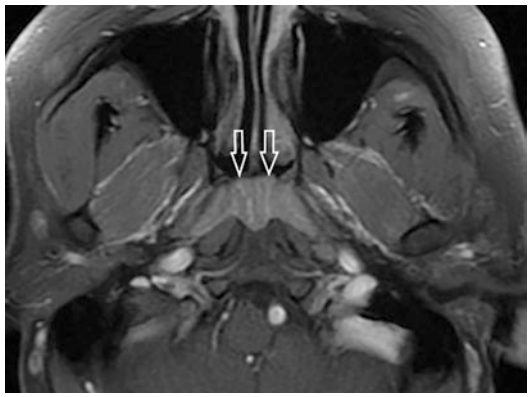

Fig. 11 Normal adenoid tissue. Axial contrast-enhanced fat-suppressed T1-W MR image shows alternating dark and bright vertical stripes typical of adenoid tissue in the nasopharynx (open arrows)

4.6 Diagnosis Confirmation

The diagnosis is confirmed by identification of AFB in smears or cultures, histopathological features consistent with TB (e.g., caseous necrosis, epithelioid giant cells) from biopsy specimens, and a response to treatment (Al-Serhani and Al-Mazrou 2001). Specimens for AFB smear and culture may be obtained from FNAC of cervical

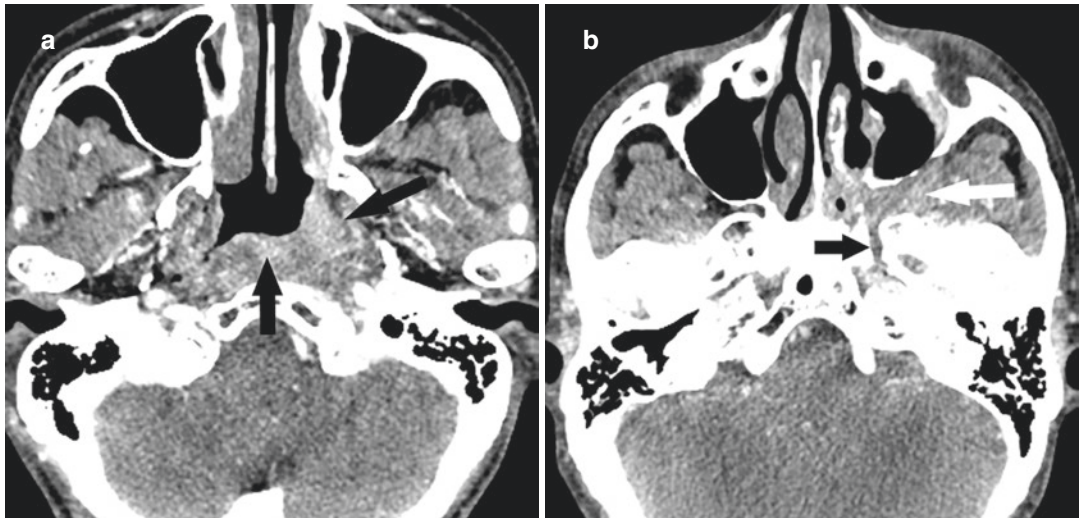

Fig. 12 Nasopharyngeal carcinoma. (**a**) Axial contrast-enhanced CT image shows infiltrative enhancing soft tissue at the posterior wall and left lateral wall of the nasopharynx (black arrows). Biopsy showed nonkeratinizing undifferentiated carcinoma. (**b**) Axial contrast-enhanced CT image at the skull base shows extension of the carcinoma into the left pterygopalatine fossa (white arrow) and left vidian canal (black arrow)

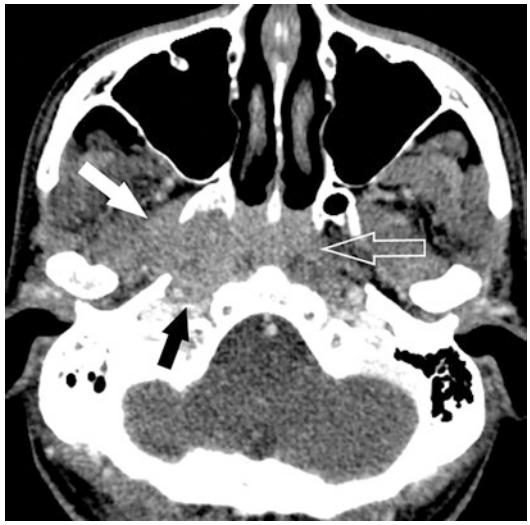

Fig. 13 Nasopharyngeal lymphoma. Axial contrast-enhanced CT image shows enhancing homogeneous soft tissue on both sides of the nasopharynx (open arrow) with involvement of the right masticator space (white arrow) and right jugular foramen (black arrow)

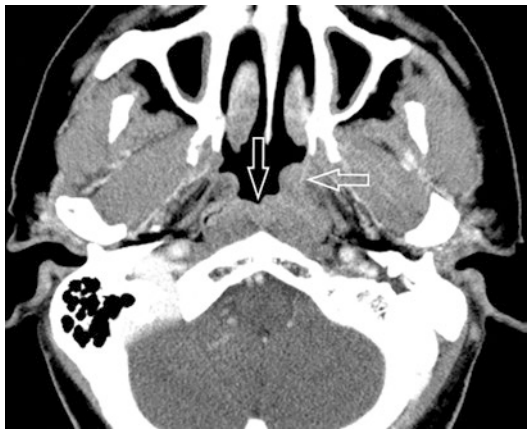

Fig. 14 Nasopharyngeal amyloidosis. Axial contrast-enhanced CT image shows infiltrative enhancing soft tissue in the posterior wall and left lateral wall of the nasopharynx (open arrows), indistinguishable from nasopharyngeal tuberculosis and malignancy

lymph nodes, if present, or tissue biopsy of the pharyngeal lesion (Krishnappa 2006). The PCR test may offer results faster than cultures (Mishra et al. 2015). Chest radiographs may reveal pulmonary TB (Madhuri et al. 2002).

4.7 Treatment

The mainstay of treatment for pharyngeal TB is similar to that for other forms of extrapulmonary head and neck TB. Adherence to treatment protocols with first-line combination anti-TB medications, namely isoniazid, rifampicin, ethambutol, and pyrazinamide, may result in resolution of lesions without the need for surgery, which is reserved for nonresponsive cases.

5 Laryngeal Tuberculosis

5.1 Introduction

Laryngeal TB is rare (Wang et al. 2007), but is the most common granulomatous disease of the larynx (Ozüdogru et al. 2005; Lucena et al. 2015), dating back to antiquity. According to Hirsch (1935), Hippocrates knew of phthisis of the larynx, and probably also noticed its connection with consumption that Galen recognized, but the first successful descriptions of the pathological changes of the larynx were made by Morgagni in the seventeenth century. Laennec drew special attention to the causal relation between laryngeal diseases and the lungs (Habershon 1905; Hirsch 1935), and Louis, Andral, and Trousseau believed tuberculous laryngitis was inseparable from simultaneous pulmonary TB (Habershon 1905).

Primary TB of the larynx is even rarer (El Kettani et al. 2010; Agarwal et al. 2019; Swain et al. 2019), and the great authorities of the latter part of last century (Heinze, Mackenzie, Shrötter, and Schnitzler of Vienna among others) all asserted that primary TB of the larynx was practically unknown, or exceedingly rare (Habershon 1905). However, changing trends show more cases without pulmonary TB, with clinical presentations different from those of classic reports (Kandiloros et al. 1997; Shin et al. 2000; Lucena et al. 2015). Most patients now diagnosed with laryngeal TB do not have any pulmonary symptoms or history of pulmonary TB (Leahy 2020).

5.2 Pathophysiology

In the preantibiotic era, laryngeal TB was caused by secondary laryngeal seeding by *M. tuberculosis* bacilli that were coughed and expectorated from the tracheobronchial tree (Ponni et al. 2019), with pooling of mycobacterium-rich sputum along the posterior airway in supine, bedridden patients; possibly explaining why the posterior larynx was most commonly affected (Rizzo et al. 2003; Ling et al. 2010). The increasing number of sputum-negative laryngeal cases without pulmonary TB suggest primary laryngeal TB or hematogenous spread, with increasing anterior laryngeal involvement (Kandiloros et al. 1997; Kenmochi et al. 2003; Ling et al. 2010). TB rarely spreads towards the larynx via lymphatic vessels (Swain et al. 2019).

Primary tuberculous laryngitis is acquired by direct inhalation and subsequent invasion of *M. tuberculosis* bacilli in the larynx. Laryngeal infection starts with exudation in the subepithelial space, which is then followed by round cell infiltration and subsequent fibrosis (Ozüdogru et al. 2005). Chronic granulomatous foci may be present, with or without caseation necrosis (Agarwal et al. 2019). Ulceration and fibrosis can interfere in the process of voice production. Involvement of the mucous lining of the vocal folds can change their flexibility and consequently change voice quality, causing dysphonia in most cases (Lucena et al. 2015).

5.3 Clinical Features, Course, and Complications

Hoarseness is the most common presenting symptom overall (Shin et al. 2000; Lim et al. 2006; Wang et al. 2007; Ling et al. 2010; Lucena et al. 2015; Swain et al. 2019; Zang et al. 2020), appearing in early-stage laryngeal TB (Dworetzky 1917), although it may be the only symptom, even in severe laryngeal TB (Kenmochi et al. 2003). Other symptoms may include dysphagia, odynophagia, sore throat, productive cough, and weight loss (El Kettani et al. 2010; Leahy 2020; Zang et al. 2020). Symptoms typically correlate with physical findings. A comparative review by Ling et al. (2010) revealed that the most frequent chief complaint of younger patients seen before 1990 was odynophagia accompanying systemic symptoms and pulmonary TB, and the posterior part of the larynx was commonly involved with multiple ulcerative lesions. In contrast, the most frequent chief complaint of older patients seen after 1998 was hoarseness (71.4%), with the most common lesion site being the true vocal cords (57.2%).

In the past, the typical patient was younger, with ulcerated laryngeal lesions, perichondritis and advanced cavitary lung disease. A series of older patients reported by Kandiloros et al. (1997) had tumor-like lesions and/or chronic non-specific laryngitis on microlaryngoscopy, with no significant ulcerations or signs of perichondritis. Similarly, separate series by Shin et al. (2000) and Ling et al. (2010) observed that patients with active pulmonary TB showed more ulcerative and multiple lesions, while patients with normal lung status showed non-specific, polypoid, and single lesions. Zang et al. (2020) also observed a higher proportion of concurrent pulmonary TB among patients with extensive and ulcerative lesions, compared to patients without concurrent pulmonary TB and with more localized and exophytic lesions.

The appearance and localization of lesions thus seem to have changed over time. The posterior glottis was previously the most common location (Rizzo et al. 2003; Ling et al. 2010; Ponni et al. 2019), but other subsites have become more common, especially the true vocal folds, followed by the false (vestibular, ventricular) vocal folds (Shin et al. 2000; Lim et al. 2006; Wang et al. 2007; El Kettani et al. 2010; Ling et al. 2010; Lucena et al. 2015; Swain et al. 2019; Leahy 2020). The epiglottis, arytenoids, aryepiglottic folds, and interarytenoid region/posterior commissure have also been involved (Lim et al. 2006; Lucena et al. 2015). These lesions may be nodular, granulomatous, exophytic, or ulcerative (Shin et al. 2000; Lim et al. 2006; Agarwal et al. 2019), but polypoid or non-specific inflammatory appearances (including swelling of the vocal

cords or epiglottis) may also be seen (Moon et al. 1996; Shin et al. 2000; Lim et al. 2006).

Laryngeal TB is usually misdiagnosed as laryngeal cancer, especially in patients with malignant signs such as enlarged cervical lymph nodes and vocal fold immobility (Kenmochi et al. 2003; Wang et al. 2007; El Kettani et al. 2010; Swain et al. 2019; Leahy 2020). Inflammatory changes may trigger laryngeal edema that, if severe enough, may obstruct the airway acutely (Cole et al. 2018). In the long term, irreversible changes in voice quality can occur due to fibrotic changes in the vocal folds, even after clinical healing of disease (Ozüdogru et al. 2005; Lucena et al. 2015).

5.4 Imaging Features

5.4.1 Computed Tomography

CT is better than laryngoscopic examination in demonstrating extension of laryngeal involvement because it shows the extension into the tissues deep to the mucosa. Three patterns of CT appearance have been described in the literature, namely diffuse thickening with enhancement, mass, and frank pus or fluid collection (Aspestrand et al. 1989; Moon et al. 1996; Kim et al. 1997; Muranjan and Kirtane 2001). Diffuse thickening with enhancement of the larynx is the most common pattern (Figs. 15 and 16). The degree of mucosal enhancement is usually pronounced. Bilateral involvement is common on CT but may be asymmetrical. The surface of the epiglottis may be smooth or irregular (Fig. 17). Clouding or infiltration of paralaryngeal fat was always present in the study of Moon et al. (1996) but none was found in the study of Kim et al. (1997).

Although a polypoid mass or fungating mass is commonly seen on laryngoscopic examination, CT finding of a mass lesion from laryngeal TB is less commonly found (Moon et al. 1996; Kim et al. 1997). The mass itself may be difficult to differentiate from early cancer on CT (Fig. 18). Diffuse, bilateral enhancement of the laryngeal mucosa, calcifications in necrotic lymph nodes, and presence of pulmonary TB may help in diagnosis of TB, if they accompany a mass lesion in the larynx, especially in young patients. But radiologists should keep in mind that laryngeal TB and cancer of the larynx can coexist, although rarely.

Tuberculous abscess rarely occurs in the larynx and if present, is seen as a low-density

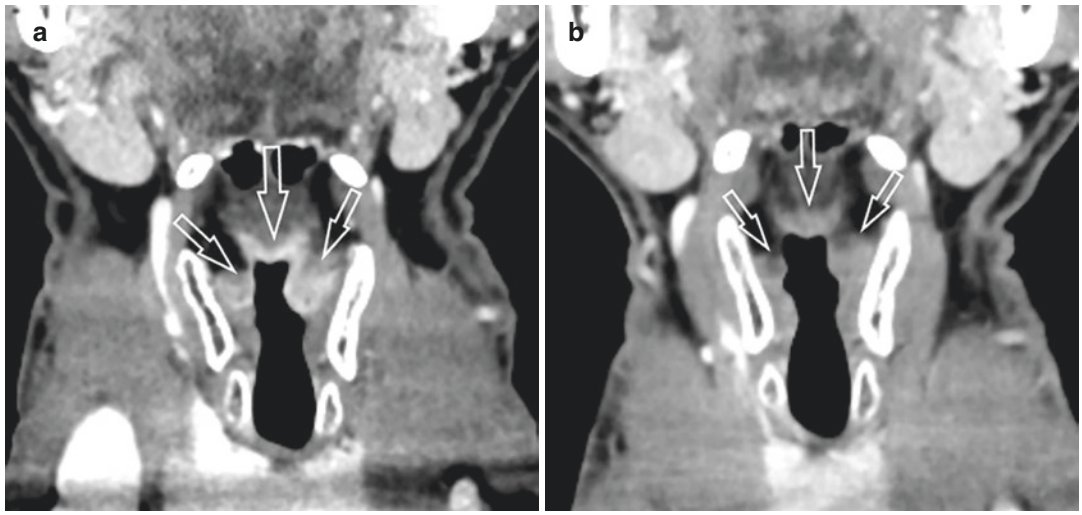

Fig. 15 Diffuse enhancement in laryngeal tuberculosis. (**a**) Coronal contrast-enhanced CT image shows diffuse, bilateral, pronounced enhancement of the supraglottis (open arrows). (**b**) Coronal contrast-enhanced CT image after 6 months of anti-tuberculosis medication shows disappearance of the supraglottic enhancement (open arrows)

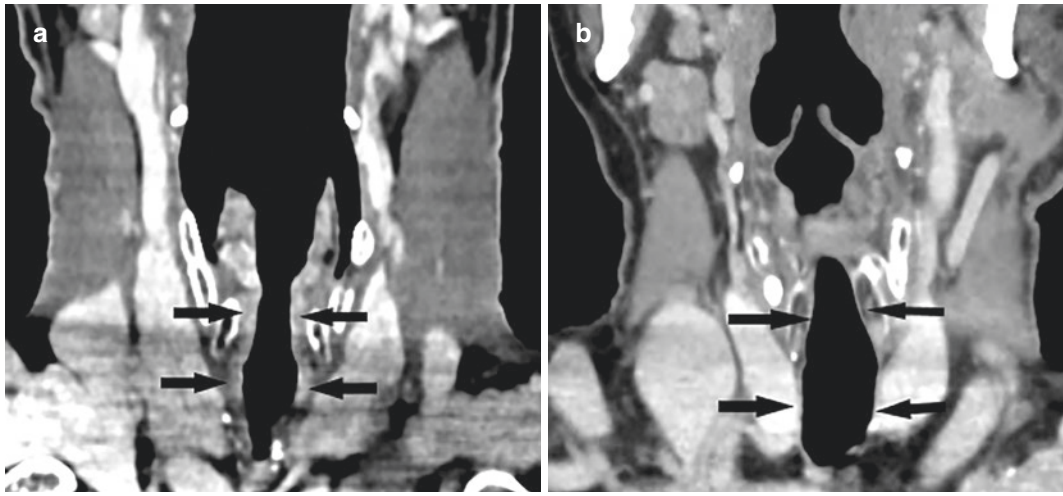

Fig. 16 Laryngeal tuberculosis with subglottic and tracheal involvement. (**a**) Coronal contrast-enhanced CT image shows thickening of subglottic and tracheal mucosa with diffuse enhancement (arrows). (**b**) Coronal contrast-enhanced CT image in a different patient shows normal subglottic airway and trachea without soft tissue thickening (arrows)

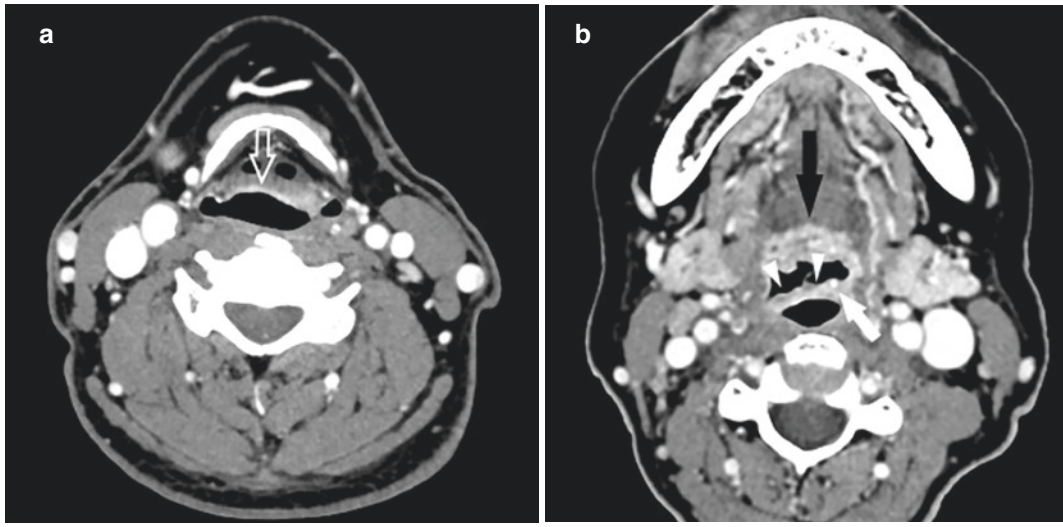

Fig. 17 Epiglottic involvement in laryngeal tuberculosis in two different patients. (**a**) Axial contrast-enhanced CT image shows diffuse, smooth thickening of the epiglottis with enhancement of the laryngeal surface (open arrow). (**b**) Axial contrast-enhanced CT image in a different patient shows thickening and irregularity of the epiglottic surface with enhancement of the epiglottis (small arrowheads) and valleculae (black arrow). A small round calcification is present at the lingual surface of epiglottis (white arrow)

fluid collection with rim enhancement (Aspestrand et al. 1989; Muranjan and Kirtane 2001). Coarse calcifications may be observed in the abscess area and may help distinguish tuberculous abscess from other causes (Fig. 19). Ulceration of the laryngeal surface is rarely seen on CT (Moon et al. 1996; Kim et al. 1997) (Fig. 20a). Laryngeal cartilages are usually intact in laryngeal TB. Reactive sclerosis of the cartilage is rarely seen (Fig. 20b). Destruction of the cartilages from laryngeal TB has not been reported. Up to

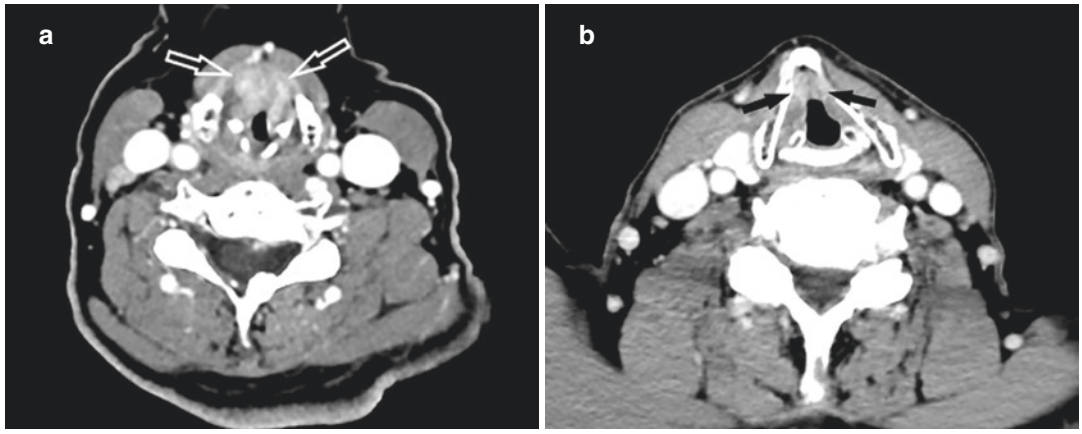

Fig. 18 Laryngeal tuberculosis presenting as a vocal cord mass mimicking cancer. (**a**) Axial contrast-enhanced CT image shows a heterogeneously enhancing mass at the anterior false and true vocal cords bilaterally (open arrows). The mass has the same appearance as a mass due to cancer. (**b**) Axial contrast-enhanced CT image of a different patient with glottic cancer shows a small enhancing mass at anterior true vocal cords with anterior commissure involvement (arrows)

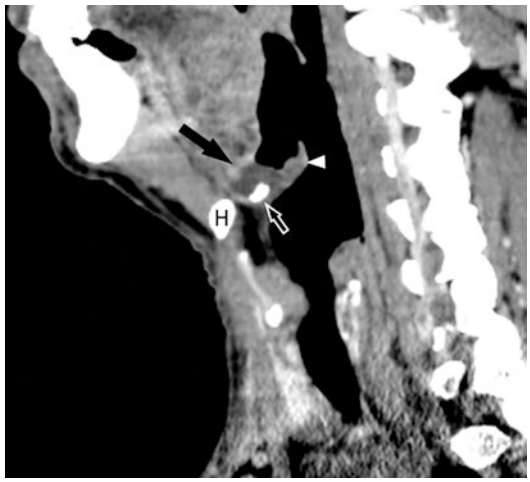

Fig. 19 Laryngeal tuberculosis with abscess formation. This patient presented with cervical lymphadenopathy which turned out to be from metastatic poorly differentiated carcinoma of unknown origin. ENT examination showed a mass at the left side of the epiglottis. Biopsy of the epiglottic mass showed granuloma and the tissue was strongly positive for acid-fast bacilli. Sagittal contrast-enhanced CT image shows thickening of the epiglottis (arrowhead) with a rim-enhancing fluid collection at the epiglottic base extending to the vallecula (black solid arrow). A calcification within the abscess wall is present (small open arrow). H = hyoid bone

50% of patients with laryngeal TB have cervical lymphadenopathy on CT (Moon et al. 1996; Kim et al. 1997).

5.4.2 Magnetic Resonance Imaging

There have only been a few reports of MRI being performed on patients with laryngeal TB. The findings are non-specific diffuse enhancement of the vocal cords and/or supraglottis with diffuse swelling (Lou and Li 2019).

5.5 Imaging Differential Diagnosis

Nontuberculosis mycobacterial (NTM) laryngitis is extremely rare. The clinical presentation and laryngoscopic examination are the same as laryngeal TB (Yan et al. 2020). The imaging findings of NTM laryngitis have not been described in the literature. Our case of NTM laryngitis showed diffuse swelling with mucosal enhancement of the free edge of the epiglottis and both aryepiglottic folds, indistinguishable from laryngeal TB (Fig. 21).

Laryngeal carcinoma can have the same appearance as laryngeal TB on laryngoscopic examination and on imaging. Early infiltrative cancer can have mucosal or deeper soft tissue enhancement, similar to the diffuse enhancement type of laryngeal TB. However, early cancer is more likely to involve only one side of the larynx, while TB frequently involves both sides

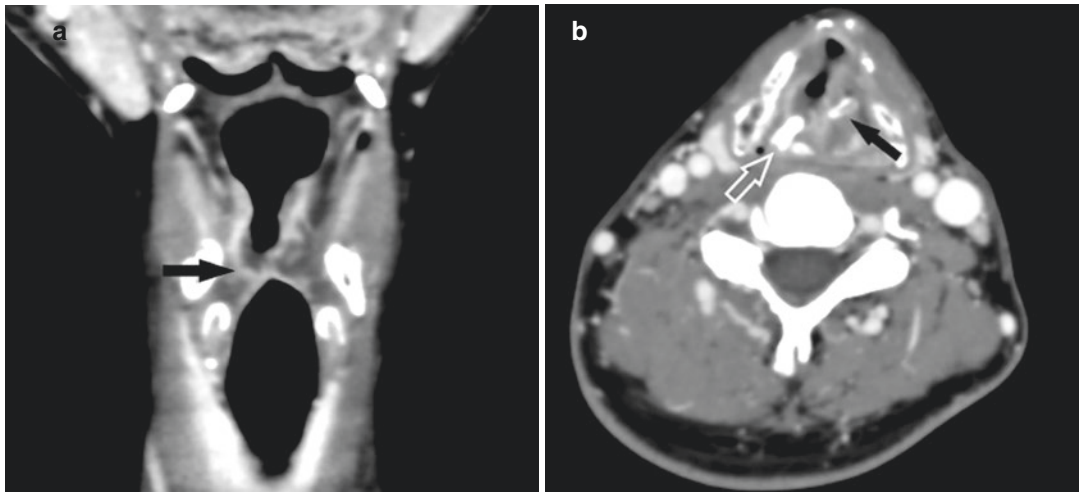

Fig. 20 Laryngeal tuberculosis with ulceration and cartilage sclerosis. (**a**) Coronal contrast-enhanced CT image shows enhancing mucosa of both false and true vocal cords with ulceration and necrotic tissue of the right true vocal cord (arrow). (**b**) Axial contrast-enhanced CT image shows sclerosis of the right arytenoid cartilage (open arrow) associated with the ulceration. The patient also has anteromedial deviation of the left arytenoid cartilage from left true vocal cord paralysis (black arrow) of unknown cause

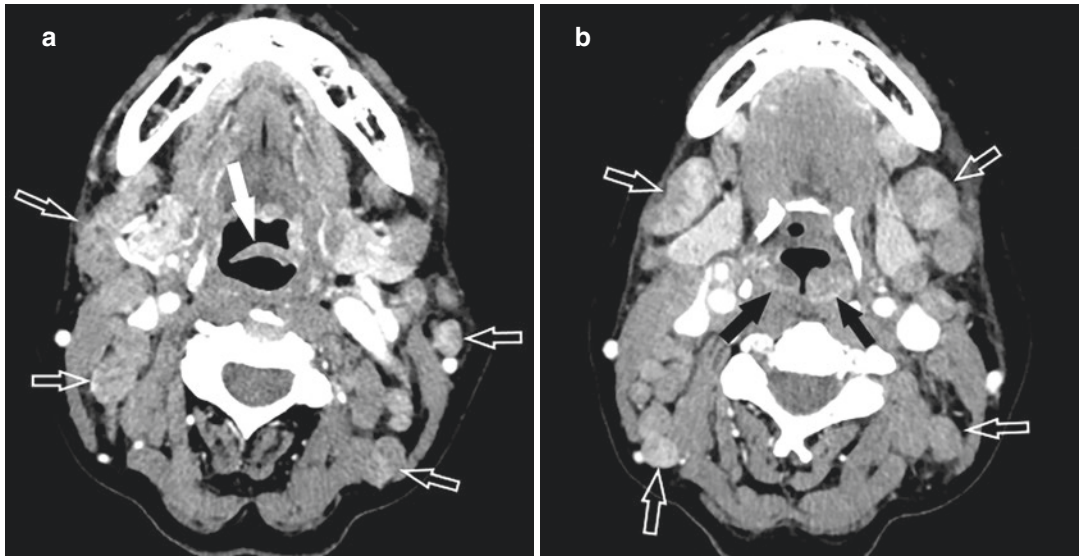

Fig. 21 Nontuberculosis mycobacterial (NTM) laryngitis. (**a**) Axial contrast-enhanced CT image shows diffuse enhancement with thickening of the epiglottis (solid arrow) and multiple bilateral heterogeneously enhancing lymph nodes (open arrows). (**b**) Axial contrast-enhanced CT image shows diffuse enhancement with thickening of bilateral aryepiglottic folds (black arrows). Multiple heterogeneously enhancing lymph nodes are present (open arrows). The patient also had enhancement at the left palatine tonsil and the pharyngeal wall (not shown)

(Fig. 22). A small cancer that presents as a mass cannot be distinguished from mass-like TB on imaging (Fig. 18b) and the diagnosis can only be made by biopsy. The presence of cartilage destruction can suggest a diagnosis of cancer (Fig. 22c). Subglottic or hypopharyngeal extension is more common in cancer than in TB (Moon et al. 1996).

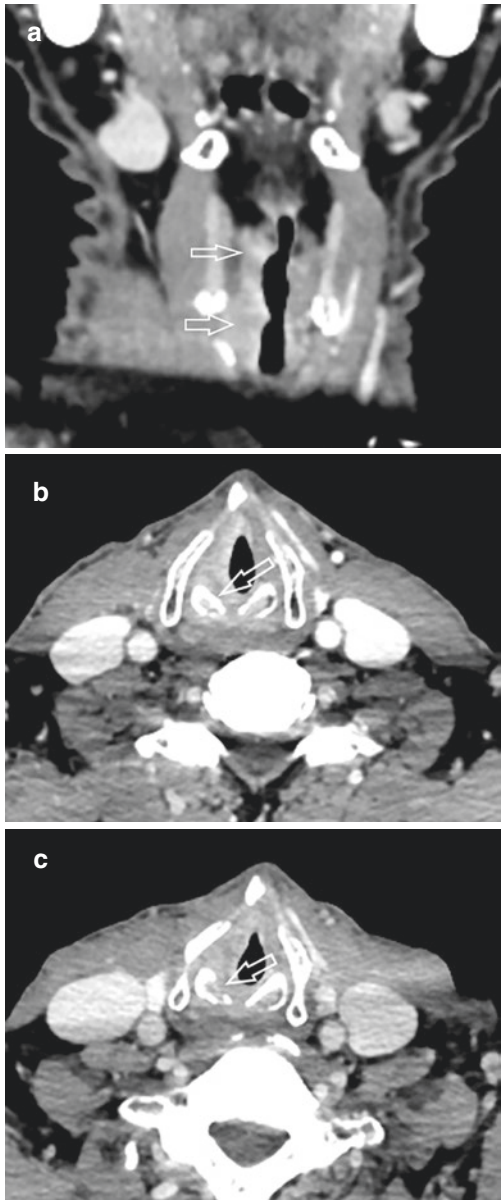

Fig. 22 Laryngeal cancer. This patient presented with hoarseness for 3 months. (**a**) Coronal contrast-enhanced CT image shows infiltrative lesions at the right supraglottis, glottis, and subglottis (open arrows). (**b**) Axial contrast-enhanced CT image taken at the level of the subglottis shows an intact cricoid cartilage (open arrow). The CT findings cannot be distinguished from those of tuberculosis. The patient also had active pulmonary tuberculosis seen on CT (not shown). Biopsy of the laryngeal lesion showed squamous cell carcinoma. The patient was lost to follow-up for 2 months after biopsy. (**c**) Axial contrast-enhanced CT image taken 2 months later at the same level as (**b**) shows cricoid cartilage destruction typical of malignancy (open arrow)

Diffuse thickening of the supraglottis with mucosal enhancement can be observed on CT in patients with acute supraglottitis from bacterial infection. The clinical presentation in supraglottitis is usually more acute and more severe, compared to the presentation of laryngeal TB. On CT, acute supraglottitis is often accompanied by subcutaneous fat clouding, platysma muscle thickening, and thickening of the retropharyngeal space (Smith et al. 1996). These findings are not features of laryngeal TB and can help in differentiating between the two entities.

Fungal laryngitis is a rare condition. Reports of CT findings are limited and include soft tissue enhancement, swelling of laryngeal tissue, and frank abscess formation (Nair et al. 2011; Kmeid et al. 2016). The findings on imaging cannot be differentiated from laryngeal TB. Other rare granulomatous diseases of the larynx which can present as infiltrative soft tissue or localized masses on imaging are sarcoidosis and amyloidosis (Ferretti et al. 2002; Parmar et al. 2010; Takumi et al. 2020). The CT and MRI findings can be similar to TB, and diagnosis should be made by biopsy.

5.6 Diagnosis Confirmation

The diagnosis of tuberculous laryngitis can be difficult due to nonpathognomonic symptoms and physical examination findings, particularly for those without pulmonary disease and in those with HIV infection, but can be confirmed by a combination of laboratory examinations (Ozüdogru et al. 2005; Leahy 2020). Endoscopic examination of the larynx in laryngeal TB is non-specific and may be confused with laryngeal cancer (Swain et al. 2019). However, laryngoscopy allows characterization and surface mapping of lesions, collection of biopsy specimens for AFB smears and cultures, as well as histopathological evaluation.

The positive rates of sputum smears and cultures are higher in patients with laryngeal TB having extensive and ulcerative lesions and concurrent pulmonary TB, than in patients without pulmonary TB (Zang et al. 2020). The histopathological features of ulcerative lesions

include fewer granulomas and more areas with caseous necrosis, and these lesions are more likely to have AFB detected with a Ziehl–Neelsen stain than exophytic lesions that rarely show detectable bacilli (Zang et al. 2020). Histopathological and bacteriological examinations are confirmatory tests for the diagnosis (Agarwal et al. 2019; Swain et al. 2019), and may be supported by a PCR test (Kenmochi et al. 2003). Chest radiographs and sputum AFB smears and cultures can rule in or exclude the presence of pulmonary TB (Agarwal et al. 2019). In cases with no pulmonary involvement, a PPD test may be positive if laryngeal TB is present (Leahy 2020).

5.7 Treatment

Similar to head and neck TB in other subsites, a six to nine-month course of a combination of anti-TB medications can cure the disease and alleviate symptoms. Particularly for tuberculous laryngitis, it can expedite and improve hoarseness, although dysphonia may persist after resolution of TB (Lucena et al. 2015). It is also prudent that in the management of patients with laryngeal TB, HIV screening be performed, given the high incidence of co-infection (Leahy 2020).

6 Conclusion

The diagnosis of TB in the ear, nose, and throat region is difficult for both clinicians (such as ENT surgeons) and radiologists. Although imaging findings are mostly non-specific, there are some clues that can help in arriving at the diagnosis. Knowing the imaging spectrum of TB in these organs is important for radiologists because they can help ENT surgeons initiate further investigation and early treatment.

References

Abes FL, Abes G, Jamir J (2011) The variable clinical presentation of tuberculosis otitis media and the importance of early detection. J Laryngol Otol 32:539–543

Agarwal R, Gupta L, Singh M et al (2019) Primary laryngeal tuberculosis: a series of 15 cases. Head Neck Pathol 13:339–343

Al-Serhani AM, Al-Mazrou K (2001) Pharyngeal tuberculosis. Am J Otolaryngol 22:236–240

Aremu SK, Alabi BS (2010, 2010) Tuberculous otitis media: a case presentation and review of the literature. BMJ Case Rep:bcr0220102721

Aspestrand F, Kolbenstvedt A, Boysen M (1989) CT findings in benign expansions of the larynx. J Comput Assist Tomogr 13:222–225

Bath AP, O'Flynn P, Gibbin KP (1992) Nasopharyngeal tuberculosis. J Laryngol Otol 106:1079–1080

Bhalla RK, Jones TM, Rothburn MM, Swift AC (2001) Tuberculous otitis media—a diagnostic dilemma. Auris Nasus Larynx 28:241–243

Bharatha A, Bartlett ES, Yu E (2010) Case 154: pharyngeal and retropharyngeal tuberculosis with nodal disease. Radiology 254:629–632

Bhatia KSS, King AD, Vlantis AC et al (2012) Nasopharyngeal mucosa and adenoids: appearance at MR imaging. Radiology 263:437–443

Birrell JF (1973) Aural tuberculosis in children. Proc R Soc Med 66:331–338

Cai PQ, Li YZ, Zeng RF et al (2013) Nasopharyngeal tuberculosis: CT and MRI findings in thirty-six patients. Eur J Radiol 82:e448–e454

Chaturvedi VN, Chaturvedi P (1986) Tuberculosis of the middle ear. Indian Pediatr 23:199–204

Chen YS, Li WY, Ho CY (2010) Localized nasopharyngeal amyloidosis. J Chin Med Assoc 73:549–552

Cho YS, Lee HS, Kim SW et al (2006) Tuberculous otitis media: a clinical and radiologic analysis of 52 patients. Laryngoscope 116:921–927

Chopra RK, Kerner MM, Calcaterra TC (1994) Primary nasopharyngeal tuberculosis: a case report and review of this rare entity. Otolaryngol Head Neck Surg 111:820–823

Cole AE, Heaton D, Chekairi A (2018) Laryngeal tuberculosis: a rare cause of critical airway obstruction. BMJ Case Rep 2018:bcr2017222841

Deenadayal DS, Kumar BN, Bommakanti V, Sameeri KL (2016) Tuberculous otitis media—a rare entity or a missed diagnosis. Int J Otolaryngol Head Neck Surg 5:65–72

Dey S, Misra S, Dutta M (2018) Primary sinonasal tuberculosis: a diagnostic challenge. Turkish Arch Otolaryngol 56:117–121

Dworetzky J (1917) The diagnosis of tuberculosis laryngitis. JAMA 69:619–625

El Kettani NEC, El Hassani MR, Chakir N, Jiddane M (2010) Primary laryngeal tuberculosis mimicking laryngeal carcinoma: CT scan features. Indian J Radiol Imaging 20:11–12

Emmett JR, Fischer ND, Biggers WP (1977) Tuberculous mastoiditis. Laryngoscope 87:1157–1163

Ferretti GR, Calaque O, Reyt E et al (2002) CT findings in a case of laryngeal sarcoidosis. Eur Radiol 12:739–741

Gean-Marton AD, Kirsch CFE, Vezina LG, Weber AL (1991) Focal amyloidosis of the head and neck: evaluation with CT and MR imaging. Radiology 181:521–525

Gleitsmann JW (1907) Tuberculosis of the accessory sinuses of the nose. Laryngoscope 17: 445–450

Goguen LA, Karmody CS (1995) Nasal tuberculosis. Otolaryngol Head Neck Surg 113:131–135

Goyal A, Nagarkar NM, Uppal KS et al (1998) Tuberculosis of the pyriform fossa—a rare entity. J Laryngol Otol 112:782–783

Gupta K, Yadav SPS, Sarita MM (2005) Primary pharyngeal tuberculosis. Lung India 22:127–129

Gupta R, Gupta A, Anand C, Garg M (2014) Tuberculous osteomyelitis of the maxilla: a rarest of rare case report. Natl J Maxillofac Surg 5:188–191

Habershon SH (1905) The treatment of laryngeal tuberculosis. Laryngol Rhinol Otol 20:630–637

Haddad NM, Zaytoun GM, Hadi U (1987) Tuberculosis of the soft palate: an unusual presentation of oral tuberculosis. Otolaryngol Head Neck Surg 97:91–92

Hajioff D, Snow MH, Thaker H, Wilson JA (1999) Primary tuberculosis of the posterior oropharyngeal wall. J Laryngol Otol 113:1029–1030

Hegarty JL, Rao VM (1993) Amyloidoma of the nasopharynx: CT and MR findings. AJNR Am J Neuroradiol 14:215–218

Hirsch C (1935) Tuberculosis of the larynx. Laryngoscope 45:269–294

Iravani K, Jahromi SB, Ashraf MJ (2015) Primary tuberculosis of the vallecula and pyriform sinus: a case report and review of literature. Iran J Otorhinolaryngol 27:171–175

Jha D, Deka RC, Sharma MC (2002) Tuberculosis of the maxillary sinus manifesting as a facial abscess. Ear Nose Throat J 81:102–104

Kahane J, Crane BT (2009) Tuberculous otitis media. Otol Neurotol 30:865–866

Kameswaran M, Anand Kumar RS, Murali S et al (2007) Primary nasal tuberculosis—a case report. Indian J Otolaryngol Head Neck Surg 59:87–89

Kameswaran M, Natarajan K, Parthiban M et al (2017) Tuberculous otitis media: a resurgence? J Laryngol Otol 131:785–792

Kandiloros DC, Nikolopoulos TP, Ferekidis EA et al (1997) Laryngeal tuberculosis at the end of the 20th century. J Laryngol Otol 111:619–621

Kant S, Srivastava R, Verma AK et al (2013) Maxillary sinus tuberculosis: various presentations. Indian J Chest Dis Allied Sci 55:175–177

Kenmochi M, Ohashi T, Nishino H et al (2003) A case report of difficult diagnosis in the patient with advanced laryngeal tuberculosis. Auris Nasus Larynx 30:s131–s134

Khan S, Pujani M, Jetley S (2017) Primary nasal tuberculosis: resurgence or coincidence—a report of four cases with review of literature. J Lab Physicians 9:26–30

Kim MD, Kim DI, Yune HY et al (1997) CT findings of laryngeal tuberculosis: comparison to laryngeal carcinoma. J Comput Assist Tomogr 21:29–34

Kim YM, Kim AY, Park YH et al (2007) Eight cases of nasal tuberculosis. Otolaryngol Head Neck Surg 137:500–504

Kim KY, Bae JH, Park JS, Lee SS (2014) Primary sinonasal tuberculosis confined to the unilateral maxillary sinus. Int J Clin Exp Pathol 7:815–818

King AD, Ahuja AT, Tse GMK et al (2003a) MR imaging features of nasopharyngeal tuberculosis: report of three cases and literature review. AJNR Am J Neuroradiol 24:279–282

King AD, Lei KIK, Richards PS, Ahuja AT (2003b) Non-Hodgkin's lymphoma of the nasopharynx: CT and MR imaging. Clin Radiol 58:621–625

Kmeid M, Azar E, Nasser S et al (2016) Invasive epiglottic aspergillosis mimicking supraglottic laryngeal carcinoma—a case report and review of the literature. Oncol Hematol Rev 12:97–100

Krishnappa BD (2006) Tuberculosis of tonsil. Indian J Otolaryngol Head Neck Surg 58:210

Leahy K (2020) Laryngeal and tracheal manifestations of systemic disease. In: Flint P, Haughey B, Lund V et al (eds) Cummings otolaryngology head and neck surgery, 7th edn. Elsevier Saunders, Philadelphia, pp 183–183

Lee PYC, Drysdale AJ (1993) Tuberculous otitis media: a difficult diagnosis. J Laryngol Otol 107:339–341

Lee MS, Kim DJ, Kim MS et al (1999) Sinonasal tuberculosis: report of two cases demonstrated with CT. J Korean Radiol Soc 41:1107–1109

Lim JY, Kim KM, Choi EC et al (2006) Current clinical propensity of laryngeal tuberculosis: review of 60 cases. Eur Arch Otorhinolaryngol 263:838–842

Ling L, Zhou SH, Wang SQ (2010) Changing trends in the clinical features of laryngeal tuberculosis: a report of 19 cases. Int J Infect Dis 14:e230–e235

Lou ZC, Li X (2019) Leukoplakia or LPR: the misdiagnosis of laryngeal tuberculosis. Ear Nose Throat J:145561319891264

Lucena MM, Da SFDS, Da CAD et al (2015) Evaluation of voice disorders in patients with active laryngeal tuberculosis. PLoS One 10:e0126876

Lugton IW (1999) Mucosa-associated lymphoid tissues as sites for uptake, carriage and excretion of tubercle bacilli and other pathogenic mycobacteria. Immunol Cell Biol 77:364–372

Madhuri, Mohan C, Sharma ML (2002) Posterior oropharyngeal wall tuberculosis. Indian J Otolaryngol Head Neck Surg 54:152–153

Maheshwari A, Panigrahi R (2017) Tubercular otitis media: an under diagnosed entity. Int J Otorhinolaryngol Head Neck Surg 3:82–87

Mahindra S, Malik GB, Sohail MA (1981) Primary tuberculosis of the adenoids. Acta Otolaryngol 92:173–180

Masterson L, Srouji I, Kent R, Bath AP (2011) Nasal tuberculosis—an update of current clinical and laboratory investigation. J Laryngol Otol 125:210–213

Mishra RK, Prasad BK, Mathew S (2015) Nasopharyngeal tuberculosis. Med J Armed Forces India 71:s586–s589

Moon WK, Han MH, Chang KH et al (1996) Laryngeal tuberculosis: CT findings. AJR Am J Roentgenol 166:445–449

Moon WK, Han MH, Chang KH et al (1997) CT and MR Imaging of head and neck tuberculosis. Radiographics 17:391–402

Muhammad S, Sule A, Wey G (2020) Sinonasal tuberculosis mimicking malignancy—case report and review of literature. Ann Trop Pathol 11:76–78

Munoz A, Ruiz-Contreras J, Jimenez A et al (2009) Bilateral tuberculous otomastoiditis in an immunocompetent 5-year-old child: CT and MRI findings. Eur Radiol 19:1560–1563

Muranjan SN, Kirtane MV (2001) Tubercular laryngeal abscess. J Laryngol Otol 115:660–662

Myerson MC, Gilbert JG (1941) Tuberculosis of the middle ear and mastoid. Arch Otolaryngol 33:231–250

Nair AB, Chaturvedi J, Venkatasubbareddy BM et al (2011) A case of isolated laryngeal candidiasis mimicking laryngeal carcinoma in an immunocompetent individual. Malays J Med Sci 18:75–78

Newcomb JE (1904) Tuberculosis of the pharynx. Laryngoscope 14:423–430

Nishiike S, Irifune M, Osaki Y et al (2003) Tuberculous otitis media: clinical aspects of 12 cases. Ann Otol Rhinol Laryngol 112:935–938

Ormerod FC (1931) Tuberculous disease of the middle ear. J Laryngol Otol 46:449–459

Ozüdogru E, Cakli H, Altuntas EE, Gürbüz MK (2005) Effects of laryngeal tuberculosis on vocal fold functions: case report. Acta Otorhinolaryngol Ital 25:374–377

Pande TK, Hiran S, Rao VVB et al (1995) Primary lingual tuberculosis caused by M. bovis infection. Oral Surg Oral Med Oral Pathol Oral Radiol Endod 80: 172–174

Parmar H, Rath T, Castillo M, Gandhi D (2010) Imaging of focal amyloid depositions in the head, neck, and spine: amyloidoma. AJNR Am J Neuroradiol 31: 1165–1170

Patil C, Kharat (Patil) R, Deshmukh P et al (2013) Primary tuberculosis of nasopharynx (adenoid)—a rare presentation. Asian Pac J Trop Med 6:246–248

Percodani J, Braun F, Arrue P et al (1999) Nasopharyngeal tuberculosis. J Laryngol Otol 113:928–931

Ponni S, Venkatesan R, Saxena SK, Suryanarayanan G (2019) Primary laryngeal tuberculosis—changing trends and masquerading presentations: a retrospective study. Int J Otorhinolaryngol Head Neck Surg 5:634–638

Rai D, Kumar S, Thakur S (2016) A rare case of tubercular pansinusitis with orbital and intracranial extension. Lung India 33:349–351

Rho MH, Kim DW, Kim SS et al (2007) Tuberculous otomastoiditis on high-resolution temporal bone CT: comparison with nontuberculous otomastoiditis with and without cholesteatoma. AJNR Am J Neuroradiol 28:493–496

Rizzo PB, Da Mosto MC, Clari M et al (2003) Laryngeal tuberculosis: an often forgotten diagnosis. Int J Infect Dis 7:129–131

Robertson K, Kumar A (1995) Atypical presentations of aural tuberculosis. Am J Otolaryngol 16:294–302

Safder S, Carpenter JS, Roberts TD, Bailey N (2010) The "black turbinate" sign: an early MR imaging finding of nasal mucormycosis. AJNR Am J Neuroradiol 31:771–774

Sanehi S, Dravid C, Chaudhary N, Venkatachalam VP (2008) Tuberculosis of paranasal sinuses. Indian J Otolaryngol Head Neck Surg 60:85–87

Selimoglu E, Sutbeyaz Y, Ciftcioglu A et al (1995) Primary tonsillar tuberculosis: a case report. J Laryngol Otol 109:880–882

Sellami M, Mnejja M, Charfi S, Ghorbel A (2017) Tuberculosis of the tonsil simulating a cancer. Lancet Infect Dis 17:1317

Shah NJ, Prashanth V, Velimuthan N (2010) Primary tuberculosis of the ethmoid and sphenoid sinuses—a rare entity. Bombay Hosp J 52:86–89

Sharma SC, Baruah P (2003) Sphenoid sinus tuberculosis in children—a rare entity. Int J Pediatr Otorhinolaryngol 67:399–401

Shin JE, Nam SY, Yoo SJ, Kim SY (2000) Changing trends in clinical manifestations of laryngeal tuberculosis. Laryngoscope 110:1950–1953

Smith MM, Mukherji SK, Thompson JE, Castillo M (1996) CT in adult supraglottitis. AJNR Am J Neuroradiol 17:1355–1358

Srivanitchapoom C, Sittitrai P (2016) Nasopharyngeal tuberculosis: epidemiology, mechanism of infection, clinical manifestations, and management. Int J Otolaryngol 2016:4817429

Swain SK, Behera IC (2020) A rare presentation of nasal tuberculosis. J Med Soc 34:47–49

Swain SK, Behera IC, Sahu MC (2017) Primary sinonasal tuberculosis: our experiences in a tertiary care hospital of eastern India. Egypt J Ear Nose Throat Allied Sci 18:237–240

Swain SK, Behera IC, Sahu MC (2019) Primary laryngeal tuberculosis: our experiences at a tertiary care teaching hospital in Eastern India. J Voice 33:812.e9–812.e14

Taci N, Yurdakul AS, Ceyhan I et al (2003) Detection of Mycobacterium tuberculosis DNA from peripheral blood in patients with HIV-seronegative and new cases of smear-positive pulmonary tuberculosis by polymerase chain reaction. Respir Med 97: 676–681

Takumi K, Staziaki PV, Hito R et al (2020) Amyloidosis in the head and neck: CT findings with clinicopathological correlation. Eur J Radiol 128:109034

Theisen CF (1899) Tuberculosis of pharynx: with preliminary report of tuberculous infection of tonsils and lymphoid tissue of naso-pharynx. JAMA XXXIII:382–385

Tisekar O, Bhaskar M, Biraris P et al (2020) Primary tonsillar tuberculosis masquerading as carcinoma of the tonsil. Indian J Tuberc 67:386–388

Upadhya IB, Dave VJ, Suratwala JN (2017) Primary tuberculosis of frontal sinus presenting as intractable headache. Clin Rhinol An Int J 10:157–159

Vital V, Printza A, Zaraboukas T (2002) Tuberculous otitis media: a difficult diagnosis and report of four cases. Pathol Res Pract 198:31–35

Wang CC, Lin CC, Wang CP et al (2007) Laryngeal tuberculosis: a review of 26 cases. Otolaryngol Head Neck Surg 137:582–588

Williams PW (1901) Diseases of the upper respiratory tract: the nose, pharynx and larynx, 4th edn. J Wright, University of Chicago

Windle-Taylor PC, Bailey CM (1980) Tuberculous otitis media: a series of 22 patients. Laryngoscope 90:1039–1044

Wolfowitz BL (1972) Tuberculous mastoiditis. Arch Otolaryngol 95:109–113

Yan K, Taxy JB, Paintal A, Friedman AD (2020) Atypical laryngeal infections: localized lesions from unusual organisms may simulate malignancy. Ann Otol Rhinol Laryngol 129:82–86

Yaniv E (1987) Tuberculous otitis: an underdiagnosed disease. Am J Otolaryngol 8:356–360

Zang J, Tian Y, Jiang X, Lin XY (2020) Appearance and morphologic features of laryngeal tuberculosis using laryngoscopy: a retrospective cross-sectional study. Medicine 99:e23770

Imaging of Thoracic Tuberculosis

Saoussen Hantous-Zannad, Henda Néji, Meriem Affes, Monia Attia, Ines Baccouche, Salma Kechaou, Fatma Tritar, and Khaoula Ben Miled-M'rad

Contents

Abstract

Tuberculosis is an airborne infectious disease caused by *Mycobacterium tuberculosis*. It is a major cause of morbidity and mortality, particularly in developing countries, and its incidence is rising in developed countries. The lungs are the most involved organ of the thorax, but other extrapulmonary thoracic structures can be affected. Imaging is fundamental in the management of the disease. The first approach of diagnosis is based on clinical symptoms. Radiological signs depend on the patient's age, immune status, and previous contact with *M. tuberculosis*. Confirmation of

S. Hantous-Zannad (✉) · H. Néji · M. Affes
M. Attia · I. Baccouche · S. Kechaou
K. B. Miled-M'rad
Department of Radiology, Abderrahmane Mami Hospital, Ariana, Tunis, Tunisia
e-mail: saoussen.hantous@fmt.utm.tn; henda.neji@fmt.utm.tn; meriem.affes@fmt.utm.tn; monia.attia@fmt.utm.tn; ines.bac@gmail.com; salmakechaou85@gmail.com; khaoulabenmiledmrad@gmail.com

F. Tritar
Department of Pneumology, Abderrahmane Mami Hospital, Ariana, Tunis, Tunisia
e-mail: fatma.tritar@gmail.com

© The Author(s), under exclusive license to Springer Nature Switzerland AG 2022

M. F. Ladeb, W. C. G. Peh (eds.), *Imaging of Tuberculosis*, Medical Radiology Diagnostic Imaging,
https://doi.org/10.1007/978-3-031-07040-2_8

the diagnosis can be made only by bacteriological and/or histological examination. Chest radiography remains the first-line imaging examination and can suggest the diagnosis based on lesion features and location. Computed tomography plays an important role in the detection of tuberculosis in patients with normal or inconclusive chest radiographs and in disease activity determination. It is also indicated for the detection of complications, evaluation of parenchyma sequelae, and prior to surgical management of multidrug-resistant tuberculosis.

Abbreviations

AIDS	Acquired immunodeficiency syndrome
CT	Computed tomography
MRI	Magnetic resonance imaging
PPTB	Post-primary tuberculosis
TB	Tuberculosis

1 Introduction

Pulmonary tuberculosis (TB) is a major cause of morbidity and mortality around the world, particularly in developing countries, even though it is a preventable disease. After exposure to *Mycobacterium tuberculosis*, an estimated 20–25% of the subjects become infected. Approximately 3–5% of these infected individuals will progress to developing active TB disease during their lifetime (Yu et al. 2019; World Health Organization 2021c). Pulmonary disease is present in more than 80% of TB cases, while extrapulmonary TB occurs in about 20% of cases (Yu et al. 2019). Its radiological manifestations may vary according to factors related to the host (e.g., age, immune status, and previous contact with *M. tuberculosis*). Imaging has a crucial role in the screening, diagnosis, and monitoring of TB. Chest radiographs may be sufficient for diagnosis in an appropriate clinical setting. Computed tomography (CT) is indicated when there are radiological-clinical discrepancies and is useful to look for signs of disease activity. It is indicated in the diagnosis of complications and the assessment of sequelae, as well as in long-term follow-up. Magnetic resonance imaging (MRI) may be performed to evaluate complications of thoracic disease, such as chest wall involvement, but is of limited value in the assessment of patients with pulmonary TB. Positron-emission tomography (PET) is not currently performed for diagnosis but has yielded promising results. This chapter aims to review the characteristic imaging findings of various forms of pulmonary and extrapulmonary thoracic TB, as well as to assess the role of CT and other modalities in the diagnosis and management of pulmonary TB.

2 Pathophysiology

2.1 Transmission of Tuberculosis

TB is a contagious interhuman disease. *M. tuberculosis* is carried in airborne particles and is transmitted through air, which leads to the spread of the disease. Infectious droplet nuclei are generated when persons with pulmonary or laryngeal TB disease cough, sneeze, shout, or sing. Depending on the environment, these tiny particles can remain suspended in air for several hours. Prolonged exposure in a closed atmosphere can lead to infection of contacts (e.g., inhabitants of the same house, coworkers in an office, clients in bars). Transmission occurs when a contact person inhales droplet nuclei containing *M. tuberculosis*, which reaches the lung alveoli. These tuberculous bacilli are phagocytosed by alveolar macrophages and are destroyed or inhibited. A small number may multiply in cells and are then released when the macrophages die. If alive, these bacilli may spread through lymphatic channels or the bloodstream to more distant tissues and organs (including areas of the body in which TB disease is most likely to develop, such as the regional lymph nodes, lung apex, kidneys, brain, and bone). This process of dissemination primes the immune system for a systemic

response (Barreira-Silva et al. 2018; Migliori et al. 2018; World Health Organization 2021c).

Other transmission modes are less frequent and include the digestive tract and the cutaneous or cutaneous-mucous routes. In the digestive tract, *M. bovis* is transmitted by ingesting unpasteurized milk products from cows with TB or by handling contaminated animal products. The cutaneous or cutaneous-mucous route is rare and is caused by an injury of the skin with direct contact with *M. tuberculosis* or by projection (e.g., conjunctiva).

2.2 Pathogenesis of Tuberculosis

2.2.1 Incubation Time

TB has two incubation times. The first concerns the primary infection. It is the time between the first contact with *M. tuberculosis* and the date of positive tuberculin test, lasting from 4 to 12 weeks. The patient is usually asymptomatic. Once the primary infection occurs, TB disease and symptoms may appear after a certain time. This second incubation time can be short (immediate) or long (up to several years). Recent research has clearly demonstrated that human TB infection, from latent infection to active TB disease, exists within a continuous spectrum of metabolic bacterial activity and antagonistic immunological responses (Pai et al. 2016; Drain et al. 2018).

2.2.2 Primary Tuberculosis

Primary TB occurs when a host is initially exposed to bacilli by inhalation. The bacilli are carried by normal airflow, mainly to the middle and lower lung fields. An early granulomatous inflammatory response occurs, known as the primary (or Ghon) focus. Within weeks after infection, the immune system is usually able to halt the multiplication of tuberculous bacilli, hence preventing further progression. As an effective cellular immune response can take weeks and varies from host to host, bacilli are initially able to grow and divide in the distal parenchyma before being transported to hilar lymph nodes by the lymphatics and possibly to more distant anatomical sites by the bloodstream. Typical epithelioid granulomas with giant cells and caseous necrosis are then organized. At this stage, the disease is called latent TB infection (LTBI) and may be detected using the tuberculin skin test (TST) or an interferon-gamma release assay (IGRA) (Barry et al. 2009).

Only 5% of people infected with TB rapidly progress to active disease. The others develop LTBI but remain at risk for progression to active disease ("reactivation") (American Thoracic Society 1990; Cadena et al. 2017). Primary or scattered foci can also be fractionated and remain quiescent with the risk of being reactivated in the future, causing post-primary disease. If the host's immune status fails upon initial containment, uncontrolled primary infection (primary progressive TB) occurs, with bacilli spreading hematogenously and endobronchially. Primary TB has classically been considered as a disease of children living in highly endemic areas, where exposure is more likely to occur during the first years of life. However, the recognition of primary TB in adults is increasing, probably due to effective public health initiatives and treatments that have created larger populations of unexposed adults (American Thoracic Society 1990).

2.2.3 Post-primary Tuberculosis

Both reactivation and reinfection with the tuberculous bacillus are categorized under post-primary TB (PPTB) or TB disease. It occurs in people who have developed immunity to primary TB. Only 5–10% of the approximately two billion people infected with *M. tuberculosis* worldwide will develop TB disease during their lifetime, most often in the first 2 years after the primary infection. TB disease can result from either a new exposure (exogenous infection) or reactivation of quiescent bacteria due to decrease in immune defenses (endogenous reinfection). The probability of developing TB disease is much higher in people with acquired immunodeficiency syndrome (AIDS). It is also higher in people having risk factors such as diabetes mellitus, undernutrition, malignancy, organ transplantation, chemotherapy, steroids, TNF-alpha

inhibitor drugs, smoking and alcohol consumption, chronic obstructive pulmonary disease, past history of TB, healthcare workers, and pregnant women (World Health Organization 2021a). The elderly and children younger than 5 years of age are also at increased risk for progression of LTBI to TB disease (Lewinsohn et al. 2017).

3 Clinical Features

The clinical features of thoracic TB are dependent on several factors, including the disease type (primary or post-primary), predominant infection location (e.g., lymph nodes, lung parenchyma, pleural space), infection duration, and host factors such as age and immune status. The symptoms are generally non-specific. As TB is a slowly progressive disease, the initial symptoms are usually discrete and become more prominent with time. The classic symptoms of pulmonary TB include persistent cough, hemoptysis, evening fever, night sweats, and weight loss. Cough, the most common symptom of pulmonary TB, may be dry in the early course of the illness, but sputum is usually produced as inflammation continues. Chest pain and dyspnea, sometimes even respiratory distress, are present in very extensive forms or forms occurring in patients with chronic lung disease. Most patients present for medical consultation after having been symptomatic for weeks or even months. In TB cases discovered by systematic screening (e.g., in migrants or during contact investigations), the prevalence of symptoms may be much lower (Migliori et al. 2018).

Clinical examination of the lungs is most frequently normal, contrasting with the reported symptoms and extent of radiological lesions. Physical signs are usually absent, except when pulmonary lesions are extensive with large areas of consolidation. Crackles, wheezing, and bronchial breath sounds may be heard. Uveitis, erythema nodosum, and other skin conditions may be the first signs of pulmonary TB (Lewinsohn et al. 2017; Migliori et al. 2018). When present, it is also possible to discover a pleural effusion or a pneumothorax on physical examination. Pleural effusion is often the only manifestation of primary TB. The frequency of effusion increases with age, occurring in about 40% of adults with primary TB. The pleural space is more likely to be involved in PPTB because of the large number of bacteria reaching the pleural space from a ruptured cavity resulting in bronchopleural fistula, localized effusions, hydropneumothorax, or tuberculous empyema (Epstein et al. 1987). The extrathoracic clinical examination should include looking for dissemination to structures such as the central nervous system, peripheral lymphadenopathy, and urogenital and musculoskeletal systems.

4 Imaging Modalities

4.1 Chest Radiography

Chest radiography has a major role in the assessment of pulmonary TB. Typically, the posterior-anterior radiograph is sufficient. Other radiographical views, such as a lordotic view or dual-energy radiography with bone subtraction, can improve the depiction of the lung apices (Sharma et al. 2015; Nachiappan et al. 2017). Chest radiographs are used for the screening of TB in general population, those with structural risk of TB development, patients with AIDS, and people younger than 15 years who are contacts of patients with TB. Radiographs have a sensitivity of 94% and specificity of 89% when considering any abnormality. The specificity rises to 96% when considering suggestive abnormalities. Chest radiographs may be normal in 15% of cases. Computer-aided detection (CAD) has now been introduced as an alternative to human interpretation of digital chest radiographs for TB screening. However, its application should be limited to patients aged 15 years or older. CAD has not shown significant differences in sensitivity and specificity, compared to human reading of chest radiographs (0.90–0.92 versus 0.82–0.93 and 0.23–0.66 versus 0.14–0.63) (World Health Organization 2021a). Chest radiographs are also useful for reactivation detection after a previous healed episode, assessment of sequelae and complications, as well as monitoring of treatment efficacy.

4.2 Ultrasound Imaging

Ultrasound (US) imaging is a non-invasive imaging tool that has proven its usefulness for the diagnosis of pneumonia, pneumothorax, and pleural as well as pericardial effusion and thickening. It is also used for the assessment of cold abscesses, thoracic bone lesions, and detection of mediastinal lymph nodes in children (Di Gennaro et al. 2018; Heuvelings et al. 2019). Many US imaging findings in lung TB have been described, such as apical consolidation and subpleural nodules. Detection of consolidation has a sensitivity ranging from 72.5% to 100% with an odds ratio of 5.29 l, while subpleural nodule detection has a sensitivity ranging from 6.7% to 80.4% with an odds ratio of 9.67. Sensitivity is lower for the detection of proven chest radiographical cavitating lesions (Giordani and Heller 2019; Montuori et al. 2019; Fentress et al. 2020; Bigio et al. 2021). Moreover, fine-needle aspiration and biopsies for diagnostic purposes can be performed under US imaging guidance with a performance accuracy that can reach 100% (Di Gennaro et al. 2018).

4.3 Computed Tomography

CT may be indicated in many situations, such as discrepancy between clinical presentation and chest radiographical findings, or smear-negative sputum (paucibacillary TB). The radiation dose can be reduced to the minimum necessary for diagnosis. Low-dose CT, performed with 50 mAs and 120 kVp, has a sensitivity of 100% and a positive predictive value of 86.4% (He et al. 2017). Ultralow-dose CT (80 kVp, 25 mAs) may offer the same diagnostic value, especially when applying iterative reconstruction (Yan et al. 2019). Moreover, CT can be performed for the evaluation of the extent of fibrotic lesions and assessment of complications (e.g., lymph node rupture in the trachea or esophagus, mediastinal fibrosis, empyema necessitans). In patients with hemoptysis, CT aortography is useful for the detection of Rasmussen aneurysm and systemic mapping of the bronchial or nonbronchial arteries prior to embolization (Hantous-Zannad et al. 2015). CT offers the possibility to assess lesions in the differential diagnosis as well as associated diseases such as lymphoma, sarcoidosis, and lung cancer. Moreover, it allows guidance of interventional procedures such as punctures, biopsies, and intracavitary treatment.

4.4 Magnetic Resonance Imaging

MRI is not commonly used for the diagnosis of pulmonary TB because of its high cost and low availability in developing countries (Hantous-Zannad et al. 2015). Moreover, it used to have a poor image quality due to the low density of protons of the lungs, motion artifacts, and susceptibility (Yan et al. 2020). Currently, the development of ultrashort time echo (UTE) sequences has enabled the assessment of various lung lesions, including TB (Delacoste et al. 2019; Yan et al. 2020). When performed, MRI is comparable to CT in detecting consolidation, cavities, and noncalcified nodules larger than 5 mm, with a sensitivity varying between 69.6% and 100% (Yan et al. 2020). MRI has also been found to be more sensitive in detecting caseous necrosis, liquefaction, active cavitation, and abnormalities of lymph nodes and pleura (Yan et al. 2020). Enlarged tuberculous lymph nodes have specific signal abnormalities on T2-weighted sequences, depending on their histological features. They have moderately hyperintense signal when inflamed. When they contain necrosis, they have a central hypointense signal surrounded by a hyperintense signal. Liquefaction results in an obvious hyperintense signal (Hantous-Zannad et al. 2015; Zeng et al. 2019). MRI is also the technique of choice for studying the impact of tuberculous pericarditis and can be used for the assessment of chest wall lesions.

4.5 Positron-Emission Tomography and Other Modalities

[Fluorine-18]-fluoro-2-deoxy-D-glucose (^{18}F-FDG) PET/CT is not currently performed for the diagnosis of TB, but it may be used for

determining the activity of disease and the response to treatment (Hantous-Zannad et al. 2015; Yu et al. 2019). It is also useful in the detection of unknown sites and allows the most appropriate site of biopsy to be selected. It plays an important role in monitoring response to therapy in cases of multidrug-resistant TB or extrapulmonary TB. However, ^{18}F-FDG PET/CT cannot reliably differentiate active TB from malignant lesions, and false positives can be due to other infective or inflammatory conditions. It is also unable to distinguish tuberculous lymphadenitis from metastatic lymph node involvement. The lack of specificity is a limitation for ^{18}F-FDG PET/CT in the management of TB (Yu et al. 2019). Angiography is no longer used for diagnostic purposes, except as the first step before embolization. This latter procedure is performed in patients with life-threatening hemoptysis.

5 Imaging Features

Even if it is more accurate to distinguish active from inactive TB (Sharma et al. 2015; Nachiappan et al. 2017), we consider it more didactic to keep the classical distinction of primary and PPTB as their clinical pathological and radiological manifestations are quite different.

5.1 Primary Tuberculosis

Primary TB commonly manifests with enlargement of the mediastinal and hilar lymph nodes and homogeneous parenchymal consolidation. Unilateral pleural effusion and a miliary appearance may also be observed.

5.1.1 Parenchymal Involvement

Parenchymal involvement most often results in a small segmental or subsegmental subpleural consolidation. More rarely, lobar pneumonia resistant to antibiotics or multifocal involvement is observed. Parenchymal involvement is classically preferentially localized in the middle, lingular, and inferior lobes in adults, corresponding to the best ventilated pulmonary territories. Location in the upper lobe is more common in children. Cavitation is observed in 10% of cases (Andreu et al. 2005). In about two-thirds of cases, parenchymal lesions resolve without leaving any sequelae, but this resolution may take up to 2 years. Pulmonary infiltrates leave a few parenchymal scars such as nodules, which can completely calcify to form a Ghon focus or an area of fibrosis. Concomitant presence of a calcified hilar or mediastinal lymph node constitutes the Ranke complex (Koh et al. 2010).

5.1.2 Lymph Node Involvement

Lymph node involvement is most frequently unilateral. It is bilateral in nearly one-third of cases. The hilar and paratracheal groups are the most affected, while subcarinal nodes are less frequently involved. Lymph node involvement is visible on chest radiographs in 96% of children and 43% of adults (Koh et al. 2010). CT is more sensitive to detect this involvement. Lymph nodes greater than 20 mm present with a central hypodensity corresponding to caseous necrosis and peripheral ring-like enhancement after intravenous contrast administration corresponding to inflammatory granulomatous tissue (Burrill et al. 2007) (Fig. 1). The frequency of lymph node involvement decreases with age, while that of parenchymal involvement increases. Lesions evolve towards regression in two-thirds of cases, with possible massive calcified scar formation (Skoura et al. 2015; Nachiappan et al. 2017).

5.1.3 Pleural Effusions

Pleural effusions are observed in about a quarter of patients with primary TB and develop 3–7 months after the first exposure. They are more common in adults (Andreu et al. 2005; Burrill et al. 2007; Nachiappan et al. 2017). Pleural effusion is often multicompartmentalized and hyperechoic on US imaging (Fig. 2).

5.1.4 Miliary Involvement

Miliary involvement is rare during primary infection, occurring in 1–7% of cases. It is mostly observed during PPTB (Andreu et al. 2005; Burrill et al. 2007; Koh et al. 2010). This can be explained by hematogenous dissemination of

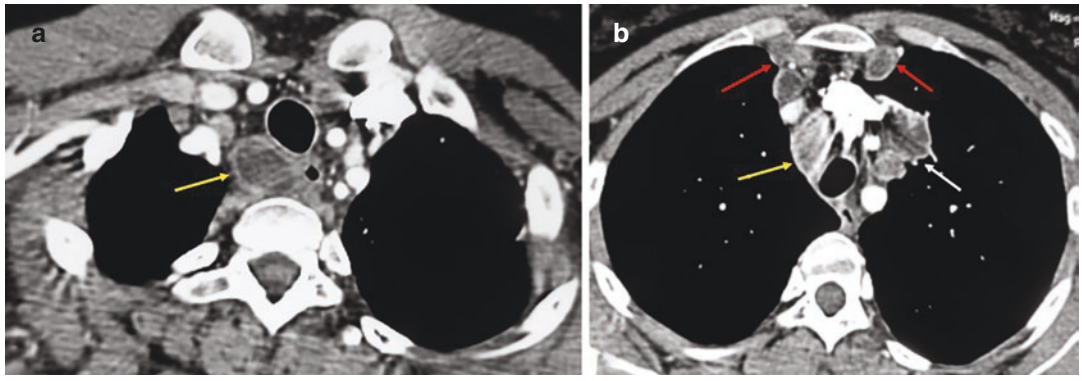

Fig. 1 Primary tuberculosis manifesting as lymph node enlargement. (**a** and **b**) Axial contrast-enhanced CT images in soft tissue window settings show retrotracheal (yellow arrow in **a**), lateral tracheal (yellow arrow in **b**), prevascular (white arrow in **b**), as well as bilateral internal mammary (red arrows in **b**) enlarged lymph nodes, all of which have central necrotic low attenuation and peripheral rim enhancement

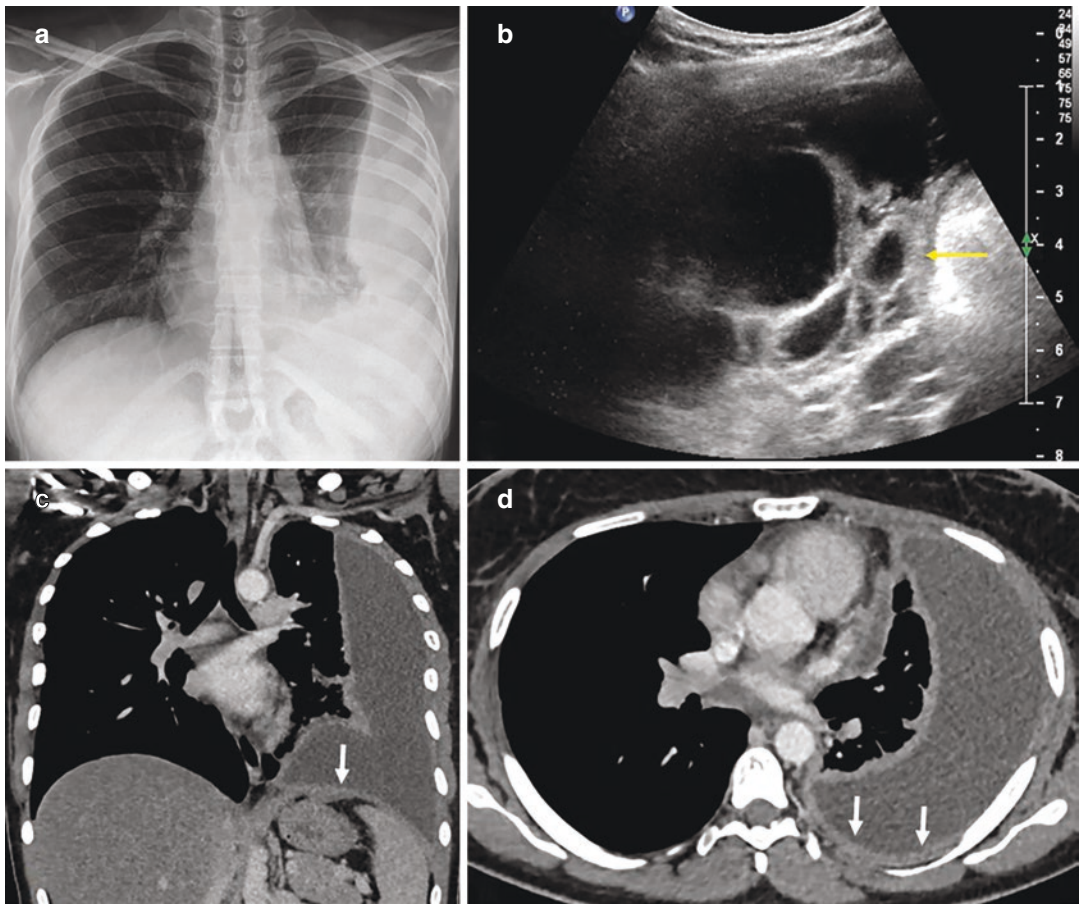

Fig. 2 Pleural tuberculosis in a 29-year-old woman. (**a**) PA chest radiograph shows a large left pleural opacity. (**b**) Lateral thoracic US image shows an anechoic pleural effusion with septations and thickening of parietal pleura (yellow arrow). (**c**) Coronal and (**d**) axial contrast-enhanced CT images confirm left pleural effusion and thickening (white arrows)

M. tuberculosis in patients whose immune system could not contain the infection (e.g., young children, immunocompromised patients). It is considered to be a severe form of the disease, with systemic spread and frequent meningeal as well as hepatosplenic involvement. It usually occurs within 6 months after the first contact with the bacteria. The TST may remain negative and could therefore be a source of diagnostic errors. In 85% of cases, radiological characteristics consist of micronodules 1–3 mm in size, with sharp contours and diffuse distribution. There is an apparent predominance in the lung bases, explained by the larger volume of parenchyma at this level (Fig. 3). CT is more sensitive for the detection of micronodules and their random diffuse distribution in both lungs. Reconstructions using maximal intensity projection (MIP) are useful for this purpose (Fig. 4). CT also allows assessment of other asymptomatic locations (Jeong and Lee 2008; Skoura et al. 2015; Nachiappan et al. 2017). MRI is more accurate than CT for the detection of brain lesions. Lesions generally heal under adequate treatment within 2–6 months (Nachiappan et al. 2017).

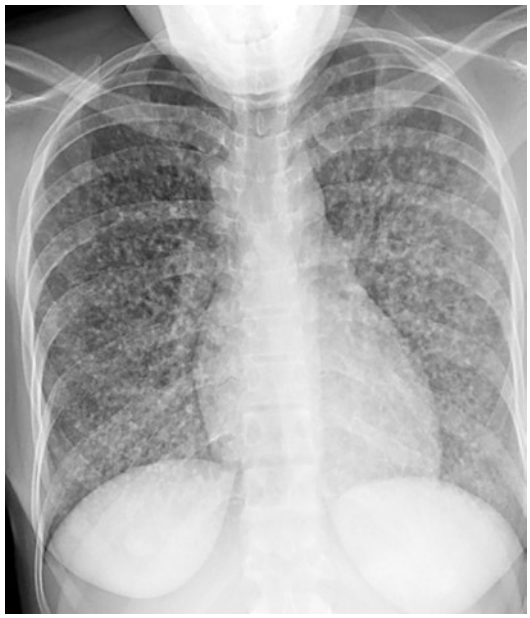

Fig. 3 Miliary tuberculosis in a 26-year-old woman. PA chest radiograph shows diffuse and randomly distributed millet-sized nodular opacities in both lungs

5.2 Post-primary Tuberculosis

Unlike primary TB, PPTB is chronic and fibrosing. It usually occurs in the apical and posterior segments of the upper lobe and less frequently in the apical segment of the lower lobe. The high intra-alveolar oxygen pressure and poor lymphatic drainage with low clearance of microorganisms help *M. tuberculosis* development in these areas. Bilateral upper lobe location is present in 32–64% of cases, with an asymmetric appearance in most cases (Skoura et al. 2015). Involvement of two or more lobes has a good positive predictive value for the diagnosis of active PPTB. Finally, multilobar involvement is common, and a progression towards a complete

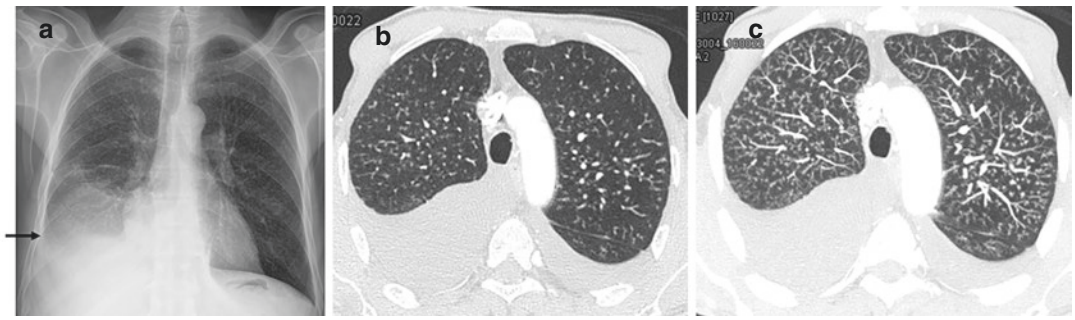

Fig. 4 Miliary tuberculosis in a 47-year-old man with right pleural effusion. (**a**) PA chest radiograph shows diffuse millet-sized nodular opacities in both lungs, with a right pleural opacity (arrow). Axial (**b**) millimeter section and (**c**) MIP-reconstructed HRCT images taken at the level of the upper lobes show uniformly sized small nodules randomly distributed in both lungs, which are better detected with MIP reconstruction. Note the presence of bilateral pleural effusions

lobar or pulmonary involvement with parenchymal destruction can be observed. Radiological features comprise nodules, cavities, and alveolar and nonalveolar opacities. Cavitation is characteristic of this form of TB. Lymph node involvement is less frequent than in the primary form, being described in only 5–10% of cases (Bomanji et al. 2015).

5.2.1 Micronodules and Nodules

Micronodules and nodules occur secondary to bronchogenic spread, which constitutes the most characteristic mode of dissemination of PPTB. This dissemination occurs when an area of caseous necrosis liquefies and communicates with the bronchial tree (Nachiappan et al. 2017). They are most often multiple with blurred boundaries, measuring 5–15 mm in diameter, and grow slowly. On CT, centrilobular micronodules are characterized by fuzzy contours, variable density, size less than 3 mm, and centrilobular topography located 2–3 mm from the pleura, with integrity of the pleuropulmonary interfaces (Fig. 5). They are best identified on CT MIP reconstructions using 6 mm thickness. This lesion results from bronchogenic dissemination of bacilli. It corresponds pathologically to the sections of bronchioles filled with granulomas in connection with the so-called cellular bronchiolitis.

These micronodules sometimes appear to be linked to distal broncho-arterial axes. This appearance has been described as "tree in bud" (Jeong and Lee 2008) (Fig. 6). It reflects thickening of the bronchiolar wall, associated with or

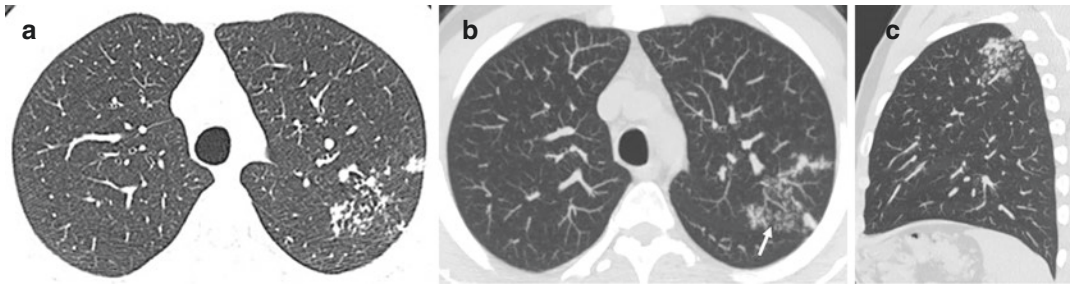

Fig. 5 Post-primary tuberculosis in a 32-year-old man. (**a**) Axial HRCT and (**b**) axial and (**c**) sagittal MIP-reconstructed HRCT images show centrilobular micronodules, and branching nodular and linear (tree-in-bud) opacities (arrow) in the dorsal segment of the left upper lobe

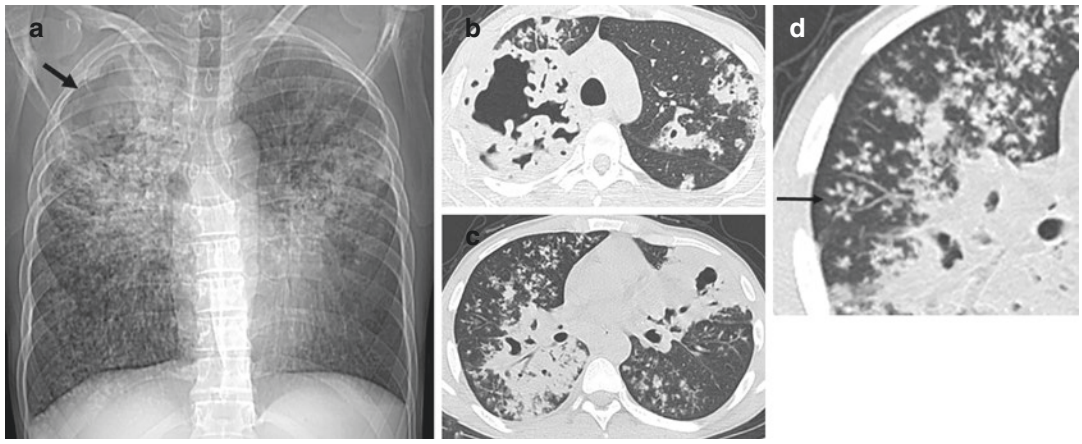

Fig. 6 Post-primary tuberculosis in a 35-year-old man. (**a**) PA chest radiograph shows bilateral alveolar opacities in the upper lungs with a cavity in a right opacity (arrow). (**b** and **c**) Axial HRCT images show bilateral cavitating consolidations and nodules, centrilobular micronodules, and acinar nodules. (**d**) Axial 4 mm MIP-reconstructed HRCT image shows branching nodular and linear (tree-in-bud) opacities (arrow) in the lateral segment of the middle lobe

without dilation of the bronchiolar lumen filled with secretions such as mucus, pus, and granulation tissue. Presence of branching centrilobular nodules with a tree-in-bud appearance is the most useful radiological feature for distinguishing active from inactive TB. However, it is not pathognomonic as it can be observed in pyogenic bronchopneumonia, atypical mycobacteria infection with bronchogenic dissemination, as well as invasive airway aspergillosis (Rossi et al. 2005). There is a clear tendency for these micronodules to congregate and cluster around the bronchioles. Their confluence will lead to the appearance of acinar nodules 5–10 mm in diameter, blurred outlines, and centrilobular location, corresponding to filling of the acini by granulomas beyond bronchiolar walls. The coalescence of these nodules results in acinary rosettes (Jeong and Lee 2008; Nachiappan et al. 2017) (Fig. 6).

5.2.2 Cavitation

Cavitation is the characteristic sign of PPTB and is considered an activity marker. Cavitation occurs in about half of affected patients (Andreu et al. 2005). The presence of cavitating lesions is significantly associated with smear-positive sputum, due to the greater bacillary richness of cavities (Singla et al. 2003). The cavities appear on chest radiographs as gas-filled spaces, rarely containing fluid, often with irregular contours and sharp and thick walls (Figs. 7 and 8). The bronchus to which they drain may be sometimes identified. On CT, the presence of bronchial micronodules located around a cavity in a typical area (apical and dorsal segments of the upper lobe and apical segment of the lower lobe) suggests the diagnosis of TB. These cavities are frequently multiple and are typically within an area of parenchymal consolidation (Fig. 9).

5.2.3 Lobar Alveolar Opacities

Lobar alveolar opacities correspond to tuberculous pneumonia. They appear as a systematized alveolar syndrome with air bronchogram, occurring in immunocompetent adults, always in the upper lobes, most often the right one. This consolidation almost always contains a cavity.

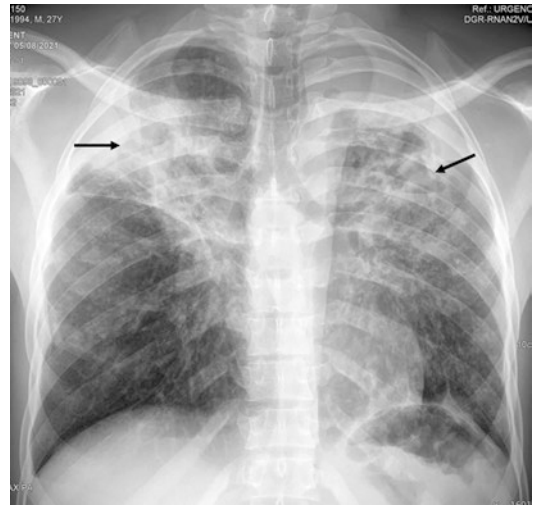

Fig. 7 Tuberculosis reactivation in a 27-year-old man. AP chest radiograph shows retractile and cavitating opacities in both upper lung lobes (arrows) as well as multiple bilateral ill-defined nodules

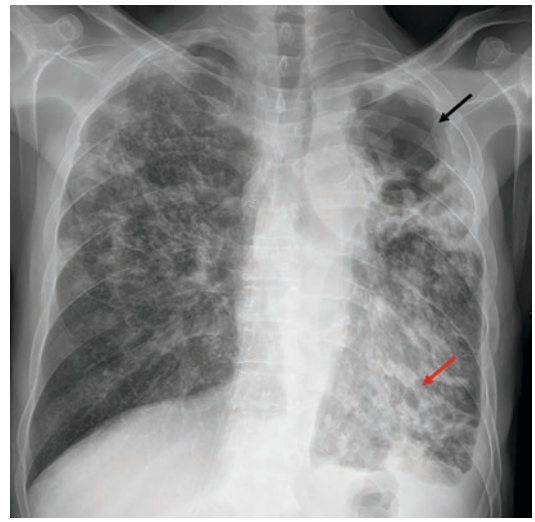

Fig. 8 Tuberculosis reactivation in a 59-year-old man. PA chest radiograph shows a cavitating consolidation in the left upper lobe (black arrow) and multiple ill-defined and confluent nodules in both lungs. Note bronchiectasis in the left lower lobe (red arrow)

5.2.4 Pneumatoceles

The development of pneumatoceles (or thin-walled cystic spaces in lung parenchyma) during PPTB is explained by the drainage of necrotic parenchymal lesions in areas of consolidation,

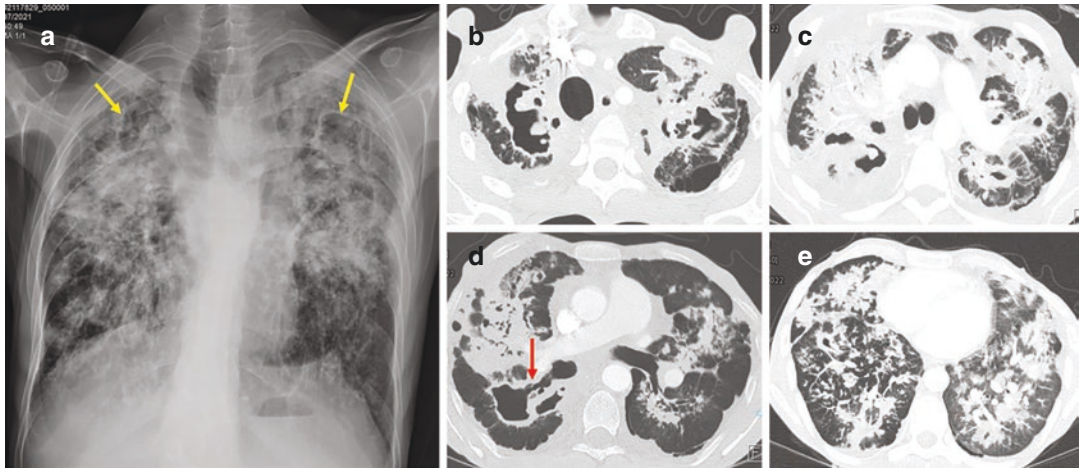

Fig. 9 Pulmonary tuberculosis reactivation in a 36-year-old man. (**a**) PA chest radiograph and (**b–e**) axial HRCT images show retracted consolidations containing several cavities predominantly in the upper lobes (yellow arrows), one of which communicates with the apical bronchus of the right lower lobe (red arrow). There are also bilateral confluent centrilobular micronodules and acinar nodules

coupled with the check-valve phenomenon caused by bronchiolar obstructions due to inflammatory edema of the walls (Burrill et al. 2007).

5.3 Extrapulmonary Tuberculosis

5.3.1 Pleural Tuberculosis

Tuberculous pleuritis is the second most common form of extrapulmonary TB after lymph node TB. It is present in 3–5% of patients with TB in developed countries and is ten times more frequent in high endemic countries (Shaw et al. 2018). In patients with AIDS, pleural TB is the primary site of infection, occurring in 30% of cases (Shaw et al. 2018). It usually develops 3–6 months after the primary infection. The pleural fluid is paucibacillary in most of the cases, but culture is positive in 76% of patients (Mazza-Stalder et al. 2012). In the first 24 h after inoculation, there is an accumulation of neutrophils in pleural fluid, followed by macrophages, whose number reaches a peak on the fourth day. After that, the fluid becomes lymphocytic (Shaw et al. 2018).

Pleural empyema results from a chronic infectious and highly bacillary process. The pleural fluid contains mainly neutrophils with a rate greater than 50%. This may result either from lymph node rupture into the pleural space or from hematogenous spread. Tuberculous empyema evolves into three phases, namely the preempyema exudative phase, the fibrinopurulent phase, and the organizing phase with granulation tissue development (Shaw et al. 2018).

Pleural TB is generally unilateral with a variable volume that is often moderate (Udwadia and Sen 2010; Shaw et al. 2018). Concomitant parenchymal involvement is observed in 20–50% of cases on chest radiographs (Shaw et al. 2018). US imaging can be used to assess the volume of pleural effusion, loculations, and pleural thickening, as well as to guide pleural punctures (Udwadia and Sen 2010; Hantous-Zannad et al. 2015). Pleural effusion may be anechoic, septated, or homogeneously echogenic in cases of empyema (Shaw et al. 2018) (Fig. 2). It can rarely be connected to the skin by a fistula, resulting in a so-called empyema necessitans (Hantous-Zannad et al. 2015) (Fig. 10). CT is the best imaging technique to assess the entire pleura and lung parenchyma, as well as for bronchopleural fistula detection (Udwadia and Sen 2010; Hantous-Zannad et al. 2015). Nodular thickening

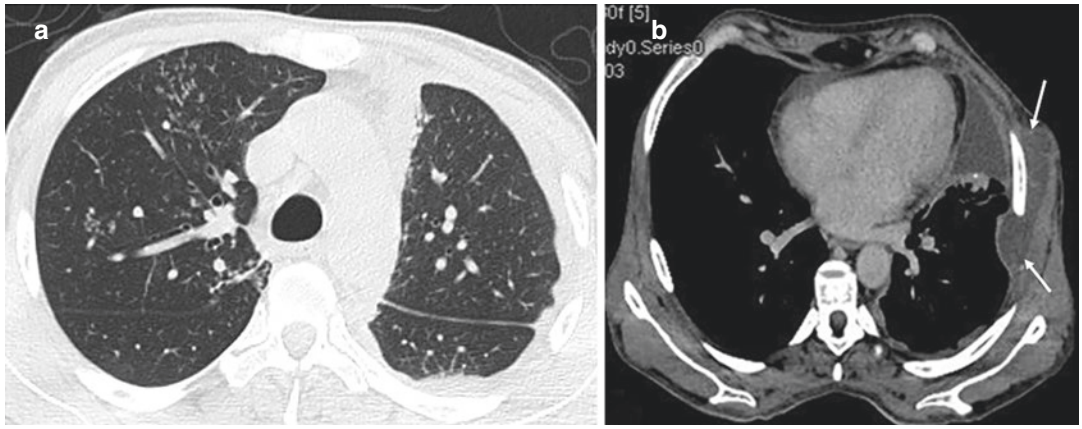

Fig. 10 Pulmonary tuberculosis and empyema necessitans. (**a** and **b**) Axial contrast-enhanced CT images in a 45-year-old patient with evolutive parenchymal tuberculosis (tree-in-bud opacities in the right upper lobe in **a**) and empyema necessitans (arrows in **b**)

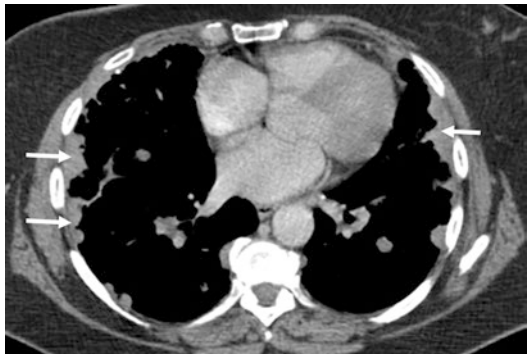

Fig. 11 Nodular pleural tuberculosis in a young woman. Axial contrast-enhanced CT image shows multiple areas of nodular pleural tuberculosis (arrows). There is no effusion. The diagnosis was confirmed by surgical biopsy

of the pleura without effusion is rare and atypical; this may mimic mesothelioma and metastases (Nèji et al. 2017) (Fig. 11).

5.3.2 Endobronchial Tuberculosis

Endobronchial TB is observed in 5–40% of patients with active TB. It results from fistulation of an interbronchial lymph node into the lumen of an airway or an extension of granulomas from peribronchial lymphatics (Pathak et al. 2016). Affected patients present most commonly with cough. Chest radiographs may show a lobar collapse, suggestive of bronchial cancer, particularly in patients at risk (Cadiñanos Loidi et al. 2014). On bronchoscopy, endobronchial TB can be classified into seven types, namely caseating, edematous-hyperemic, fibrostenotic, tumoral, granular, ulcerative, and non-specific bronchitis type, with most of them evolving into stenosis (Chung and Lee 2000).

5.3.3 Cardiovascular Tuberculosis

In autopsy studies of patients who died from TB, the heart is involved in 2% of immunocompetent patients and in 80% of patients with HIV co-infection (Mutyaba and Ntsekhe 2017). Pericardial TB is the most frequent expression of heart involvement and represents 1–2% of all tuberculous locations, but is associated with mortality close to 40% (Hantous-Zannad et al. 2015; Mutyaba and Ntsekhe 2017; López-López et al. 2021). It is more common in immunocompromised patients, especially those with AIDS who present with tuberculous pericardial effusion in 85% of cases (Mutyaba and Ntsekhe 2017; López-López et al. 2021). It results more from retrograde lymphatic dissemination than a hematogenous route. It can also result from direct rupture of adjacent pulmonary or pleural foci (Mutyaba and Ntsekhe 2017). Pericardial fluid is typically paucibacillary (Mutyaba and Ntsekhe 2017). Patients may present with one of these four syndromes: acute pericarditis, effusive pericarditis, myopericarditis, and constrictive

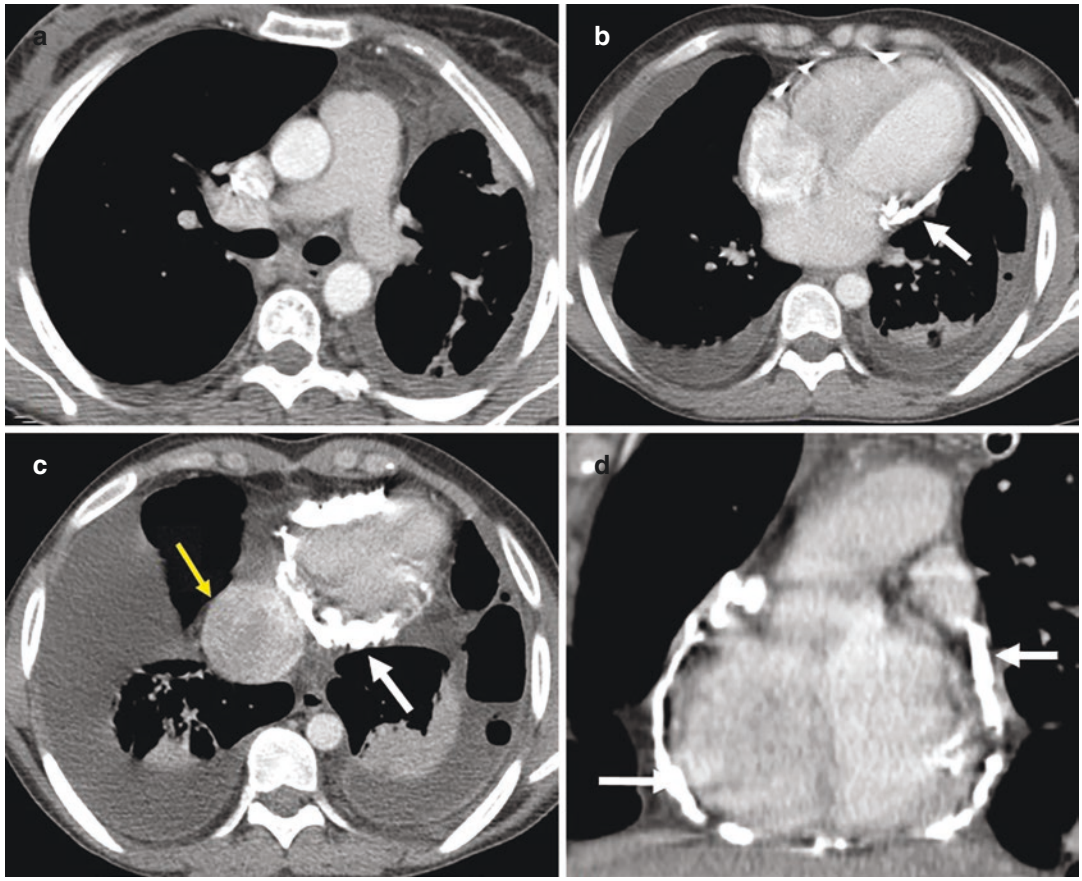

Fig. 12 Chronic calcified pericarditis. (**a–c**) Axial and (**d**) coronal contrast-enhanced CT images show circumferential calcifications of the pericardium (white arrows), and dilatation of the atria, pulmonary artery, and inferior vena cava (yellow arrow)

pericarditis. TB accounts for 38–83% of causes of constrictive pericarditis in endemic countries, and pericardial TB evolves to constriction in 20–50% of cases, despite adequate treatment (López-López et al. 2021).

US imaging, CT, and MRI can show pericardial effusion and thickening and can be used to assess their effect on the heart cavities. CT is the best technique to show calcifications of the pericardium, which is the final stage in the development of tuberculous pericarditis (Hantous-Zannad et al. 2015) (Fig. 12). Left ventricle myocardial involvement results from hematogenous spread most of the time. The right ventricle myocardium is involved by contiguous spread from right mediastinal lymph nodes. Patterns include myocarditis, tuberculomas, miliary tubercles, or diffuse infiltration (Mutyaba and Ntsekhe 2017) (Fig. 13). Endocarditis is extremely rare, with only few cases having been reported (López-López et al. 2021).

Tuberculous aortitis is exceptional and accounts for 0.004% of 22,792 post-mortem examinations performed over 50 years (Mutyaba and Ntsekhe 2017). *M. tuberculosis* reaches the aortic wall via the vasa vasorum and implants on atheromatous plaques. Patients may present with mycotic aneurysms of the thoracic or abdominal aorta. Stenotic lesions are less frequent (Mutyaba and Ntsekhe 2017; López-López et al. 2021).

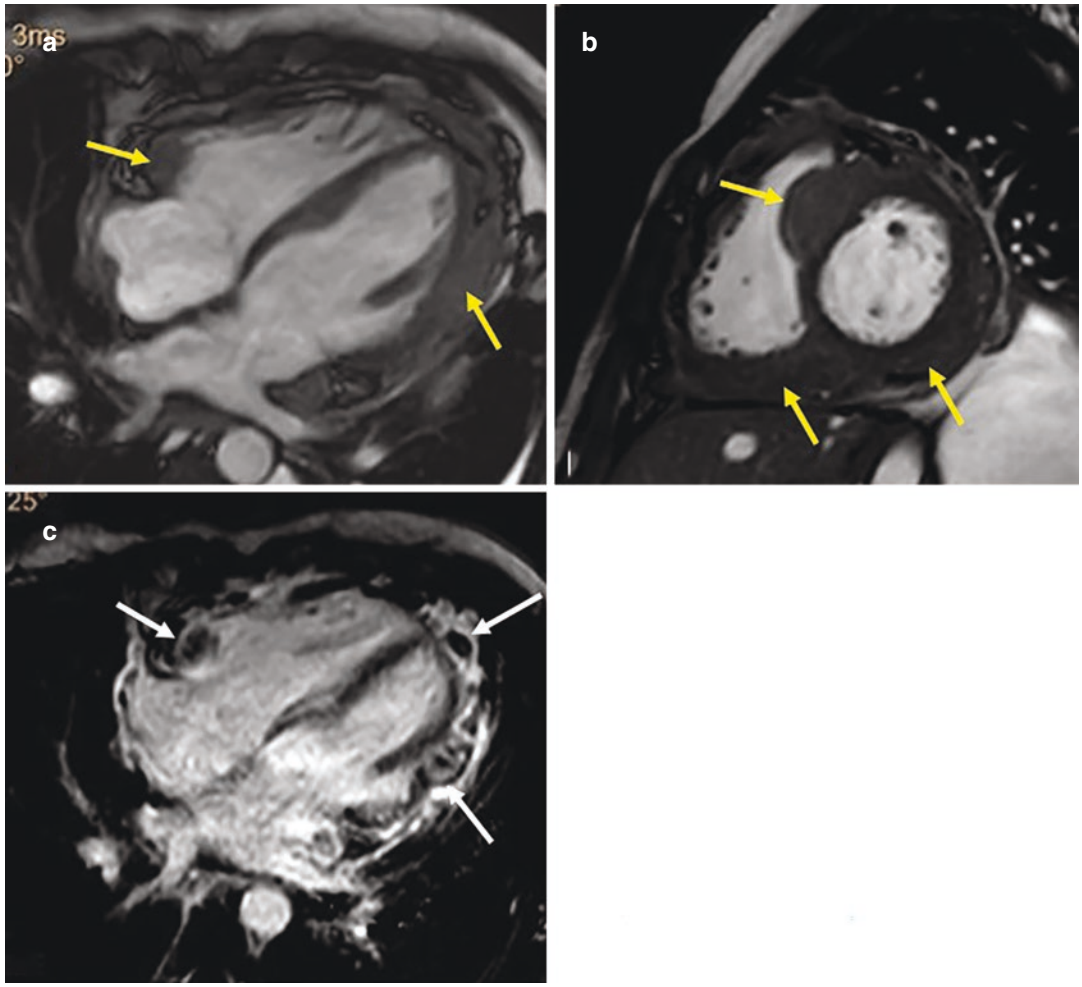

Fig. 13 Cardiac tuberculosis with myocardial tuberculomas in a 24-year-old woman. Cardiac (**a**) four-chamber, (**b**) short-axis cine, and (**c**) delayed-enhancement MR images show myocardial and pericardial thickening (yellow arrows) as well as many tuberculomas with peripheral enhancement (white arrows)

5.3.4 Anterolateral Chest Wall Tuberculosis

TB of the anterolateral chest wall represents less than 5% of osteoarticular TB and 15% of extrapulmonary thoracic TB (Hantous-Zannad et al. 2015). It mainly affects the ribs and intercostal spaces (2%). Sternal and clavicular involvement is rarer. Primary TB of the sternum occurs in 0.3% (Fig. 14). Chest wall TB is exceptionally an isolated location (Bouslama et al. 1998). A history of TB is found in 83% of cases, and associated active pulmonary TB is found in 17% of cases (Bouslama et al. 1998). Chest wall involvement results either from hematogenous and lymphatic spread or from contiguous mediastinal lymph nodes and pleural empyema (Kakamad et al. 2020). Patients generally present with a fluctuant painless mass without inflammatory signs (Bouslama et al. 1998; Kakamad et al. 2020).

On imaging, presumptive signs of chest wall TB infection include extensive osteolysis without osteoblastic reaction and presence of bone sequestra or fine soft tissue calcifications on radiographs and CT (Chelli Bouaziz et al. 2009). Pathological sternal or rib fractures may occur. On US imaging, a cold abscess may manifest as a thick-walled fluid collection containing bone

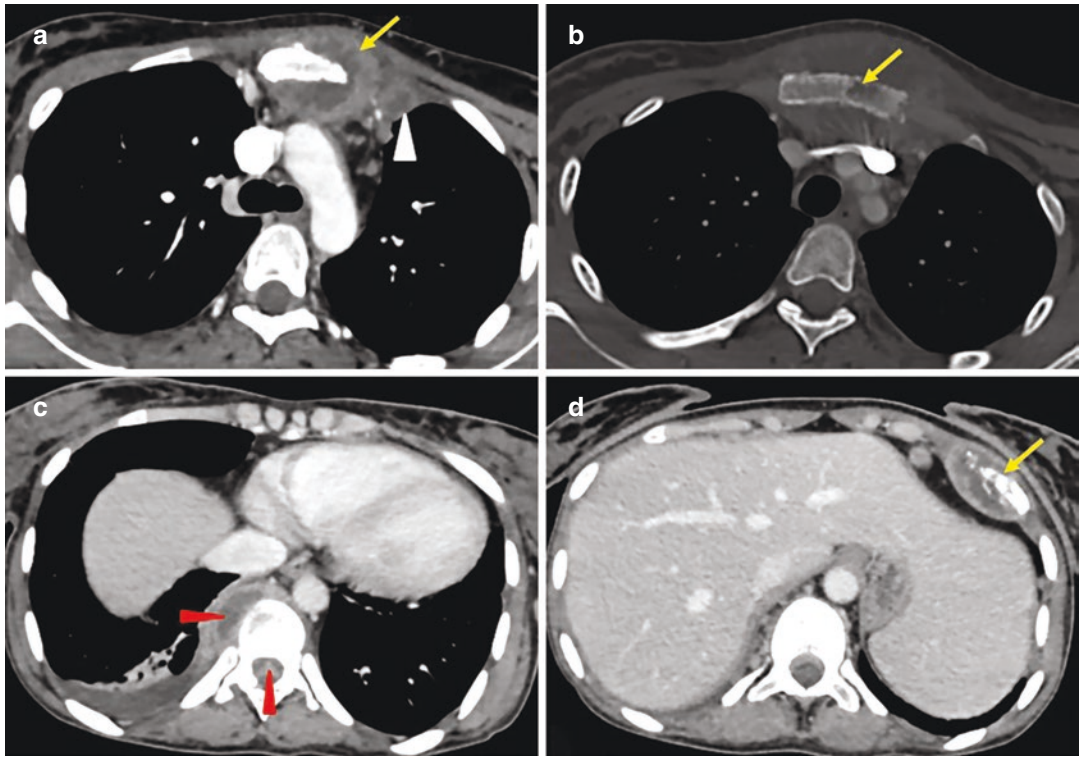

Fig. 14 Multifocal anterolateral chest wall tuberculosis in a 19-year-old woman. (**a–d**) Axial contrast-enhanced CT images show osteitis with associated collections of the sternum (yellow arrows in **a** and **b**) and left sixth rib (yellow arrow in **d**). Note the necrotic internal mammary lymph node (white arrowhead in **a**), right paravertebral and intraspinal epidural collections (red arrowheads in **c**), as well as a right pleural effusion

sequestra or a heterogeneous tissue mass, most often one that is largely necrotic (Hantous-Zannad et al. 2015; Kabiri et al. 2020; Kakamad et al. 2020). The walls of a cold abscess typically show a regular enhancing rim after contrast administration on CT and MRI (Chelli Bouaziz et al. 2009). Needle aspiration or core biopsy is sometimes needed to confirm the diagnosis (Kakamad et al. 2020).

5.4 Atypical Forms of Pulmonary Tuberculosis

5.4.1 Tumorlike Pulmonary Tuberculosis

Tumorlike pulmonary TB accounts for 3.5–4.5% of cases in immunocompetent patients (Hantous-Zannad et al. 2015). It is more common in immunocompromised patients. Mycobacterial infections account for 27% of all lesions mimicking lung cancer (Hammen 2015). This form of pulmonary TB occurs at an average age of 45 years (Hantous-Zannad et al. 2015). However, it may also occur in children (Chen et al. 2018b). The period taken for diagnosis varies between 30 and 70 days, due to the negativity of direct examination of the common samples (Hantous-Zannad et al. 2015). The diagnosis is made based on cultures of bacteriological samples and on pathological examination of fragments of bronchial and transparietal biopsies and operative resection specimens. The diagnostic accuracy, sensitivity, specificity, positive predictive value, and negative predictive value of CT-guided percutaneous biopsies for the diagnosis of TB are 90%, 79.6%, 100%, 100%, and 88.9%, respectively (Chen et al. 2018a).

There are two forms of pseudotumoral TB, namely the parenchymal form and the

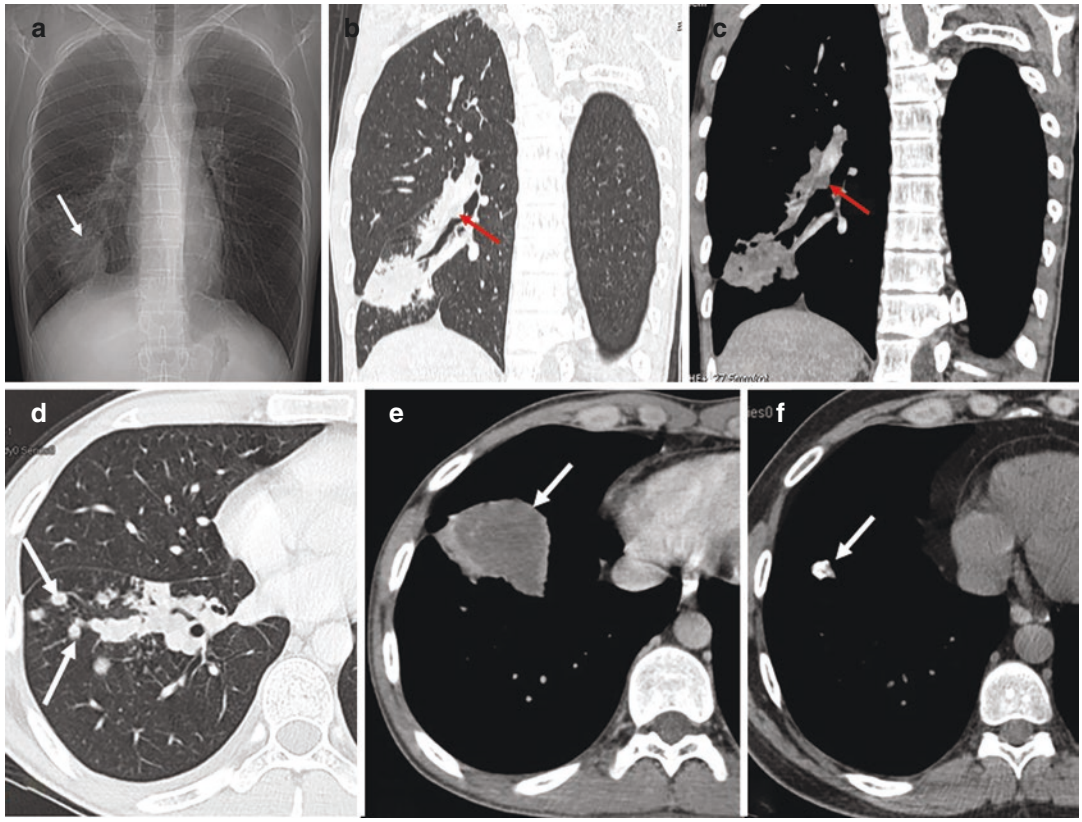

Fig. 15 Tumorlike tuberculosis in a 23-year-old man who presented with chest pain. (**a**) PA chest radiograph shows a rounded right lower zone opacity (white arrow). (**b** and **c**) Coronal and (**d** and **e**) axial CT images show an endobronchial mass (red arrows in **b** and **c**), pulmonary nodules (white arrows in **d**), and a necrotic mass (white arrow in **e**) in the right lower lobe. (**f**) Follow-up axial CT image shows that the disease has healed after treatment with sequela of a calcified nodule (white arrow)

endobronchial form (Fig. 15). The parenchymal form may present either as a single mass, as well as a rounded consolidation, mimicking a primary lung cancer, or as many nodules simulating metastases (Kaur 2021). Lesions are generally predominantly found in the apical and dorsal segments of the upper lobe and the apical segment of the lower lobe. However, these locations are not specific. Some signs may suggest the diagnosis of TB, such as peripheral contrast enhancement of masses; coexistence of diffuse, central, or lamellar calcifications; necrotic or calcified lymph nodes; and centrilobular micronodules producing a tree-in-bud appearance and acinar nodules (Hantous-Zannad et al. 2015).

5.4.2 Paucibacillary Tuberculosis

Paucibacillary TB is defined by a negative acid-fast bacilli (AFB) smear microscopy. AFB smear microscopy has a sensitivity of only 34–80% for the diagnosis of pulmonary TB (Park et al. 2019). Hence, the confirmation of paucibacillary TB is made on cultures or on pathological examination of a biopsy sample. It represents 41–49% of all new cases of TB in countries with a high endemicity for this disease and is responsible for 10–20% of TB transmission (Li et al. 2013; Campos et al. 2016). It is more common in men than in women and in HIV-positive patients (Li et al. 2013; Campos et al. 2016). The World Health Organization recommends the diagnosis

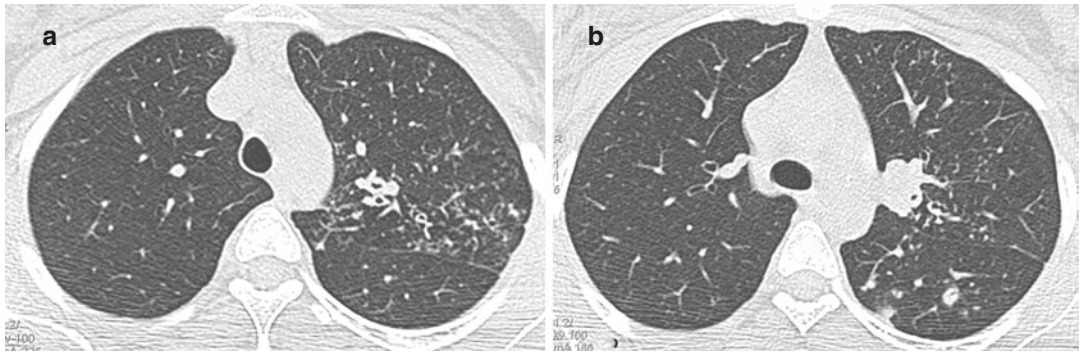

Fig. 16 Paucibacillary tuberculosis in an 18-year-old patient who presented with chronic cough. (**a** and **b**) Axial CT images show micronodules and nodules of the left upper and lower lobes

of these forms in immunocompromised and immunocompetent patients to be based on clinical symptoms and chest radiographical features (World Health Organization 2007; Huerga et al. 2012; Walusimbi et al. 2013). However, only 55% of patients can be treated based on this approach (Huerga et al. 2012).

Patients with smear-negative TB have less typical chest radiographical features. CT is more sensitive and is particularly indicated in patients with normal or nonsuggestive chest radiographical findings (Matsuoka et al. 2004). Its sensitivity and specificity for detecting signs of disease activity in paucibacillary patients range from 70% to 88%. Its positive predictive value is in the 70–92% range, and its negative predictive value is in the order of 80%. It can be used to look for signs of TB disease activity such as centrilobular micronodules with a "tree-in-bud" appearance, acinar nodules, cavitating nodules, consolidation, and areas of ground-glass opacities (Caliskan et al. 2014) (Fig. 16). Centrilobular micronodules are the most frequently seen lesions and are as common in paucibacillary patients as in bacilliferous patients (Alsowey et al. 2017; Kim et al. 2019). Consolidation, cavitation, and involvement of the upper lobes and of multiple lobes are more frequent in bacilliferous patients (Alsowey et al. 2017). Peripheral location and lower zone involvement are associated with smear-negative TB (Lee et al. 2021). CT is more sensitive but less specific than polymerase chain reaction (PCR) test and less sensitive and less specific than IGRA for the diagnosis of smear-negative TB (Lee et al. 2010; Shaarrawy et al. 2013; Alsowey et al. 2017).

5.4.3 Tuberculosis of the Lung Bases

TB of the lung bases is an atypical form of TB and is defined by lesions located inferior to the hilum, i.e., involving the right middle lobe, the lingula, and the lower lobes without involvement of the upper lung (Halawar and Sudhindraswamy 2019; Ben Miled-M'Rad et al. 2002). It represents almost 5% of all cases of pulmonary TB, with diabetes mellitus as the main risk factor and predominance to the right side. The main radiological findings are patchy opacities and homogeneous consolidations. Cavities may also be observed (Halawar and Sudhindraswamy 2019) (Fig. 17). Mechanisms of involvement of the lung bases include inoculation from apical foci, fistulation of a hilar lymph node in a bronchus, or retrograde lymph flow from the hilum to the lower lung territories (Ben Miled-M'Rad et al. 2002).

5.4.4 Multidrug-Resistant Tuberculosis

Multidrug-resistant tuberculosis (MDR-TB) is defined as resistance to at least isoniazid and rifampicin. Extensively drug-resistant

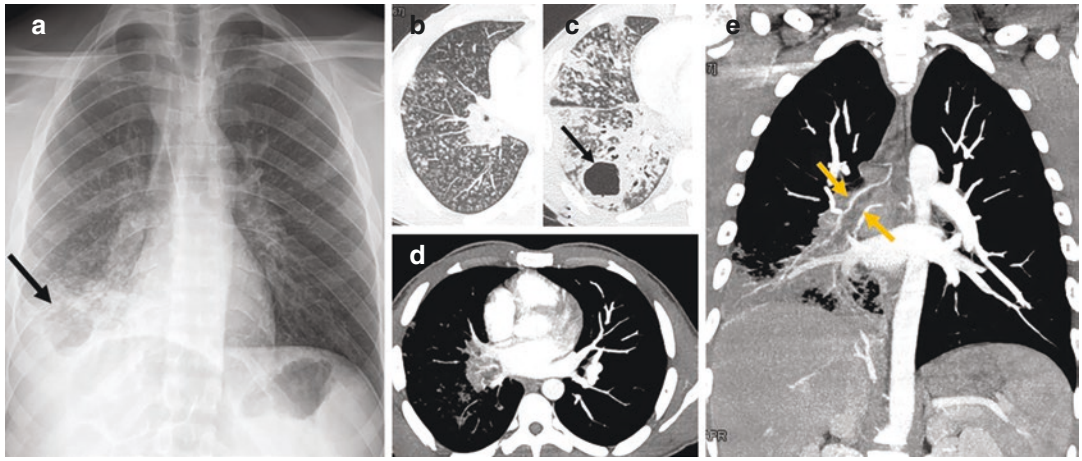

Fig. 17 Tuberculosis of the lower lungs. (**a**) PA chest radiograph shows a cavitating opacity in the right lower lung (black arrow). (**b** and **c**) Axial MIP-reconstructed HRCT images show tree-in-bud opacities with a cavitating consolidation of the right lower lobe (black arrow). (**d**) Axial and (**e**) coronal MIP-reconstructed contrast-enhanced CT images show right chronic pulmonary embolism (seen as the absence of opacification of the right pulmonary arteries, compared to the left side in **d**) and hypertrophy of the bronchial arteries (yellow arrows in **e**)

tuberculosis (XDR-TB) has been defined, since January 2021, by resistance to any fluoroquinolone and at least one additional Group A drug (Group A drugs comprise levofloxacin, moxifloxacin, bedaquiline, and linezolid) (World Health Organization 2021b). Surgery has changed the prognosis of patients with MDR-TB and XDR-TB. However, the indications for surgery are restricted to only 2% of these patients. Only patients with unilateral involvement or limited to operable locations can benefit from surgical treatment, which has a cure rate of up to 90–98% (Mordant et al. 2012). CT has an essential place in the pre-operative assessment of the disease extent (Fig. 18).

5.4.5 Tuberculosis in Immunocompromised Patients

TB can occur in patients with impaired cellular immunity. Patients with organ transplant and AIDS are 20 to 30 times more likely to develop TB (Nachiappan et al. 2017). TB occurs at a stage where the CD4 level is most often between 200 and 500/mm^3 and is responsible for 12% of deaths in patients with AIDS (Hantous-Zannad et al. 2015; Guedes 2018). Chest radiographical signs vary according to the CD4 count (Hantous-Zannad et al. 2015; Nachiappan et al. 2017). When the CD4 level exceeds 350/mm^3, TB has a classic presentation with occurrence of upper lobar cavities. However, radiographs may be normal in patients with a CD4 count below 200/mm^3, explaining the absence of AFB in sputum (Hantous-Zannad et al. 2015; Nachiappan et al. 2017). The apical location is less frequent than in immunocompetent patients. Mediastinal lymph node enlargement, hematogenous dissemination, and extrapulmonary involvement are more frequent in immunosuppressed patients (Guedes 2018). Miliary TB can occur in patients with severe immunosuppression. Worsening of pulmonary lesions can occur within 60 days after anti-retroviral therapy, which is associated with immune reconstitution inflammatory syndrome observed when the CD4 level is less than 5/mm^3 (Nachiappan et al. 2017). CT may suggest the diagnosis and evaluate the disease extent (Hantous-Zannad et al. 2015).

Cancers and their treatment are also recognized to promote the development of TB (Fig. 19). In fact, the incidence of TB in patients with cancers is higher than that in a control population, with a hazard ratio of 1.64 and

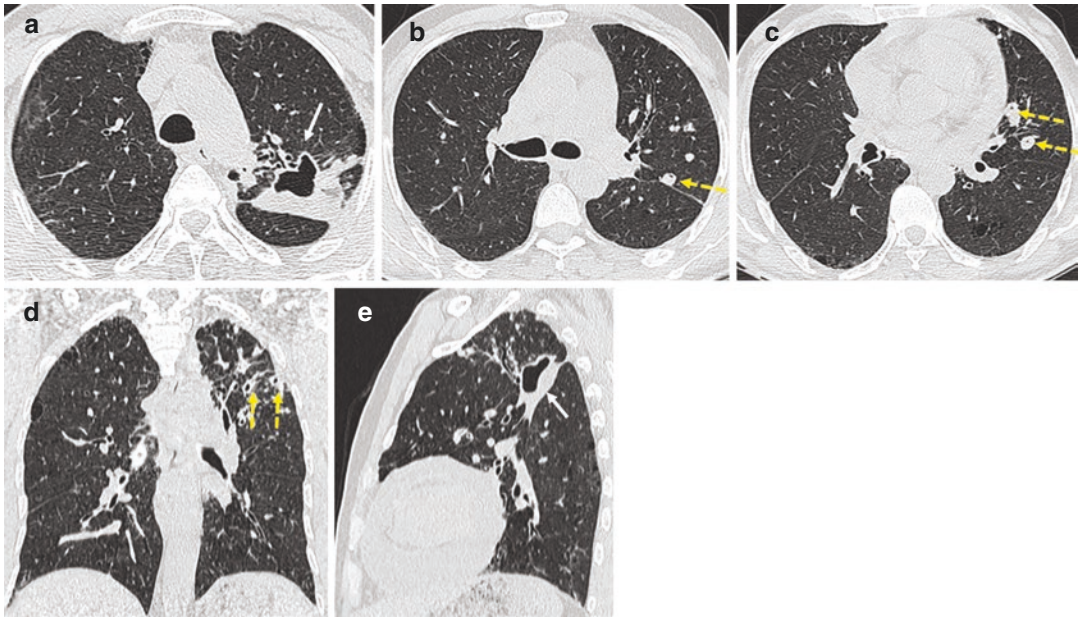

Fig. 18 Multidrug-resistant tuberculosis in a 54-year-old patient. (**a–c**) Axial, (**d**) coronal, and (**e**) sagittal CT images show a cavitating consolidation (white arrow) and nodules located mainly in the left upper lung (yellow arrows)

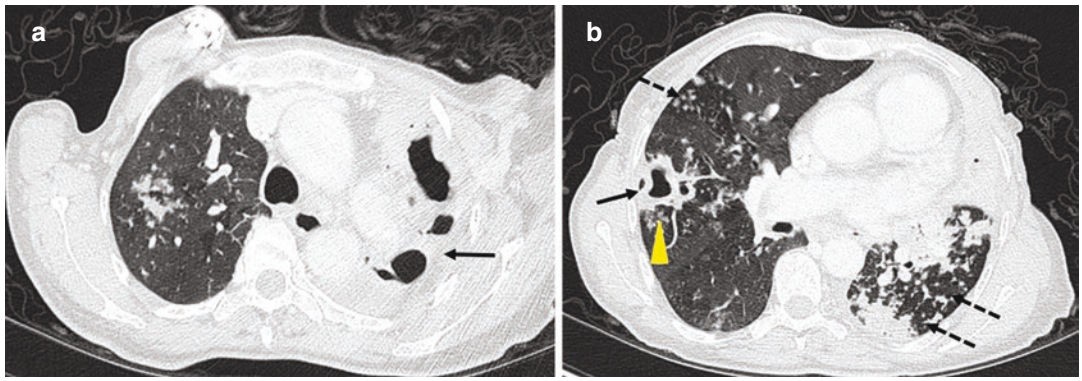

Fig. 19 Pulmonary tuberculosis in a 60-year-old woman who was treated for breast cancer. She underwent surgery, chemotherapy, radiotherapy, and hormonotherapy. (**a** and **b**) Axial CT images show cavitating consolidations (black arrows), acinar nodules (black dashed arrows), and centrilobular micronodules (yellow arrowhead)

incidence rate ratio (IRR) of 1.47 (Vento and Lanzafame 2011; Shen et al. 2021). It is more often observed in patients with aerodigestive tract and hematological cancers (Vento and Lanzafame 2011). The IRR of TB for adult patients is 2.61. In hematological cancers, the IRR is 3.53, and in solid cancers in adults, it is 2.25. The highest IRR is observed in children with hematological malignancies or solid cancers (IRR 16.82) (Dobler et al. 2017). Its development is explained by malnutrition and alteration of the local and systemic immunity that is caused by cancer itself or by chemotherapy and radiotherapy (Vento and Lanzafame 2011). TB occurs most frequently in the year before and the year after the diagnosis of cancer (Shen and Lin 2021). Recurrence of TB is observed in 3% and 5% of cases, respectively, in the first year and the first 2 years after treatment completion (Shu et al. 2019).

6 Imaging Differential Diagnosis

6.1 Pulmonary Tuberculosis

The imaging differential diagnosis depends on the infection type and pattern.

6.1.1 Miliary Involvement

Miliary involvement is seen in a wide variety of diseases. Chest radiographs alone cannot distinguish among the differential diagnoses. CT may identify the hematogenous distribution of micronodules and associated signs, thus restricting the etiological diagnostic range.

In infections, several microorganisms can manifest as military involvement. Viral pneumonitis has been reported, particularly the herpes group of viruses (Agrawal 2011; Franquet 2011). Other causes such as fungal infections, nocardiosis, and salmonellosis have also been described. Miliary metastases (Agrawal 2011; Chaddha et al. 2017) may be caused by many tumors, especially thyroid carcinoma, osteosarcoma, renal cell carcinoma, breast carcinoma, pancreatic cancer, and lung cancer. Other histological types are less frequent, such as malignant melanoma and trophoblastic disease.

Miliary involvement has been described as a rare presentation of sarcoidosis (Rajagopala et al. 2020). With the advent of high-resolution CT (HRCT), perilymphatic nodule distribution is better recognized, and the diagnosis of sarcoidosis is more easily considered (Koyama et al. 2004). However, random micronodules have been described in sarcoidosis (Criado et al. 2010; Chaddha et al. 2017). Associated signs such as peribronchovascular thickening and symmetrical nonnecrotic enlarged mediastinal lymph nodes help in the diagnosis (Criado et al. 2010; Chaddha et al. 2017) (Fig. 20).

Pneumoconioses such as silicosis, berylliosis, and coal workers' pneumoconiosis may also manifest as a miliary pattern. Hypersensitivity pneumonitis may appear miliary on chest radiographs. CT is able to highlight the centrilobular distribution of micronodules and their ground-glass appearance (Fahim and Khan 2011). Langerhans cell histiocytosis may rarely manifest as a miliary pattern (Chaddha et al. 2017) (Fig. 21).

6.1.2 Cavitating Lesions

Cavitating lesions can occur in other diseases including infection, vasculitis, and sarcoidosis. There is a huge number of species of nontuberculous mycobacteria, and only a few have a proven pulmonary pathogenicity in humans: *Mycobacterium avium* complex (MAC/*M. avium* and *M. intracellular*), *M. kansasii*, *M. xenopi*, and *M. abscessus*. The diagnosis is difficult, requiring a concordance of clinical,

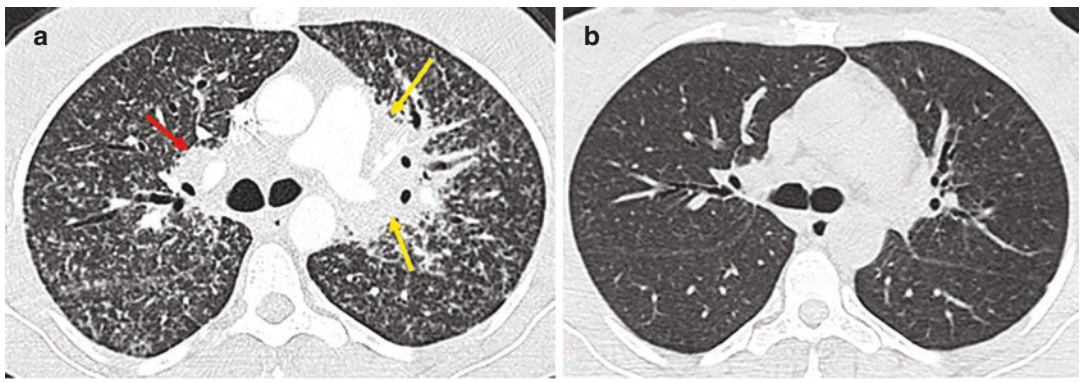

Fig. 20 Miliary sarcoidosis in a 32-year-old woman. (**a** and **b**) Axial HRCT images show randomly distributed micronodules in both lungs (**a**) that disappeared after treatment with corticosteroids (**b**). Note also peribronchovascular thickening (yellow arrows) and hilar lymphadenopathy (red arrow) on the initial HRCT image (**a**)

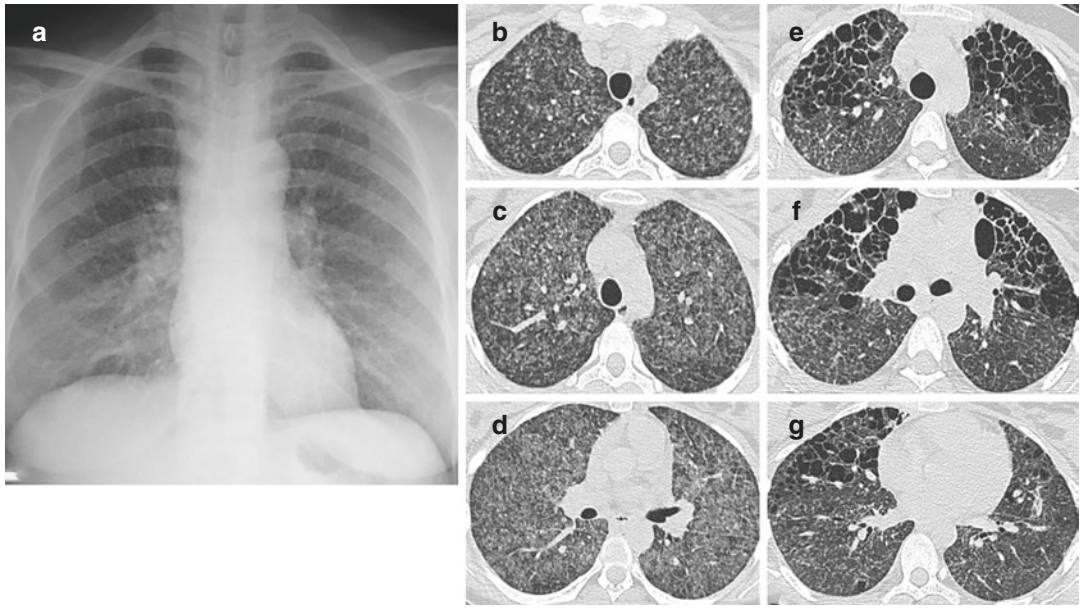

Fig. 21 Langerhans cell histiocytosis. (**a**) PA chest radiograph shows a miliary pattern. (**b–d**) Axial CT images show diffuse ground-glass micronodules. (**e–g**) Follow-up CT images show appearance of confluent cysts. Association of miliary tuberculosis and pneumocystosis was suggested. Diagnosis of Langerhans cell histiocytosis was confirmed by high CD1a count from the bronchoalveolar lavage. *Pneumocystis jirovecii* test was negative

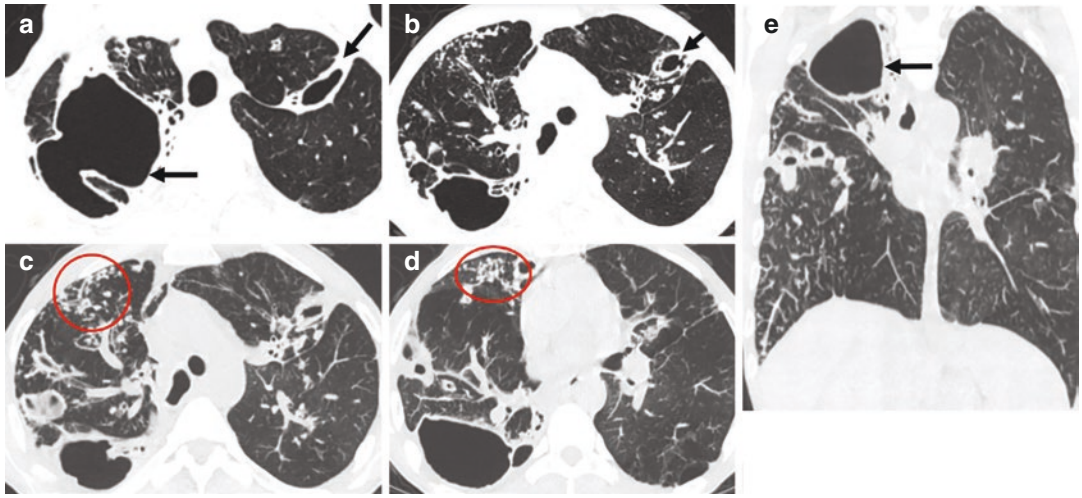

Fig. 22 Atypical mycobacterial infection in a 48-year-old man who presented with fever and night sweats. He was previously treated for gastric lymphoma in 1996 and pulmonary tuberculosis in 2016. (**a** and **b**) Axial and (**c** and **d**) axial and (**e**) coronal MIP-reconstructed CT images show bilateral cavitating consolidations (arrows) and tree-in-bud opacities (circled). Sputum bacteriological examination showed *Mycobacterium kansasii*

radiological, and bacteriological criteria. Three radiological presentations have been described. *M. avium* and *M. kansasii* cause the "tuberculosis-like" form with nodules, "tree-in-bud" appearance, and cavities, which predominate in the upper lobes (Andréjak et al. 2011) (Figs. 22 and 23). Uncommon bacterial infections that have been reported to have a cavitary

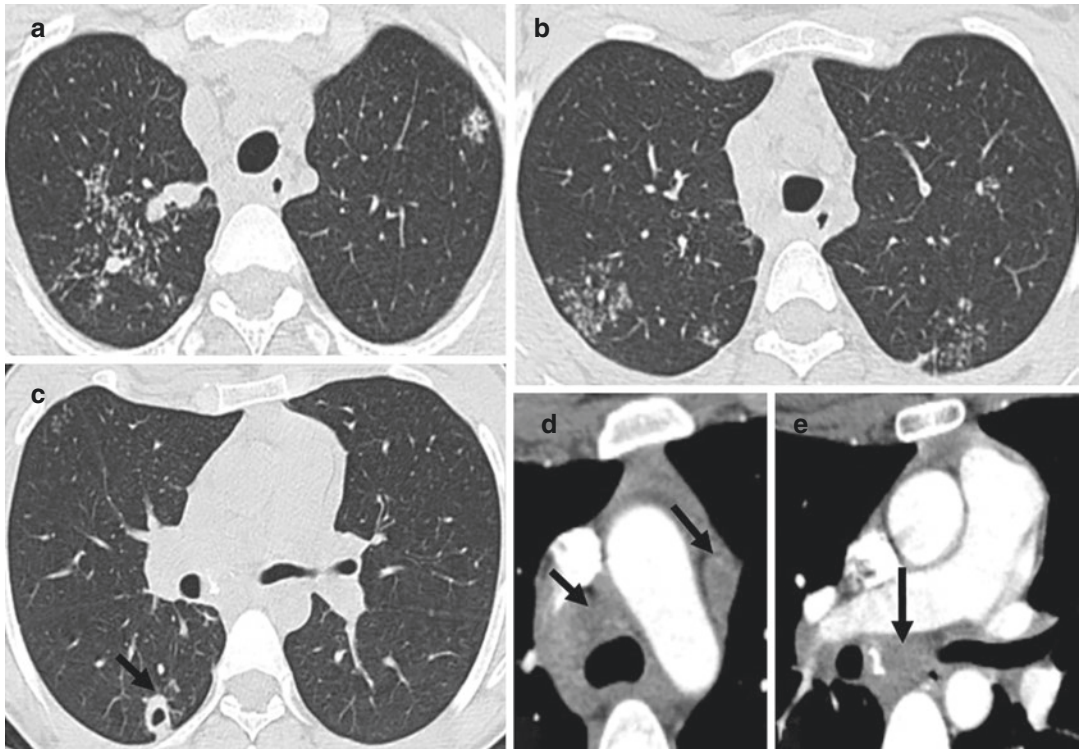

Fig. 23 Atypical mycobacteria infection (*Mycobacterium fortuitum*) in a 22-year-old man with no past medical history who presented with dry cough and weight loss. (**a–e**) Axial contrast-enhanced CT images show tree-in-bud opacities in the upper lungs (**a** and **b**), a cavitating nodule (arrow in **c**), and multiple enlarged mediastinal lymph nodes (arrows in **d** and **e**)

pattern are actinomycosis (Fig. 24) and nocardia (Fig. 25). Fungal infections that may manifest as a chronic cavitating consolidation include aspergillosis, mucormycosis, histoplasmosis, blastomycosis, cryptococcosis, and pneumocystosis (Fig. 26).

Common imaging findings in vasculitis (granulomatosis with polyangiitis) include multiple, bilateral pulmonary masses that may cavitate in larger lesions. These cavitating nodules and masses have thick and irregular walls (Cho et al. 2019). Very active forms of sarcoidosis may cavitate and mimic TB. However, they remain very rare, comprising fewer than 1% of cases. The diagnosis is sometimes difficult, and even more so in the presence of micronodules and upper zone predominance of lesions. Bullae in advanced fibrotic sarcoidosis may simulate the sequelae of TB (Fig. 27).

6.1.3 Lung Cancer

The diagnosis of TB and lung cancer can be difficult as symptoms of both diseases are often similar. Some radiological features can help in differentiating cancer from pseudotumoral TB. Malignant lesions have irregular or spiculated margins (Bhatt et al. 2012), whereas centrilobular micronodules around lesions with a "tree-in-bud" appearance are the most characteristic CT features suggestive of pulmonary TB. Tuberculoma can also mimic lung cancer, especially in the absence of calcifications. However, the presence of benign-looking calcification within the nodule, adjacent tree-in-bud lesions, or satellite nodules may help in differentiating tuberculomas from malignant nodules.

PET/CT has been suggested to distinguish between both diagnoses. However, increased FDG intake is also observed in granulomatous inflammation and tuberculomas. Maximum

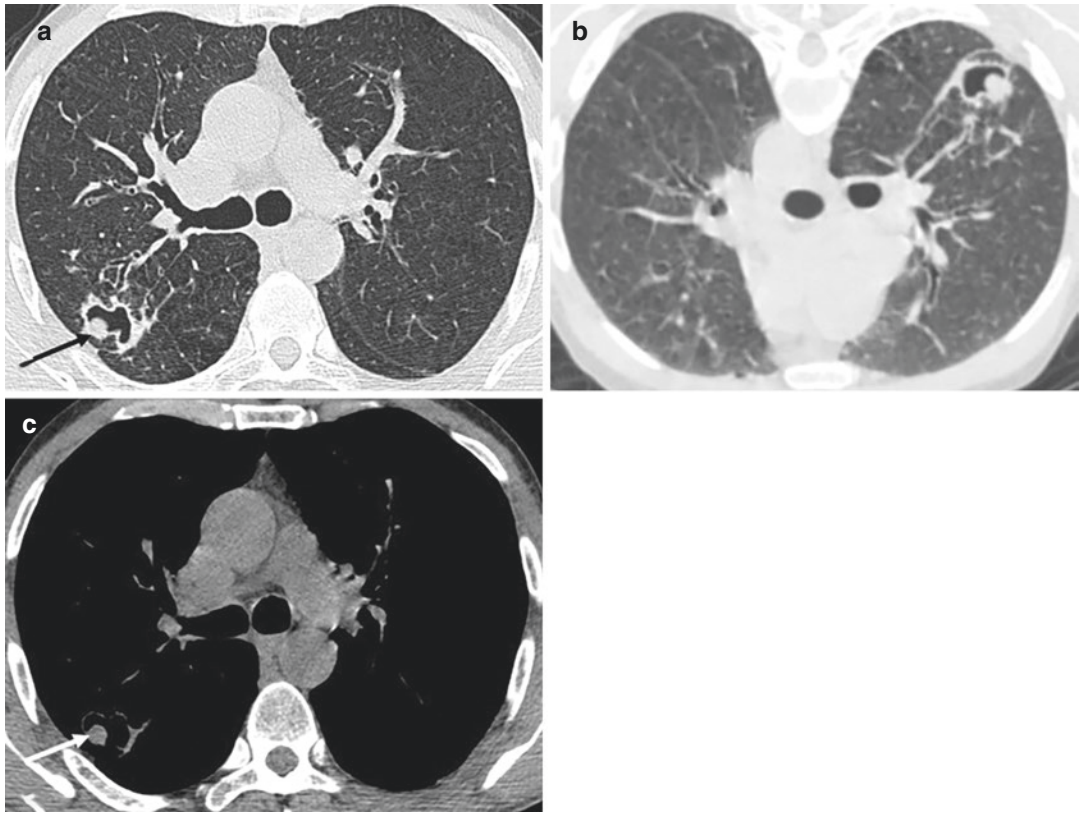

Fig. 24 Actinomycosis in a 60-year-old man, a cigarette smoker, who presented with hemoptysis. (**a–c**) Axial CT images show an irregular-walled air-filled cavity with hypodense content (arrows in **a** and **c**) that shifts to a dependent position on the prone image (**b**). The diagnosis was pathologically confirmed after upper right lobectomy

standardized uptake values (SUVmax) tend not to be significantly different for TB and malignant lesions (Goo et al. 2000; Zheng et al. 2011; Ankrah et al. 2016). Thus, positive ^{18}F-FDG PET/CT findings should be interpreted with caution in TB-endemic regions. Besides ^{18}F-FDG, other PET tracers have been investigated for imaging of TB. ^{11}C-choline has been evaluated for differentiation of lung cancer and other lesions, including active TB, and has been proven to be an accurate tool for this differentiation, especially in cases of combining ^{11}C-choline and ^{18}F-FDG (Hara et al. 2003; Ankrah et al. 2016). Nevertheless, this tool is not generally used in our mainstream practice.

6.2 Lymph Node Tuberculosis

Many conditions can produce enlarged mediastinal nodes with low attenuation on CT.

6.2.1 Sarcoidosis

Typically, the lymphadenopathies observed in sarcoidosis are well defined, homogeneous, with hilar and right paratracheal predominant locations (Criado et al. 2010). Symmetry is an important diagnostic feature to differentiate sarcoidosis from TB. The lymph node pattern of enhancement is an important criterion in the differentiation of a tuberculous node from one due to sarcoidosis. Sarcoidosis lymphadenopathy typically enhances homogeneously. However, it should be noted that even sarcoidosis lymphadenopathy may have heterogeneous enhancement with the "cluster of black pearls" sign. This sign corresponds to tiny round hypodense nodules scattered uniformly within an enlarged node (Venkata Ramanan et al. 2017) (Fig. 28). Lymph node calcification may be present in long-standing sarcoidosis. When calcifications have amorphous,

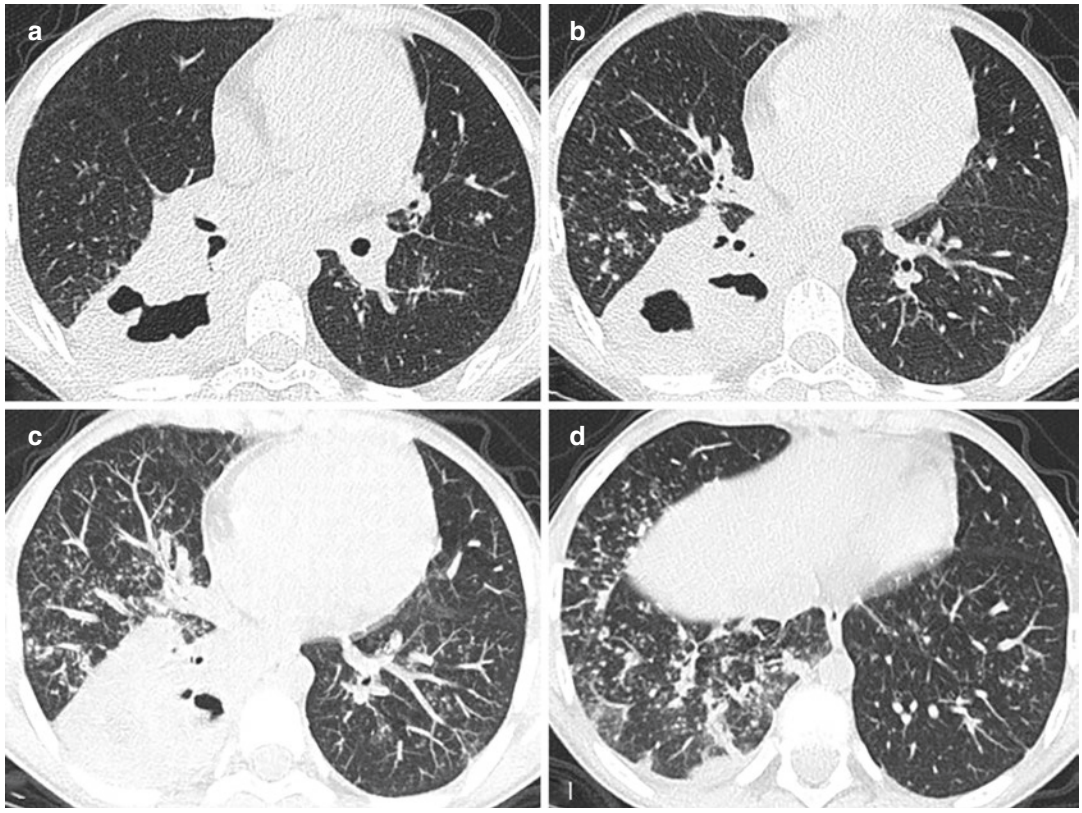

Fig. 25 Nocardiosis in an 11-year-old patient with a history of chronic septic granulomatosis. (**a** and **b**) Axial CT images show multiple cavitating consolidations in the right lower lobe without obvious communication with the bronchial tree. (**c** and **d**) Axial MIP-reconstructed CT images show bilateral confluent centrilobular micronodules predominantly in the middle and right lower lobes. Favorable outcome was achieved after appropriate antibiotic treatment with cotrimoxazole.

punctuate, or popcorn-like appearances, it becomes indistinguishable from those seen in other infectious granulomatous diseases such as TB (Suwatanapongched and Gierada 2006; Criado et al. 2010). Eggshell-like calcifications are more suggestive of sarcoidosis (Criado et al. 2010).

6.2.2 Fungal Infections

Fungal infections, most notably histoplasmosis and pulmonary coccidioidomycosis, can be considered in cases of lymph node enlargement (Nin et al. 2016). In the acute form of histoplasmosis, lymphadenopathy is a common finding. In the chronic form, calcifications may be seen (Nin et al. 2016).

6.2.3 Lymphoma and Lymph Node Metastases

Like TB, lymphomatous adenitis appears asymmetrical (Suwatanapongched and Gierada 2006). The enhancement pattern can be helpful in distinguishing TB from lymphoma. Commonly, lymphoma shows homogenous enhancement, which is very rarely described in lymph node TB (Tang et al. 2012) (Fig. 29a, b). The association between lymphoma and TB should be considered in endemic countries because of immunity suppression due to lymphoma, and the similarities in clinical course as well as imaging findings (Narasimhan et al. 2014). Lymph node metastases are characterized by asymmetrical involvement and low-density attenuation (Fig. 29c, d).

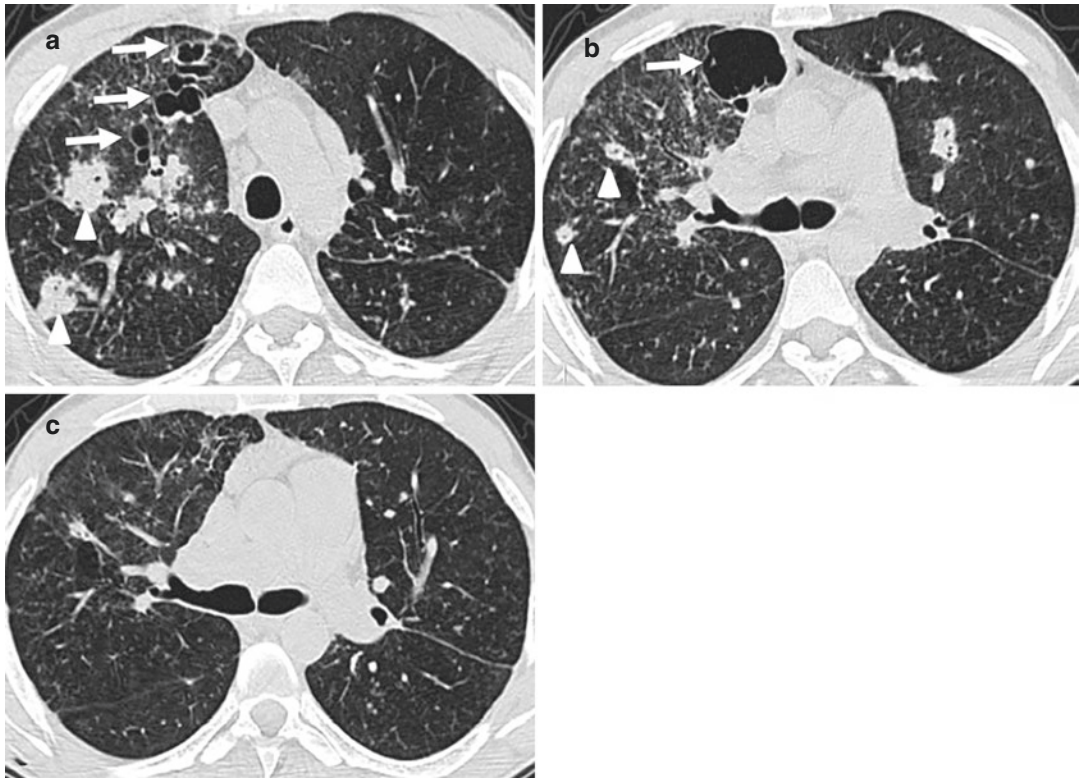

Fig. 26 Atypical form of pneumocystosis. (**a** and **b**) Axial CT images show right upper lobe cystic lesions (arrows) associated with nodules, most of which are cavitating (arrowheads). (**c**) Follow-up axial CT image shows clear regression of lesions after treatment

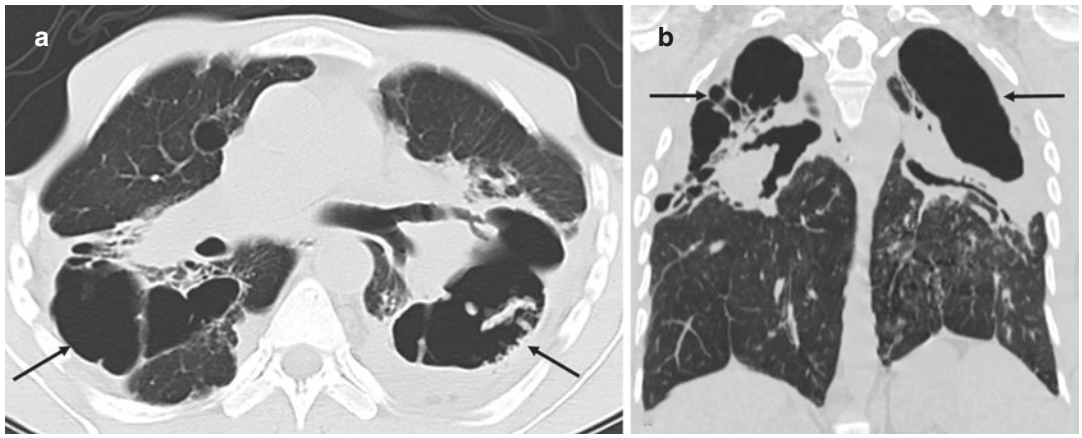

Fig. 27 Cavitating sarcoidosis mimicking tuberculosis sequelae. (**a**) Axial and (**b**) coronal CT images show bilateral cavitating consolidations of the upper lobes and the upper segments of the lower lobes with bronchiectasis (arrows)

^{18}F-FDG PET is not useful in distinguishing TB from malignant lymphadenopathy. A high focal uptake of FDG has been reported in mediastinal, supraclavicular, and intra-abdominal tuberculous lymphadenitis (Harkirat et al. 2008; Pelletier-Galarneau et al. 2017).

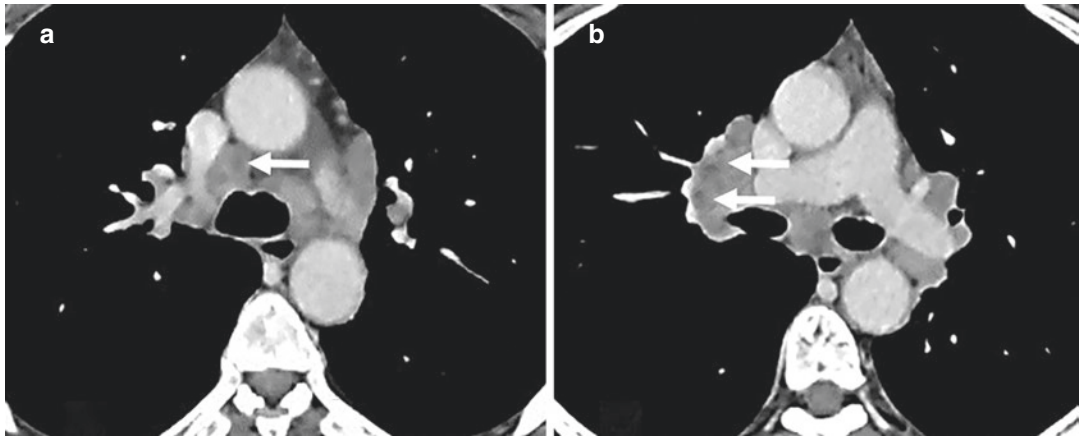

Fig. 28 Sarcoidosis mediastinal lymphadenitis. (**a** and **b**) Axial contrast-enhanced CT images show heterogeneous enhancement of enlarged mediastinal lymph nodes with the "cluster of black pearls" sign (arrows)

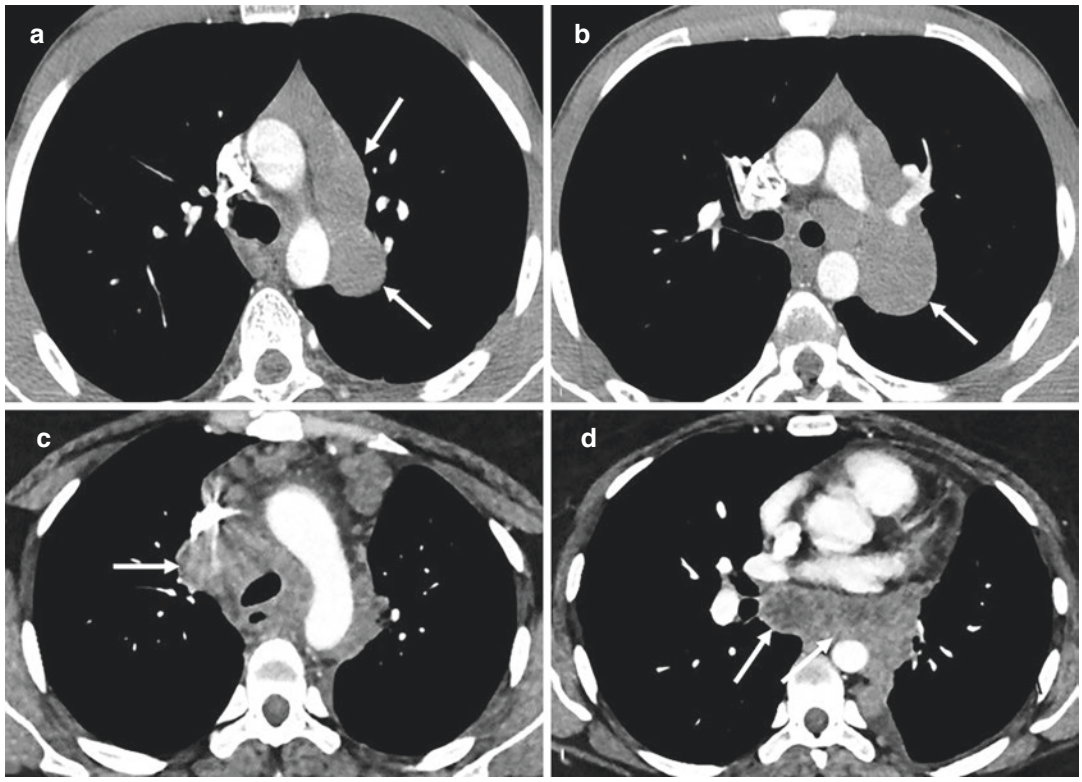

Fig. 29 Different malignant conditions mimicking mediastinal lymph node tuberculosis. Axial contrast-enhanced CT images show (**a** and **b**) Hodgkin lymphoma with asymmetrical and homogeneous enlarged mediastinal lymph nodes (arrows) and (**c** and **d**) melanoma metastases with heterogeneous and confluent enlarged lymph nodes (arrows)

6.3 Pleural Tuberculosis

Pleural TB can be confused with several differential diagnoses, mainly malignant pleural disease. In fact, it can mimic metastatic pleural disease, mesothelioma, and primary pleural lymphoma. Common imaging signs suggestive of malignant pleural disease are circumferential pleural thickening, nodular thickening (with unique or multiple nodules), pleural thickening >10 mm, and mediastinal pleural involvement (Kim et al. 2016). In some cases, distinguishing between pleural TB and malignant pleural disease is challenging, especially in cases of extensive pleural TB with mediastinal pleural involvement (Kim et al. 2014). In a recent study, the phlegmonous appearance of paracardiac fat (defined as a combination of paracardiac fat stranding and multiple fluid collections) with no lymph nodes in the ipsilateral paracardiac fat has been found to be more frequent in pleural TB than in malignant pleural effusion (Lee et al. 2020). Pleural TB may also mimic some benign pleural diseases such as non-specific pleural empyema, inflammatory disease, asbestosis, or silicosis.

7 Diagnosis Confirmation

Sputum smear and culture of AFB are considered the first step for the diagnosis of pulmonary TB. Sputum should be spontaneously produced by the patient in the morning immediately after waking up and before breakfast, i.e., on an empty stomach. Otherwise, induced expectoration should be performed. Gastric tube insertion is indicated in cases where there is difficulty in producing sputum, particularly in children and women. If sputum samples are negative, bronchial endoscopy with bronchoalveolar lavage can be performed. Sputum produced immediately after bronchoscopy should be collected for smear and culture to optimize the diagnostic yield. Samples can be obtained by tracheal or tracheobronchial aspiration in intubated patients. Specimens from associated extrapulmonary locations can also be considered. In case of mediastinal lymphadenopathy, endobronchial US-guided transbronchial needle aspiration may be helpful for diagnosis (Nachiappan et al. 2017). In patients with AIDS (with a CD4 count <100 cells/mm^3), it is also recommended to perform mycobacterial cultures of blood and urine (George et al. 2011).

There are several identification techniques available for the diagnosis of TB. Direct microscopy still plays a major role in the diagnosis and follow-up of TB. The demonstration of acid-alcohol-resistant bacteria by Ziehl–Neelsen stain (fuchsin) or by auramine is considered as the reference technique. In rapid molecular tests, the direct detection of *M. tuberculosis* by genomic amplification (PCR) is very specific, allowing diagnostic confirmation within hours. Culture-based methods (Löwenstein-Jensen) improve the results of direct examination, taking up to 8 weeks to provide results but remaining as the reference standard. The use of liquid media and automated reading systems can shorten culture detection times to between 7 and 12 days (Lewinsohn et al. 2017). Although multiple advances have been made in the diagnosis of TB, no reliable and simple test exists to definitively diagnose the disease. Pathological examination of tissue samples can be a diagnostic method by demonstration of epithelioid granulomas with caseous necrosis (Lewinsohn et al. 2017; World Health Organization 2021c).

8 Treatment

The current recommended treatment for cases of drug-susceptible TB disease is 6 months of first-line regimen including the following drugs: isoniazid (H), rifampicin (R), ethambutol (E), and pyrazinamide (Z), consisting of 2 months of initial phase with all four drugs (HRZE) followed by a 4-month maintenance phase with two drugs (HR): 2HRZE/4HR. The use of fixed dose combinations is recommended rather than separate drugs. Anti-retroviral therapy should be started during TB treatment in all people living with HIV

(World Health Organization 2017). It is feasible and safe to start anti-retroviral therapy within 2 weeks of TB treatment initiation, regardless of CD4 cell count. For people with drug-susceptible TB, treatment success rates are at least 85%. Treatment for people with rifampicin-resistant TB (RR-TB) and MDR-TB is longer and requires drugs that are more expensive and more toxic. The latest World Health Organization data show a global treatment success rate of 59% for MDR-TB (World Health Organization 2021c).

The best way to make sure that patients get their treatment is to ensure that they take the medication under direct observation. All comorbidities should be addressed, especially any psychiatric illnesses that might affect adherence to TB treatment. Efficiency monitoring is based on clinical signs, chest radiography, and bacteriology (microscopy and cultures). The bacteriology control must be done at 2 months, at the end of the fifth month to look for treatment failure, and at the sixth month (Fitzwater et al. 2010; World Health Organization 2013). A chest radiograph should be obtained in all patients at the completion of treatment to establish a new baseline. Patients responsive to pulmonary TB treatment and normal chest radiographs do not require any follow-up. Those with an abnormal chest radiograph at the end of the treatment should have a new one two months later to decide whether the patient needs further follow-up. Relapse occurs in 1–3% of cases and is defined by a positive culture 1–2 years after treatment completion (Alffenaar et al. 2018).

For LTBI, recommended options for TB-preventive treatment include a weekly dose of rifapentine and isoniazid for 3 months (3HP), a daily dose of rifampicin and isoniazid for 3 months (3HR), a daily dose of rifapentine and isoniazid for 1 month (1HP), a daily dose of rifampicin for 4 months (4R), and a daily dose of isoniazid for 6 months (6H) or longer (Migliori et al. 2018; World Health Organization 2018). The unique licensed vaccine helpful in protecting against TB disease in children is the bacille Calmette–Guérin (BCG) vaccine. No vaccine is effective in preventing TB disease in adults, either before or after exposure to TB infection (World Health Organization 2021c).

9 Disease Course, Complications, and Sequelae

With treatment, nonresistant TB disease cure is obtained in 96% of patients. Treatment failure is defined by bacillus persistence in the sputum for at least 5 months after treatment onset. Complications and sequelae may appear during or after treatment.

9.1 Imaging of Tuberculosis Complications

Sometimes, vital complications can occur, whatever the evolutionary stage of the disease. The role of CT is fundamental in diagnosis, treatment guidance, and monitoring.

9.1.1 Hemoptysis

Hemoptysis occurs more frequently in cases of TB sequelae than in active TB disease (Carette et al. 2012). The bleeding originates in most cases from the bronchial arteries. CT angiography aims to locate the bleeding in some cases and to assess its etiology and mechanism. Several lesions are responsible for hemoptysis, namely bronchiectasis, broncholithiasis, systemic hypervascularization, Rasmussen aneurysm, and aspergilloma (Carette et al. 2012; Almeida et al. 2020). Systemic hypervascularization leads to hypertrophy of systemic bronchial and nonbronchial (intercostal, diaphragmatic, internal mammary) arteries. Thoracic CT angiography, performed in the systemic arterial phase, allows clear visualization of these arteries and specification of their number, origin, and course. It is also useful to identify ectopic vessels or nonbronchial collaterals and to locate the artery of Adamkiewicz (Carette et al. 2012).

9.1.2 Aspergilloma

Aspergilloma is a mycelial tuft associated with mucus and cellular debris, developing mainly in a residual cavity. Hemoptysis is the most common clinical manifestation. Aspergilloma presents radiographically as the "air crescent sign." CT shows a hypodense, mobile, and gravity-dependent mass in a parenchymal cavity

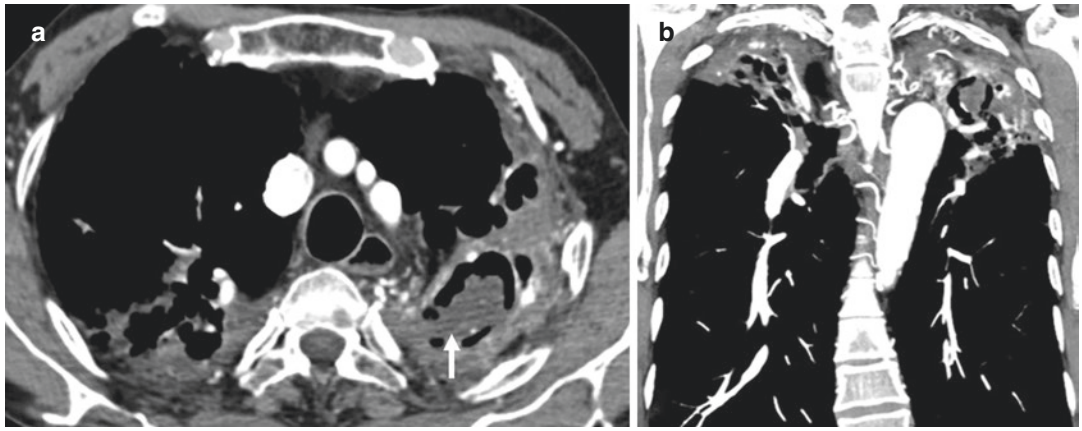

Fig. 30 Aspergilloma in a 74-year-old patient with a history of pulmonary tuberculosis. (**a**) Axial and (**b**) coronal CT angiography images show resultant lesions in the upper lobes with a left cavity containing a mycetoma (arrow in **a**). Note the surrounding systemic bronchial and nonbronchial bilateral hypervascularization, particularly around this cavity (**b**)

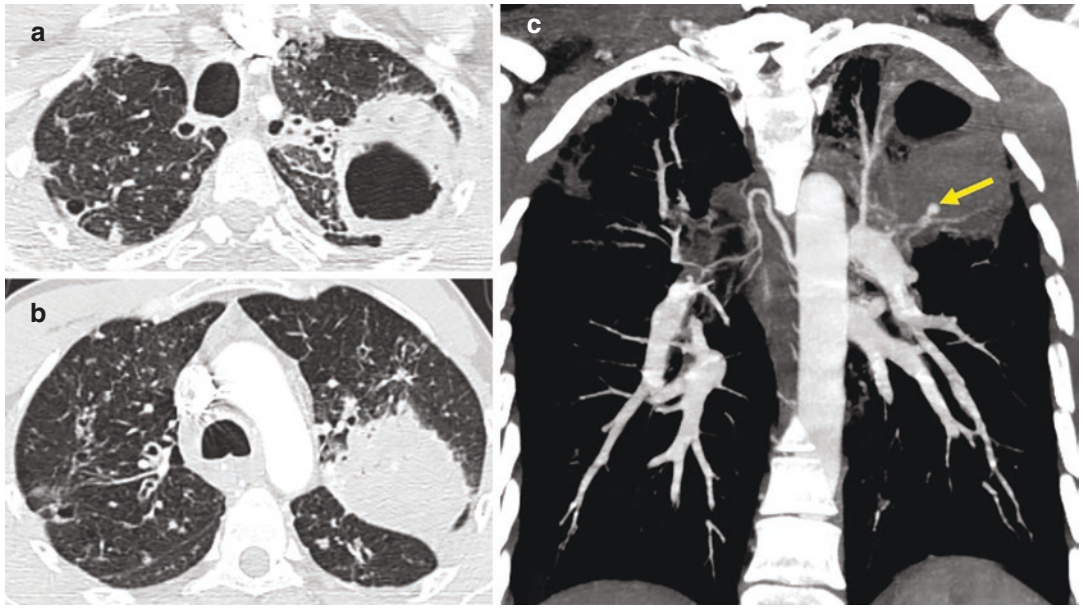

Fig. 31 Rasmussen aneurysm in a 42-year-old man. (**a** and **b**) Axial contrast-enhanced CT images show active pulmonary tuberculosis with cavitating consolidation of the left upper lobe. (**c**) Coronal MIP-reconstructed contrast-enhanced CT image shows the Rasmussen aneurysm (arrow)

(Fig. 30). Thickening of the cavity wall or of the adjacent pleura, as well as the appearance of fluid contents, may be the first sign of aspergillus development (Khan et al. 2020).

9.1.3 Rasmussen Aneurysm

Rasmussen aneurysm is a rare complication of TB due to the weakening of the wall of a pulmonary artery at the boundary of an adjacent cavity. It can be responsible for a fatal hemoptysis. Thoracic CT angiography can be used to diagnose Rasmussen aneurysm (Fig. 31) and to show signs of active bleeding such as spontaneously hyperdense contents of a cavity or extravasation of contrast agent. Pulmonary arterial vaso-occlusion is recommended for the treatment of

this complication (Carette et al. 2012; Hantous-Zannad et al. 2015).

9.1.4 Thromboembolic Complications

Pulmonary thromboembolism (PTE) or deep vein thrombosis (DVT), or both, may be observed in association with TB in active disease (Khan et al. 2020) (Fig. 17). The prevalence of DVT and PTE among patients with active TB is 2.07% and 0.95%, respectively, against 0.72% and 0.27%, respectively, among control patients without TB (Dentan et al. 2013). Hypercoagulability during TB is attributed to associated factors such as inflammatory syndrome, disorders of hemostasis (protein S deficiency, protein C and antithrombin III resistance), and chronic hypoxia (Berthe et al. 2014). Careful attention to PTE/DVT should be paid at the time of diagnosis of TB and during anti-TB therapy (Ha et al. 2019). The diagnosis of PTE and DVT is confirmed by CT angiography and Doppler US imaging, respectively.

9.1.5 Cancer Complicating Parenchymal Sequelae of Tuberculosis

The association between TB and cancer is not accidental. Chronic inflammation and the process of fibrous scarring lead to metaplasia predisposing to malignant transformation. The diagnosis is suggested by the modification of pre-existing lesions, convexity of the contours of parenchymal consolidation, and appearance or existence of a pleural extension or bone osteolysis by contiguity or by occurrence of lymphadenopathies (Hantous-Zannad et al. 2015; Khan et al. 2020).

9.1.6 Bronchopleural Fistulae

A bronchopleural fistula is a direct communication between the pleural cavity and the bronchial tree or lung parenchyma. This may develop either during the active stage of TB infection or as a complication of chronic tuberculous empyema. Multiplanar reconstructed CT images help in identifying and recognizing these fistulas (Choi et al. 2001; Khan et al. 2020).

9.1.7 Complications of Lymph Node Involvement

Complications of lymph node involvement such as broncholithiasis and rupture into the bronchus or esophagus (Fig. 32) are easily recognized on CT, which is facilitated by multiplanar reconstructions. CT can also help suggest the diagnosis of mediastinal fibrosis resulting from coalescence of granulomatous mediastinal nodes and the development of multiple foci of tuberculous granulomas in the mediastinum. Chest radiographs show few abnormalities, which contrast with obvious clinical signs such as the superior vena cava syndrome. CT angiography shows mediastinal fibrosis and its impact on mediastinal vessels and the air–tracheobronchial axis by demonstrating thrombosis of the superior vena cava, compression of the arteries and pulmonary veins, and compression of the trachea and the

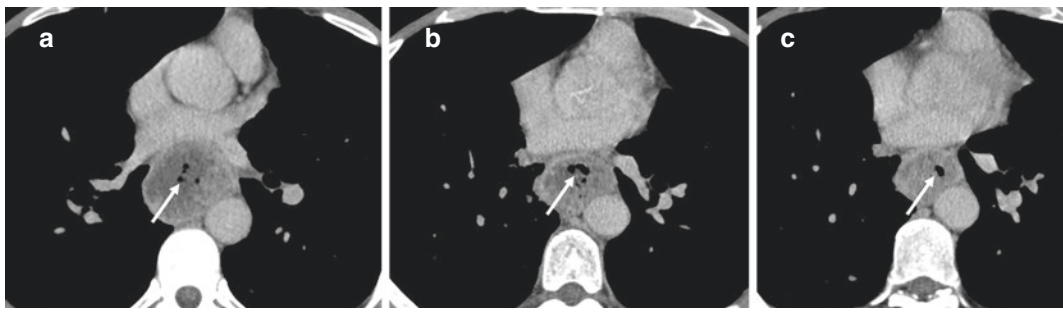

Fig. 32 Nodal-esophageal fistula in a patient with active tuberculosis who presented with dysphagia. (**a–c**) Axial contrast-enhanced CT images show necrotic enlarged mediastinal lymph nodes communicating with the esophagus lumen and containing air (arrows)

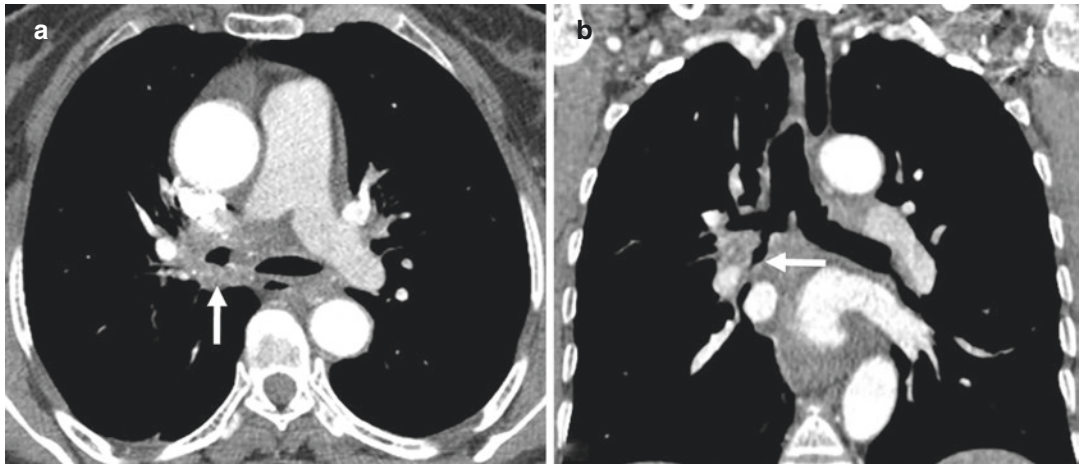

Fig. 33 Mediastinal fibrosis confirmed by surgical biopsy in a 65-year-old woman who was previously treated for pulmonary tuberculosis. (**a**) Axial and (**b**) coronal contrast-enhanced CT images show a partially calcified mediastino-pulmonary mass sheathing the right bronchial tree (arrow in **a**) with parietal irregularity and lumen narrowing (arrow in **b**)

large bronchial trunks (Fig. 33). Associated pulmonary sequelae evoke the tuberculous origin of mediastinal fibrosis (Khan et al. 2020).

9.2 Interventional Radiology Treatment of Tuberculosis Complications

9.2.1 Hemoptysis

TB results in chronic inflammation of the lungs, which leads to recruitment of systemic vessels, either bronchial or nonbronchial, in the inflamed regions. These vessels may rupture, resulting in hemoptysis that may threaten the patient's life. Patients with hemoptysis due to TB may be treated by embolization. TB represents 50% of causes of hemoptysis in patients undergoing bronchial arterial embolization. This technique results in immediate clinical course improvement in 86–96% of patients (Shin et al. 2011; Pei et al. 2014). Recurrence of hemoptysis after embolization is observed in 30.6–50% of patients, particularly in those with active TB, mycetoma, and incomplete embolization. The risk of recurrence increases with time. In fact, cumulative recurrence-free rate shifts from 98.5% at 1 month to 65.7% at 48 months (Shin et al. 2011; Peng et al. 2019). Endovascular treatment is also a common procedure for the management of Rasmussen aneurysm. Embolization should be done by systemic and pulmonary arterial approaches because of the development of pulmonary-to-systemic arterial anastomoses produced by chronic inflammation (Tanahashi et al. 2016; Giraldo-Montoya et al. 2018).

9.2.2 Intracavitary Treatment of Aspergillomas

Aspergillomas developing in tuberculous cavities are complex and may cause life-threatening hemoptysis. The gold standard treatment of aspergillomas remains to be surgical excision. However, patients with contraindications to surgery may undergo nonsurgical alternatives such as systemic administration of antifungal medication, transbronchial removal of aspergilloma, and endobronchial and intracavitary instillation of antifungal medication. The latter is performed under CT guidance via catheter placement in the cavity containing the aspergilloma (Lang et al. 2020). The aim of this technique is to completely fill the cavity, therefore creating an anaerobic environment that is inappropriate for aspergillus development (Giron et al. 1998) (Fig. 34). Technical success is achieved in 95–100% of cases, with clinical cessation of hemoptysis in 85–100% of patients (Giron et al. 1998; Kravitz

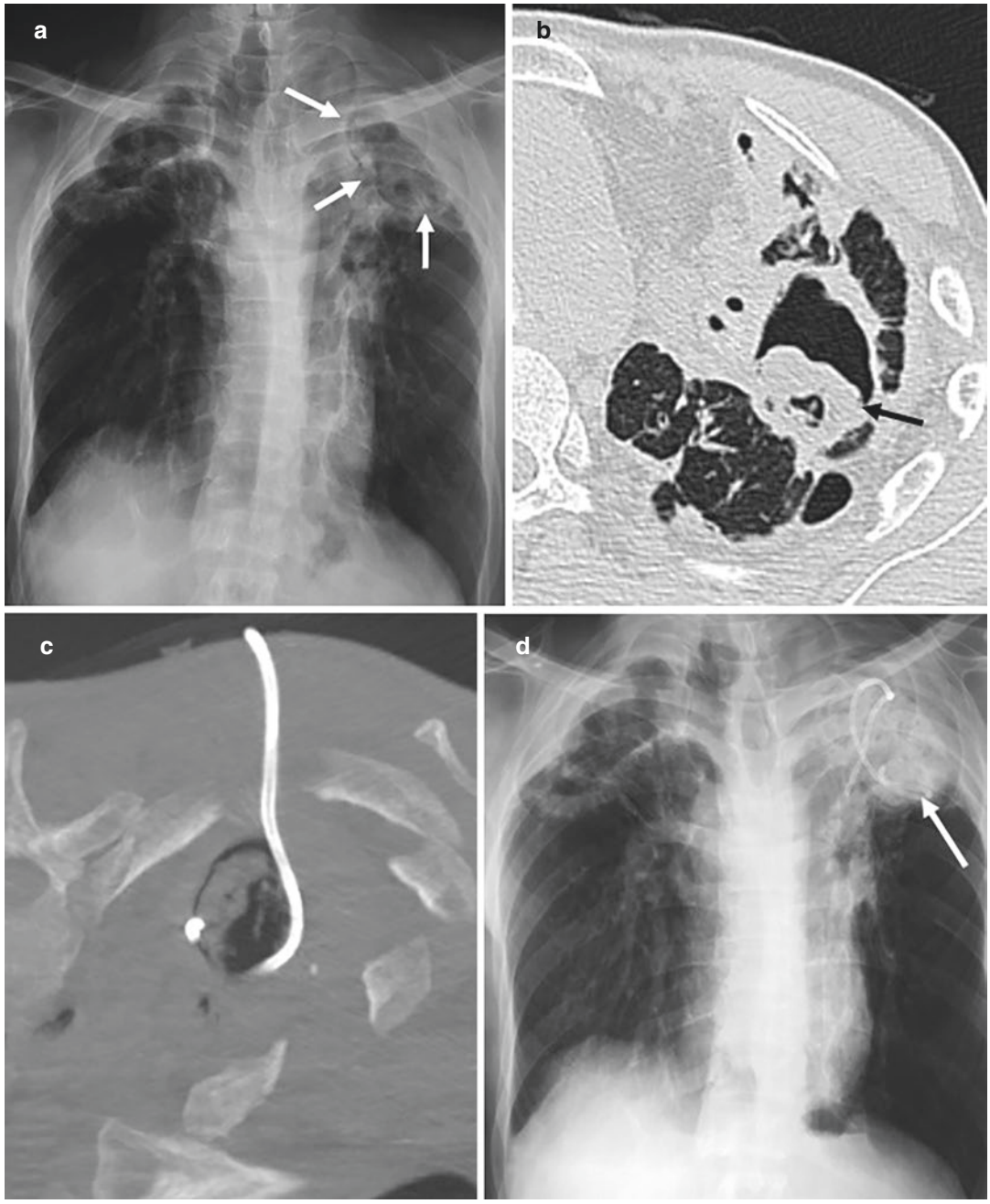

Fig. 34 Intracavitary treatment of an aspergilloma in a 58-year-old man who presented with recurrent tuberculosis. (**a**) PA chest radiograph shows a cavitating lesion with an internal mass suspicious of aspergilloma (white arrows). (**b**) Axial CT image shows the aspergilloma (black arrow) more precisely. The diagnosis was confirmed by serology. The patient had a functional contraindication to surgery. (**c**) Axial CT image and (**d**) PA chest radiograph show a pigtail catheter introduced into the cavity, which was filled by contrast material and amphotericin B (white arrow)

et al. 2013). Disappearance of the fungal ball occurs in 72.5% of cases (Giron et al. 1998).

9.3 Imaging of Post-tuberculosis Sequelae

Post-TB sequelae are due to the anatomical and pathophysiological changes in the chest following TB infection, even after completion of treatment and achievement of bacteriological cure. They depend on the interaction between the virulence of tuberculous bacilli and the host's immune response, duration of the disease, and delay in diagnosis. Various sequelae lesions can persist in both primary and post-primary TB and can be the cause of complications. These sequelae can be categorized into parenchymal lesions, airway disease, pleural and chest wall lesions, mediastinal lesions, and vascular abnormalities (Khan et al. 2020). CT evaluation at the end of the treatment, possibly repeated, with search for tuberculous bacilli may be necessary before concluding that there is inactive TB.

9.3.1 Parenchymal Lesions

Tuberculomas can be observed after primary or post-primary TB and are often located in the upper lobes. They appear as single or multiple solid nodules, usually with smooth margins, measuring between a few mm to 3 cm in size (Fig. 35). They may contain calcifications, which may be nodular or diffuse, are found in 20–30% of cases, and are better visualized on CT (Hantous-Zannad et al. 2015). Tuberculomas can manifest as an eccentric cavity or a hypodense lesion with peripheral contrast enhancement. Any change in the CT appearance, such as an increase in volume and the appearance of surrounding bronchiolar or acinar micronodules, should suggest TB reactivation (Carette et al. 2012; Hantous-Zannad et al. 2015; Khan et al. 2020).

With anti-TB treatment, the cavitary lesions retract, their walls become thinner, and the surrounding lesions tend to disappear. These cavities may persist and usually have regular walls, usually of less than 1 cm and even 1 mm thickness, making them difficult to distinguish on CT from an emphysematous bulla, cystic bronchiectasis, air cyst, or pneumatocele (Hantous-Zannad et al. 2015) (Fig. 36). They can be complicated by secondary pyogenic infection or aspergillus development or be the site of TB reactivation (Khan et al. 2020).

The process of healing tuberculous parenchymal lesions may lead to fibrous bands and retractile stellar or linear scarring. These fibrous lesions may be associated with traction bronchiectasis

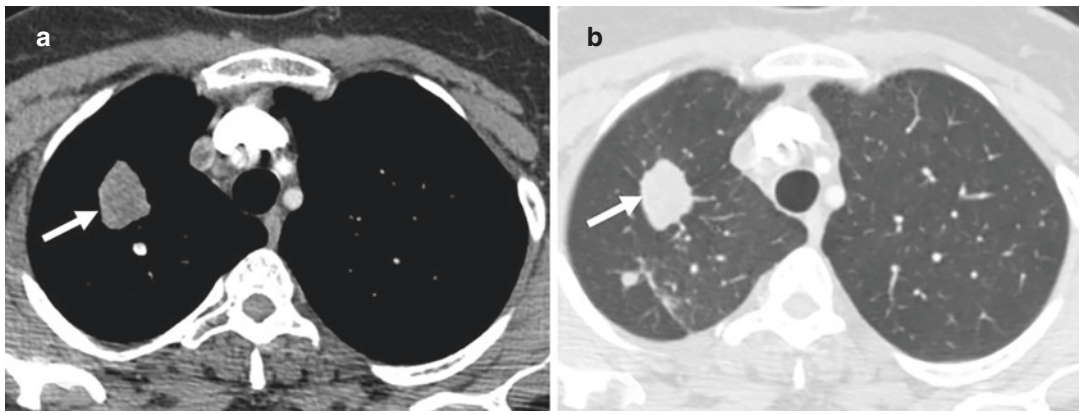

Fig. 35 Tuberculoma in a 42-year-old woman. Axial contrast-enhanced CT images taken in (**a**) soft tissue and (**b**) lung window settings show a tuberculoma of the right upper lobe (arrows)

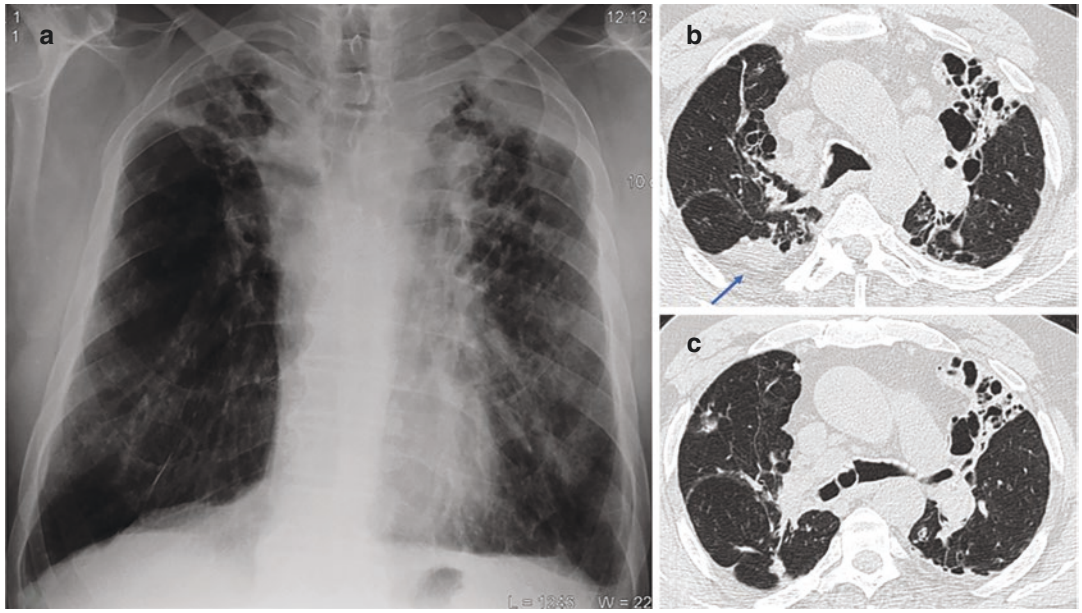

Fig. 36 Tuberculosis sequelae. (**a**) PA chest radiograph shows retractile bilateral apical opacities with bilateral hilar elevation. (**b** and **c**) Axial HRCT images show destruction of the upper lobes with cavities and bronchiectasis. Note the extrapleural fat hypertrophy (arrow)

and paracicatricial emphysema, which has a characteristic appearance on CT (Hantous-Zannad et al. 2015). Extensive parenchymal destruction may appear as atelectasis of an entire lobe or entire lung. It may be the site of bronchiectasis and cavitary images associated with retraction of the mediastinum; enlargement of the trachea, the remaining lung, and the esophagus; and retraction of the parietal pleura with hypertrophy of extrapleural fat (Fig. 36). Compensatory expansion of the healthy lung as well as bronchovascular and scissural distortion are observed. Lobar or segmental atelectasis may also occur secondary to proximal bronchial obstruction (Pathak et al. 2016).

9.3.2 Tracheobronchial Stenosis

Tracheobronchial stenosis may result from fibrous parietal involvement caused by bronchial TB. This appears on CT as regular circumferential wall thickening with narrowing of the bronchial lumen. The stenosis may be secondary to compression of the bronchus by a residual lymph node. Erosion of the bronchial wall by a calcified compressive lymph node causes broncholithiasis (Hantous-Zannad et al. 2015; Pathak et al. 2016; Khan et al. 2020) (Fig. 37). CT is ideal to aid diagnose and assess the impact of bronchial obstruction downstream, i.e., obstructive pulmonary disease, atelectasis, expiratory trapping, and bronchiectasis. Constrictive bronchiolitis associated with fibrous involvement of the bronchioles leads to air trapping and emphysematous lesions. CT reveals areas of hypoattenuation reflecting air trapping and pulmonary arterial vasoconstriction, which is accentuated on expiration (Hantous-Zannad et al. 2015).

9.3.3 Mediastinal Lesions

Residual lymph nodes may persist after tuberculous lymph node involvement, even when properly treated. Caseous lesions are gradually replaced by fibrous tissue and calcification. The Ranke complex is a sequel of primary TB, comprising a Ghon lesion that has undergone calcification and an ipsilateral calcified mediastinal

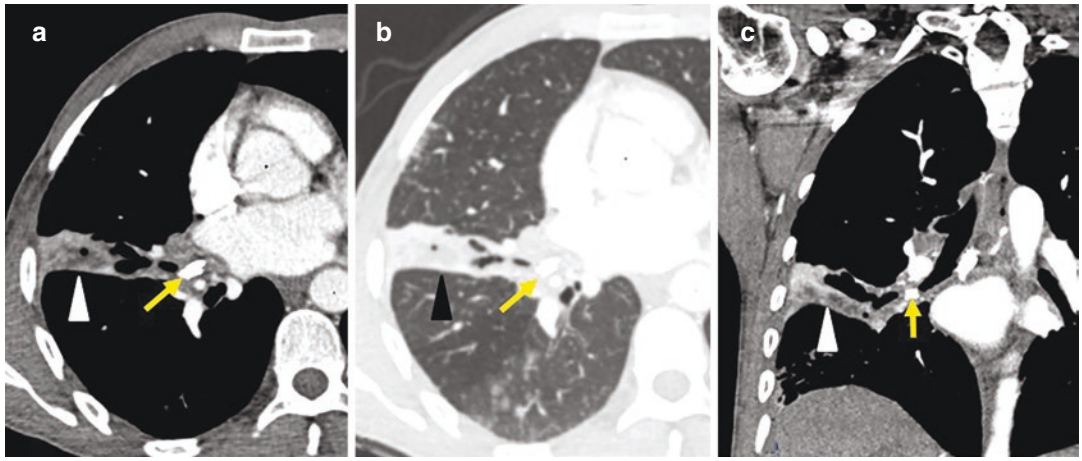

Fig. 37 Broncholithiasis in a 45-year-old patient with a history of pulmonary tuberculosis who presented with recurrent hemoptysis. Axial contrast-enhanced CT images taken in (**a**) soft tissue and (**b**) lung window settings and (**c**) coronal contrast-enhanced CT images taken in the soft tissue setting show broncholithiasis in the middle lobe bronchus (yellow arrows) with collapse of the middle lobe containing bronchiectasis (arrowheads)

node (Choi et al. 2001; Carette et al. 2012; Khan et al. 2020). Fibrous or calcified thickening of the pericardium may complicate pericardial effusion, resulting in constrictive pericarditis in about 10% of patients. CT shows pericardial thickening of more than 3 mm and can identify calcifications (Khan et al. 2020). MRI enables studying the effects of constrictive pericarditis on right cardiac function (Hantous-Zannad et al. 2015).

9.3.4 Pleural Lesions

Fibrothorax refers to an extensive and regular thickening of the pleura, which can be partially or totally calcified. It presents as diffuse pleural thickening but without effusion, suggesting inactivity, and is associated with volume loss of the ipsilateral lung. Patients with diffuse pleural thickening may develop restrictive lung disease (Khan et al. 2020). Empyema may persist and cannot be confirmed to be inactive on imaging. It may be complicated by empyema necessitans, bronchopleural fistula, and pneumothorax. More rarely, they can form the basis of neoplastic degeneration (Choi et al. 2001). Chyliform effusion is also a known post-TB pleural complication. CT findings include air-fluid, fat-fluid, or fat-calcium levels in the pleural cavity (Khan et al. 2020). A pleural fibrinous body is a characteristic but non-specific lesion, producing the appearance of a pseudopleural mass. Its diagnosis is suggested on CT by the presence of a hyperdense lesion and absence of enhancement after contrast administration (Choi et al. 2001; Khan et al. 2020).

9.3.5 Chest Wall Sequelae

Osteitis, osteoarthritis, and tuberculous spondylodiscitis can leave sequelae in the form of bone or cartilage destruction and spinal deformity with dorsal kyphosis. Soft tissue calcifications can also be seen.

10 Conclusion

The radiological manifestations of thoracic TB are variable and depend on factors related to the host. Chest radiography remains the first-line examination showing a characteristic appearance in most cases. CT is an effective diagnostic method when chest radiographs are normal or inconclusive and provides valuable information for the diagnosis and management of TB. In patients with positive findings on TST or IGRA,

imaging and especially CT play an important role in risk stratification by helping to distinguish latent infection, previous inactive disease, and active disease. In addition to the diagnosis of TB, HRCT is useful in determining disease activity. Its role is essential in the management of complications dominated by hemoptysis due to its severity and in the evaluation of sequelae. MRI may be performed to evaluate some complications.

References

Agrawal G (2011) Miliary nodules due to secondary pulmonary hemosiderosis in rheumatic heart disease. World J Radiol 3:51–54

Alffenaar JWC, Akkerman OW, Bothamley G (2018) Monitoring during and after treatment. Eur Respir Monogr 82:308–325

Almeida J, Leal C, Figueiredo L (2020) Evaluation of the bronchial arteries: normal findings, hypertrophy and embolization in patients with hemoptysis. Insights Imaging 11:70. https://doi.org/10.1186/s13244-020-00877-4

Alsowey AM, Amin MI, Said AM (2017) The predictive value of multidetector high resolution computed tomography in evaluation of suspected sputum smear negative active pulmonary tuberculosis in Egyptian Zagazig University Hospital patients. Pol J Radiol 82:808–816

American Thoracic Society (1990) Diagnostic standards and classification of tuberculosis. Am Rev Respir Dis 142:725–735

Andréjak C, Lescure FX, Schmit JL, Jounieaux V (2011) Diagnostic et traitement des mycobactérioses atypiques d'expression respiratoire. Rev Mal Respir 28:1293–309

Andreu J, Cáceres J, Pallisa E, Martinez-Rodriguez M (2005) Manifestations radiologiques de la tuberculose pulmonaire. EMC-Radiologie 2:121–132

Ankrah AO, van der Werf TS, de Vries EFJ et al (2016) PET/CT imaging of mycobacterium tuberculosis infection. Clin Transl Imaging 4:131–144

Barreira-Silva P, Torrado E, Nebenzahl-Guimaraes H et al (2018) Aetiopathogenesis, immunology and microbiology tuberculosis. Eur Respir Monogr 82:62–82

Barry CE, Boshoff HI, Dartois V et al (2009) The spectrum of latent tuberculosis: rethinking the biology and intervention strategies. Nat Rev Microbiol 7:845–855

Ben Miled-M'Rad K, Kara M, Hantous-Zannad S et al (2002) Tuberculose des bases pulmonaires. Rev Mal Respir 19:161–165

Berthe A, Diop MM, Touré PS et al (2014) Tuberculose et maladie thromboembolique, une association redoutable non fortuite. Revue Africaine de Médecine Interne 1:38–40

Bhatt M, Kant S, Bhaskar R (2012) Pulmonary tuberculosis as differential diagnosis of lung cancer. South Asian J Cancer 1:36–42

Bigio J, Kohli M, Klinton JS et al (2021) Diagnostic accuracy of point-of-care ultrasound for pulmonary tuberculosis: a systematic review. PLoS One 16(5):e0251236

Bomanji JB, Gupta N, Gulati P, Das CJ (2015) Imaging in tuberculosis. Cold Spring Harb Perspect Med 5(6):a017814

Bouslama K, Bakir L, Ben M'Rad S et al (1998) Tuberculose de la paroi thoracique: à propos d'un cas et revue de la littérature. Med Mal Infect 28: 666–667

Burrill J, Williams CJ, Bain G et al (2007) Tuberculosis: a radiologic review. Radiographics 27:1255–1273

Cadena AM, Fortune SM, Flynn JL (2017) Heterogeneity in tuberculosis. Nat Rev Immunol 17:691–702

Cadiñanos Loidi J, Abad Pérez D, de Miguel BR (2014) Endobronchial tuberculosis simulating lung cancer. Arch Bronconeumol 50:126–127

Caliskan T, Ozkisa T, Aribal S et al (2014) High resolution computed tomography findings in smear-negative pulmonary tuberculosis patients according to their culture status. J Thorac Dis 6:706–712

Campos LC, Rocha MVV, Willers DMC, Silva DR (2016) Characteristics of patients with smear-negative pulmonary tuberculosis (TB) in a region with high TB and HIV prevalence. PLoS One 11(1):e0147933

Carette MF, Mizouni L, El Amri A et al (2012) Imagerie typique et atypique de la tuberculose bronchopulmonaire. La Lettre du Pneumologue 15:32–43

Chaddha U, English R, Daniels J et al (2017) A 58-year-old man with fatigue, weight loss, and diffuse miliary pulmonary opacities. Chest 151:e131–e134

Chelli Bouaziz M, Jelassi H, Chaabane S et al (2009) Imaging of chest wall infections. Skeletal Radiol 38:1127–1135

Chen J, Byanju S, Zhang H et al (2018a) CT-guided percutaneous core needle biopsy of pulmonary tuberculosis: diagnostic accuracy and complications. Radiol Infect Dis 5:69–75

Chen Y, Yang Y, Chen L, Fan M (2018b) Large pulmonary solitary mass caused by mycobacterium tuberculosis mimicking a malignant tumor in a child. Radiol Infect Dis 5:131–134

Cho Y, Lee J, Vassiliou C, von Borstel D (2019) TB or not TB: differential diagnosis and imaging findings of pulmonary cavities. J Am Osteopath Coll Radiol 8:18–27

Choi JA, Hong KT, Oh YW et al (2001) CT manifestations of late sequelae in patients with tuberculous pleuritis. AJR Am J Roentgenol 176:441–445

Chung HS, Lee JH (2000) Bronchoscopic assessment of the evolution of endobronchial tuberculosis. Chest 117:385–392

Criado E, Sánchez M, Ramírez J et al (2010) Pulmonary sarcoidosis: typical and atypical manifestations at

high-resolution CT with pathologic correlation. Radiographics 30:1567–1586
Delacoste J, Dournes G, Dunet V et al (2019) Ultrashort echo time imaging of the lungs under high-frequency noninvasive ventilation: a new approach to lung imaging. J Magn Reson Imaging 50:1789–1797
Dentan C, Epaulard O, Seynaeve D et al (2013) Active tuberculosis and venous thromboembolism: association according to international classification of diseases, ninth revision hospital discharge diagnosis codes. Clin Infect Dis 58:495–501
Di Gennaro F, Pisani L, Veronese N et al (2018) Potential diagnostic properties of chest ultrasound in thoracic tuberculosis—a systematic review. Int J Environ Res Public Health 15(10):2235
Dobler CC, Cheung K, Nguyen J, Martin A (2017) Risk of tuberculosis in patients with solid cancers and haematological malignancies: a systematic review and meta-analysis. Eur Respir J 50(2):1700157
Drain PK, Bajema KL, Dowdy D et al (2018) Incipient and subclinical tuberculosis: a clinical review of early stages and progression of infection. Clin Microbiol Rev 31(4):e00021–e00018
Epstein DM, Kline LR, Albelda SM, Miller WT (1987) Tuberculous pleural effusions. Chest 91: 106–109
Fahim A, Khan MN (2011) An unusual cause of miliary radiographic pattern. BMJ Case Rep 2011:bcr1020115060
Fentress M, Ugarte-Gil C, Cervantes M et al (2020) Lung ultrasound findings compared with chest X-ray findings in known pulmonary tuberculosis patients: a cross-sectional study in Lima, Peru. Am J Trop Med Hyg 103:1827–1833
Fitzwater SP, Caviedes L, Gilman RH et al (2010) Prolonged infectiousness of tuberculosis patients in a directly observed therapy short-course program with standardized therapy. Clin Infect Dis 51:371–378
Franquet T (2011) Imaging of pulmonary viral pneumonia. Radiology 260:18–39
George PM, Mehta M, Dhariwal J et al (2011) Post-bronchoscopy sputum: improving the diagnostic yield in smear negative pulmonary TB. Respir Med 105:1726–1731
Giordani MT, Heller T (2019) Role of ultrasound in the diagnosis of tuberculosis. Eur J Intern Med 66:27–28
Giraldo-Montoya ÁM, Rodríguez-Morales AJ, Hernández-Hurtado JD et al (2018) Rasmussen aneurysm: a rare but not gone complication of tuberculosis. Int J Infect Dis 69:8–10
Giron J, Poey C, Fajadet P et al (1998) CT-guided percutaneous treatment of inoperable pulmonary aspergillomas: a study of 40 cases. Eur J Radiol 28: 235–242
Goo JM, Im JG, Do KH et al (2000) Pulmonary tuberculoma evaluated by means of FDG PET: findings in 10 cases. Radiology 216:117–121
Guedes G (2018) Tuberculosis and immunosuppression. J Microbiol Exp 6:145–146
Ha H, Kim KH, Park JH et al (2019) Thromboembolism in mycobacterium tuberculosis infection: analysis and literature review. Infect Chemother 51:142–149
Halawar RS, Sudhindraswamy VB (2019) Radiography and HRCT in lower lobe tuberculosis. Radiol Infect Dis 6:142–146
Hammen I (2015) Tuberculosis mimicking lung cancer. Respir Med Case Rep 16:45–47
Hantous-Zannad S, Zidi A, Néji H et al (2015) Apport de l'imagerie dans la tuberculose thoracique. Rev Pneumol Clin 71:93–109
Hara T, Kosaka N, Suzuki T et al (2003) Uptake rates of 18F-Fluorodeoxyglucose and 11C-choline in lung cancer and pulmonary tuberculosis. Chest 124:893–901
Harkirat S, Anand S, Indrajit I, Dash A (2008) Pictorial essay: PET/CT in tuberculosis. Indian J Radiol Imaging 18:141–147
He W, Chen BD, Lv Y et al (2017) Use of low-dose computed tomography to assess pulmonary tuberculosis among healthcare workers in a tuberculosis hospital. Infect Dis Poverty 6(1):68
Heuvelings CC, Bélard S, Andronikou S et al (2019) Chest ultrasound compared to chest X-ray for pediatric pulmonary tuberculosis. Pediatr Pulmonol 54:1914–1920
Huerga H, Varaine F, Okwaro E et al (2012) Performance of the 2007 WHO algorithm to diagnose smear-negative pulmonary tuberculosis in a HIV prevalent setting. PLoS One 7(12):e51336
Jeong YJ, Lee KS (2008) Pulmonary tuberculosis: up-to-date imaging and management. AJR Am J Roentgenol 191:834–844
Kabiri EH, Alassane EA, Kamdem MK et al (2020) Tuberculous cold abscess of the chest wall: a clinical and surgical experience. Report of 16 cases (case series). Ann Med Surg 51:54–58
Kakamad FH, Hassan MN, Salih AM et al (2020) Primary chest wall tuberculosis mimicking gynecomastia: a case report. Int J Surg Case Rep 75:473–475
Kaur H (2021) Pulmonary tuberculosis mimicking lung cancer and metastasis radiologically—a case report. J Clin Med Res 3(1):1–4
Khan R, Malik NI, Razaque A (2020) Imaging of pulmonary post-tuberculosis sequelae. Pak J Med Sci 36:S75–S82
Kim JS, Shim SS, Kim Y et al (2014) Chest CT findings of pleural tuberculosis: differential diagnosis of pleural tuberculosis and malignant pleural dissemination. Acta Radiol 55:1063–1068
Kim YK, Kim JS, Lee KW et al (2016) Multidetector CT findings and differential diagnoses of malignant pleural mesothelioma and metastatic pleural diseases in Korea. Korean J Radiol 17:545–553
Kim JH, Kim MJ, Ham SY (2019) Clinical characteristics and chest computed tomography findings of smear-positive and smear-negative pulmonary tuberculosis in hospitalized adult patients. Medicine 98(34):e16921
Koh WJ, Jeong YJ, Kwon OJ et al (2010) Chest radiographic findings in primary pulmonary tuberculosis: observations from high school outbreaks. Korean J Radiol 11:612–617

Koyama T, Ueda H, Togashi K et al (2004) Radiologic manifestations of sarcoidosis in various organs. Radiographics 24:87–104

Kravitz JN, Berry MW, Schabel SI, Judson MA (2013) A modern series of percutaneous intracavitary instillation of amphotericin B for the treatment of severe hemoptysis from pulmonary aspergilloma. Chest 143:1414–1421

Lang M, Lang AL, Chauhan N, Gill A (2020) Non-surgical treatment options for pulmonary aspergilloma. Respir Med 164:105903

Lee HM, Shin JW, Kim JY et al (2010) HRCT and whole-blood interferon-γ assay for the rapid diagnosis of smear-negative pulmonary tuberculosis. Respiration 79:454–460

Lee D, Son MJ, Yoo SM et al (2020) Phlegmonous appearance in the ipsilateral paracardiac fat without paracardiac lymph node enlargement on chest CT favors the diagnosis of pleural tuberculosis over malignant pleural effusion. Diagnostics (Basel) 10(12):1041

Lee HN, Kim JI, Kim YH (2021) Clinical and CT characteristics of Xpert MTB/RIF-negative pulmonary tuberculosis. PLoS One 16(5):e0250616

Lewinsohn DM, Leonard MK, LoBue PA et al (2017) Official American Thoracic Society/Infectious Diseases Society of America/Centers for Disease Control and Prevention clinical practice guidelines: diagnosis of tuberculosis in adults and children. Clin Infect Dis 64:1–33

Li XX, Jiang SW, Zhang H et al (2013) Clinical and radiographic predictors in diagnosing sputum smear-negative pulmonary tuberculosis in HIV-negative patients: a cross-sectional study in China. Chin Med J (Engl) 126:3662–3667

López-López JP, Posada-Martínez EL, Saldarriaga C et al (2021) Tuberculosis and the heart. J Am Heart Assoc 10(7):e019435

Matsuoka S, Uchiyama K, Shima H et al (2004) Relationship between CT findings of pulmonary tuberculosis and the number of acid-fast bacilli on sputum smears. Clin Imaging 28:119–123

Mazza-Stalder J, Nicod L, Janssens JP (2012) La tuberculose extrapulmonaire. Rev Mal Respir 29: 566–578

Migliori GB, Sotgiu G, Rosales-Klintz S et al (2018) ERS/ECDC statement: European Union standards for tuberculosis care, 2017 update. Eur Respir J 51:1702678

Montuori M, Casella F, Casazza G et al (2019) Lung ultrasonography in pulmonary tuberculosis: a pilot study on diagnostic accuracy in a high-risk population. Eur J Intern Med 66:29–34

Mordant P, Badia A, Le Pimpec-Barthes F, Riquet M (2012) Chirurgie pulmonaire dans la tuberculose et les mycobactérioses atypiques. Rev Pneumol Clin 68:77–83

Mutyaba AK, Ntsekhe M (2017) Tuberculosis and the heart. Cardiol Clin 35:135–144

Nachiappan AC, Rahbar K, Shi X et al (2017) Pulmonary tuberculosis: role of radiology in diagnosis and management. Radiographics 37:52–72

Narasimhan R, Reddy R, Mathew M, Parameswaran A (2014) A case of concomitant Hodgkin's lymphoma with tuberculosis. Lung India 31:59–62

Nèji H, Affes M, Attia M et al (2017) Atypical pleuropulmonary tuberculosis mimicking a malignant disease. J Thorac Oncol 12:e145–e147

Nin CS, de Souza VVS, do Amaral RH et al (2016) Thoracic lymphadenopathy in benign diseases: a state of the art review. Respir Med 112:10–17

Pai M, Behr MA, Dowdy D et al (2016) Tuberculosis. Nat Rev Dis Primers 2:16076

Park JH, Choe J, Bae M et al (2019) Clinical characteristics and radiologic features of immunocompromised patients with pauci-bacillary pulmonary tuberculosis receiving delayed diagnosis and treatment. Open Forum Infect Dis 6(2):ofz002

Pathak V, Shepherd RW, Shojaee S (2016) Tracheobronchial tuberculosis. J Thorac Dis 8:3818–3825

Pei R, Zhou Y, Wang G et al (2014) Outcomes of bronchial artery embolization for life-threatening hemoptysis secondary to tuberculosis. PLoS One 9(12):e115956

Pelletier-Galarneau M, Martineau P, Zuckier LS et al (2017) 18 F-FDG-PET/CT imaging of thoracic and extrathoracic tuberculosis in children. Semin Nucl Med 47:304–318

Peng Y, Zhu Y, Ao G et al (2019) Effect of bronchial artery embolisation on the management of tuberculosis-related haemoptysis. Int J Tuberc Lung Dis 23:1269–1276

Rajagopala S, Sankari S, Kancherla R et al (2020) Miliary sarcoidosis: does it exist? A case series and systematic review of literature. Sarcoidosis Vasc Diffuse Lung Dis 37:53–65

Rossi SE, Franquet T, Volpacchio M et al (2005) Tree-in-bud pattern at thin-section CT of the lungs: radiologic-pathologic overview. Radiographics 25:789–801

Shaarrawy H, Zeidan M, Nasr A, Nouh M (2013) Assessment of the role of high resolution computed tomography in the diagnosis of suspected sputum smear negative active pulmonary TB. Egypt J Chest Dis Tuberc 62:263–268

Sharma M, Sandhu MS, Gorsi U et al (2015) Role of digital tomosynthesis and dual energy subtraction digital radiography in detection of parenchymal lesions in active pulmonary tuberculosis. Eur J Radiol 84:1820–1827

Shaw JA, Irusen EM, Diacon AH, Koegelenberg CF (2018) Pleural tuberculosis: a concise clinical review. Clin Respir J 12:1779–1786

Shen BJ, Lin HH (2021) Time-dependent association between cancer and risk of tuberculosis: a population-based cohort study. Int J Infect Dis 108:340–346

Shen BJ, Lo WC, Lin HH (2021) Global burden of tuberculosis attributable to cancer in 2019: global, regional, and national estimates. J Microbiol Immunol Infect 8:S1684–1182(21)00048–7

Shin BS, Jeon GS, Lee SA, Park MH (2011) Bronchial artery embolisation for the management of haemoptysis in patients with pulmonary tuberculosis. Int J Tuberc Lung Dis 15:1093–1098

Shu CC, Liao KM, Chen YC et al (2019) The burdens of tuberculosis on patients with malignancy: incidence, mortality and relapse. Sci Rep 9(1):11901

Singla R, Osman MM, Khan N et al (2003) Factors predicting persistent sputum smear positivity among pulmonary tuberculosis patients 2 months after treatment. Int J Tuberc Lung Dis 7:58–64

Skoura E, Zumla A, Bomanji J (2015) Imaging in tuberculosis. Int J Infect Dis 32:87–93

Suwatanapongched T, Gierada DS (2006) CT of thoracic lymph nodes. Part II: diseases and pitfalls. Br J Radiol 79:999–1000

Tanahashi Y, Kondo H, Osawa M et al (2016) Transcatheter embolization of a Rasmussen aneurysm via pulmonary artery with n-butyl cyanoacrylate and iodized oil mixture injection with balloon occlusion. J Vasc Surg Cases Innov Tech 2:161–164

Tang SS, Yang ZG, Deng W et al (2012) Differentiation between tuberculosis and lymphoma in mediastinal lymph nodes: evaluation with contrast-enhanced MDCT. Clin Radiol 67:877–883

Udwadia ZF, Sen T (2010) Pleural tuberculosis: an update. Curr Opin Pulm Med 16:399–406

Venkata Ramanan R, Pudhiavan A, Venkataramanan A (2017) The "cluster of black pearls" sign of sarcoid lymphadenopathy: a new sign on thin-section contrast-enhanced multidetector CT. Clin Radiol 72:729–736

Vento S, Lanzafame M (2011) Tuberculosis and cancer: a complex and dangerous liaison. Lancet Oncol 12:520–522

Walusimbi S, Bwanga F, De Costa A et al (2013) Meta-analysis to compare the accuracy of GeneXpert, MODS and the WHO 2007 algorithm for diagnosis of smear-negative pulmonary tuberculosis. BMC Infect Dis 13(1):507

World Health Organization (2007) Improving the diagnosis and treatment of smear-negative pulmonary and extrapulmonary tuberculosis among adults and adolescents: recommendations for HIV-prevalent and resource-constrained settings/stop TB department; department of HIV/AIDS. World Health Organization, Geneva. https://apps.who.int/iris/handle/10665/69463

World Health Organization (2013) Definitions and reporting framework for Tuberculosis-2013 revision: updated December 2014 and January 2020. World Health Organization, Geneva. https://apps.who.int/iris/handle/10665/79199

World Health Organization (2017) Guidelines for treatment of drug-susceptible tuberculosis and patient care 2017 update. World Health Organization, Geneva. https://apps.who.int/iris/handle/10665/255052

World Health Organization (2018) Latent tuberculosis infection: updated and consolidated guidelines for programmatic management. World Health Organization, Geneva. https://apps.who.int/iris/handle/10665/260233

World Health Organization (2021a) WHO consolidated guidelines on tuberculosis module 2: screening–systematic screening for tuberculosis disease. World Health Organization, Geneva. https://www.who.int/publications/i/item/9789240022676

World Health Organization (2021b) Meeting report of the WHO expert consultation on the definition of extensively drug-resistant tuberculosis, 27–29 October 2020. World Health Organization, Geneva. https://apps.who.int/iris/handle/10665/338776

World Health Organization (2021c) Global tuberculosis report 2021. World Health Organization, Geneva. https://www.who.int/teams/global-tuberculosis-programme/tb-reports/global-tuberculosis-report-2021

Yan C, Liang C, Xu J et al (2019) Ultralow-dose CT with knowledge-based iterative model reconstruction (IMR) in evaluation of pulmonary tuberculosis: comparison of radiation dose and image quality. Eur Radiol 29:5358–5366

Yan Q, Yang S, Shen J et al (2020) 3T magnetic resonance for evaluation of adult pulmonary tuberculosis. Int J Infect Dis 93:287–294

Yu WY, Lu PX, Assadi M et al (2019) Updates on 18 F-FDG-PET/CT as a clinical tool for tuberculosis evaluation and therapeutic monitoring. Quant Imaging Med Surg 9:1132–1146

Zeng J, Liu Z, Shen G et al (2019) MRI evaluation of pulmonary lesions and lung tissue changes induced by tuberculosis. Int J Infect Dis 82:138–146

Zheng Z, Pan Y, Guo F et al (2011) Multimodality FDG PET/CT appearance of pulmonary tuberculoma mimicking lung cancer and pathologic correlation in a tuberculosis-endemic country. South Med J 104:440–445

Imaging of Abdominal Solid Organ and Peritoneal Tuberculosis

Shalini Govil, Sanjay Govil, and Anu Eapen

Contents

S. Govil (✉)
Department of Radiology, Naruvi Hospital, Vellore, Tamil Nadu, India
e-mail: shalagovil@gmail.com

S. Govil
Department of Surgery, Apollo Hospital, Bengaluru, Karnataka, India
e-mail: s4govil@gmail.com

A. Eapen
Department of Radiology, Christian Medical College, Vellore, Tamil Nadu, India
e-mail: anuepn@yahoo.com

Abstract

Compared to pulmonary tuberculosis (TB), extrapulmonary TB occurs much less frequently, with abdominal TB comprising a small subset of extrapulmonary TB. Although a variety of imaging modalities are available, computed tomography is the single most useful technique for evaluating TB involving the abdominal solid organs and peritoneal cavity. The miliary, macronodular, serohepatic, and cholangitic forms of hepatobiliary TB present as rim-enhancing parenchymal hypodensities, subcapsular lesions that sugar-coat and scallop the liver surface, as well as bile duct thickening, strictures, and periductal miliary calcifications. Gall bladder and pancreatic TB are very rare and mimic malignancy but the presence of necrotic lymphadenopathy, ascites, liver, spleen, or ileocecal lesions may

© The Author(s), under exclusive license to Springer Nature Switzerland AG 2022

M. F. Ladeb, W. C. G. Peh (eds.), *Imaging of Tuberculosis*, Medical Radiology Diagnostic Imaging,
https://doi.org/10.1007/978-3-031-07040-2_9

suggest the diagnosis. Splenic TB presents as rim-enhancing hypodensities, calcifications, or endarteritis-related infarcts. Peritoneal TB, a relatively common form of abdominal TB, involves the peritoneal lining, mesentery, and omentum, and is caused by contiguous spread from the fallopian tube, bowel, or psoas abscess. The four forms of peritoneal TB are wet-ascitic, dry-plastic, fixed-fibrotic, and "abdominal cocoon." Tuberculous lymphadenitis, the commonest form of abdominal TB, occurs secondary to small bowel or right colon infection and presents as enlarged, matted, enhancing peripancreatic and superior mesenteric nodes that progress to fibrosis and calcification following treatment and healing.

Abbreviations

CT	Computed tomography
HIV	Human immunodeficiency virus
MRI	Magnetic resonance imaging
TB	Tuberculosis
US	Ultrasound

1 Introduction

Tuberculosis (TB) is a disease of antiquity, described as a consumptive illness ("phthisis") from as far back as the sixth century BC. After achieving epidemic proportions as the "White Plague" in the Western world in the seventeenth, eighteenth, and nineteenth centuries, its recognition as a bacterial disease and consequent susceptibility to antibiotics resulted in a brief period of control in the twentieth century. In the last three decades, however, there has been a resurgence of this "Captain of all these men of death," particularly in patients infected with the human immunodeficiency virus (HIV) (Herzog 1998).

The World Health Organization (WHO) estimated that approximately ten million people fell ill with TB in 2020 and 1.3 million died from the disease over the same period. The South-East Asia region, as defined by the WHO, accounts for 43% of the global burden; with India alone harboring 26% of all patients, 8% of whom are HIV-positive. The incidence of extrapulmonary TB has also steadily increased over the last three decades. Up to two-thirds of patients with acquired immunodeficiency syndrome (AIDS) and TB have extrapulmonary involvement. The WHO reports an extrapulmonary TB average incidence of 16%, with an additional 10–15% having coexistent pulmonary and extrapulmonary TB (Evans et al. 2016; CDC 2019; World Health Organization 2021). Abdominal TB accounts for 5–17% of all extrapulmonary TB; with the small bowel most commonly affected (34%), followed by the peritoneum (31%), large bowel (22%), liver (15%), and the upper gastrointestinal tract (9%), with overlapping tuberculous lymphadenitis in 55–66% of cases (Al Karawi et al. 1995).

In this chapter, we discuss the imaging of hepatobiliary, pancreatic, splenic, peritoneal, and lymph node TB, focusing on pathophysiology, clinical presentation, and differential diagnosis as they pertain to imaging features and choice of imaging modality.

2 Hepatobiliary Tuberculosis

2.1 Pathophysiology and Classification

Tuberculous bacilli most commonly reach the liver by hematogenous arterial dissemination during primary infection with *Mycobacterium tuberculosis* or on reactivation of pulmonary infection. Isolated hepatobiliary infection can occur via the portal vein, from bowel or mesenteric TB. Less commonly, the liver may be infected via the amniotic vein during prenatal or perinatal dissemination. Regardless of the pathway to the liver, the bacilli are contained within granulomas (Chaudhary 2014). In isolated hepatobiliary TB, the primary complex is formed within hepatic hilar lymph nodes. If the host

immune response is overwhelmed by the bacterial load, granulomas develop with central caseation that may coalesce to form larger masses.

Pulmonary TB is associated with granulomas in the liver in up to 20% of patients. Miliary TB involves the liver in 20–50% (McMullan and Lewis 2017), with patients with advanced preterminal pulmonary TB being more likely to have liver involvement. Biliary system involvement is usually secondary to rupture of liver granulomas and release of bacteria into the bile, or involvement of the bile ducts by lymph node masses (Chaudhary 2014). Other pathological findings that are associated with hepatic TB and may be apparent on imaging include hepatic steatosis, amyloidosis, and peliosis hepatis (McMullan and Lewis 2017).

Many attempts have been made to classify hepatobiliary TB with a view to differentiate miliary multisystem involvement from localized involvement of the hepatobiliary system and abdominal organs. Some also differentiate microscopic disease revealed only on liver biopsy from gross disease apparent on imaging. From an imaging standpoint, hepatobiliary TB can be classified into four distinct patterns of involvement, namely miliary, macronodular, serohepatic, and cholangitic forms that cover all manifestations observed on imaging (Alvarez 1998; Vanhoenacker et al. 2004; Amarapurkar et al. 2008; Kakkar et al. 2015; Evans et al. 2016) (Table 1).

2.2 Clinical Features

Hepatobiliary TB is most commonly seen in younger patients between 30 and 50 years of age. The most common symptom is right upper quadrant abdominal pain (65–87%), with non-specific symptoms such as fever, anorexia, and weight loss (55–90%). Symptoms are often present for a year or more; and jaundice (35%), hepatomegaly (70–96%), and splenomegaly (25–55%) may be found on physical examination (Chong 2008; Chaudhary 2014). Laboratory tests reveal abnormal liver function tests, with a disproportionate elevation of serum alkaline phosphatase and gamma glutamyl peptidase in the infiltrative miliary or granulomatous forms.

2.3 Imaging

2.3.1 Chest Radiograph

An abnormal chest radiograph is seen in 65–75% of patients with hepatobiliary TB. Findings include apical cavitation and

Table 1 Classification of hepatobiliary tuberculosis

Miliary tuberculosis	• Most common pattern • Disseminated disease • Concurrent involvement of abdominal organs • Random, miliary micronodular lesions ≤2 cm • Miliary calcification	**Mixed** • Miliary calcifications • Nodular lesions • Different stages • Coexisting granulomas • Liquefaction necrosis • Fibrosis • Calcification
Macronodular tuberculosis	• Rare compared to miliary • Macronodular lesions >2 cm • Solitary or multiple • Variable-sized • Punctate calcification	
Serohepatic tuberculosis	• Rarest variant • Subserosal tissue inseparable from the fibrous Glisson capsule • Subcapsular hypodense lesions • Thickened capsule	
Tuberculous cholangitis	• Rare • Irregular dilated intrahepatic ducts • Diffuse miliary peribiliary calcifications	

fibrosis, miliary nodules, and pleural effusions. Subdiaphragmatic calcifications may be seen on the chest radiographs in up to 50% of patients (Alvarez 1998).

2.3.2 Ultrasound Imaging

The transabdominal ultrasound (US) imaging features of hepatobiliary TB vary, depending on the type of lesion.

2.3.2.1 Miliary Lesions

In the most common miliary form of the disease, the only finding may be hepatosplenomegaly. However, US imaging, with its high contrast resolution, may reveal miliary disease with a diffusely echogenic and heterogeneous "bright liver" containing multiple hyperechoic, nonshadowing specks (Akhan and Pringot 2002; Gupta et al. 2019).

2.3.2.2 Macronodular Lesions

Macronodular liver lesions have a variable appearance on US imaging and can appear hypoechoic, mixed echogenicity with anechoic foci of necrosis, hyperechoic or rarely, hypoechoic with a hyperechoic caseous center. The lesion can be fairly ill-defined, gaining definition as multiple small hypoechoic lesions coalesce to form a large mass and develop a well-defined wall. Some of these lesions may show a pseudocapsule due to compressed parenchyma. Larger masses demonstrate echogenic debris, shaggy septations, and a "honeycomb" appearance. Calcifications may be apparent in late-stage disease, either within or along the rim of the mass (Batra et al. 2000; Akhan and Pringot 2002).

2.3.2.3 Tuberculous Cholangitis

On US imaging, tuberculous cholangitis presents as intrahepatic biliary dilatation, hilar lymph nodal masses, intrinsic bile duct wall thickening, and stricture. Gall bladder TB has hypoechoic irregular wall thickening, shaggy echogenic intraluminal septations, and regional hypoechoic lymphadenopathy (Akhan and Pringot 2002; Kakkar et al. 2015).

2.3.3 Computed Tomography

2.3.3.1 Miliary Lesions

Miliary tubercles are often too small and isodense to be detected by computed tomography (CT) and usually present as hepatosplenomegaly. Sometimes, larger tubercles may be visible as small, subcentimeter, hypodense (30–40 HU) nodular or cystic focal lesions in the liver, showing minimal peripheral enhancement. Calcification in chronic disease is more easily discernible as small nodular foci of calcification (Fig. 1). Miliary TB may be suspected when on abdominal CT, the lung bases show miliary nodules; or a chest radiograph reveals features of concurrent pulmonary TB (Alvarez 1998; Evans et al. 2016). However, miliary metastases, lymphoma, and sarcoidosis still need to be included in the differential diagnosis of tiny liver hypodensities, and excluded definitively with biopsy.

2.3.3.2 Macronodular Lesions

The granulomatous and nodular forms of TB are solid, hypodense, and heterogeneous (14–45 HU) lesions of varying sizes, with the larger nodular forms presenting as single solid pseudotumors (Gulati et al. 1999; Evans et al. 2016; Gupta et al.

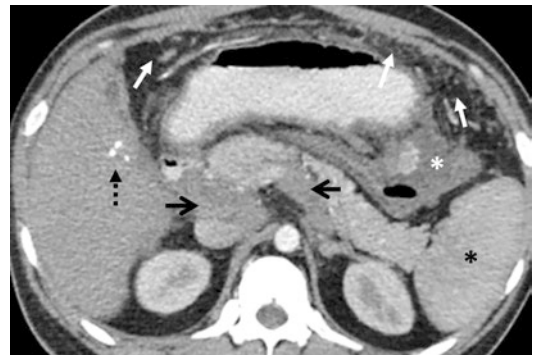

Fig. 1 Calcification in hepatic tuberculosis. Axial contrast-enhanced CT image shows chronic tuberculous disease that is more discernible as small nodular foci of calcification (dashed black arrow). There are enlarged retropancreatic nodes (black arrows), thickened omentum (white arrows), loculated perigastric peritoneal fluid (white asterisk), and splenomegaly (black asterisk). (Courtesy of Dr. Jansi Sekar, Naruvi Hospital, Vellore, India)

2019). Noncaseating granulomas are hypodense and show minimal, non-specific peripheral rim enhancement; while caseating granulomas show necrosis, liquefaction, and calcification. In the less common mode of infection, where bacilli travel from the intestine into the liver via the portomesenteric venous circulation, extrahepatic and intrahepatic portal phlebitis may be visible in the form of thickened, narrowed, and enhancing portal venous walls that can progress to a portal cavernoma (Fig. 2).

Individual and coalescing hepatic abscesses surrounding portal radicles may give rise to the characteristic "cluster sign." "Honeycomb" lesions are larger, multiseptated, peripherally enhancing lesions with septal enhancement and central necrosis. These appearances are non-specific and more often associated with pyogenic or cholangitic abscesses; but when combined with enhancing peritoneal thickening, necrotic lymph nodes and splenic hypodensities, the possibility of TB should be considered. The rim of some lesions may be hyperdense due to granulation tissue in the wall of necrotic collections, or due to coexistent calcification (*calcificans puncta*). Dominant necrosis without obvious peripheral enhancement can be misdiagnosed as cysts. When necrotic and confined to the liver, TB can closely mimic pyogenic abscess, especially when complicated by rupture, perihepatic collections, and peritonitis. Tuberculous granulomas can also exhibit washout which,

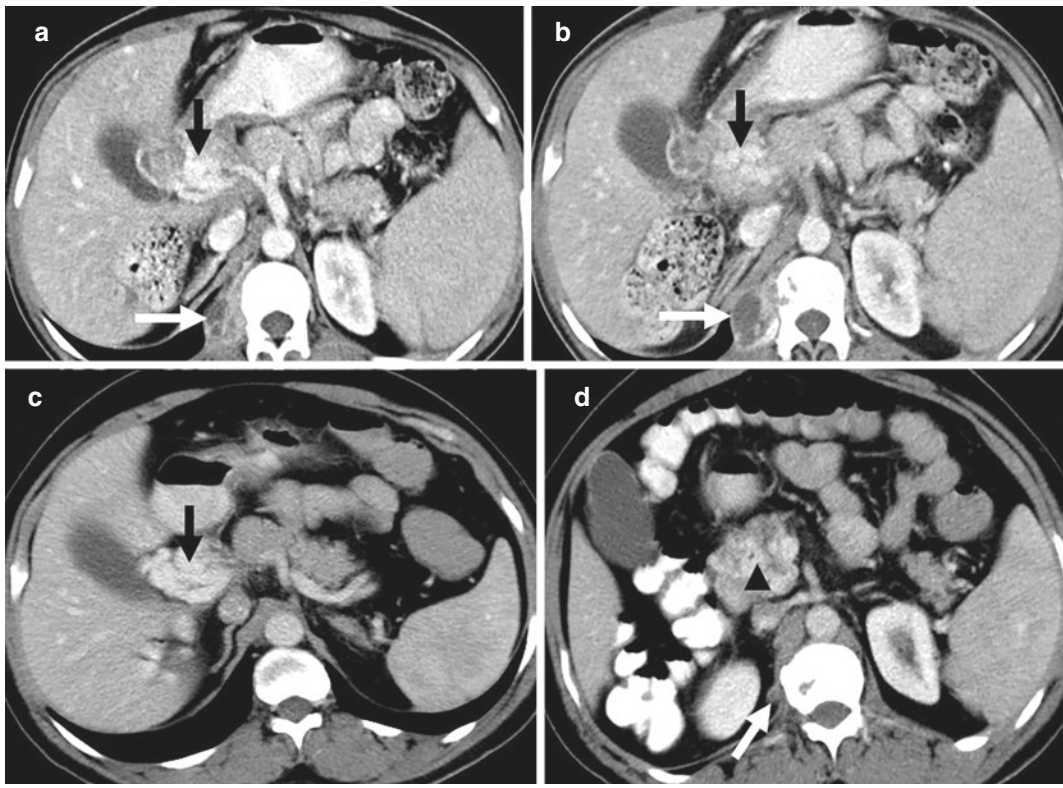

Fig. 2 Periportal tuberculous lymphadenitis causing portal cavernoma in a 46-year-old man with spinal tuberculosis. (**a** and **b**) Axial contrast-enhanced CT images show a right paraspinal abscess (white arrows) and periportal nodal mass encasing a portal cavernoma (black arrow). (**c** and **d**) Axial contrast-enhanced CT images at 2 years follow-up show resolution of the periportal nodal mass and also resolution of the right paraspinal lesion (white arrow). Portal cavernoma at the porta hepatis (black arrow) and in the head of pancreas (black arrowhead) is still present

when associated with portal vein thrombosis, can mimic hepatocellular carcinoma (HCC) (Kakkar et al. 2015).

2.3.3.3 Serohepatic Tuberculosis

In this characteristic but rare form of hepatobiliary TB, conglomerated subcapsular lesions overlie a thickened enhancing capsule and give rise to a "sugar-coated" or "frosted liver" appearance that is often associated with bulky necrotic gastrohepatic and retroperitoneal lymphadenopathy. Scalloping of the liver and other solid organs, previously thought to be pathognomonic of pseudomyxoma peritonei or peritoneal carcinomatosis, can also occur in TB (Jain et al. 2016; Gupta et al. 2019) (Fig. 3).

2.3.3.4 Tuberculous Cholangitis

Tuberculous cholangitis can be primary or secondary due to compression by periportal nodes and hepatic granulomas. Both intrahepatic and extrahepatic bile ducts may be involved, with bile duct thickening and strictures leading to obstructive biliopathy (Fig. 4), sometimes associated with an ill-defined periportal mass. Extensive periductal miliary calcifications are characteristic, when evident. Synchronous hypodense liver granulomas, cholangitic abscesses, retroperitoneal nodal masses, periportal granulomatous infiltration, or splenic nodules may suggest TB. Ductal TB presents as single or multiple biliary strictures and focal dilatations, giving rise to a "beaded" appearance that can mimic sclerosing cholangitis; while parenchymal atrophy and hilar masses can mimic cholangiocarcinoma (Gulati et al. 1999; Evans et al. 2016; Gupta et al. 2019).

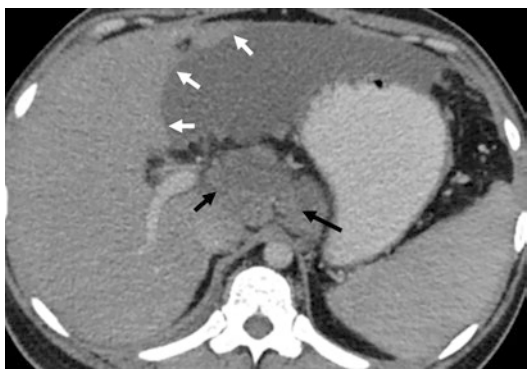

Fig. 3 Serohepatic tuberculosis. Axial contrast-enhanced CT image shows a large subcapsular hypodense collection indenting and "scalloping" the left lobe of liver (white arrows). There are bulky, necrotic, conglomerated gastrohepatic, and retroperitoneal lymphadenopathy extending along the subcapsular plane (black arrows). (Courtesy of Dr. Jansi Sekar, Naruvi Hospital, Vellore, India)

2.3.3.5 Gall Bladder Tuberculosis

Gall bladder TB is extremely rare, and has a nonspecific appearance that resembles the irregular wall thickening and mass of gall bladder malignancy. Multiple foci of necrosis or calcifications and evidence of TB elsewhere may suggest the diagnosis of gall bladder TB.

Types of gall bladder TB that have been described are the micronodular/polypoid type, thickened wall type, and mass-forming type. The polypoid type is broad-based and < 1 cm in size, as opposed to carcinoma >1 cm in size and benign epithelial polyps that are narrow-based. The most common thickened wall type closely resembles cholecystitis and carcinoma with varying appearances; being diffuse or focal, uniform or irregular, with homogeneous or heterogeneous enhancement. A "halo" of edema has been described in gall bladder TB, a feature not seen in carcinoma. The mass-forming type is also similar to gall bladder carcinoma, although foci of low-density necrosis and flecked calcifications may be suggestive of gall bladder TB. Low-density foci in a thickened gall bladder wall associated with calculi can also be due to xanthogranulomatous cholecystitis (Xu et al. 2011).

2.3.4 Magnetic Resonance Imaging

2.3.4.1 Miliary Lesions

Due to the wider availability and accuracy of contrast-enhanced CT, magnetic resonance imaging (MRI) is less commonly performed for hepatobiliary TB. Disseminated and miliary TB

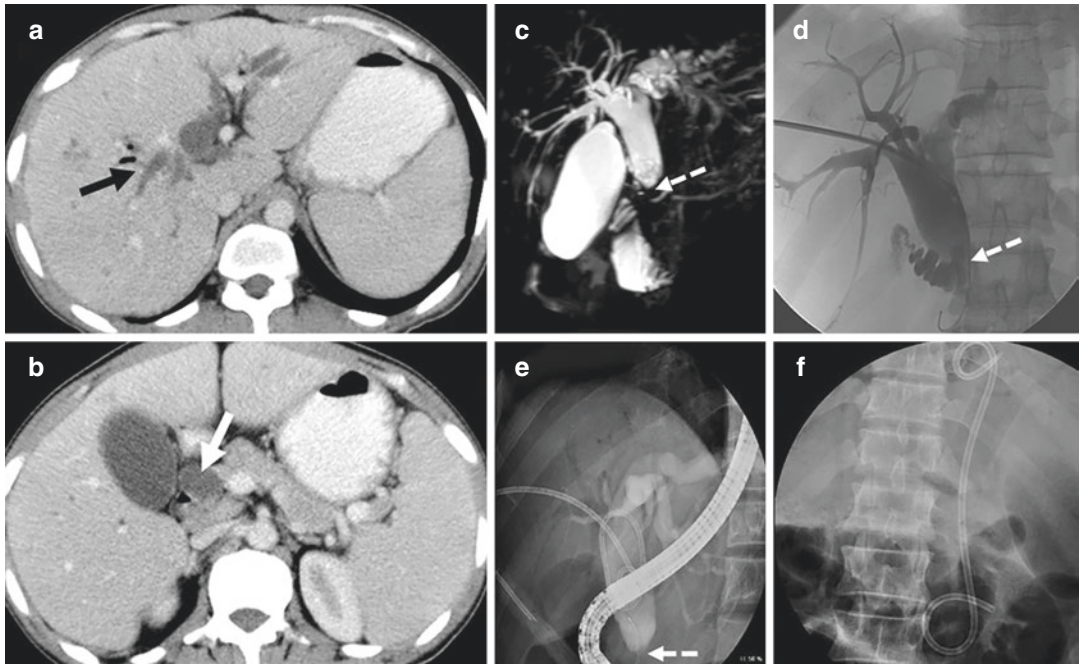

Fig. 4 Tuberculous stricture of the bile duct in a 40-year-old man with hepatic tuberculosis confirmed on histology. (**a** and **b**) Axial contrast-enhanced CT images taken in the portal venous phase show dilated intrahepatic biliary radicles (black arrow) and a dilated common bile duct (white arrow). (**c**) MRCP, (**d**) PTC, and (**e**) ERCP images prior to stent placement show a tightly obstructing mid common bile duct stricture (dashed white arrows). (**f**) Postprocedure radiograph following internal bile duct stent placement shows satisfactory position of the internal bile duct stent

involving the liver and spleen most commonly present with hepatosplenomegaly (Fig. 5) on MRI, with a few visible tiny granulomas when they are T2-hyperintense.

2.3.4.2 Macronodular Lesions

Unlike CT, where all lesions are hypodense regardless of disease stage, MRI findings correlate well with the stage of TB. In the early stages, granuloma with or without caseation/ liquefaction necrosis appears T1-hypointense and T2-hyperintense; while the later fibrous stages reveal both T1 and T2 signal hypointensity. On contrast-enhanced MRI, there is peripheral and internal enhancement resulting in "honeycomb" lesions that are T2-hyperintense and surrounded by a T2-hypointense rim (Evans et al. 2016; Gupta et al. 2019).

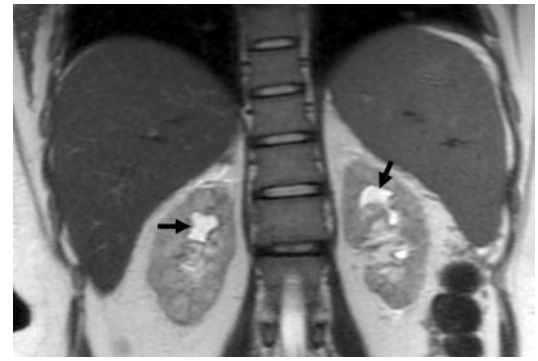

Fig. 5 Hepatosplenomegaly in disseminated tuberculosis. Coronal T2-W MR image shows disseminated and miliary tuberculosis presenting as hepatosplenomegaly. Both kidneys are heterogeneously hyperintense with irregular parenchymal thinning and asymmetrical hydrocalycosis (black arrows). (Courtesy of Dr. Ashok Mithra, Naruvi Hospital, Vellore, India)

2.3.4.3 Tuberculous Cholangitis

Magnetic resonance cholangiopancreatography (MRCP) accurately depicts biliary anatomy and pathology non-invasively, while endoscopic ultrasonography (EUS) and endoscopic retrograde cholangiopancreatography (ERCP) provide opportunities for tissue sampling and stent placement. MRI and MRCP can demonstrate a necrotic or nonnecrotic lymph nodal mass at the hilum, smaller mildly-enhancing peribiliary nodes, thickened enhancing bile duct wall, or tight narrowing of the common bile duct (Fig. 4). Focal biliary radical dilatation is well depicted on MRCP.

2.3.4.4 Serohepatic Tuberculosis

Serohepatic TB presents as peripherally placed, subcapsular lesions with thickening of the adjacent liver capsule and overlying peritoneum. These lesions are T1-hypointense and T2-hyperintense, producing a "sugar-coated" or "frosted liver" appearance (Jain et al. 2016; Gupta et al. 2019).

2.3.5 Other Imaging Modalities

ERCP and EUS can complement findings of cross-sectional imaging in hepatobiliary TB. ERCP is useful for biliary analysis, brush cytology, and stenting of dominant extrahepatic biliary strictures (Fig. 4). On rare occasions, the diagnosis of TB can be made by detecting acid-fast bacilli (AFB) in bile samples or brush cytology. EUS is helpful in obtaining needle biopsies of lymph nodal masses or left lobe liver lesions, and can guide biliary duct cannulation when transpapillary cannulation proves technically difficult.

The sclerosing cholangitis-like changes occasionally encountered in tuberculous cholangitis are best displayed on ERCP, given the inherent high spatial resolution of conventional contrast radiography. Intrahepatic and extrahepatic bile duct irregularities, strictures, and dilatations have been described; mimicking primary sclerosing cholangitis in immunocompetent patients, and HIV-cholangiopathy or atypical mycobacterial cholangitis in those who are immunocompromised (Karaosmanoglu et al. 2016).

The role of Fluorine-18-2′-Deoxy-2-fluoro-d-glucose ([^{18}F] FDG) positron-emission tomography (PET)/CT is unclear but since granulomas are [^{18}F] FDG-avid, there may be some benefit in the evaluation of pyrexia of unknown origin, determining disease extent in HIV-positive patients, and evaluating response to anti-TB therapy (Sathekge et al. 2013; Pai et al. 2016).

2.4 Differential Diagnosis

The miliary form of hepatic TB is identical to the miliary form of other disseminated granulomatous disease such as fungal infection and sarcoidosis. Characteristic appearances that include the "sand-like" hypodensities of sarcoidosis and the "wheel-within-wheel" US imaging appearance of hepatosplenic candidiasis may help in differentiating these entities, as well as calcification and evidence of TB elsewhere.

The granulomatous nodular form of hepatic TB can be mistaken for a pyogenic liver abscess, while the portobiliary findings closely resemble hilar cholangiocarcinoma. Serohepatic TB may be misdiagnosed as pseudomyxoma peritonei or peritoneal carcinomatosis because of scalloping of the liver. Low-density visceral scalloping in the setting of a low-density liver mass usually indicates biliary cystadenoma or cystadenocarcinoma but biliary stricturing is not the dominant feature of these pathologies (Sharma et al. 2017). Ascites, diffuse peritoneal thickening and enhancement, necrotic or matted lymph nodes, splenic and bowel involvement, particularly in the clinical setting of a young patient with a long history, may raise the possibility of abdominal TB. In the vast majority, malignancy remains the most common and important differential diagnosis, with biopsy and histopathological examination the only final arbiter for a definitive diagnosis.

CT is more sensitive than US imaging in the diagnosis of hepatobiliary TB but neither modality is very specific. The diagnosis of malignancy, other inflammatory and infective etiologies such as fungal abscess, sarcoidosis, and sclerosing cholangitis must be considered and excluded though biopsy or bile fluid sampling for AFB (Evans et al. 2016). Tuberculous granulomas at an early or medium stage, and fibro-proliferous lesions, all appear hypodense on CT but on T2-weighted MRI, have various signal intensities that can be an advantage when diagnosing hepatic TB. However, MRI is of limited value in detecting calcification, although large calcific lesions may appear T2-hypointense (Fig. 6). Contrast-enhanced MRI shows minimally enhancing, non-specific honeycomb lesions. In endemic countries and in the right clinical setting, calcification and concurrent involvement of extrahepatic sites may suggest the diagnosis of TB, even when liver imaging is non-specific (Joshi et al. 2014).

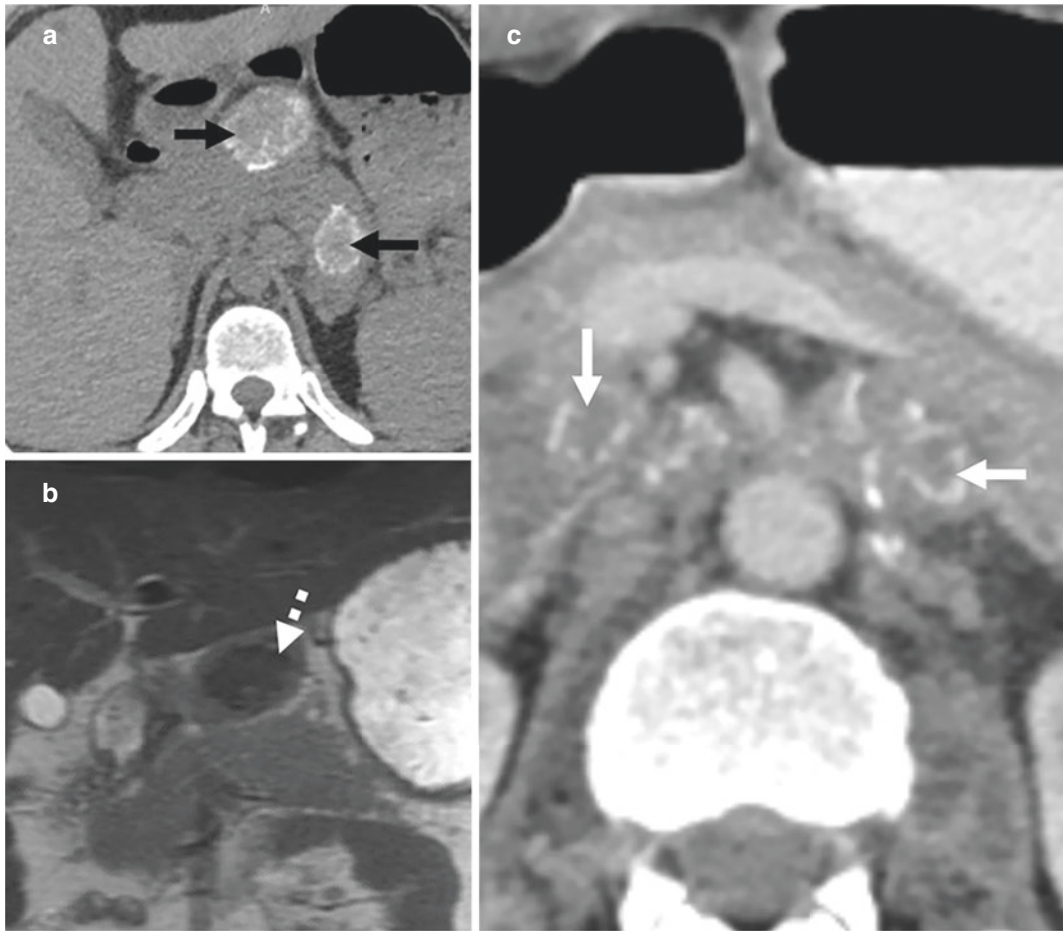

Fig. 6 Tuberculous lymphadenitis. (**a**) Axial unenhanced CT, (**b**) coronal T2-W MR, and (**c**) axial contrast-enhanced CT images show small and large centrally (black arrows) and peripherally (white arrows) calcified nodes in the coeliac, splenic, and lesser curve nodal regions. The large node along the lesser curve in the gastrohepatic ligament (dashed white arrow) is T2-hypointense on MRI. (Courtesy of Dr. Ashok Mithra, Naruvi Hospital, Vellore, India)

3 Pancreatic Tuberculosis

3.1 Clinical Features

Pancreatic TB is extremely uncommon, with an incidence of only 2–5% of autopsies of patients with miliary TB. However, the incidence is rising, especially in developing countries, due to the increasing number of immunocompromised patients. Patients with pancreatic TB usually present in the fourth decade with abdominal pain (81%), weight loss (55%), fever (36%), vomiting (19%), or jaundice (17%). Fever and an abnormal chest radiograph should raise the possibility of TB, with abnormal chest radiographs being reported in up to 50% of patients with pancreatic TB. Pancreatic TB can develop from direct extension, lympho-hematogenous dissemination or reactivation of previous abdominal TB. In patients with HIV infection or those with miliary TB, US imaging may demonstrate a bulky heterogeneous pancreas with multiple small hypoechoic (90%) or isoechoic (10%) lesions, sometimes with fine intralesional echoes (Woodfield et al. 2004; Nagar et al. 2009; Sharma et al. 2016).

3.2 Imaging

CT shows hypodense pancreatic masses associated with peripancreatic lymphadenopathy (75%) (Fig. 7) that can form a confluent, contiguous, complex, lobulated, mixed solid, and cystic pancreatic mass. The head and body of the pancreas are the most common sites, with multiple lesions found in 30% of patients. Cystic masses can, in fact, be mistaken for macrocystic mucinous cystic neoplasms. Smaller lesions (<3 cm) are more likely to be homogeneous, while larger lesions are heterogeneous. On dynamic contrast-enhanced CT, initial mild enhancement can progress to delayed, intense enhancement of the cyst wall or solid component. Calcification, biliary dilatation, and main pancreatic duct (MPD) dilatation are uncommon; while ascites (40%) and involvement of the liver, spleen, and ileocecal region are more common (15%). Necrotic peripancreatic nodes and adjacent vascular involvement can also occur (Nagar et al. 2009).

MRI shows T1-hypointense or isointense focal lesions that are heterogeneous on T2-weighted images. On contrast-enhanced fat-suppressed T1-weighted MRI, there is peripheral enhancement around foci of central necrosis. A diffuse enlargement of the pancreas with T2-hyperintense signal has also been described. On MRCP, biliary or MPD dilation is rarely identified (9%). ERCP is rarely necessary but EUS provides visualization of mediastinal lymphadenopathy and periduodenal adenopathy that may be amenable to EUS-guided biopsy.

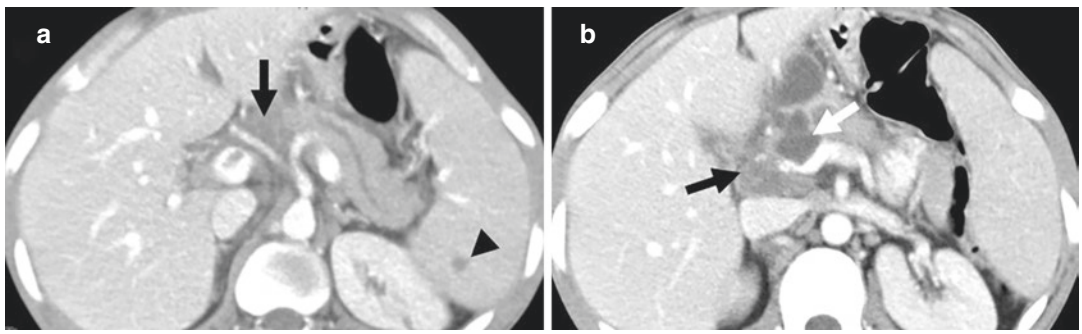

Fig. 7 Pancreatic tuberculosis in a 48-year-old immunocompromised man with disseminated tuberculosis that was confirmed on cytology. (**a** and **b**) Axial contrast-enhanced CT images show enlarged hypodense periportal portocaval nodes (black arrow). There is contiguous involvement of the pancreas as fluid-density foci in the neck of pancreas, indenting the splenoportal confluence (white arrow). Tuberculous granuloma is seen in the spleen (black arrowhead)

3.3 Differential Diagnosis

The differential diagnosis includes carcinoma, cystic neoplasms, walled-off necrosis, and abscess. Vascular involvement in the form of contiguous portal thrombophlebitis can occur in pancreatic or peripancreatic TB, and is therefore not useful in differentiation from pancreatic carcinoma (Joshi et al. 2014).

4 Splenic Tuberculosis

4.1 Clinical Features

Splenic TB is rare and occurs in 5–8% of patients with TB, being more common in those with HIV infection. Patients present with fever (82%), weight loss (44%), and splenomegaly (13–100%). Types of splenic TB include the miliary pattern, multiple nodular granulomas, and a solitary mass. Mass-forming tuberculomas and splenic calcifications are seen in the later phase of the disease.

Miliary TB occurs more often in immunocompromised patients, with the spleen being the third most common organ infected (75%), after the lung (100%) and liver (82%,). The spleen is more commonly involved than the lymph nodes (55%) and bone marrow (41%) (Chablou et al. 2021). The spleen is enlarged by multiple varying-sized tiny nodules scattered throughout the parenchyma, with some nodules coalescing into microabscesses. Isolated primary involvement in immunocompetent patients is extremely rare. Splenic TB is often misdiagnosed on imaging as metastasis, lymphoma, hemangioma, sarcoidosis, or splenic abscess, and hence requires histopathological diagnosis (Lin et al. 2016).

4.2 Imaging

4.2.1 Ultrasound Imaging

Splenic lesions are first detected on US imaging, although this modality is limited in lesion characterization, displaying most pathologies as nonspecific hypoechoic nodules. Micronodular forms of splenic TB are seen in association with miliary TB and demonstrate a diffusely hyperechoic "bright spleen." Larger lesions are often multiple and hypoechoic, with some lesions showing a hyperechoic rim, calcification, and internal debris. Single lesions, when present (15%), are hypoechoic and heterogeneous, and contain calcification. In early stages of the disease, the mass can be hyperechoic and with progressive liquefaction, develop into a "honeycomb" lesion. US imaging, with its inherent high contrast resolution, may occasionally display splenic lesions more obviously than other modalities. US imaging can also provide real-time guidance of percutaneous aspiration done to confirm TB.

4.2.2 Computed Tomography

The miliary pattern consists of innumerable subcentimeter hypodense microabscesses, often too small to be perceptible, producing a non-specific, heterogeneous, enlarged spleen. A few lesions may coalesce to form a heterogeneous hypodense mass (35–45 HU) with moderate rim enhancement and a nonenhancing central portion (Fig. 8). Dense nodular calcification and multiple calcified lesions in the spleen suggest healed prior TB. Splenic infarcts secondary to endarteritis can also occur. The combination of splenic infarcts, splenic hypodensities, rim-enhancing lesions, and calcifications should raise the possibility of splenic TB (Fig. 9).

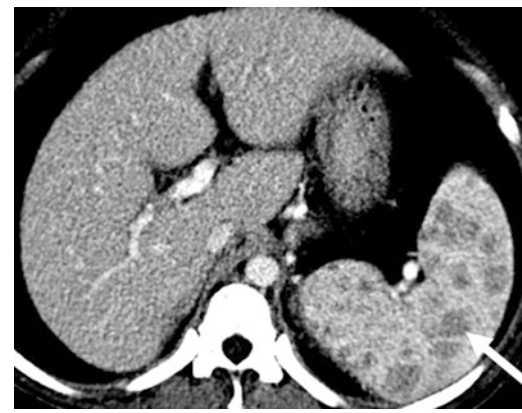

Fig. 8 Splenic tuberculosis in a 23-year-old woman with fever and loss of weight. Axial contrast-enhanced CT image shows splenomegaly with multiple hypodense lesions (white arrow)

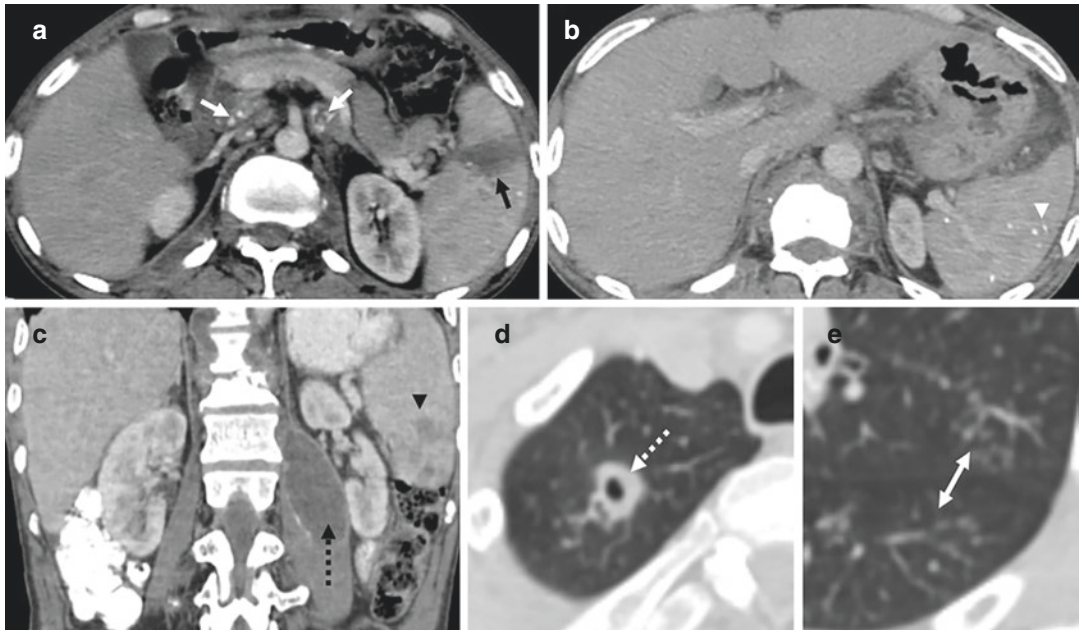

Fig. 9 Pulmonary and extrapulmonary tuberculosis. (**a–e**) Contrast-enhanced CT images show retropancreatic nodes that are (**a**) enlarged with punctate calcifications (white arrows). In the spleen, there is (**a**) an infarct (black arrow), (**b**) punctate calcifications (white arrowhead), and (**c**) irregular, hypodense nodules (black arrowhead). The lungs show (**d**) a small thick-walled right apical cavity (dashed white arrow) and (**e**) "tree-in-bud" bronchiolitis (double white arrow). (**c**) A left psoas muscle collection (dashed black arrow) is also present. (Courtesy of Dr. Jansi Sekar, Naruvi Hospital, Vellore, India)

4.2.3 Magnetic Resonance Imaging

MRI is more helpful for lesion characterization with higher soft tissue contrast resolution and capacity for tissue characterization; often serving as the arbiter when US imaging and CT are equivocal or when malignancy cannot be excluded. The use of diffusion-weighted imaging (DWI) is limited, because the normal spleen physiologically restricts diffusion, and because both splenic abscesses and malignancy also restrict diffusion. Focal splenic tuberculous lesions are of variable signal intensities and enhancement patterns. This spectrum of variable imaging findings represents different phases of disease progression with signal intensities dependent on the extent of fibrosis, granuloma formation, caseation, and liquefaction necrosis.

On T1-weighted images, tuberculomas in the spleen appear as hypointense nodules with a relatively less hypointense rim. On T2-weighted images, they appear as nodules with a hyperintense central area, also surrounded by a less intense rim; this appearance correlates with a caseating granuloma, having a semiliquid center and peripheral reactive fibrosis. Nodules with extensive central liquefaction necrosis, and minimal peripheral granuloma and fibrosis, appear as hyperintense lesions without rim hypointensity on T2-weighted images. The sensitivity for detecting granulomas is higher on MRI than on CT. Larger masses with heterogeneous signal intensity show heterogeneous enhancement on contrast-enhanced T1-weighted images (Joshi et al. 2014).

Contrast-enhanced imaging of the spleen on both CT and MRI has pitfalls due to the unique splenic blood flow pattern. The "zebra pattern," pseudonodular hypodense and pseudoinfiltrative hypodense lesions seen in the early arterial phase mimic pathology that disappear in the late venous phase, resulting in complete homogenization of the organ.

4.3 Differential Diagnosis

The imaging features of miliary TB involving the spleen are non-specific and include a wide differential diagnosis of inflammatory, infective, and neoplastic diseases (Table 2). The presence of pulmonary and extrapulmonary TB, along with splenic calcification, enlarged lymph nodes and soft tissue collections are the best discriminators among these entities (Fig. 9). Lymphoma and nodular tuberculomas of the spleen have similar clinical and imaging presentations, especially when associated with enlarged periportal, omental, and mesenteric lymph nodes. Other similar nodular appearances are seen in splenic metastases and primary aggressive splenic tumors such as the angiosarcoma; however, these are rarely encountered. Peripheral target-like enhancement favors metastases. Although splenic infections have largely non-specific appearances, a few characteristic findings listed in Table 3 can be useful as discriminators. The definitive diagnosis, however, can be made only on histopathological examination of tissue obtained by percutaneous image-guided aspiration, biopsy, or splenectomy.

Table 2 Differential diagnosis of splenic tuberculosis

Miliary type
Sarcoidosis
Histoplasmosis
Brucellosis
Berylliosis
Hodgkin disease
Parasitic diseases
Metastatic carcinoma
Nodular granuloma
Lymphoma
Metastases
Primary splenic tumors, e.g., angiosarcoma

Table 3 Characteristic imaging features of various splenic infections (Ref: Karaosmanoglu et al. 2021)

Infectious disease	Imaging characteristics
Pyogenic abscess	Air
	Restricted diffusion on MRI
Brucellosis	Splenic infarcts
	Calcifications: snowflake, concentric lamellated patterns
Mycobacterium avium-intracellulare complex	T2-hypointense signal on MRI
	Progressive peripheral enhancement
Melioidosis	Hypointense signal on T2-W, T1 in-phase MRI, DWI
	Multiloculated lesions
Malaria	Perisplenic extension
	Splenic rupture
	Splenic infarction
	Massive splenomegaly
	Infarction
	Rupture
	Chronic: "onion skin" from healed, recurrent bleeds
Echinococcosis	Cyst-within-cyst "cartwheel" sign
	Water-lily sign
	Laminated wall
	Pericyst T2-hypointense signal on MRI
Candidiasis	Wheel-within-wheel
	T2-hypointense signal on MRI
	Delayed contrast media retention
	Calcifications
Pneumocystis	T2-hypointense signal
	Annular calcifications

5 Peritoneal Tuberculosis

5.1 Pathophysiology and Classification

Peritoneal TB is a relatively common form of abdominal TB that involves the peritoneal lining, mesentery, and omentum. Although 38% of patients will have an abnormal chest radiograph, active pulmonary TB is present in only 15% of patients. Patients with cirrhosis, HIV infection, or chronic renal failure on continuous ambulatory peritoneal dialysis are at increased risk for peritoneal TB. Mechanisms of pathogenesis of tuberculous peritonitis include reactivation of latent foci of peritoneal infection, rupture of caseous abdominal lymph nodes, blood-borne spread from active pulmonary disease, and direct contiguous spread from the fallopian tube, bowel or psoas abscess. Ingested or blood-borne tuberculous bacilli infect the mucosa, form submucosal tubercles, undergo caseous necrosis, ulcerate the overlying mucosa, and spread transmurally into adjacent lymph nodes and peritoneum.

There are four types of peritoneal TB. The wet-ascitic type (90%) presents as free or loculated ascites containing strands of fine adhesions and floating membranes. The dry-plastic type (3%) primarily involves the mesentery demonstrating thickening, caseous nodules, lymph node enlargement, and bowel adhesions. The fixed-fibrotic type (7%) primarily involves the omentum and is associated with matted bowel loops, small-volume ascites, and sometimes a clinically palpable mass. Most often, these forms overlap each other and differentiation among them is clinically irrelevant.

The "abdominal cocoon," or sclerosing encapsulating peritonitis, is considered a distinct fourth form. Arising secondary to peritoneal TB, the tuberculous abdominal cocoon is composed of diffuse, thickened, enhancing bowel encapsulated by thickened, enhancing peritoneum. This differs from the primary or congenital cocoon, where localized malfixation of the peritoneum results in an internal hernia of small bowel prone to closed loop obstruction. In congenital cocoon, the hernial sac is thin walled and the bowel within is normal in thickness (Fig. 10). Tuberculous ascites may be free or loculated, and is present in 30–100% of patients with tuberculous peritonitis (Sanai and Bzeizi 2005).

5.2 Clinical Features

Patients with peritoneal TB can present with fever, abdominal pain, anorexia, weight loss, malaise, abdominal tenderness, a "doughy" abdomen and ascites. Ascites from peritoneal TB is exudative and can mimic peritoneal carcinomatosis. Clinical presentation and fluid analysis often cannot distinguish TB from carcinoma, with yield from fluid AFB being variable (Debi et al. 2014). Given the low sensitivity of other non-invasive methods such as ascitic fluid AFB stain and culture (4–8%), biopsy is the best option at laparoscopy. However, US-guided localization of a peritoneal nodule for core biopsy is possible, when sufficient ascites outlines an anteriorly located nodule on high frequency scanning. Extensive adhesions demonstrated on imaging should be anticipated, when performing laparoscopy or surgery (Demir et al. 2001).

5.3 Imaging

5.3.1 US imaging

US imaging typically shows fixed membranes, septa and debris (17%), floating debris (13%), mobile strands or membranes (9%), and fixed septa (9%), with a moderate or large amount of ascites with clear or complex fluid (83%). US imaging also shows an omental "cake" (26%), thickened mesentery with adherent small bowel loops (22%), splenomegaly (20%), pleural effusion (17%), lymphadenopathy (13%), and thickening of the ileal wall (7%). Free floating debris, fine echo exudates, and mobile septae are not easily visible on CT. Chylous ascites, though rarely present, demonstrates a fat-fluid level, with the echogenic supernatant that is more echogenic than the sediment layer. Peritoneal thickening is

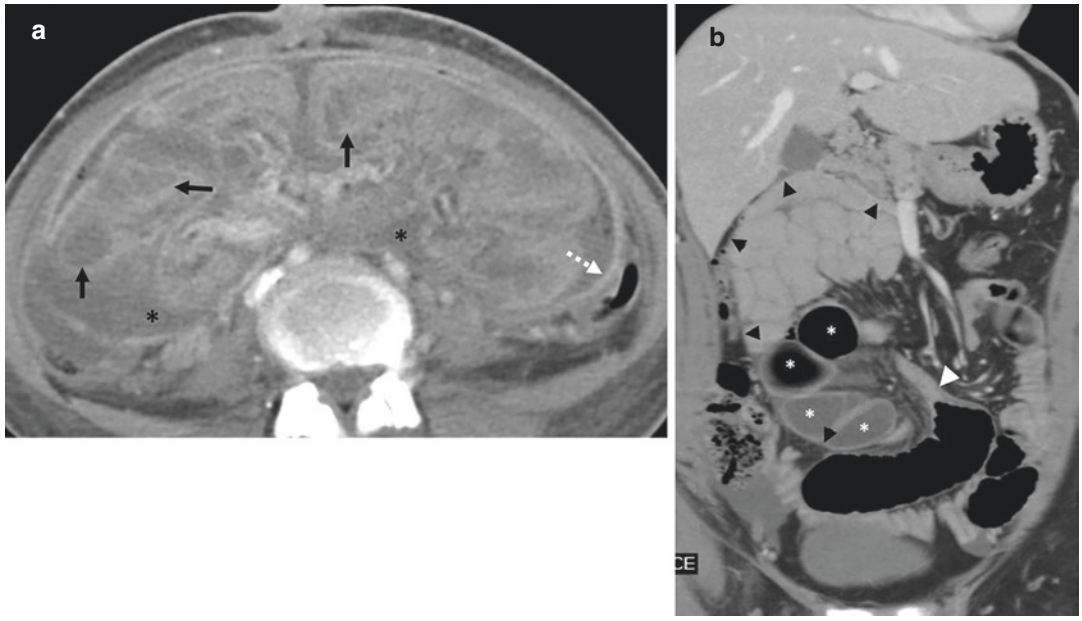

Fig. 10 Abdominal cocoon: comparison of secondary versus primary types. (**a**) Cocoon secondary to peritoneal tuberculosis. Axial contrast-enhanced CT image shows encapsulation of thickened enhancing small bowel (black arrows) and locules of fluid (black asterisks) by thickened enhancing peritoneum (dashed white arrow). (**b**) Congenital cocoon/internal hernia causing closed loop obstruction due to small bowel malrotation. Coronal contrast-enhanced CT image shows encapsulation of normal thickness small bowel by a thin sac in the right side of the abdomen (black arrowheads). There is "beaking" (white arrowhead) of the afferent jejunal loop obstructed at the mouth of the cocoon. Dilated and obstructed jejunal loops in the lower half of the sac (white asterisks) and collapsed loops in the upper half of the sac are present

present in 14–100%, more evident when highlighted by surrounding ascites. Smooth, diffuse, regular, hypoechoic 2–6 mm thickening, or irregular peritoneal thickening with nodules <5 mm can be found. Omental abnormality is observed in 14–55% of patients on US imaging and 36–82% on CT. The omentum may have a "smudged," "dirty" or much less often, a "caked" appearance (Fig. 11). Nodular omentum is not a feature of TB. The mesentery is thickened >15 mm, echogenic and nodular. Enlarged lymph nodes and sometimes caseous, centrally echogenic nodules may be apparent within or adjacent to the mesentery (Lee et al. 1991).

5.3.2 Computed Tomography

On CT, ascites has high density (20–45 HU) due to the high protein and cellular content. When a chylous fat-fluid level is present, it is clearly demonstrated on CT and the rare combination of chylous ascites with abdominal

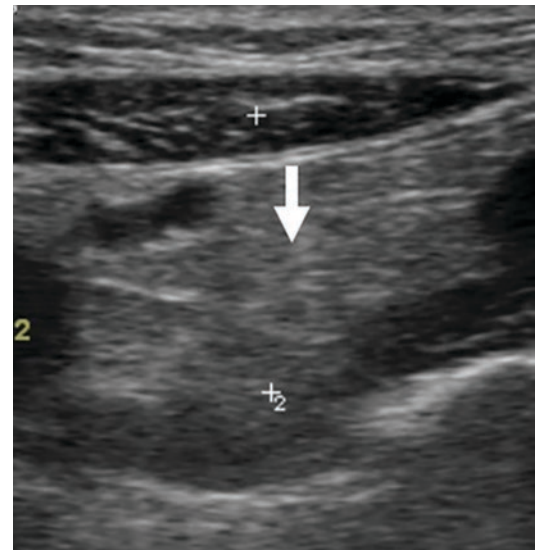

Fig. 11 Peritoneal tuberculosis. US image shows chalky thickening of greater omentum, seen as an "omental cake" (white arrow). Tuberculosis was confirmed on histopathology

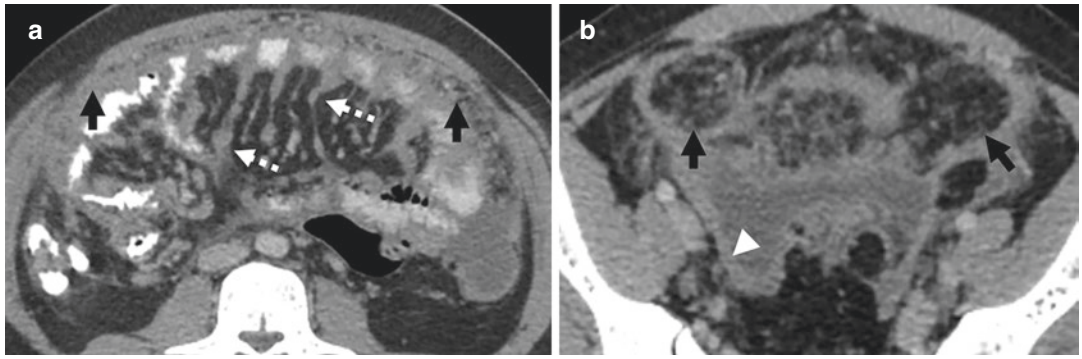

Fig. 12 Peritoneal tuberculosis. (**a** and **b**) Axial contrast-enhanced CT images show diffuse peritoneal (white arrowhead), omental (black arrows), and mesenteric (dashed white arrows) thickening, nodularity and enhancement. (Courtesy of Dr. Jansi Sekar, Naruvi Hospital, Vellore, India)

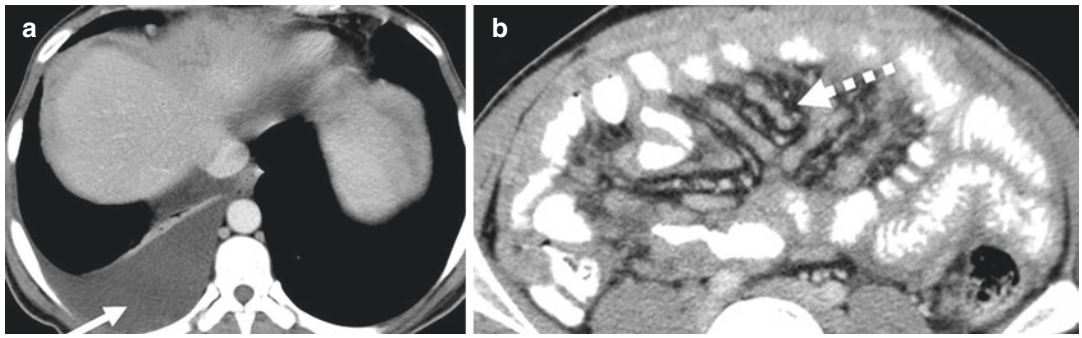

Fig. 13 Peritoneal tuberculosis in a 35-year-old man with anorexia and weight loss for 6 months. (**a** and **b**) Axial contrast-enhanced CT images show a right pleural effusion (white arrow). There is mesenteric nodularity and thickening (dashed white arrow) and diffuse small bowel wall thickening due to serosal involvement

lymphadenopathy is pathognomonic of TB (Prasad and Patankar 1999). On CT, peritoneal thickening, nodularity, and enhancement are seen (Fig. 12), along with mesenteric hypervascularity, patchy or diffuse hyperdensity (Fig. 13). Clumped and matted bowel, together with thickened adhesive mesentery, can cause closed loop obstruction. Interloop abscess, loculations of ascites, and peritoneal and mesenteric nodal calcification (Fig. 14) can occur, along with calcifications in the wall of encysted ascites. Fixed loops of bowel and mesentery can stand out as spokes of a wheel radiating from the mesenteric root, giving rise to the "stellate sign." In advanced disease, the peritoneal layers

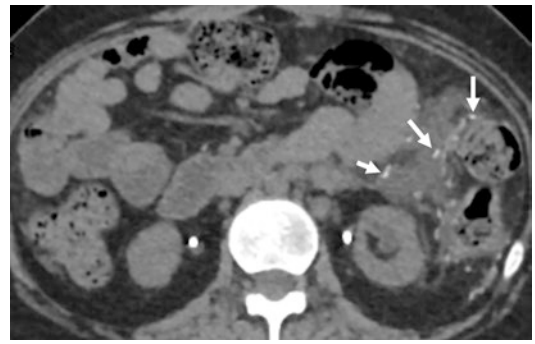

Fig. 14 Calcifications in peritoneal tuberculosis. Axial unenhanced CT image shows multiple punctate calcifications (white arrows) within conglomerate peritoneal nodes, medial to the descending colon. (Courtesy of Dr. Ashok Mithra, Naruvi Hospital, Vellore, India)

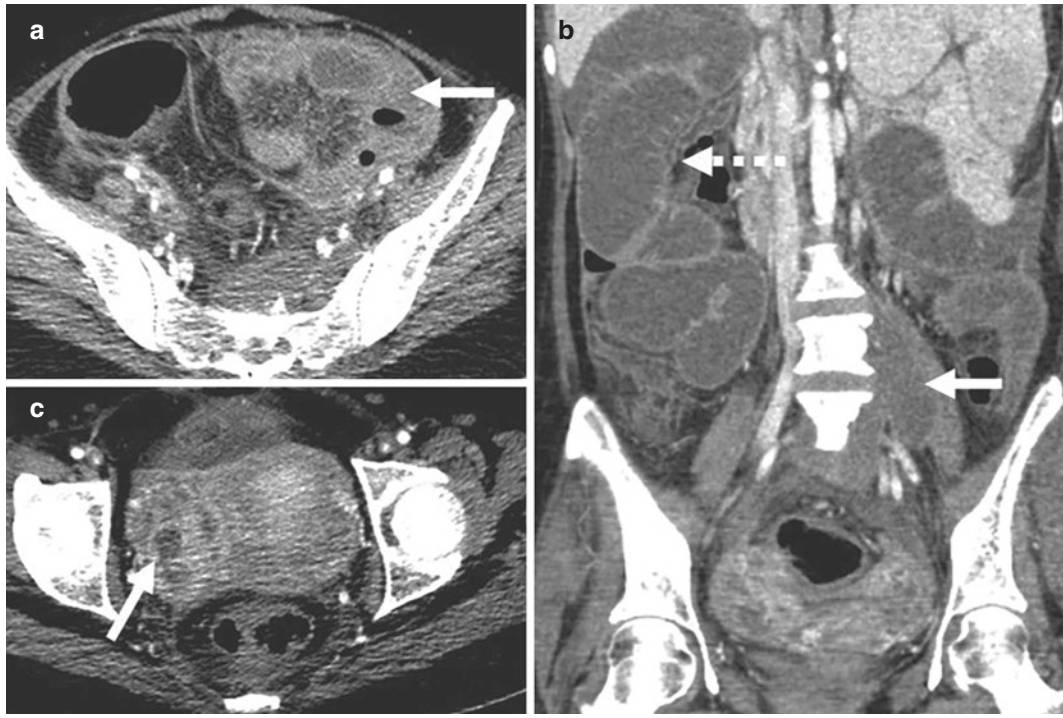

Fig. 15 Disseminated tuberculosis of the abdomen in a 31-year-old woman presenting with low-grade fever and abdominal pain for 2 weeks. She also has diabetes mellitus. (**a** and **c**) Axial and (**b**) coronal contrast-enhanced CT images show (**a**) clumping of small bowel with mesenteric thickening (white arrow) forming a cocoon and causing bowel obstruction, with (**b**) dilated proximal small bowel (dashed white arrow). There is a (**b**) left psoas abscess (white arrow) and (**c**) right tubo-ovarian mass (white arrow)

can lose their definition and form an abdominal cocoon. An enhancing mantle of thickened peritoneum envelops thickened and matted small bowel, forming the cocoon. Abdominal cocoon secondary to TB differs from the idiopathic or primary cocoon that resembles an internal hernia, with a smaller clump of bowel encased by a thin, smooth membranous sac that may be associated with small bowel malrotation (Rastogi 2008; Sharma et al. 2013) (Figs. 11 and 15).

5.3.3 Magnetic Resonance Imaging

On MRI, thickened enhancing peritoneum that is T2-iso- or hyperintense can be seen, although peritoneal and mesenteric nodes are not well delineated due to poor spatial resolution. Conversely, mildly-enhancing, thick and thin septae within the loculated fluid on T2-weighted images are not always evident on CT. Thickened omentum shows heterogeneously hyperintense T2 signal (Joshi et al. 2014).

5.4 Differential Diagnosis

The differential diagnosis of peritoneal TB includes disseminated peritoneal carcinomatosis, ovarian carcinoma, peritoneal mesothelioma, and nontuberculous peritonitis. Differentiating peritoneal TB from carcinomatosis is difficult given the considerable overlap in findings, with no single distinctive finding favoring one or the other diagnosis. However, the combination of distinctive findings can lead to a specific diagnosis. Mesenteric macronodules (>5 mm) are found more frequently in TB (52%), while the omentum is more irregularly infiltrated in peritoneal carcinomatosis. A thin omental line covering the

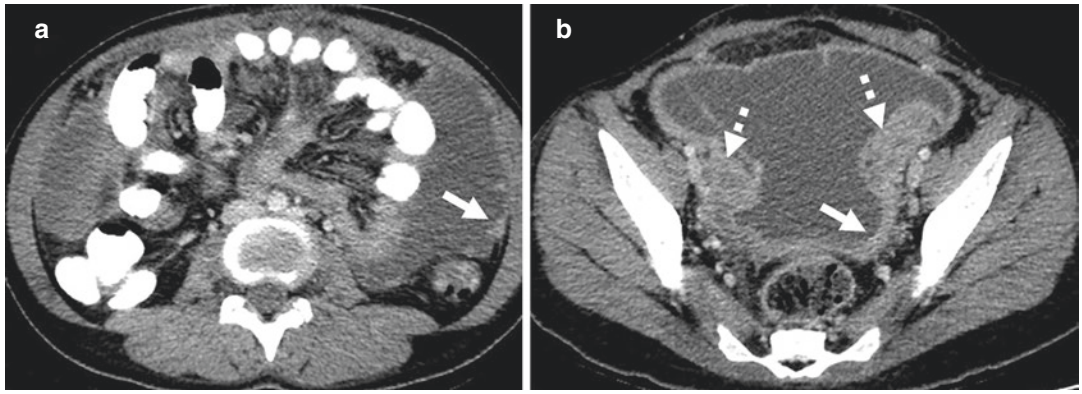

Fig. 16 Peritoneal tuberculosis in a 22-year-old woman with abdominal distension for 6 months. (**a** and **b**) Axial contrast-enhanced CT images show (**a**) ascites with peritoneal nodules (white arrow) and (**b**) diffuse thickening and enhancement of the pelvic peritoneum (white arrow) with enlarged and enhancing adnexal masses (dashed white arrows)

infiltrated omentum and peritoneal or extraperitoneal masses with a low-density center (43%) favors TB, as also splenomegaly and calcification (14%) (Ha et al. 1996).

Significant ovarian capsular change and greater ovarian parenchymal attenuation are also useful findings in differentiating between peritoneal TB and peritoneal carcinomatosis with normal-sized cancer of the ovary (Shim et al. 2017) (Fig. 16). Occasionally, peritoneal thickening, enhancement, and nodularity can occur secondary to a bile leak or urinary leak and unless there is a clinical suspicion, the peritoneal abnormalities may be mistaken for TB or carcinomatosis. On CT, finding fluid around the bile duct, gall bladder, kidneys, ureters, or bladder or identifying a hematoma or a tongue of omentum adherent to the dome of bladder or fundus of gall bladder, can suggest a leak as the cause of peritonitis (Titton et al. 2003).

6 Tuberculous Abdominal Lymphadenopathy

6.1 Pathophysiology and Classification

Tuberculous infection and inflammation of the lymph nodes, also called tuberculous lymphadenitis, are the most common presentation of abdominal TB, being present in 55–66% of cases. Approximately 5.7–17.2% of patients with peripheral tuberculous lymphadenopathy also have involvement of abdominal lymph nodes (Leder and Low 1995). Tuberculous lymphadenitis occurs more commonly in females and immigrants from endemic countries, with an age range of 30–40 years old (Salvador et al. 2015).

There are three major routes of infection, namely oral ingestion, blood-borne infection, and direct spread from contiguous infection. The oral route is most common and happens after the ingestion of sputum or milk infected with tuberculous bacilli. Bacilli are carried by intestinal lymphatics from a lesion in the intestinal submucosa into lymph nodes that drain that segment of bowel, usually the ileocecum, jejunum, ileum, and right side of colon, into peripancreatic and superior mesenteric lymph nodes (L1 vertebral level), but rarely from the left colon into the inferior mesenteric nodes (L3 vertebral level) or the lower para-aortic lymph nodes. Duodenal TB drains into the periduodenal nodes, lesser omental or hepatoduodenal ligament nodes, and the peripancreatic nodes. The lymphatic drainage from the bowel explains why lower para-aortic lymph node involvement is uncommon in the nondisseminated form of intra-abdominal TB lymphadenitis. The blood-borne route brings bacilli from a distant site, usually the lungs, to the blood and entire abdominal lymphatic system;

and therefore involves all groups of intra-abdominal nodes, including the lower para-aortic lymph nodes.

The direct route is from adjacent infected glands or structures such as the reproductive organs that drain into the para-aortic and anterior pararenal nodes. Therefore, para-aortic and paracaval node involvement occurs in disseminated TB or direct spread from reproductive organs. 80% of nondisseminated or localized TB drains into the mesenteric, lesser omental, anterior pararenal, and upper para-aortic lymph nodes; while only 20% of disseminated TB involve the lower para-aortic lymph nodes. Rarely, isolated periportal lymphadenopathy can be the only sign of TB, and while TB involves the mesenteric root and the periportal nodes in isolation, para-aortic or paracaval lymph node involvement does not happen in isolation, as it does in lymphoma.

Tuberculous lymphadenitis progresses through different stages which can be reflected on CT. The first stage of lymphoid proliferation is marked by lymph node enlargement with homogeneous enhancement. With disease progression, the central part of the lymph node undergoes caseous necrosis, resulting in a centrally nonenhancing node with peripheral capsular rim enhancement. Capsular degeneration results in perinodal cloudiness and fat stranding, and fusion of adjacent lymph nodes which appear as a multilocular enhancement and "matting." In the final stage, after treatment or healing, the lymph nodes undergo fibrosis, and calcifications can be seen. Caseation or liquefactive necrosis in the center of the enlarged lymph nodes show a 28–84 HU low attenuation related to the insufficient blood supply, while the peripheral inflammatory lymphatic tissue shows a higher attenuation reflecting the preserved blood supply (Fig. 17).

Infected lymph nodes are usually never larger than 4 cm, with a mean size of 2 cm, in line with self-limiting growth. Even when large conglomerate masses are formed, tuberculous lymphadenitis does not produce significant ureteric or bowel obstruction, but can cause biliary obstruction because of periductal inflammation and mass effect. Tuberculous lymph nodes can cause portal or splenic vein thrombophlebitis, extrahepatic portal vein obstruction, and cavernoma formation (Fig. 2). Calcification and scarring may be a dominant feature (Fig. 6) (Pereira et al. 2005).

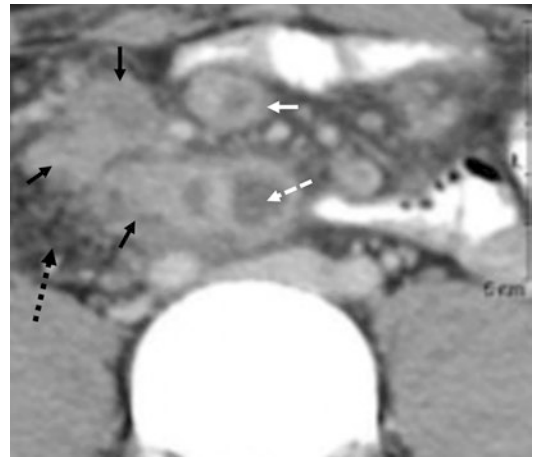

Fig. 17 Tuberculous lymphadenitis. Axial contrast-enhanced CT image shows multiple confluent enlarged mesenteric lymph nodes (black arrows) with associated perinodal fat stranding and cloudiness (dashed black arrow). Caseation in the center of the enlarged lymph nodes shows low density (dashed white arrow) due to insufficient blood supply, while peripheral inflammatory lymphatic tissue shows higher density due to preserved blood supply and enhancement (white arrow)

6.2 Clinical Features

The clinical presentation of abdominal tuberculous lymphadenitis comprises malaise, low-grade fever, weight loss, abdominal pain, and diarrhea related to small bowel involvement. In addition, symptoms based on the site of lymphadenopathy can cause localized pain and tenderness that mimics appendicitis, diverticulitis, or cholecystitis. Necrotic nodes, capsular disruption, and ensuing perinodal inflammation can be extensive and lead to bile duct obstruction, portal vein thrombosis and portal hypertension, fistula formation, duodenal stricture, and stenosis. Rarely, aortitis and renal arteritis secondary to ruptured caseating periaortic nodes lead to renovascular hypertension. In a review of 21 cases of mesenteric TB reported in the literature, all patients were females with a mean age of 43 years (range 23–69 years). Abdominal disten-

sion was the most common presenting feature (57%), while 52% of patients presented with abdominal pain. Fever was present in 19% of individuals, while dyspnea was present in 9% (Mehmood et al. 2019).

6.3 Imaging

6.3.1 Abdominal Node Size and Stations

The threshold size for lymph node enlargement depends on node location. Intra-abdominal lymphadenopathy should be diagnosed only when the nodal measurement exceeds the threshold size for that specific location. In countries with a high TB prevalence, wrongly diagnosed intra-abdominal lymphadenopathy will inevitably lead to a diagnosis of abdominal TB and ensuing clinical missteps ranging from biopsy, laparoscopy, and open surgery to empirical anti-TB therapy. Table 4 lists the threshold short-axis sizes for the main intra-abdominal nodal locations (Dorfman et al. 1991).

In the setting of intra-abdominal TB lymphadenitis, where CT will be the likely modality employed for treatment follow-up, the use of standard terminology when describing the location of enlarged lymph nodes is equally important. As TB often involves the peripancreatic region, a description of "enlarged peripancreatic nodes" actually covers many nodal stations, and a lack of specific location can lead to confusion when comparing node sizes from prior reports. Therefore, it would be prudent to describe lymph node location using nodal station nomenclature in cases likely to undergo follow-up imaging. Abdominal nodal station nomenclature is based on the accompanying vessel, as is given in Table 5 (Morón and Szklaruk 2007).

Table 4 Abdominal lymph nodes: upper limit of normal short-axis sizes by location (Ref: Dorfman et al. 1991)

Location	Size
Retrocrural space	6 mm
Paracardiac	8 mm
Gastrohepatic ligament	8 mm
Celiac axis to renal artery	9 mm
Renal artery to aortic bifurcation	11 mm
Portacaval space	10 mm
Porta hepatis	7 mm
Mesenteric	5 mm

6.3.2 Ultrasound Imaging

The relative insensitivity of US imaging in the detection of enlarged intra-abdominal nodes has long been known, with CT outperforming US imaging in the detection of enlarged para-aortic and iliac lymph nodes by a 29–33% increased sensitivity (Munker et al. 1995). Despite this relatively low sensitivity, the safe, portable, inexpensive, and non-invasive nature of US imaging is a distinct advantage in resource-limited settings where CT and MRI are not widely available. US imaging is increasing in accessibility, particularly with the growing practice of point-of-care ultrasonography (POCUS). In the last few decades, the overlap of the HIV and TB epidemics in sub-Saharan Africa has contributed to an increase in abdominal TB; this has created a challenge in this resource-limited setting to dif-

Table 5 Nomenclature for abdominal lymph node stations (Ref: Morón and Szklaruk 2007)

Station	Nodes
1	Right cardia lymph nodes
2	Left cardia lymph nodes
3	Lymph nodes along the lesser curvature
4	Lymph nodes along the greater curvature
4sa	Lymph nodes along the short gastric vessels
4sb	Lymph nodes along the left gastroepiploic vessels
4d	Lymph nodes along the right gastroepiploic vessels
5	Suprapyloric group of lymph nodes or nodes along the right gastric artery
6	Infrapyloric groups of lymph nodes
7	Lymph nodes along the left gastric artery
8	Lymph nodes along the common hepatic artery
9	Lymph nodes around the celiac artery
10	Lymph nodes at the splenic hilum
11	Lymph nodes along the splenic artery
12	Lymph nodes in the hepatoduodenal ligament
13	Lymph nodes behind the pancreatic head
14	Lymph nodes at the root of the mesentery or the superior mesenteric artery
15	Lymph nodes along the middle colic artery
16	Para-aortic group of lymph nodes

ferentiate between HIV-related opportunistic infection or neoplasm and the onset of abdominal TB. In sub-Saharan countries, POCUS and focused assessment with sonography for HIV-associated TB (FASH) are increasingly used to diagnose abdominal TB (Heller et al. 2010).

76% of patients with culture-positive TB demonstrate at least one or more of three features, namely long-axis lymph node length ≥ 10 mm, splenic hypoechoic lesions, and abdominal/pleural/pericardial effusions (Griesel et al. 2019). In a study done in India evaluating POCUS in abdominal TB, a positive FASH in the form of abdominal lymphadenopathy and splenic microabscesses was strongly associated with a diagnosis of TB (Weber et al. 2018). Ascites, lymphadenopathy, and mesenteric thickening are the main findings in abdominal TB. Lymph nodes, when necrotic, can appear nearly cystic and even demonstrate posterior acoustic enhancement, providing a target for US-guided fine-needle aspiration cytology (FNAC) (Ghazinoor et al. 2004). On US imaging, the caseous center of the enlarged lymph node may also appear hyperechoic and heterogeneous (Dorfman et al. 1991; Morón and Szklaruk 2007); while on CT, the central part of the enlarged node is hypodense (<30 HU) (Fig. 18) or sometimes isodense to skeletal muscle (35 HU).

6.3.3 Computed Tomography

The types of contrast-enhanced CT patterns in abdominal TB lymphadenitis (Pombo et al. 1998) are as follows:

(a) Peripheral rim enhancement with hypodense center
(b) Inhomogeneous enhancement
(c) Homogeneous enhancement
(d) Nonenhancing lymph nodes
(e) Conglomerate lymph node masses with areas of necrosis secondary to perinodal inflammation
(f) Increased number (>3 in one CT section) of normal-sized or mildly enlarged mesenteric nodes of homogeneous density
(g) Calcified lymph nodes

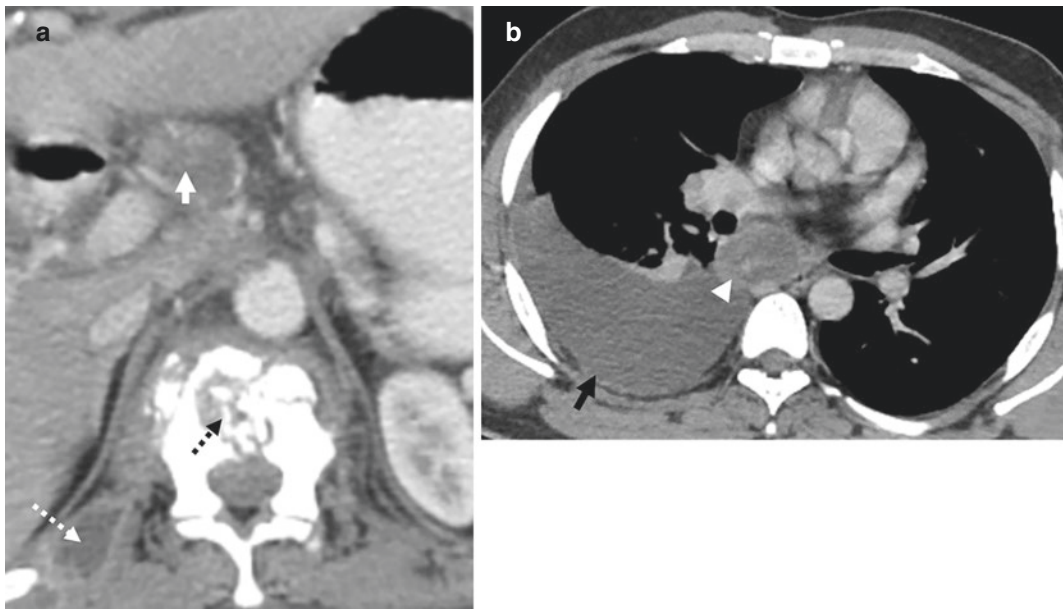

Fig. 18 Disseminated tuberculous lymphadenitis. (**a** and **b**) Axial contrast-enhanced CT images show enlarged peripherally enhancing centrally hypodense lymph nodes in the lesser omentum (white arrow) and subcarinal regions (white arrowhead). There is destruction of the vertebral body (dashed black arrow) with a right paraspinal abscess (dashed white arrow) and a right pleural effusion (black arrow). (Courtesy of Dr. Jansi Sekar, Naruvi Hospital, Vellore, India)

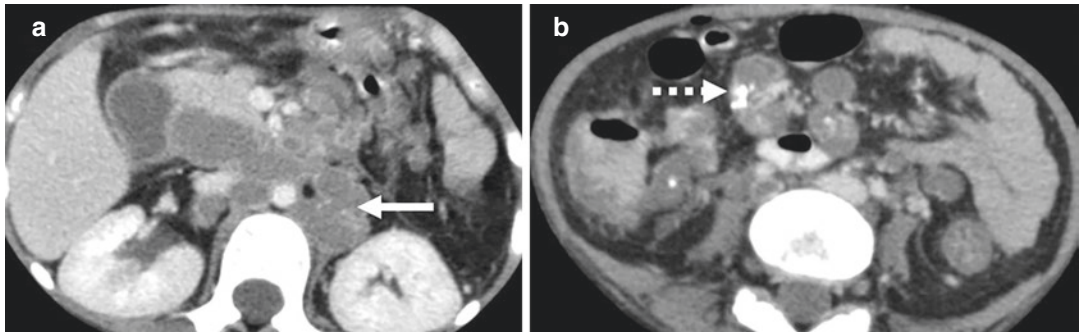

Fig. 19 Necrotic tuberculous lymphadenitis in a 19-year-old girl with fever, loss of weight, and appetite. (**a** and **b**) Axial contrast-enhanced CT images show multiple enlarged, hypodense, necrotic abdominal nodes in the portocaval, mesenteric, and para-aortic regions. Note the necrotic left para-aortic nodes (white arrow) and matted, necrotic and calcified mesenteric nodes (dashed white arrow)

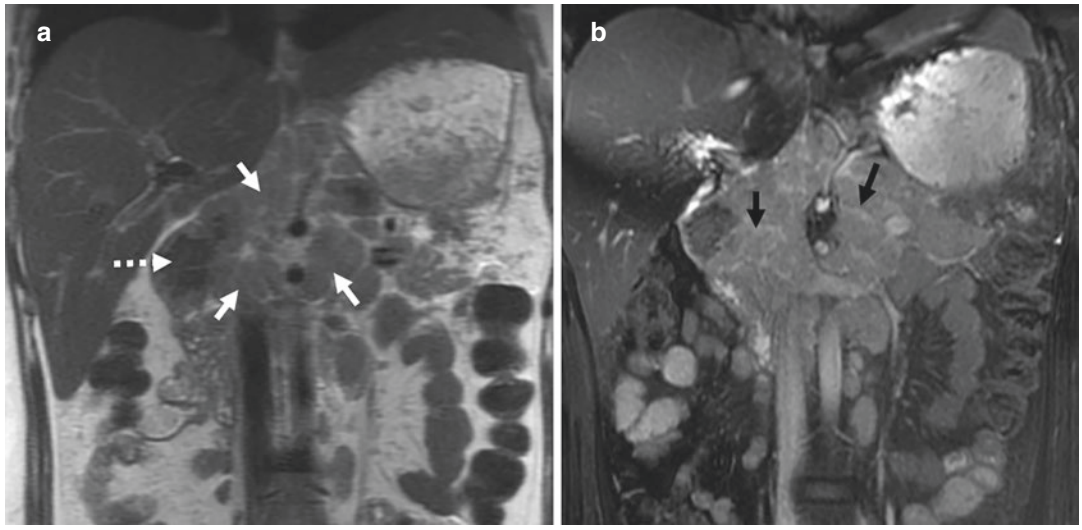

Fig. 20 Tuberculous lymphadenitis. Coronal (**a**) T2-W SSFE and (**b**) FIESTA MR images show conglomerated, matted T2-hyperintense nodes (white arrows) with perinodal T2-hyperintensity (black arrows) and central T2-hypointensity (dashed white arrow). (Courtesy of Dr. Ashok Mithra, Naruvi Hospital, Vellore, India)

Peripheral enhancement, with or without central low attenuation (Fig. 17), is the most common form of lymphadenopathy that is highly suggestive of TB, but cannot be reliably differentiated from testicular cancer metastases, squamous cell cancer metastases, treated lymphoma, Crohn disease, or Whipple disease. The other less common patterns are heterogeneous enhancement, homogeneous enhancement, and nonenhanced low-density lymph nodes (Fig. 19), most often encountered in patients with AIDS. Indicators of a tuberculous etiology include conglomerate or matted lymph node masses with foci of necrosis and perinodal inflammation, increased number (>3 in one CT section) of normal-sized or mildly enlarged, homogeneous or calcified mesenteric nodes. Calcified lymph nodes can be also found in metastatic testicular tumors and non-Hodgkin lymphoma after treatment (Joshi et al. 2014).

6.3.4 Magnetic Resonance Imaging

Tuberculous nodes are T2-hyperintense from liquefactive necrosis and show perinodal T2-hyperintensity due to capsular disruption, with a central T2-hypointense area related to paramagnetic free radicals from active phagocytic cells (Fig. 20). On T1-weighted images, lymph nodes that are hypointense show thin or thick, complete or incomplete, rim-like peripheral enhancement; while the nodes that are isointense enhance homogeneously. Conglomerate group of nodes show peripheral and central areas of enhancement (Joshi et al. 2014).

6.4 Differential Diagnosis

The differential diagnosis for the cause of enlarged lymph nodes with low-density centers and calcification is listed in Table 6. Although evidence of AFB is ideally required for the definitive diagnosis of TB, this is not always possible in abdominal TB. Currently, diagnostic criteria include clinical manifestations suggestive of TB, imaging evidence indicative of TB, histopathological or microbiological evidence of TB, and/or therapeutic response to treatment. Multiplicity, matting, and caseation are three features that indicate nodal TB. Diagnosis can be established using FNAC and a core biopsy under US, EUS, or CT guidance (Joyati Tarafder et al. 2015).

Table 6 Differential diagnosis for abdominal lymphadenopathy with low-density centers and calcification

Differential diagnosis of lymph nodes with low-density centers
Metastatic malignancy
Lymphoma after treatment
Inflammatory conditions (e.g., Crohn disease)
Pyogenic infection
Whipple disease
Differential diagnosis of calcified lymph nodes
Metastases
Teratomatous testicular tumors
Non-Hodgkin lymphoma after treatment

7 Conclusion

With the resurgence of TB and concomitant increase in extrapulmonary TB, abdominal TB is currently not an infrequent diagnosis, especially in countries where TB is prevalent. Although the bowel, lymph nodes and peritoneum are more commonly involved, hepatobiliary, pancreatic, and splenic forms of the disease can occur, often mimicking malignancy or acute abscess. Coexisting pulmonary TB, splenic involvement, rim-enhancing low-density lesions, "cobweb" ascites, scalloped or "sugar-coated" liver, peripancreatic nodal involvement, periductal miliary calcifications or an "abdominal cocoon" are all features that should raise the index of suspicion for a tuberculous etiology.

References

Akhan O, Pringot J (2002) Imaging of abdominal tuberculosis. Eur Radiol 12:312–323

Al Karawi MA, Mohamed AE, Yasawy MI et al (1995) Protean manifestation of gastrointestinal tuberculosis: report on 130 patients. J Clin Gastroenterol 20:225–232

Alvarez SZ (1998) Hepatobiliary tuberculosis. J Gastroenterol Hepatol 13:833–839

Amarapurkar DN, Patel ND, Amrapurkar AD (2008) Hepatobiliary tuberculosis in Western India. Indian J Pathol Microbiol 51:175–181

Batra A, Gulati MS, Sarma D et al (2000) Sonographic appearances in abdominal tuberculosis. J Clin Ultrasound 28:233–245

Centers for Disease Control and Prevention (2019) Tuberculosis in the United States. www.cdc.gov/tb/statistics/surv/surv2019/default.htm

Chablou M, Jabi R, Id M'barek A et al (2021) Isolated splenic tuberculosis in an immunocompetent patient: a rare case. Cures 13(2):e13463. https://doi.org/10.7759/cureus.13463

Chaudhary P (2014) Hepatobiliary tuberculosis. Ann Gastroenterol 27:207–211

Chong VH (2008) Hepatobiliary tuberculosis: a review of clinical presentations and outcomes. South Med J 101:356–361

Debi U, Ravisankar V, Prasad KK et al (2014) Abdominal tuberculosis of the gastrointestinal tract: revisited. World J Gastroenterol 20:14831–14840

Demir K, Okten A, Kaymakoglu S et al (2001) Tuberculous peritonitis—reports of 26 cases, detailing diagnostic and therapeutic problems. Eur J Gastroenterol Hepatol 13:581–585

Dorfman RE, Alpern MB, Gross BH et al (1991) Upper abdominal lymph nodes: criteria for normal size determined with CT. Radiology 180:319–322

Evans RP, Mourad MM, Dvorkin L et al (2016) Hepatic and intra-abdominal tuberculosis: 2016 update. Curr Infect Dis Rep 18(12):45. https://doi.org/10.1007/s11908-016-0546-5

Ghazinoor S, Desser T, Jeffrey RB (2004) Increased through-transmission in abdominal tuberculous lymphadenitis. J Ultrasound Med 23:837–841

Griesel R, Cohen K, Mendelson M et al (2019) Abdominal ultrasound for the diagnosis of tuberculosis among human immunodeficiency virus-positive inpatients with World Health Organization danger signs. Open Forum Infect Dis 6(4):ofz094. https://doi.org/10.1093/ofid/ofz094

Gulati MS, Sarma D, Paul SB (1999) CT appearance in abdominal tuberculosis. A pictorial essay. Clin Imaging 23:51–59

Gupta P, Kumar S, Sharma V et al (2019) Common and uncommon imaging features of abdominal tuberculosis. J Med Imaging Radiat Oncol 63:329–339

Ha HK, Jung JI, Lee MS et al (1996) CT differentiation of tuberculous peritonitis and peritoneal carcinomatosis. AJR Am J Roentgenol 167:743–748

Heller T, Goblirsch S, Wallrauch C et al (2010) Abdominal tuberculosis: sonographic diagnosis and treatment response in HIV-positive adults in rural South Africa. Int J Infect Dis 14(Suppl 3(6)):e108–e112

Herzog BH (1998) History of tuberculosis. Respiration 65:5–15

Jain N, Rissam HK, Puri SK et al (2016) The 'frosted liver' appearance in hepatic tuberculosis. A rare presentation. BJR Case Rep 2:20150367

Joshi AR, Basantani AS, Patel TC (2014) Role of CT and MRI in abdominal tuberculosis. Curr Radiol Rep 2:66. https://doi.org/10.1007/s40134-014-0066-8

Joyati Tarafder A, Mahtab MA, Ranjan Das S et al (2015) Abdominal tuberculosis: a diagnostic dilemma. Euroasian J Hepatogastroenterol 5:57–59

Kakkar C, Polnaya AM, Koteshwara P et al (2015) Hepatic tuberculosis: a multimodality imaging review. Insights Imaging 6:647–658

Karaosmanoglu AD, Onur MR, Sahani DV et al (2016) Hepatobiliary tuberculosis: imaging findings. AJR Am J Roentgenol 207:694–704

Karaosmanoglu AD, Uysal A, Onder O et al (2021) Cross-sectional imaging findings of splenic infections: is differential diagnosis possible? Abdom Radiol (NY) 28:1–25

Leder RA, Low VH (1995) Tuberculosis of the abdomen. Radiol Clin North Am 33:691–705

Lee DH, Lim JH, Ko YT et al (1991) Sonographic findings in tuberculous peritonitis of wet-ascitic type. Clin Radiol 44:306–310

Lin SF, Zheng L, Zhou L (2016) Solitary splenic tuberculosis: a case report and review of the literature. World J Surg Oncol 14:154–157

McMullan GS, Lewis JH (2017) Tuberculosis of the liver, biliary tract, and pancreas. Microbiol Spectr 5(1). https://doi.org/10.1128/microbiolspec.TNMI7-0025-2016

Mehmood A, Ehsan A, Mukhtar M et al (2019) Acute mesenteric tuberculous lymphadenitis: a comparative analysis of twenty-one cases. Cureus 11(4):e4454. https://doi.org/10.7759/cureus

Morón FE, Szklaruk J (2007) Learning the nodal stations in the abdomen. Br J Radiol 80:841–848

Munker R, Stengel A, Stäbler A et al (1995) Diagnostic accuracy of ultrasound and computed tomography in the staging of Hodgkin's disease: verification by laparotomy in 100 cases. Cancer 76:1460–1466

Nagar AM, Raut AA, Morani AC et al (2009) Pancreatic tuberculosis: a clinical and imaging review of 32 cases. J Comput Assist Tomogr 33:136–141

Pai M, Behr MA, Dowdy D et al (2016) Tuberculosis. Nat Rev Dis Primers 2:16076. https://doi.org/10.1038/nrdp.2016.76

Pereira JM, Madureira AJ, Vieira A et al (2005) Abdominal tuberculosis. imaging features. Eur J Radiol 55:173–180

Prasad S, Patankar T (1999) Computed tomography demonstration of a fat-fluid level in tuberculous chylous ascites. Australas Radiol 43:542–543

Pombo F, DiazCandamio M, Rodriguez E et al (1998) Pancreatic tuberculosis: CT findings. Abdom Imaging 23:394–397

Rastogi R (2008) Abdominal cocoon secondary to tuberculosis. Saudi J Gastroenterol 14:139–141

Titton RL, Gervais DA, Hahn PF et al (2003) Urine leaks and urinomas: diagnosis and imaging-guided intervention. Radiographics 23:1133–1147

Salvador F, Los-Arcos I, Sánchez-Montalvá A et al (2015) Epidemiology and diagnosis of tuberculous lymphadenitis in a tuberculosis low-burden country. Medicine (Baltimore) 94:e509

Sanai FM, Bzeizi KI (2005) Systematic review: tuberculous peritonitis—presenting features, diagnostic strategies and treatment. Aliment Pharmacol Ther 22:685–700

Sathekge M, Maes A, Van der Wiele C (2013) FDG PET imaging in HIV infection and tuberculosis. Semin Nucl Med 43:349–366

Sharma D, Nair RP, Dani T et al (2013) Abdominal cocoon: a rare cause of intestinal obstruction. Int J Surg Case Rep 4:955–957

Sharma V, Bhatia A, Malik S et al (2017) Visceral scalloping on abdominal computed tomography due to abdominal tuberculosis. Ther Adv Infect Dis 4:3–9

Sharma V, Rana SS, Kumar AA et al (2016) Pancreatic tuberculosis. J Gastroenterol Hepatol 31:310–318

Shim SW, Shin SH, Kwon WJ et al (2017) CT differentiation of female peritoneal tuberculosis and peritoneal carcinomatosis from normal-sized ovarian cancer. J Comput Assist Tomogr 41:32–38

Vanhoenacker FM, De Backer AI, de Beeck BO et al (2004) Imaging of gastrointestinal and abdominal tuberculosis. Eur Radiol 14(Suppl 3):E103–E115

Weber SF, Saravu K, Heller T et al (2018) Point-of-care ultrasound for extrapulmonary tuberculosis in India:

a prospective cohort study in HIV-positive and HIV-negative presumptive tuberculosis patients. Am J Trop Med Hyg 98:266–273

Woodfield JC, Windsor JA, Godfrey CC et al (2004) Diagnosis and management of isolated pancreatic tuberculosis: recent experience and literature review. ANZ J Surg 74:368–371

World Health Organization (2021) Global tuberculosis report 2021. World Health Organization, Geneva. www.who.int/teams/global-tuberculosis-programme/tb-reports/global-tuberculosis-report-2021

Xu XF, Yu RS, Qiu LL et al (2011) Gallbladder tuberculosis: CT findings with histopathologic correlation. Korean J Radiol 12:196–202

Imaging of Gastrointestinal Tuberculosis

Nidhi Prabhakar and Naveen Kalra

Contents

Abstract

Gastrointestinal tuberculosis may manifest as an isolated disease or may occur as a part of disseminated disease. The most commonly afflicted region is the ileocecal junction, followed by the ascending colon, jejunum, appendix, duodenum, stomach, sigmoid colon, and rectum. As gastrointestinal tuberculosis has a wide spectrum of imaging features, knowledge of these imaging appearances on various imaging modalities enables the early diagnosis of tuberculosis in the appropriate clinical settings. Involvement of the ileocecal region with concomitant bowel lesions and necrotic lymphadenopathy is diagnostic of tuberculosis. Isolated involvement of the colon, stomach, duodenum, esophagus, and anorectum is rare; hence, the diagnosis requires a high degree of clinical suspicion. The role of the radiologist is in timely recognition of the imaging features of tuberculosis, so that further strategies can be planned to confirm the diagnosis and/or start appropriate anti-tuberculosis treatment.

Abbreviations

CT	Computed tomography
GI	Gastrointestinal
MRI	Magnetic resonance imaging
TB	Tuberculosis
US	Ultrasound

N. Prabhakar · N. Kalra (✉)
Department of Radiodiagnosis, Post Graduate Institute of Medical Education and Research, Chandigarh, India
e-mail: nidhirajpalprabhakar@gmail.com; naval2004@yahoo.com

© The Author(s), under exclusive license to Springer Nature Switzerland AG 2022

M. F. Ladeb, W. C. G. Peh (eds.), *Imaging of Tuberculosis*, Medical Radiology Diagnostic Imaging,
https://doi.org/10.1007/978-3-031-07040-2_10

1 Introduction

Abdominal tuberculosis (TB) is the sixth most common location of extrapulmonary TB, after lymph node, urogenital, bone, miliary, and central nervous system TB (Malikowski et al. 2018). Abdominal TB encompasses the gastrointestinal (GI) tract, peritoneum, and associated viscera. GI TB can manifest as an isolated disease or may occur as a part of disseminated disease. In the GI system, the ileocecal junction is the most common site affected by TB, followed by the ascending colon, jejunum, appendix, duodenum, stomach, sigmoid colon, and rectum (Kim et al. 2018). In this chapter, we focus on the pathogenesis and imaging features of GI TB, particularly of the ileocecal region. Abdominal solid organ and peritoneal TB has been addressed in the preceding chapter.

2 Pathophysiology

GI TB is caused by the pathogenic bacteria *Mycobacterium tuberculosis*. The possible routes of infection are direct infection of mucosa through swallowed respiratory tract secretions, hematogenous spread, extension from neighboring infected viscera and lymph nodes, or uncommonly through ingestion of contaminated dairy products (Ma et al. 2019; Zhu et al. 2020). These bacteria invade through the epithelium of the GI tract and into the submucosa. The areas within the GI tract which have more lymphoid tissue and M cells, such as the ileum, are more susceptible. In addition to the pathological involvement of the bowel wall, the vessels of the mesentery are also involved. Microscopic examination shows granulomatous inflammation within the arterial wall and arterial thrombosis. Ischemia exacerbates the damage initiated by localized granulomatous inflammation. Complications of GI TB include obstruction, perforation, formation of fistulae and perianal fistulae, and hemorrhage (Lee et al. 2012; Debi et al. 2014).

3 Role of Imaging

Imaging plays an important role in indicating the diagnosis of GI TB. If the radiological findings are suggestive of TB, confirmatory diagnosis is usually achieved by endoscopy and biopsy. Imaging not only helps in the diagnosis of TB, but is also used to evaluate the extent of disease. It has a crucial role in diagnosing the complications of GI TB, which include obstruction, bleeding, and perforation. After commencement of treatment, imaging helps assess the treatment response.

4 Ileocecal and Small Bowel Tuberculosis

The ileocecal junction is the most commonly involved site in GI TB, being seen in 64% of patients with GI TB (Bhatt et al. 2017). Infected patients present clinically with protean colicky abdominal pain and vomiting. The most common complication is obstruction due to mural thickening, stricture, and edematous bowel. Patients can also present with perforation (Debi et al. 2014). The ileocecal junction is more commonly involved because of stasis in this area, presence of abundant lymphoid tissue in the bowel wall, increased rate of absorption, and closer contact of bacilli with the mucosa (Prakash 2009). The imaging features reflect the pathological findings. The pathological forms of GI TB can be hypertrophic (10%), ulcero-proliferative (30%), or ulcerative (60%) (Bhatt et al. 2017). The ulcerative form manifests as circumferential transverse ulcers, and the ulcero-proliferative form shows inflammatory pseudotumor formation along with ulcerative thickening of the intestinal wall. The hypertrophic form presents with scarring, fibrosis, and pseudotumor formation and is most commonly seen in the ileocecal region.

4.1 Abdominal Radiography

The role of abdominal radiographs in emergency situations is for the primary evaluation of suspected cases of intestinal obstruction or perforation, which are known complications in patients with GI TB. Radiographical findings of TB include enteroliths, calcified granulomas, abdominal calcified lymph nodes, and hepatosplenomegaly (Nagi et al. 2004). Dilated bowel loops with multiple air–fluid levels are a feature in

patients with intestinal obstruction. The presence of air under the diaphragm is seen in cases of perforation. Intussusception can be sometimes detected on abdominal radiographs as a soft tissue mass, proximal to which dilated bowel loops are seen. The specific signs of intussusception are the "target" and "meniscus" signs. The "target" sign is seen as a circular lucency within the soft tissue representing the fat of the intussusceptum, while the "meniscus" sign is seen as a crescent of air outlining the intussusceptum.

4.2 Barium Studies

The barium meal and follow-through study (BMFT) is important for the early diagnosis of small bowel TB. Barium enema can also be used concomitantly for the evaluation of the cecum and ileocecal junction, as well as for colonic TB. The advantages of barium studies are that they provide physiological information about the flow of food in the GI tract, transit time, and presence of motility disorders. The disadvantages are that they are lengthy procedures, with less sensitivity due to poor distensibility and overlapping of bowel segments. Miller and Sellink introduced barium enteroclysis in 1979, which has better sensitivity compared to BMFT, as intubation of the jejunum by a nasogastric tube leads to better small bowel distension (Miller and Sellink 1979). It is relatively fast to perform, and the mucosal abnormalities, particularly the smaller lesions, are better visualized. It is especially useful in patients with subacute intestinal obstruction, as it can detect partial or incomplete strictures.

The barium study findings correspond to the pathological stages (Prakash 2009). The first stage, which is due to the superficial invasion of the mucosa, is seen as accelerated intestinal transit time or spasmodic contractions of the intestine on the barium study. Disturbances in tone and peristaltic contractions lead to hypersegmentation of the barium column. Disturbances in secretions also result in flocculation or dilution of the barium suspension. There can be changes in the contours of the intestine, which may be irregular, crenated, or spiculated. The small bowel may show soft and thick folds, or hypermobility with edema of the ileocecal valve.

The second stage is seen as ulceration in the small bowel on the barium study. Ulcers can be stellate or linear in shape. Barium specks surrounded by thick or converging folds can be seen in stellate ulcers. Linear ulcers are perpendicular to the long axis. The third stage manifests as hypertrophy. Penetrating ulcers cause short, hourglass-like strictures. Multiple circumferential strictures with multifocal areas of bowel dilatation may also occur. Fixity, spiculation, and hyper- or hypomotility of bowel loops may be seen (Prakash 2009). The cecum becomes contracted, conical, and pulled upwards out of the iliac fossa, due to contraction of the mesocolon (Fig. 1).

The signs of ileocecal TB described on barium studies include the Fleischner or "inverted umbrella" sign, "gooseneck deformity," "purse-string" stenosis, Stierlin sign, and string sign.

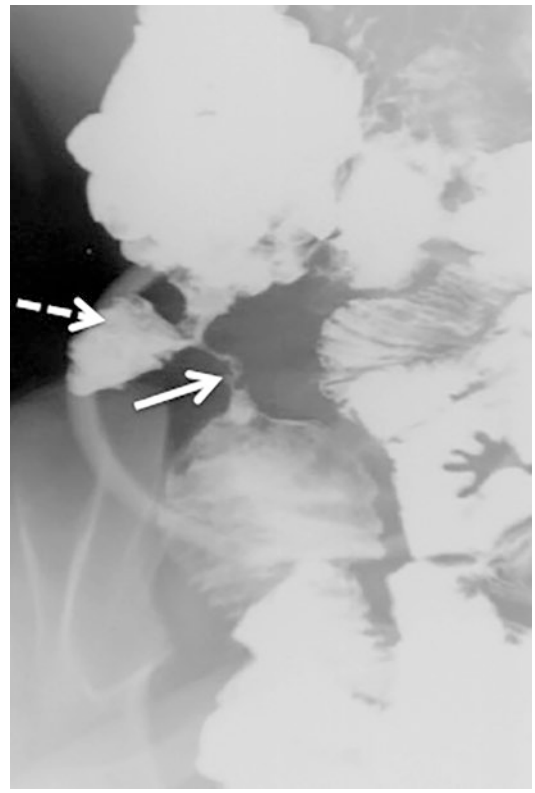

Fig. 1 46-year-old man who presented with clinical features of intestinal obstruction. Barium meal follow-through image shows luminal narrowing of the terminal ileum and ileocecal junction (solid arrow). The cecum is also contracted and distorted in shape (dashed arrow). Features are typical of ileocecal tuberculosis

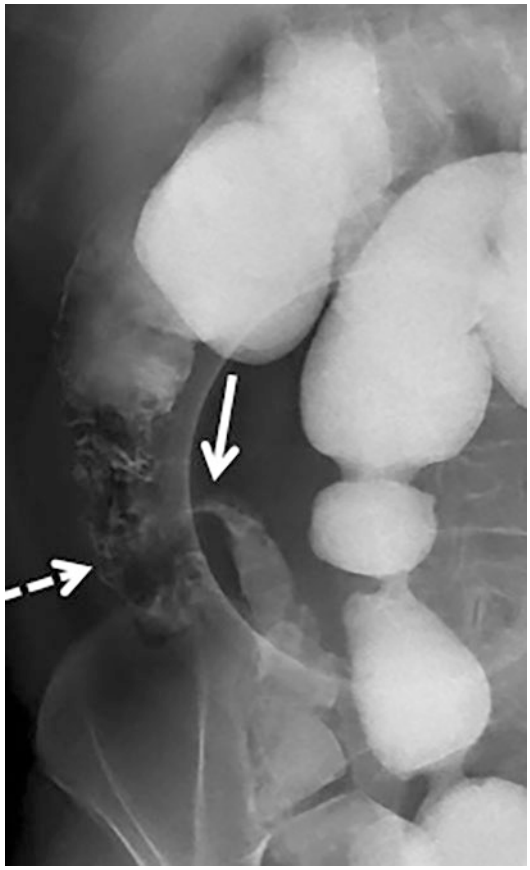

Fig. 2 56-year-old man, known case of abdominal tuberculosis, who presented with clinical features of intestinal obstruction. Barium meal follow-through image shows a contracted and distorted cecum (dashed arrow) with narrowing of ileocecal junction and dilated terminal ileum, with resultant "gooseneck" deformity (solid arrow)

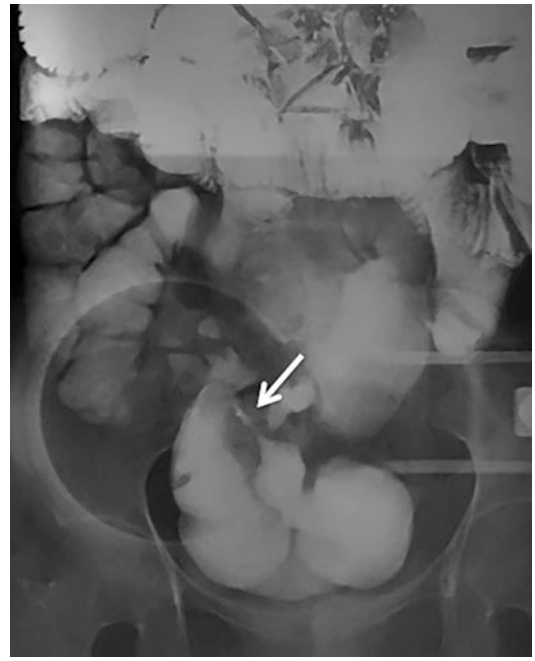

Fig. 3 36-year-old woman who had clinical features of intestinal obstruction. Barium enteroclysis image shows multiple segmental strictures in the small bowel loops due to intestinal tuberculosis. The "string sign" (arrow) is seen as a persistent area of luminal narrowing with dilated bowel loops proximal and distal to it

The Fleischner or "inverted umbrella" sign is present when a thick ileocecal valve which is gaping, together with associated narrowing of the terminal ileum, is seen. The "gooseneck" deformity occurs when there is loss of the normal ileocecal angle, dilated terminal ileum, and retracted fibrosed caecum (Fig. 2). "Purse-string" stenosis is due to localized stenosis at the ileocecal valve, with a round smooth cecum and dilated terminal ileum. The Stierlin sign is due to acute-on-chronic inflammation and is seen as lack of barium retention in the inflamed segments of ileum, cecum, and variable length of ascending colon, with normal column of barium on either side. The string sign is seen as a persistent narrow stream of barium due to bowel stenosis (Fig. 3). Barium enteroclysis is more sensitive than BMFT for demonstrating the findings of small bowel TB. Barium enteroclysis followed by barium enema may be the best protocol for the early detection of ileocecal TB (Debi et al. 2014).

4.3 Ultrasound Imaging

The advantages of abdominal ultrasound (US) imaging are that it is readily available, does not involve ionizing radiation, and can be done at the bedside of the patient. Although it cannot evaluate the intestinal findings of TB as well as barium studies, it is useful for assessing extraluminal abnormalities such as necrotic lymph nodes, peritoneal thickening, and ascites (Fig. 4). Moreover, it can diagnose possible complications

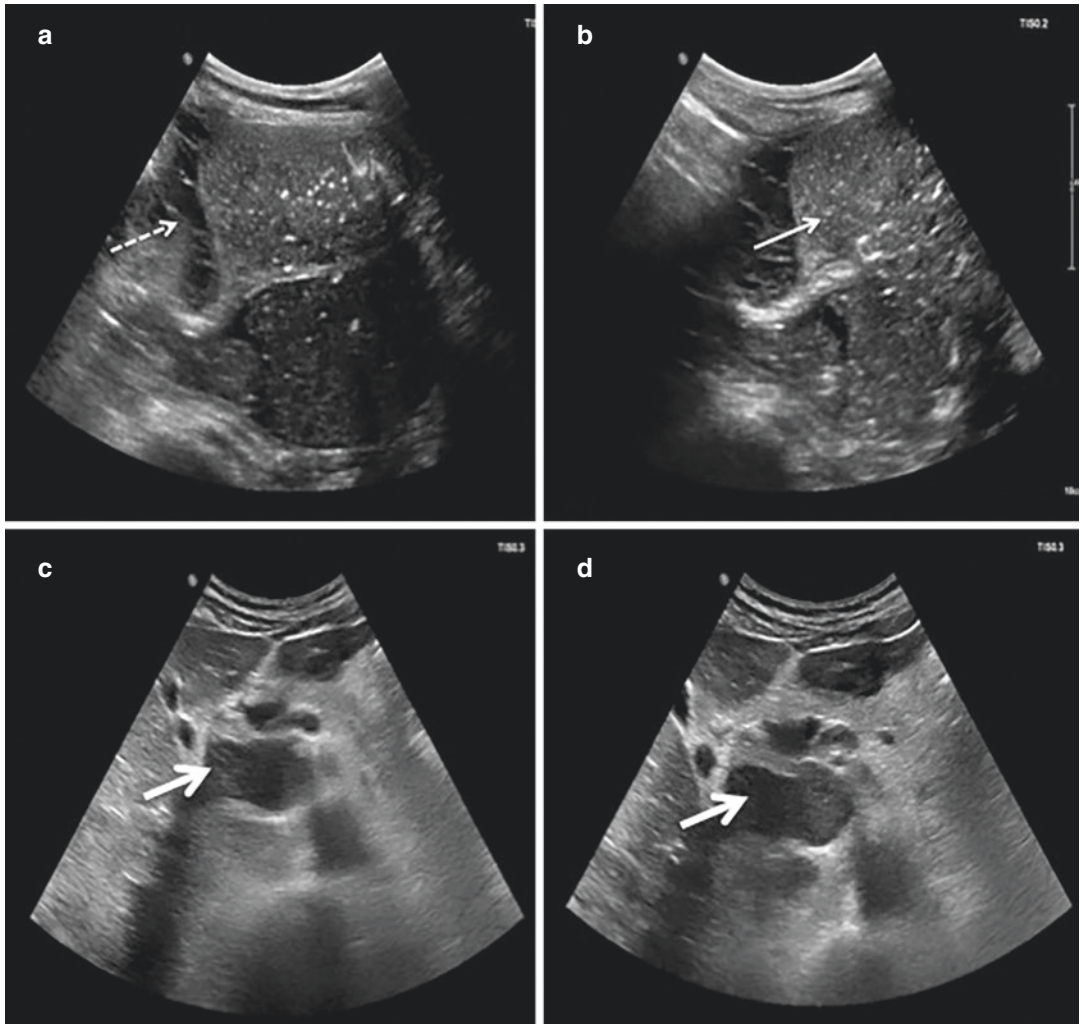

Fig. 4 23-year-old woman who presented with symptoms of obstipation. (**a** and **b**) US images of the abdomen show multiple dilated small bowel loops (thin solid arrow) with echogenic contents showing "to-and-fro" movements, and septated ascites (dashed arrow). (**c** and **d**) US images of the upper abdomen show multiple enlarged necrotic periportal lymph nodes (thick solid arrows). The patient underwent explorative laparotomy and was found to have a distal ileal stricture, which was resected. Histopathology confirmed tuberculosis

of TB such as obstruction and perforation. The disadvantage is that the findings are subjective, with much interobserver differences. Endoluminal US imaging is being used more commonly and helps in clearer visualization of intestinal wall abnormalities. More recently, contrast-enhanced US imaging has been found to be useful in evaluating patients with TB. Nagi et al. (2006) described the technique of sonoenteroclysis, in which US imaging is done after injection of isotonic nonabsorbable electrolyte solution with polyethylene glycol through a nasogastric tube, which is placed to the level of the jejunum. The small bowel lesions are visualized with greater clarity because of better distension, with findings comparable to barium enteroclysis (Nagi et al. 2006).

The early changes of small bowel TB are not visible on US imaging. However, a deep ulcer can be seen as the extension of echogenic

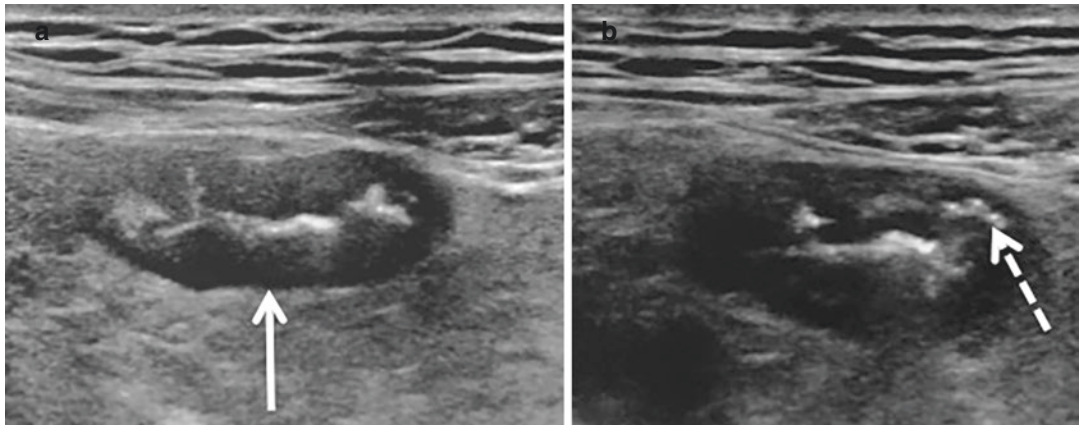

Fig. 5 36-year-old woman who was diagnosed with intestinal tuberculosis. US images show (**a**) circumferential mural thickening of the distal ileal loops producing the "pseudokidney" sign (solid arrow) and (**b**) a deep ulcer seen as extension of echogenic foci into the bowel wall (dashed arrow)

material into the wall. Hyperplastic ileocecal TB can be seen on US imaging as asymmetrical thickening of cecum and ileocecal valve. The "pseudokidney" sign may be seen when ileocecal wall thickening is present in a subhepatic location (Fig. 5). It is difficult to evaluate jejunal and ileal involvement because of the overlapping bowel loops. In cases of obstruction, however, thick-walled and short strictures may be seen, proximal to which bowel loops are dilated and show abnormal peristaltic movements. Associated peritoneal findings that can be seen on US imaging include necrotic lymph nodes, ascites, and omental thickening. Sometimes, free intraperitoneal air can be detected, indicating perforation. US imaging can be used for the follow-up of patients who are on anti-TB treatment to check for resolution of the disease. Contrast-enhanced US imaging findings in bowel TB are type 1 enhancement when the serosa enhances first and mucosa enhances gradually and type 2 enhancement when the whole bowel shows diffuse and quick enhancement (Yang et al. 2015).

4.4 Computed Tomography

As computed tomography (CT) is a cross-sectional imaging modality, it provides information about not only the bowel lumen, but also the extraintestinal abnormalities. The presence of extraintestinal abnormalities helps in arriving at a confident diagnosis of TB, when the intestinal findings are equivocal. The other benefits of CT are that the whole bowel can be visualized in one single examination, the complete extent of disease can be evaluated, and the associated complications can be diagnosed. CT is also more objective, the information provided is more reliable, and there are fewer interobserver differences. In addition, most patients tolerate CT better than barium studies.

CT is the modality of choice for evaluation of suspected cases of complications such as perforation and obstruction, because of its greater spatial resolution and the speed of acquisition (Figs. 6 and 7). Another advantage is the capability to generate multiplanar reformatted images, which help in visualizing the entire bowel in different planes. Intravenous iodinated contrast agent is administered to differentiate abnormal infected segments of bowel from normal segments. A water-soluble contrast agent can also be given orally in specific cases to facilitate the differentiation of distended bowel segments from intra-abdominal collections and to evaluate the site of perforation. The disadvantages of CT are that it cannot provide detailed evaluation of intraluminal and mucosal abnormalities, which are better seen on barium studies and endoscopy.

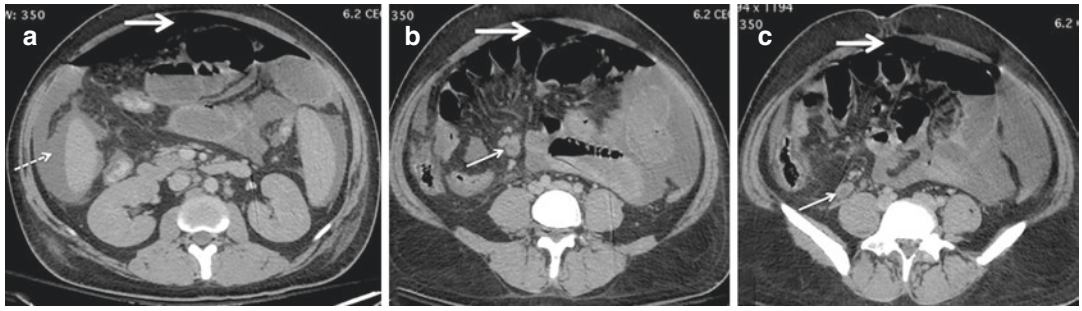

Fig. 6 26-year-old man who presented with acute abdominal pain. (**a–c**) Axial contrast-enhanced CT images show free air in the nondependent part of the peritoneal cavity (thick solid arrows). Moderate ascites (dashed arrow) and multiple enlarged mesenteric lymph nodes are seen, a few of which are necrotic (thin solid arrows). The patient underwent explorative laparotomy, with resection of the perforated ileal segment and end ileostomy. Histopathology confirmed ileal tuberculosis

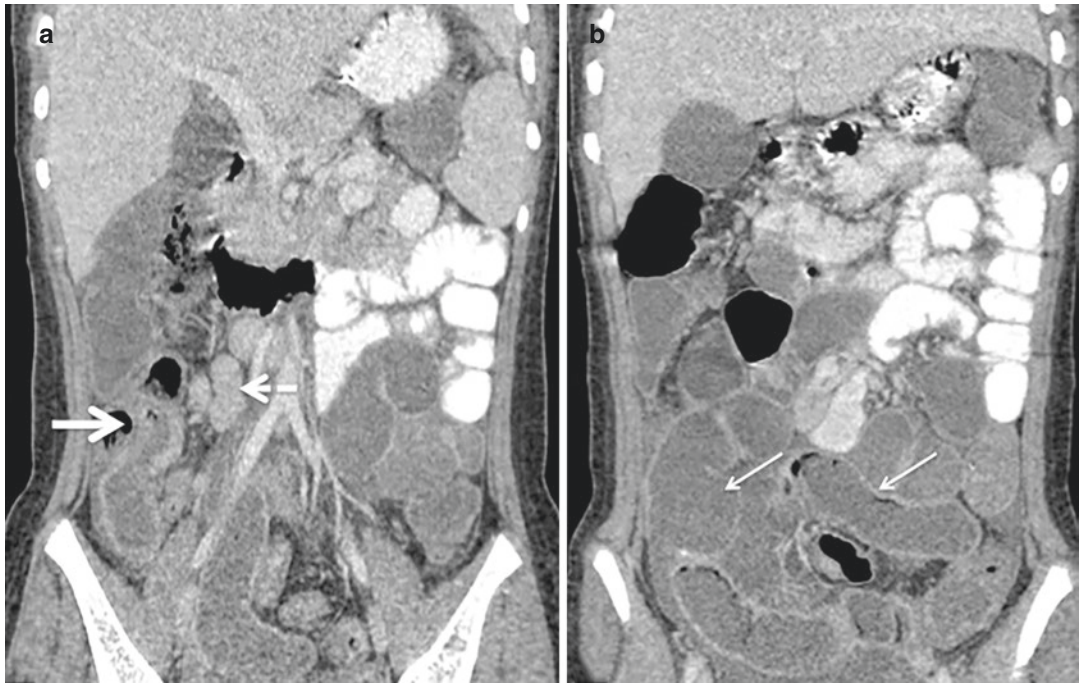

Fig. 7 13-year-old girl who presented with abdominal distension, pain, and constipation. (**a** and **b**) Coronal contrast-enhanced CT images show a long segment of mural thickening involving the distal ileal loop, ileocecal junction, and cecum (thick solid arrow). Dilated small bowel loops (thin solid arrows) are seen. Multiple enlarged lymph nodes are present in the ileocolic mesentery (dashed arrow)

CT shows thickening of the ileocecal valve, terminal ileum, and cecum in patients with ileocecal TB. Ileocecal junction abnormalities, together with the involvement of the cecum and ileum, are highly suggestive of TB (Fig. 8). Mural wall thickening can be as much as 3 cm in the cecum and terminal ileum. Mild circumferential bowel thickening in the early stages, and severe and asymmetrical wall thickening in late stages, may be seen in the ileocecal region. Sometimes, thickening is limited to the ileocecal valve and medial wall of the cecum. The ileocecal junction

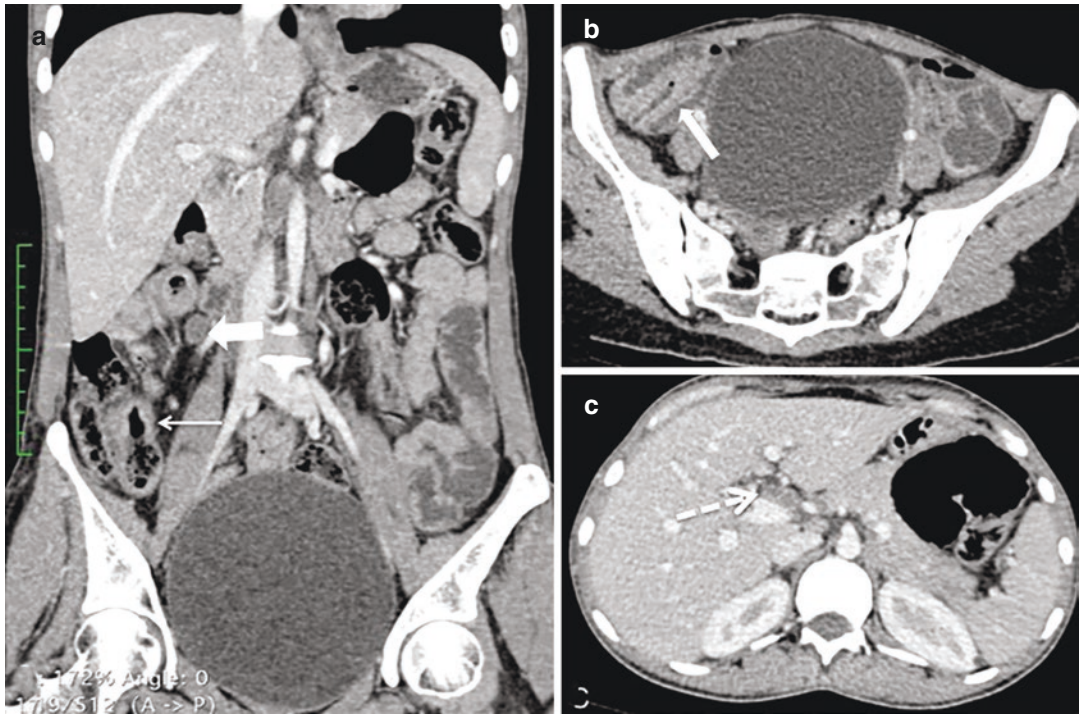

Fig. 8 27-year-old woman who presented with abdominal pain and loss of appetite for 2 months. (**a**) Coronal contrast-enhanced CT image shows smooth circumferential thickening of the distal ileum and ileocecal junction (thin solid arrow). Enlarged necrotic ileocolic lymph nodes are seen (thick solid arrow). (**b**) Axial contrast-enhanced CT image of the pelvis shows smooth circumferential thickening of the distal ileal loops (solid arrow). (**c**) Axial contrast-enhanced CT image of the upper abdomen shows necrotic periportal lymph nodes (dashed arrow)

can also display abnormal position and angulation. On CT, a small bowel lesion with concurrent ileocecal involvement strongly suggests the diagnosis of TB. However, small bowel involvement without involvement of ileocecal region may also be seen. CT may show skip lesions of concentric mural thickening and enhancement, with associated luminal narrowing in the small bowel, with or without proximal dilatation. The ileum is more frequently involved, compared to the jejunum.

Concomitant jejunal and ileal involvement may be seen in the form of multiple short or long strictures. Wall thickening is usually homogeneous with no stratification. Strictures can lead to obstruction and proximal dilatation. Perforation of bowel can occur, leading to ascites and air in the peritoneal cavity. CT can demonstrate the site of obstruction or perforation. CT may also show fistula formation, which is another known complication of TB. Active bowel disease is seen as areas of enhancement and thickening, while lack of enhancement indicates fibrosis.

The most important advantage of CT is that it can show extraintestinal findings in patients with TB. Disease activity also correlates with peritoneal changes, including excessive fat stranding, ascites, and increased vascularity (Bhatt et al. 2017) (Fig. 9). CT also shows enlarged enhancing lymph nodes in the mesentery, with 30–60% having a necrotic center in the involved lymph nodes (Bhatt et al. 2017). The periportal and mesenteric lymph nodes are most commonly involved. Peritoneal TB can also lead to bowel involvement. Peritoneal thickening and fat stranding can lead to matting of bowel loops and cocoon formation (Fig. 10). The cocoon, also known as sclerosing encapsulating peritonitis, refers to encapsulation of bowel loops within the fibrocollagenous peritoneal membrane and may lead to intestinal obstruction (Singhal et al. 2019).

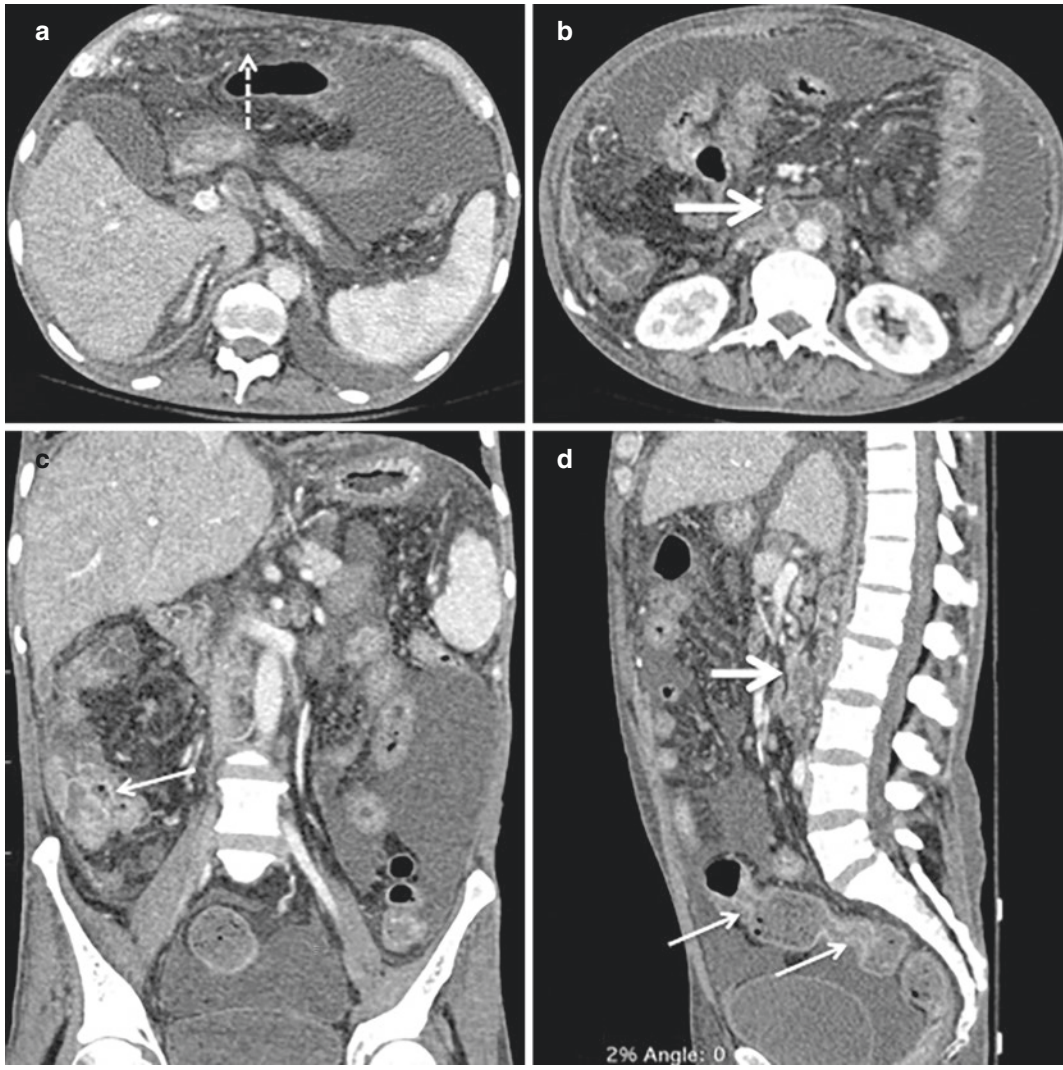

Fig. 9 53-year-old man who presented with clinical features of subacute intestinal obstruction. (**a** and **b**) Axial contrast-enhanced CT images of the abdomen show omental thickening and fat stranding (dashed arrow), gross ascites, and enlarged necrotic retroperitoneal lymph nodes (thick solid arrow). (**c**) Coronal contrast-enhanced CT image shows circumferential wall thickening of terminal ileum and ileocecal junction (thin solid arrow). (**d**) Sagittal contrast-enhanced CT image shows circumferential areas of wall thickening and luminal narrowing in the colon (thin solid arrows) and necrotic, matted, and enlarged retroperitoneal lymph nodes (thick solid arrow). The patient was confirmed to have abdominal tuberculosis on peritoneal fluid analysis

In addition to peritoneal involvement, solid organs, such as the liver and spleen, can show enlargement and hypodense lesions if they are involved. In the chronic stage of the disease, a contracted and distorted cecum of small caliber, which may be pulled up, may be seen. The fibrotic cecum will not show significant mural thickening. A patulous ileocecal valve and loss of ileocecal junction angulation are other findings. Fibrotic strictures of the ileocecal region and small bowel may lead to recurrent episodes of obstruction. Calcified bowel wall, calcified lymphadenopathy, and calcified granulomas in the liver and spleen are other sequelae of abdominal TB.

CT enterography is an improvement over the traditional CT techniques for evaluation of the

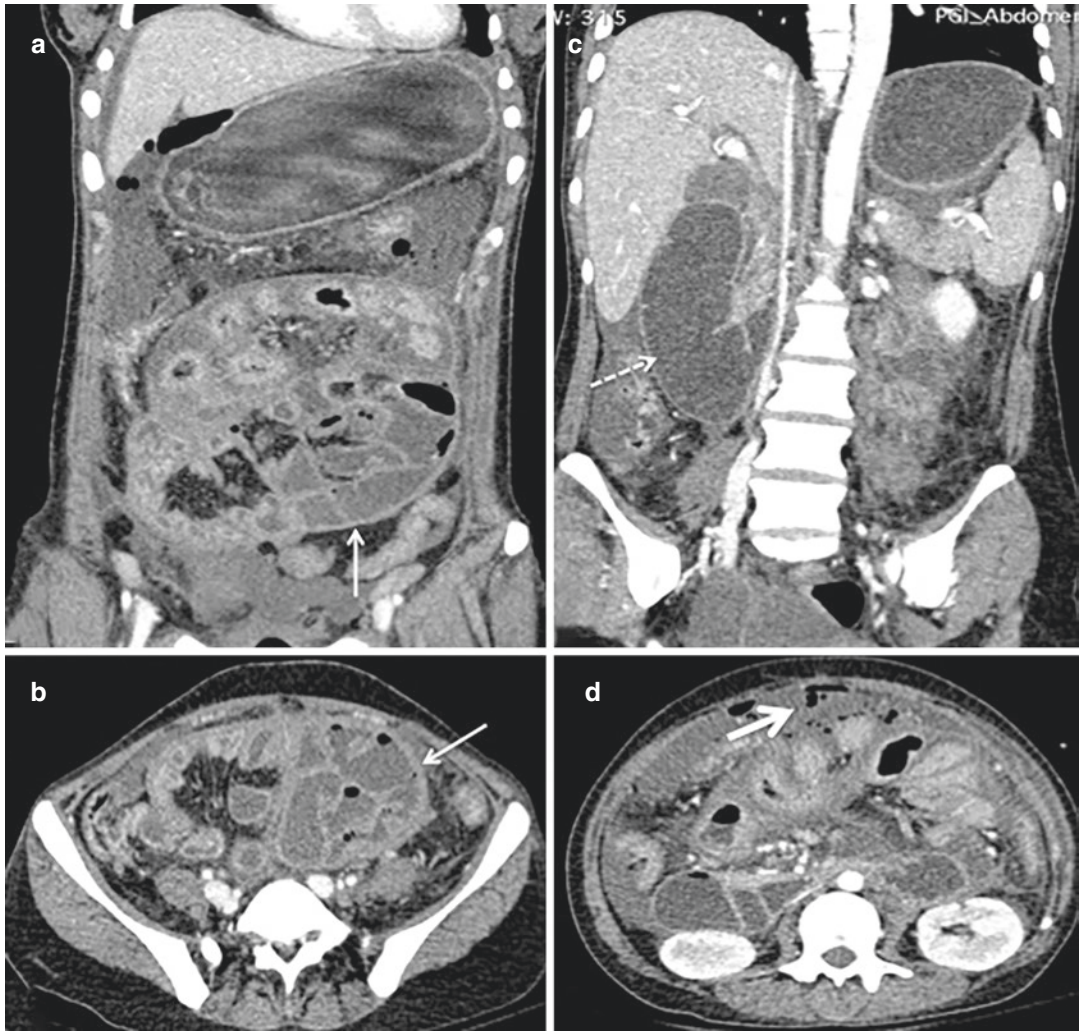

Fig. 10 31-year-old woman, a known case of abdominal tuberculosis on anti-tuberculosis treatment, who presented with abdominal distension and nonpassage of stools. (**a**) Coronal and (**b**) axial contrast-enhanced CT images show peritoneal thickening and "cocoon" (sclerosing encapsulating peritonitis) formation (thin solid arrows), leading to encapsulation of jejunal and ileal bowel loops. Moderate ascites is also present. (**c**) Coronal contrast-enhanced CT image shows a dilated duodenum (dashed arrow) consistent with intestinal obstruction. (**d**) Axial contrast-enhanced CT image shows free air in the peritoneal cavity (thick solid arrow) due to associated bowel perforation

small bowel. It involves ingestion of 1,500–2000 ml of neutral or low-density contrast material over 45–60 min, which enables good small bowel distension, allowing better visualization of wall and intraluminal abnormalities. Water–methylcellulose solution, polyethylene glycol, and low-density barium are some of the oral contrast agents which can be used for CT enterography. CT enterography helps in diagnosing incomplete or partial structure, which may lead to episodes of subacute obstruction (Kalra et al. 2014; Bhatt et al. 2017). CT enteroclysis involves intubation of the jejunum using a nasogastric tube, followed by injection of hyperosmolar fluid (Dave-Verma et al. 2008; Aiyappan et al. 2012). As the latter causes more discomfort to the patient, CT enterography is preferred to CT enteroclysis. Both methods are equally

useful for the evaluation of subacute obstruction.

Both CT enteroclysis and enterography are more sensitive than barium enteroclysis for detecting multiple strictures, which may be missed on barium examination due to overlapping ileal loops. Early and partial strictures of TB are better visualized due to better distension of small bowel (Figs. 11 and 12). Mild bowel wall thickening and enhancement are also seen with greater clarity. Another very recent advanced technique is virtual CT enteroscopy. In this procedure, the

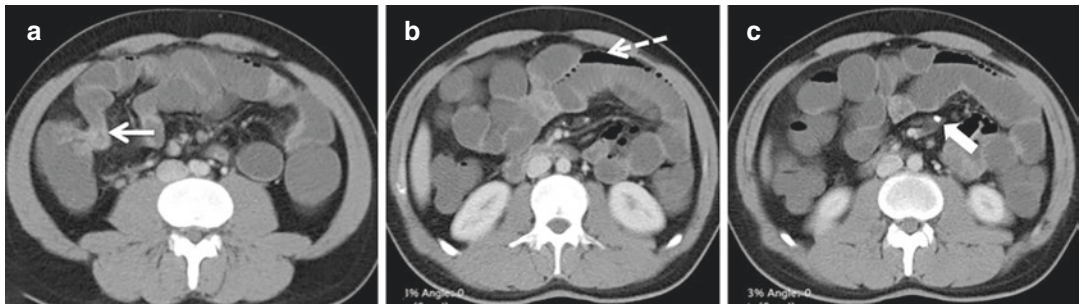

Fig. 11 32-year-old man who presented with recurrent abdominal distension. CT enterography was done after ingestion of 2 L of Peglec solution (an osmotic laxative) by the patient. (**a–c**) Axial CT enterography images show circumferential mural thickening of the terminal ileum and ileocecal junction (thin solid arrow) causing obstruction with dilatation of small bowel loops (dashed arrow). Calcified lymph nodes are seen in the mesentery (thick solid arrow)

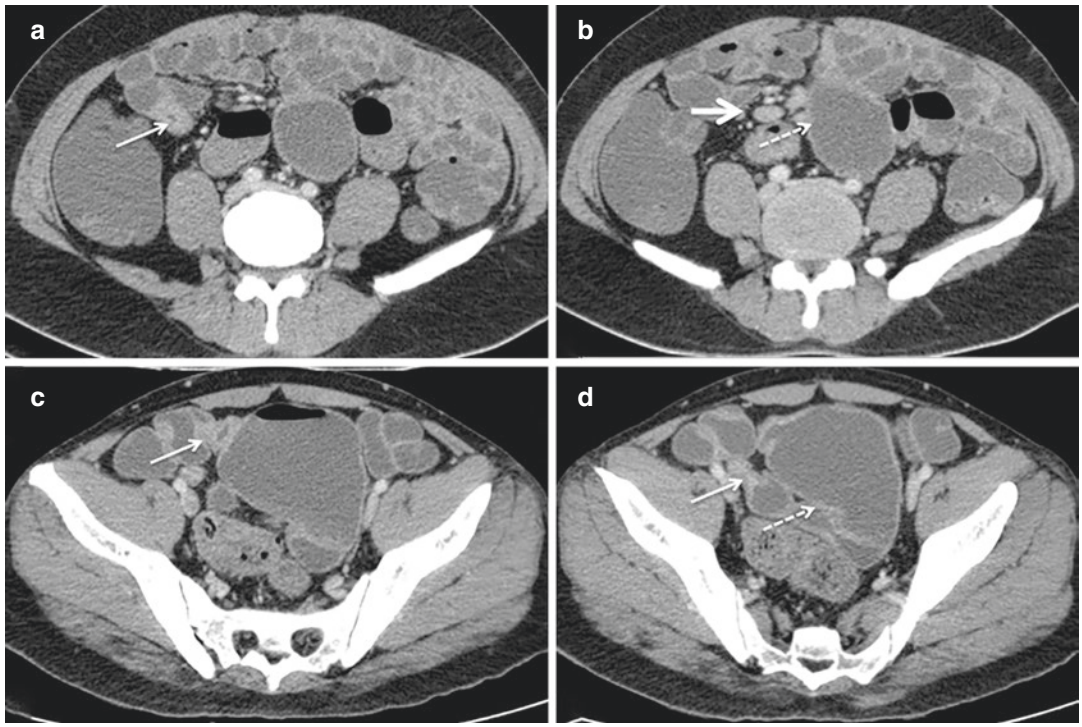

Fig. 12 44-year-old man who presented with iron deficiency anemia. (**a–d**) Axial contrast-enhanced CT enterography images show multiple areas of short-segment circumferential mural thickening and narrowing in the ileal loops (thin solid arrows) with multifocal dilatation of bowel loops (dashed arrows). Enlarged mesenteric lymph nodes are also seen (thick solid arrow)

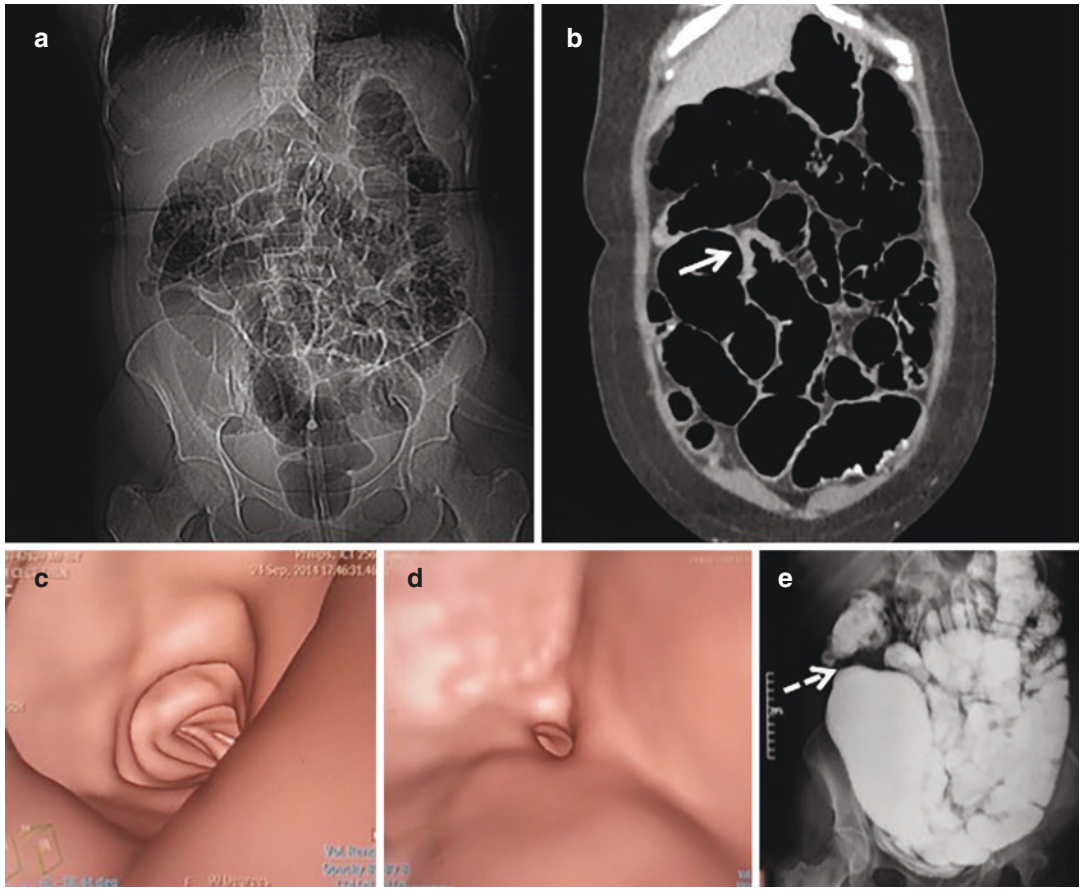

Fig. 13 30-year-old woman who presented with subacute episodes of intestinal obstruction. CT virtual enteroscopy was performed. (**a**) CT scanogram shows the small and large bowel distended with carbon dioxide. (**b**) Coronal contrast-enhanced CT image shows circumferential mural thickening with hyperenhancement of one of the ileal loops (solid arrow). (**c**) CT enteroscopy endoluminal 3D image shows a normal small bowel loop. (**d**) CT enteroscopy endoluminal 3D image shows a stricture in the ileum. (**e**) Small bowel barium enteroclysis image shows a stricture (dashed arrow) in the corresponding ileal loop with dilatation of the proximal bowel

small bowel is cannulated with a nasogastric tube and distended using carbon dioxide. CT is then acquired, and advanced reconstruction software is used to obtain endoluminal images of the small bowel, similar to those obtained in endoscopy (Kalra et al. 2021) (Fig. 13). This leads to better evaluation of intraluminal and mucosal abnormalities of the small bowel.

4.5 Magnetic Resonance Imaging

The main disadvantage of CT is the hazard of ionizing radiation. Patients with abdominal TB may need to undergo repeat imaging in order to evaluate the extent of disease and response to treatment. Magnetic resonance imaging (MRI) is a cross-sectional modality that has no radiation hazard and has better soft tissue contrast compared to CT. Findings which can be seen on MRI include an exophytic soft tissue mass around a narrow segment or a minimally symmetric or asymmetric area of thickening, which is associated with bowel tethering. The involved bowel wall is T1-hypointense and T2-hyperintense and shows heterogeneous enhancement. One of the additional advantages of MRI is that it can differentiate between acute ulcerative and subacute

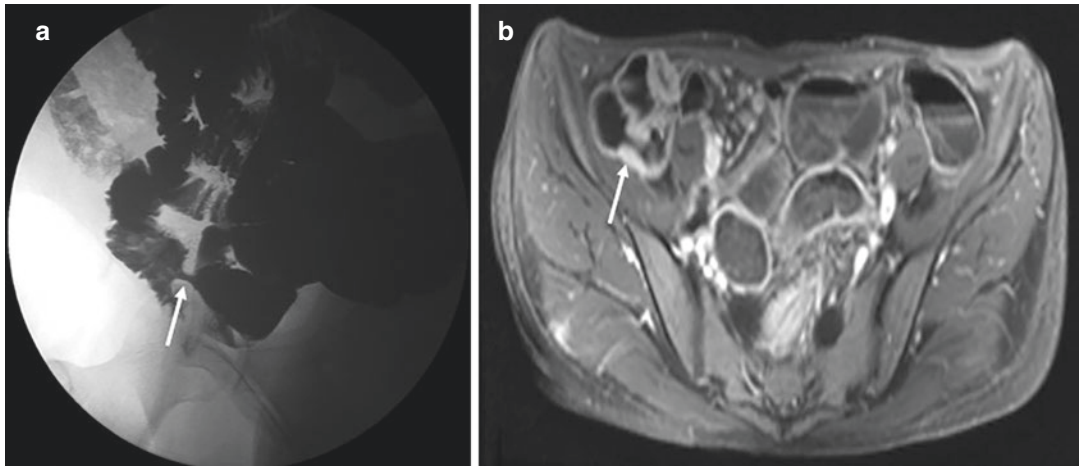

Fig. 14 34-year-old man who presented with recurrent episodes of abdominal distension. (**a**) Barium meal and follow-through image shows a short-segment "hourglass" stricture (arrow) in the ileum. (**b**) MR enterography image shows the corresponding stricture with associated wall thickening and hyperenhancement (arrow)

scarring stages, based on the difference in signal intensity and enhancement patterns (Krishna et al. 2016).

Recent advances in MRI include MR enterography and MR enteroclysis. These advances in MRI techniques lead to better evaluation of intraluminal and wall abnormalities because of better distension. MR enterography has been found to correlate well with BMFT findings (Krishna et al. 2016) (Fig. 14). In addition, similar to CT enterography, MR enterography can provide extraintestinal information together with better soft tissue contrast. MR enterography can become the one-stop radiation-free tool for the evaluation of small bowel TB. Advanced MRI techniques such as diffusion-weighted images can help in assessing the disease activity of intestinal TB. A rise in apparent diffusion coefficient (ADC) values has been found to directly correlate with good response to treatment (Mathur et al. 2019).

4.6 Differential Diagnosis

The imaging differential diagnosis of ileocecal TB includes Crohn disease, lymphoma, carcinoma, and amebiasis. Early tuberculous changes are difficult to differentiate from these clinical entities. However, advanced TB can usually be differentiated on imaging. In lymphoma, there is significantly more bowel wall thickening, as compared to the wall thickening in TB. Secondly, bowel wall thickening in lymphoma does not lead to obstruction. Thirdly, extraintestinal findings such as homogeneously enlarged lymph nodes are seen in lymphoma, while necrotic lymph nodes are seen in TB. Hepatosplenomegaly and small focal lesions in the liver and spleen can occur in both TB and lymphoma.

One important differential diagnosis of small bowel TB is Crohn disease. It is difficult to differentiate ileocecal and small bowel TB from Crohn disease. The presence of skip lesions (>3), long lesions, stratification, asymmetrical thickening, mesenteric fat proliferation, increased mesenteric vascularity, and no necrotic lymph nodes on CT can help in differentiating Crohn disease from TB (Lundstedt et al. 1996; Kedia et al. 2015; Goyal et al. 2019). Amebiasis may show involvement of the cecum, but the terminal ileum is usually not involved. Carcinoma of the cecum will typically not involve the terminal ileum. In addition, it will show predominantly locoregional metastatic lymphadenopathy, vis-à-vis TB, which has infected abdominal lymph nodes which are at a site remote from the ileocecal region (Pereira et al. 2005).

5 Esophageal Tuberculosis

Esophageal TB is rare. It accounts for 2.8% of all cases of GI TB (Prasant et al. 2019). The first case of esophageal TB was diagnosed post-mortem in 1890. The first case of esophageal TB to be diagnosed ante-mortem occurred in 1907. An autopsy series reported secondary involvement of the esophagus in 25 of 16,489 patients who died of TB (Dahale et al. 2018). The modes of spread for esophageal TB are through swallowed sputum, retrograde lymphatic spread, blood-borne spread, and direct spread through mediastinal lymph nodes, tuberculous lung cavity, and tuberculous spondylodiscitis (Pott disease). The mid-esophagus is the most commonly-affected site (Dahale et al. 2018).

Esophageal TB can be primary or secondary. Primary TB involves only the esophagus, without involvement of any other site. Primary esophageal TB is very rare, because of the inherent properties of the esophagus that protect it. These protecting factors include stratified squamous epithelium, esophageal peristalsis, mucus-coated epithelium, saliva, and erect posture (Dahale et al. 2018). Secondary esophageal TB is more common and is caused by secondary involvement of the esophagus through spread from mediastinal, lung parenchymal, or spinal TB. The most common presenting symptom is dysphagia, followed by odynophagia (Dahale et al. 2018). Complications such as esophageal fistula may lead to symptoms such as coughing and dyspnea on swallowing.

Nagi et al. (2003b) evaluated 23 patients with esophageal TB, finding that the chest radiographs were abnormal in 65% of the patients. Chest radiographs may therefore be normal in patients with primary esophageal TB. However, those with secondary esophageal TB may show features of pulmonary and mediastinal TB. Nodules, cavities, and consolidation may be seen on chest radiographs. The barium swallow findings of patients with esophageal TB are extrinsic compression by enlarged lymph nodes, traction diverticula, smooth strictures, mucosal ulcerations, sinus/fistulous tracts, kinking, and pseudotumors. Sinus tracts/fistulous communications with the mediastinum or tracheobronchial tree may be seen (Prakash 2009). Esophageal perforation into the mediastinum may also occur.

The diagnostic modality of choice is CT. Mediastinal lymphadenopathy is seen in most patients with esophageal TB. In patients with primary esophageal TB, CT shows mural thickening of the esophagus with adjacent lymphadenopathy. In secondary esophageal TB, there is secondary involvement of the esophagus from adjacent sites, such as the mediastinum, lung parenchyma, or vertebrae. A feature of mediastinal TB is necrotic lymphadenopathy, while in lung parenchymal TB, cavities, consolidation, and centrilobular or miliary nodules may be seen. CT also assists in diagnosing complications such as fistula, perforation, or stricture. Imaging (including chest radiographs, barium swallow, and CT) also helps in determining the extent of disease. Endoscopy with mucosal biopsy confirms the diagnosis, showing ulcers, elevated lesions, and fistula (Dahale et al. 2018). Endoscopic US imaging shows hypoechoic lesions with indistinct margins, interruption of the five-layer structure, and mediastinal lymphadenopathy (Xiong et al. 2020). The differential diagnosis includes eosinophilic granulomas, Crohn disease, candidiasis, actinomycosis, syphilis, esophageal malignancy, and esophageal injury (Prasant et al. 2019).

6 Gastric Tuberculosis

Gastric TB is usually associated with pulmonary TB. The incidence of gastric TB has been found to be 0.03–0.21% of all routine biopsies (Kim et al. 2018). Gastric involvement occurs in 2% of patients with pulmonary TB (Kim et al. 2018). Gastric TB is rare because of the bactericidal properties of gastric acid, scarcity of lymphoid tissue in gastric wall, and intact mucosa of the stomach wall (Mukhopadhyay et al. 2010; Lv et al. 2020). The most common mode of spread is from adjacent affected lymph nodes. The most frequent location is the pyloric antrum and lesser curvature near the pyloric region, due to increased lymphoid tissue in this location. This area is also common for peptic ulcer disease as this site is prone to mucosal breech, gastritis damage,

erosions, and ecchymosis. Abnormal gastric conditions such as injury, erosion, and/or ulcer in the gastric mucosa, reduction in gastric acid, and delayed gastric emptying increase the time of TB bacilli in the stomach, leading to increased risk of gastric TB. Gastric TB can be primary or secondary. Regardless of whether it is primary or secondary, gastric TB is very rare, though the secondary infection is more common than the primary form (Ma et al. 2019). The clinical presentation is non-specific and includes epigastric pain, vomiting, and weight loss. Sometimes, patients present with gastric outlet obstruction, perforation, and dysphagia.

The barium meal may show ulceration and irregular filling defects in the antral and pyloric regions (Chazan and Aitchison 1960; Guirguis et al. 1983; Zengin et al. 2003). Features of gastric outlet obstruction can be detected on barium studies (Amarapurkar et al. 2003). In addition, gastrocolic fistula formation has also been reported (Nagi et al. 2002). CT is helpful in determining the lesion and its relationship with surrounding structures such as paragastric or abdominal lymph nodes (Fig. 15). Endoscopic US imaging may show a poorly defined gastric wall or a hypoechoic lesion in the submucosa of the stomach wall with irregular boundaries and nonhomogeneous echogenicity. Enlarged para-aortic or abdominal lymph nodes, and connection between the stomach wall lesion and enlarged gastric or abdominal lymph nodes, may be seen. Endoscopic US imaging facilitates the determination of the layer of origin. However, on endoscopic US imaging, TB can be misdiagnosed as a submucosal tumor (Kim et al. 2018; Zhu et al. 2020).

Lack of specific clinical, radiological, and endoscopy features makes the diagnosis of gastric TB difficult. It can mimic peptic ulcer disease, cancer, and lymphoma. The gold standard is endoscopic biopsy, which shows caseating epithelioid granulomas or presence of acid-fast bacilli (AFB). The diagnosis is challenging, and only 50% may be diagnosed after biopsy. The positivity rate of biopsy is low because the lesions are primarily submucosal. Molecular techniques such as polymerase chain reaction (PCR) test and DNA sequencing are helpful (Ma et al. 2019).

7 Duodenal Tuberculosis

Only 2–2.5% of GI TB affects the duodenum. The second and third parts of the duodenum are most commonly involved (Nagi et al. 2015). Involvement can be extrinsic or intrinsic. Extrinsic involvement is most commonly due to adhesions or surrounding lymph nodes, while intrinsic involvement is less common and can be ulcerative or hyperplastic (De et al. 2016). The

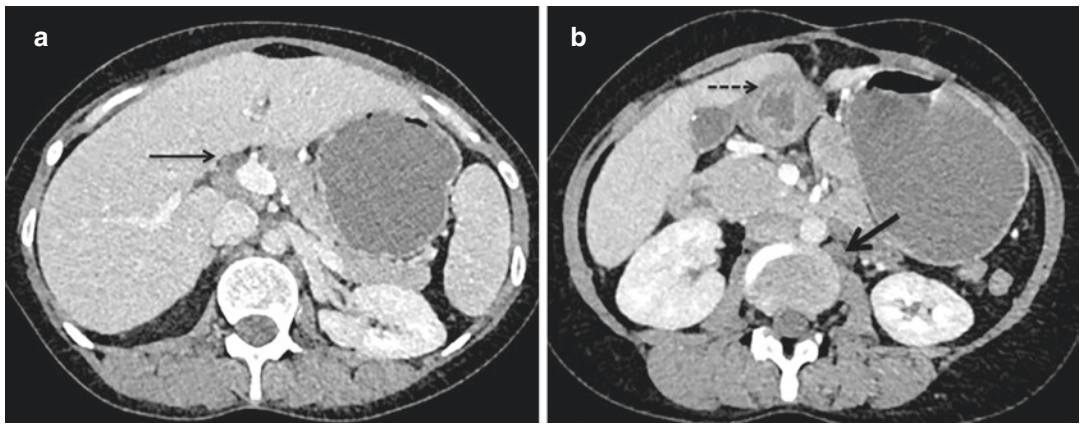

Fig. 15 24-year-old woman, a known case of gastrointestinal tuberculosis who previously underwent operation for small bowel obstruction, now presented with recurrent upper abdominal pain. (**a**) Axial contrast-enhanced CT image shows necrotic periportal lymph nodes (thin solid arrow) (**b**) Axial contrast-enhanced CT image shows circumferential wall thickening of the stomach in the region of pylorus (dashed arrow). Enlarged para-aortic lymph nodes are also seen (thick solid arrow). Endoscopic biopsy confirmed gastric tuberculosis

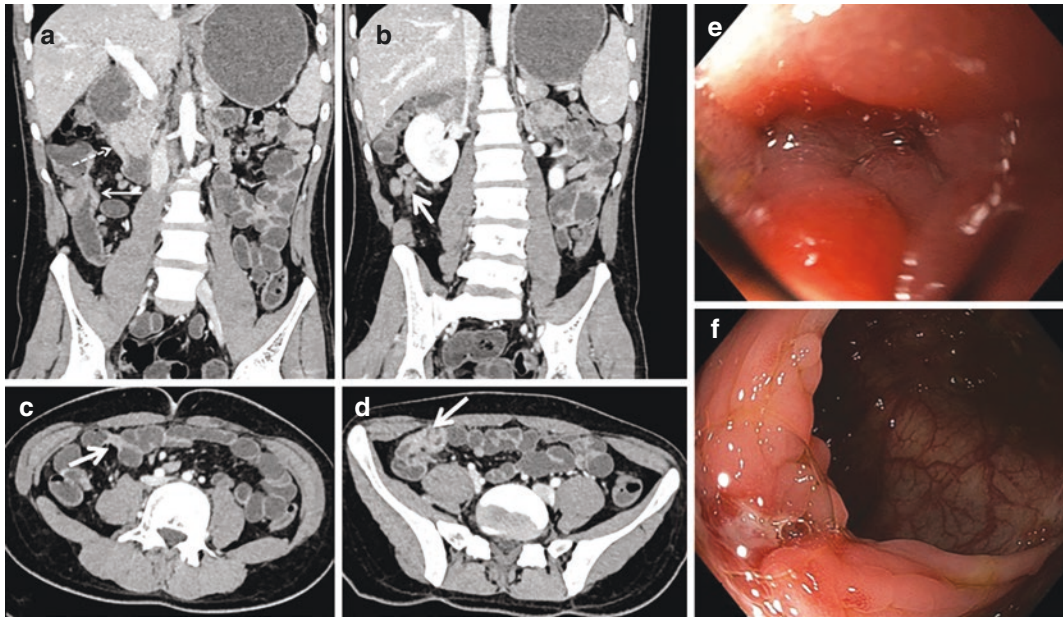

Fig. 16 46-year-old man who presented with loss of weight and appetite for 3 months. (**a** and **b**) Coronal contrast-enhanced CT images show circumferential thickening of the ileocecal junction and terminal ileum (thin solid arrow), with a contracted and thick-walled cecum. There is circumferential thickening of the second part of the duodenum (dashed arrow) leading to proximal dilatation of the stomach. Enlarged ileocolic lymph nodes are also seen (thick solid arrow). (**c** and **d**) Axial contrast-enhanced CT images show other areas of circumferential wall thickening and luminal narrowing in the small bowel loops (solid arrows). (**e**) Gastroscopy photograph shows thickening of folds in the second part of the duodenum. (**f**) Colonoscopy photograph shows an ulcer in the cecum close to the ileocecal valve and pseudopolyps. Biopsy in both these regions showed granulomas. (Endoscopy images courtesy of Dr. Vishal Sharma, Department of Gastroenterology, PGIMER, Chandigarh, India)

most common presenting symptoms are obstruction and dyspepsia.

Barium studies are non-specific but can delineate the level and extent of involvement of duodenal TB. The most common barium study findings in patients who present with obstructive symptoms are strictures, extrinsic compression, and polypoidal intraluminal masses. The most common feature in patients who present with dyspeptic symptoms is ulceration. Other barium findings include perforation and fistulas (Nagi et al. 2015). There may be widening of the duodenal C-loop or impressions on the medial aspect of the C-loop, due to adjacent enlarged lymph nodes. Extrinsic involvement is most common in the third part of duodenum, and it can sometimes simulate the superior mesentery artery syndrome (Lundstedt et al. 1996). The incompetence of the sphincter of Oddi can lead to passage of air or reflux of intraluminal contrast agent into the biliary tree (Chavhan 2003).

US imaging may show circumferential mural thickening at the point of obstruction or necrotic lymph nodes in the region. Other associated findings such as ascites and peritoneal thickening can also be seen on US imaging. CT shows the thickened wall of the duodenum and necrotic lymph nodes (Fig. 16). Necrotic lymph nodes can be seen in both intrinsic and extrinsic duodenal TB (Gulati et al. 1999). Complications of duodenal TB are obstruction, fistula formation, and perforation; these are well evaluated on CT. The imaging differential diagnosis includes lymphoma, pancreatic carcinoma, and peptic ulcer disease.

8 Colonic Tuberculosis

Colonic TB is usually contiguous with ileocecal involvement. Isolated colonic TB is rare and is seen in only 10.8% of cases of abdominal TB (Debi et al. 2014). The ascending colon has been

reported to be the most commonly involved segment (Mukewar et al. 2012), while others have found the transverse colon to be more commonly involved (Nagi et al. 2003a). Affected patients most frequently present with weight loss and abdominal pain, while some present with fever, abdominal mass, and bleeding per rectum. Most patients respond to anti-TB drug therapy. About 10% of patients with colonic TB require surgery for lower GI bleeding (Mukewar et al. 2012).

Barium enema shows segmental involvement with associated spiculation, spasm, rigidity, ulcers, symmetrical annular strictures, and sometimes polyps (Nagi et al. 2003a). Complications include perforation, fistulae, and pericolic abscesses. Double-contrast barium enema is more sensitive than single-contrast barium enema and can show shallow ulcers with elevated margins. These ulcers are transversely oriented. The confluence of these ulcers may create larger girdle ulcers and affect large segments of colon (Nakano et al. 1992). CT can show short- or long-segment involvement and circumferential mural thickening, with associated luminal narrowing. Short-segment involvement is usually seen around the hepatic flexure (Fig. 17). Advanced TB can cause shortening of bowel with distortion. Complications of TB such as

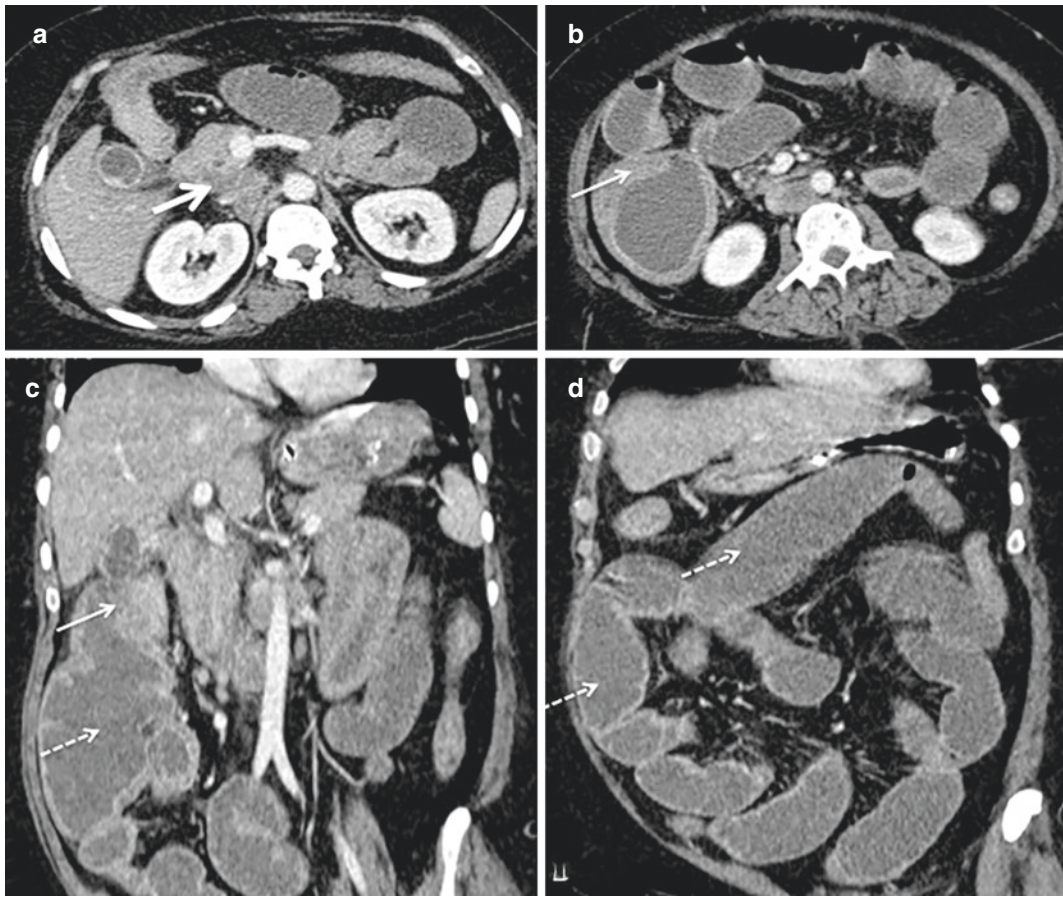

Fig. 17 42-year-old man who presented with clinical features of intestinal obstruction. (**a**) Axial contrast-enhanced CT image shows enlarged necrotic peripancreatic lymph nodes (thick solid arrow). (**b**) Axial and (**c**) coronal contrast-enhanced CT images show asymmetrical circumferential wall thickening of the colonic hepatic flexure (thin solid arrows) as well as dilated ascending colon and cecum (dashed arrow). (**d**) Coronal contrast-enhanced CT image shows dilated small bowel loops (dashed arrows). There is symmetrical thickening with stratification in the ascending colon, cecum, and terminal ileum

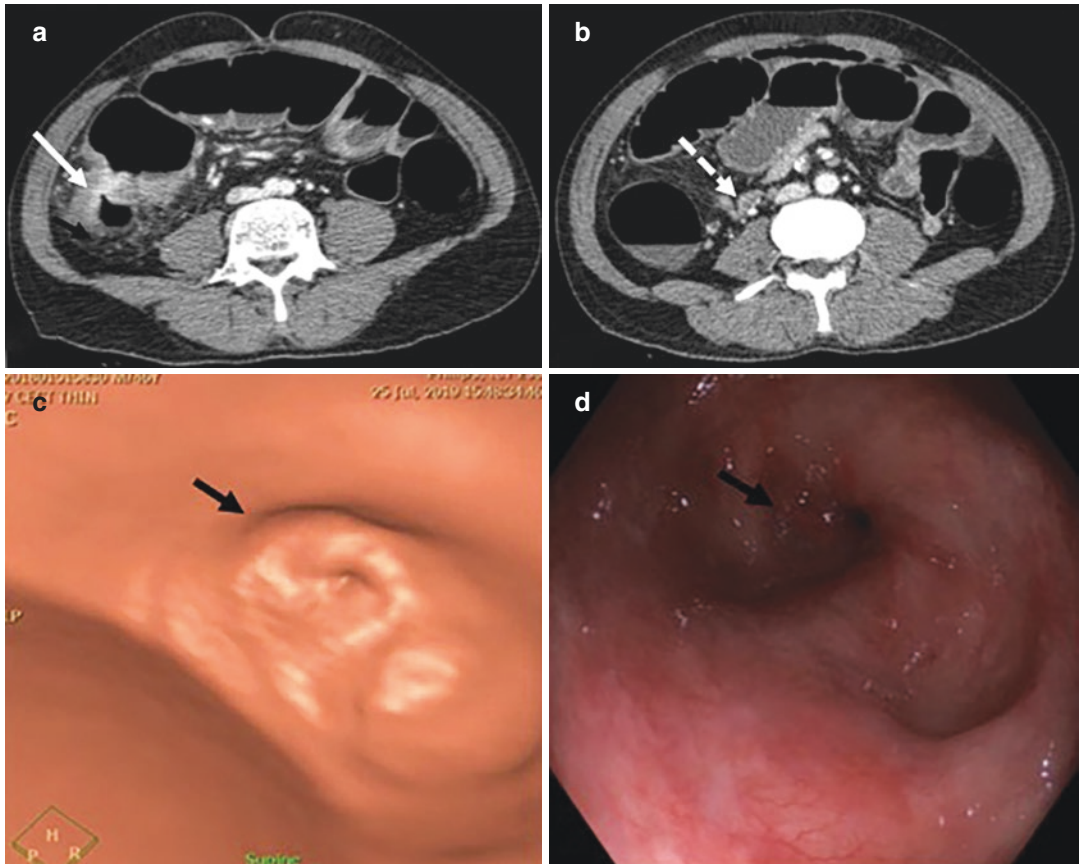

Fig. 18 CT colonography images with colonoscopic correlation in a 40-year-old man. (**a**) Axial contrast-enhanced CT image shows asymmetrical mural thickening in the proximal ascending colon causing luminal narrowing (white solid arrow) (**b**) Axial contrast-enhanced CT image shows a few subcentimeter-sized lymph nodes (white dashed arrow) in the ileocecal mesentery. (**c**) CT colonography endoluminal 3D image shows luminal narrowing with wall irregularity (black arrow). (**d**) Conventional colonoscopy photograph shows a stricture at the corresponding site (black arrow). Biopsy confirmed tuberculosis

perforation, obstruction, pericolic abscess, sinuses, and fistulae can be well visualized on CT (Gulati et al. 1999).

CT colonography is an alternative to barium enema for the evaluation of colonic TB. CT colonography is an advanced CT technique, which involves distension of the colon using air or carbon dioxide, followed by CT acquisition and reconstruction of images using 3D reconstruction techniques (Prabhakar et al. 2015). The advantages of CT colonography are that it is more sensitive to smaller mucosal lesions and provides information about the lumen, colonic wall, and extraluminal abnormalities (Fig. 18). CT colonography has been advocated in differentiating TB from Crohn disease. The ulcers are circumferential in TB and longitudinal in Crohn disease. In addition, the ileocecal valve is more commonly found to be incompetent in TB than in Crohn disease (Kim et al. 2009). The differential diagnosis of colonic TB includes inflammatory bowel disease, amebic colitis, pseudomembranous colitis, ischemic colitis, and malignancy.

9 Anorectal Tuberculosis

Anorectal TB is the rarest site of GI TB. Affected patients present with anal pain, discharge, multiple and/or recurrent fistulae, and inguinal

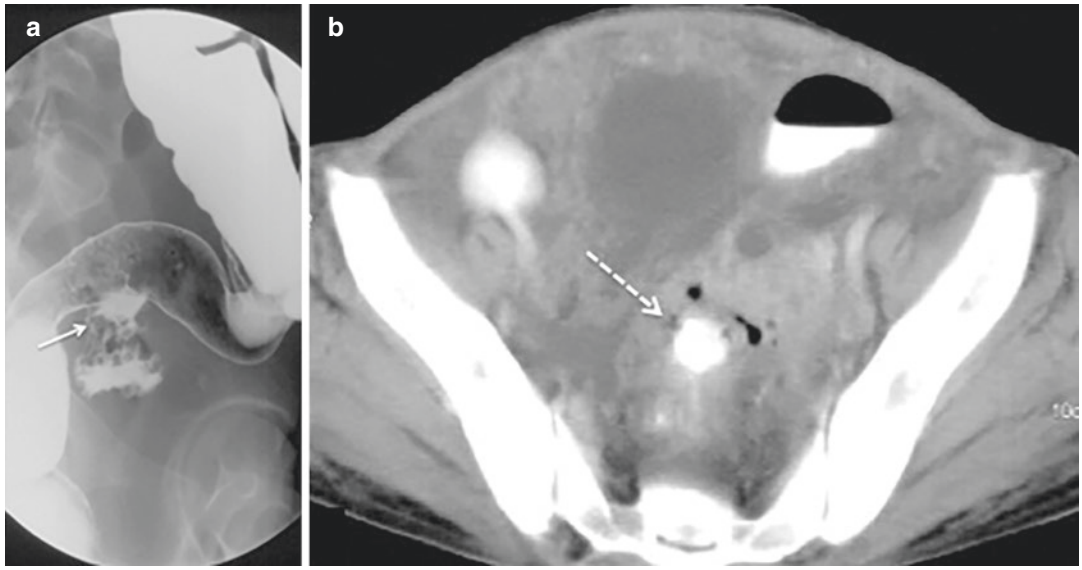

Fig. 19 58-year-man who had recurrent episodes of anorectal bleeding and constipation. (**a**) Double-contrast barium enema image shows a focal area of localized perforation along left lateral wall of the rectum (solid arrow). (**b**) Axial contrast-enhanced CT image shows asymmetrical circumferential wall thickening of the rectum (dashed arrow). Extensive fat stranding and ascites are also seen in the pelvis

lymphadenopathy. Six forms of perianal TB have been described, namely fistula-in-ano, ulcer with undermined edges, short and annular strictures, multiple small mucosal ulcers, lupoid form with submucosal nodule and mucosal ulceration, and verrucose form with wartlike excrescences (Pandit et al. 2018). The most common form is fistula-in-ano. Tuberculous fistulae are usually complex, involve the external sphincter, and have multiple tracks. The diagnosis is made by detection of AFB on routine microscopy of rectal discharge or by histological examination of tissue obtained from the lesion (Gupta 2005). The management includes both medical and surgical treatment.

Anorectal TB leads to significant luminal narrowing with areas of deep ulcers, which are located approximately 10 cm from the anal verge. Barium enema shows strictures, which are of variable length, and also deep ulcers. The presacral space can be increased (Puri et al. 1996), due to inflammation or fibrosis. CT shows wall thickening, which can be circumferential or focal (Gulati et al. 1999) (Fig. 19). The rectum is usually not well distended by contrast material, due to ulceration, spasm, or fibrosis. In addition, there may be fistulae, strictures, and chronic ischiorectal abscesses. MRI is routinely used for the evaluation of perianal fistulas because of its superior soft tissue contrast. The advantages of MRI are that it can better define the primary and secondary tracks, localize the internal openings, and identify the complications such as abscesses, communications with other viscera, and involvement of sphincters (Balci et al. 2019). The differential diagnosis includes Crohn disease, malignancy, lymphogranuloma venereum, amebiasis, actinomycosis, and schistosomiasis.

10 Diagnosis and Treatment

Tuberculin skin testing is used for initial evaluation, but it cannot differentiate between active and latent cases of TB. Smear microscopy and mycobacterial culture should be performed in all cases of TB. Histopathology is used for confirmatory diagnosis (Khanna et al. 2017), showing epithelioid granulomas with Langhans cells and caseous necrosis. AFB may be present. The diagnosis is challenging, as the clinical utility of culture is limited by its relatively low yield and the

prolonged period required for growth to be detected. Molecular techniques such as PCR test and DNA sequencing may help. Anti-TB therapy using a combination of four drugs consisting of rifampicin, isoniazid, pyrazinamide, and ethambutol is the treatment of choice. This drug therapy helps in the resolution of the disease and also any fistula. However, some complications, e.g., perforation and obstruction, may require surgical management.

11 Conclusion

Imaging has a pivotal role in the diagnosis, evaluation of disease extent, and assessment of the treatment response of GI TB. As GI TB has a wide spectrum of imaging features, knowledge of these imaging appearances on various imaging modalities will enable an early diagnosis in the appropriate clinical settings. Confirmatory diagnosis requires tissue culture and/or histological examination. The ileocecal junction is the most commonly involved site in GI TB. The involvement of the ileocecal region with concomitant lesions in bowel and necrotic lymphadenopathy is diagnostic of TB. Though GI TB can affect any site, isolated involvement of the colon, stomach, duodenum, esophagus, and anorectum is rare; hence, the diagnosis requires a high degree of clinical suspicion. The role of the radiologist is in timely recognition of the imaging features of TB, so that further strategies can be planned to confirm the diagnosis and/or start appropriate anti-TB treatment.

References

Aiyappan SK, Kalra N, Sandhu MS et al (2012) Comparison of neutral and positive enteral contrast media for MDCT enteroclysis. Eur J Radiol 81:406–410

Amarapurkar DN, Patel ND, Amarapurkar AD (2003) Primary gastric tuberculosis report of 5 cases. BMC Gastroenterol 3:6

Balci S, Onur MR, Karaosmanoglu AD (2019) MRI evaluation of anal and perianal diseases. Diagn Interv Radiol 25:21–27

Bhatt S, Roy S, Bhardwaj N et al (2017) Kaleidoscopic view of bowel tuberculosis on multi-detector computed tomography (CT) enterography—a novel technique unfolding an archaic disease. Pol J Radiol 82:783–791

Chavhan GE (2003) Duodenal tuberculosis: radiological features on barium studies and their clinical correlation in 28 cases. J Postgrad Med 49:214–217

Chazan BI, Aitchison JD (1960) Gastric tuberculosis. Br Med J 2:1288–1290

Dahale AS, Kumar A, Srivastava S et al (2018) Esophageal tuberculosis: uncommon of common. JGH Open 2:34–38

Dave-Verma H, Moore S, Singh A et al (2008) Computed tomographic enterography and enteroclysis: pearls and pitfalls. Curr Probl Diagn Radiol 37: 279–287

De A, Lamoria S, Dhawan S et al (2016) Duodenal tuberculosis: dig deep to diagnose. Trop Doct 46:172–174

Debi U, Ravisankar V, Prasad KK (2014) Abdominal tuberculosis of the gastrointestinal tract: revisited. World J Gastroenterol 20:14831–14840

Goyal P, Shah J, Gupta S et al (2019) Imaging in discriminating intestinal tuberculosis and Crohn's disease: past, present and the future. Expert Rev Gastroenterol Hepatol 13:995–1007

Guirguis MM, Ghaly AF, Abadir L (1983) Gastric tuberculosis. Bristol Med Chir J 98:73–76

Gulati MS, Sarma D, Paul SB (1999) CT appearances in abdominal tuberculosis. A pictorial essay. Clin Imaging 23:51–59

Gupta PJ (2005) Ano-perianal tuberculosis—solving a clinical dilemma. Afr Health Sci 5:345–347

Kalra N, Agrawal P, Mittal V et al (2014) Spectrum of imaging findings on MDCT enterography in patients with small bowel tuberculosis. Clin Radiol 69:315–322

Kalra N, Gulati A, Gupta P (2021) Comparison of virtual computed tomography enteroscopy using carbon dioxide with small bowel enteroclysis and capsule endoscopy in patients with small bowel tuberculosis. Eur Radiol 31:3297–3305

Kedia S, Sharma R, Nagi B et al (2015) Computerized tomography-based predictive model for differentiation of Crohn's disease from intestinal tuberculosis. Indian J Gastroenterol 34:135–143

Khanna V, Kumar A, Alexander N (2017) A case report on esophageal tuberculosis—a rare entity. Int J Surg Case Rep 35:41–43

Kim TH, Kim JK, Lee JH (2009) Education and imaging. Gastrointestinal: CT colonography in ileocecal tuberculosis. J Gastroenterol Hepatol 24:699

Kim TU, Kim SJ, Ryu H et al (2018) Gastric tuberculosis presenting as a subepithelial mass: a rare cause of gastrointestinal bleeding. Korean J Gastroenterol 72:304–307

Krishna S, Kalra N, Singh P et al (2016) Small-bowel tuberculosis: a comparative study of MR enterography and small-bowel follow-through. AJR Am J Roentgenol 207:571–577

Lee WK, Van Tonder F, Tartaglia CJ et al (2012) CT appearances of abdominal tuberculosis. Clin Radiol 67:596–604

Lundstedt C, Nyman R, Brismar J (1996) Abdominal manifestations in 112 patients. Acta Radiol 37: 489–495

Lv M, Tang K, Meng Y et al (2020) Primary isolated asymptomatic gastric tuberculosis of the cardia mimicking gastric stromal tumor: a rare case report and literature review. BMC Gastroenterol 20:108

Ma J, Yin H, Xie H (2019) Critical role of molecular test in early diagnosis of gastric tuberculosis: a rare case report and review of literature. BMC Infect Dis 19:589

Malikowski T, Mahmood M, Smyrk T et al (2018) Tuberculosis of the gastrointestinal tract and associated viscera. J Clin Tuberc Other Mycobact Dis 12:1–8

Mathur P, Sharma R, Kandasamy D et al (2019) Can ADC be used as a surrogate marker of response to therapy in intestinal tuberculosis? Abdom Radiol 44: 3006–3018

Miller RE, Sellink JL (1979) Enteroclysis: the small bowel enema. Gastrointest Radiol 4:269–283

Mukewar S, Mukewar S, Ravi R et al (2012) Colon tuberculosis: endoscopic features and prospective endoscopic follow-up after anti-tuberculosis treatment. Clin Transl Gastroenterol 3:e24

Mukhopadhyay M, Rahaman QM, Mallick NR et al (2010) Isolated gastric tuberculosis: a case report and review of literature. Indian J Surg 72:412–413

Nagi B, Lal A, Kochhar R et al (2002) Perforations and fistulae in gastrointestinal tuberculosis. Acta Radiol 43:501–506

Nagi B, Kochhar R, Bhasin DK et al (2003a) Colorectal tuberculosis. Eur Radiol 13:1907–1912

Nagi B, Lal A, Kochhar R et al (2003b) Imaging of esophageal tuberculosis: a review of 23 cases. Acta Radiol 44:329–333

Nagi B, Sodhi KS, Kochhar R et al (2004) Small bowel tuberculosis: enteroclysis findings. Abdom Imaging 29:335–340

Nagi B, Rana SS, Kochhar R et al (2006) Sonoenteroclysis: a new technique for the diagnosis of small bowel diseases. Abdom Imaging 31:417–424

Nagi B, Lal A, Gupta P et al (2015) Radiological findings in duodenal tuberculosis: a 15-year experience. Abdom Imaging 40:1104–1109

Nakano H, Jaramillo E, Watanabe M et al (1992) Intestinal tuberculosis: findings on double-contrast barium enema. Gastrointest Radiol 17:108–114

Pandit K, Khanal S, Bhatta S et al (2018) Anorectal tuberculosis as a chronic rectal mass mimicking rectal prolapse in a child—a case report. Ann Med Surg (Lond) 36:264–266

Pereira JM, Madureira AJ, Vieira A et al (2005) Abdominal tuberculosis: imaging features. Eur J Radiol 55:173–180

Prabhakar N, Kalra N, Bhasin DK et al (2015) Comparison of CT colonography with conventional colonoscopy in patients with ulcerative colitis. Acad Radiol 22:296–302

Prakash A (2009) Abdominal tuberculosis. In: Gupta AK, Chowdhury V, Khandelwal N (eds) Diagnostic radiology: gastrointestinal and hepatobiliary imaging, 3rd edn. Jaypee Brothers Medical Publishers, New Delhi, pp 112–133

Prasant P, Kajal N, Dadra R et al (2019) Esophageal tuberculosis: a rare case report. Int J Mycobacteriol 8:409–411

Puri AS, Vij JC, Chaudhary A et al (1996) Diagnosis and outcome of isolated rectal tuberculosis. Dis Colon Rectum 39:1126–1129

Singhal M, Krishna S, Lal A et al (2019) Encapsulating peritoneal sclerosis: the abdominal cocoon. Radiographics 39:62–77

Xiong J, Guo W, Guo Y et al (2020) Clinical and endoscopic features of esophageal tuberculosis: a 20-year retrospective study. Scand J Gastroenterol 55:1200–1204

Yang G, Zhang W, Yu T et al (2015) The features of intestinal tuberculosis by contrast-enhanced ultrasound. Jpn J Radiol 33:577–584

Zengin K, Taskin M, Cicek Y et al (2003) Primary gastric tuberculosis mimicking gastric tumor that results in pyloric stenosis. Eur Surg 35:220–221

Zhu R, Zhou Y, Wang H et al (2020) Gastric tuberculosis mimicking submucosal tumor: a case series. BMC Gastroenterol 20:23

Imaging of Urogenital, Adrenal, and Breast Tuberculosis

Thanat Kanthawang, Malai Muttarak, and Puwitch Charoenchue

Contents

Abstract

Many patients presenting with extrapulmonary tuberculosis (TB) have urogenital TB. Urogenital TB can easily be overlooked owing to non-specific symptoms, chronic and cryptic or protean clinical manifestations, and lack of clinician awareness of the possibility of TB. Although the definitive diagnosis of urogenital TB is established by culturing *Mycobacterium tuberculosis* or by DNA identification, the diagnosis is often difficult and delayed. Abnormal abdominal or chest radiographs are useful as the initial diagnostic investigation in a large proportion of infected patients. Intravenous urography and hysterosalpingography, the standard imaging modalities for the evaluation of urogenital TB in the past, are infrequently used nowadays in the era of cross-sectional imaging. Computed tomography, magnetic resonance imaging, and ultrasound imaging are useful, depending on which urogenital organs are investigated. Imaging features of TB affecting the adrenal gland and breast are also addressed. Awareness of the imaging findings enables the radiologist to raise the diagnostic suspicion in a timely manner, for initiation of prompt treatment and prevention of complications. Imaging can aid in localizing the site, extent, and effect of the disease, obtaining tissue samples for diagnosis, planning medical or surgical management, and monitoring the response to treatment.

T. Kanthawang (✉) · M. Muttarak · P. Charoenchue
Department of Radiology, Faculty of Medicine, Chiang Mai University, Chiang Mai, Thailand
e-mail: thanatkanthawang@gmail.com; thanat.kanthawang@cmu.ac.th; malai.muttarak@gmail.com; Puwitch.c@cmu.ac.th; Puwitch.c@gmail.com

© The Author(s), under exclusive license to Springer Nature Switzerland AG 2022

M. F. Ladeb, W. C. G. Peh (eds.), *Imaging of Tuberculosis*, Medical Radiology Diagnostic Imaging,
https://doi.org/10.1007/978-3-031-07040-2_11

Abbreviations

BCG	Bacillus Calmette–Guérin
CT	Computed tomography
CTU	Computed tomographic urography
HIV	Human immunodeficiency virus
HSG	Hysterosalpingography
IVU	Intravenous urography
MRI	Magnetic resonance imaging
PET	Positron-emission tomography
TB	Tuberculosis
US	Ultrasound

1 Introduction

More than a century after the isolation of the causative organism *Mycobacterium tuberculosis*, tuberculosis (TB) continues to produce considerable patient morbidity and mortality globally. Although developing countries bear the brunt of the disease at present, the emergence of the human immunodeficiency virus (HIV) epidemic, multidrug resistance, and population migration have caused a resurgence in the developed countries. Countries in South-East Asia and Africa are particularly affected (Chakaya et al. 2021). Annually, 15–40% of patients newly infected with TB have features of extrapulmonary TB (Kulchavenya 2014; Chakaya et al. 2021). TB affecting the kidneys, ureters, bladder, prostate, urethra, penis, scrotum, testicles, epididymis, vas deferens, ovaries, fallopian tubes, uterus, cervix, and vulva were initially grouped as "genitourinary TB." Currently, the term "urogenital TB" is preferred because renal and urinary tract TB is more common than genital TB (Kulchavenya et al. 2016).

The proportion of urogenital TB among all forms of extrapulmonary TB reported in the literature ranges from 15% to 20% in Africa, Asia, Eastern Europe, and the Russian Federation, to 2–10% in Western Europe and the USA (Muneer et al. 2019). The urogenital tract is among the most common sites of extrapulmonary TB, together with lymph nodes and pleura (Kulchavenya 2014). Urogenital TB is a neglected clinical problem and can easily be undiagnosed owing to non-specific symptoms or asymptomatic, chronic and cryptic or protean clinical manifestations, and a lack of clinician awareness of the possibility of TB. Delay in making a diagnosis results in disease progression and complications. Moreover, TB has a variety of radiological presentations that can mimic numerous other disease entities. A high level of clinical suspicion and familiarity with various radiological features of TB enables an early diagnosis, hence allowing commencement of prompt and efficient treatment aimed at reducing patient morbidity.

In this chapter, we describe the pathogenesis, clinical features, imaging findings, and differential diagnosis of urogenital TB, including the urinary system, and both male and female genitalia. Imaging findings and the differential diagnosis of adrenal and breast TB are also described.

2 Pathophysiology

Following primary infection, the mycobacteria evoke a complex array of immune responses, which result in either elimination (eradication) or containment via primary granuloma formation. Primary tuberculous lesions are mostly found in the lungs, tonsils, or intestines. In the majority of people with primary infection, the mycobacteria are eventually either eliminated or contained as latent TB infection which is still at risk of reactivation (Furin et al. 2019). If no containment occurs at this stage, the mycobacteria can seed to all organs of the body. This is known as extrapulmonary TB, and accounts for 5–10% of people with the primary disease (Chakaya et al. 2021).

The main route of urogenital infection is via the blood and lymphatic systems. Mycobacteria can lodge in urogenital organs and form granulomas, such as at the corticomedullary junction of kidney or epididymal tail. These granulomas, with or without caseous necrosis, remain stable for many years. But if reactivation or disease progression occurs, further tissue destruction can be

extensive, with resultant cavities or abscesses which can drain into surrounding tissues and form fistulae. Calcification, scarring, and fibrosis are manifestations of the healing process. The result of the disease is destruction, loss of function, and calcification of the target organ. Imaging findings are therefore widely variable, depending on the extent and stage of the disease.

Urinary spread from infected urine and semen is common and can cause multiple secondary infections in the lower urinary tract and genitalia. The different routes for tuberculous infection in the upper urinary tract and female genitalia are commonly initiated by hematogenous or lymphatic spread. However, in the lower urinary tract and male genitalia, TB can result from both hematogenous and urinary spread (Muttarak et al. 2005; Muneer et al. 2019).

The lower urinary tract and male genitalia may be complicated by iatrogenic Bacillus Calmette–Guérin (BCG)-induced urogenital TB, especially affecting the bladder and prostate. BCG is, in fact, attenuated *Mycobacteria bovis*, and is widely used for intravesical therapy of superficial bladder cancer but less than 5% of patients treated have complications (Lamm et al. 1986). In rare cases, BCG sepsis is possible and live BCG vaccination in immunosuppressed individuals can also cause local and disseminated BCG disease (Furin et al. 2019). Other rare modes of urogenital TB that have been reported include congenital transmission (including transplacental transmission via blood or lymphatics from a mother with active TB or ingestion of Mycobacterium-infected amniotic fluid during birth), sexual transmission from an ulcer or secretion of infected partners, and accidental inoculation (Muneer et al. 2019).

3 Clinical Features and Complications

Urogenital TB can present at any age in men and women. However, owing to the long latency period before reactivation, it commonly affects those aged 30–50 years and is infrequently reported in children (Chattopadhyay et al. 1997). Risk factors for developing TB after infection include malnutrition, HIV infection, diabetes mellitus, chronic renal and liver disease, alcohol and substance abuse, smoking, homelessness, poor housing, pneumoconiosis, genetics, vitamin deficiency, immunosuppressive drugs, renal transplantation and dialysis (Kulchavenya et al. 2016; Furin et al. 2019).

Urogenital TB can present with a range of clinical manifestations, from asymptomatic, subclinical, non-specific symptoms and signs, to complications such as obstructive uropathy and renal failure (Figueiredo et al. 2008). The latent period between the primary infection and clinical presentation varies from 5 to 40 years, resulting in an insidious disease onset (Kulchavenya and Kholtobin 2015; Ramachandran et al. 2021). A large percentage of urogenital TB remains subclinical and has probably never been diagnosed ante-mortem (Zachoval et al. 2018). In addition, up to 50% of cases are diagnosed incidentally when patients are investigated for a range of other urinary tract and genital disorders (Muneer et al. 2019).

Urogenital TB can occur concurrently in up to 20% of individuals with evidence of either active or inactive pulmonary TB (Yadav et al. 2017). Clinical and autopsy studies have shown that unilateral involvement is more common, but bilateral disease and combined involvement of urinary and genital infections can also occur (Chattopadhyay et al. 1997; Figueiredo et al. 2008). Genital TB coexists with urinary tract involvement in two-thirds of affected cases (Yadav et al. 2017). As a rule, all patients with genital TB should be screened for urinary tract involvement and vice versa, as well as for pulmonary involvement.

Urogenital TB can cause many complications, including chronic renal failure, stricture, fistulous formation from the urogenital tract to adjacent organs and skin, obstructive uropathy, infertility, sexual dysfunction, and urinary bladder dysfunction. A high clinical awareness of the possibility of underlying TB is therefore important. Some clinical features should raise the suspicion of

urogenital TB, especially in patients with risk factors, history of TB contact, or active or cured infection (Kulchavenya et al. 2016). These include:

- Urinary tract infection (UTI) with frequent recurrences and resistance to standard antibiotic therapy.
- UTI with persistent dysuria and decreasing bladder volume.
- Sterile pyuria is present on urine examination.
- Leucocytes in all portions of a three-glass test in a patient with epididymo-orchitis.
- Chronic epididymitis or chronic prostatitis that does not resolve with standard antibiotics.
- Pyospermia and/or hematospermia.
- Scrotal, perineal, and lumbar fistulas.

4 Imaging Features and Differential Diagnosis

The role of imaging in urogenital TB is to help localize the site of disease or tissue destruction, assess the extent of involvement, monitor response to treatment, and discover complications. Imaging is also useful for guiding tissue sampling and drainage.

Abdominal and chest radiographs are initial investigations in the diagnostic work-up for urogenital TB. All patients with urogenital TB should undergo a chest radiograph to look for concurrent active pulmonary TB. Abdominal or chest radiographs may show abnormalities caused by active TB or healed TB in up to 50% of patients with urogenital TB (Merchant et al. 2013). Evidence of chronic active TB or previous healed TB often manifests as calcifications in the lung, hilar lymph nodes, kidney, spleen, liver, and adrenal glands.

Positron-emission tomography (PET) imaging using [Fluorine-18]-fluoro-2-deoxy-D-glucose (^{18}F-FDG) can provide functional information about sites with active inflammatory and immune cells that use glucose during metabolism (Subramanyam and Palaniswamy 2015). PET/CT can help identify multifocality of tuberculous disease, but there are limitations to reaching a specific diagnosis. PET/CT cannot distinguish TB from cancer and other infections because FDG is taken up by all metabolically active cells (Subramanyam and Palaniswamy 2015; Gambhir et al. 2017). PET/CT may have a role to help to localize disease sites for guiding biopsies and monitoring treatment response.

Intravenous urography (IVU) has long contributed to the diagnosis of urinary TB and many radiologists, particularly the more senior ones, are familiar with its findings. However, IVU is infrequently used nowadays and has been replaced by cross-sectional imaging, including computed tomography (CT), magnetic resonance imaging (MRI), and ultrasound (US) imaging. These cross-sectional techniques can provide information regarding changes in the renal parenchyma, surrounding tissues, and genital organs that are not readily visualized on IVU (Kenney 1990; Wang et al. 1997).

Cross-sectional imaging also provides more anatomical details and IVU may not be able to optimally evaluate the collecting system in obstructive uropathy, especially in patients with poor renal excretory function. In addition, the involvement of the other organs included in the cross-sectional images can help to suggest a diagnosis of tuberculous infection, such as spondylodiscitis or lung infection. US imaging is also a useful modality to identify abscesses and provide real-time guidance for drainage and tissue sampling. In this chapter, we will focus on cross-sectional imaging of urogenital TB.

4.1 Urinary Tract Tuberculosis

It is important to understand the pathological basis for disease in order to understand the radiological features of urinary tract TB. *Mycobacterium tuberculosis* bacilli lodge in the corticomedullary junction of the kidney during hematogenous seeding, and form cortical granulomas. If the disease progresses or reactivates, the organisms spread into the medulla causing papillitis. As the disease progresses, extensive papillary necrosis may develop, with the formation of frank cavities

destroying the renal parenchyma, and may then extend into the pelvicalyceal system, ureter and urinary bladder, respectively.

Advanced disease leads to cortical scarring, parenchymal atrophy, and infundibular and pelvic strictures causing caliectasis. Single or multiple calyces may be involved in one or both kidneys. The end result of the disease is atrophy, loss of function, and dystrophic calcification of the kidney. The process may spread beyond the kidney with perinephric and retroperitoneal involvement, and fistulas may extend into the gastrointestinal tract or to the skin.

Up to 50% of patients with renal TB have ureteric involvement and up to 21% have bladder TB (Figueiredo et al. 2008). Bladder TB can also spread from male genital TB (secondary infection) or less commonly, primary infection from hematogenous spread or intravesical BCG therapy (Figueiredo et al. 2008; Kulchavenya et al. 2016). Hence, concomitant abnormal imaging findings along the urinary tract support the infectious process of TB.

Currently, CT urography (CTU) is progressively replacing IVU for the assessment of urinary lesions and new techniques have been used for improving the assessment of renal and urinary tract lesions including multiplanar reconstruction (MPR) (Fig. 1a, b, and d), maximum intensity projection (MIP) (Fig. 1e), and curved reformatted

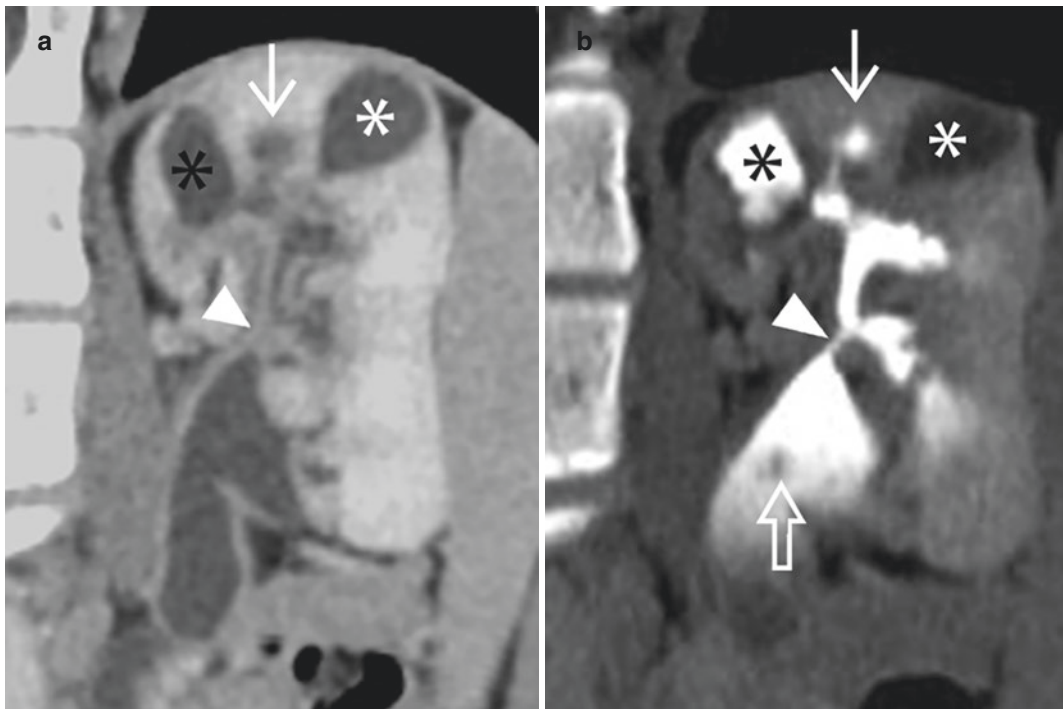

Fig. 1 Urinary tract TB. Coronal CT images of the (**a**) nephrographic and (**b**) excretory phases show a cavity in the renal medulla of the left kidney on the nephrographic phase (arrow) with late opacification by iodinated urine in the excretory phase (arrow), representing papillary necrosis. The pelvicalyceal system shows thickened wall, luminal narrowing (arrowheads) and caliectasis which may be opacified (black asterisk) or nonopacified (white asterisk) on the excretory phase. Filling defect within the renal pelvis is observed (open arrow). (**c**) Longitudinal US image taken 1 year after treatment shows caliectasis and a contracted renal pelvis (arrowhead) in the upper pole. Moderate hydronephrosis in the lower pole and hydroureter (arrow) is due to distal ureteral stricture. (**d**) Coronal CT image of the nephrographic phase taken 2 years after treatment shows multiple infundibular strictures (arrowhead) with parenchymal atrophy and the nonopacified caliectasis in the upper pole of the left kidney, appearing as a multiloculated cyst. (**e**) Coronal MIP CT image of the excretory phase, also obtained at 2 years, shows a beaded appearance of the left ureter

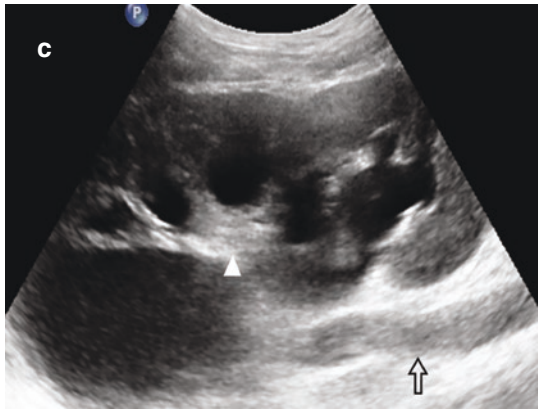

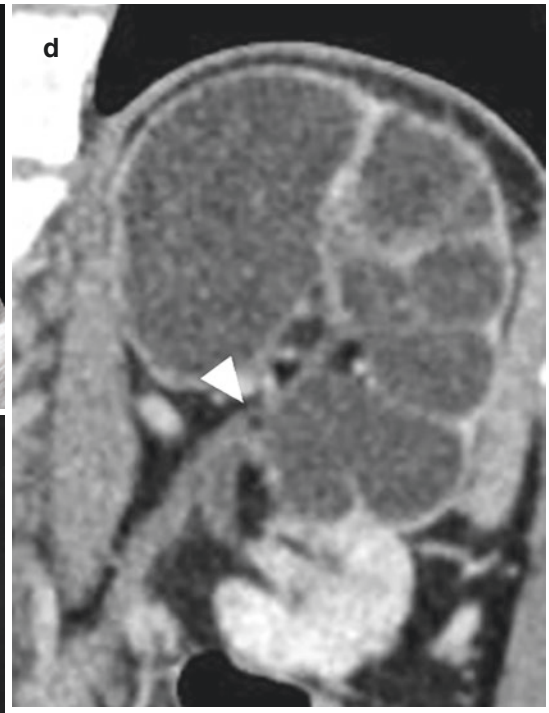

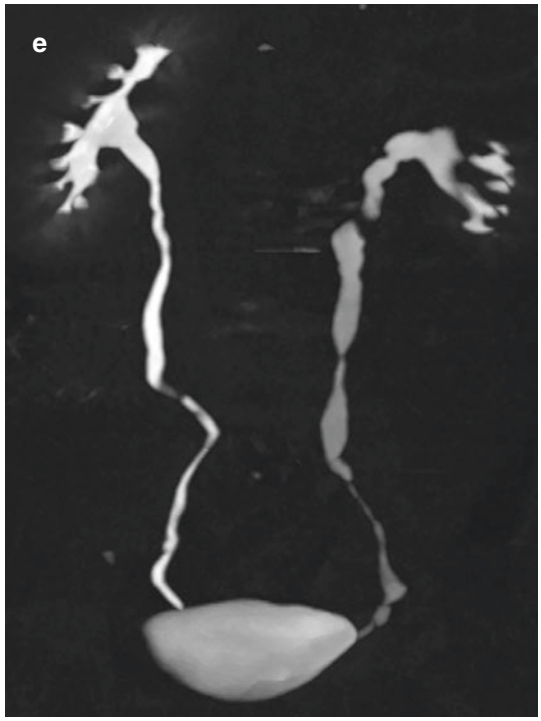

Fig. 1 (continued)

images (Gaudiano et al. 2017) (Fig. 2a, b). CTU allows the detection of almost all the radiological signs of urogenital TB with great accuracy. The main limitation of CTU is its inability to identify very early changes such as small parenchymal granulomas (<3 mm), subtle urothelial thickening, and minimal papillary necrosis (Merchant et al. 2013). MRI may be used to evaluate renal parenchymal change due to its superior soft tissue resolution compared to CT and US imaging, especially in patients with impaired renal function (Fig. 3a–d).

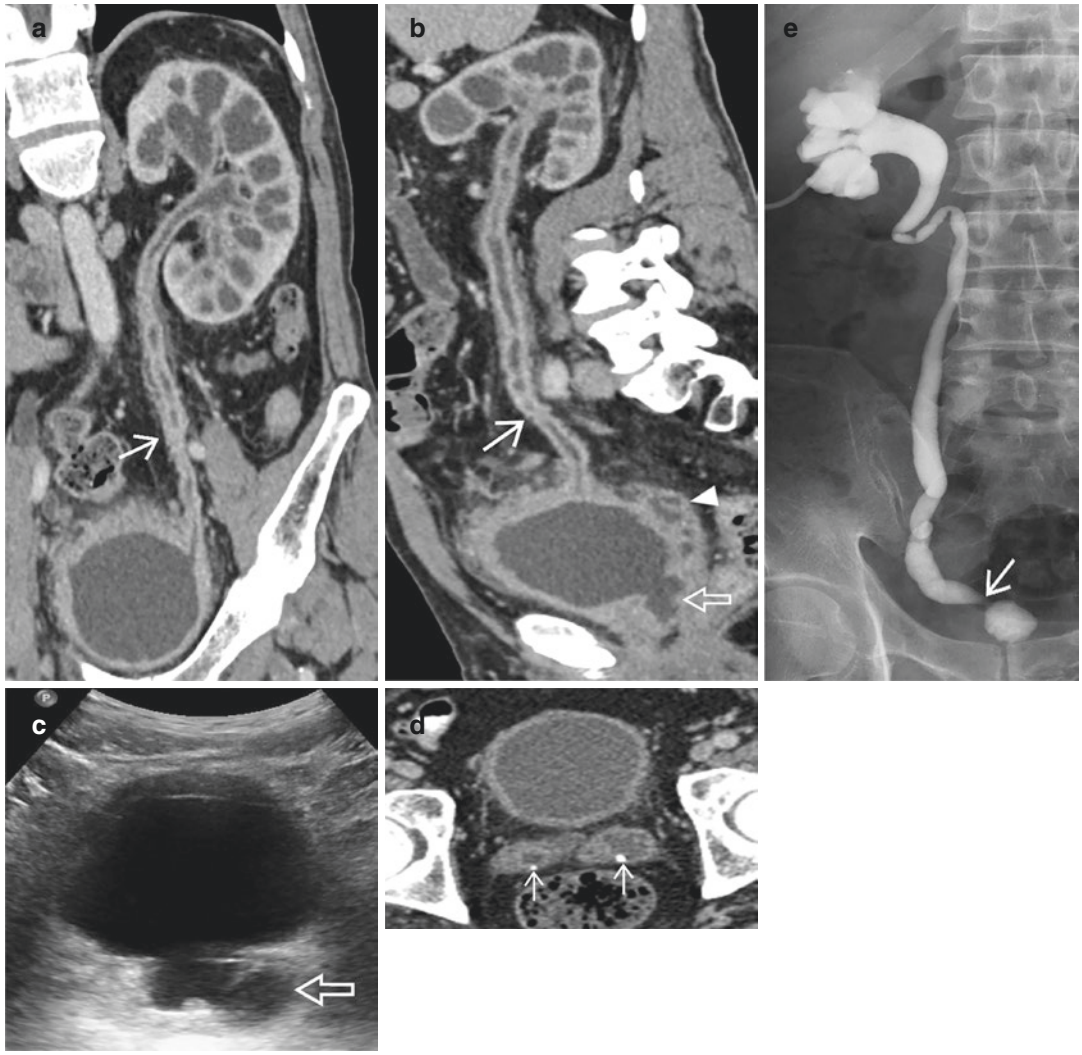

Fig. 2 TB of the urinary tract and male genitalia. Curved MPR images taken in the (**a**) coronal and (**b**) sagittal oblique planes of the nephrographic phase show thickened wall and fat stranding along the left pelvicalyceal system and ureter. Marked thickened wall with luminal narrowing at the distal ureter (arrows) causes mild upstream hydroureteronephrosis. There is a wall thickening and fat stranding involving the urinary bladder and left seminal vesicle (arrowheads) with an abscess in the prostate gland (open arrow). (**c**) Transverse US image shows thickened wall of the urinary bladder and a fluid collection in the prostate gland (open arrow). (**d**) Axial contrast-enhanced CT image of the lower pelvis taken 1 year after treatment shows decreased degree of wall thickening of the urinary bladder and seminal vesicles with new calcifications (arrows) in both seminal vesicles. (**e**) Right tube nephrography obtained 1.5 years after treatment shows right distal ureteric stricture (arrow) and a small capacity bladder causing marked upstream hydroureteronephrosis

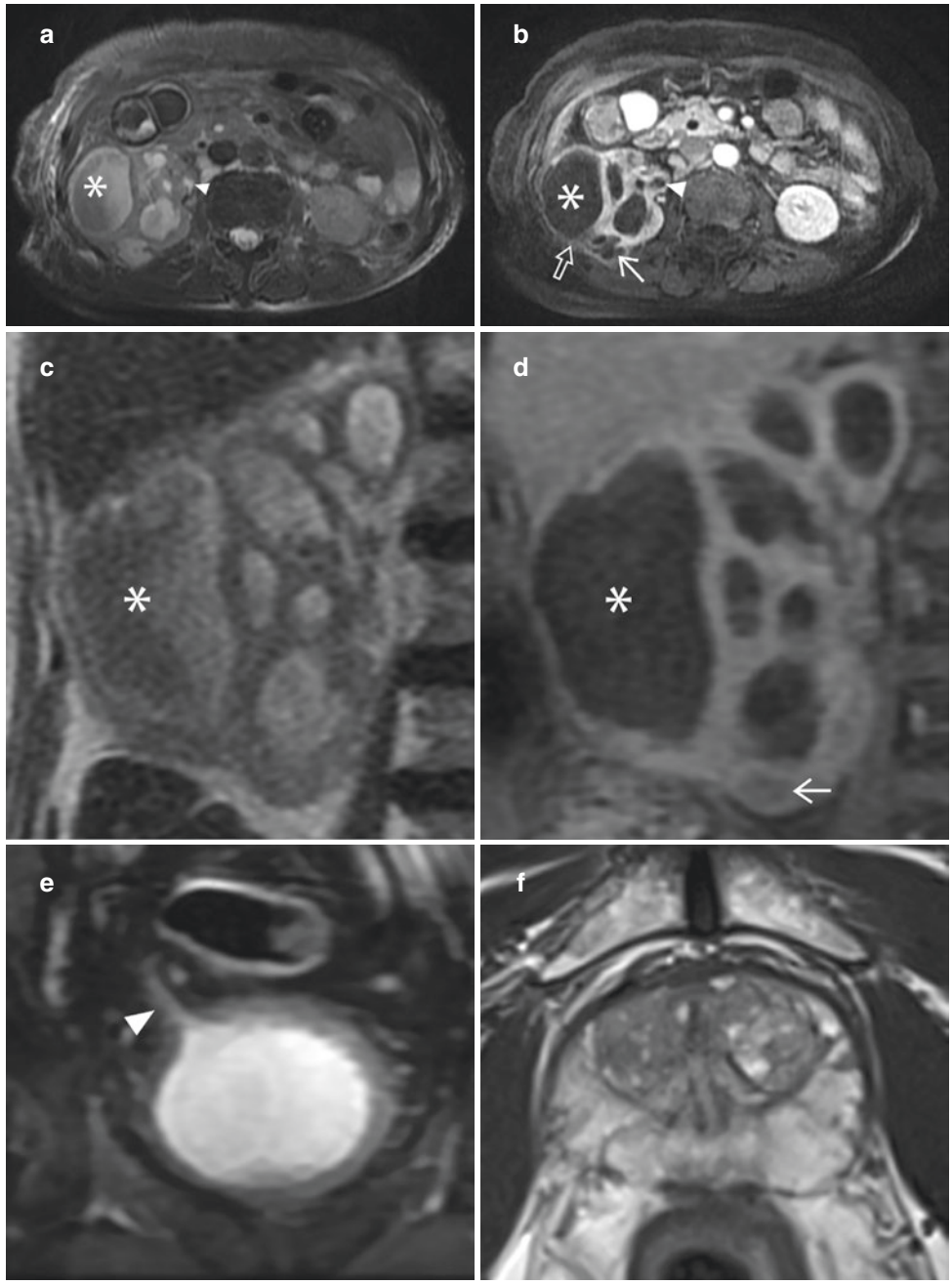

Fig. 3 TB of the urinary tract and male genitalia. Axial fat-suppressed (**a**) T2-weighted and (**b**) contrast-enhanced T1-weighted and coronal (**c**) T2-weighted and (**d**) contrast-enhanced fat-suppressed T1-weighted MR images show a large subcapsular abscess (asterisks) in the right kidney and a parenchymal abscess ruptured into right perinephric space (arrow in **b**). There is focal hypoperfusion in renal parenchyma (open arrow in **b**). A small granuloma with central caseous necrosis in renal parenchyma at the lower pole (arrow in **d**) is not well seen on the T2-weighted image (**c**). Thickened wall of the right upper ureter is also present (arrowhead). (**e**) Coronal fat-suppressed T2-weighted MR image of the pelvis shows thickened wall of the right distal ureter (arrowhead) and urinary bladder. (**f**) Axial T2-weighted MR image of the prostate gland shows diffuse, radiating hypointense streaks in the peripheral zone (watermelon skin sign)

4.1.1 Renal Tuberculosis

The radiological changes of renal TB can be divided into parenchymal and collecting system involvement. In about two-thirds of patients with renal TB, multiple abnormalities are present (Kenney 1990). Concomitant parenchymal and collecting system involvement is suggestive of the diagnosis.

In the acute phase, imaging findings are indistinguishable from nontuberculous infection. Features of parenchymal involvement include focal hypoperfusion (Fig. 3b), granuloma, papillary necrosis (Fig. 1a, b), and abscess. Focal hypoperfusion due to localized tissue edema and vasoconstriction is caused by active inflammation. Cortical granulomas can be seen as solid hypoenhancing masses in the parenchyma (Fig. 3d). In rare cases, a single nodule or multiple nodules can be seen in the renal parenchyma without other urinary tract involvement; this is known as the pseudotumoral type (Jung et al. 2005). This type may mimic renal neoplasms and lead to unnecessary surgery.

Rupture and caseation of granulomas result in cortical abscesses which may extend to the subcapsular or retroperitoneal spaces (Fig. 3a–d). For collecting system involvement, imaging may show an uneven appearance, with a thickened wall with increased contrast enhancement (Figs. 1a, b and 2a, b). Filling defects secondary to the accumulation of granulomatous material within the lumen may be observed (Gaudiano et al. 2017) (Fig. 1b).

In the chronic phase, healing of acute inflammation results in multifocal strictures and calcification, which are considered characteristic features and suggest the diagnosis. Development of infundibular and renal pelvic stricture (Fig. 1d) is a common finding and is almost pathognomonic of TB (Kenney 1990). The stricture causes uneven caliectasis that may be opacified or nonopacified (known as phantom calyx on IVU) by iodinated urine, depending on the excretory function of that segment of the kidney (Muttarak et al. 2005) (Fig. 1a, b). Various patterns of hydronephrosis can be seen, depending on the site of the stricture, and includes caliectasis. When the renal pelvis and ureter are involved, associated hydronephrosis becomes severe (Fig. 1c, d). In long-standing TB, as atrophy of the renal parenchyma and hydronephrosis progresses, the kidney loses its morphology and appears as multiple thin-walled cysts or as a multiloculated cyst (Jung et al. 2005) (Fig. 1d).

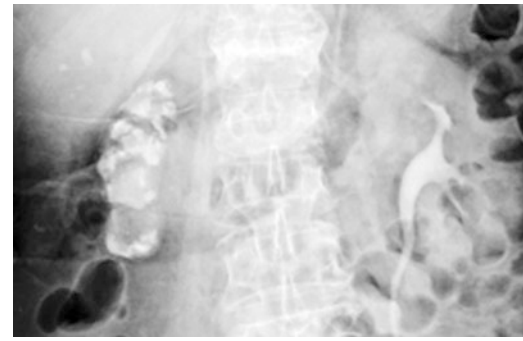

Fig. 4 Tuberculous autonephrectomy. IVU image shows a nonfunctional and atrophic right kidney with extensive lobar calcifications (putty kidney). This typical appearance of end-stage renal TB is also called autonephrectomy. Normal excretory function of the left kidney is noted. (Courtesy of Associate Professor Kobkun Muangsomboon, Faculty of Medicine, Siriraj Hospital, Mahidol University, Bangkok, Thailand)

Calcification is present in >50% of patients with renal TB, and CT is the best imaging modality to detect this (Wang et al. 1997; Merchant et al. 2013). In end-stage TB, extensive lobar calcifications involving the entire kidney are seen; known as "putty kidney" which is a characteristic finding (Dyer et al. 1998) (Fig. 4). Other patterns of renal calcification in TB include amorphous, spotted, curvilinear, and triangular ring-like calcifications within the collecting system, representing papillary necrosis (Muttarak et al. 2005). A range of differential diagnosis for renal calcification should be considered, such as helminth infections, healed renal abscesses, renal calculi, and aneurysms of the renal artery (Kenney 1990; Dyer et al. 1998).

US imaging has less sensitivity than CT or IVU because of difficulties in detecting subtle pelvicalyceal or ureteric changes, difficulties in

recognizing isoechoic parenchymal masses or infiltrative parenchymal disease, lesser sensitivity to calcifications, and inability to evaluate the function of the kidney (Vijayaraghavan et al. 2004). However, US imaging can be used as a screening modality for the upper urinary tract in suspected instances of TB (Rui et al. 2008) (Fig. 1c).

4.1.2 Ureteric Tuberculosis

TB of the ureters can involve any part of the ureter, although the lower third is the most frequently affected site, followed by the pelviureteric junction (Goel and Dalela 2008) (Figs. 2e and 3e). Early ureteric infection produces ulcers causing mucosal irregularity. Fibrosis occurs during the healing process which causes ureteric stricture. A long segment of a thickened wall with increased contrast enhancement of the ureter can be seen on imaging during the acute stage (Fig. 2a, b). Ureteric involvement by itself, i.e., without renal TB, has not been described (Muneer et al. 2019). Hence, isolated ureteric involvement raises the possibility of urothelial tumor in the differential diagnosis, in particular when there is short segmental involvement. Multiple strictures may produce a series of alternating dilatations and narrowing, giving a beaded appearance which is the typical sign of ureteric TB (Muttarak et al. 2005) (Fig. 1e). As the areas of fibrosis coalescence, the ureter appears shortened and straightened, producing a pipe-stem appearance.

4.1.3 Tuberculous Cystitis

Urinary bladder involvement usually manifests initially as interstitial cystitis, which leads to mucosal ulceration and mural thickening (Figs. 2a–c and 3e). If there is nodular, mass-like or asymmetrical wall thickening, urothelial cancer is an important differential diagnosis and tissue sampling is required. Mucosal edema at the trigone of bladder TB can cause ureteric obstruction without ureter involvement. In advanced disease, inflammation progresses to involve the muscular layer, and subsequent mural fibrosis leads to wall thickening and a contracted bladder (thimble bladder) which is the most common imaging appearance (Merchant et al. 2013) (Fig. 2e). Advanced bladder involvement also may be complicated by vesicoureteric reflux due to fibrosis at the ureteric orifice (Jung et al. 2005). In rare cases, calcifications of the bladder wall may be seen, which must be differentiated from other causes of bladder calcifications, such as schistosomiasis of the bladder, cyclophosphamide cystitis, radiation-induced bladder calcification, calcified bladder carcinoma, or encrusted foreign body (Harisinghani et al. 2000).

4.2 Male Genital Tuberculosis

The epididymis and prostate are the most frequently affected sites of male genital TB (Ramachandran et al. 2021). Most cases of epididymal and prostate TB occur by the hematogenous route from a primary focus in the lungs or kidneys, and urinary spread from infected urine and semen (Borthwick 1946). Thus, prostatic TB commonly coexists with renal and scrotal TB, and hence should be screened for concomitant involvement (Kulchavenya et al. 2014). CT has a limited role in male genital TB.

4.2.1 Tuberculous Epididymo-orchitis

The epididymis is the most common site of clinically evident genital TB (Borthwick 1946). The involvement is usually unilateral, although bilateral involvement may be seen in 25–40% of cases (Ramachandran et al. 2021). The presence of a nontender scrotal testicular mass with hard consistency or scrotal edema is suggestive of scrotal TB but clinically differentiating this from malignant swelling can be difficult (Yang et al. 2001). Scrotal fistulae and sinuses discharging pus are suggestive of TB (Muttarak et al. 2001; Yang et al. 2001).

Epididymal infection usually begins in the tail, due to its rich vascularity and predisposition to frequent urinary reflux. Infection is limited to the epididymal tail in 40% of cases (Ramachandran et al. 2021). As the infection progresses, the body and head are involved and

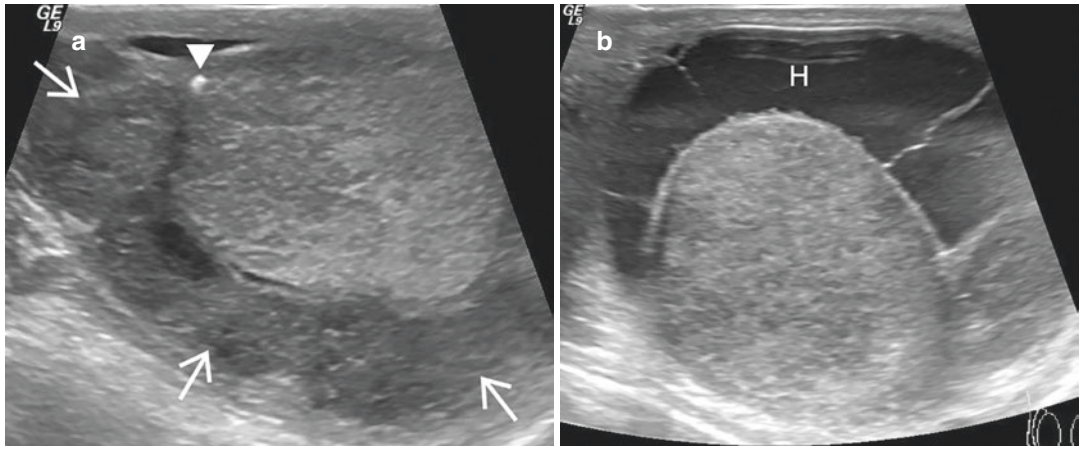

Fig. 5 Tuberculous epididymo-orchitis. (**a**) Longitudinal and (**b**) transverse US images of the left hemiscrotum show diffusely enlarged heterogeneously hypoechoic epididymis (arrows) and testis with calcification (arrowhead). Overlying skin thickening and a large septated hydrocele (H in **b**) are also seen

abscess formation occurs. Testicular involvement is less common and occurs by contiguous spread from the epididymis (epididymo-orchitis), particularly if appropriate treatment has not been initially given. Rupture of the abscess through the scrotal skin leads to sinuses and fistulae.

US imaging is the best imaging modality for assessing the epididymis, testis, and scrotum. Tuberculous epididymitis can be seen as diffusely enlarged homo- or heterogeneously hypoechoic (Figs. 5a and 6a–c), and nodular enlarged heterogeneously hypoechoic lesions (Muttarak et al. 2001) (Fig. 7a, b). The bipolar form involving the epididymal tail and head, with sparing of the body, has also been reported (Drudi et al. 1997). US imaging features of tuberculous orchitis include a diffusely enlarged homo- or heterogeneously hypoechoic testis (Figs. 5a, b and 6c), nodular enlarged testis with a heterogeneously hypoechoic testis, and multiple small hypoechoic nodules in the enlarged testis producing a miliary pattern (Drudi et al. 1997; Muttarak et al. 2001) (Fig. 6a, b).

On US imaging, most cases have a heterogeneous texture due to admixture of inflammatory edema, granulomas, caseation, and fibrosis. Other US imaging features of scrotal TB include hydrocele (Figs. 5b and 7a), scrotal wall thickening (Figs. 5a, b and 8a, b), scrotal wall abscess (Fig. 8a, b), sinus tract formation (Fig. 8a, b), and intrascrotal extratesticular calcifications (Muttarak et al. 2001) (Figs. 5a and 7a, b).

The US features of tuberculous epididymo-orchitis must be differentiated from nontuberculous infection and tumor. The presence of skin thickening and epididymal involvement in conjunction with testicular lesions is suggestive of an infection rather than a tumor because orchitis is almost always caused by epididymitis. Isolated tuberculous orchitis is extremely rare and in such cases, primary testicular malignancy needs to be ruled out. Nontuberculous epididymitis is more likely to be homogeneous (Fig. 9) with a higher degree of blood flow around the abscess, whereas tuberculous epididymitis is usually heterogeneous or nodular (Yang et al. 2001). Moreover, epididymal tumor also tends to be homogeneous and less commonly encountered, compared to infection (Yang et al. 2003). Failure of conventional antibiotic therapy with the presence of the aforementioned US features is suggestive of tuberculous epididymo-orchitis.

4.2.2 Tuberculous Prostatitis

The large majority of patients with tuberculous prostatitis are asymptomatic, resulting in significant underestimation of the true prevalence

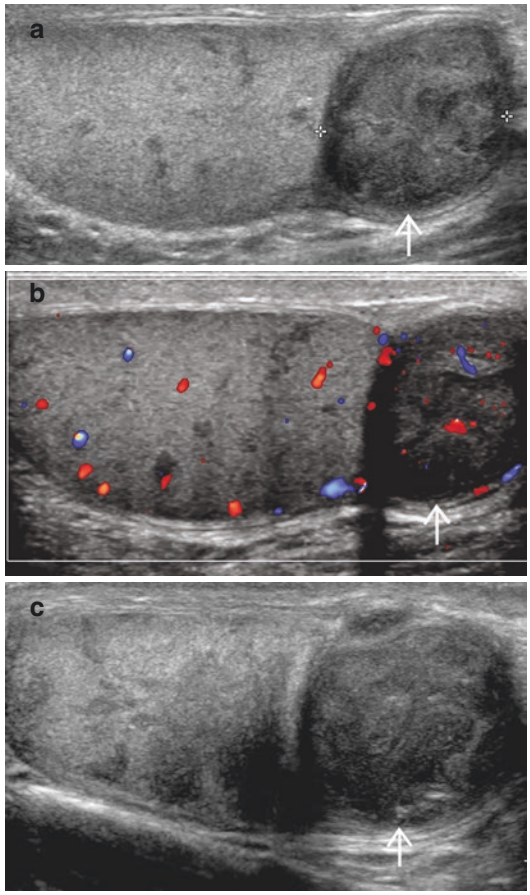

Fig. 6 Bilateral tuberculous epididymo-orchitis. Longitudinal (**a**) gray-scale and (**b**) color Doppler US images of the left hemiscrotum show an enlarged heterogeneously hypoechoic epididymis (arrow) with concomitant multiple small hypoechoic nodules in the testis, compatible with a miliary pattern. Increased vascular flow in epididymis and testis is also seen. (**c**) Longitudinal US image of the right hemiscrotum shows an enlarged heterogeneously hypoechoic epididymis (arrow) and testis

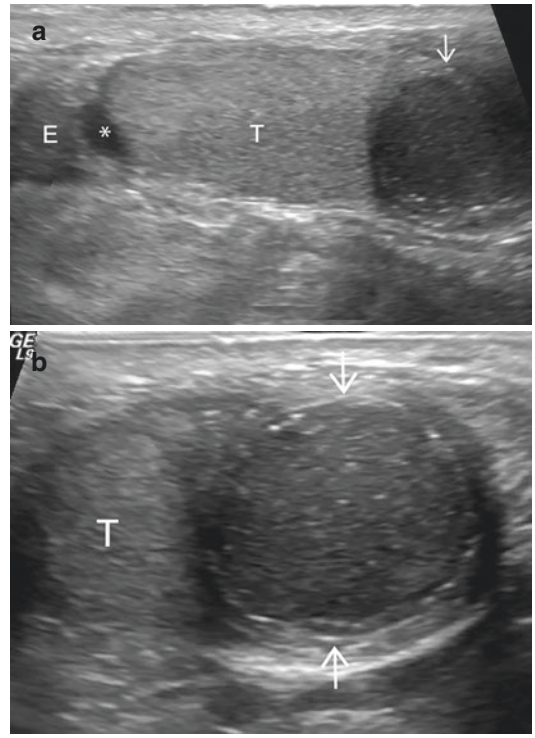

Fig. 7 Tuberculous epididymitis. (**a**) Longitudinal and (**b**) transverse US images of the left hemiscrotum show nodular enlargement in the epididymal tail with a heterogeneously hypoechoic pattern and rim calcifications (arrows). Small hydrocele (asterisk) is also seen. The epididymal head (E) and testis (T) appear normal

(Muneer et al. 2019). Many cases are incidentally detected during work-up for urinary tract TB or prostate cancer using multiparametric MRI, or retrospectively during pathological analysis of a transurethral resection specimen. Clinical symptoms and digital rectal examination are non-specific. An indurated prostate during the digital rectal examination and elevated serum prostate-specific antigen levels may be found, and hence be mistaken for prostate cancer.

Multiparametric MRI is the best imaging modality to assess the prostate, seminal vesicles, and ejaculatory ducts. MRI is more sensitive than CT and US imaging for demonstrating tuberculous prostatitis, which has two distinct imaging appearances, namely nodular and diffuse forms. In the nodular form, one or multiple enhancing small, markedly T2-hypointense nodules are present in the peripheral zone (Fig. 10a–c). The markedly hypointense T2 signal (signal slightly higher than muscle) is characteristic of TB, differentiating from prostate cancer (Engin et al. 2000; Cheng et al. 2015). This T2-hypointense signal has been attributed to macrophage-laden oxygen free radicals in granuloma or fibrosis, and should be distinguished from calcification. Diffusion restriction can be variable in nodular form (Bour et al. 2013; Cheng et al. 2015) (Fig. 10d).

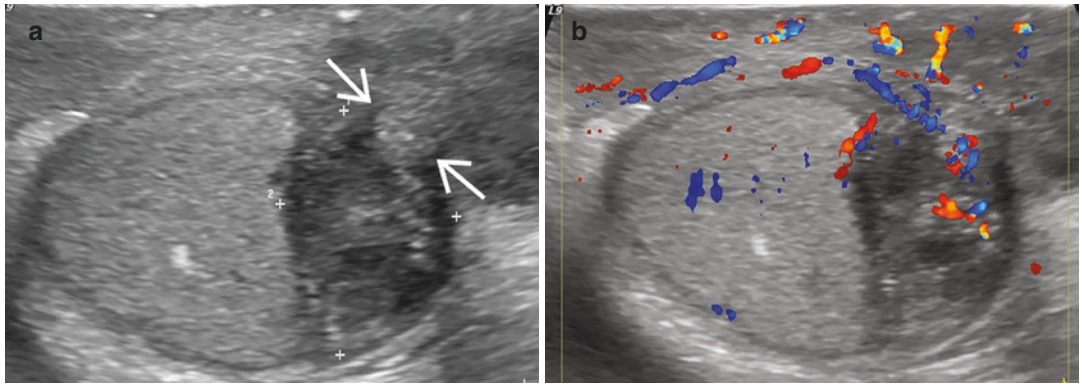

Fig. 8 Tuberculous epididymitis with sinus tract and scrotal wall abscess. (**a**) Transverse US image of the right hemiscrotum shows thickening of the scrotal skin, and an enlarged heterogeneously hypoechoic epididymis with a sinus tract extending to the scrotal wall (arrows). (**b**) Corresponding transverse color Doppler US image shows nonvascularized areas within the epididymis and scrotal wall which represent abscess formation

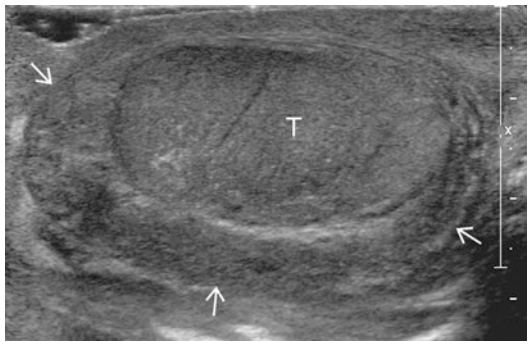

Fig. 9 Bacterial epididymo-orchitis. Longitudinal US image of the left hemiscrotum shows a diffusely enlarged homogeneously hypoechoic epididymis (arrows) and testis (T). Scrotal skin thickening is also seen

The diffuse pattern is more common and characterized by diffuse glandular enlargement, T2-hypointensity, mild-moderate enhancement and diffusion restriction; and may be indistinguishable from bacterial prostatitis (Cheng et al. 2015). Streaky, diffuse, and radiating areas of hypointense signal in the prostate (referred to as "watermelon skin") on T2-weighted MR images has been reported to be specific for tuberculous prostatitis (Engin et al. 2000) (Fig. 3f). Evolving abscesses, more common in HIV patients, are identified as T2-hyperintense foci showing marked central diffusion restriction and rim enhancement (Ramachandran et al. 2021) (Fig. 11a–d). The abscesses and inflammatory soft tissue can also be identified on CT. These findings are not specific for TB and cannot be distinguished from a pyogenic abscess in the absence of calcifications (Wang et al. 1997) (Fig. 2b). The seminal vesicles and the vas deferens also can be involved by TB, with cross-sectional images showing wall thickening, contraction, or intraluminal or wall calcifications (Jung et al. 2005) (Fig. 2b, d).

Extraprostatic extension may be found in both prostate cancer and florid granulomatous prostatitis. Deformation of the prostate contour and marked early contrast enhancement are features of malignancy (Ramachandran et al. 2021). MR spectroscopy is useful in differentiating TB from malignancy. Since malignant cells show elevated choline due to increased cell turnover and lose the ability to synthesize citrate, the choline-to-citrate ratio is elevated in malignancy beyond two standard deviations (>0.86) (Chen et al. 2010). Tuberculous abscesses may show a lipid-lactate peak.

Transrectal ultrasonography (TRUS) can also be used to evaluate prostate TB. Common findings in prostate TB on TRUS are poorly defined hypoechoic areas in the posterolateral peripheral zones (Engin et al. 2000). US-guided prostate biopsies of the hyperechoic lesions are required to confirm the diagnosis and exclude an underlying adenocarcinoma (Aziz et al. 2016).

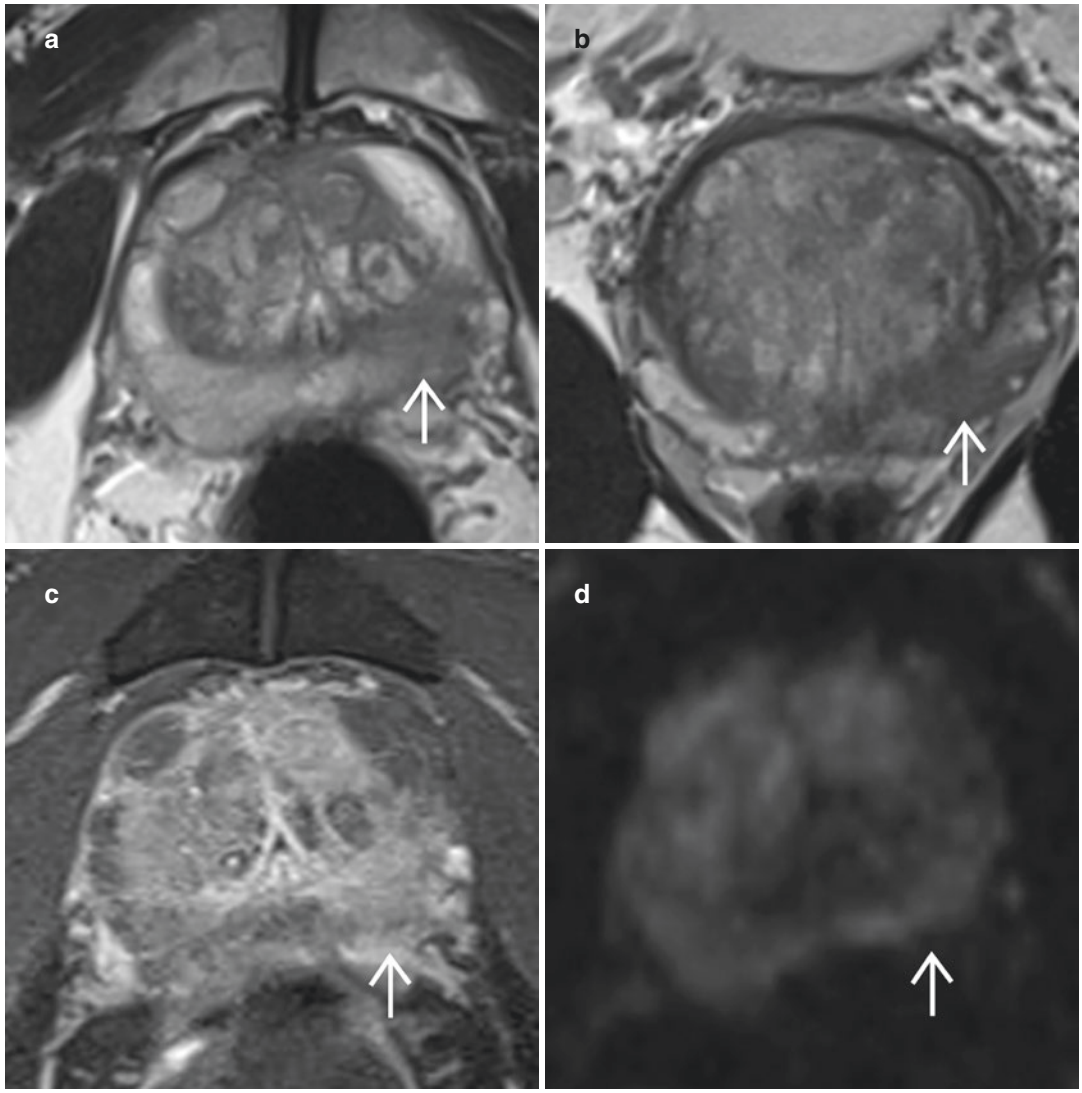

Fig. 10 Prostatic TB in a 64-year-old asymptomatic man who had a mild elevation of serum prostate-specific antigen (12 ng/mL) during his annual health check. (**a**) Axial and (**b**) coronal T2-weighted and (**c**) axial contrast-enhanced fat-suppressed T1-weighted MR images show a rectangular-shaped, T2-hypointense focus with moderate enhancement (arrow) in the left posterolateral peripheral zone of the apex, not causing any prostate contour deformation. (**d**) The lesion has mildly restricted diffusion on the high *b*-value diffusion-weighted image (*b*-value = 1400, arrow). The diagnosis of prostatic TB was confirmed with histopathological analysis

4.3 Female Genital Tuberculosis

The female genitalia are commonly affected by hematogenous and lymphatic transmission. The disease can also spread from abdominal and peritoneal TB. Genital TB is an important cause of female infertility in up to 17% of cases, especially in developing countries (Zhao and Hao 2014). The majority involve the fallopian tube (95–100%), endometrial cavity (50–60%), and ovaries (20–30%); while cervical and vulvovaginal TB are uncommon (Gatongi et al. 2005). Salpingitis caused by hematogenous dissemination is almost always bilateral (Engin et al. 2000).

Hysterosalpingography (HSG) is primarily used for identifying pathology and evaluating

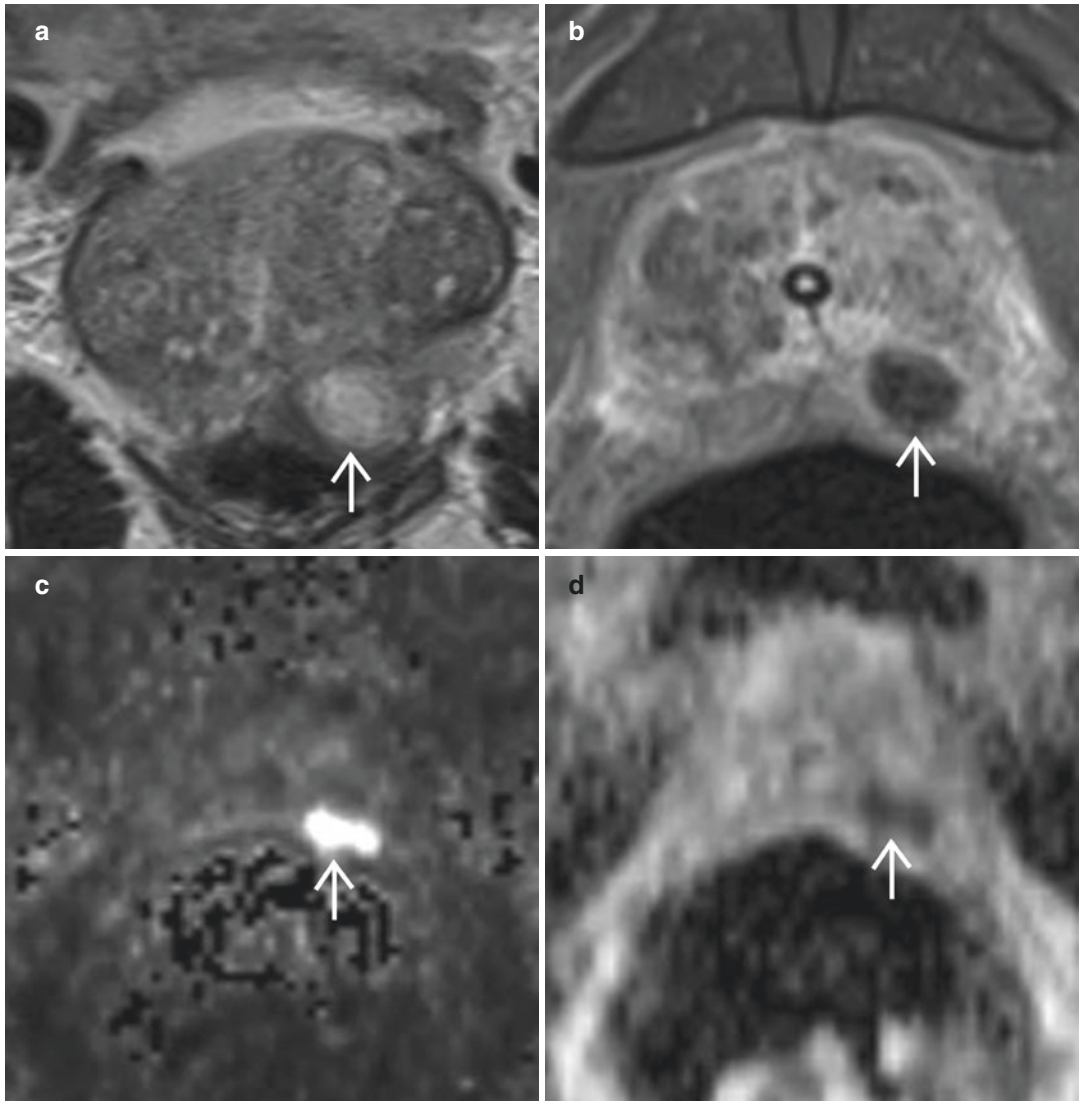

Fig. 11 Prostatic TB with abscess formation in a 72-year-old man who had TB epididymo-orchitis and mild raised serum prostate-specific antigen (10.7 ng/mL). (**a**) Coronal T2-weighted and (**b**) axial contrast-enhanced fat-suppressed T1-weighted MR images show a round T2-hyperintense fluid-pocket in the left posterior peripheral zone of the prostate with rim enhancement (arrow), representing the abscess. Axial (**c**) high *b*-value diffusion-weighted (*b*-value = 1400) and (**d**) ADC images show restricted diffusion (arrow)

patency of the uterus and fallopian tube, and is used for the investigation of infertility (Shah et al. 2015) (Fig. 12). Most changes are non-specific and related to chronic inflammation and fibrosis, including fallopian tube dilatation from hydrosalpinx or pyosalpinx (Fig. 12a), tubal stenosis, fallopian tube nodular scarring (salpingitis isthmic nodosa), endometrial adhesions with deformity, and obliteration of the endometrial cavity (Shah et al. 2015). Genital TB can be suspected when multiple adhesions are present at the fallopian tubes and uterine cavity, or when associated calcifications are observed (Grace et al. 2017).

US and cross-sectional imaging (CT or MRI) allows simultaneous evaluation of genital organs and extrapelvic involvement, such as ascites or thickened peritoneum in associated peritoneal

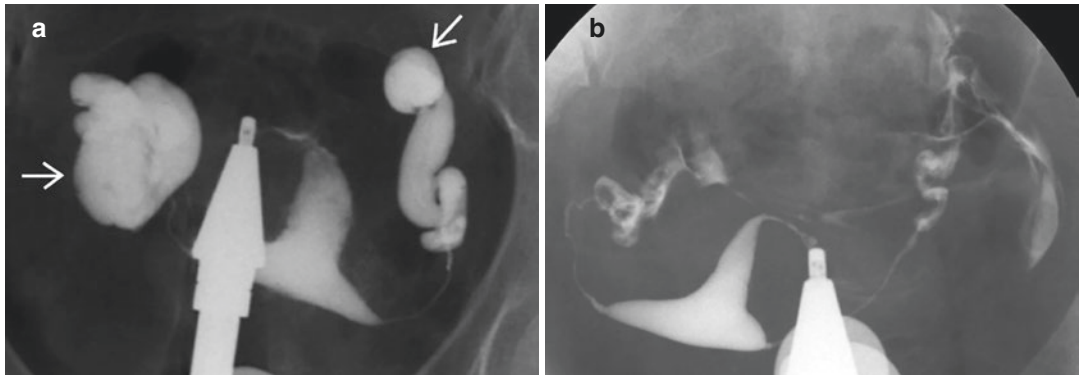

Fig. 12 (**a**) Hydrosalpinges in a 35-year-old woman with infertility who had history of pulmonary TB. HSG image shows diffuse dilatation of both fallopian tubes (arrows). The left fallopian tube is vertically oriented and fixed. There is no spillage of contrast media into the peritoneal cavity. (**b**) Normal HSG image in another patient shows a normal anteflexed uterus with patent bilateral fallopian tubes seen as a spillage of contrast media into the peritoneal cavity

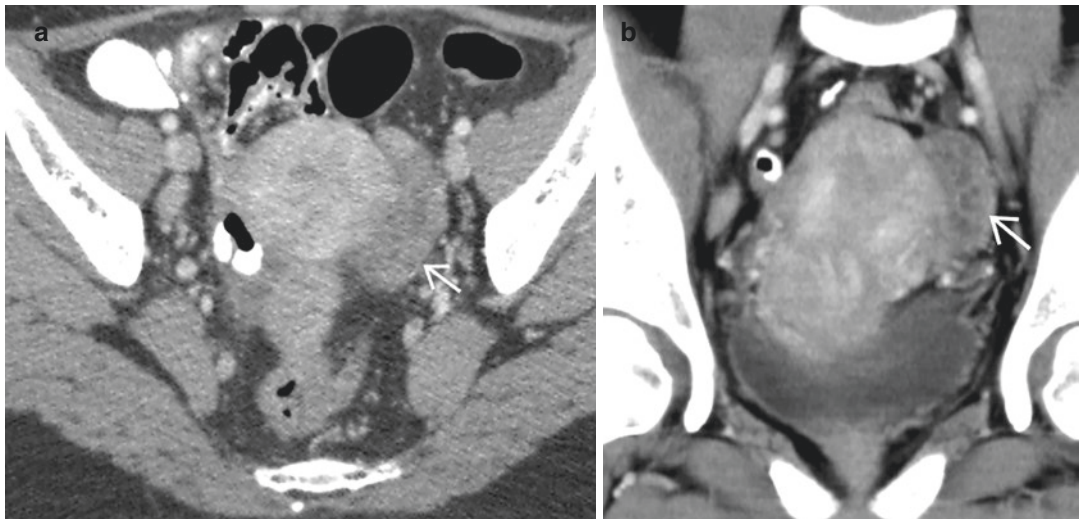

Fig. 13 Left tuberculous salpingitis in a 34-year-old woman. (**a**) Axial and (**b**) coronal contrast-enhanced CT images show a fluid-filled dilated left fallopian tube or hydrosalpinx (arrow)

disease. Presence of a tubo-ovarian abscess that extends through the peritoneum into the extraperitoneal compartment is suggestive of TB but may mimic ovarian tumor with peritoneal carcinomatosis (Engin et al. 2000; Harisinghani et al. 2000) (Figs. 13 and 14). The combination of abscess formation in the ovary and smooth peritoneal thickening supports the diagnosis of TB over peritoneal carcinomatosis (Fig. 14). The most frequent finding of tuberculous endometritis is a distended uterine cavity filled with heterogeneous material in the acute stage, which is a non-specific finding (Grace et al. 2017) (Fig. 14).

4.4 Adrenal Tuberculosis

From autopsy studies, adrenal gland infection accounts for 6% of cases with active TB and is the most common endocrine organ involved (Lam and Lo 2001). Bilateral adrenal involvement is expected, due to the hematogenous

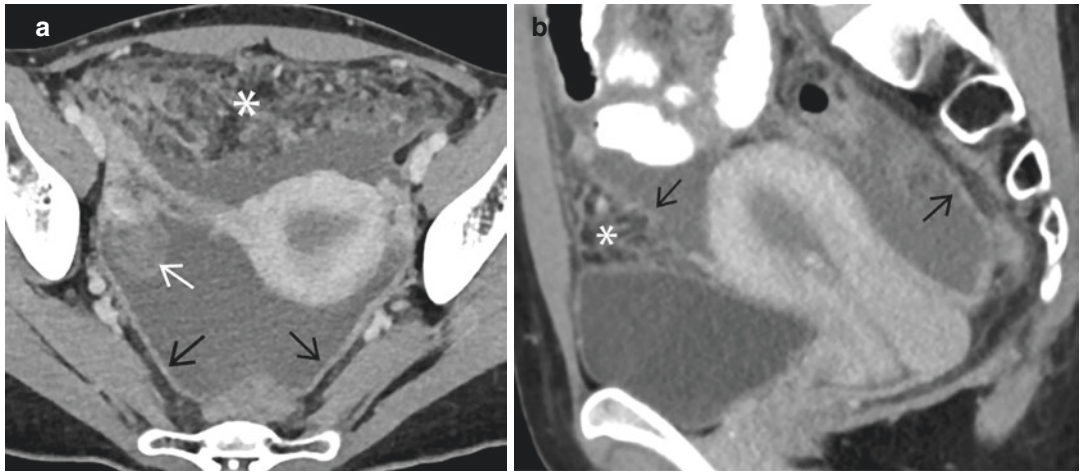

Fig. 14 Endometrial and right ovarian TB in a 38-year-old woman who had peritoneal TB. (**a**) Axial and (**b**) sagittal contrast-enhanced CT images show a prominent uterus with a fluid-filled uterine cavity and a prominent right ovary (white arrow). There is smooth peritoneal thickening (black arrows) and soft tissue infiltration of the omental fat (asterisk), representing peritoneal TB

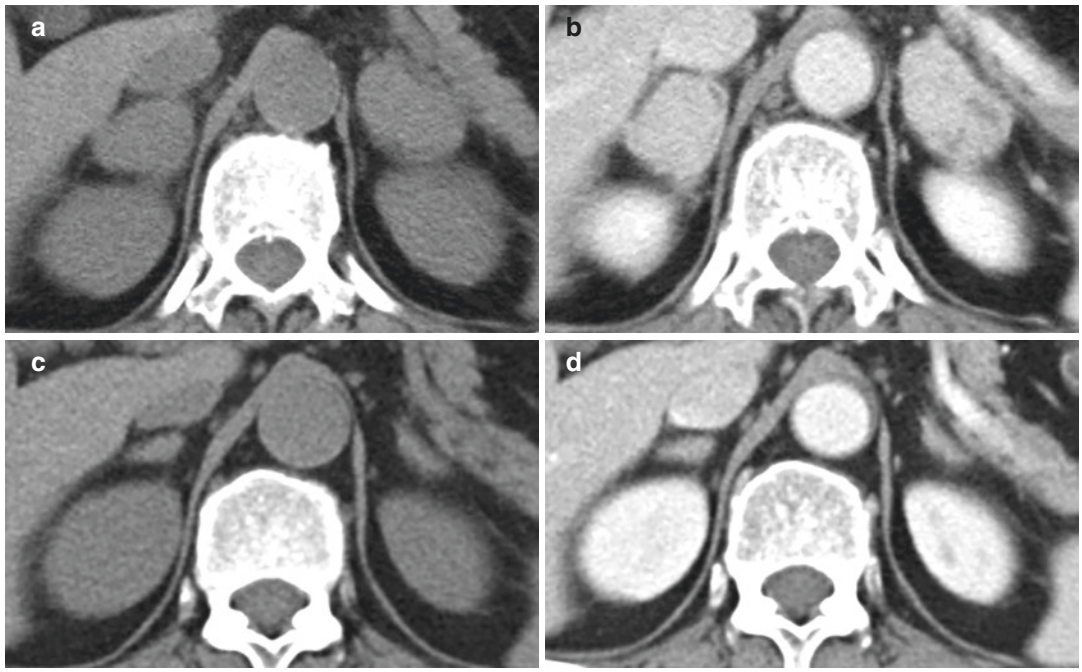

Fig. 15 Bilateral adrenal TB in a 73-year-old woman with pulmonary TB. Axial (**a**) unenhanced and (**b**) contrast-enhanced CT images show bilateral adrenal enlargement with homogeneous enhancement. Follow-up axial (**c**) unenhanced and (**d**) contrast-enhanced CT images obtained at 3 months following anti-TB treatment show normal adrenal glands

spread of TB. Adrenal TB is one of the common causes of adrenal insufficiency (or Addison disease) (Guo et al. 2007). During the early stages, the glands may appear enlarged with necrotic changes (Fig. 15). Calcifications and atrophy develop later (Engin et al. 2000; Harisinghani

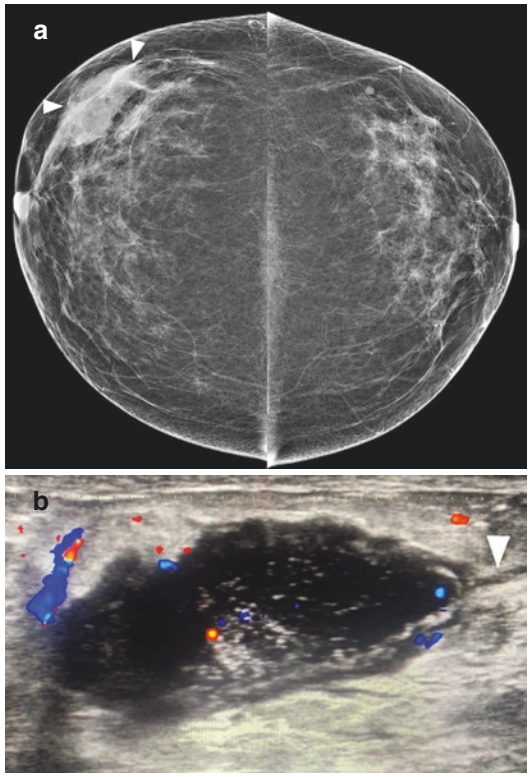

Fig. 16 Right tuberculous mastitis in a 36-year-old woman who presented with a recent palpable lesion. (**a**) Bilateral craniocaudal (CC) mammograms show an ill-defined mass (arrowheads) and trabecular thickening in right breast. (**b**) Corresponding color Doppler US image shows parenchymal edema in the right breast with an abscess and fistula tract (arrowhead). (Courtesy of Dr. Tanvi Jakhi, Mammocare, Mumbai, India)

et al. 2000). The radiological differential diagnosis includes metastases, lymphoma, primary neoplasm, hemorrhage, or other chronic infection such as histoplasmosis.

4.5 Tuberculous Mastitis

Tuberculous mastitis is a rare manifestation of extrapulmonary TB. The diagnosis is difficult because of non-specific clinical and imaging features. It is usually overlooked diagnostically and often misdiagnosed as malignancy or pyogenic inflammatory disease of the breast (Gon et al. 2013). Tuberculous mastitis may occur by direct inoculation of bacilli through the lactiferous ducts, secondary to primary tuberculous infection elsewhere in the body, or rarely, from direct extension from TB of the chest wall (Sakr et al. 2004; Teo et al. 2009). The disease commonly affects women of reproductive age (Shinde et al. 1995; Farrokh et al. 2019). Farrokh et al. (2019) found the mean age of affected patients to be 33.7 years. Tuberculous mastitis mostly presents as a painless or painful lump. Infrequent presentations include inflammatory changes such as skin discoloration, skin ulcer, sinus tract, and nipple discharge.

There are three forms of mammographic appearances, namely nodular, diffuse, and sclerosing. The nodular form is the most common finding. The mass can have well-defined margins mimicking benign breast lesions in the early stage; while in the later stage, the mass can have ill-defined or spiculated margins mimicking carcinoma (Fig. 16a). The diffuse form is seen as an area of diffusely increased density with skin thickening and edema, resembling inflammatory breast carcinoma. The sclerosing form may appear as an ill-defined irregular dense mass with focal or diffuse skin thickening. Associated nipple retraction and reduced breast volume may occur, which means that it cannot be differentiated from malignancy (Sakr et al. 2004; Farrokh et al. 2019). If there is localized skin thickness and sinus formation associated with an ill-defined breast mass, breast TB needs to be included in the differential diagnosis (Baykan et al. 2021) (Fig. 16b). US imaging can better identify masses hidden by dense fibroglandular breast tissue at mammography, differentiate cystic from solid lesions, hence adding confidence in excluding malignancy.

In our experience, we have seen many cases of tuberculous axillary lymphadenitis without evidence of mastitis (Muttarak et al. 2002). We have also seen a few cases of chest wall TB presenting as a palpable breast mass (Pattamapaspong et al. 2011). Patients with tuberculous axillary

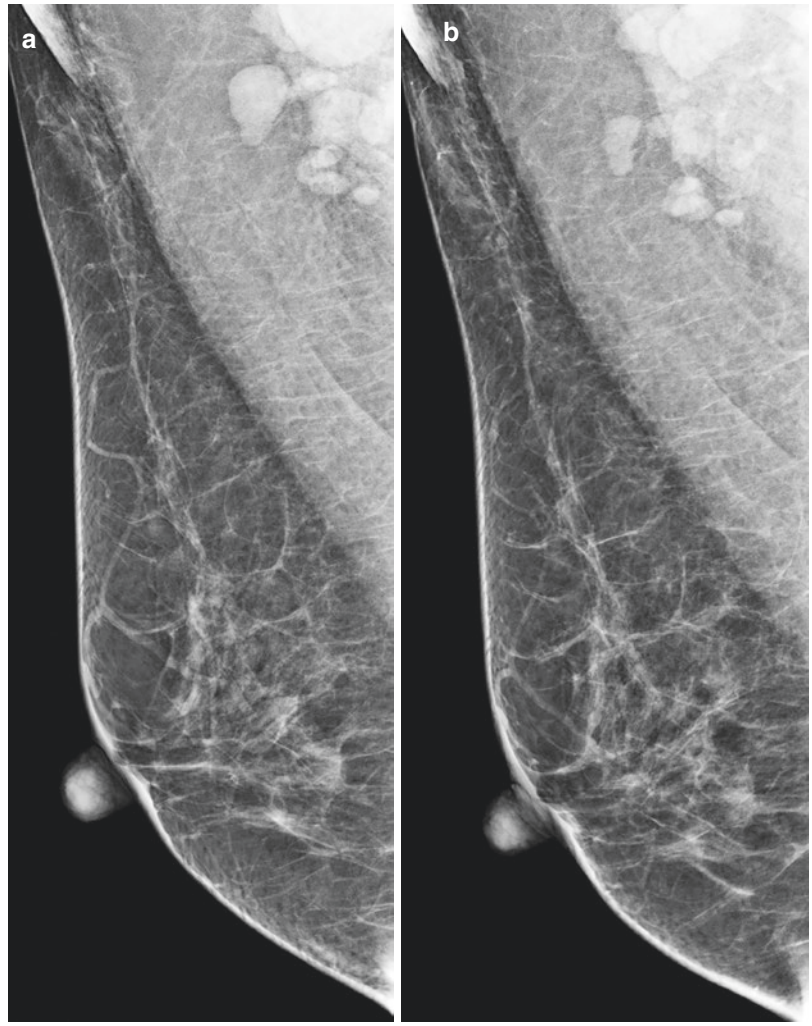

Fig. 17 Tuberculous lymphadenitis in a 49-year-old woman who had a palpable right axillary mass. (**a**) Right mediolateral oblique (MLO) mammogram shows multiple enlarged, dense axillary nodes without abnormality in the breast. US-guided fine-needle aspiration of the node showed caseous necrotic material with positive acid-fast bacilli. (**b**) Right MLO mammogram 6 months following anti-TB therapy shows smaller size of the axillary nodes

lymphadenitis most commonly present with a palpable axillary mass, and mammography is usually performed to search for occult breast cancer. On mammography, tuberculous axillary lymphadenitis appears as large homogeneous dense nodes with either well- or ill-defined margins and may be matted (Fig. 17). These findings cannot be differentiated from other causes of lymphadenopathy. The presence of macrocalcifications is suggestive of tuberculous lymphadenitis (Muttarak et al. 2002).

Patients with chest wall TB may present as a palpable breast mass mimicking breast cancer or abscess (Teo et al. 2009; Pattamapaspong et al. 2011). Mammography and US imaging are usually indicated in women presenting with a palpable breast mass. On mammography, the mass may not be distinguishable from cancer or abscess. US imaging identifies a fluid collection rather than a solid mass (Figs. 18 and 19). Nevertheless, CT is more helpful than US to evaluate the extent of the lesion and identify

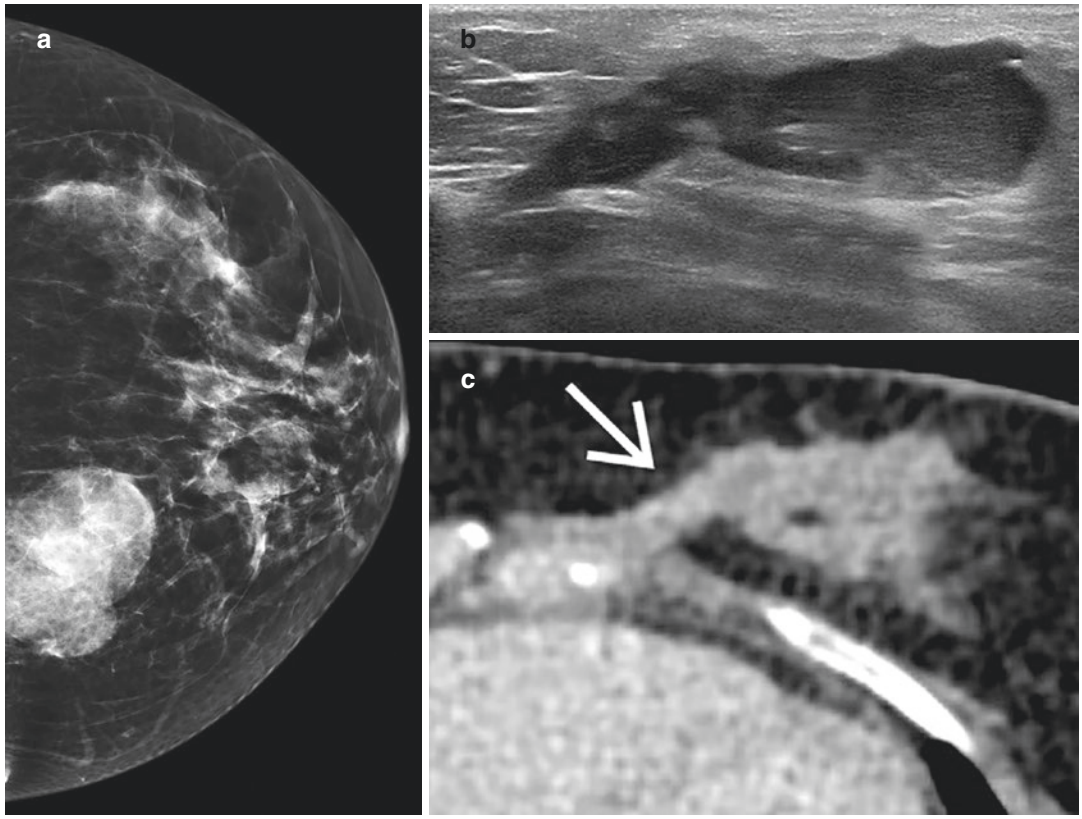

Fig. 18 Chest wall TB in a 49-year-old woman who had a history of tuberculous arthritis and presented with a palpable left breast mass. (**a**) Left craniocaudal (CC) mammogram shows a circumscribed high-density mass at the posterior inner quadrant. (**b**) Composite US images show an ill-defined hypoechoic collection at the posterior aspect of the breast. (**c**) Axial contrast-enhanced CT image shows an ill-defined hypodense mass lesion with connection (arrow) to the costochondral junction

associated chest wall and intrathoracic lesions (Figs. 18c and 19c).

5 Diagnosis Confirmation

The diagnosis is established by the demonstration of acid-fast bacilli or positive cultures from the urine, semen, pus, or biopsy specimens. However, the diagnostic yield is often not satisfactory because of the paucity of microorganisms. The diagnostic yield of urine microscopy is about 10% and urine culture is about 30–40% (Berta et al. 2011). At least three, but preferably five, serial microbiological studies with early morning urine (including postejaculate and postmassage urine), ejaculate and prostate secretion, including smears and cultures, should be performed to confirm the diagnosis of urogenital TB (Kulchavenya et al. 2016).

Molecular methods examining for the presence of *M. tuberculosis*-specific DNA in biopsy specimens or urine samples provide more reliable diagnostic results and early identification of drug-resistant strains (Kohli et al. 2018; Chen et al. 2019). Histological finding of granulomatous inflammation, although non-specific, helps to suggest the diagnosis of TB. Identification of acid-fast bacilli in tissue specimens does not confirm that the organism is mycobacterium, and confirmation by culture or molecular methods is still required (Muneer et al. 2019). In patients suspected of

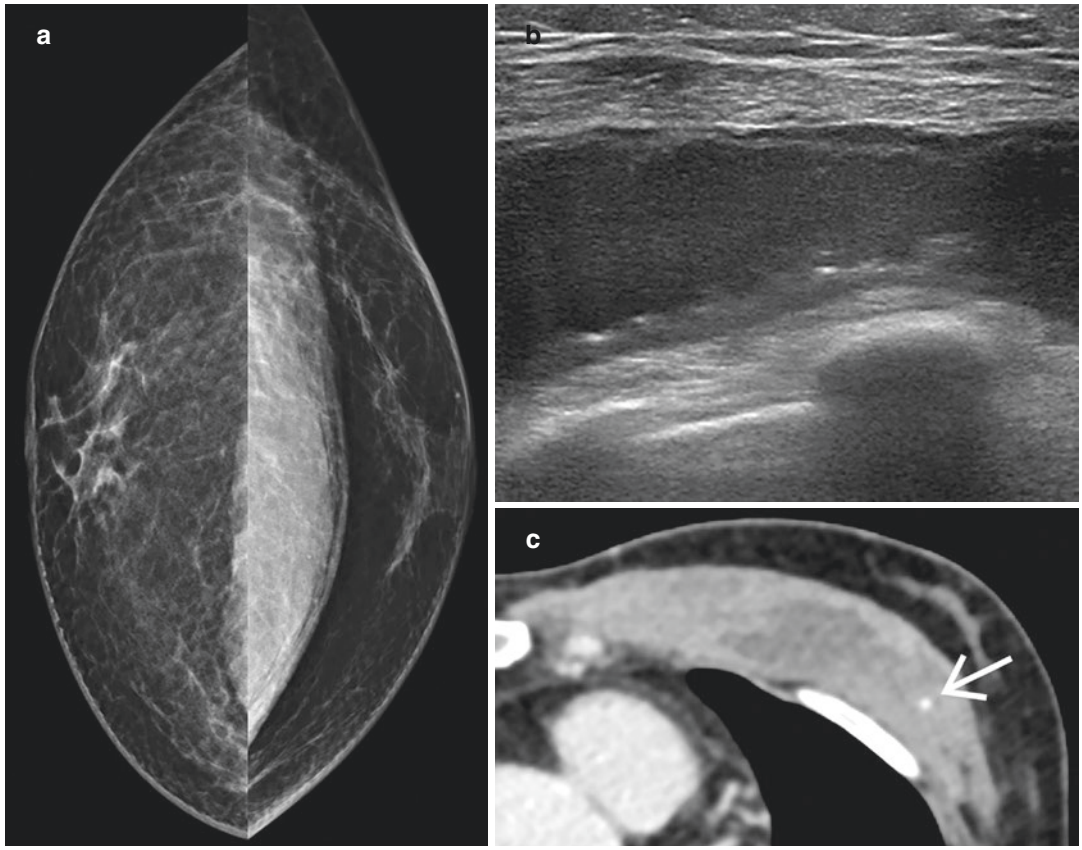

Fig. 19 Tuberculous pyomyositis in a 53-year-old man who had a history of disseminated TB and presented with bilateral breast enlargement. (**a**) Bilateral craniocaudal (CC) mammograms show bilateral gynecomastia and an enlarged, dense left pectoralis muscle. (**b**) US image of the left breast shows a hypoechoic mass in the pectoralis muscle. (**c**) Axial contrast-enhanced CT image shows enlargement of the left pectoralis muscle with an irregular hypodense mass and calcification (arrow)

having urogenital TB, but without documented evidence of mycobacterium, the diagnosis of urogenital TB has to be made based on other features such as histological findings, imaging findings, or clinical features (Kulchavenya et al. 2016).

6 Treatment

Generally, urogenital TB is treated with anti-TB drugs, similar to pulmonary TB. Drug-sensitive TB requires 6–9 months of World Health Organization (WHO)-recommended standard treatment regimens (Furin et al. 2019). Drug-resistant TB requires 12–24 months of therapy with toxic drugs with close monitoring (Furin et al. 2019). Surgical management is an adjunctive treatment for certain circumstances, such as drainage of abscess, correction of urinary tract obstruction, resection of nonfunctioning kidney, correction of tubal obstruction, or neobladder creation for a contracted bladder (Bansal and Bansal 2015).

Surgical treatment is required in up to 50% of patients during or after anti-TB drug therapy (Kulchavenya 2013). Patients with urogenital TB should be followed up for control or eradication, or if symptoms persist or recur after completion of the therapy. Patients should be seen every 6 months for 1–3 years, depending on the

form and stage of the disease (Bansal and Bansal 2015). Serial monitoring with US imaging or IVU enables an early diagnosis of progression or worsening of hydronephrosis, enabling early surgical intervention (Bansal and Bansal 2015). Following the full course of the therapy, patients should be under surveillance for 3–5 years, with an annual check-up for relapse (Kulchavenya 2013).

7 Conclusion

Urogenital TB remains a neglected clinical problem due to its cryptic and protean clinical manifestations. Imaging findings are widely variable, and depend on the extent and stage of the disease. However, concomitant involvement along the urogenital tract with combined stricture and dilatation of the collecting system, calcification, and sinus tract formation are suggestive of TB. Combined with the appropriate clinical context, imaging can support the diagnosis of urogenital TB, as well as guide tissue sampling which is still required for a definitive diagnosis. Knowing these characteristic imaging findings can lead to early diagnosis and help establish prompt and efficient treatment.

Acknowledgements We would like to thank Associate Professor Suwalee Pojchamarnwiputh and Assistant Professor Wittanee Na Chiangmai for their invaluable advice.

References

Aziz EM, Abdelhak K, Hassan FM (2016) Tuberculous prostatitis: mimicking a cancer. Pan Afr Med J 25:130

Bansal P, Bansal N (2015) The surgical management of urogenital tuberculosis our experience and long-term follow-up. Urol Ann 7:49–52

Baykan AH, Sayiner HS, Inan I et al (2021) Primary breast tuberculosis: imaging findings of a rare disease. Insights Imaging 12:19

Berta M, Sturm G, Juri L et al (2011) Bacteriological diagnosis of renal tuberculosis: an experience at the regional tuberculosis laboratory in Cordoba Province, Argentina. Rev Argent Microbiol 43:191–194

Borthwick WM (1946) The pathogenesis of tuberculous epididymitis. Edinb Med J 53:55–70

Bour L, Schull A, Delongchamps NB et al (2013) Multiparametric MRI features of granulomatous prostatitis and tubercular prostate abscess. Diagn Interv Imaging 94:84–90

Chakaya J, Khan M, Ntoumi F et al (2021) Global Tuberculosis Report 2020—reflections on the global TB burden, treatment and prevention efforts. Int J Infect Dis 11. S1201-9712(21)00193-4

Chattopadhyay A, Bhatnagar V, Agarwala S et al (1997) Genitourinary tuberculosis in pediatric surgical practice. J Pediatr Surg 32:1283–1286

Chen Y, Liu M, Guo Y (2010) Proton magnetic resonance spectroscopy in prostate tuberculosis. Urology 75:1065–1066

Chen Y, Wu P, Fu L et al (2019) Multicentre evaluation of Xpert MTB/RIF assay in detecting urinary tract tuberculosis with urine samples. Sci Rep 9:11053

Cheng Y, Huang L, Zhang X et al (2015) Multiparametric magnetic resonance imaging characteristics of prostate tuberculosis. Korean J Radiol 16:846–852

Drudi FM, Laghi A, Iannicelli E et al (1997) Tubercular epididymitis and orchitis: US patterns. Eur Radiol 7:1076–1078

Dyer RB, Chen MY, Zagoria RJ (1998) Abnormal calcifications in the urinary tract. Radiographics 18:1405–1424

Engin G, Acunas B, Acunas G et al (2000) Imaging of extrapulmonary tuberculosis. Radiographics 20:471–488. quiz 529-530,532

Farrokh D, Alamdaran A, Feyzi Laeen A et al (2019) Tuberculous mastitis: a review of 32 cases. Int J Infect Dis 87:135–142

Figueiredo AA, Lucon AM, Junior RF et al (2008) Epidemiology of urogenital tuberculosis worldwide. Int J Urol 15:827–832

Furin J, Cox H, Pai M (2019) Tuberculosis. Lancet 393:1642–1656

Gambhir S, Ravina M, Rangan K et al (2017) Imaging in extrapulmonary tuberculosis. Int J Infect Dis 56:237–247

Gatongi DK, Gitau G, Kay V et al (2005) Female genital tuberculosis. Obstet Gynaecol 7:75–79

Gaudiano C, Tadolini M, Busato F et al (2017) Multidetector CT urography in urogenital tuberculosis: use of reformatted images for the assessment of the radiological findings. A pictorial essay. Abdom Radiol (NY) 42:2314–2324

Goel A, Dalela D (2008) Options in the management of tuberculous ureteric stricture. Indian J Urol 24:376–381

Gon S, Bhattacharyya A, Majumdar B et al (2013) Tubercular mastitis—a great masquerader. Turk Patoloji Derg 29:61–63

Grace GA, Devaleenal DB, Natrajan M (2017) Genital tuberculosis in females. Indian J Med Res 145:425–436

Guo YK, Yang ZG, Li Y et al (2007) Uncommon adrenal masses: CT and MRI features with histopathologic correlation. Eur J Radiol 62:359–370

Harisinghani MG, Mcloud TC, Shepard JA et al (2000) Tuberculosis from head to toe. Radiographics 20: 449–470. quiz 528–529, 532

Jung YY, Kim JK, Cho KS (2005) Genitourinary tuberculosis: comprehensive cross-sectional imaging. AJR Am J Roentgenol 184:143–150

Kenney PJ (1990) Imaging of chronic renal infections. AJR Am J Roentgenol 155:485–494

Kohli M, Schiller I, Dendukuri N et al (2018) Xpert((R)) MTB/RIF assay for extrapulmonary tuberculosis and rifampicin resistance. Cochrane Database Syst Rev 8:CD012768

Kulchavenya E (2013) Best practice in the diagnosis and management of urogenital tuberculosis. Ther Adv Urol 5:143–151

Kulchavenya E (2014) Extrapulmonary tuberculosis: are statistical reports accurate? Ther Adv Infect Dis 2:61–70

Kulchavenya E, Kholtobin D (2015) Diseases masking and delaying the diagnosis of urogenital tuberculosis. Ther Adv Urol 7:331–338

Kulchavenya E, Brizhatyuk E, Khomyakov V (2014) Diagnosis and therapy for prostate tuberculosis. Ther Adv Urol 6:129–134

Kulchavenya E, Naber K, Bjerklund Johansen TE (2016) Urogenital tuberculosis: classification, diagnosis, and treatment. Eur Urol Suppl 15:112–121

Lam KY, Lo CY (2001) A critical examination of adrenal tuberculosis and a 28-year autopsy experience of active tuberculosis. Clin Endocrinol (Oxf) 54:633–639

Lamm DL, Stogdill VD, Stogdill BJ et al (1986) Complications of bacillus Calmette-Guerin immunotherapy in 1278 patients with bladder cancer. J Urol 135:272–274

Merchant S, Bharati A, Merchant N (2013) Tuberculosis of the genitourinary system-urinary tract tuberculosis: renal tuberculosis—part I. Indian J Radiol Imaging 23:46–63

Muneer A, Macrae B, Krishnamoorthy S et al (2019) Urogenital tuberculosis—epidemiology, pathogenesis and clinical features. Nat Rev Urol 16:573–598

Muttarak M, Peh WCG, Lojanapiwat B et al (2001) Tuberculous epididymitis and epididymo-orchitis: sonographic appearances. AJR Am J Roentgenol 176:1459–1466

Muttarak M, Pojchamarnwiputh S, Chaiwun B (2002) Mammographic features of tuberculous axillary lymphadenitis. Australas Radiol 46:260–263

Muttarak M, Chiangmai WN, Lojanapiwat B (2005) Tuberculosis of the genitourinary tract: imaging features with pathological correlation. Singapore Med J 46:568–575

Pattamapaspong N, Muttarak M, Sivasomboon C (2011) Tuberculosis arthritis and tenosynovitis. Semin Musculoskelet Radiol 15:459–469

Ramachandran A, Das CJ, Razik A (2021) Male genital tract tuberculosis: a comprehensive review of imaging findings and differential diagnosis. Abdom Radiol (NY) 46:1677–1686

Rui X, Li XD, Cai S et al (2008) Ultrasonographic diagnosis and typing of renal tuberculosis. Int J Urol 15:135–139

Sakr AA, Fawzy RK, Fadaly G et al (2004) Mammographic and sonographic features of tuberculous mastitis. Eur J Radiol 51:54–60

Shah HU, Sannananja B, Baheti AD et al (2015) Hysterosalpingography and ultrasonography findings of female genital tuberculosis. Diagn Interv Radiol 21:10–15

Shinde SR, Chandawarkar RY, Deshmukh SP (1995) Tuberculosis of the breast masquerading as carcinoma: a study of 100 patients. World J Surg 19:379–381

Subramanyam P, Palaniswamy SS (2015) Dual time point (18)F-FDG PET/CT imaging identifies bilateral renal tuberculosis in an immunocompromised patient with an unknown primary malignancy. Infect Chemother 47:117–119

Teo TH, Ho GH, Chaturverdi A et al (2009) Tuberculosis of the chest wall: unusual presentation as a breast lump. Singapore Med J 50:e97–e99

Vijayaraghavan SB, Kandasamy SV, Arul M et al (2004) Spectrum of high-resolution sonographic features of urinary tuberculosis. J Ultrasound Med 23:585–594

Wang LJ, Wong YC, Chen CJ et al (1997) CT features of genitourinary tuberculosis. J Comput Assist Tomogr 21:254–258

Yadav S, Singh P, Hemal A et al (2017) Genital tuberculosis: current status of diagnosis and management. Transl Androl Urol 6:222–233

Yang DM, Yoon MH, Kim HS et al (2001) Comparison of tuberculous and pyogenic epididymal abscesses: clinical, gray-scale sonographic, and color Doppler sonographic features. AJR Am J Roentgenol 177:1131–1135

Yang DM, Kim SH, Kim HN et al (2003) Differential diagnosis of focal epididymal lesions with gray scale sonographic, color Doppler sonographic, and clinical features. J Ultrasound Med 22:135–142. quiz 143–144

Zachoval R, Nencka P, Vasakova M et al (2018) The incidence of subclinical forms of urogenital tuberculosis in patients with pulmonary tuberculosis. J Infect Public Health 11:243–245

Zhao WH, Hao M (2014) Pelvic inflammatory disease: a retrospective clinical analysis of 1922 cases in North China. Gynecol Obstet Invest 77:169–175

Imaging of Spinal Tuberculosis

Mouna Chelli Bouaziz, Mohamed Fethi Ladeb, Wafa Achour, and Mohamed Chakroun

Contents

M. Chelli Bouaziz (✉) · M. F. Ladeb
Department of Radiology, MT Kassab Institute of Orthopaedics, Tunis, Tunisia

Faculty of Medicine of Tunis, Tunis-El Manar University, Tunis, Tunisia
e-mail: bouaziz_mouna@yahoo.fr; fethiladeb@hotmail.fr

W. Achour
Laboratory Department, National Bone Marrow Transplant Center, Tunis, Tunisia

Faculty of Medicine of Tunis, Tunis-El Manar University, Tunis, Tunisia
e-mail: wafaachour@gmail.com

M. Chakroun
Department of Infectious Diseases, Fattouma Bourguiba Hospital, Monastir, Tunisia

Faculty of Medicine of Monastir, University of Monastir, Monastir, Tunisia
e-mail: chakrounme@gmail.com

Abstract

Spinal tuberculosis remains frequent in low- and middle-income countries, with an increased incidence of infections having been recently observed in developed countries. It represents 25–60% of all musculoskeletal tuberculosis. Tuberculous spondylodiscitis (also called Pott disease), isolated tuberculous vertebral osteomyelitis and primitive neural arch tuberculosis are the three main anatomico-radiological patterns. Magnetic resonance imaging is the gold standard imaging technique for the assessment of spinal tuberculosis, allowing an early and precise diagnosis. In the absence of early and adequate treatment, the disease may progress, leading to spinal deformities and/or neurological impairment. The diagnosis is usually straightforward when the patient already has existing extraskeletal tuberculosis. Otherwise, spinal tuberculosis is typically confirmed by bacteriological and/or histopathological tests.

© The Author(s), under exclusive license to Springer Nature Switzerland AG 2022

M. F. Ladeb, W. C. G. Peh (eds.), *Imaging of Tuberculosis*, Medical Radiology Diagnostic Imaging,
https://doi.org/10.1007/978-3-031-07040-2_12

Abbreviations

AFB	Acid-fast bacilli
CT	Computed tomography
MRI	Magnetic resonance imaging
TB	Tuberculosis

1 Introduction

Tuberculosis (TB) remains endemic in most developing countries. Its incidence varies between 191 every 100,000 inhabitants in sub-Saharan Africa to 237 every 100,000 inhabitants in South-East Asia (Durieux 1990; Lacut et al. 1995; Billo 1996; Huchon 1997). A resurgence of TB, with a rising incidence of spinal TB, has also been reported in the recent decades. Since 1980, cases in the industrialized countries of Europe and the USA have emerged, mainly in immigrants from endemic countries with a high prevalence of TB, in some groups with poor social conditions and in immunocompromised patients, such as those with acquired immunodeficiency syndrome (AIDS) (Durieux 1990; Aït Khaled et al. 1997; Garg and Somvanshi 2011; Moon 2014).

2 Epidemiology

Musculoskeletal involvement accounts for 1–5% of all tuberculous locations and 9–19% of extrapulmonary TB (Eschard et al. 1993; Lacut et al. 1995; Murray 1996; Aït Khaled et al. 1997; Bernard and Perronne 1997; Pertuiset et al. 1997; Moon 2014). Spinal TB represents 25–60% of musculoskeletal TB (Hamza 1993; Resnick 1995; Cotten et al. 1996; Engin et al. 2000; Tuli 2002; Ben Taarit et al. 2003; De Backer et al. 2006). However, the exact incidence and prevalence of spinal TB are unknown in most parts of the world. Currently, most of the patients with spinal TB in developed countries are immigrants from countries where TB is endemic (Garg and Somvanshi 2011). In Europe, the mean age of musculoskeletal TB varies from 45 to 72 years in native patients, and from 27 to 39 years in patients coming from developing countries (Aït Khaled et al. 1997). Children are more frequently affected in developing countries (Lacut et al. 1995; Garg and Somvanshi 2011). No gender predilection has been observed in most European and American series, as the disease involves males and females equally (Aït Khaled et al. 1997; Garg and Somvanshi 2011).

3 Pathophysiology

Musculoskeletal TB is generally due to *Mycobacterium tuberculosis*. In our experience, *Mycobacterium bovis* is observed in about 20% of cases (Chebbi et al. 2019). Musculoskeletal TB results from reactivation of a pulmonary primary infection focus (Murray 1996; Aït Khaled et al. 1997) after a variable delay, which is usually shorter in children (Eschard et al. 1993; Lacut et al. 1995; Aït Khaled et al. 1997; Pertuiset et al. 1997; Garg and Somvanshi 2011; Moon 2014). Tuberculous bacillus spreads hematogenously and infects the spine, hips, and knees (Moon 2014). Direct inoculation is rare (Lacut et al. 1995; Garg and Somvanshi 2011; Moon 2014). Spinal involvement usually results from hematogenous spread of *Mycobacterium tuberculosis* into the vasculature of the cancellous vertebral body. The primary infection site is usually either a pulmonary or a genitourinary lesion. Spread occurs either via the arterial or venous route (Garg and Somvanshi 2011). The vertebrae are extremely well vascularized, even in adulthood, which may explain the predilection for spinal disease (Agrawal et al. 2010).

Local or general predisposing factors are noted in 17–50% of cases; including poverty, overcrowding, illiteracy, malnutrition, alcoholism, drug abuse, diabetes mellitus, chronic hemodialysis, immunosuppressive therapy, and human immunodeficiency virus (HIV) infection (Eschard et al. 1993; Lacut et al. 1995; Aït Khaled et al. 1997; Moon 2014). However, musculoskeletal TB seems to be less frequent compared to infections due to atypical mycobacteria in people living with HIV (up to 9%) with severe immunodepression (Durieux 1990; Lacut et al. 1995; Aït

Khaled et al. 1997; Pertuiset et al. 1997; Garg and Somvanshi 2011; Moon 2014). Genetic susceptibility to spinal TB has recently been demonstrated, with an association found between FokI polymorphism in the vitamin D receptor gene and susceptibility to spinal TB (Garg and Somvanshi 2011).

4 Anatomico-radiological Patterns

Three main anatomico-radiological patterns of spinal TB have been described, namely tuberculous spondylodiscitis, also called Pott disease; solitary vertebral involvement, also called tuberculous spondylitis or vertebral osteomyelitis; and primitive neural arch tuberculosis. Spondylodiscitis indicates the involvement of the disc and vertebra, and accounts for 47–94% of spinal TB (Davies et al. 1984; Eschard et al. 1993; Cotten et al. 1996; Chebbi et al. 2019). Spondylitis or vertebral osteomyelitis refers to exclusive involvement of the vertebra, with sparing of the adjacent discs. These "skip lesions" are due to spread of infection along the Batson perivertebral plexus of veins (Agrawal et al. 2010). They may result in a vertebral collapse or extend into the spinal canal (Stabler and Reiser 2001). Subligamentous extension to contiguous or noncontiguous vertebrae without disc involvement is quite frequent, resulting in a multilevel tuberculous spondylitis. In a series of 206 cases of spinal TB, spondylitis accounted globally for 50%, varying from 30% in autochthonous inhabitants to 61% in immigrants (Aït Khaled et al. 1997). In spinal TB studied by MRI, spondylitis accounted for 28–54% of cases (Pertuiset et al. 1999).

Primitive neural arch TB represents 1–37% of spinal TB. It is characterized by the increased frequency of epidural abscesses, spinal instability, and spinal cord compression (Eschard et al. 1993; Cotten et al. 1996; Naim-Ur-Rahaman et al. 1999; Ansari et al. 2001; Stabler and Reiser 2001; Boussel et al. 2002; Chebbi et al. 2019). Other patterns of spinal TB seem to be rare, although limited data are available in the literature. Subligamentous TB is a rare presentation in which infection is initially located under the anterior longitudinal ligament and results in anterior erosion of multiple vertebral bodies with adjacent abscess formation (Morvan et al. 1998; Ansari et al. 2001; Stabler and Reiser 2001; Narlawar et al. 2002; Nassar et al. 2002). This presentation is more frequently observed in children (Sharif et al. 1995; Mahboubi and Morris 2001; Moorthy and Prabhu 2002; Chebbi et al. 2019). Primitive tuberculous epidural abscesses usually involve males and are located in the thoracic spine (Stabler and Reiser 2001; Ben Taarit et al. 2003). Spinal cord and nerve root involvement may be isolated or associated with spondylodiscitis. They may be observed at any age but usually occur in young adults (Ben Taarit et al. 2003; Gupta et al. 2015; Mishra et al. 2015).

4.1 Tuberculous Spondylodiscitis

Tuberculous spondylodiscitis was first described by Sir Percival Pott in 1779.

4.1.1 Pathogenesis

The subchondral bone of the vertebral body anterior corners, which is the most vascularized region, is usually the initial location of TB. The disease then extends to the adjacent vertebral body by contiguity beneath the anterior or posterior longitudinal ligament or through vascular anastomoses (Eschard et al. 1993; Lacut et al. 1995), causing progressive destruction of the disc and vertebra (Morvan et al. 1998; Ben Taarit et al. 2003; Chebbi et al. 2019). More than one vertebra is usually involved because of spread via the longitudinal vascular anastomosis. In children, the disc can be primarily involved by the hematogenous route, due to its vascularized nature (Morvan et al. 1998; Engin et al. 2000; Rasouli et al. 2012).

The disease may extend to the paravertebral soft tissues or to the spinal canal (Lacut et al. 1995), where tissue necrosis results in perivertebral abscess formation (Narlawar et al. 2002). Tuberculous abscesses are typically large, surrounded by a smooth wall, and may result in sinus tract formation (Dorcas and David 1995;

Huchon 1997). A lack of proteolytic enzymes in mycobacterial infections, in comparison with pyogenic infections, has been suggested as the possible cause of the subligamentous spread and would also explain the abscess delimitation. The abscess extension is related to the site of vertebral infection, adjacent soft tissue anatomy and gravity (Resnick 1995). At the cervical spine, abscesses develop anteriorly and laterally; whereas thoracic abscesses develop beneath the longitudinal spinal ligament. Lumbar abscesses develop along the psoas muscle and may reach the iliac fossa and the Scarpa triangle. The presence of central or peripheral calcifications is characteristic of tuberculous abscesses (Resnick 1995; Naim-Ur-Rahaman et al. 1999; Stabler and Reiser 2001; Moorthy and Prabhu 2002; Chelli Bouaziz et al. 2013).

4.1.2 Topography (Fig. 1)

The lower thoracic and upper lumbar spine are the most frequently involved sites (80%) (Turgut

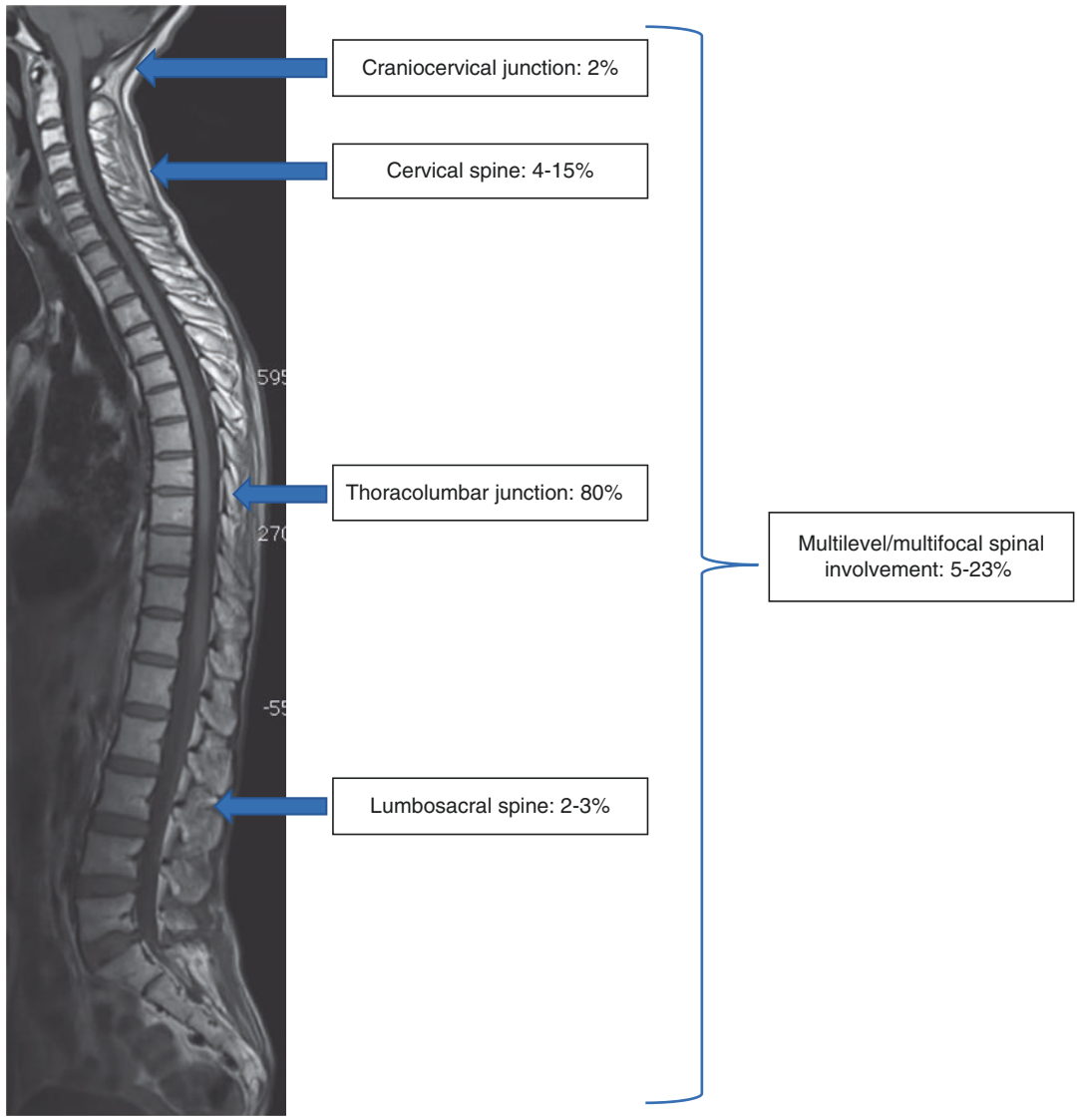

Fig. 1 Location of spinal tuberculosis

2001; Ben Taarit et al. 2003; Teo and Peh 2004). The cervical spine is involved in only 4–15% of cases (Cotten et al. 1996; Pertuiset et al. 1997) and the lumbosacral spine in 2–3% of cases (Pertuiset et al. 1999; Harisinghani et al. 2000; Moore and Rafii 2001). Multiple vertebrae are involved in 5–23% of cases, mainly in children, immigrants, and immunocompromised persons (Pertuiset et al. 1997; Lamer et al. 1998; Papavero et al. 1999; Turgut 2001; Colmenero et al. 2004; Golden and Vikram 2005; Le Roux et al. 2005). The vertebral body is more frequently involved than the posterior arch.

4.1.3 Clinical Features

The onset of spinal TB is very gradual and the clinical presentation is typically insidious. The delay between the first symptoms and the diagnosis has decreased from 6 to 24 months in the past, to a mean of 3 months in recent studies (Hamza 1993; Pertuiset et al. 1997). Spinal pain, usually marked, may be mechanical at the early stages, becoming inflammatory later on (Lacut et al. 1995; Murray 1996; Ben Taarit et al. 2003; Colmenero et al. 2004). Night sweats are observed in 20% of cases, with fatigue and gradual weight loss. A moderate evening fever is observed in about 50% of cases. Neurological impairment is frequent (35–60% of cases) with variable patterns and severity (e.g., radicular pain, paraplegia). Spinal cord compression and cauda equina syndrome are observed in about 25–30% of cases (Pertuiset et al. 1997). Spinal TB revealed by a sinus tract is exceptional in developed countries (Davies et al. 1984; Resnick 1995; Cotten et al. 1996; Pertuiset et al. 1999; Rasouli et al. 2012). Clinical examination shows segmental spine stiffness with paravertebral contracture or soft tissue abscesses (15–30% of cases). Spinal deformity is unusual (Ladeb et al. 2019).

4.1.4 Imaging Features

4.1.4.1 Radiographs

Radiographs are usually the first imaging examination to be performed when spinal TB is suspected. Subchondral bone resorption and osteolysis of the anterior vertebral corners are the first radiographical signs (Fig. 2). As the disease progresses, large intravertebral cavities continuous with the disc may be observed, typically limited by thin sclerosis and containing sequestra in half of the cases (Hamza 1993; Dorcas and David 1995) (Fig. 3). Bone sclerosis is seen less frequently than in brucellar or pyogenic spondylodiscitis (Moore and Rafii 2001; Stabler and Reiser 2001; Dinc et al. 2002).

The intervertebral disc height is initially preserved. Subsequently, partial or complete disc narrowing may appear, usually involving the anterior aspect (Fig. 4). The association of a normal disc height with intravertebral cavities is highly suggestive of spinal TB (Davies et al. 1984; Naim-Ur-Rahaman et al. 1999; Mahboubi and Morris 2001). Spontaneous evolution may

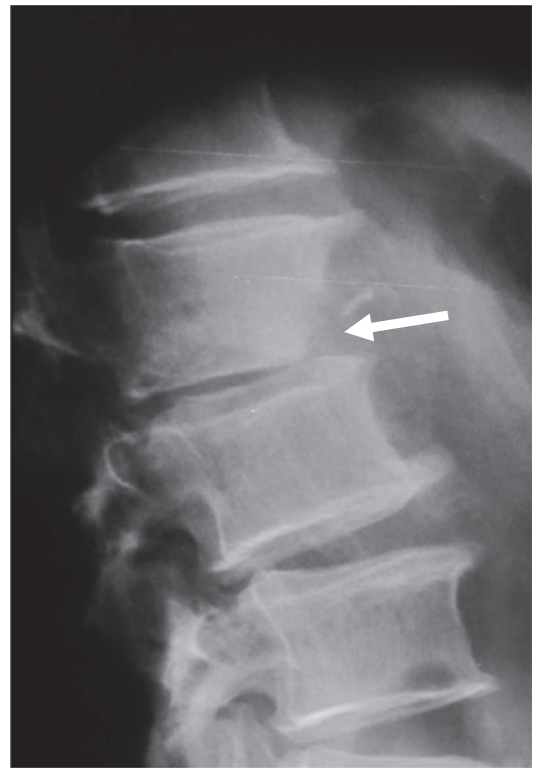

Fig. 2 Tuberculous spondylodiscitis of the lumbar spine. Lateral radiograph shows narrowing of the intervertebral disc space with subchondral bone resorption and osteolysis of the adjacent anterior-inferior vertebral body (arrow)

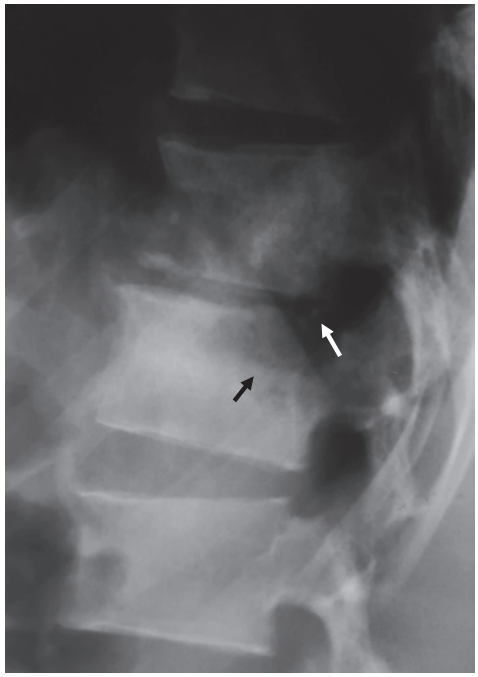

Fig. 3 Tuberculous spondylodiscitis of the lumbar spine. Lateral radiograph shows a large intravertebral cavity at the superior aspect of L1 vertebral body (black arrow), continuous with the disc and containing a sequestrum (white arrow). There is adjacent sclerosis and narrowing of T12/L1 intervertebral space

result in vertebral collapse or anterior vertebral fusion, causing subsequent kyphosis (Fig. 5). Paravertebral abscess of the cervical spine appears on radiographs as a thickening of the prevertebral soft tissues (Fig. 6); whereas in the thoracic spine, it appears as a mediastinal opacity (Fig. 7) that may extend far from the discovertebral lesion. In the lumbar spine, paravertebral abscess may be seen as convexity of the lateral aspect of the psoas muscle (Dorcas and David 1995; Boussel et al. 2002; Dinc et al. 2002).

4.1.4.2 Ultrasound Imaging

Ultrasound imaging has a limited role in the diagnosis of spinal TB. It may be used at the cervical or lumbar level in the assessment of paravertebral abscesses and/or to guide needle aspiration or biopsy of these abscesses (Harisinghani et al. 2000) (Fig. 8).

4.1.4.3 Magnetic Resonance Imaging

Magnetic resonance imaging (MRI) is the method of choice for the assessment and follow-up of spinal TB (Sharif et al. 1995; Ridley et al.

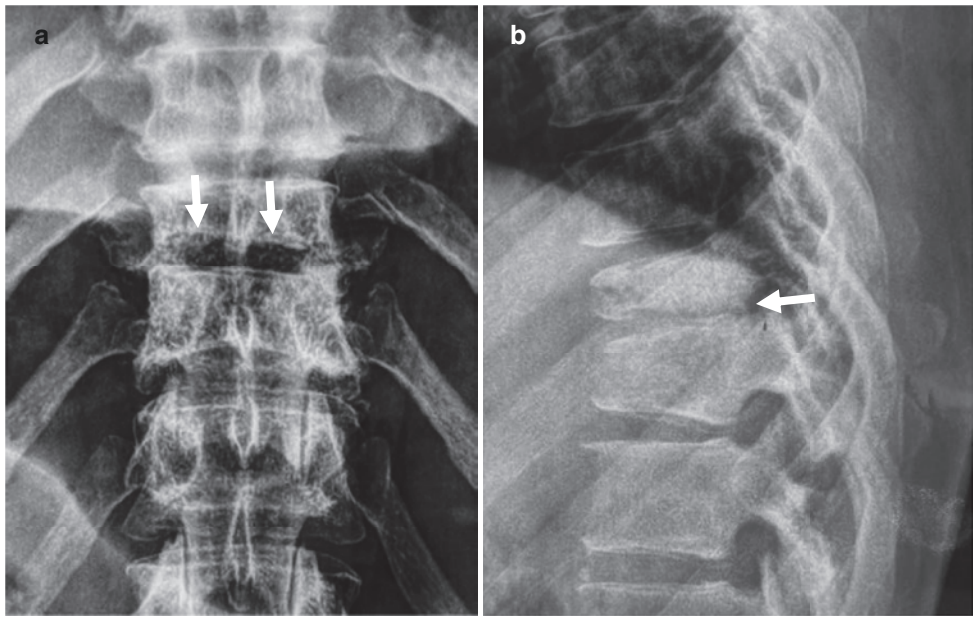

Fig. 4 Tuberculous spondylodiscitis of the lower thoracic spine. (**a**) Anteroposterior and (**b**) lateral radiographs show moderate T10 and mild T11 vertebral body compression, T10/T11 intervertebral disc narrowing with adjacent end-plate destruction, worse at the T10 vertebra (arrows)

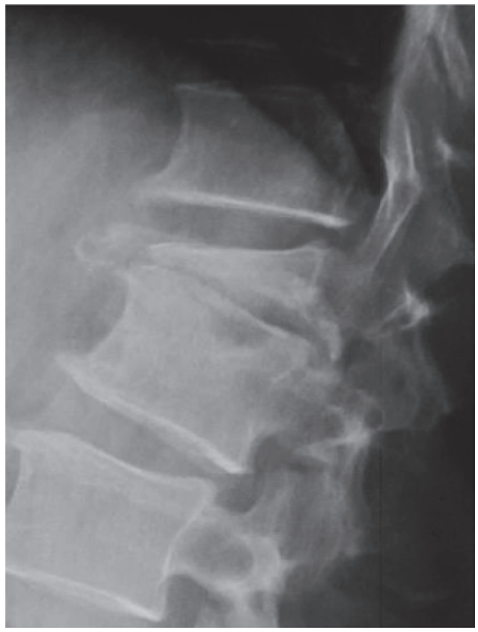

Fig. 5 Tuberculous spondylodiscitis of the lumbar spine. Lateral radiograph shows L1/L2 vertebral fusion with angular kyphosis

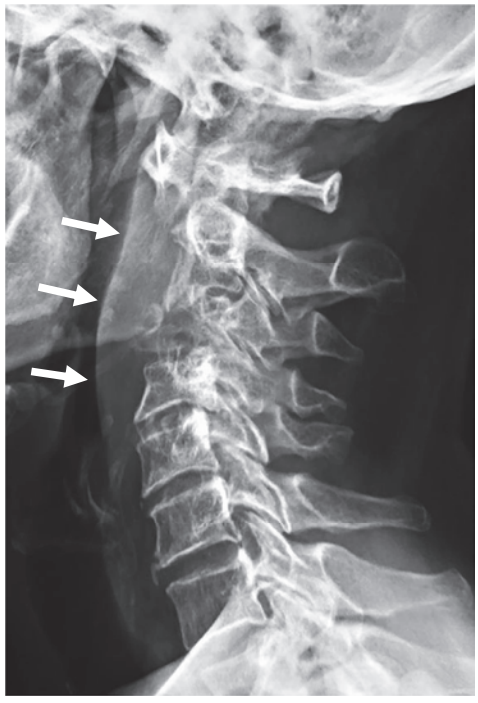

Fig. 6 Tuberculous spondylitis of the cervical spine. Lateral radiograph shows compression of C3 vertebral body and marked thickening of the prevertebral soft tissues (arrows). Note the anterior atlanto-axial subluxation

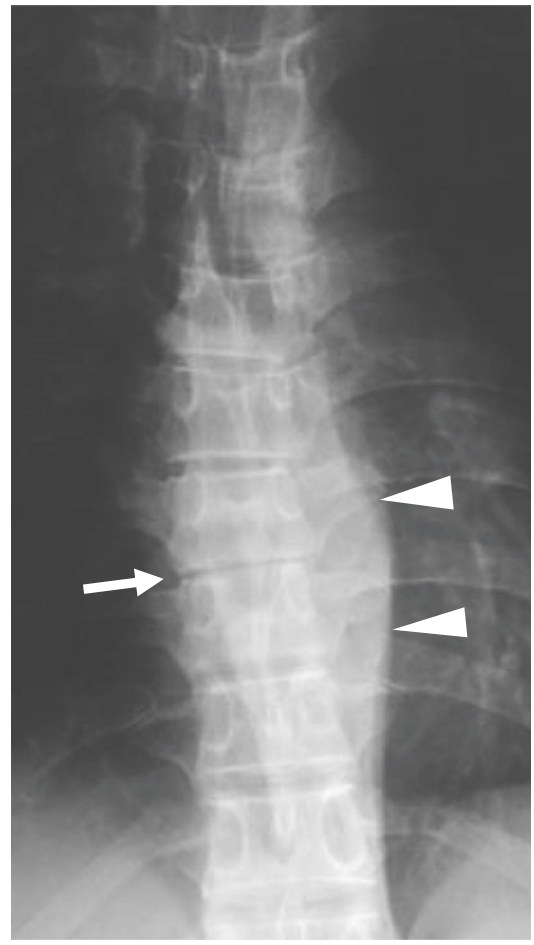

Fig. 7 Tuberculous spondylodiscitis of the thoracic spine. Anteroposterior radiograph shows T8/T9 disc narrowing (arrow) with paravertebral soft tissue thickening (arrowheads)

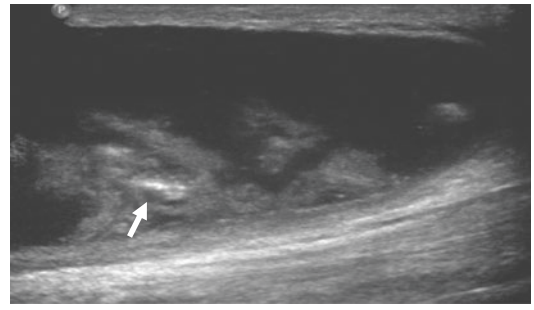

Fig. 8 Tuberculous spondylodiscitis of the thoracic spine. Ultrasound image shows a large soft tissue abscess surrounded by a thin and smooth wall and containing thin calcifications (arrow)

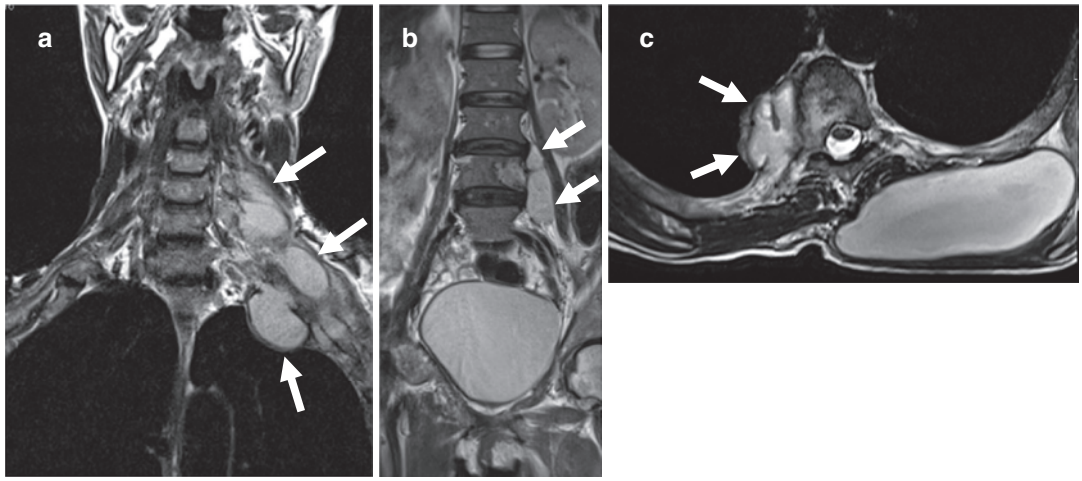

Fig. 9 Multifocal spinal tuberculosis. (**a** and **b**) Coronal and (**c**) axial T2-W MR images show multilevel spinal involvement with skip lesions involving the cervical (**a**), thoracic (**c**), and lumbar (**b**) spine (arrows)

1998; Moore and Rafii 2001; Stabler and Reiser 2001; Boussel et al. 2002; Moorthy and Prabhu 2002; Nassar et al. 2002; Teo and Peh 2004). The sensitivity of MRI enables early detection of bone changes before they appear on radiographs and CT. Moreover, this nonirradiating imaging method allows an assessment of the whole spine to look for additional asymptomatic spine locations, also called "skip infections," which may be observed in 16–70% of cases (Cotten et al. 1996; Morvan et al. 1998; Engin et al. 2000; Harisinghani et al. 2000; Jain 2010; Rivas-Garcia et al. 2013) (Fig. 9).

MRI is performed using a spine array coil, and the protocol usually includes spin-echo T1-weighted sequences before and after intravenous gadolinium-based contrast administration in at least two orthogonal planes. The coronal plane is particularly useful to assess the extension of paravertebral abscesses and to rule out additional involvement of sacro-iliac and/or coxo-femoral joints (Sharif et al. 1995; Boussel et al. 2002). Spin-echo or fast spin-echo T2-weighted images with fat suppression or contrast-enhanced fat-suppressed T1-weighted MR images are more sensitive to detect early abnormalities of bone, spinal canal, and paravertebral soft tissues (Narlawar et al. 2002).

The involved vertebral body usually appears T1-hypointense and T2-hyperintense, with heterogeneous enhancement on contrast-enhanced T1-weighted images (Morvan et al. 1984; Ridley et al. 1998; Harisinghani et al. 2000; Nassar et al. 2002; Teo and Peh 2004). Intraosseous abscesses appear as areas of T1-hypointensity and T2-hyperintensity, with rim enhancement (Figs. 10 and 11). The penumbra sign described on T1-weighted sequences represents a relatively high T1 intensity of the internal layer of the abscess wall due to the presence of paramagnetic free radicals produced by activated macrophages. This sign appears to be very specific (99%) for abscess (Fig. 12) (Moser et al. 2012). Atypical MRI patterns have been reported, including intermediate to hypointense T2 signal or hyperintense T1 signal of the vertebral body (Pertuiset et al. 1999). This latter sign, usually observed in young patients, may be explained by the increased level of proteins in the caseum (central necrotic material of tuberculous lesions) (Boussel et al. 2002).

Upon infection, the T2 signal of the intervertebral disc remains normal for a long time, then the signal increases with disappearance of the disc cleft. On T1-weighted images, the intervertebral disc is of intermediate signal intensity (Pertuiset et al. 1999; Boussel et al. 2002). Intravenous

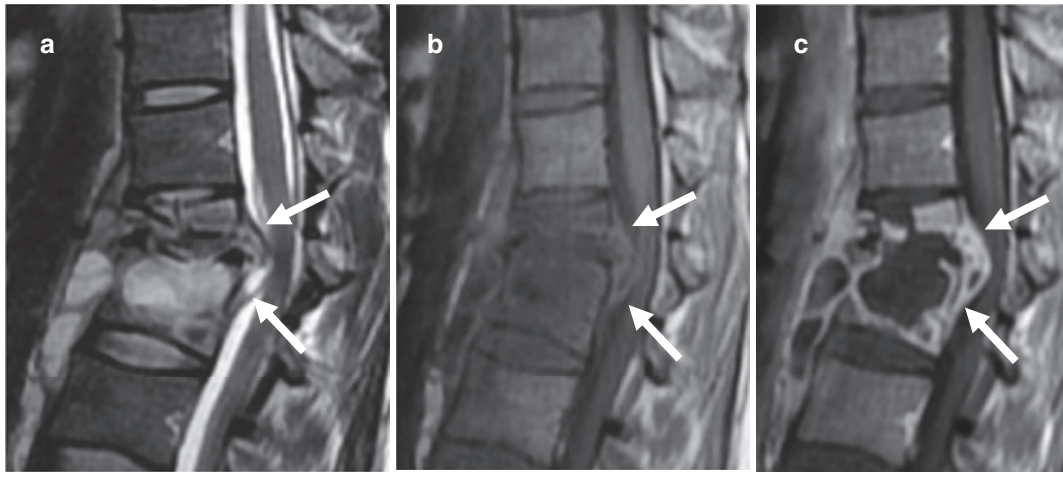

Fig. 10 Tuberculous spondylodiscitis with intraosseous abscess and epidural extension. Sagittal (**a**) T2-W, (**b**) T1-W, and (**c**) contrast-enhanced T1-W MR images show T2-hyperintense and T1-hypointense signal of the disc and adjacent vertebral bodies with peripheral enhancement. This extends to the epidural abscess (arrows) causing spinal cord compression

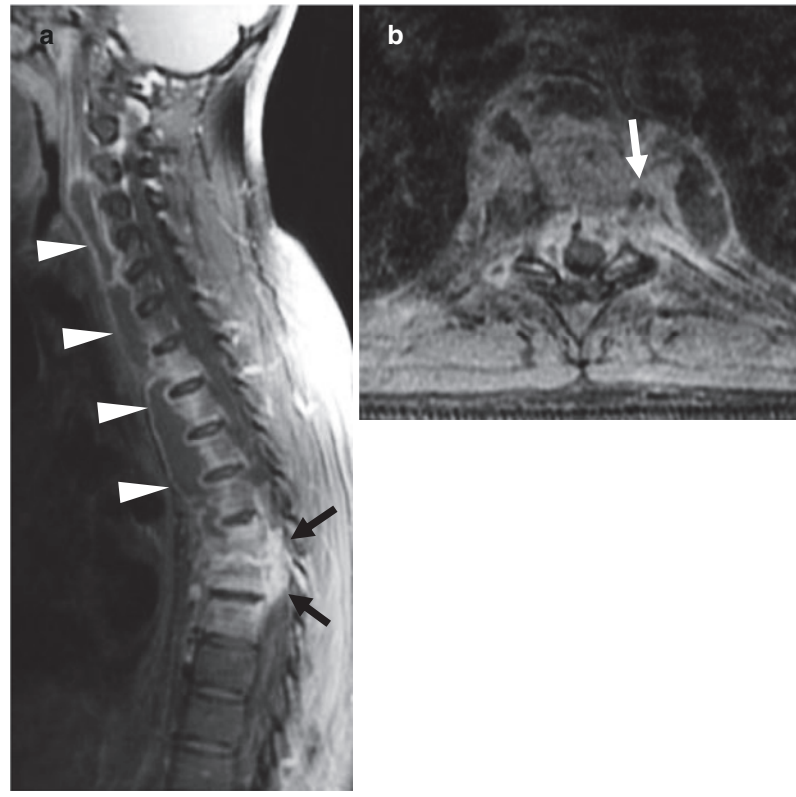

Fig. 11 Multilevel tuberculous spondylodiscitis of the thoracic spine. (**a**) Sagittal and (**b**) axial contrast-enhanced fat-suppressed T1-W MR images show multilevel vertebral body and intervertebral disc enhancement with epidural extension (black arrows). Note the extensive subligamentous spread of prevertebral abscesses (arrowheads), bilobed appearance of the epidural abscess, and the extension to the left costovertebral joint (white arrow)

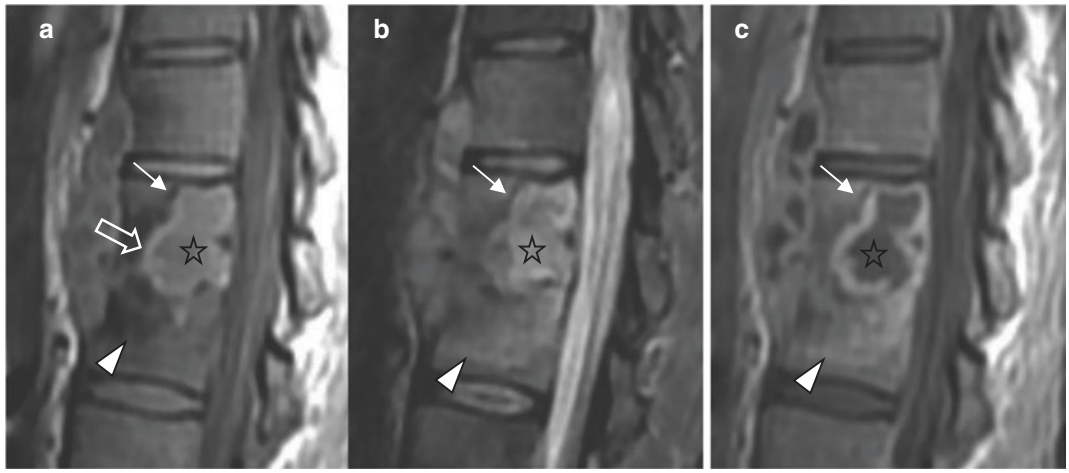

Fig. 12 Tuberculous spondylodiscitis with penumbra sign. Sagittal (**a**) T1-W, (**b**) T2-W, and (**c**) contrast-enhanced T1-W MR images show a target appearance of a vertebral body abscess at the T12-L1 level with four concentric layers: abscess center (pus) with T1-hypointense and T2-hyperintense signal (star), abscess wall with T1-hyperintense signal corresponding to granulation tissue (penumbra sign) (open arrow), reactive sclerosis with T1- and T2-hypointense signal (white arrow), and peripheral bone edema with T1-hypointense and T2-hyperintense signal (arrowhead)

contrast administration results either in a diffuse or rim enhancement. A normal or T2-hypointense disc signal may be observed in children at the early stage of the disease, in granulomatous spondylodiscitis or in vertebral spondylitis (Teo and Peh 2004; Chelli Bouaziz et al. 2013; Chelli Bouaziz et al. 2017). MRI allows a precise assessment of disease extension to the paravertebral soft tissues and the spinal canal.

Abscesses show hyperintense T2 signal and hypointense to intermediate T1 signal, surrounded by smooth well-defined and well-vascularized walls (Morvan et al. 1984; Boussel et al. 2002; Teo and Peh 2004). Epidural phlegmon appears as an epidural mass of intermediate T1 and hyperintense T2 signal, with enhancement on contrast-enhanced T1-weighted images (Boussel et al. 2002). Epidural abscess and phlegmon typically show a "bilobed" shape (Madhok and Sachdeva 2016) (Fig. 13). MRI is an excellent tool to assess the longitudinal extent of the epidural abscess or mass, and its effects on the spinal cord or the cauda equina (Morvan et al. 1998; Boussel et al. 2002).

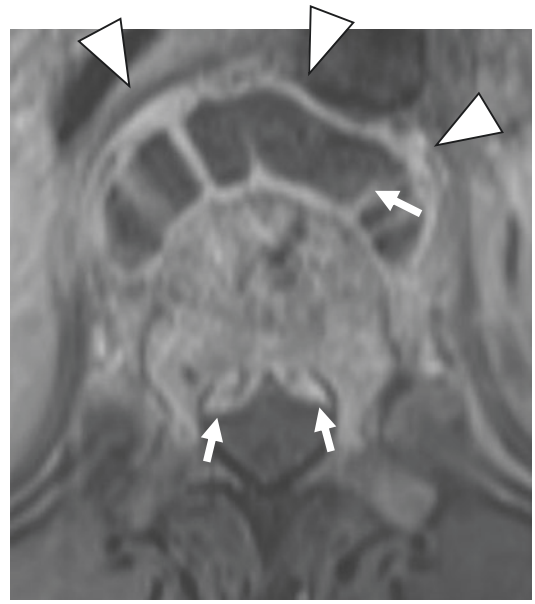

Fig. 13 Tuberculous spondylodiscitis with bilobed epidural abscess. Axial contrast-enhanced T1-W MR image shows a bilobed epidural abscess (arrows). There is also a large anterior abscess (arrowheads)

Associated lesions, including arachnoiditis, myelitis, or intramedullary tuberculomas, are well depicted by MRI, particularly on contrast-enhanced T1-weighted images. They appear as linear or nodular enhancement of the subarachnoid space, spinal cord, or nerve roots

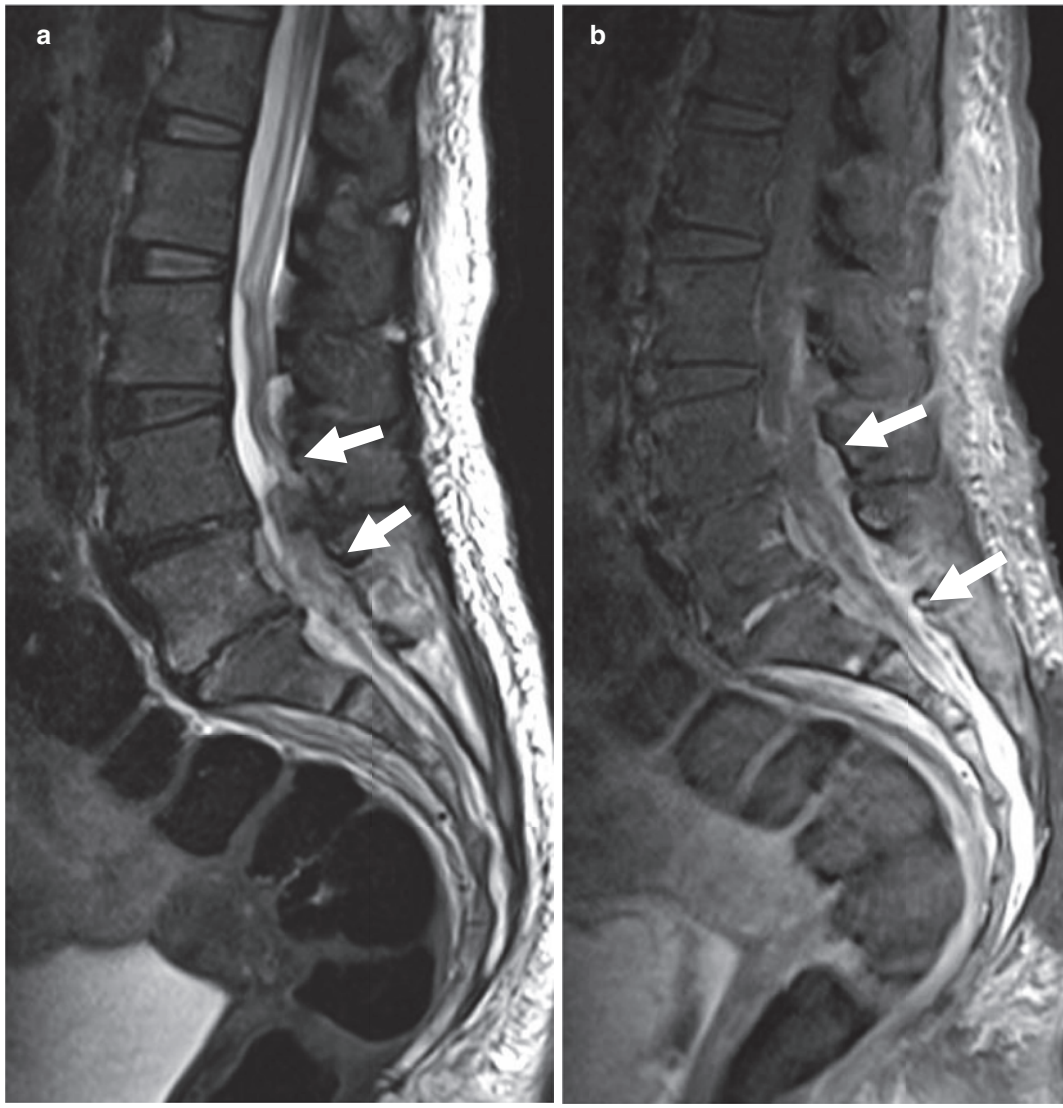

Fig. 14 Tuberculous arachnoiditis. Sagittal (**a**) T2-W and (**b**) contrast-enhanced T1-W MR images of the lumbar spine show T2-hyperintense nodularity and nodular enhancement of the subarachnoid space (arrows)

(Davies et al. 1984) (Fig. 14). Intramedullary tuberculomas are characterized by areas of central hypointensity and rim enhancement on contrast-enhanced T1-weighted MR images, with or without central T2-hyperintensity (Mishra et al. 2015). Nerve root involvement may present as meningeal enhancement, clumping of nerve roots or nerve radicles, a soft tissue mass replacing subarachnoid space, or a mixed pattern (Gupta et al. 2015).

Currently, functional MRI sequences are generally not used in routine practice. Diffusion MRI has been proposed to distinguish tuberculous spondylitis from vertebral metastases by demonstrating the absence of restriction in cases of infection. However, some doubtful cases have

been observed (Ansari et al. 2013; Ladeb et al. 2013). Some authors have evaluated the role of magnetic resonance spectroscopy and showed an increased lipid-lactate peaks in the diagnosis of spinal TB (Rauf et al. 2015).

4.1.4.4 Computed Tomography

Computed tomography (CT) is more sensitive than radiographs for detecting early bone destruction. It also allows a precise assessment of disease extension to the spinal canal and posterior elements, and to look for an associated posterior arthritis (Cotten et al. 1996). The details of vertebral collapse are better assessed by sagittal and coronal CT images (Dorcas and David 1995; Sharif et al. 1995; Pertuiset et al. 1999; Boussel et al. 2002; Dinc et al. 2002; Teo and Peh 2004). Calcifications and bone sequestra are better seen on CT than MRI (Cotten et al. 1996) (Fig. 15). The involved disc may show intradiscal hypodensity which is better depicted on sagittal and coronal images (Boussel et al. 2002).

Paravertebral tuberculous abscesses are usually large and bilateral (Cotten et al. 1996; Ridley et al. 1998; Naim-Ur-Rahaman et al. 1999; Mahboubi and Morris 2001; Stabler and Reiser 2001). They appear on CT as hypodense collections limited by thin, smooth, and well-vascularized walls (Fig. 16). The presence of calcifications at the center or the periphery of the abscess is characteristic of TB (Figs. 15, 17, and 18) (Sharif et al. 1995; Cotten et al. 1996; Pertuiset et al. 1999). Epidural extension is inconstant and visible as an epidural abscess or mass of spontaneously high density that is homogeneously enhanced after contrast administration. Abscesses and phlegmons are limited by the posterior longitudinal ligament and show a bilobed pattern on axial images (Stabler and Reiser 2001; Boussel et al. 2002) (Figs. 13 and 18).

CT is more frequently performed than MRI for the assessment of bone destruction. In our practice, CT is reserved for spinal cord compression secondary to vertebral destruction that extends to the neural arch, for suspicion of spinal instability, and when MRI is contraindicated. It is also used to guide percutaneous biopsy for obtaining histological and bacteriological specimens. It is also indicated in the pre-operative assessment of secondary spine deformities (Sharif et al. 1995; Harisinghani et al. 2000; Stabler and Reiser 2001; Turgut 2001; Teo and Peh 2004).

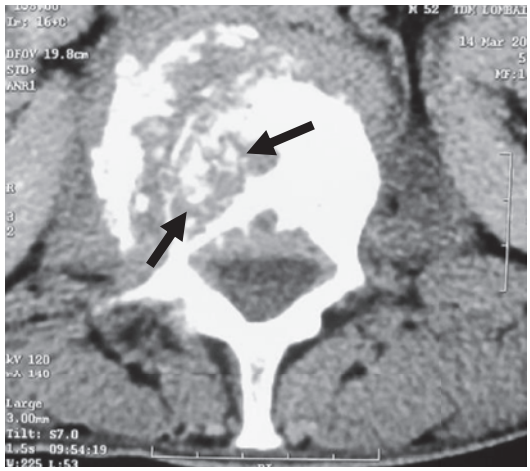

Fig. 15 Tuberculous spondylodiscitis of the lumbar spine. Axial CT image shows multiple calcifications at the abscess wall and central area. Several sequestra (black arrows) are present in the vertebral osteolytic lesion. Epidural component is also noted

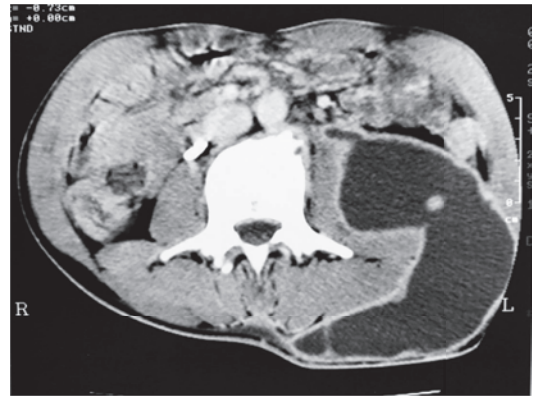

Fig. 16 Tuberculous spondylodiscitis of the lumbar spine with huge paravertebral abscess. Axial CT image taken in soft tissue window shows a large left paravertebral abscess with thin and smooth walls, which extends to the subcutaneous plane

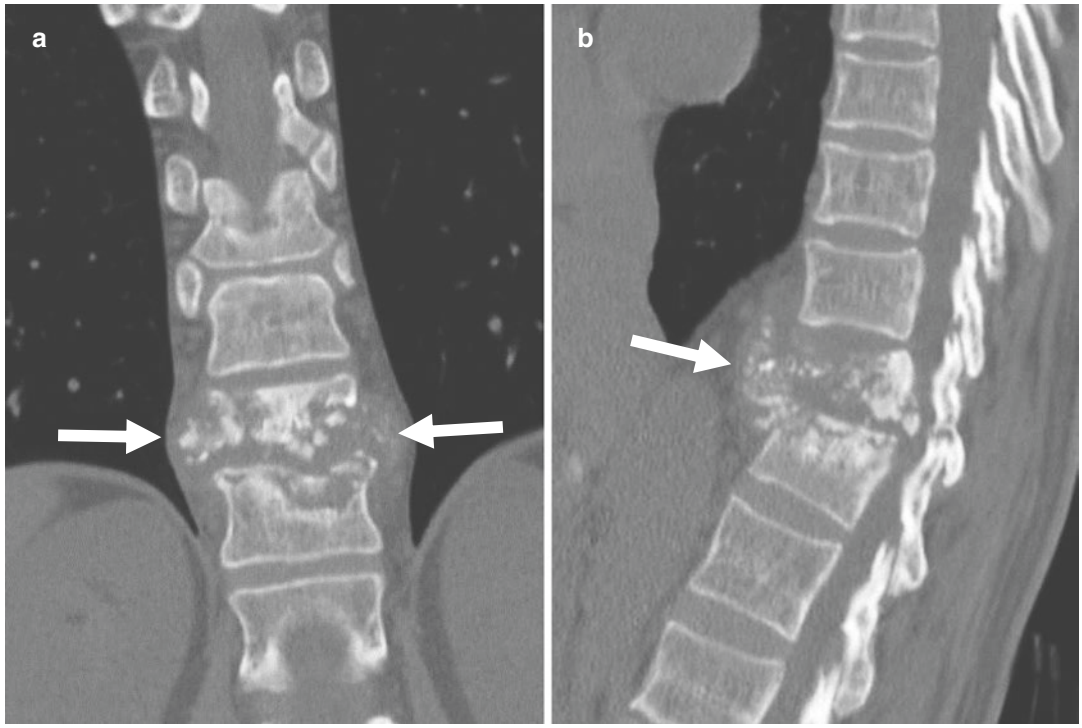

Fig. 17 Tuberculous spondylodiscitis of the thoracolumbar junction with abscess calcifications. (**a**) Coronal and (**b**) sagittal CT images taken in bone window show discovertebral destruction and small calcifications of the paravertebral soft tissue abscesses (arrows)

4.1.4.5 Scintigraphic Imaging

Scintigraphic imaging is particularly recommended in patients with suspected primary or postsurgical spinal infection, when MRI cannot be obtained or is contraindicated (Berbari et al. 2015; Kannivelu et al. 2021). Technetium-99m (^{99m}Tc) scintigraphy has a place in the diagnosis of spinal TB. It allows early diagnosis of spinal infection and detection of other asymptomatic locations, with a sensitivity varying from 65% to 100% but has a low specificity. The most commonly used tracers are ^{99m}Tc-diphosphonates and Gallium-67 (^{67}Ga)-citrate, with both being sensitive but not specific (Cotten et al. 1996; Pertuiset et al. 1999; Boussel et al. 2002; Shikhare et al. 2011).

Three-phase bone scintigraphy may demonstrate hyperemia and increased blood pool activity. Single-photon emission tomography (SPET) and single-photon emission computed tomography (SPECT) have a better spatial resolution than bone scintigraphy, and may thus reveal abnormalities not seen on the planar images (Shikhare et al. 2011). Bone scintigraphy is being gradually replaced by Fluorine-18 2′-deoxy-2-fluoro-D-glucose positron-emission tomography ([^{18}F] FDG PET), which is now considered as the preferred non-invasive nuclear medicine imaging modality of choice in the diagnosis, management, and clinical decision-making process in spinal infection. The role of hybrid PET/MRI, although promising, needs to be evaluated (Kannivelu et al. 2021).

PET using [^{18}F] FDG has a sensitivity of 97.5% and a specificity of 86.3% in the diagnosis of musculoskeletal infections. At the moment of diagnosis, it detects additional tuberculous foci in 60–80% of patients which has, in certain cases, an impact on the treatment

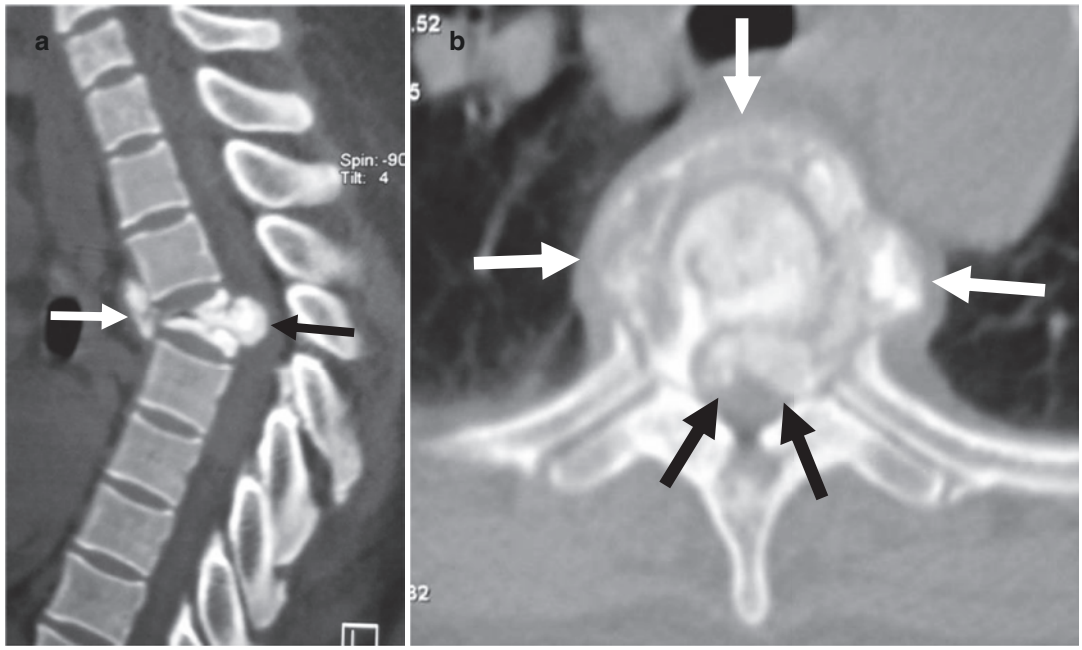

Fig. 18 Long-standing tuberculous spondylodiscitis at T4–6 vertebral levels. (**a**) Sagittal and (**b**) axial CT images taken in bone window show disco-vertebral destruction with bone sclerosis and calcified paravertebral (white arrows) and epidural (black arrows) abscesses. [Reproduced with permission from: Bouaziz MC, Ladeb MF, Labbene E et al. (2021) Imaging of spinal tuberculosis. In: Ladeb MF, Peh WCG (eds) Imaging of spinal infection. Springer International, https://doi.org/10.1007/978-3-030-70459-9_12]

(Ladeb et al. 2015). Some authors have noted elevated standardized uptake values (SUV) (>21) compared to pyogenic infections but other studies did not confirm these results (Yang et al. 2003; Heysell et al. 2013; Kannivelu et al. 2021). Recent studies showed that [^{18}F] FDG PET/CT had a superior diagnostic value for detecting spondylodiscitis within the first 2 weeks (Smids et al. 2017). After this period, for the diagnosis of spondylodiscitis, the diagnostic value of [^{18}F] FDG PET/CT is comparable to that of MRI for the evaluation of the entire spine (Altini et al. 2020).

[^{18}F] FDG PET appears to be superior to ^{67}Ga scintigraphy and MRI at diagnosing or ruling out spondylodiscitis in the presence of severe degenerative changes of the vertebral end-plates and intervertebral discs, or in patients with previous trauma. However, it is important to note that the specificity is moderately reduced in patients with spinal instrumentation (Kannivelu et al. 2021). PET allows follow-up after treatment, as FDG uptake returns to its normal value in 3–4 months and quantification of SUV has been proposed to detect residual lesions (Rivas-Garcia et al. 2013).

4.1.5 Craniocervical Junction Tuberculosis

TB of the craniocervical junction (Figs. 19 and 20) accounts for 2% of tuberculous spondylodiscitis. It involves the first two cervical vertebrae, as well as occipito-atlantal and atlanto-axial joints (Resnick 1995; Boussel et al. 2002). Two hypotheses have been suggested to explain its pathogenesis, namely (1) initial involvement of lateral C1 masses with destruction of the transverse ligament and extension of the infection to the retropharyngeal space and neighboring joints; and (2) initial involvement of the retropharyngeal space followed by extension to C1–C2 vertebrae by lymphatic and venous pharyngo-periodontal anastomoses. Craniocervical junction TB may cause spinal cord compression by C1–C2

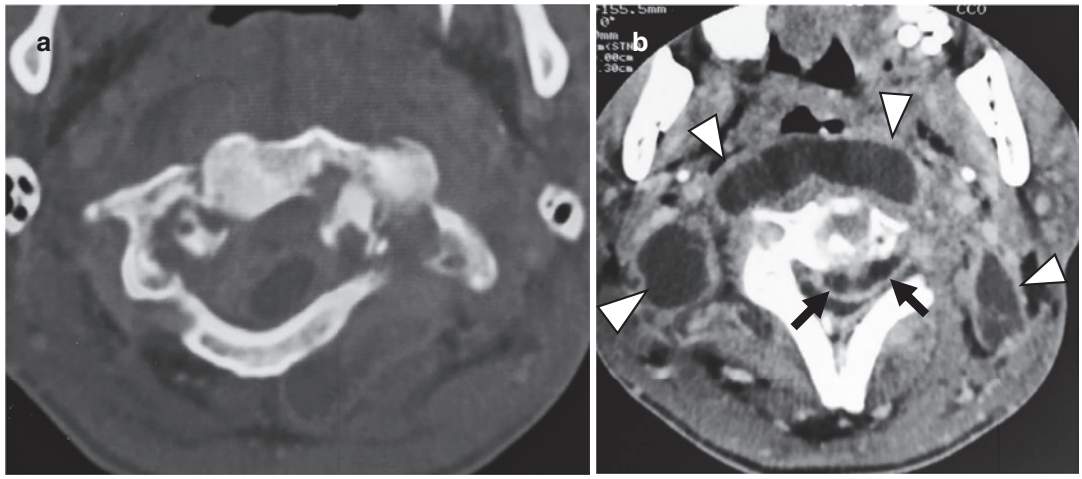

Fig. 19 Craniocervical junction tuberculosis. Axial CT images taken in (**a**) bone and (**b**) soft tissue windows show destruction of C1 and C2 vertebrae with atlanto-axial dislocation, epidural (black arrows) and paravertebral (white arrowheads) abscesses

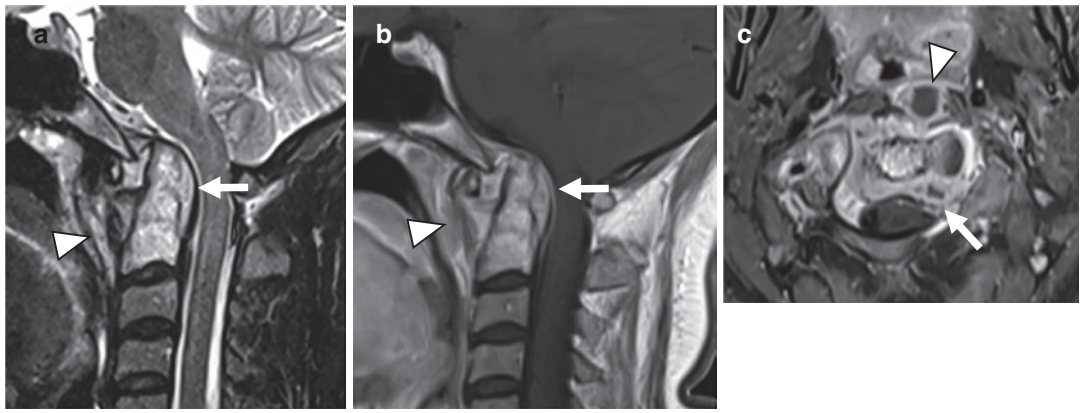

Fig. 20 Craniocervical junction tuberculosis. Sagittal (**a**) T2-W and (**b**) contrast-enhanced T1-W and (**c**) axial contrast-enhanced fat-suppressed T1-W MR images show signal hyperintensity of C1 and C2 vertebral bodies with epidural (arrows) and paravertebral (arrowheads) extension

dislocation (disruption of the transverse ligament), by ascending dislocation of the odontoid or by extension of an anterior epidural abscess (Boussel et al. 2002). Radiographical assessment of this condition may be rather difficult. CT is useful to depict bone destruction, especially of the neural arch, and MRI is the method of choice for the assessment of spinal canal extension.

4.1.6 Differential Diagnosis

The differential diagnosis of Pott disease mainly includes other spondylodiscitis (Table 1) and erosive degenerative disc disease (Table 2) (Resnick 1995; Cotten et al. 1996; Narlawar et al. 2002; Nassar et al. 2002). Clinical findings may help but the distinction between tuberculous, brucellar, mycotic, and pyogenic spinal infections may be difficult (Morvan et al. 1984; Ridley et al. 1998; Harisinghani et al. 2000; Moore and Rafii 2001; Attia et al. 2004).

In typical cases, the differential diagnosis between tuberculous and brucellar spinal infection is quite straightforward. However, brucellar spondylodiscitis may mimic TB (multifocal

Table 1 Main differentiating signs among tuberculous spondylodiscitis (Pott disease), brucellar spondylodiscitis, and pyogenic spondylodiscitis

	Tuberculous spondylodiscitis	Brucellar spondylodiscitis	Pyogenic spondylodiscitis
Disc narrowing	Late and marked	Late and moderate	Early and moderate
Vertebral destruction	Important	Discrete	Important
Bone sclerosis	Late and moderate	Early and marked	Early and marked
Vacuum phenomenon	Absent	Possible	Absent
Soft tissue abscesses	Frequent, large and well defined	Inconstant, small, well defined	Variable size, ill-defined
Preferential location	Thoracic and thoracolumbar spine	Lower lumbar spine	Lumbar spine

Table 2 Main differentiating MRI features between Pott disease and erosive degenerative disc disease

	Erosive degenerative disc disease	Pott disease
Disc	Vacuum phenomenon T2-hypointense ± linear T2-hyperintense signal Linear enhancement	Diffuse T2-hyperintense signal Diffuse or rim enhancement
Vertebral body	Marked sclerosis Superficial erosions Homogeneous enhancement	Moderate and late sclerosis Important bone destruction Heterogeneous enhancement
Paravertebral abscess	Absent	50–70% of cases

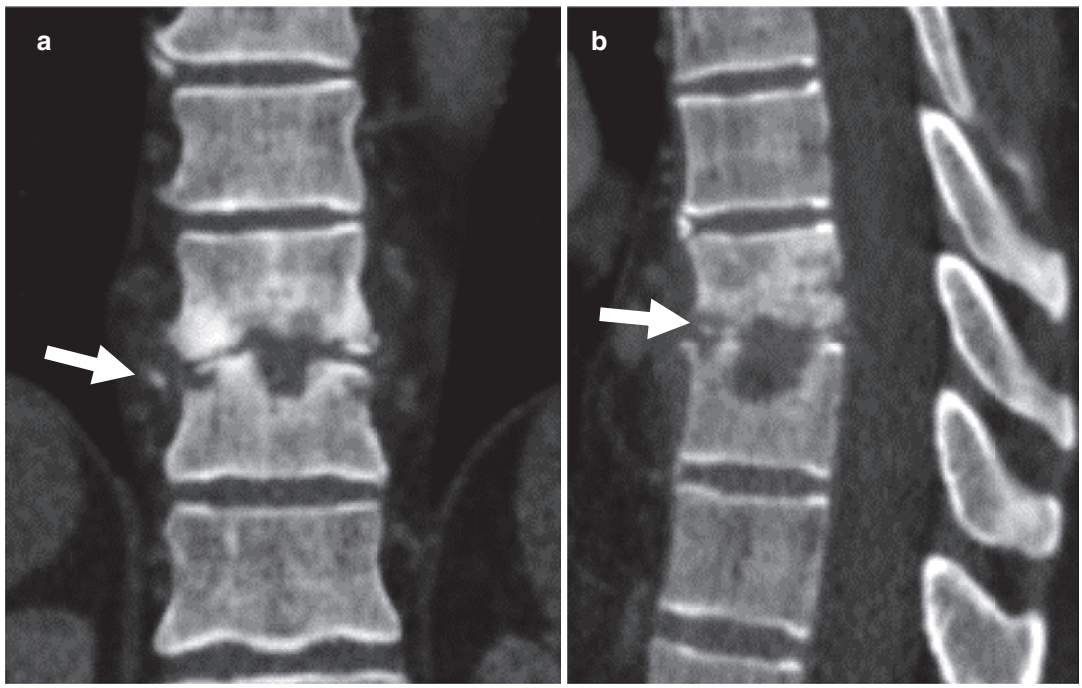

Fig. 21 Pseudo-Pott brucellar spondylodiscitis. (**a**) Coronal and (**b**) sagittal CT images show extensive vertebral destruction surrounded by bone sclerosis with small calcifications (arrows)

spinal involvement, disco-vertebral extensive destruction, large abscesses with or without calcifications), the so-called pseudo-Pott brucellar spondylodiscitis (Fig. 21). Bacteriological and/or immunological tests are needed to make a positive diagnosis (Madkour et al. 1988; Sharif et al. 1989; Al-Shahed et al. 1994; Chelli Bouaziz et al. 2008; Chelli Bouaziz et al. 2010).

Fungal spondylodiscitis is a very uncommon condition, accounting for 0.6–1.6% of infective

spondylodiscitis (Fig. 22). However, their incidence has recently been increasing, due to rise in immunosuppressive conditions such as diabetes mellitus, AIDS, and patients undergoing chemotherapy (Comacle et al. 2016). The most frequently encountered agents are *Candida* and *Aspergillus* spp. Clinical and radiological findings are not specific, and the diagnosis is often delayed and made on pathological study of the disco-vertebral specimen (Williams et al. 1999; Wrobel et al. 2001). Blood cultures are negative in 24–50% of cases (Arias et al. 2004).

Antigen and antibody assays based on the detection of circulating cell wall fungal antigens are useful in fungal infections, where they have a high positive predictive value for the diagnosis of *Candida albicans*. Molecular techniques have also been used with fungal infection and have enhanced the sensitivity of conventional methods utilized in diagnostic mycology (Skaf et al. 2010). The imaging appearances of fungal spondylodiscitis often mimic tuberculous spondylodiscitis due to the frequency of subligamentous extension and involvement of multiple contiguous or noncontiguous vertebral bodies (skip lesions). The T2-hypointense signal of the disc and subchondral bone may be observed in both conditions. However, the abscess wall is typically thin and smooth in spinal TB, and thick and irregular in fungal spondylodiscitis.

Bone sarcoidosis usually involves the small tubular bones of the hands and feet but may also involve the axial or appendicular skeleton, with an incidence varying from 1% to 14% (Rua-Figueroa et al. 2002). Bone lesions may be single or multiple; or osteolytic, sclerotic, or mixed (Fig. 23). On MRI, the vertebral body shows T1-hypointense and T2-hyperintense signal, with

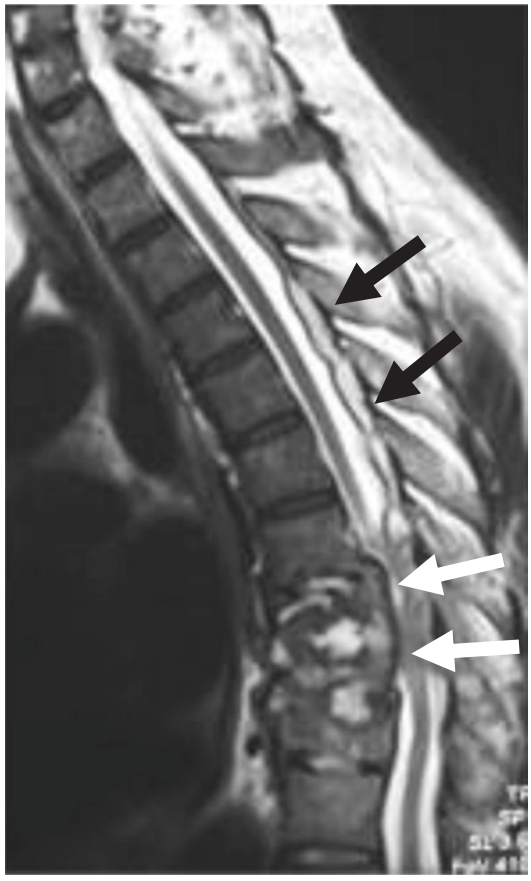

Fig. 22 Fungal spondylodiscitis. Sagittal T2-W MR image shows gross destruction of T8, T9, T10, and T11 vertebral bodies and posterior elements with an epidural component (white arrows) and cranial tracking (black arrows)

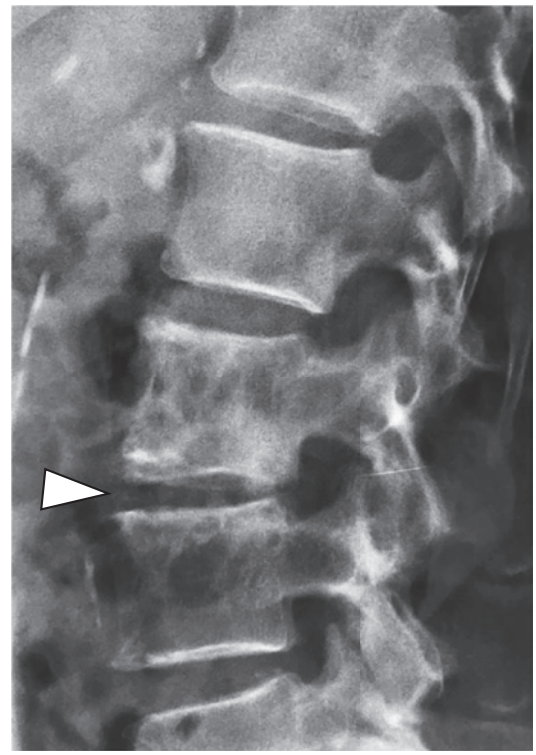

Fig. 23 Spinal sarcoidosis. Lateral radiograph of the lumbar spine shows mild disc narrowing (arrowhead) and heterogeneous osteolytic-sclerotic appearance of the adjacent vertebrae

variable enhancement after contrast administration. The posterior elements and intervertebral discs are rarely involved (Lefere et al. 2014). Chest CT is indicated to show mediastinal and pulmonary abnormalities that are suggestive of sarcoidosis. Bone scintigraphy and PET/CT are sensitive but not specific (Valencia et al. 2009).

Spinal hydatidosis (caused by the parasite *Echinococcus granulosus*) may mimic TB at an advanced stage of the disease, with disc involvement. The conservation of vertebral body height and shape is suggestive of echinococcosis, as well as the presence of multiple intra- and extraosseous vesicles on ultrasound imaging, CT, and MRI. Other features are the lack of bone marrow edema and the frequent extension to the neighboring bones (e.g., ribs, iliac bone) (Ladeb et al. 2013).

4.1.7 Imaging Follow-Up

The radiological follow-up of tuberculous spondylodiscitis evolves in three steps. Firstly, a progression of the lesions may be observed (progression of disc narrowing, bone destruction, and vertebral collapse), indicating a diagnostic error or a resistance to antibiotics. After 1 or 2 months of treatment, the disease is stabilized, with subsequent signs of bone healing (peripheral sclerosis and osteophytes). The late phase depends on the importance of disco-vertebral lesions at the time of treatment restoration. Complete vertebral fusion (Fig. 24) results from bone destruction which exposes the vertebral cancellous bone. In cases of moderate bone destruction, vertebral fusion may be incomplete. Restoration to original condition can be obtained only in cases of early treatment. On MRI, the disc and the vertebral body signal decrease on T2-weighted and contrast-enhanced T1-weighted images. Fatty reconversion of the vertebral bone marrow correlates to a favorable clinical outcome (Fig. 25). The abscesses should disappear in 1–12 months. Signal abnormalities may remain but does not indicate failure of treatment. PET/CT allows follow-up of spondylodiscitis after treatment.

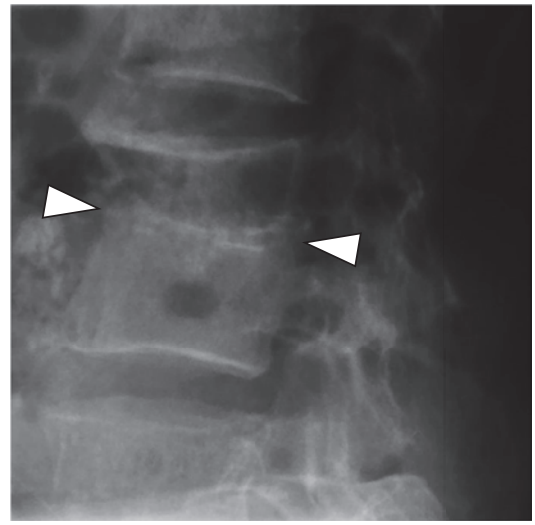

Fig. 24 Treated tuberculous spondylodiscitis. 2-year follow-up lateral radiograph shows complete vertebral fusion of two adjacent vertebral bodies (arrowheads)

4.1.8 Complications

The main complications of tuberculous spondylodiscitis are kyphosis and spinal cord compression. Spinal cord compression following tuberculous spondylodiscitis is observed in 30–40% of cases (Hamza 1993; Pertuiset et al. 1997; Lolge et al. 2003). Early compression following an evolutive TB must be distinguished from late compression appearing several years after recovery. Early compression may result from epidural abscesses, bone sequestra, subluxation, arachnoiditis, spinal cord ischemia or from a combination of these, whereas late compression mainly results from kyphosis (Martini 1988). Neurological impairment in tuberculous spondylodiscitis is usually symmetrical and progressive (Ridley et al. 1998). Pott paraplegia usually regresses after medical treatment. CT (Fig. 18) and MRI (Fig. 26) are useful to identify the cause of compression, with osseous causes being better depicted by CT than MRI (Sharif et al. 1995; Cotten et al. 1996; Morvan et al. 1998; Pertuiset et al. 1999; Dinc et al. 2002; Moorthy and Prabhu 2002; Narlawar et al. 2002; Teo and Peh 2004). Kyphosis is the consequence of spondylodiscitis with destruction of several

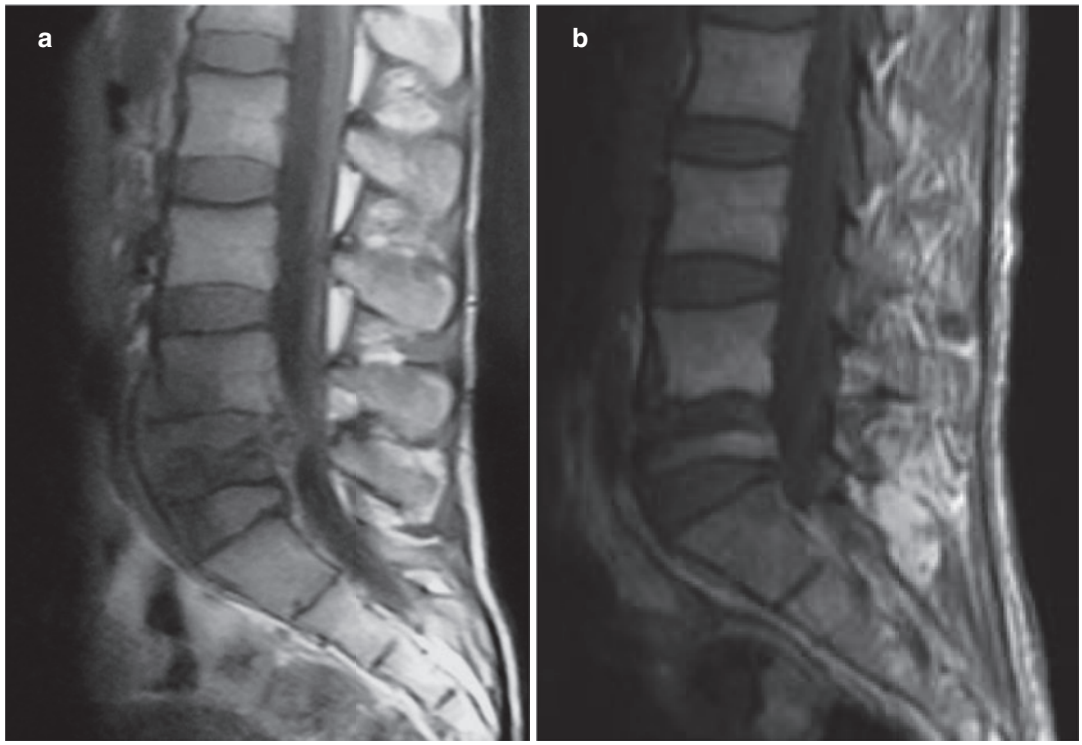

Fig. 25 Treated tuberculous spondylodiscitis. Sagittal T1-W MR images obtained (**a**) pre-treatment and at (**b**) 2-year follow-up post-treatment shows fatty reconversion of L4 and L5 vertebral bodies indicative of healing. (Fig. 25b is reproduced with permission from: Bouaziz MC, Ladeb MF, Labbene E et al. (2021) Imaging of spinal tuberculosis. In: Ladeb MF, Peh WCG (eds) Imaging of spinal infection. Springer International. https://doi.org/10.1007/978-3-030-70459-9_12)

vertebral bodies. It is radiologically assessed by the Cobb method. Kyphosis progression may be caused by incomplete bone repair, more frequent in children than in adults. Kyphosis may cause chronic pain, spinal cord compression or cardio-respiratory issues.

4.2 Vertebral Osteomyelitis (Solitary Vertebral Involvement)

In solitary spinal involvement, the infection exclusively involves the vertebra, with sparing of the intervertebral disc. However, one or more vertebrae, contiguous or not, may be involved. Radiographs are normal in about 45% of cases (Lolge et al. 2003). Otherwise, they may show a round or oval osteolytic lesion, usually at the center of the vertebral body, with a peripheral sclerotic rim (Cotten et al. 1996; Pertuiset et al. 1999; Boussel et al. 2002). Moth-eaten osteolysis may also be observed, sometimes resulting in vertebral collapse, with homogeneous or heterogeneous bone sclerosis that may hide the underlying osteolysis (Fig. 27). The differential diagnosis includes lymphoma, myeloma, metastasis, and eosinophilic granuloma.

Clinical and biological findings, as well as the presence of paravertebral and/or epidural abscesses, are helpful to make the diagnosis. Vertebral destruction is better depicted by CT. MRI usually shows intermediate T1 and hyperintense T2 signal of one or more vertebral

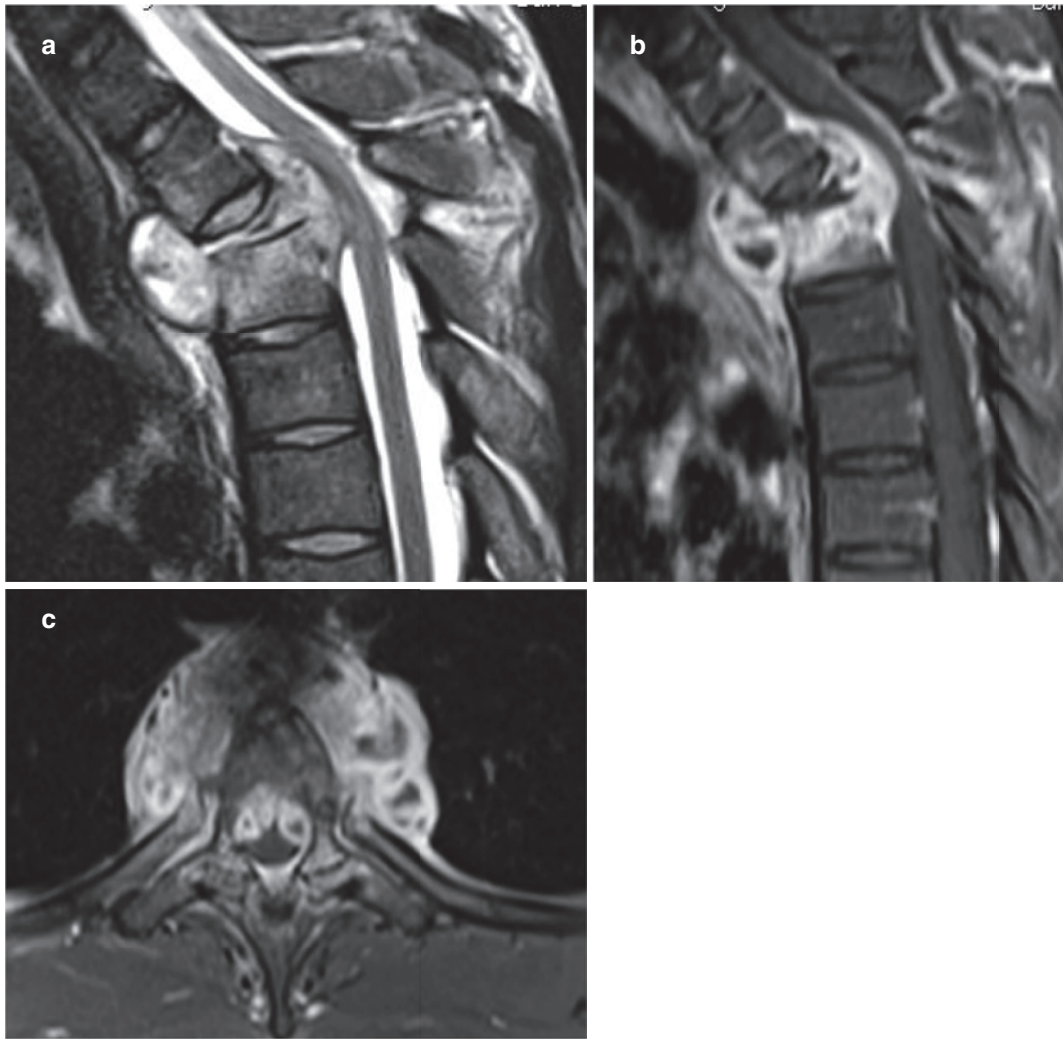

Fig. 26 Spinal tuberculosis with cord compression. Sagittal (**a**) T2-W and (**b**) contrast-enhanced fat-suppressed T1-W and (**c**) axial contrast-enhanced fat-suppressed T1-W MR images show disco-vertebral destruction with severe vertebral collapse, large paravertebral and epidural abscesses, and spinal cord compression. Note that the epidural abscess has a bilobed configuration on the axial image

bodies, with sparing of the intervertebral discs. Contrast administration produces diffuse or heterogeneous vertebral enhancement, and allows assessment of intraspinal and paravertebral extension of the disease. The presence of disco-vertebral and/or perivertebral abscesses is essential to distinguish tuberculous solitary vertebral involvement from the other differential diagnosis of a solitary vertebral lesion (metastases, myeloma, sarcoidosis). When abscesses are not present and when there is no clinical and biological evidence of infection, percutaneous biopsy may be required to obtain diagnostic confirmation.

4.3 Primitive Neural Arch Tuberculosis

Neural arch tuberculosis is usually observed in the cervicothoracic spine and may involve one or more spinal levels (Fig. 28) (Resnick 1995;

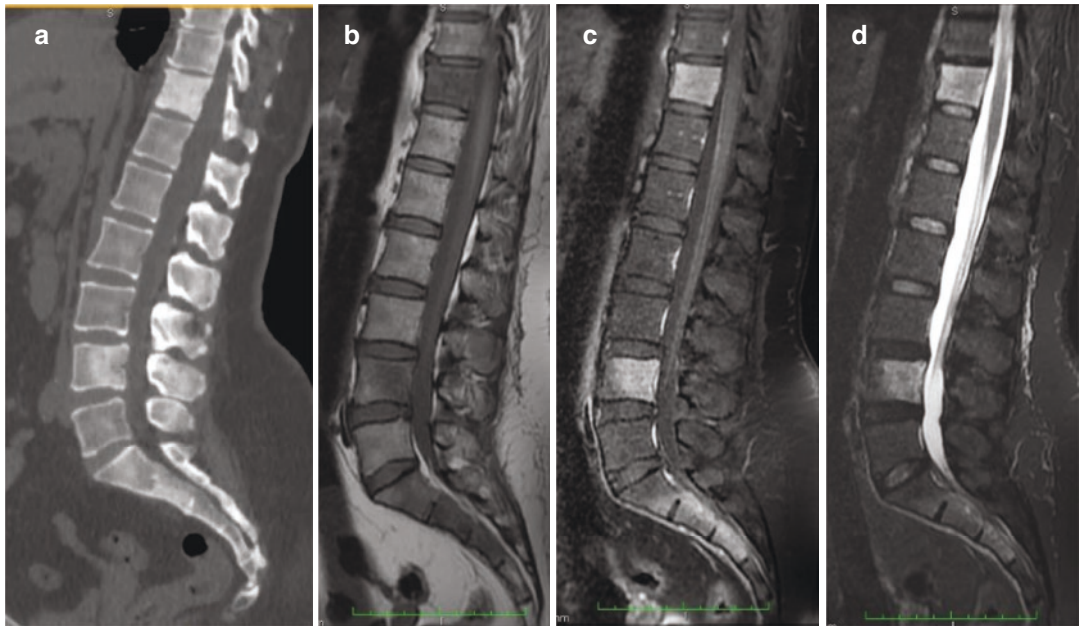

Fig. 27 Multifocal tuberculous spondylitis (vertebral osteomyelitis). Sagittal (**a**) CT and (**b**) T1-W, (**c**) contrast-enhanced fat-suppressed T1-W, and (**d**) STIR MR images show multiple involvement of thoracic, lumbar, and sacral vertebrae, with sparing of the adjacent discs

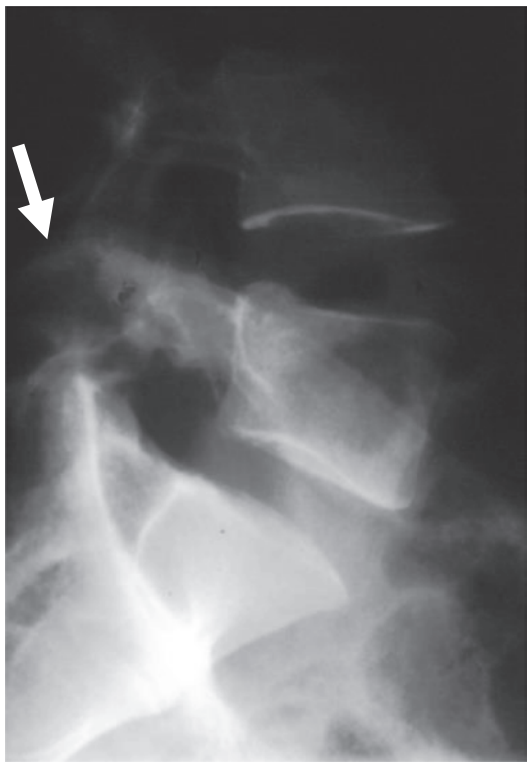

Fig. 28 Neural arch tuberculosis. Lateral radiograph of the lower lumbar spine shows osteolysis of L5 neural arch (arrow)

Sharif et al. 1995; Cotten et al. 1996; Pertuiset et al. 1999; Boussel et al. 2002; Ben Taarit et al. 2003). The neural arch may occasionally be the initial site to be involved (Resnick 1995). Involvement of a single vertebral arch is far more common (Wallace and Cohen 1976; Kumar 2017). Imaging plays an important role in the diagnosis (Morvan et al. 1998; Nassar and al 2002). The analysis of radiographs is not always easy and the detection of neural arch abnormalities is possible in less than 10% of the cases (Morvan et al. 1998; Narlawar et al. 2002). Radiographs may show osteolysis of a spinous process, lamina, or pedicle. Bone destruction may extend to the posterior cortex of the vertebral body or the adjacent ribs with relative sparing of the intervertebral discs (Resnick 1995; Morvan et al. 1998). Well-defined or ill-defined bone sclerosis may also be observed (Cotten et al. 1996).

CT allows a more precise assessment of bone and adjacent soft tissues. It shows intraspinal and extraspinal extension of the infection, which is particularly frequent in this presentation (Cotten et al. 1996; Narlawar et al. 2002; Nassar et al. 2002). The

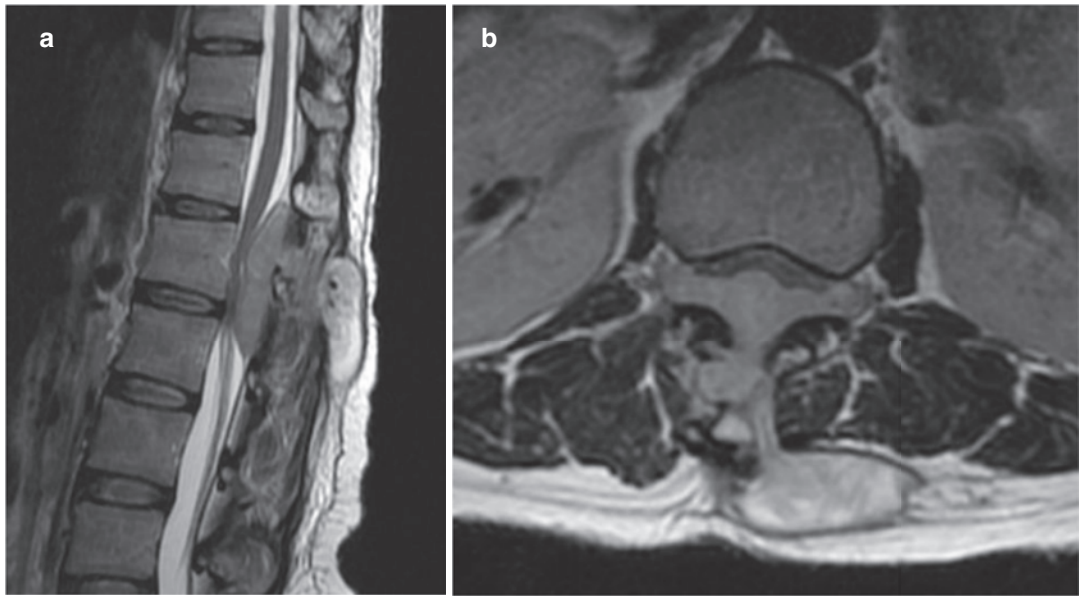

Fig. 29 Neural arch tuberculosis. (**a**) Sagittal and (**b**) axial T2-W MR images show involvement of posterior elements with epidural extension and spinal cord compression. There is also a large soft tissue component which extends posteriorly into the subcutaneous tissues

presence of a sequestrum, and associated zygoapophyseal, costovertebral, or costotransversal arthritis is of great diagnostic value (Cotten et al. 1996). On MRI, the lesions show T1-hypointense and T2-hyperintense signal with contrast enhancement (Morvan et al. 1998) (Fig. 29). Neural arch involvement may result in spinal instability, in which case imaging diagnosis is important for surgical planning (Narlawar et al. 2002). The differential diagnosis includes metastases and primitive spinal tumors (Garg and Somvanshi 2011; Momjian and George 2014).

5 Spinal Tuberculosis Diagnosis

5.1 Presumptive Diagnostic Signs

TB is suspected when there is a history of recent primary infection (30%), another active TB focus (19–30%), satellite lymphadenopathy (10%), and positive tuberculin skin test (75–100%). When there is tuberculous spondylodiscitis, increase in erythrocyte sedimentation rate and C-reactive protein is observed in 55% and 75% of cases, respectively. The radiological presumptive signs are listed in Table 3.

5.2 Diagnosis Confirmation

Diagnostic confirmation is usually established by either the demonstration of acid-fast bacilli (AFB) on microscopy/culture or by histological examination of material obtained following biopsy. Even though the histological examination is highly suggestive of spinal TB when caseating granulomas are observed and diagnostic when AFB are found (Lacerda et al. 2017), definite diagnosis requires positive microbiology (Garg and Somvanshi 2011). The diagnosis can be based on extraspinal clinical specimens (e.g., sputum, urine, lymph node aspirates) since 20–40% of patients have active TB at other sites. (Merino et al. 2012). When these tests are negative, imaging-guided percutaneous aspiration biopsy from the affected site is the gold standard technique for diagnosis of spinal TB. It usually yields sufficient material from the spine

Table 3 Radiological signs suggesting spinal TB

Location	Thoracolumbar junction or distal thoracic spine
Extension	Multifocal Subligamentous extension at three vertebra or more
Vertebra	Bone osteolysis adjacent to the disc Sequestra Involvement of vertebral bodies sparing the disc Intravertebral abscess Neural arch involvement: frequent (68% in children, 52% in adults). May be isolated Heterogeneous enhancement of the vertebral body
Disc	Late involvement
Epidural extension	Bilobed appearance of the epidural abscess or phlegmon
Soft tissue abscesses	Frequent, large, well-defined and smooth walls Calcifications at the center or the periphery of the abscess
Extraosseous locations	Pulmonary, urogenital, lymph nodes

and/or adjacent abscess (Garg and Somvanshi 2011). Open biopsy of the spine, when required, has a slightly higher diagnostic yield either for culture or histological study (Garg and Somvanshi 2011).

It is also important to search for other associated microorganisms (Merino et al. 2012). Diagnostic sensitivity of AFB smear microscopy (Ziehl–Neelsen and fluorescent staining) is about 17–30% but can be as high as 58% in some studies. This low sensitivity is explained by the paucibacillary nature of osteoarticular TB (Lacerda et al. 2017). Culture sensitivity can reach 83% in solid media but the time to culture (3–8 weeks) is a limitation. Liquid media is more sensitive and has a shorter time to detection (2–3 weeks). Sensitivity of *M. tuberculosis* detection in pus from paravertebral abscesses is 42% (Wallace and Cohen 1976). Culture is necessary for an accurate drug susceptibility testing (DST) which is crucial for the treatment of spinal TB, especially in countries with high prevalence of drug resistance (Merino et al. 2012).

Historically, identification of positive mycobacterial cultures was based on colony morphology and select biochemical reactions; however, molecular methods must be used for definitive identification of most mycobacterial isolates from culture (Caulfield and Wengenack 2016). Nucleic acid amplification tests (NAAT) may be useful for rapid diagnosis and can distinguish between *Mycobacterium tuberculosis* complex and atypical mycobacteria (Lacerda et al. 2017). It is more sensitive than conventional methods when low numbers of bacilli are present (Merino et al. 2012). A positive result can be used as evidence of extrapulmonary TB because false-positive results are unlikely. However, a negative result may not be used to exclude TB because false-negative results are exceedingly common.

In bone and joint TB, the Cepheid Xpert MTB/RIF test achieves a sensitivity of 82% and a specificity of 100% in the diagnosis, and a 100% concordance with culture-DST for the detection of rifampin resistance. The GenoType MTBDRplus (MTBDR) assay, detecting both rifampicin and isoniazid resistances, shows a sensitivity of 72% in these infections (Lacerda et al. 2017). Nevertheless, these tests are not available in all laboratories, especially in low- and middle-income countries (Merino et al. 2012). Tuberculin skin test and interferon-γ release assays are not routinely used in the diagnosis of extrapulmonary TB (Lacerda et al. 2017) since they cannot differentiate latent from active TB infection. However, in difficult cases of spinal osteomyelitis, their high negative predictive value may be helpful in rule out TB (Trecarichi et al. 2012).

Improvements in percutaneous biopsy techniques have reduced the number of surgical biopsies. Disco-vertebral biopsy allows rapid histopathological examination by showing epithelioid and giant cell granulomas, with or without necrosis, in approximately 90% of cases (Trecarichi et al. 2012). False negatives are seen at an advanced stage of the disease when fibrosis

sets in (Francis et al. 1999). Cytological puncture is a cheap, rapid, and fairly nonaggressive technique with a very low risk of complications (Masood 2013). In countries with a high endemicity of TB, cytopathological examination can constitute an alternative to histopathology, provided that the proceduralist and the cytopathologist are well trained (Masood 2013). It is particularly recommended for paravertebral abscesses and osteolytic lesions with cortical interruption, as these are frequently observed in tuberculous spondylodiscitis. (Gupta et al. 1999).

In cytology, epithelioid granulomas, giant cells, and caseous necrosis are observed with frequencies varying from 50% to 68% (Ben Taarit et al. 2003). If there is a discrepancy between clinico-radiological and cytological results, a vertebral or disco-vertebral biopsy is necessary for diagnosis (Kang et al. 1999; Jorda et al. 2000; Handa et al. 2009; Gasbarrini et al. 2012). The histopathological differential diagnosis of spinal TB arises with other granulomatous infections, such as other bacterial infection (brucellosis, syphilis, *Yersinia pseudotuberculosis* infection), fungal infection (histoplasmosis), and sarcoidosis. Suppurative forms are rare and can be considered in the absence of an epithelioid granuloma for an infection with pyogenic bacteria. It is the positivity of Ziehl–Nielsen staining on the histological sections, and especially the bacteriological examination, which allows the correct diagnosis to be made.

Conventionally, the inflammatory infiltrate of brucellosis is polymorphic, rich in lymphocytes, associated with plasma cells and neutrophils, and the small histiocytic granuloma is made up of small groups of histiocytes but cases of associated granulomatous brucellosis with necrosis have been reported (Halimi et al. 1999). Mycotic spondylodiscitis can also be granulomatous and necrotizing. Demonstration by special stains of spores and mycelial filaments in yeast infections and hyphae in filamentous fungal infections confirms the mycotic origin. In the absence of caseous necrosis, the histological distinction between spinal sarcoidosis and TB is not easy.

6 Treatment

Anti-TB drug treatment is the gold standard for the treatment of tuberculous spondylodiscitis, whereas surgical treatment plays an important role as adjunctive therapy.

6.1 Anti-tuberculosis Treatment

The treatment of spinal TB is mainly medical. It consists of a combination of four antibiotics (isoniazid, rifampicin, ethambutol, and pyrazinamide) for 2 months, followed by two antibiotics (isoniazid and rifampicin) for 7–10 months, for a total treatment duration of 9–12 months (Eschard et al. 1993; Ramachandran et al. 2005). The duration of anti-TB treatment varies according to the clinical course and the improvement of the radiological imaging findings. Adherence to treatment is crucial for efficacy and recovery; it must be continuously reinforced and maintained throughout the course of treatment. The frequency of side effects to anti-TB drugs requires regular clinical and biological monitoring.

6.2 Associated Treatment

Vertebral immobilization is necessary in cervical spine TB and in TB complicated by spinal compression or instability (Hamza 1993). Rehabilitation must be considered after the acute phase of rest and stabilization of the bone lesions. It is necessary to prevent muscular atrophy (Eschard et al. 1993). The aim of surgery is to completely remove a lesion, achieve spinal decompression and stability, and restore a normal spinal balance (De Backer et al. 2006). The indications for surgery are: (1) Acute spinal compression, compression of bone origin and flaccid paraplegia (Hamza 1993); (2) Large paravertebral abscesses resistant to medical treatment and percutaneous drainage; and (3) Progressive kyphosis with spinal instability (Golden et al. 2005; Ramachandran et al. 2005).

7 Conclusion

Spinal TB accounts for 25–60% of musculoskeletal TB. The three main anatomo-radiological patterns are tuberculous spondylodiscitis (Pott disease), tuberculous spondylitis, and primary neural arch TB. Time to diagnosis has improved from 6 to 24 months in the past to 3 months on average in the more recent series, thanks to advances in imaging. Imaging also helps to clarify the extent of the infection and its impact on the spinal cord and nerve roots but it only provides presumptive diagnosis of spinal TB. In the absence of active extraspinal TB, confirmation of diagnosis of TB is provided by histology and/or bacteriology.

References

Agrawal V, Patgaonkar PR, Nagariya SP (2010) Tuberculosis of spine. J Craniovertebr Junction Spine 1:74–85

Aït Khaled N, Enarson D, Billo N (1997) Epidémiologie de la tuberculose et de la résistance aux antituberculeux. Rev Mal Resp 14:5S8–5S18

Al-Shahed MS, Sharif HS, Haddad MC et al (1994) Imaging features of musculoskeletal brucellosis. Radiographics 14:333–348

Altini C, Lavelli V, Niccoli-Asabella A et al (2020) Comparison of the diagnostic value of MRI and whole body ^{18}F-FDG PET/CT in diagnosis of spondylodiscitis. J Clin Med 9:1581. https://doi.org/10.3390/jcm9051581

Ansari S, Ashraf AN, Al-Moutaery K (2001) Spinal infection: a review. Neurosurg Q 11:112–123

Ansari S, Amanullah MF, Ahmad K, Rauniyar RK (2013) Pott's spine: diagnostic imaging modalities and technology advancements. N Am J Med Sci 5:404–411

Arias F, Mata-Essayag S, Landaeta ME et al (2004) Candida albicans osteomyelitis: case report and literature review. Int J Infect Dis 8:307–314

Attia M, Harnof S, Knoller N et al (2004) Cervical Pott's disease presenting as a retropharyngeal abscess. Isr Med Assoc J 6:438–439

Ben Taarit C, Turki S, Ben Maïz H (2003) La tuberculose ostéoarticulaire en Tunisie: étude rétrospective de 180 cas. Med Mal Infect 33:210–214

Berbari EF, Kanj SS, Kowalski TJ et al (2015) Infectious Diseases Society of America (IDSA) clinical practice guidelines for the diagnosis and treatment of native vertebral osteomyelitis in adults. Clin Infect Dis 61:e26–e46

Bernard L, Perronne C (1997) La tuberculose ostéo-articulaire aujourd'hui. Presse Med 26:308–310

Billo NE (1996) Tendances épidémiologiques de la tuberculose. Rev Prat 46:1332–1335

Boussel L, Marchand B, Blineau N et al (2002) Imagerie de la tuberculose ostéo-articulaire. J Radiol 83:1025–1034

Caulfield AJ, Wengenack NL (2016) Diagnosis of active tuberculosis disease: from microscopy to molecular techniques. J Clin Tuberc Other Mycobact Dis 4:33–43

Chebbi Y, Riahi H, Bouaziz MC et al (2019) Mycobacterium bovis spondylodiscitis: report of 4 cases. J Clin Rheumatol 10:1097

Chelli Bouaziz M, Ladeb MF, Chakroun M, Chaabane S (2008) Spinal brucellosis: a review. Skeletal Radiol 37:785–790

Chelli Bouaziz M, Bougamra I, Kaffel D, Hamdi W, Ghannouchi M, Kchir MM (2010) Non-contiguous multilevel spondylitis: an exceptional presentation of spinal brucellosis. Tunis Med 88:280–284

Chelli Bouaziz M, Ladeb MF, Chakroun M (2013) Tuberculose rachidienne. In: Laredo JD, Wybier M, Petrover D (eds) Imagerie rhumatologique et orthopédique. Sauramps Medical, Montpellier, pp 523–538

Chelli Bouaziz M, Riahi H, Ladeb MF, Chakroun M, Rammeh S (2017) Imagerie de la tuberculose rachidienne. Encycl Med Chir Radiologie et imagerie médicale-musculosquelettique-neurologique-maxillofaciale, 31–670-C-10

Colmenero JD, Jimenez-Mejias ME, Reguera JM et al (2004) Tuberculous vertebral osteomyelitis in the new millennium: still a diagnostic and therapeutic challenge. Eur J Clin Microbiol Infect Dis 23:477–483

Comacle P, Le Govic Y, Hoche-Delchet C et al (2016) Spondylodiscitis due to Aspergillus terreus in an immunocompetent host: case report and literature review. Mycopathologia 181:575–581

Cotten A, Flipo RM, Drouot MH et al (1996) La tuberculose vertébrale. Etude des aspects cliniques et radiologiques à partir d'une série de 82 cas. J Radiol 77:419–426

Davies PD, Humphries MJ, Byfield SP et al (1984) Bone and joint tuberculosis. A survey of notifications in England and Wales. J Bone Joint Surg Br 66:326–330

De Backer AI, Mortelé KJ, Vanhoenacker FM, Parizel PM (2006) Imaging of extraspinal musculoskeletal tuberculosis. Eur J Radiol 57:119–130

Dinc H, Ahmetoglu A, Baykal S et al (2002) Image-guided percutaneous drainage of tuberculous iliopsoas and spondylodiskitic abscesses: midterm results. Radiology 225:353–358

Dorcas CY, David JS (1995) Musculoskeletal tuberculosis. Radiol Clin North Am 33:679–689

Durieux P (1990) Epidémiologie de la tuberculose. Rev Prat 40:703–705

Engin G, Acunas B, Acunas G, Tunaci M (2000) Imaging of extrapulmonary tuberculosis. Radiographics 20:471–488

Eschard JP, Leone J, Etienne JC (1993) Tuberculose osseuse et articulaire des membres. Encycl Méd Chir, Appareil locomoteur, 14–185-A-10:15

Francis IM, Das DK, Luthra UK et al (1999) Value of radiologically guided fine needle aspiration cytology (FNAC) in the diagnosis of spinal tuberculosis: a study of 29 cases. Cytopathology 10:390–401

Garg RK, Somvanshi DS (2011) Spinal tuberculosis: a review. J Spinal Cord Med. 34:440–454

Gasbarrini A, Boriani L, Salvadori C et al (2012) Biopsy for suspected spondylodiscitis. Eur Rev Med Pharmacol Sci 16:26–34

Golden MP, Vikram HR (2005) Extrapulmonary tuberculosis: an overview. Am Fam Physician 72:1761–1768

Gupta S, Takhtani D, Gulati M et al (1999) Sonographically guided fine-needle aspiration biopsy of lytic lesions of the spine: technique and indications. J Clin Ultrasound 27:123–129

Gupta R, Garg RK, Jain A et al (2015) Spinal cord and spinal nerve root involvement (myeloradiculopathy) in tuberculous meningitis. Medicine (Baltimore) 94(3):e404

Halimi C, Bringard N, Boyer N et al (1999) Brucellome hépatique: deux nouveaux cas et revue de la littérature. Gastroenterol Clin Biol 23:513–517

Hamza M (1993) Tuberculose articulaire et vertébrale. Rev Rhum (Ed Fr) 60:115–118

Handa U, Garg S, Mohan H, Garg SK (2009) Role of fine-needle aspiration cytology in tuberculosis of bone. Diagn Cytopathol 38:1–4

Harisinghani MG, Mcloud TC, Shepard JA et al (2000) Tuberculosis from head to toe. Radiographics 20:449–470

Heysell SK, Thomas TA, Sifri CD, Rehm PK, Houpt ER (2013) 18-fluorodeoxyglucose positron emission tomography for tuberculosis diagnosis and management: a case series. BMC Pulm Med 13:14

Huchon G (1997) Tuberculose et mycobactérioses non tuberculeuses Encycl Med Chir, Maladies Infectieuses, 8–038-C-10:20

Jain AK (2010) Tuberculosis of the spine: a fresh look at an old disease. J Bone Joint Surg Br 92:905–913

Jorda M, Rey L, Hanly A, Ganjei-Azar P (2000) Fine-needle aspiration cytology of bone: accuracy and pitfalls of cytodiagnosis. Cancer 90:47–54

Kang M, Gupta S, Khandelwal N et al (1999) CT-guided fine-needle aspiration biopsy of spinal lesions. Acta Radiol 40:474–478

Kannivelu A, Tong AKT, Loke KSH, Ng DCE (2021) Nuclear medicine imaging of spinal infection. In: Ladeb MF, Peh WCG (eds) Imaging of spinal infection. Springer Nature Switzerland, pp 71–88

Kumar K (2017) Posterior spinal tuberculosis: a review. Mycobact Dis 7:243. https://doi.org/10.4172/2161-1068.1000243

Lacerda C, Linhas R, Duarte R (2017) Tuberculous spondylitis: a report of different clinical scenarios and literature update. Case Rep Med. https://doi.org/10.1155/2017/4165301

Lacut JY, Dupon M, Paty MC (1995) Tuberculoses extrapulmonaires. Revue et possibilités de diminution des délais d'intervention thérapeutiques. Méd Mal Infect 25:304–320

Ladeb MF, Chelli Bouaziz M, Chakroun M, Loussaief C (2013) Atteintes parasitaires de l'appareil locomoteur. Encycl Med Chir Radiologie et imagerie médicale-musculosquelettique-neurologique-maxillofaciale 31–225-A-10

Ladeb MF, Chelli Bouaziz M, Riahi H, Chakroun M (2015) Imagerie de la tuberculose articulaire extra-rachidienne. Encycl Med Chir Radiologie et imagerie médicale-musculosquelettique-neurologique-maxillofaciale 31–220-A-10

Ladeb MF, Riahi H, Chelli Bouaziz M, Mechri M (2019) Clinical evolution of tuberculous spondylodiscitis in Tunisia. Bull Acad Natl Med 203:328–333

Lamer S, Garel C, Holvoet-Vernaut L, Hassan M (1998) Lésion lytique épiphyso-métaphysaire. Presse Med 27:1197–1198

Le Roux P, Quinque K, Bonnel AS, Le Luyer B (2005) Les atteintes extrapulmonaires de la tuberculose de l'enfant. Arch Pédiatrie 12:S122–S126

Lefere M, Larbi A, Malghem J, Vande Berg B, Dallaudière B (2014) Vertebral sarcoidosis: long-term follow-up with MRI. Skeletal Radiol 43:1185–1190

Lolge S, Maheshwari M, Shah J, Patkar D, Chawla A (2003) Isolated solitary vertebral body tuberculosis—study of seven cases. Clin Radiol 58:545–550

Madhok R, Sachdeva P (2016) Evaluation of apparent diffusion coefficient values in spinal tuberculosis by MRI. J Clin Diagn Res 10:TC19–TC23

Madkour MM, Sharif HS, Abed M, Al-Fayez MA (1988) Osteoarticular brucellosis. AJR Am J Roentgenol 150:1101–1105

Mahboubi S, Morris MC (2001) Imaging of spinal infections in children. Radiol Clin North Am 39: 215–222

Martini M (1988) Tuberculosis of bone and joints. Springer Verlag, Berlin

Masood S (2013) Ultrasound guided fine needle aspiration biopsy: the new challenges and opportunities for cytopathologists. Diagn Cytopathol 41:1017–1018

Merino P, Candel FJ, Gestoso I, Baos E, Picazo J (2012) Microbiological diagnosis of spinal tuberculosis. Int Orthop 36:233–238

Mishra SS, Das D, Das S, Mohanta I, Tripathy SR (2015) Spinal cord compression due to primary intramedullary tuberculoma of the spinal cord presenting as paraplegia: a case report and literature review. Surg Neurol Int 6:42

Momjian R, George M (2014) Atypical imaging features of tuberculous spondylitis: case report with literature review. J Radiol Case Rep 8:1–14

Moon MS (2014) Tuberculosis of spine: current views in diagnosis and management. Asian Spine J 8:97–111

Moore SL, Rafii M (2001) Imaging of musculoskeletal and spinal tuberculosis. Radiol Clin North Am 39:329–342

Moorthy S, Prabhu NK (2002) Spectrum of MR imaging findings in spinal tuberculosis. AJR Am J Roentgenol 179:979–983

Morvan G, Martin N, Massare C, Nahum H (1984) La tuberculose du rachis cervical : étude radiologique à propos d'une série multicentrique de 53 cas. Rev Chir Orthop Reparatrice Appar Mot 70:76–80

Morvan G, Laredo JD, Wibier M (1998) Imagerie ostéo-articulaire, vol 2. Médecine-Sciences-Flammarion, Paris, pp 756–763

Moser T, Ehlinger M, Chelli Bouaziz M, Ladeb MF, Durckel J, Dosch JC (2012) Pitfalls in osteoarticular imaging: how to distinguish bone infection from tumour? Diagn Interv Imaging 93:351–359

Murray JF (1996) Expressions cliniques actuelles de la tuberculose. Rev Prat 46:1344–1349

Naim-Ur-Rahaman, El Bakry A, Jamjoom ZA, Kolawole TM (1999) Atypical forms of spinal tuberculosis: case report and review of the literature. Surg Neurol 51:602–607

Narlawar RS, Shah JR, Pimple MK et al (2002) Isolated tuberculosis of posterior elements of spine: magnetic resonance imaging findings in 33 patients. Spine 27:275–281

Nassar I, Mahi M, Semlali S et al (2002) Tuberculose de l'arc vertebral postérieur. J Neuroradiol 29:204–207

Papavero R, Bissuel F, Gruel S et al (1999) Tuberculose vertébrale de l'enfant. Place de l'imagerie dans la démarche diagnostique et thérapeutique. Presse Med 28:1980–1982

Pertuiset E, Beaudreuil J, Horusitzky F et al (1997) Aspects épidémiologiques de la tuberculose ostéo-articulaire de l'adulte. Etude rétrospective de 206 cas diagnostiqués en région parisienne de 1980 à 1994. Presse Med 26:311–315

Pertuiset E, Beaudreuil J, Liote F et al (1999) Spinal tuberculosis in adults. A study of 103 cases in a developed country, 1980–1994. Medicine 78:309–320

Ramachandran S, Clifton IJ, Collyns TA, Watson JP, Pearson SB (2005) The treatment of spinal tuberculosis: a retrospective study. Int J Tuberc Lung Dis 9:541–544

Rasouli MR, Mirkoohi M, Vaccaro AR, Yarandi KK, Rahimi-Movaghar V (2012) Spinal tuberculosis: diagnosis and management. Asian Spine J 6:294–308

Rauf F, Chaudhry UR, Atif M, ur Rahaman M (2015) Spinal tuberculosis: our experience and a review of imaging methods. Neuroradiol J 28:498–450

Resnick D (1995) Osteomyelitis, septic arthritis and soft tissue infection: organisms. In: Resnick D (ed) Diagnosis of bone and joint disorders, vol 4, 3rd edn. Saunders, Philadelphia, PA, pp 2448–2558

Ridley N, Shaikh MI, Remedios D, Mitchell R (1998) Radiology of skeletal tuberculosis. Orthopaedics 21:1213–1220

Rivas-Garcia AI, Sarria-Estrada S, Torrents-Odin C, Casas-Gomila L, Franquet E (2013) Imaging findings of Pott's disease. Eur Spine J 22(Suppl 4): 567–578

Rua-Figueroa I, Gantes MA et al (2002) Vertebral sarcoidosis: clinical and imaging findings. Semin Arthritis Rheum 31:346–352

Sharif HS, Aideyan OA, Clark DC et al (1989) Brucellar and tuberculous spondylitis: comparative imaging features. Radiology 171:419–425

Sharif HS, Morgan JL, Al Shahed MS, Al Thagafi MY (1995) Role of CT and MR imaging in the management of tuberculous spondylitis. Radiol Clin North Am 33:787–804

Shikhare SN, Singh DR, Shimpi TR, Peh WCG (2011) Tuberculous osteomyelitis and spondylodiscitis. Semin Musculoskelet Radiol 15:446–458

Skaf GS, Kanafani ZA, Araj GF, Kanj SS (2010) Non-pyogenic infections of the spine. Int J Antimicrob Agents 36:99–105

Smids C, Kouijzer IJ, Vos FJ et al (2017) A comparison of the diagnostic value of MRI and ^{18}F-FDG-PET/CT in suspected spondylodiscitis. Infection 45:41–49

Stabler A, Reiser MF (2001) Imaging of spinal infection. Radiol Clin North Am 39:115–135

Teo HEL, Peh WCG (2004) Skeletal tuberculosis in children. Pediatr Radiol 34:853–860

Trecarichi EM, Di Meco E, Mazzotta V, Fantoni M (2012) Tuberculous spondylodiscitis: epidemiology, clinical features, treatment, and outcome. Eur Rev Med Pharmacol Sci 16:58–72

Tuli SM (2002) General principles of osteoarticular tuberculosis. Clin Orthop 398:11–19

Turgut M (2001) Multifocal extensive spinal tuberculosis (Pott's disease) involving cervical, thoracic and lumbar vertebrae. Br J Neurosurg 15:142–146

Valencia MP, Deaver PM, Mammarappallil MC (2009) Sarcoidosis of the thoracic and lumbar vertebrae, mimicking metastasis or multifocal osteomyelitis by MRI: case report. Clin Imaging 33:476–481

Wallace R, Cohen AS (1976) Tuberculous arthritis: a report of two cases with review of biopsy and synovial fluid findings. Am J Med 61:277–282

Williams RL, Fukui MB, Meltzer CC et al (1999) Fungal spinal osteomyelitis in the immunocompromised patient: MR findings in three cases. AJNR Am J Neuroradiol 20:381–385

Wrobel CJ, Chappell ET, Taylor W (2001) Clinical presentation, radiological findings, and treatment results of coccidioidomycosis involving the spine: report on 23 cases. J Neurosurg 95(1 Suppl):33–39

Yang CM, Hsu CH, Lee CM, Wang FC (2003) Intense uptake of [F-18]- fluoro-2 deoxy-D-glucose in active pulmonary tuberculosis. Ann Nucl Med 17:407–410

Imaging of Extraspinal Musculoskeletal Tuberculosis

Nuttaya Pattamapaspong and Wilfred C. G. Peh

Contents

N. Pattamapaspong (✉)
Department of Radiology, Faculty of Medicine, Chiang Mai University, Chiang Mai, Thailand
e-mail: nuttaya@gmail.com; nuttaya.p@cmu.ac.th

W. C. G. Peh
Department of Diagnostic Radiology, Khoo Teck Puat Hospital, Singapore, Republic of Singapore
e-mail: Wilfred.peh@gmail.com; Wilfred.peh@ktph.com.sg

Abstract

Tuberculosis can lead to serious destruction of musculoskeletal structures such as the bones, joints, and soft tissues. Early diagnosis of musculoskeletal tuberculosis is important in order to minimize structural damage and prevent permanent complications. The diagnosis requires a high degree of awareness as the clinical presentation may be indolent, non-specific, and may mimic other disease processes. Tissue destruction from tuberculous granulomas produces some characteristic patterns which can be demonstrated by imaging studies. Radiography, ultrasound imaging, computed tomography, and magnetic resonance imaging help in detection of the disease, guide appropriate laboratory investigation and surgical management, as well as in the evaluation of treatment outcome. Whole-body [Fluorine-18]-fluoro-2-deoxy-D-glucose positron-emission tomography has a gradually increasing role in the detection of multifocal lesions and disease monitoring. Knowing the characteristic imaging features and potential mimics aids in timely diagnosis and treatment of musculoskeletal tuberculosis.

© The Author(s), under exclusive license to Springer Nature Switzerland AG 2022

M. F. Ladeb, W. C. G. Peh (eds.), *Imaging of Tuberculosis*, Medical Radiology Diagnostic Imaging,
https://doi.org/10.1007/978-3-031-07040-2_13

Abbreviations

CT	Computed tomography
MRI	Magnetic resonance imaging
TB	Tuberculosis

1 Introduction

Musculoskeletal tuberculosis (TB) is an important cause of mortality and morbidity worldwide. Cases are rising because of the steadily increasing number of immunocompromised hosts such as patients with human immunodeficiency virus (HIV) infection, immunosuppressive treatment, advanced age, and also a rise in immigration from countries with a high disease prevalence (Arora and Chopra 2019; Suarez et al. 2019; World Health Organization 2021). Appendicular involvement, although less common than spinal TB, can lead to serious bone and joint destruction. The indolent and diverse clinical presentation often mimics many other diseases, and may cause a delay in diagnosis. The emergence of multidrug-resistant strains increases the difficulty in treatment and control of disease spread. Early imaging diagnosis plays an important role in directing appropriate laboratory investigation, hence allowing timely diagnosis and treatment.

2 Pathophysiology

TB affects the musculoskeletal system, causing osteomyelitis, arthritis, or soft tissue infection. The organism reaches the musculoskeletal system via hematogenous spread or by direct inoculation. Hematogenous spread is more common and will be discussed in more detail in the following paragraphs. The disease either presents during the primary spread of the organism or as a reactivation, usually when host immunity decreases. At the site of infection, the TB bacilli induce a granulomatous inflammatory reaction that consists of epithelioid cells, lymphocytes, and multinucleated giant cells, forming either caseating or noncaseating granulomas (Natarajan et al. 2020). The host inflammatory response results in liquefactive and caseous necrosis, tissue destruction, and abscess formation. The infective focus then spreads to the surrounding structures. In the late stage of the disease, the granulomatous lesions may calcify (Sharma et al. 1978).

The metaphysis of long bones and large weight-bearing joints, such as the hip and knee, are commonly affected because of their rich vascular supply (Pigrau-Serrallach and Rodríguez-Pardo 2013; Natarajan et al. 2020). The predilection for the location of osteomyelitis depends on the distribution of intraosseous vascular structures according to age. In infants younger than 1.5 years of age, transphyseal spread is common, due to vessels crossing the growth plate. In children aged between one and 16 years, the metaphysis is the most common site, as the epiphyseal growth plate acts as a natural barrier to the spread of infection. However, isolated epiphyseal lesions may still occur, owing to the presence of the nutrient artery of the epiphysis. In adults, vascular distribution in form of communicating metaphyseal and epiphyseal vessels allows the infection to reach subchondral bone (Wang et al. 1999; Resnick 2002a; Ranson 2009) (Fig. 1).

Tuberculous arthritis may result from primary spread via subsynovial vessels, or be secondary to osteomyelitis or infected para-articular tissue (De Backer et al. 2006) (Fig. 2). As the exudative fluid in tuberculous arthritis lacks proteolytic enzymes, the cartilage is usually spared until later stages of the disease (Akeson et al. 2002). The pattern of cartilage destruction reflects the growth of granulation tissue which can be along the free surface of cartilage, between the cartilage and subchondral bone, or result from penetration through the cartilage (Resnick 2002b) (Fig. 2).

Soft tissue infections, including pyomyositis, bursitis, tenosynovitis, and subcutaneous tissue abscesses, can present as a primary affected site but is more commonly a complication of

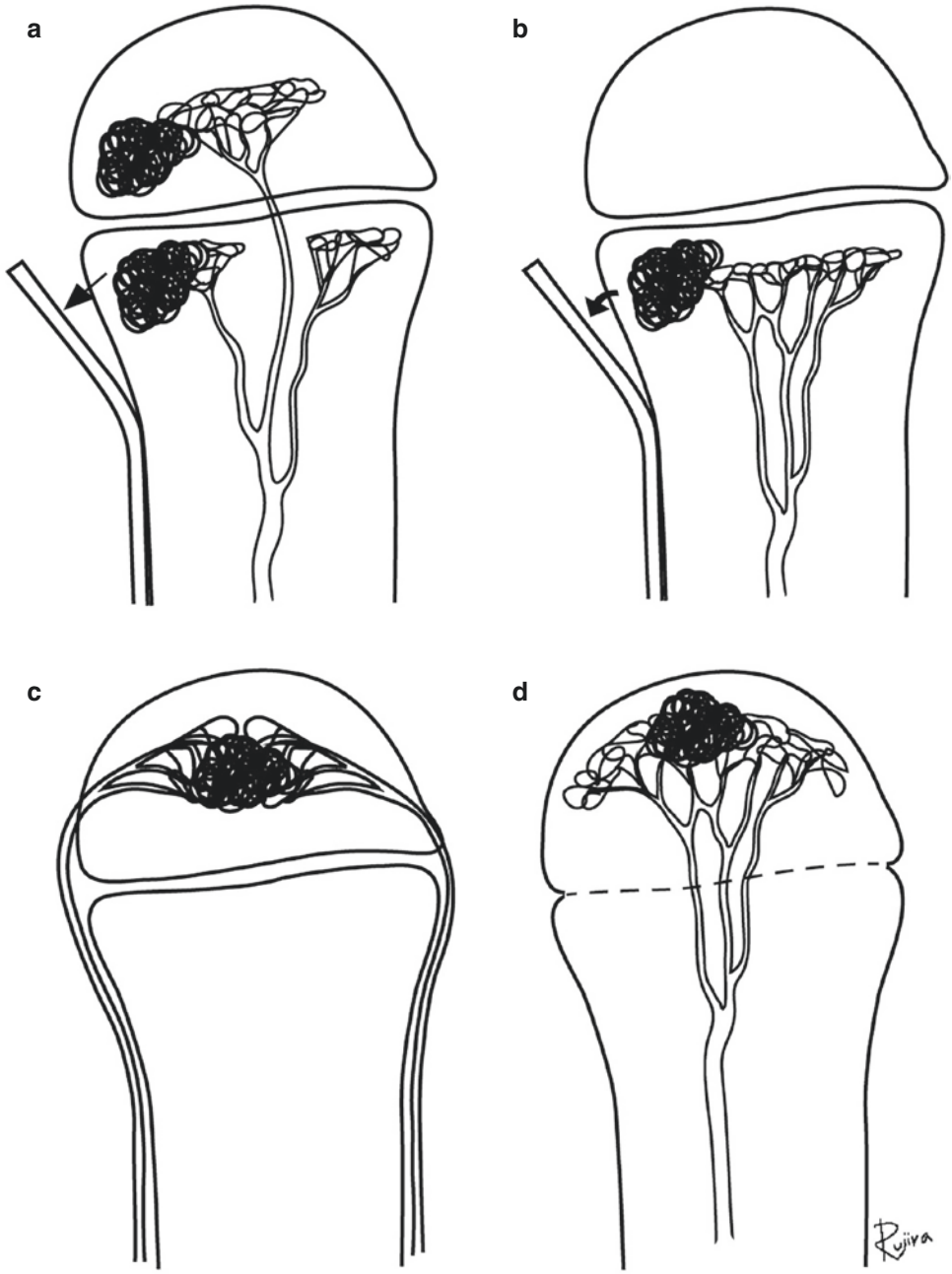

Fig. 1 Location of osteomyelitis and distribution of intraosseous vascular structures according to age. (**a**) In infants aged less than 1.5 years, infection in the metaphysis spreads via vessels traversing the growth plate leading to infection of the epiphysis. (**b**) In children aged 1–16 years, infection has predilection for the metaphysis because of its rich vascular supply. The growth plate acts as a natural barrier to infection spreading to the epiphysis. The infection in the metaphysis may spread under the periosteum and extend to the surrounding soft tissues (arrows in **a** and **b**). (**c**) Isolated epiphyseal osteomyelitis may occur due to spread via the epiphyseal nutrient artery. (**d**) In adults, epiphyseal vessels passing through the closed physis allow infection to reach subchondral bone. Osteomyelitis in the epiphysis and subchondral bone can spread to the joint resulting in tuberculous arthritis

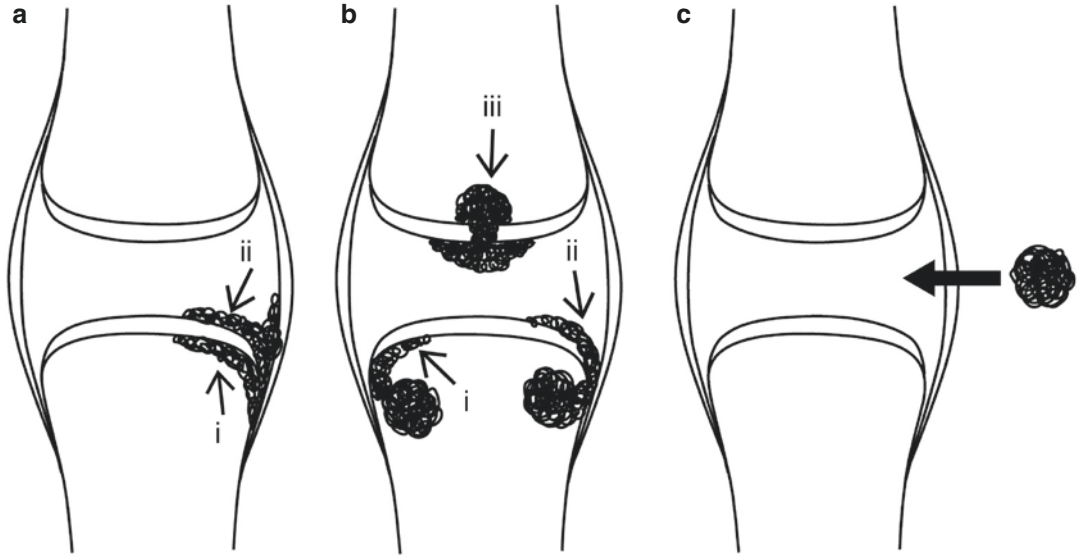

Fig. 2 Patterns of spread causing tuberculous arthritis and cartilage destruction. Joint infection spreads from (**a**) subsynovial vessels, (**b**) osteomyelitis, or (**c**) infected para-articular soft tissues. Destruction of the cartilage by granulation tissue can be (i) deep from subchondral bone, (ii) over the cartilage surface, or (iii) through penetration of the cartilage

osteomyelitis or arthritis. Tuberculous tenosynovitis and bursitis initially develop as a serous effusion, followed by synovial thickening, and accumulation of tissue debris and caseous material. Eventually, debris and synovial thickening become prominent and there is minimal effusion. Tenosynovitis may lead to tendon tethering or rupture (Jaovisidha et al. 1996).

3 Clinical Features and Complications

Musculoskeletal TB is a disease that affects all age groups but there is a predilection for children and the elderly (Perez-Velez and Marais 2012; Arora and Chopra 2019). Clinical features of musculoskeletal TB are variable and non-specific. Infected patients can present with chronic pain, limb deformity, dislocation, pathological fracture, palpable mass as a result of abscess formation, or draining skin sinus. Fever is infrequent and is mostly associated with disseminated infection (Naidoo et al. 2017). Multifocal lesions occur in 7–11% of patients and are commonly associated with HIV infection, children, or poor physical status (Prasad et al. 2012; Pigrau-Serrallach and Rodríguez-Pardo 2013; Naidoo et al. 2017; Suarez et al. 2019). Not all lesions are symptomatic, and different stages of destruction and healing can be expected as a result of multiple episodes of hematogenous seeding of the organism and variable local tissue immunity.

The major predisposing factors of musculoskeletal TB are conditions leading to immunosuppression, caused by diseases or treatment (Hodkinson et al. 2009; Lin et al. 2009). Tissue injury, either by trauma or surgery, is a predisposing factor because of increased vascular supply and impairment of the local immune system. Tuberculous infection has been reported following different types of surgery such as fracture fixation (Kumar et al. 2006), reconstruction of the anterior cruciate ligament of the knee (Nag et al. 2009), and sternotomy (Gopal et al. 2007). Inflammatory joint disease may also predispose to tuberculous arthritis (Bryan et al. 1982; Hortas et al. 1988). Prosthetic joint infection due to TB

is uncommon. Three pathogenic mechanisms have been reported: (1) Active tuberculous arthritis present at the time of surgery but not known to clinician; (2) Hematogenous spread from a distant focus; and (3) Surgical trauma resulting in activation of previous unknown TB (Hugate and Pellegrini 2002; Khater et al. 2007; Carrega et al. 2013; Harwin et al. 2013).

Bone and joint infections often subsequently progress to soft tissue abscesses. Tuberculous abscess typically has a minimal inflammatory response, and is also called a cold abscess. If untreated, the soft tissue abscess may form a sinus tract which drains to the skin. In the immature skeleton, bone and joint tuberculosis may cause limb length discrepancy and deformity. In tenosynovitis of the wrist, thickened synovial tissue and debris can envelop the median nerve, resulting in the carpal tunnel syndrome (Hassanpour and Gousheh 2006).

4 Imaging Features

4.1 Radiography

Radiographs are the main modality used in the detection of musculoskeletal infection. Due to the typically late and indolent clinical presentation, radiographs commonly reveal the advanced stages of disease with considerable structural destruction. The features of tuberculous osteomyelitis are a well-defined osteolytic lesion usually located in the metaphysis of long bones with or without sclerotic reaction, cortical expansile remodeling, sequestrum, and periostitis. Transphyseal spread is a characteristic feature of tuberculous osteomyelitis, a finding which is unusual for bacterial infection (De Vuyst et al. 2003) (Figs. 3, 4, and 5). An isolated epiphyseal lesion resulting from epiphyseal vessel spread may sometimes occur (Fig. 6)

Multifocal tuberculous osteomyelitis, also called osteitis cystica tuberculosa multiplex, is an unusual form of osteomyelitis that occurs in children more often than in adults (Shikhare et al.

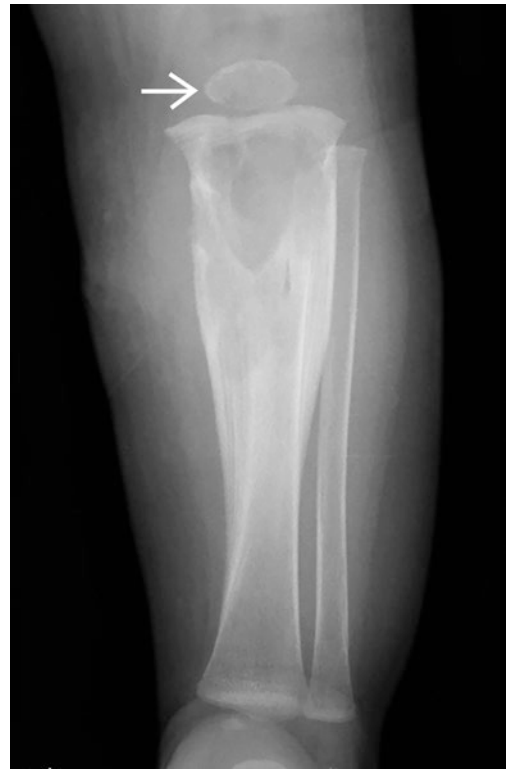

Fig. 3 Tuberculous osteomyelitis with transphyseal spread in an 8-month-old male infant who had swelling of the leg for 1 month. Frontal radiograph shows an osteolytic lesion in the metaphysis with bone expansion and thick laminated periosteal reaction. Note the osteolytic lesion in the epiphysis (arrow) indicating transphyseal spread

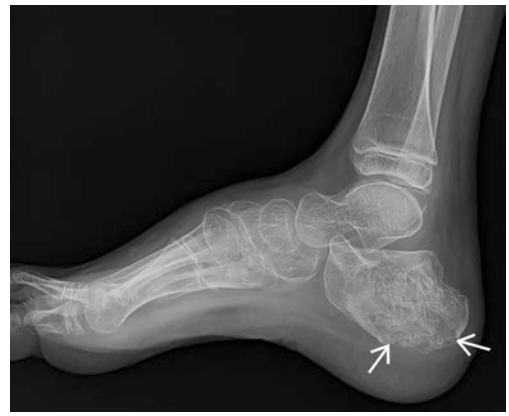

Fig. 4 Tuberculous osteomyelitis of the calcaneus in a 10-year-old girl who presented with a draining sinus in the heel. Lateral radiograph shows an osteolytic lesion with sclerotic reaction. Note the cortical bone destruction corresponding to the location of the sinus (arrows)

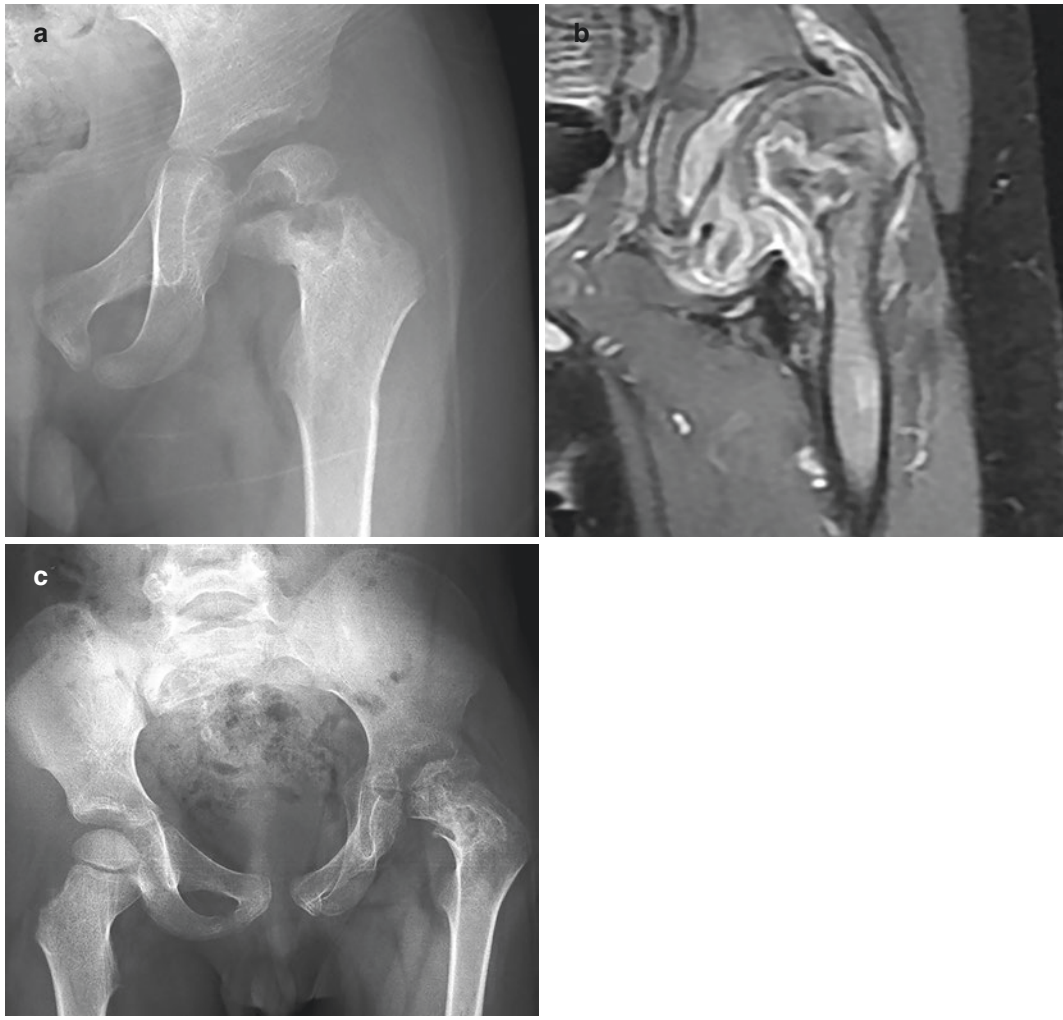

Fig. 5 Tuberculous osteomyelitis with transphyseal spread and arthritis in a 4-year-old girl. (**a**) Frontal radiograph shows an osteolytic lesion in the metaphysis with extension to the proximal femoral epiphysis. (**b**) Coronal contrast-enhanced fat-suppressed T1-weighted MR image shows transphyseal extension of the intraosseous abscess and synovial enhancement indicating joint involvement. (**c**) Frontal radiograph taken at 2-year follow-up after treatment shows a flattened left femoral epiphysis mimicking the changes of Perthes disease. Note the sclerotic changes due to healed osteomyelitis. (Courtesy of Dr. Thanat Kanthawang, Faculty of Medicine, Chiang Mai University, Thailand)

2011). The disease manifests radiographically as well-defined osteolytic lesions resembling bone cysts of variable sizes. Sclerotic changes at the lesion margins are usually minimal and when present support evidence of healing (Tiwari et al. 2007) (Fig. 7).

Tuberculous dactylitis or osteomyelitis of the short tubular bone of hands and feet commonly occurs in younger patients, particularly children aged less than 6 years (Ranjan et al. 2019). These patients often present with soft tissue swelling and flexion deformity. Characteristic

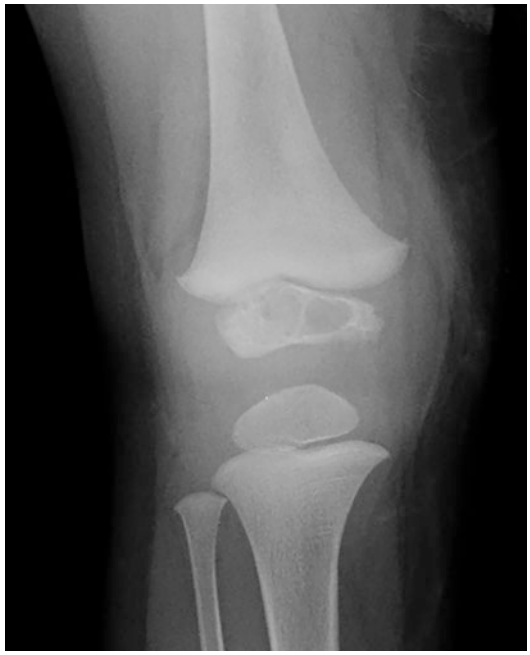

Fig. 6 Tuberculous epiphyseal osteomyelitis in a 2-year-old boy who had right knee swelling for 4 months. Frontal radiograph of the knee shows an osteolytic lesion in the femoral epiphysis

radiographic features include an osteolytic lesion, fusiform expansion of the bone and thick periosteal reaction, leading to the term spina (short bone) ventosa (inflated with air) (Fig. 8). In the mild form of the disease, dactylitis causes soft tissue swelling and periosteal reaction.

The radiographic hallmark of tuberculous arthritis, described as the Phemister triad, consists of marginal bone erosions, juxta-articular osteoporosis, and relatively preserved joint space (Phemister and Hatcher 1933) (Figs. 9, 10, and 11). Large subchondral bone destruction, due to intraosseous abscesses, may be present (Fig. 10). Widespread disease may also occur in the interconnecting joints of the wrist and midfoot (Dhillon and Nagi 2002; Hsu et al. 2004) (Fig. 11). Soft tissue abscesses, tenosynovitis, or bursitis can lead to a large soft tissue mass detectable on radiographs (Fig. 10a). Associated soft tissue calcification is a suggestive sign of tuberculous infection (Sharma et al. 1978) (Fig. 12).

Apart from structural damage by granulomatous formation, radiographs can demonstrate

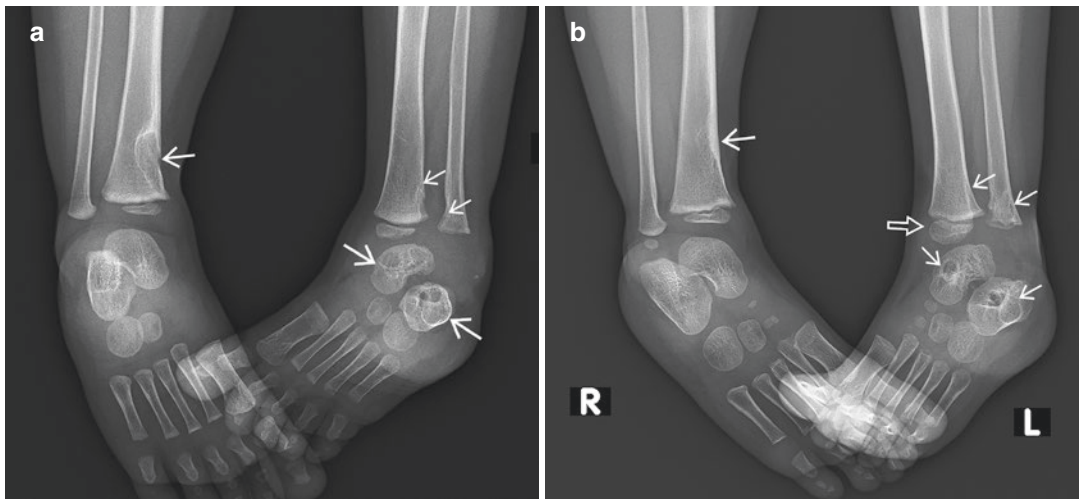

Fig. 7 Multifocal tuberculous osteomyelitis in a 16-month-old boy. (**a**) Frontal radiograph of both ankles shows multifocal osteolytic lesions (arrows). (**b**) 8-month follow-up frontal radiograph shows variable degrees of sclerotic change around the lesions indicating different stages of healing. Note overgrowth of the medial left tibial epiphysis (open arrow)

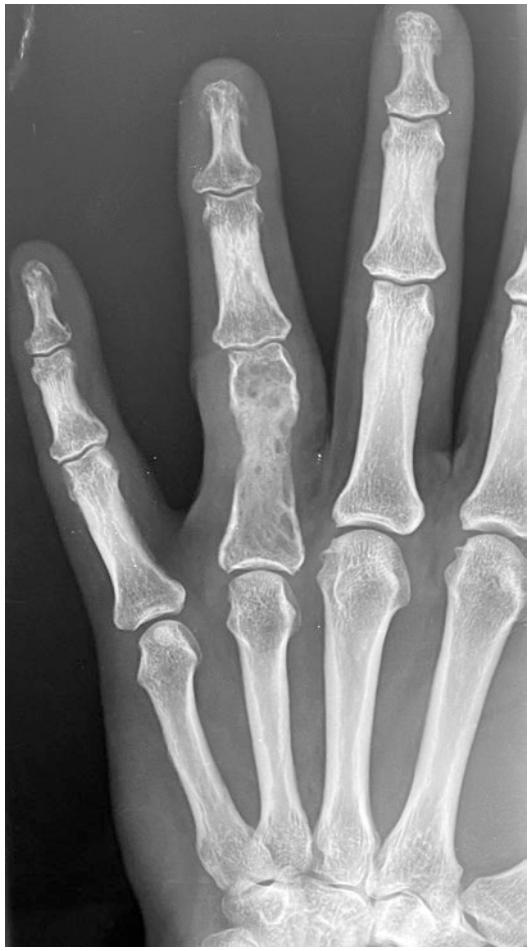

Fig. 8 Tuberculous dactylitis (or spina ventosa). Frontal radiograph of the ring finger shows an ill-defined osteolytic lesion of the proximal phalanx with cortical destruction. There is surrounding soft tissue swelling. (Courtesy of Prof. Mohamed Fethi Ladeb, MT Kassab Institute of Orthopaedics, Tunis, Tunisia)

complications such as pathological fracture (Fig. 13), dislocation (Figs. 14 and 15), limb length discrepancy, and deformities. Enlarged epiphyses result from reactive hyperemia affecting the growing ossification center (Fig. 7b). In the hip, gradual joint destruction in the weight-bearing joint causes bone remodeling and acetabular protrusion (Fig. 16a). Fibrous ankylosis occurs as an end-stage of the disease (De Vuyst et al. 2003). Bony ankylosis is uncommon in tuberculosis except in cases with surgical intervention (Parsa et al. 2018).

4.2 Computed Tomography

Computed tomography (CT) helps better demonstrate the features of TB detected by radiographs, particularly bone erosions, sequestrum (Fig.10b–d), pyomyositis, and soft tissue calcification (Figs. 15b, c and 17). CT enables detailed evaluation of abscess extension, internal organ involvement, and disseminated disease (Fig. 18). CT is particularly useful in the assessment of chest wall infection, which has a predilection for the sternal margin because of spread of infection via the internal mammary lymph nodes (Bergeron et al. 2017) (Fig. 19a). Other affected sites are the sternoclavicular joint, costochondral junction, rib shafts, and costovertebral joints (Morris et al. 2004). Mediastinal extension is well demonstrated by CT (Fig. 20). CT is also useful for guiding biopsy.

4.3 Magnetic Resonance Imaging

Magnetic resonance imaging (MRI) is the most useful modality for the evaluation of musculoskeletal TB, as it provides a good demonstration of inflammatory processes in bones, joints, and soft tissues (Figs. 5b, 9b–d, and 19b, c). The minimal inflammatory response of the tissues around an abscess is a characteristic finding of tuberculous infection (Fig. 21). Sinus formation is seen as "tram-track" enhancement extending from the infected site to the skin (Figs. 14c, d and 22). In children, MRI allows better evaluation of transphyseal spread, articular involvement, and infection of the unossified part of the epiphysis (Figs. 5b and 23).

A characteristic sign of abscess formation on MRI is the presence of a penumbra, which refers to the T1-hyperintense wall of abscess

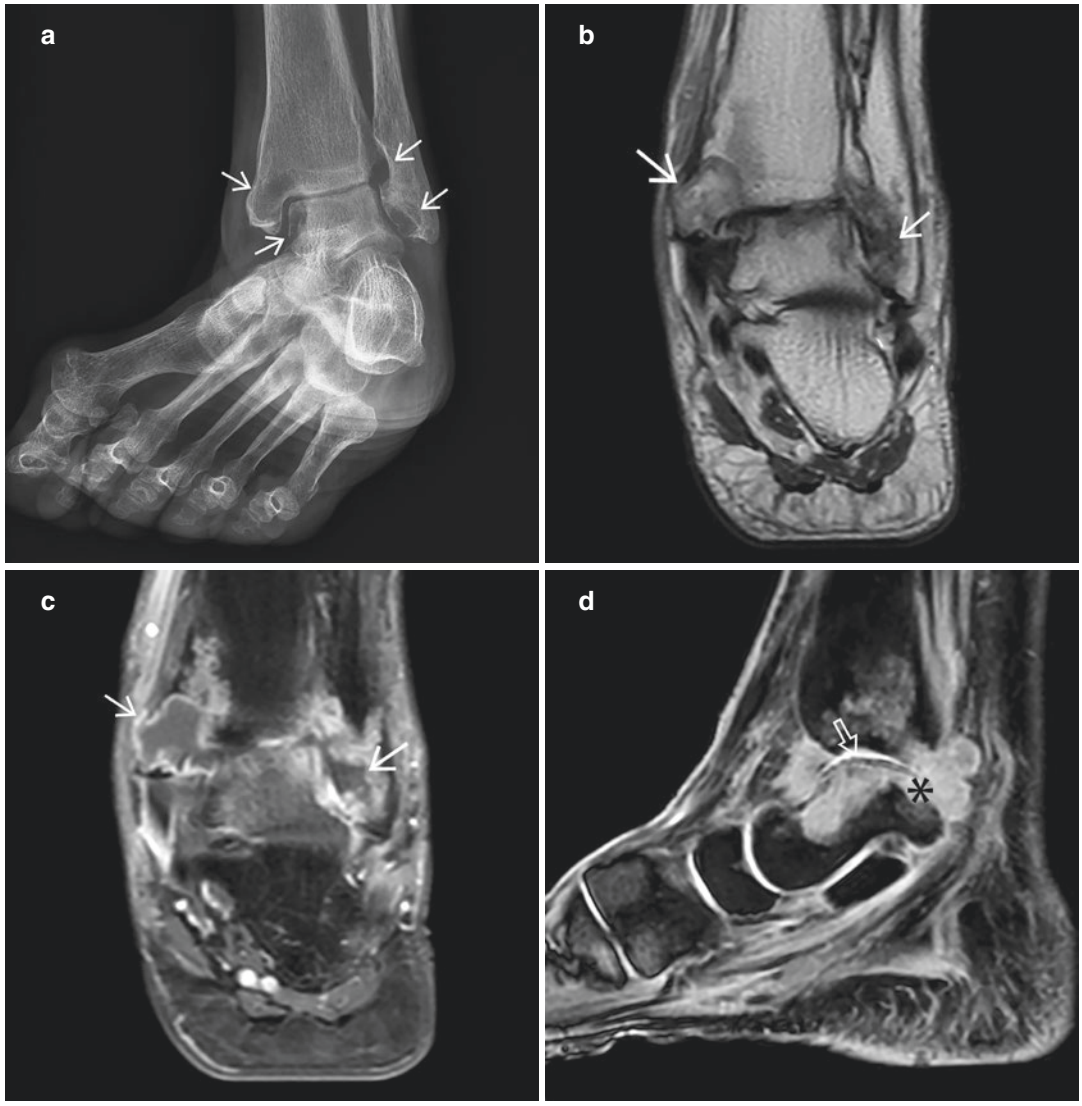

Fig. 9 Tuberculous arthritis in a 68-year-old woman who had chronic left ankle pain. (**a**) Frontal radiograph shows erosions (arrows) with relatively spared joint spaces. Coronal (**b**) T2-weighted and (**c**) contrast-enhanced fat-suppressed T1-weighted MR images show large bone erosions with enhanced granulation tissue (arrows). (**d**) Sagittal MR image using the water-selective cartilage (WATSc) sequence shows a relatively intact cartilage surface (open arrow) with subchondral extension of the granulation tissue (*)

representing vascularized granulation tissue (Grey et al. 1998) (Fig. 23). This penumbra sign has a high specificity (96%) for chronic abscesses and helps in differentiating musculoskeletal infection from tumors (McGuinness et al. 2007). However, the sign is not specific to TB, and abscess formation from other organisms can also produce this sign. Rarely, this sign has also been reported in chondrosarcoma, eosinophilic granuloma, fibrous dysplasia, pigmented villonodular synovitis, and benign cystic lesions (Grey et al. 1998; McGuinness et al. 2007).

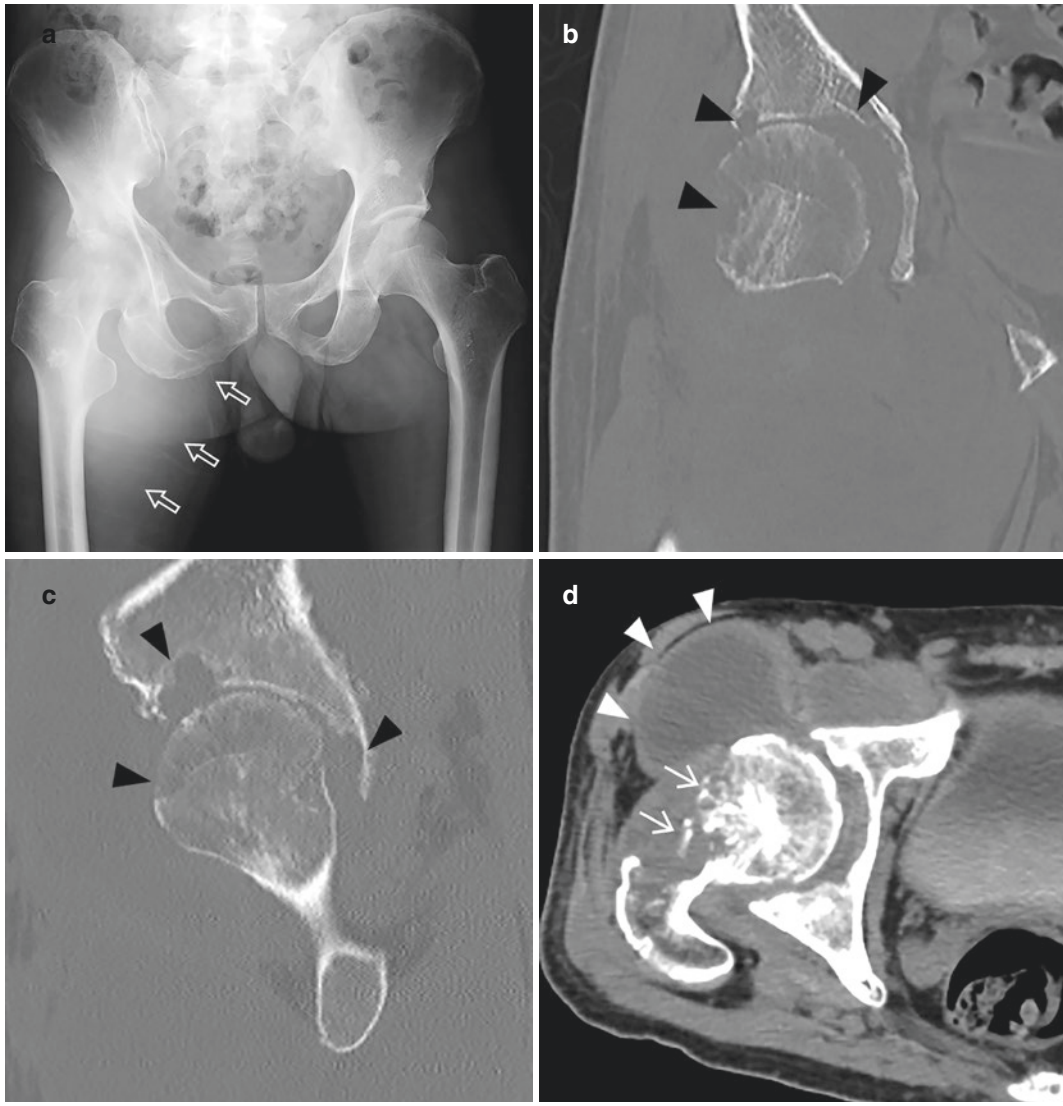

Fig. 10 Tuberculous arthritis in a 54-year-old man who had right hip pain and a groin mass for 4 months. (**a**) Frontal radiograph shows right hip joint destruction and juxta-articular osteoporosis. Note the large soft tissue shadow in the right upper thigh (open arrows). (**b**) Coronal and (**c**) sagittal CT images show large bone erosions around the right hip joint (black arrowheads). (**d**) Axial contrast-enhanced CT image shows sequestra (arrows) and a large para-articular abscess (arrowheads)

In tuberculous arthritis, MRI can demonstrate the cartilage and bone destruction caused by granulation tissue. With the lack of proteolytic enzymes, focal areas of relatively intact cartilage may be present between the areas of granulation tissue (Fig. 9d). Synovial proliferation with heterogeneous intermediate to hypointense signal on T2-weighted images is found in approximately 40% of tuberculous arthritis (Sawlani et al. 2003) (Fig. 16b). Tissue components in caseous necrosis, including fibrosis, macrophage infiltration, and free radicals from macrophage by-products, contribute to T2-hypointense signal in tuberculous synovitis

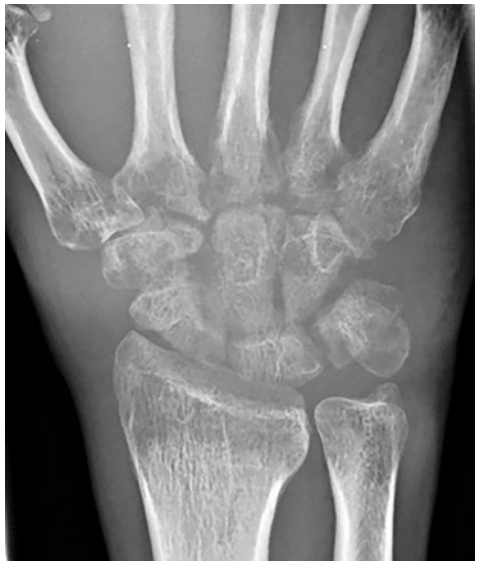

Fig. 11 Tuberculous arthritis in a 33-year-old man who had a right wrist pain for 3 weeks. Frontal radiograph shows extensive bone erosions in the interconnecting joints of the wrist, and prominent juxta-articular osteoporosis with relatively preserved joint spaces

(Suh et al. 1996; Sawlani et al. 2003) (Fig. 16b). Presence of rice bodies in the joint, bursa, or tendon sheath is a sign of chronic synovitis, a feature also sometimes seen in tuberculous infection. Rice bodies have been described in various rheumatic diseases including rheumatoid arthritis, juvenile idiopathic arthritis, or osteoarthritis (Griffith et al. 1996; Forse et al. 2012; Subramaniam et al. 2012). Rice bodies represent debris whose shape resembles grains of rice, and consists of fibrin collagen and mononuclear cells (Popert 1985) (Fig. 24).

4.4 Ultrasound Imaging

Ultrasound (US) imaging is a good modality for the detection of joint effusion, synovial thickening, bone erosion, and soft tissue extension. There is often very marked synovial thickening which contrasts with low volume joint effusion. Para-articular

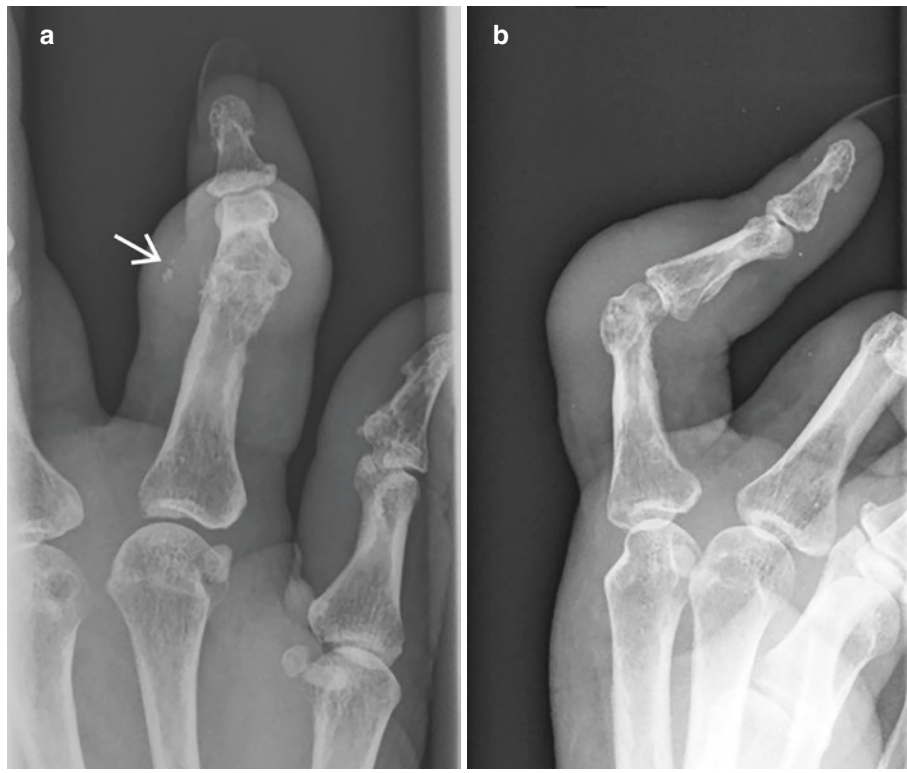

Fig. 12 Soft tissue tuberculosis with calcification in a 57-year-old woman who had index finger swelling for 1 month. (**a**) Frontal and (**b**) lateral radiographs show soft tissue swelling, flexion deformity, subluxation of the proximal interphalangeal joint, and small soft tissue calcifications (arrow). Surgery revealed soft tissue abscess, and rupture of the extensor digitorum tendon and joint capsule

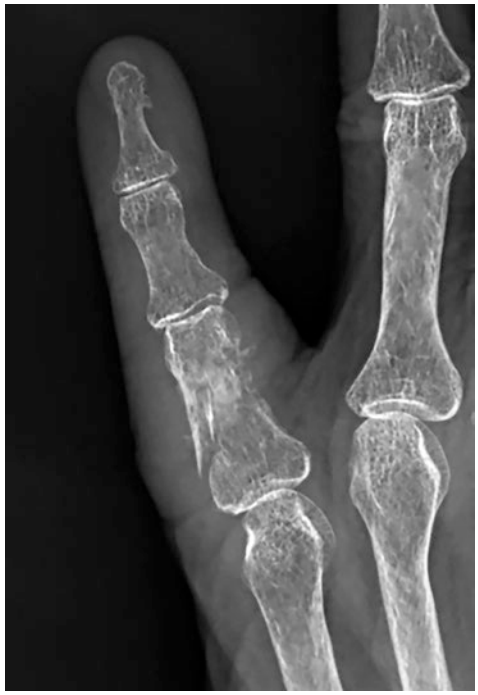

Fig. 13 Tuberculous osteomyelitis with pathological fracture in a 91-year-old woman. Frontal radiograph shows an oblique fracture through a permeative osteolytic lesion in the proximal phalanx of the finger

abscess, rice bodies, and granulomatous calcifications are well detected (Fig. 25). US imaging can also be used for guiding fluid aspiration.

4.5 Nuclear Medicine Imaging

Nuclear medicine imaging studies allow detection of multifocal infection and monitoring of disease but its utility limited by low specificity. Three-phase ^{99M}technetium (Tc) methylene diphosphonate (MDP) bone scintigraphy is positive in active and healing osteomyelitis. Gallium scintigraphy and labeled leukocyte imaging help identification of active infection (Palestro et al. 2006). Whole-body [Fluorine-18]-fluoro-2-deoxy-D-glucose positron-emission tomography (^{18}F-FDG PET) has a gradually increasing role in detecting multifocal lesions, assessing disease activity, and monitoring response to treatment (Ankrah et al. 2016). Active TB has avid tracer uptake (Fig. 26). Since ^{18}F-FDG is a non-specific tracer, it may cause a false-positive diagnosis in patients being evaluated for tumor metastasis.

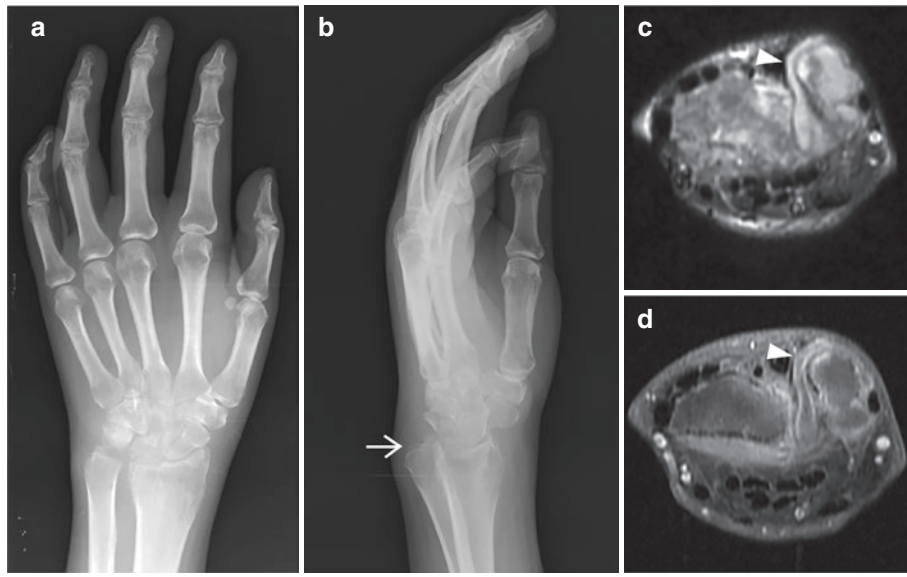

Fig. 14 Tuberculous arthritis with joint subluxation in a 49-year-old woman with connective tissue disease who had left wrist pain and draining sinus. (**a**) Frontal radiograph shows extensive destruction of the carpal and adjacent bones of the wrist with juxta-articular osteoporosis. (**b**) Lateral radiograph shows dorsal subluxation of the distal radioulnar joint (arrow). Axial (**c**) short tau inversion recovery (STIR) and (**d**) contrast-enhanced fat-suppressed T1-weighted MR images show a "tram-track" sinus tract (arrowheads)

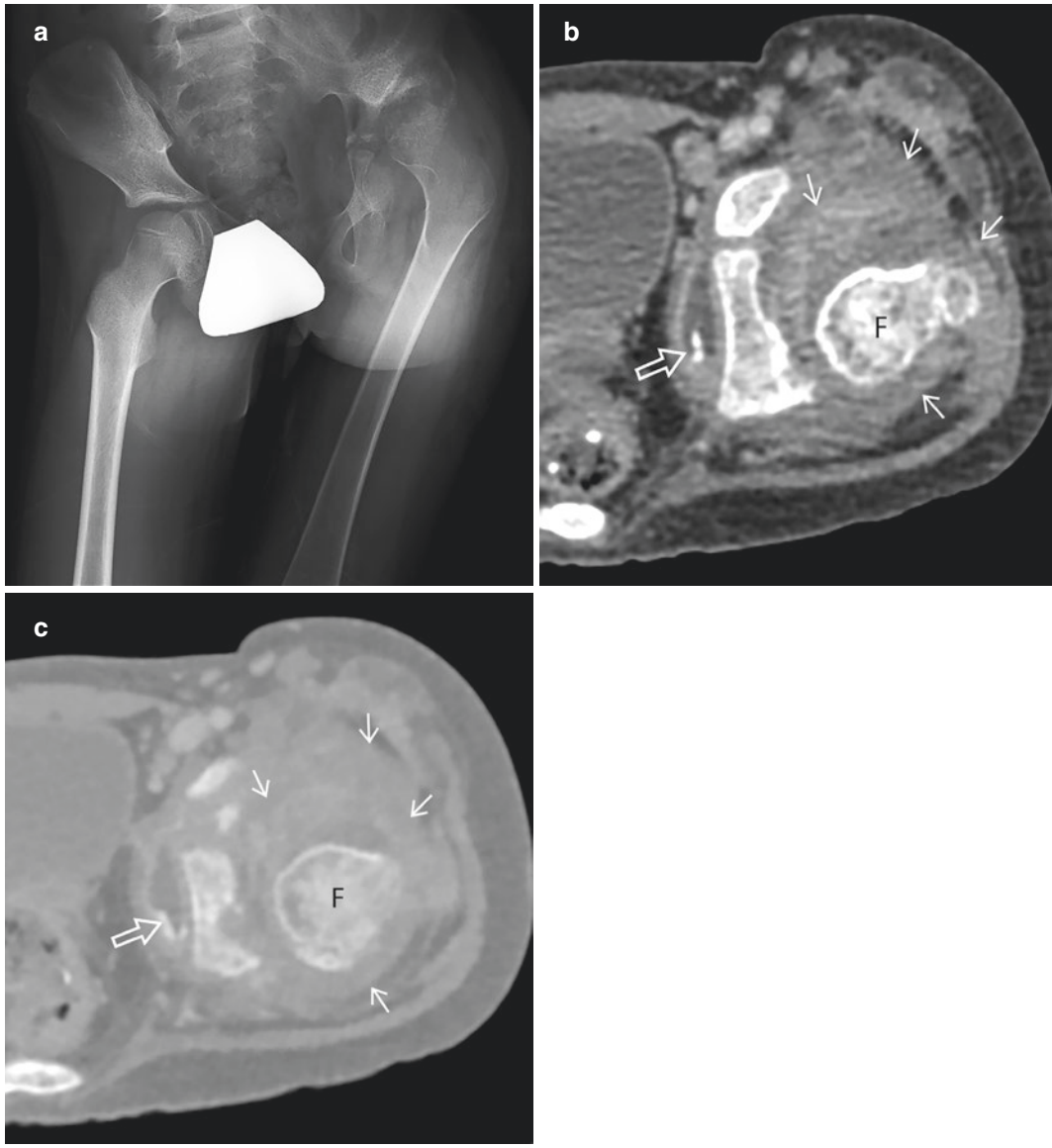

Fig. 15 Tuberculous arthritis with subluxation in a 6-year-old girl who had left hip pain and limb length discrepancy. (**a**) Frontal radiograph shows destruction of the left hip joint and shortening of the left limb. Axial CT images obtained in (**b**) soft tissue and (**c**) bone window settings show distension of the joint by a large effusion (arrows), posterior subluxation of the femoral head (F), and a calcified abscess (open arrow)

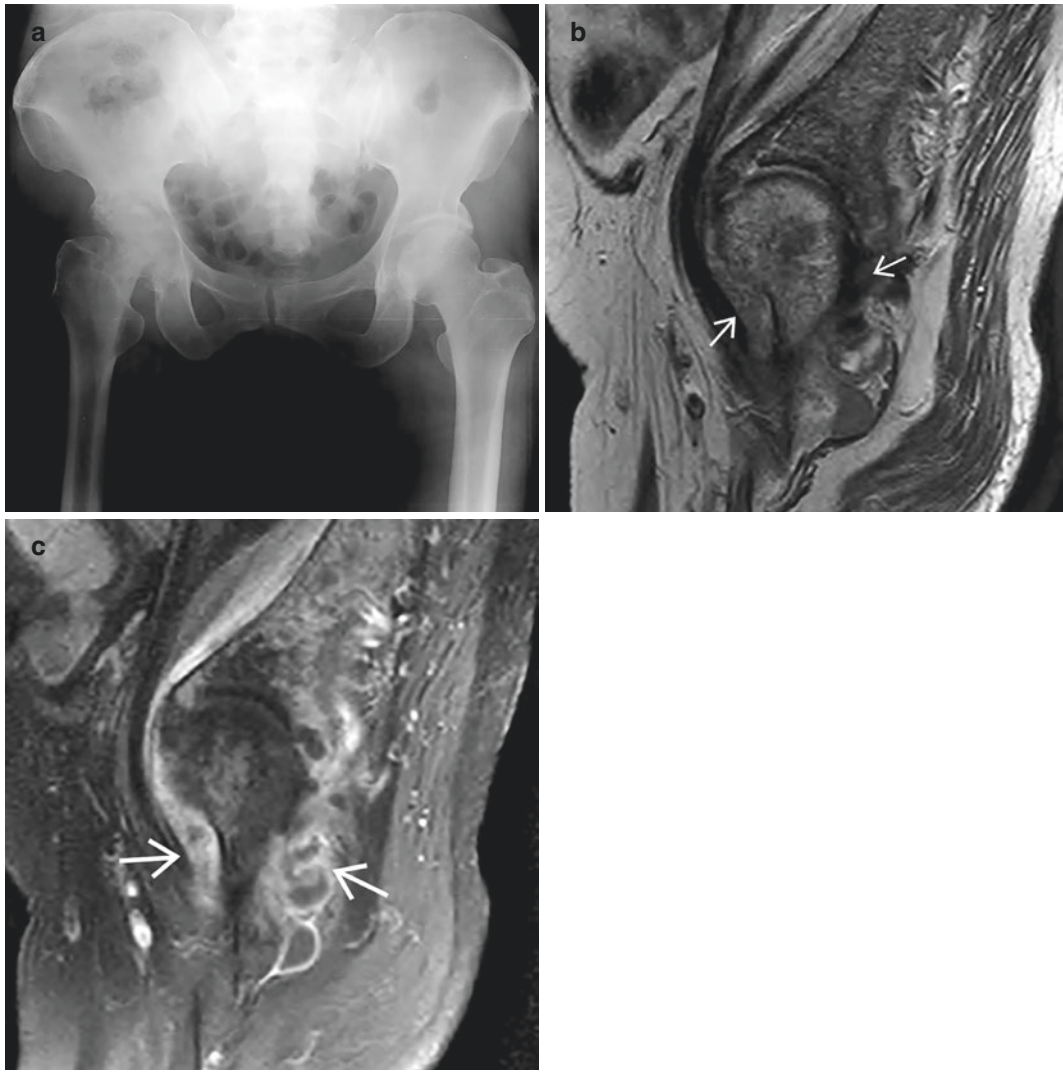

Fig. 16 Tuberculous arthritis in a 74-year-old woman who had a right hip pain for 2 weeks. (**a**) Frontal radiograph shows destruction of the right hip joint with medial wall deformity of the acetabulum (protrusio acetabuli). Sagittal (**b**) T2-weighed and (**c**) contrast-enhanced fat-suppressed T1-weighted MR images show T2-hypointense synovitis with rim enhancement (arrows)

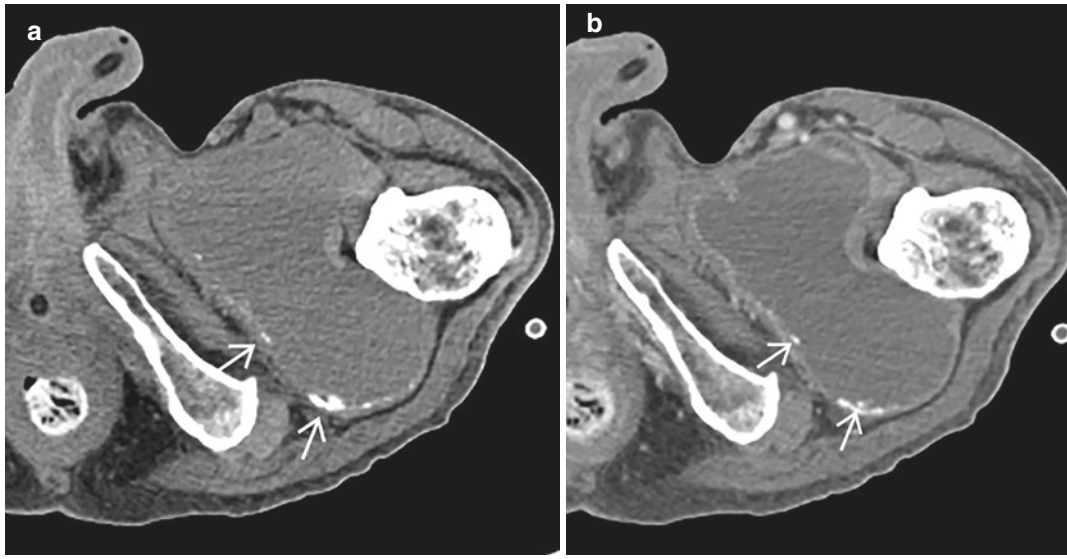

Fig. 17 Tuberculous soft tissue abscess in a 65-year-old man who had a slow-growing mass in the left thigh for 1 year. Axial (**a**) unenhanced and (**b**) contrast-enhanced CT images show a large abscess with rim-enhancing wall and calcifications (arrows)

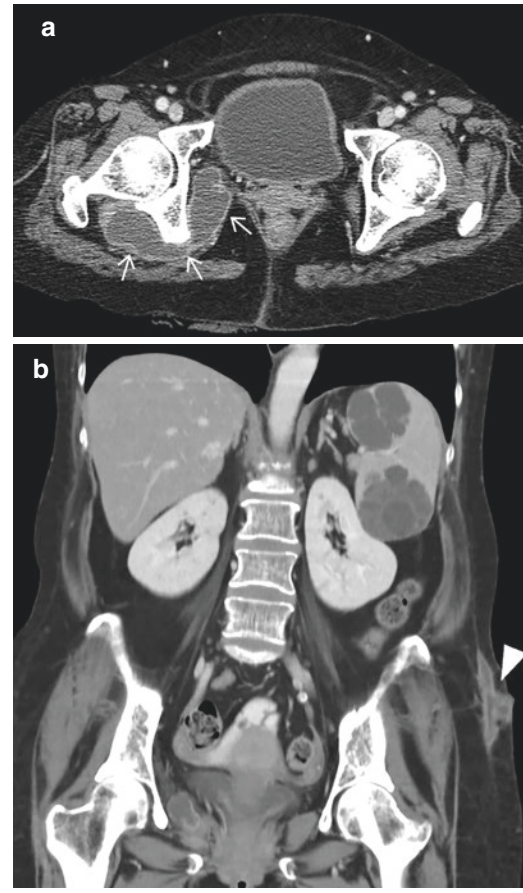

Fig. 18 Disseminated tuberculosis in a 50-year-old woman with connective tissue disease. (**a**) Axial contrast-enhanced CT image shows a deep soft tissue abscess adjacent to the right posterior hip joint and posterior ischium with extension deep to the gluteus minimus and obturator internus muscles (arrows), lateral to the ischiorectal fossa. (**b**) Coronal contrast-enhanced CT image shows splenic abscesses and a subcutaneous tissue abscess with a sinus tract in the left buttock (arrowhead)

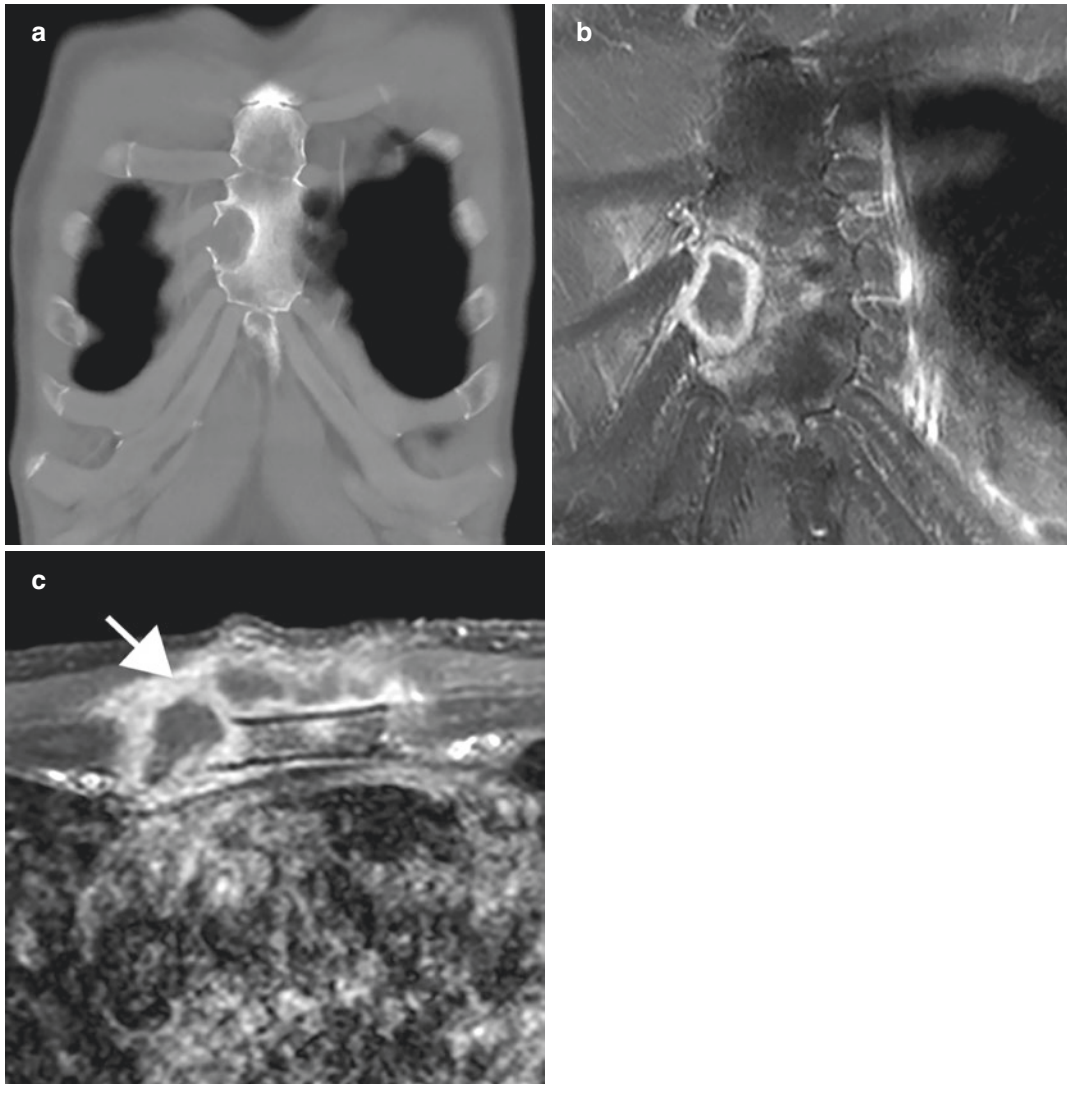

Fig. 19 Tuberculous osteomyelitis of the sternum in a 44-year-old woman who presented with a painless anterior chest wall mass. (**a**) Coronal CT image shows an osteolytic lesion at the right sternal border. (**b**) Coronal and (**c**) axial contrast-enhanced fat-suppressed T1-weighted MR images of the sternum show an intraosseous abscess with anterior soft tissue extension (arrow)

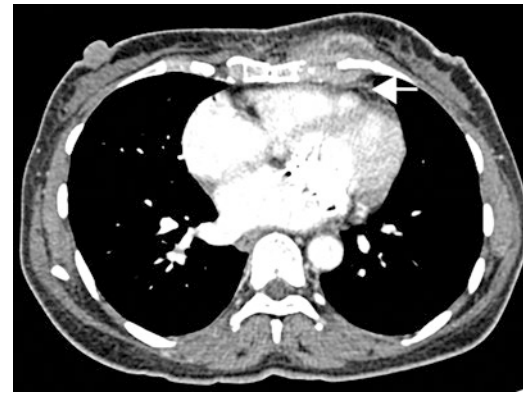

Fig. 20 Tuberculous osteomyelitis of the chest wall in a 47-year-old woman with tricuspid valve replacement who presented with a painful left breast mass. Axial contrast-enhanced CT image shows a chest wall abscess at the left costochondral junction and mediastinal extension abutting the pericardium (arrow)

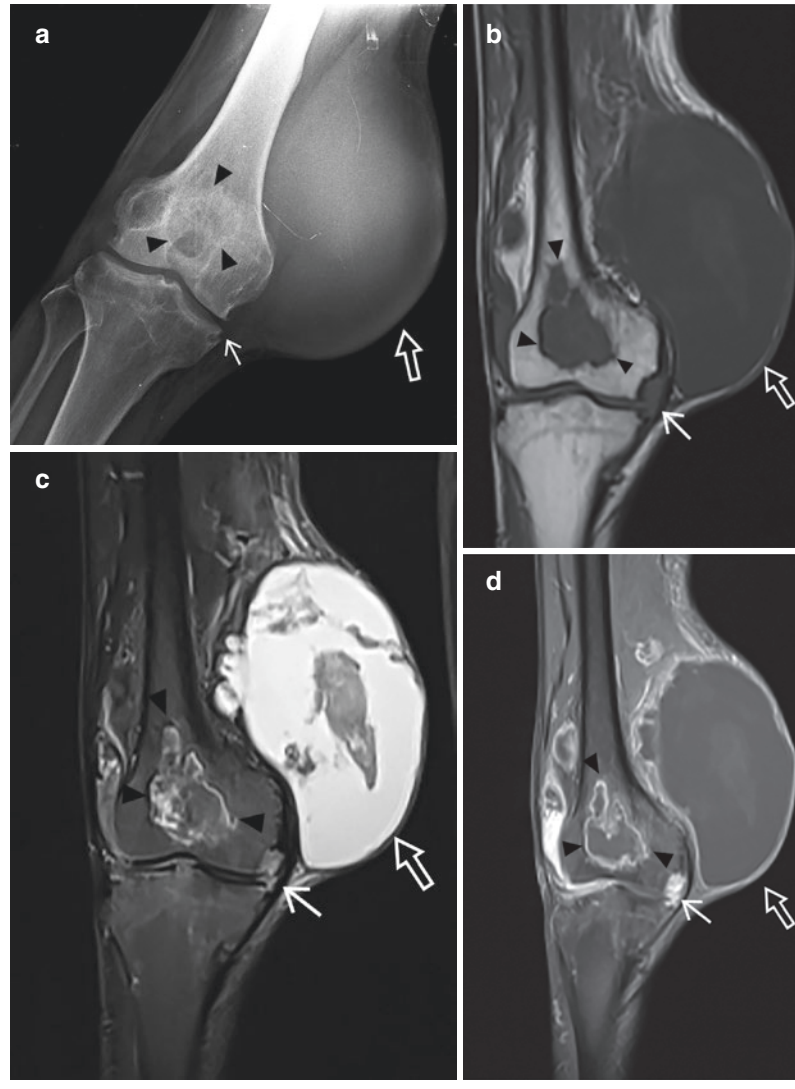

Fig. 21 Tuberculous osteomyelitis and arthritis, with an associated large soft tissue abscess in a 71-year-old man who had slow-growing thigh mass for the past 1 year. (**a**) Frontal radiograph of the right knee shows an osteolytic lesion in the femur with sclerotic borders (arrowheads), marginal bone erosion (arrow), and a large soft tissue mass (open arrow). Coronal (**b**) T1-weighted, (**c**) fat-suppressed T2-weighted, and (**d**) contrast-enhanced fat-suppressed T1-weighted MR images show osteomyelitis in the distal femur (arrowheads), synovial enhancement with bone erosion (arrows), and a large subcutaneous abscess (open arrows)

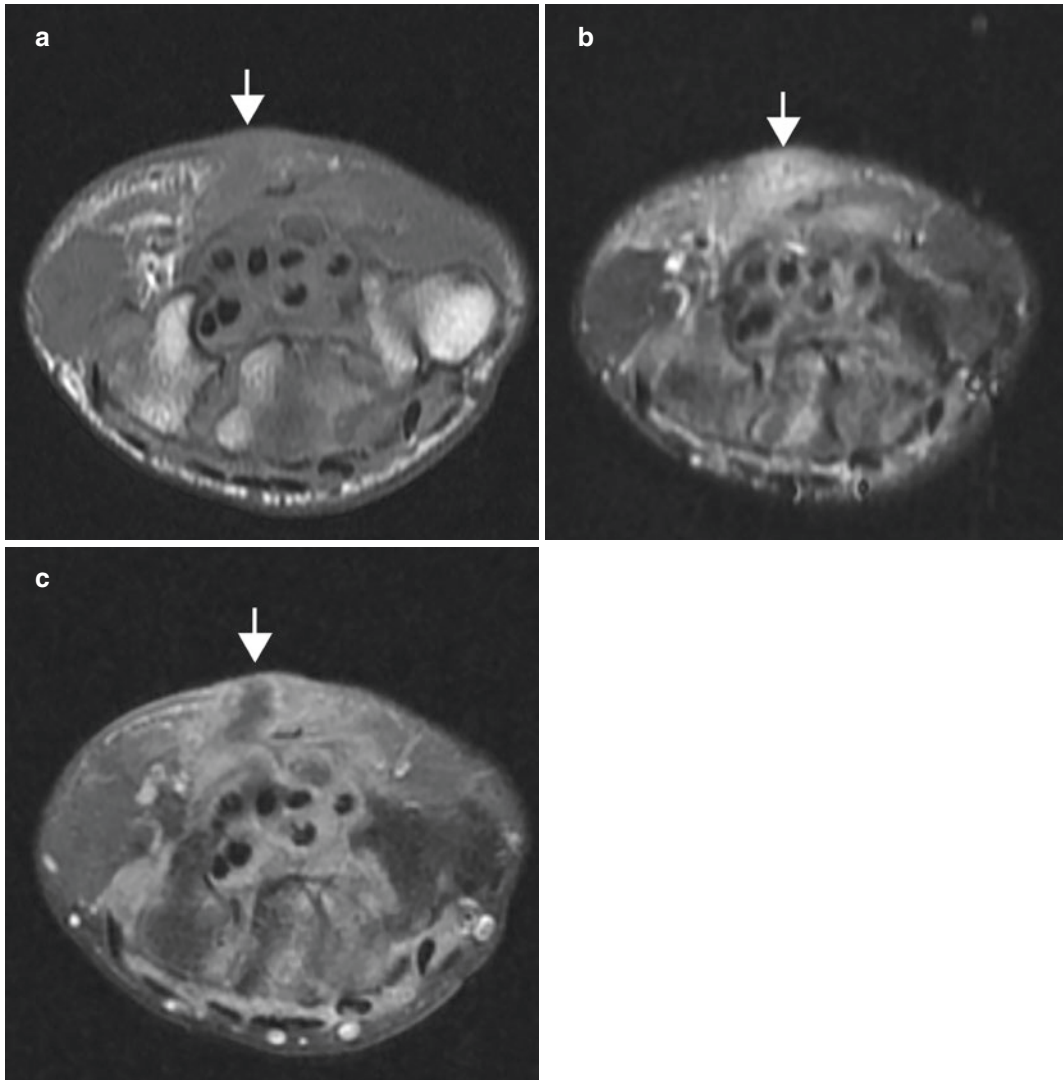

Fig. 22 Tuberculous arthritis and tenosynovitis with a sinus tract in a 41-year-old man who had wrist pain and a draining sinus for 6 months. Axial (**a**) T1-weighted, (**b**) STIR, and (**c**) contrast-enhanced fat-suppressed T1-weighted MR images show bone marrow signal abnormality in the carpal bones, synovitis in the flexor tendon sheath, and a "tram-track" sinus tract (arrows)

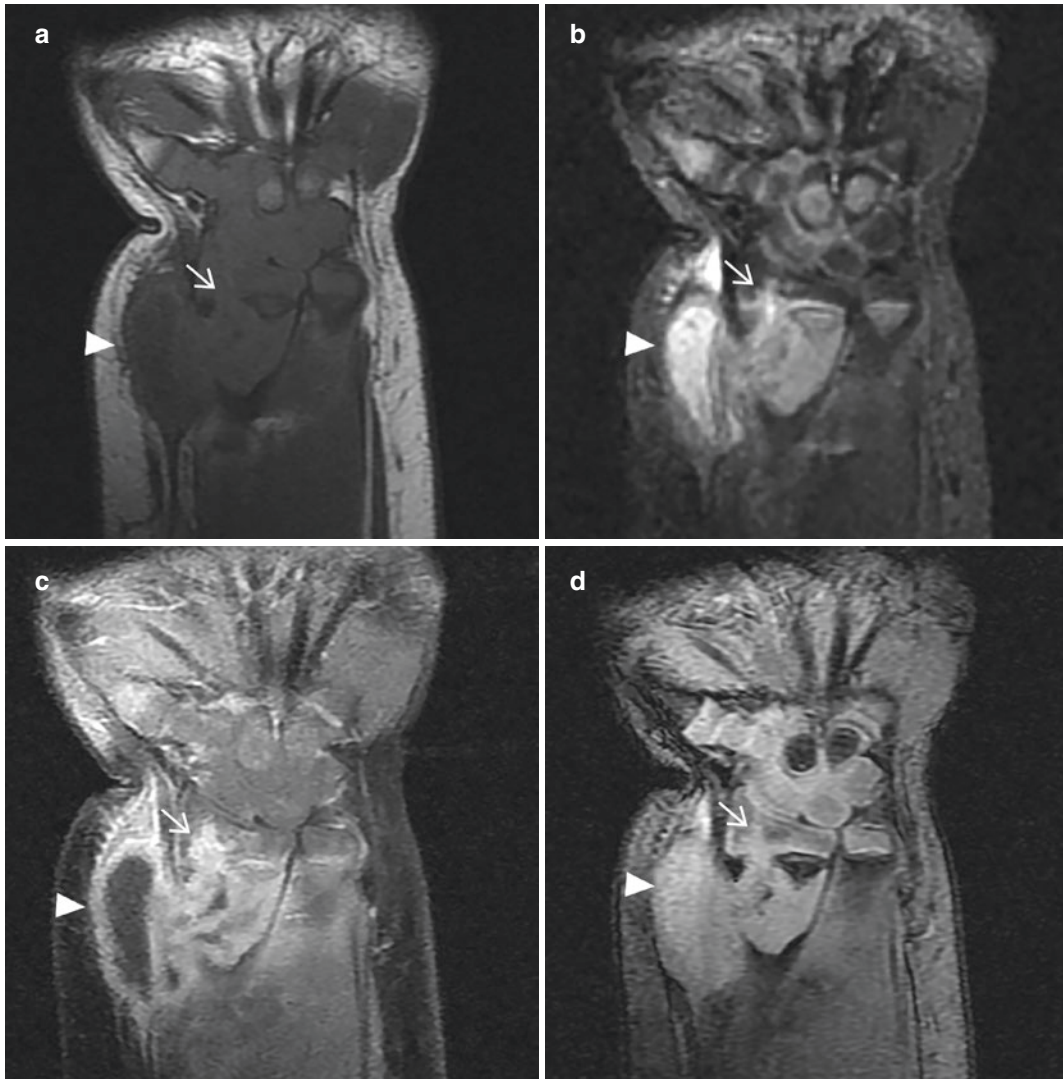

Fig. 23 Tuberculous osteomyelitis with transphyseal spread in a 1-year-old girl who had wrist pain and swelling for 1 month. Coronal (**a**) T1-weighted, (**b**) STIR, (**c**) contrast-enhanced fat-suppressed T1-weighted, and (**d**) 3D spoiled gradient-recalled (SPGR) MR images show osteomyelitis in the metaphysis of the radius with transphyseal spread into the unossified epiphysis (arrows). Note extension to form an adjacent soft tissue abscess with the penumbra sign (arrowheads)

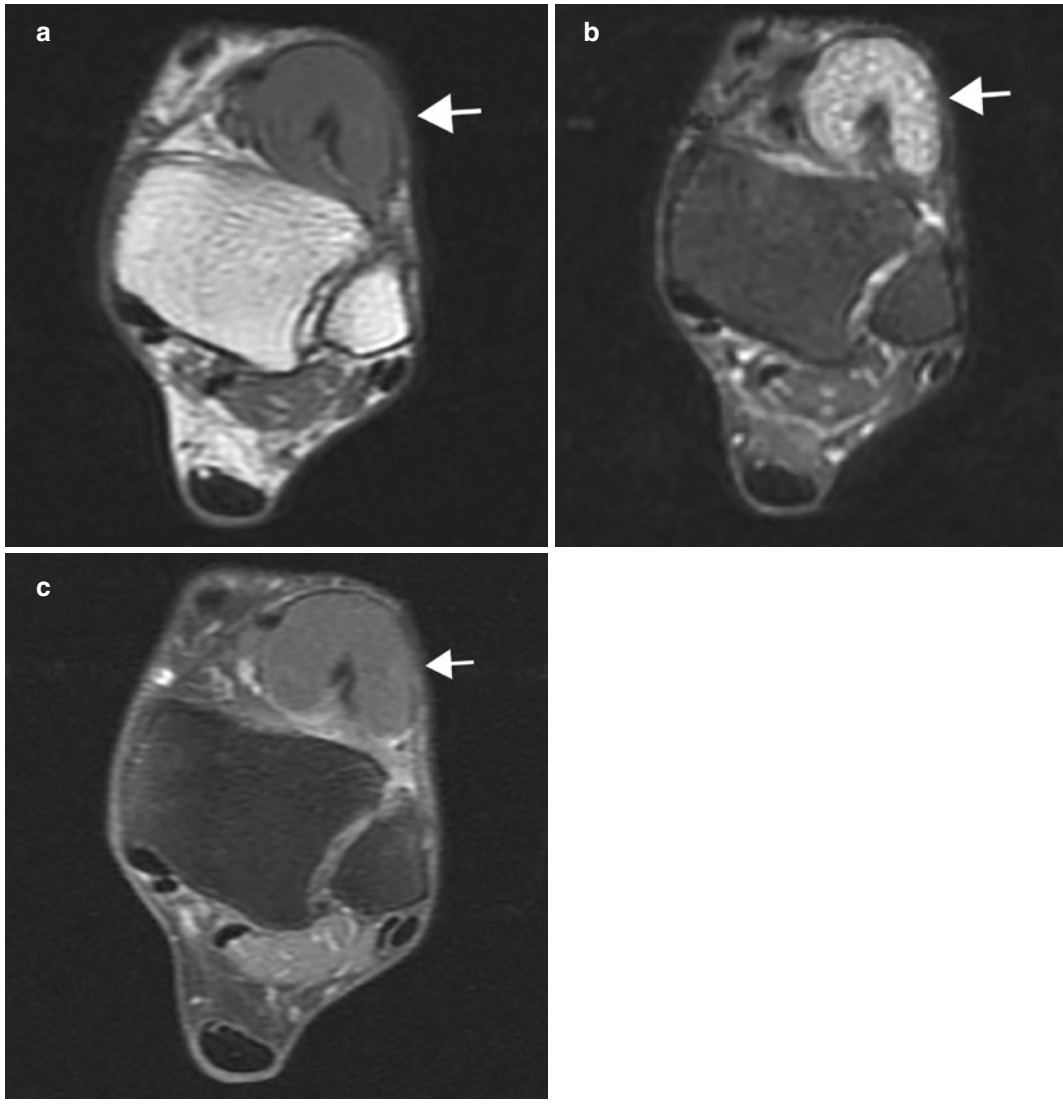

Fig. 24 Tuberculous tenosynovitis with rice bodies in a 70-year-old woman who had a soft tissue mass at the ankle for 1 year. Axial (**a**) T1-weighted, (**b**) T2-weighted, and (**c**) contrast-enhanced fat-suppressed T1-weighted MR images show T2-hypointense rice bodies in the extensor digitorum tendon sheath (arrows). Note the rice bodies are imperceptible on the T1-weighted image and do not enhance

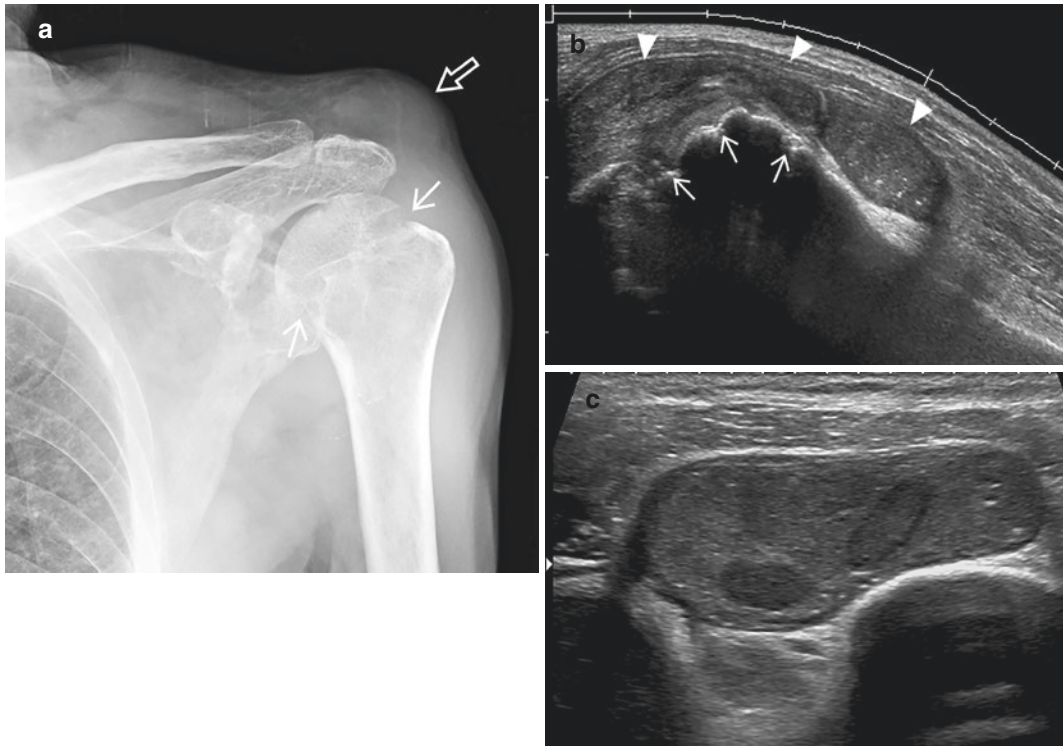

Fig. 25 Tuberculous arthritis of the left shoulder with subdeltoid bursitis in a 68-year-old man who had left shoulder pain for 10 months. (**a**) Frontal radiograph shows bone erosions (arrows) in the humeral head and soft tissue swelling (open arrow) superior to the shoulder joint. (**b**) Longitudinal US image shows erosions in the humeral head (arrows) with echogenic effusion in the subdeltoid bursa (arrowheads). (**c**) Transverse US image of the shoulder shows rice bodies in the echogenic joint fluid within the subdeltoid bursa

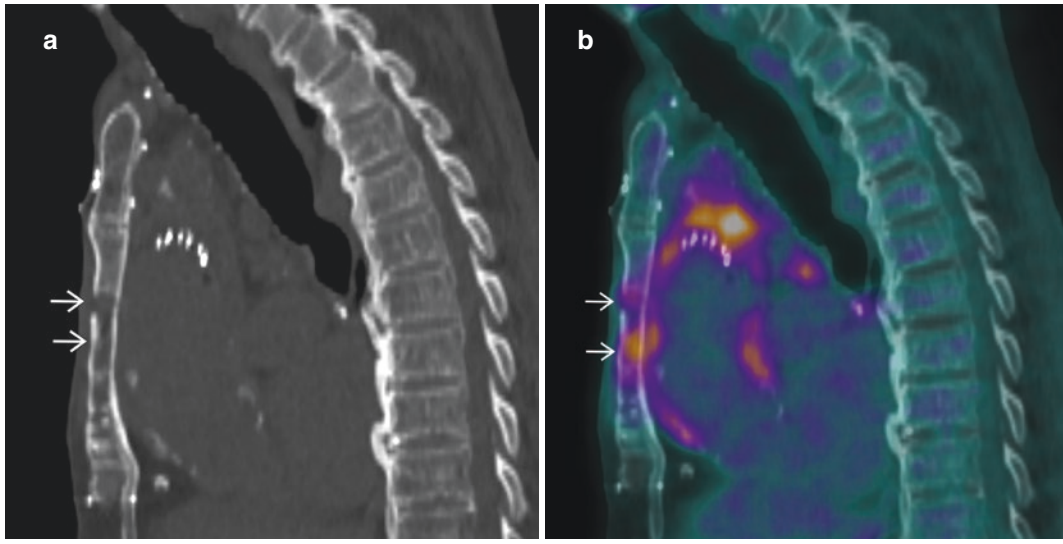

Fig. 26 ^{18}F-FDG PET/CT of tuberculous osteomyelitis. 83-year-old man with thoracic aortic dissection who had prolonged fever after thoracic aortic stent-graft placement. Sagittal (**a**) CT and (**b**) PET/CT fusion images show an intense metabolic-active destructive osteolytic lesion in the sternum (arrows). Biopsy revealed caseating granulomatous inflammation. (Courtesy of Dr. Tawika Kaewchur, Faculty of Medicine, Chiang Mai University, Thailand)

5 Imaging Differential Diagnosis

5.1 Tuberculous Osteomyelitis

Intraosseous abscesses cause well-defined osteolytic lesions mimicking tumor or tumor-like conditions such as simple bone cyst, aneurysmal bone cyst, chondroblastoma, or intraosseous tophi. Multifocal tuberculous osteomyelitis shares similar imaging features with eosinophilic granuloma, bone metastases, and multiple myeloma. The differential diagnosis of tuberculous dactylitis includes other conditions affecting short tubular bones such as vaso-occlusive insult of sickle cell disease, eosinophilic granuloma, and enchondroma (Ejindu et al. 2007; Ranjan et al. 2019). Tuberculous osteomyelitis of the femoral capital epiphysis in children can cause flattening and sclerotic changes, with an imaging appearance similar to Perthes disease (Agarwal 2020) (Fig. 5c). Presence of abscess formation, penumbra sign, and track-like transphyseal spread help in distinguishing abscesses from other conditions.

5.2 Tuberculous Arthritis

The clinical and radiological appearances of pyogenic arthritis and inflammatory arthritis share some similar features with tuberculous arthritis. Bone erosions, subchondral bone marrow edema, and inflammatory changes of the surrounding soft tissues due to pyogenic arthritis are more prominent than those of TB. The abscess walls in TB tend to be smooth and thin, while they are typically irregular and thick in pyogenic arthritis (Hong et al. 2001). Although rare, coexistent TB and pyogenic arthritis have been reported (Dojode et al. 2018). The main presumptive imaging signs of tuberculous arthritis are summarized in Table 1.

Rheumatoid arthritis typically presents as a symmetrical polyarticular disease. However, the disease may initially manifest as a monoarticular involvement and persist in that stage for a long time. Both rheumatoid and tuberculous arthritis can cause juxta-articular osteoporosis and heterogeneous T2-hypointense synovitis. Synovitis related to rheumatoid arthritis tends to be uneven and thick, while tuberculous synovitis is smooth and thin. Large bone erosions and para-articular abscesses favor tuberculosis (Choi et al. 2009).

Table 1 Presumptive imaging signs of tuberculous arthritis

Subchondral bone	Osteopenia Mild bone sclerosis Large bone erosions containing sequestra Mild bone edema (on MRI)
Joint space	Slow and progressive narrowing Prominent synovial thickening Synovial calcifications Different age of synovitis (on MRI) Mild effusion with T2-hypointense signal (on MRI)
Soft tissues	Smooth wall abscess, with calcifications of the abscess wall

The destruction pattern of TB in the foot may mimic neuropathic joint disease. Tuberculous arthritis, particularly in the interconnected joints of midfoot, has potential for widespread destruction, similar to the pattern seen in neuropathic joint disease. In contrast to neuropathic joint, severe osteoporosis is the hallmark of tuberculous arthritis during the active stage (Dhillon and Nagi 2002). The presence of para-articular abscesses and draining sinus leads to the diagnosis of infectious arthritis (Zacharia et al. 2003) (Fig. 27).

On MRI, synovial chondromatosis manifests as intra-articular loose bodies with hypointense signal on T2-weighted images, similar to that of rice bodies. However, on T1-weighted images, the signal intensity of synovial chondromatosis loose bodies is hyperintense, while that of rice bodies of TB are almost imperceptible (Chen et al. 2002) (Fig. 28).

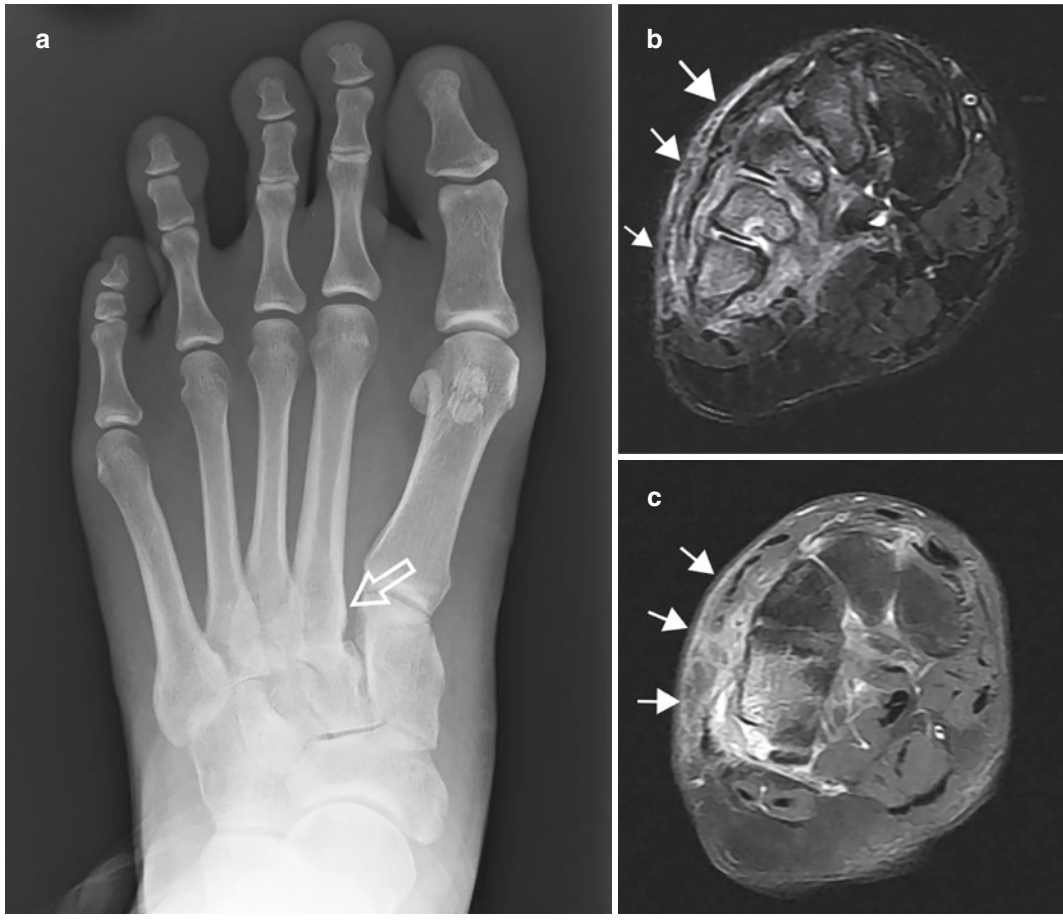

Fig. 27 Tuberculous arthritis in a 33-year-old woman who had left foot pain and a draining sinus in the dorsal foot for 1 month. (**a**) Frontal radiograph shows narrowing of the joint spaces of the midfoot and Lisfranc joint subluxation (open arrow), resembling a neuropathic joint. Coronal (**b**) fat-suppressed T2-weighted and (**c**) contrast-enhanced fat-suppressed T1-weighted MR images show extensive bone marrow edema and enhancement of the midfoot bones. Note the inflammation of the dorsal subcutaneous soft tissues (arrows) corresponding to the location of the sinus tract

5.3 Tuberculous Soft Tissue Infection

Tuberculous myositis and bursitis can present as a slow-growing mass that clinically simulates a tumor (Batra et al. 2007). Infection tends to spread along the low resistant space under the fascia (Soler et al. 2001). CT, MRI, and US imaging allow detection of the abscess and evaluation of the extent of disease. The calcification of granulomatous tissue at the wall of abscesses is characteristic of TB, but can also be a feature of other chronic bacterial infections (Coppola et al. 1987; Pattamapaspong and Muttarak 2011). Tuberculous abscesses of the anterior chest wall can be clinically confused with breast masses (Chung et al. 1996; Arslan et al. 1999; Jain et al. 2009; Teo et al. 2009) (Fig. 20). CT and MRI help confirm the precise location of the disease.

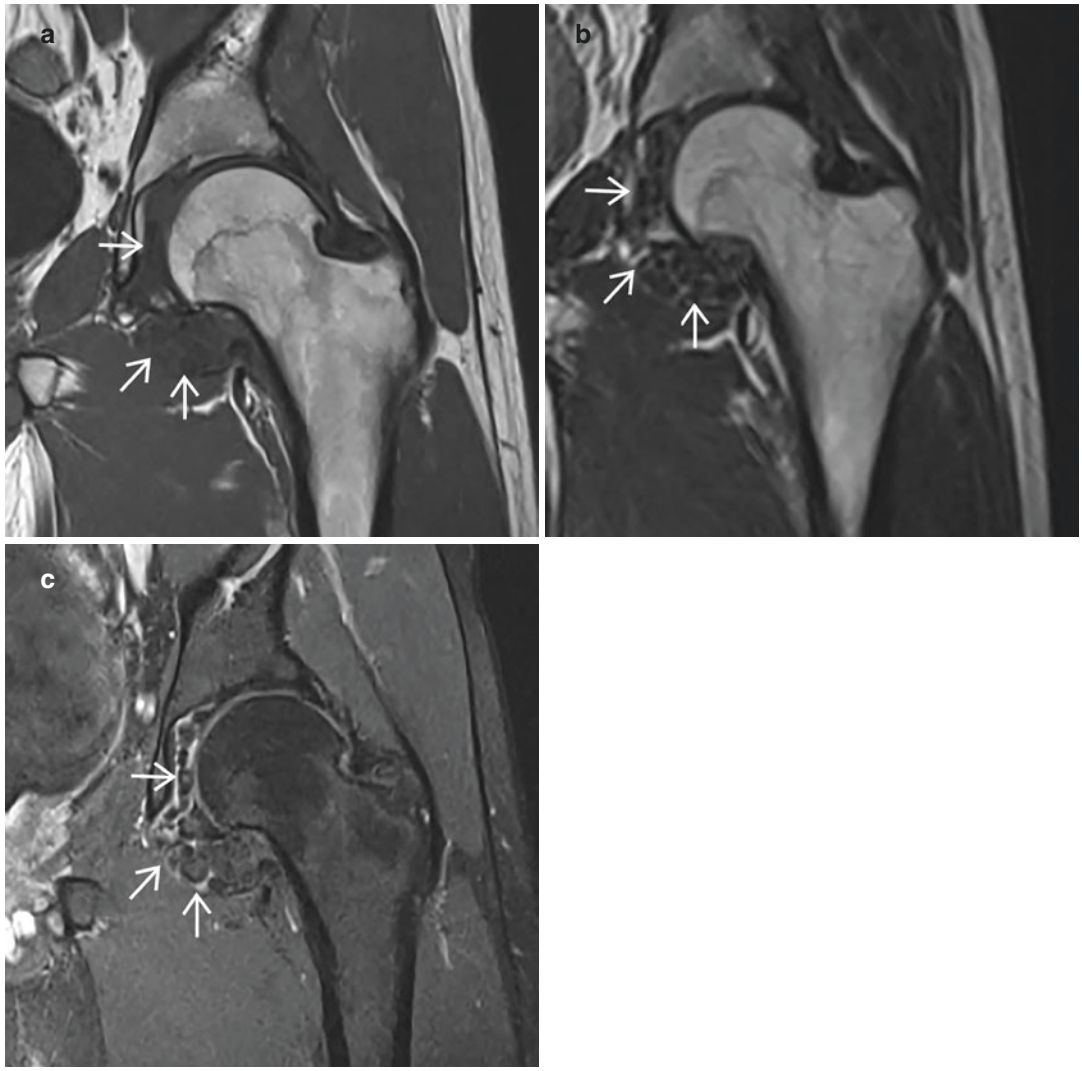

Fig. 28 Synovial chondromatosis. Coronal (**a**) T1-weighted, (**b**) T2-weighted, and (**c**) contrast-enhanced fat-suppressed T1-weighted MR images of the left hip show osteochondral bodies which show faintly T1-hyperintense signal, T2-hypointense signal and do not enhance (arrows)

6 Diagnosis Confirmation

The definite diagnosis of musculoskeletal TB requires positive culture or smear microscopy from pus or infected tissue. However, smear microscopy has a low sensitivity (less than 40%), causing difficulty in diagnosis (Natarajan et al. 2020). Culture may yield 80% sensitivity but takes 6–8 weeks, resulting in a delay of treatment and potential further structural damages (Gardam and Lim 2005). Molecular methods examining for the presence of *M. tuberculosis*-specific DNA in biopsy and cytology specimens provide timely reliable diagnostic results and early identification of drug-resistant strains (Ghanekar et al. 2019; Natarajan et al. 2020). The histopathological findings of granulomatous and necrotizing inflammatory reaction, although non-specific, help suggest the diagnosis of TB. Infected specimens should be taken from the depth of the infected site to avoid contamination by other

organisms at the sinus tract. In endemic areas or in patients with a risk of exposure to TB, diagnosis that is based on the combination of clinical, imaging, and histopathological findings is practically acceptable (Ghanekar et al. 2019).

7 Treatment

Musculoskeletal TB is typically treated using anti-TB drugs. The optimal treatment duration remains debatable but a 9–12 month course is recommended (Nahid et al. 2016). Surgical intervention aims to facilitate healing, prevent the spread of the infection, and maintain function. If performed, debridement needs to include sinus tracts which may not be possible by the standard incision; thus imaging plays a role in surgical planning (Dhillon et al. 2017). Arthrodesis or arthroplasty may be necessary in order to relieve pain and maintain function. Surgery can provide successful outcome when combined with adequate anti-TB drug treatment (Dhillon et al. 2017; Parsa et al. 2018).

The response to treatment is judged by clinical and radiological improvement. Clinically, fever, night sweats, weight loss, and draining sinuses should resolve. Radiological signs of healing include resolution of abscesses and bone marrow edema, with gradual remineralization of affected bones. No improvement or deterioration of the disease after five months of treatment should raise the concern of treatment failure. Follow-up for at least 2 years after completing the course of treatment is recommended for monitoring of possible disease relapse (World Health Organization and Ministry of Health and Family Welfare, Government of India 2016).

8 Conclusion

Extraspinal musculoskeletal TB has various clinical manifestations and imaging findings, depending on whether the affected sites are the bone, joint, or soft tissues. Imaging studies are valuable tools in lesion detection and achieving an accurate diagnosis, bearing in mind that TB can mimic a number of other musculoskeletal diseases. Although non-specific, certain patterns of structural destruction accompanied by abscesses with minimal inflammatory reaction, soft tissue calcification and sinus tracts are suggestive of TB. When combined with the appropriate clinical context, these characteristic imaging features lead to timely diagnosis and appropriate treatment.

References

Agarwal A (2020) Paediatric osteoarticular tuberculosis: a review. J Clin Orthop Trauma 11:202–207

Akeson WH, Chu CR, Bugbee W (2002) Articular cartilage: morphology, physiology, and function. In: Resnick D (ed) Diagnosis of bone and joint disorders, 4th edn. W.B. Saunders, Philadelphia, pp 793–815

Ankrah AO, Van der Werf TS, De Vries EF et al (2016) PET/CT imaging of Mycobacterium tuberculosis infection. Clin Transl Imaging 4:131–144

Arora VK, Chopra KK (2019) Geriatric TB: Needs focussed attention under RNTCP. Indian J Tuberc 66:516–519

Arslan A, Ciftci E, Yildiz F et al (1999) Multifocal bone tuberculosis presenting as a breast mass: CT and MRI findings. Eur Radiol 9:1117–1119

Batra S, Ab Naell M, Barwick C et al (2007) Tuberculous pyomyositis of the thigh masquerading as malignancy with concomitant tuberculous flexor tenosynovitis and dactylitis of the hand. Singapore Med J 48:1042–1046

Bergeron EJ, Meguid RA, Mitchell JD (2017) Chronic infections of the chest wall. Thorac Surg Clin 27:87–97

Bryan WJ, Doherty JH Jr, Sculco TP (1982) Tuberculosis in a rheumatoid patient. A case report. Clin Orthop Relat Res 171:206–208

Carrega G, Bartolacci V, Burastero G, Finocchio GC, Ronca A, Riccio G (2013) Prosthetic joint infections due to *Mycobacterium tuberculosis*: a report of 5 cases. Int J Surg Case Rep 4:178–181

Chen A, Wong LY, Sheu CY et al (2002) Distinguishing multiple rice body formation in chronic subacromial-subdeltoid bursitis from synovial chondromatosis. Skeletal Radiol 31:119–121

Choi JA, Koh SH, Hong SH et al (2009) Rheumatoid arthritis and tuberculous arthritis: differentiating MRI features. AJR Am J Roentgenol 193:1347–1353

Chung SY, Yang I, Bae SH et al (1996) Tuberculous abscess in retromammary region: CT findings. J Comput Assist Tomogr 20:766–769

Coppola J, Muller NL, Connell DG (1987) Computed tomography of musculoskeletal tuberculosis. Can Assoc Radiol J 38:199–203

De Backer AI, Mortele KJ, Vanhoenacker FM et al (2006) Imaging of extraspinal musculoskeletal tuberculosis. Eur Radiol 57:119–130

De Vuyst D, Vanhoenacker F, Gielen J et al (2003) Imaging features of musculoskeletal tuberculosis. Eur Radiol 13:1809–1819

Dhillon MS, Agashe V, Patil SD (2017) Role of surgery in management of osteo-articular tuberculosis of the foot and ankle. Open Orthop J 11:633–650

Dhillon MS, Nagi ON (2002) Tuberculosis of the foot and ankle. Clin Orthop Relat Res 398:107–113

Dojode CMR, Joseph G, Shah NN (2018) A deceptive presentation of tuberculosis hip as staphylococcal infection, its successful management and literature review. BMJ Case Rep 2018:bcr-2018-224558. https://doi.org/10.1136/bcr-2018-224558

Ejindu VC, Hine AL, Mashayekhi M et al (2007) Musculoskeletal manifestations of sickle cell disease. Radiographics 27:1005–1021

Forse CL, Mucha BL, Santos MLZ, Ongcapin EH (2012) Rice body formation without rheumatic disease or tuberculosis infection: a case report and literature review. Clin Rheumatol 31:1753–1756

Gardam M, Lim S (2005) Mycobacterial osteomyelitis and arthritis. Infect Dis Clin North Am 19:819–830

Ghanekar C, Patel D, Abhyankar M et al (2019) Role of line probe assay in detection of extra-pulmonary tuberculosis: experience from a tertiary care hospital in western Maharashtra. Indian J Tuberc 66:325–330

Gopal K, Raj A, Rajesh MR et al (2007) Sternal tuberculosis after sternotomy for coronary artery bypass surgery: a case report and review of the literature. J Thorac Cardiovasc Surg 133:1365–1366

Grey AC, Davies AM, Mangham DC et al (1998) The 'penumbra sign' on T1-weighted MR imaging in subacute osteomyelitis: frequency, cause and significance. Clin Radiol 53:587–592

Griffith JF, Peh WCG, Evans NS, Smallman LA, Wong RW, Thomas AM (1996) Multiple rice body formation in chronic subacromial/subdeltoid bursitis: MR appearances. Clin Radiol 51:511–514

Harwin SF, Banerjee S, Issa K et al (2013) Tubercular prosthetic knee joint infection. Orthopedics 36:e1464–e1469

Hassanpour SE, Gousheh J (2006) Mycobacterium tuberculosis-induced carpal tunnel syndrome: management and follow-up evaluation. J Hand Surg Am 31:575–579

Hodkinson B, Musenge E, Tikly M (2009) Osteoarticular tuberculosis in patients with systemic lupus erythematosus. QJM 102:321–328

Hong SH, Kim SM, Ahn JM et al (2001) Tuberculous versus pyogenic arthritis: MR imaging evaluation. Radiology 218:848–853

Hortas C, Ferreiro JL, Galdo B et al (1988) Tuberculous arthritis of peripheral joints in patients with previous inflammatory rheumatic disease. Br J Rheumatol 27:65–67

Hsu CY, Lu HC, Shih TT (2004) Tuberculous infection of the wrist: MRI features. AJR Am J Roentgenol 183:623–628

Hugate R Jr, Pellegrini VD Jr (2002) Reactivation of ancient tuberculous arthritis of the hip following total hip arthroplasty: a case report. J Bone Joint Surg Am 84:101–105

Jain S, Shrivastava A, Chandra D (2009) Breast lump, a rare presentation of costochondral junction tuberculosis: a case report. Cases J 2:7039

Jaovisidha S, Chen C, Ryu KN et al (1996) Tuberculous tenosynovitis and bursitis: imaging findings in 21 cases. Radiology 201:507–513

Khater FJ, Samnani IQ, Mehta JB, Moorman JP, Myers JW (2007) Prosthetic joint infection by *Mycobacterium tuberculosis*: an unusual case report with literature review. South Med J 100:66–69

Kumar S, Agarwal A, Arora A (2006) Skeletal tuberculosis following fracture fixation. A report of five cases. J Bone Joint Surg Am 88:1101–1106

Lin JN, Lai CH, Chen YH et al (2009) Risk factors for extra-pulmonary tuberculosis compared to pulmonary tuberculosis. Int J Tuberc Lung Dis 13:620–625

McGuinness B, Wilson N, Doyle AJ (2007) The "penumbra sign" on T1-weighted MRI for differentiating musculoskeletal infection from tumour. Skeletal Radiol 36:417–421

Morris BS, Maheshwari M, Chalwa A (2004) Chest wall tuberculosis: a review of CT appearances. Br J Radiol 77:449–457

Nag HL, Neogi DS, Nataraj AR et al (2009) Tubercular infection after arthroscopic anterior cruciate ligament reconstruction. Arthroscopy 25:131–136

Nahid P, Dorman SE, Alipanah N et al (2016) Official American Thoracic Society/Centers for Disease Control and Prevention/Infectious Diseases Society of America Clinical Practice Guidelines: Treatment of drug-susceptible tuberculosis. Clin Infect Dis 63:e147–e195

Naidoo J, Mahomed N, Moodley H (2017) A systemic review of tuberculosis with HIV coinfection in children. Pediatr Radiol 47:1269–1276

Natarajan A, Beena PM, Devnikar AV et al (2020) A systemic review on tuberculosis. Indian J Tuberc 67:295–311

Palestro CJ, Love C, Miller TT (2006) Infection and musculoskeletal conditions: imaging of musculoskeletal infections. Best Pract Res Clin Rheumatol 20:1197–1218

Parsa A, Mirzaie M, Ebrahimzadeh MH et al (2018) Hip surgery in quiescent or active tubercular hip arthritis: is reactivation risk really a matter. Arch Bone Jt Surg 6:169–175

Pattamapaspong N, Muttarak M (2011) Musculoskeletal melioidosis. Semin Musculoskelet Radiol 15:480–488

Perez-Velez CM, Marais BJ (2012) Tuberculosis in children. N Engl J Med 367:348–361

Phemister DB, Hatcher CH (1933) Correlation of pathological and roentgenological findings in the diagnosis of tuberculous arthritis. AJR Am J Roentgenol 29:736–752

Pigrau-Serrallach C, Rodríguez-Pardo D (2013) Bone and joint tuberculosis. Eur Spine J 22(Suppl. 4):556–566

Popert J (1985) Rice-bodies, synovial debris, and joint lavage. Br J Rheumatol 24:1–2

Prasad A, Manchanda S, Sachdev N et al (2012) Imaging features of pediatric musculoskeletal tuberculosis. Pediatr Radiol 42:1235–1249

Ranjan R, Goel L, Sud A et al (2019) Bilateral tubercular dactylitis: unusual presentation of an usual disease. Indian J Tuberc 66:346–352

Ranson M (2009) Imaging of pediatric musculoskeletal infection. Semin Musculoskelet Radiol 13:277–299

Resnick D (2002a) Osteomyelitis, septic arthritis, and soft tissue infection: mechanisms and situations. In: Resnick D (ed) Diagnosis of bone and joint disorders, 4th edn. W.B. Saunders, Philadelphia, pp 2377–2480

Resnick D (2002b) Osteomyelitis, septic arthritis, and soft tissue infection: organisms. In: Resnick D (ed) Diagnosis of bone and joint disorders, 4th edn. W.B. Saunders, Philadelphia, pp 2510–2624

Sawlani V, Chandra T, Mishra RN et al (2003) MRI features of tuberculosis of peripheral joints. Clin Radiol 58:755–762

Sharma SV, Varma BP, Khanna S (1978) Dystrophic calcification in tubercular lesions of bursae. Acta Orthop Scand 49:445–447

Shikhare SN, Singh DR, Shimpi TR, Peh WCG (2011) Tuberculous osteomyelitis and spondylodiscitis. Semin Musculoskelet Radiol 15:446–458

Soler R, Rodriguez E, Remuinan C et al (2001) MRI of musculoskeletal extraspinal tuberculosis. J Comput Assist Tomogr 25:177–183

Suarez I, Maria Funger S, Jung N et al (2019) Severe disseminated tuberculosis in HIV-negative refugees. Lancet Infect Dis 19:e352–e359

Subramaniam R, Tan JWL, Chau CYP, Lee KT (2012) Subacromial bursitis with giant rice bodies as initial presentation of rheumatoid arthritis. J Clin Rheumatol 18:352–355

Suh JS, Lee JD, Cho JH (1996) MR imaging of tuberculous arthritis: clinical and experimental studies. J Magn Reson Imaging 6:185–189

Teo TH, Ho GH, Chaturverdi A et al (2009) Tuberculosis of the chest wall: unusual presentation as a breast lump. Singapore Med J 50:e97–e99

Tiwari A, Sud A, Mehta S (2007) Multifocal skeletal tuberculosis presenting as multiple bone cysts. Ann Acad Med Singapore 36:1038–1039

Wang MN, Chen WM, Lee KS (1999) Tuberculous osteomyelitis in young children. J Pediatr Orthop 19:151–155

World Health Organization (2021) Global tuberculosis report 2021. World Health Organization, Geneva. Available at: https://www.who.int/teams/global-tuberculosis-programme/tb-reports/global-tuberculosis-report-2021

World Health Organization and Ministry of Health and Family Welfare, Government of India (2016) Index—TB Guidelines. In: Guidelines on extrapulmonary tuberculosis for India. World Health Organization, Geneva. Available at: https://tbcindia.gov.in/showfile.php?lid=3245. Accessed 17 May 2021

Zacharia TT, Shah JR, Patkar D et al (2003) MRI in ankle tuberculosis: review of 14 cases. Australas Radiol 47:11–16

Tuberculosis and Human Immunodeficiency Virus Co-infection

Mohamed Chakroun, Ikbel Kooli, Wafa Marrakchi, Hajer Ben Brahim, Abir Aouam, and Adnene Toumi

Contents

M. Chakroun (✉) · I. Kooli · W. Marrakchi
H. B. Brahim · A. Aouam · A. Toumi
Department of Infectious Diseases, Fattouma Bourguiba Hospital, Monastir, Tunisia

Faculty of Medicine of Monastir, University of Monastir, Monastir, Tunisia
e-mail: chakrounme@gmail.com

Abstract

Tuberculosis (TB) and human immunodeficiency virus (HIV) co-infection is frequent in many countries. People living with HIV are 15–22 times more likely to develop active TB than people without HIV. Active TB disease can develop after recent exposure to *Mycobacterium tuberculosis* (primary disease) or with reactivation of latent infection. TB screening must be done in all people living with HIV before starting isoniazid prophylaxis therapy. Diagnosis is difficult because tests are often negative. Sputum smear and culture are the gold standard but have low sensitivity. Interferon-gamma release assay is very helpful because if it is negative, it eliminates TB. Radiological examinations are good tools to help in the diagnosis. Among people living with HIV, chest radiographical signs vary according to the CD4 count: a classical presentation of upper lobe cavitations occurs if CD4 exceeds 350 cells/mm^3 and may be normal in patients with a CD4 count below 200 cells/mm^3. Anti-TB treatment should be given to adults living with HIV, regardless of their CD4 cell count and whether they are or not on antiviral therapy.

© The Author(s), under exclusive license to Springer Nature Switzerland AG 2022

M. F. Ladeb, W. C. G. Peh (eds.), *Imaging of Tuberculosis*, Medical Radiology Diagnostic Imaging,
https://doi.org/10.1007/978-3-031-07040-2_14

Abbreviations

AIDS	Acquired immunodeficiency syndrome
ART	Anti-retroviral therapy
CD4	Lymphocyte T CD4
CD8	Lymphocyte T CD8
DR-TB	Drug-resistant tuberculosis
EPTB	Extrapulmonary tuberculosis
HIV	Human immunodeficiency virus
INH	Isoniazid
LTBI	Latent TB infection
MDR-TB	Multidrug-resistant tuberculosis
PLHIV	People living with human immunodeficiency virus
TB	Tuberculosis
XDR-TB	Extensively drug-resistant tuberculosis

1 Introduction

Tuberculosis (TB) is a serious disease found mainly in low- and middle-income countries, where it is a challenge in terms of diagnosis and treatment. TB is a communicable disease that is a major cause of ill health, one of the top ten causes of death worldwide and the leading cause of death from a single infectious agent. The human immunodeficiency virus (HIV) epidemic has led to increased TB notification rates as well as increased morbidity and mortality of TB (Mukadi et al. 2001). Moreover, HIV infection has been found to be the most significant risk factor for developing active TB and for TB reactivation in persons with latent TB infection (LTBI) (Styblo 1991). Anti-retroviral therapy (ART) has been proven to reduce mortality in patients with HIV-associated TB (World Health Organization 2019). The World Health Organization (WHO) recommends systematic screening for TB among people living with HIV (PLHIV).

2 Epidemiology of Tuberculosis in People Living with HIV

Globally, approximately 10 million people fell ill with TB in 2020, with around 1.3 million TB deaths among HIV-negative people and an additional 214,000 deaths among HIV-positive people (World Health Organization 2021a). HIV infection increases the TB rates in all countries. TB is still the most common opportunistic infection worldwide (World Health Organization 2021a). The TB-HIV co-infection rate is different according to various subgroups, being higher for vulnerable populations. The prevalence of TB-HIV co-infection is 6% among prisoners and 24% among migrants (Dememew et al. 2020; Semá Baltazar et al. 2020). Furthermore, TB-HIV co-infection is still frequent despite the use of ART (Moore et al. 2007). For people with TB, 56% are men and 8.2% are HIV co-infected (World Health Organization 2021b).

Recently, the WHO has recommended starting ART for all PLHIV who are co-infected with TB as soon as possible, within 2 weeks of initiating TB treatment, regardless of CD4 count (World Health Organization 2021b). HIV co-infection with multidrug/extensively drug-resistant TB (MDR/XDR-TB) is a potential threat with challenging management. HIV is responsible for all forms of MDR/XDR-TB epidemics (World Health Organization 2008). The treatment success rates are different in different countries. Overall, the treatment success rate for PLHIV co-infection with TB is 76%, and the proportion of HIV-positive patients with TB who die during TB treatment is 11% (Izudi et al. 2019).

3 Clinical Issues in the Care of People with HIV-TB Co-infection

The four symptoms (recurrent cough, night sweats, weight loss, fever) in the screening tool integrated in the WHO guidelines for intensified

TB case finding have poor specificity and suboptimal sensitivity. Subclinical TB among HIV-infected people is frequent (Oni et al. 2011). Cases of subclinical TB present with an intermediate degree of immunosuppression, as reflected by a median CD4 of more than 200/mm^3 (Bajema et al. 2019).

3.1 Latent Tuberculosis Infection

LTBI is defined as a state of persistent immune response to stimulation by *Mycobacterium tuberculosis* antigens without evidence of clinically manifested TB. The vast majority of infected people have no signs or symptoms of TB (Ilievska-Poposka et al. 2018). The WHO and the United States Department of Health and Human Services recommend screening all PLHIV for LTBI at the time of HIV diagnosis, regardless of their epidemiological risk factors or TB exposure history. The two currently available methods for diagnosis of LTBI are the tuberculin skin test (TST) and interferon-gamma release assay (IGRA) (Bares and Swindells 2020).

3.2 Active Tuberculosis

3.2.1 Pulmonary Tuberculosis

PLHIV are 15–22 times more likely to develop active TB than people without HIV, and active TB disease can develop after recent exposure to *M. tuberculosis* (primary disease) or with reactivation of latent infection (Bares and Swindells 2020). The increased risk of active TB begins in the first year after HIV infection and rises with progressive immunodeficiency (Sonnenberg et al. 2005). In fact, TB can occur at any stage of HIV disease, and its manifestations depend largely on the level of immunosuppression (Wondimeneh et al. 2012). In patients with relatively intact immune function (CD4 cell count >200/mm^3), pulmonary TB is more frequently seen than extrapulmonary TB (EPTB) (Zumla et al. 2000). During early HIV disease, symptoms and signs are similar to those in HIV-uninfected people. The lungs are most commonly affected, with cough, fever, and respiratory signs along with chest radiographical lesions, often with cavitations (Swaminathan et al. 2010).

3.2.2 Extrapulmonary Tuberculosis

HIV infection and immunological status of the patient are determinant factors in clinical features and outcome of TB disease. Multiple studies have suggested that among PLHIV, EPTB is more frequent than localized pulmonary TB in patients with CD4 cell count <100/mm^3 (Leeds et al. 2012). This same level of CD4 cell count is also retained as an independent associated risk factor for severe EPTB (Leeds et al. 2012; Denkinger et al. 2014). To explain the association between low CD4 cell count and occurrence of EPTB and severe involvement, Leeds et al. (2012) have suggested that severe immunodeficiency status is associated with the decrease of T lymphocyte activation and interferon-gamma production, which increases the risk of TB reactivation. Among all TB cases in PLHIV, 25% are EPTB and lymph nodes are the most frequent site (Denkinger et al. 2014).

4 Diagnosis

Many tools can be used in the diagnosis of TB-HIV co-infection. TB screening is very important among PLHIV in order to start isoniazid prophylaxis therapy (IPT) or TB treatment, and to reduce mortality. Several tools may be used, such as molecular tests and IGRA among others.

4.1 Latent Tuberculosis Infection

The available tests for the diagnosis of LTBI have limitations that pose great challenges for both the diagnosis and treatment of these patients (Klautau and Kuschnaroff 2005). The main diagnostic criteria for active TB are microbiological, i.e., presence of sputum with positive direct bacilli smear

and culture, or pathological examination showing caseating granulomas, and acid-fast bacilli (AFB) in tissue specimens. ART initiation constitutes the best timing for the screening and treatment of LTBI.

4.1.1 Tuberculin Skin Test

TST is performed with intradermal administration of 0.1 ml purified protein derivative. The WHO concludes that TST may be inadequate for diagnosing LTBI in immunocompromised individuals due to HIV infection (World Health Organization 2021b). The chronic state of immunosuppression in PLHIV may lead to false-negative TST results. That is the reason why the CDC recommends retesting PLHIV when the CD4 count is more than 200/mm^3.

4.1.2 Interferon-Gamma Release Assay

IGRA is a blood test which evaluates the production of interferon-gamma by lymphocytes after stimulation by specific antigens of *M. tuberculosis*. IGRA is a sensitive test when screening PLHIV for LTBI. A negative IGRA test in PLHIV strongly excludes LTBI. In contrast, those with positive IGRA are more likely to have LTBI (Klautau et al. 2018).

4.2 Active Tuberculosis

4.2.1 Chest Radiography

The WHO still considers chest radiographs to be an important modality in the diagnosis of TB. However, this exam has low specificity and may be associated with overdiagnosis of TB, resulting in unnecessary TB treatment (Cudahy et al. 2017). Chest radiographs remain a useful adjuvant test in smear-negative pulmonary TB to guide further patient management in high TB-HIV prevalence settings. But it has low specificity in the diagnosis of culture-confirmed TB-HIV-co-infected individuals (Davis et al. 2010). Tiamiyu et al. (2020) noted that chest radiographs were reported as typical of TB in only 24 (16%) of patients, while the rest (126, 84%) were reported as atypical. This makes diagnosis of TB even more challenging to clinicians. This poor performance may be attributed to the non-specific chest radiographical patterns and difficulty in interpretation (Jaeger et al. 2013). Other HIV-related pulmonary diseases (e.g., *Pneumocystis carinii* pneumonia, bacterial pneumonia) may complicate chest radiographical interpretation in PLHIV with co-infection (Kanaya et al. 2001). Computed tomography (CT) may suggest the diagnosis and evaluate the disease extent.

Among PLHIV, chest radiographical signs vary according to the CD4 count (Kouassi et al. 2013). When this level exceeds 350 cells/mm^3, TB has a classical presentation with the occurrence of upper lobar cavitations. However, radiographs may be normal in patients with a CD4 count below 200 cells/mm^3, explaining the absence of AFB in the sputum (Hadadi et al. 2011). Apical location involvement is less frequent than in immunocompetent patients. Mediastinal lymph node enlargement, hematogenous dissemination, and extrapulmonary involvement are more frequent in immunosuppressed patients (Kouassi et al. 2013). This can be explained by the low level of immunosuppression (CD4 cell count <200/mm^3) (Grover et al. 2020). Kouassi et al. (2013) showed that pulmonary cavitation (59.3%), infiltrates (38.7%), and location of the lesions at the lung apex (72%) are more common in patients with relatively intact immune function (CD4 cell count >350/mm^3). In contrast, mediastinal lymphadenopathy, pleural effusion, and normal chest radiographs (9.3%) are more common in PLHIV with CD4 cell count <200/mm^3. The scarcity of cavitation (22.3% compared to 59.3% in PLHIV with CD4 cell count >350/mm^3) and the increase in associated lesions become more marked if patients are immunocompromised (Kouassi et al. 2013). Like the infiltrates, cavitating lesions are more often bilateral, and this suggests that more than one lobe is involved in most of the cases. Therefore, a diffuse pattern in the chest radiograph of a patient with known pulmonary TB should alert the physician to the possi-

bility of concurrent HIV infection and would probably harden the differential diagnosis with regard to other opportunistic infections (Hadadi et al. 2011).

Miliary TB and pleural effusion can occur in patients with severe immunosuppression. Miliary dissemination occurs in 10% of PLHIV (Esteve et al. 2010). Pleural effusion occurs in 10–23.2% of cases, and can present on its own or bilaterally (Hadadi et al. 2011; Kouassi et al. 2013). Lymphadenopathies have also been reported as an unusual mode of presentation of pulmonary TB in PLHIV and have been found in 12.5% of cases (Hadadi et al. 2011). Worsening of pulmonary lesions can occur within 60 days after ART, which is associated with the immune reconstitution inflammatory syndrome observed when the CD4 level is less than 50 cells/mm^3 (Müller et al. 2010).

4.2.2 Computed Tomography

Computed tomography (CT) is not routinely performed in pulmonary TB. It may be indicated in a number of clinical situations, such as discrepancy between symptoms and chest radiographical findings or in paucibacillary TB with smear-negative sputum. Moreover, CT can be performed to evaluate the extent of fibrotic lesions and to assess complications as well as associated diseases such as lymphoma, sarcoidosis, aspergillosis, and lung cancer (Hantous-Zannad et al. 2015). For pulmonary TB, CT of the thorax has a sensitivity of 100% and a positive predictive value of 86.4% (He et al. 2017).

4.2.3 Positron-Emission Tomography

[Fluorine-18]-fluoro-2-deoxy-glucose positron-emission tomography/CT (^{18}F-FDG PET/CT) identifies areas of active inflammation by mapping where cells with high metabolic demand take up the radioactively labeled glucose analogue (FDG). For people recently infected with TB, there is increased FDG uptake in the lungs and lymph nodes (Geadas et al. 2018). Among HIV-co-infected individuals with LTBI, lung abnormalities on ^{18}F-FDG PET may be observed. Therefore, ^{18}F-FDG PET allows early diagnosis of TB (Sathekge et al. 2013). In rare cases of HIV-TB co-infection, ^{18}F-FDG PET cannot differentiate TB from malignancy or any other infectious process and cannot avoid the need for biopsy or thoracotomy (Geadas et al. 2018). Moreover, ^{18}F-FDG PET can be used to evaluate TB treatment response in ART (Sathekge et al. 2011). Goyal et al. (2021) found that in addition to diagnosis, ^{18}F-FDG PET/CT is an excellent tool in estimating the total disease burden, assessing response to ART and identification of the treatment endpoint (Goyal et al. 2021).

4.2.4 Sputum Smear and Culture

Smear microscopy is a point-of-care measure of bacillary burden in patients with TB. The bacillary burden of TB in sputum is a key marker of transmission risk and disease severity. Until recently, smear microscopy has been the mainstay of rapid TB diagnosis but lacks sensitivity, particularly in PLHIV (Bark et al. 2011). Culture remains the gold standard for diagnosis of TB, but its sensitivity is lower among PLHIV compared to HIV-negative individuals. Sputum is rarely positive when patients are co-infected with HIV and TB, as this may be secondary to the low bacillary load in sputum from HIV-infected patients (Zürcher et al. 2019). However, nucleic acid amplification test (NAAT) in sputum has demonstrated superior performance with 97% accuracy (Feliciano et al. 2019).

4.2.5 Nucleic Acid Amplification Test

The sensitivity of NAAT for TB diagnosis in PLHIV is comparable to that in the general population (Chang et al. 2012). NAAT can replace smear culture as the initial diagnostic test for TB. NAAT in sputum has demonstrated superior performance with 97% accuracy (Feliciano et al. 2019). However, it is less sensitive in PLHIV than in HIV-negative patients. GeneXpert *Mycobacterium tuberculosis*/rifampicin (Xpert MTB/RIF) is one of the NAATs used in several countries. Many studies provide evidence of the

much-improved performance of the Xpert MTB/RIF test compared to smear microscopy. In addition, the Xpert MTB/RIF test can detect mutations in the rpoB gene, which occurs in 95–99% of RIF-resistant isolates, and it is considered a good indicator for MDR-TB (Ling et al. 2008).

5 Treatment

5.1 LTBI Treatment

PLHIV with LTBI are more likely to develop active TB. Thus, it is recommended to treat LTBI among PLHIV, as part of their care; after excluding active TB. LTBI treatment reduces the overall risk for TB in PLHIV with positive TST by 64% (World Health Organization 2018).

5.1.1 Adults

LTBI treatment should be given to adults living with HIV, regardless of their CD4 cell count and whether they are or not on ART (Lee et al. 2013). Isoniazid (INH) monotherapy, given at the dosage of 5 mg/kg of body weight for 6 months, is the standard regimen to treat LTBI in PLHIV. Pyridoxine is coadministrated at a dosage of 25–50 mg per day, to prevent peripheral neuropathy (Lee et al. 2013; World Health Organization 2018). Recently, shorter regimens based on rifampicin alone or INH + rifampicin or INH + rifapentine have also been proposed (World Health Organization 2018).

5.1.2 Pregnant Women

Because of the high risk of TB reactivation in pregnancy and the post-partum period, pregnant women living with HIV should be treated for LTBI. The use of INH is preferred. However, INH side effects and hepatotoxicity are more frequent in pregnancy. Thus, close monitoring of liver function is necessary. Rifampicin-based regimens are not recommended because of limited information about the safety of rifampicin in pregnancy (Malhamé et al. 2016; Miele et al. 2020).

5.1.3 Children

LTBI treatment should be considered for all children living with HIV aged more than 12 months and living in countries with either high or low TB incidence. Daily INH is recommended for 6 months. Short-course treatment based on rifampicin-INH or rifapentine-INH is also possible (Harries et al. 2020).

5.1.4 Patients in Contact with Active Cases of Multidrug-Resistant Tuberculosis

There is currently no efficacious treatment of LTBI caused by MDR-TB. INH monotherapy is not effective. Fluoroquinolone monotherapy is possible, according to the drug susceptibility tests. Either pyrazinamide-ethambutol or pyrazinamide-fluoroquinolone should be considered for treating LTBI for patients at risk of MDR-TB. The duration of treatment is six to 12 months (Vernon 2013).

5.2 Active Tuberculosis Treatment

5.2.1 Drug Regimen and Side Effects

The anti-TB drugs used to treat drug-susceptible TB have remained largely unchanged since the HIV epidemic. The current preferred regimen includes a 2-month intensive phase of INH, a rifamycin (rifampin or rifabutin), pyrazinamide, and ethambutol, followed by a 4-month continuation phase of INH plus rifampin or rifabutin. The use of fixed dose combination (FDC) is also recommended for PLHIV to reduce the pill burden (World Health Organization 2018). Fluoroquinolone-containing regimens have also been evaluated to treat TB in PLHIV, and it is possible to substitute ethambutol with moxifloxacin. Treatment interruptions for drug adverse effects are more frequent among PLHIV co-infected with TB. Immune activation secondary to HIV has been associated with impaired INH and pyrazinamide clearance (Vinnard et al. 2017). That would explain why adverse effects are more frequent for PLHIV with TB co-infection.

5.2.2 Drug Combinations and Interactions

ART is recommended for all PLHIV, with or without TB co-infection. In cases of TB co-infection, ART must be started during TB treatment. It is feasible and safe to start ART within 2 weeks of TB treatment initiation, regardless of CD4 cell count. Using efavirenz with rifampicin is safe and does not reduce efavirenz efficacy. The WHO recently recommended that dolutegravir replaces efavirenz as the preferred drug in first-line ART regimen because it is better tolerated and has a higher genetic barrier for resistance (World Health Organization 2019). Because of significant drug-drug interaction between dolutegravir and rifampicin, it is important to double the dose of dolutegravir to 50 mg every 12 h (Dooley et al. 2013). Double dose of raltegravir is an option for ART during simultaneous rifampicin-containing regimen of TB treatment in children (Meyers et al. 2019).

5.2.3 Drug Resistance

XDR-TB-HIV treatment involves complex medication regimens with potential drug-drug interactions and adverse drug reactions (Shean et al. 2013). Improved adherence to ART is associated with improved survival in XDR-TB-HIV patients (O'Donnell et al. 2014).

5.2.4 Duration of Treatment

The WHO recommends that PLHIV with TB co-infection should receive at least the same duration of TB treatment as HIV-negative patients with TB (6 months).

5.2.5 Immune Reconstitution Inflammatory Syndrome

Simultaneous TB treatment and ART use can be associated with the immune reconstitution inflammatory syndrome (IRIS) (Müller et al. 2010). IRIS has been associated with a variety of pathogens, but associated TB-HIV IRIS has been noted in 4–54% of patients starting ART during TB treatment (Bana et al. 2016). Some clinical risk factors are associated with IRIS pathogenesis, such as low baseline CD4 cell count (<50–100 cells/mm^3), short time interval between the beginning of TB treatment and ART, dissemination of TB to extrapulmonary sites, and a high bacterial load (Lai et al. 2015; Meya et al. 2016). IRIS treatment is based on the use of corticosteroids. IRIS affecting the central nervous system or producing acute respiratory distress syndrome can be lethal, if not diagnosed in a timely manner and treated appropriately (Karmakar et al. 2011).

6 Prevention

Without a preventive strategy, more than 30% of PLHIV will develop TB. ART decreases the risk of active TB, including XDR- and MDR-TB (Granich et al. 2010). The most effective strategy of prevention is to diagnose and treat active and latent TB infection as soon as possible. Moreover, the use of isoniazid prophylaxis therapy (IPT) for PLHIV in high-TB-incidence countries is recommended as a preventive strategy. Adults and children living with HIV are susceptible to TB. However, children are at higher risk for active TB than adults. Thus, IPT reduces the risk of TB among children older than 15 years old (Ayieko et al. 2014). For immunocompromised PLHIV, it is recommended to detect TB reinfection which may occur with low CD4 count (Ayele et al. 2015). Despite the use of the *Mycobacterium bovis* bacille Calmette–Guérin (BCG) vaccine, TB is still frequent (Delany et al. 2014). Indeed, the BCG vaccine is more effective in low-TB-incidence countries and is more effective to prevent severe TB in young children (Khoshnood et al. 2018).

7 Outcome

TB-HIV co-infection is a main cause of mortality in PLHIV because of the mutual modification of the evolution of each infection (Duarte et al. 2018). Early diagnosis of both HIV and TB is a key component of favorable outcomes of TB-HIV co-infection (Nliwasa et al. 2018). Mortality remains high in PLHIV with active TB, especially

in high-TB-incidence areas. This co-infection is the principal cause of early and long-term mortality in PLHIV (Pecego et al. 2016). Patients with advanced TB-HIV co-infection have high rates of morbidity and mortality despite the initiation of both ART and TB treatment (Pecego et al. 2016).

The risk factors for unfavorable outcomes and mortality are multiple. Late HIV stage, absence of ART or poor adherence to treatment (Sileshi et al. 2013; Magnabosco et al. 2019; Tola et al. 2019), delayed diagnosis (Tola et al. 2019), nadir CD4 cell count less than 50 cells/mm^3 (Sileshi et al. 2013; Pecego et al. 2016), people older than 60 years of age (Sileshi et al. 2013; Ji et al. 2018; Tola et al. 2019), absence of cotrimoxazole prophylaxis (Sileshi et al. 2013), co-infection with other opportunistic infections (Pecego et al. 2016; Ji et al. 2018), association with other comorbidities, and lower education (Magnabosco et al. 2019) are predictive of early and 6-month mortality. According to Sileshi et al. (2013), smear-positive pulmonary TB and EPTB are associated with a high rate of mortality among TB-HIV patients. Complications with bacterial pneumonia and pulmonary atelectasis are risk factors of unfavorable outcomes among PLHIV with pulmonary TB (Ji et al. 2018). High mortality is also associated with the failure of first-line TB treatment and with DR-TB. The second-line treatment success rate is lower in PLHIV, compared to HIV-negative patients (Chem et al. 2019).

8 Conclusion

HIV-TB co-infection is still common in many countries, particularly among vulnerable populations. HIV infection increases the TB rates, making it the most common opportunistic infection worldwide. TB screening should be offered to all PLHIV. When the diagnosis of TB is ruled out, INH prophylaxis should be provided. All cases of confirmed TB should be promptly treated. Treatment is very efficient and reduces mortality in PLHIV; hence it is very important to make an early diagnosis of HIV-TB co-infection. Although helpful, radiological examinations alone do not confirm the diagnosis of TB infection. Microbiological examination, sputum, and culture are needed for confirmation. The use of NAAT is expanding, as this test can confirm TB diagnosis and detect rifampicin resistance mutations.

References

Ayele HT, van Mourik NSM, Debray TPA et al (2015) Isoniazid prophylactic therapy for the prevention of tuberculosis in HIV infected adults: a systematic review and meta-analysis of randomized trials. PLoS One 10:e0142290

Ayieko J, Abuogi L, Simchowitz B et al (2014) Efficacy of isoniazid prophylactic therapy in prevention of tuberculosis in children: a meta–analysis. BMC Infect Dis 14:91

Bajema KL, Bassett IV, Coleman SM et al (2019) Subclinical tuberculosis among adults with HIV: clinical features and outcomes in a south African cohort. BMC Infect Dis 19:14

Bana TM, Lesosky M, Pepper DJ et al (2016) Prolonged tuberculosis-associated immune reconstitution inflammatory syndrome: characteristics and risk factors. BMC Infect Dis 16:518

Bares SH, Swindells S (2020) Latent tuberculosis and HIV infection. Curr Infect Dis Rep 22:17

Bark CM, Thiel BA, Johnson JL (2011) Pretreatment time to detection of mycobacterium tuberculosis in liquid culture is associated with relapse after therapy. J Clin Microbiol 50:538

Chang K, Lu W, Wang J et al (2012) Rapid and effective diagnosis of tuberculosis and rifampicin resistance with Xpert MTB/RIF assay: a meta-analysis. J Infect 64:580–588

Chem ED, Van Hout MC, Hope V (2019) Treatment outcomes and antiretroviral uptake in multidrug-resistant tuberculosis and HIV co-infected patients in sub Saharan Africa: a systematic review and meta-analysis. BMC Infect Dis 19:723

Cudahy PGT, Dawson R, Allwood BW et al (2017) Diagnostic outcomes after chest radiograph interpretation in patients with suspected tuberculosis and negative sputum smears in a high-burden human immunodeficiency virus and tuberculosis setting. Open Forum Infect Dis 4:ofx123

Davis JL, Worodria W, Kisembo H et al (2010) Clinical and radiographic factors do not accurately diagnose smear-negative tuberculosis in HIV-infected inpatients in Uganda: a cross-sectional study. PLoS One 5:e9859

Delany I, Rappuoli R, De Gregorio E (2014) Vaccines for the 21st century. EMBO Mol Med 6: 708–720

Dememew ZG, Jerene D, Datiko DG et al (2020) The yield of community-based tuberculosis and HIV among key populations in hotspot settings of Ethiopia: a cross-sectional implementation study. PLoS One 15:e0233730

Denkinger CM, Schumacher SG, Boehme CC et al (2014) Xpert MTB/RIF assay for the diagnosis of extrapulmonary tuberculosis: a systematic review and meta-analysis. Eur Respir J 44:435–446

Dooley KE, Sayre P, Borland J et al (2013) Safety, tolerability, and pharmacokinetics of the HIV integrase inhibitor dolutegravir given twice daily with rifampin or once daily with rifabutin: results of a phase 1 study among healthy subjects. J Acquir Immune Defic Syndr 62:21–27

Duarte R, Lönnroth K, Carvalho C et al (2018) Tuberculosis, social determinants and co-morbidities (including HIV). Pulmonology 24: 115–119

Esteve E, Supervía A, Pallàs O et al (2010) Miliary tuberculosis coinfection with human immunodeficiency virus. West J Emerg Med 11:405–407

Feliciano CS, LJB M, Anselmo LMP et al (2019) Xpert MTB/RIF performance to diagnose tuberculosis and rifampicin resistance in a reference centre in southern Brazil. ERJ Open Res 5:00043–02019

Geadas C, Acuna-Villaorduna C, Mercier G et al (2018) FDG-PET/CT activity leads to the diagnosis of unsuspected TB: a retrospective study. BMC Res Notes 11:464

Goyal D, Shriwastav R, Mittal R et al (2021) Role of 18F-FDG PET/CT in the assessment of response to antitubercular chemotherapy and identification of treatment endpoint in patients with tuberculosis of the joints. Clin Nucl Med 46:449–455

Granich R, Akolo C, Gunneberg C et al (2010) Prevention of tuberculosis in people living with HIV. Clin Infect Dis 50:215–S222

Grover S, Chawla G, Parihar HL et al (2020) Human immunodeficiency virus infection amongst newly diagnosed tuberculosis patients and their clinico-radiological profile: a prospective study from Western India. J Family Med Prim Care 9:2475

Hadadi A, Tajik P, Rasoolinejad M et al (2011) Pulmonary tuberculosis in patients with HIV/AIDS in Iran. Iran J Public Health 40:100–106

Hantous-Zannad S, Zidi A, Néji H et al (2015) Apport de l'imagerie dans la tuberculose thoracique. Rev Pneumol Clin 71:93–109

Harries AD, Kumar AMV, Satyanarayana S et al (2020) Treatment for latent tuberculosis infection in low- and middle-income countries: progress and challenges with implementation and scale-up. Expert Rev Respir Med 14:195–208

He W, Chen BD, Lv Y et al (2017) Use of low-dose computed tomography to assess pulmonary tuberculosis among healthcare workers in a tuberculosis hospital. Infect Dis Poverty 6:68

Ilievska-Poposka B, Metodieva M, Zakoska M et al (2018) Latent tuberculosis infection—diagnosis and treatment. Open Access Maced J Med Sci 6:651–655

Izudi J, Semakula D, Sennono R et al (2019) Treatment success rate among adult pulmonary tuberculosis patients in sub-Saharan Africa: a systematic review and meta-analysis. BMJ Open 9:e029400

Jaeger S, Karargyris A, Candemir S et al (2013) Automatic screening for tuberculosis in chest radiographs: a survey. Quant Imaging Med Surg 3:89–99

Ji YJ, Liang PP, Shen JY et al (2018) Risk factors affecting the mortality of HIV-infected patients with pulmonary tuberculosis in the cART era: a retrospective cohort study in China. Infect Dis Poverty 7:25

Kanaya AM, Glidden DV, Chambers HF (2001) Identifying pulmonary tuberculosis in patients with negative sputum smear results. Chest 120:349–355

Karmakar S, Sharma S, Vashishtha R et al (2011) Clinical characteristics of tuberculosis-associated immune reconstitution inflammatory syndrome in north Indian population of HIV/AIDS patients receiving HAART. Clin Dev Immunol 2011:1–9

Khoshnood S, Heidary M, Haeili M et al (2018) Novel vaccine candidates against mycobacterium tuberculosis. Int J Biol Macromol 120:180–188

Klautau GB, Kuschnaroff TM (2005) Clinical forms and outcome of tuberculosis in HIV-infected patients in a tertiary hospital in São Paulo—Brazil. Braz J Infect Dis 9:464–478

Klautau GB, da Mota NVF, Salles MJC et al (2018) Interferon-γ release assay as a sensitive diagnostic tool of latent tuberculosis infection in patients with HIV: a cross-sectional study. BMC Infect Dis 18:585

Kouassi B, N'Gom A, Horo K et al (2013) Correlation of the manifestations of tuberculosis and the degree of immunosuppression in patients with HIV. Rev Mal Respir 30:549–554

Lai RPJ, Meintjes G, Wilkinson KA et al (2015) HIV–tuberculosis-associated immune reconstitution inflammatory syndrome is characterized by toll-like receptor and inflammasome signalling. Nat Commun 6:8451

Lee SS, Meintjes G, Kamarulzaman A, Leung CC (2013) Management of tuberculosis and latent tuberculosis infection in human immunodeficiency virus-infected persons: TB/HIV co-infection. Respirology 18:912–922

Leeds IL, Magee MJ, Kurbatova EV et al (2012) Site of extrapulmonary tuberculosis is associated with HIV infection. Clin Infect Dis 55:75–81

Ling DI, Flores LL, Riley LW et al (2008) Commercial nucleic-acid amplification tests for diagnosis of pulmonary tuberculosis in respiratory specimens: meta-analysis and meta-regression. PLoS One 3:e1536

Magnabosco GT, de Paula Andrade RL, Arakawa T et al (2019) Desfecho dos casos de tuberculose em pessoas com HIV: subsídios para intervenção. Acta Paul Enferm 32:554–563

Malhamé I, Cormier M, Sugarman J et al (2016) Latent tuberculosis in pregnancy: a systematic review. PLoS One 11:e0154825

Meya DB, Manabe YC, Boulware DR et al (2016) The immunopathogenesis of cryptococcal immune reconstitution inflammatory syndrome: understanding a conundrum. Curr Opin Infect Dis 29:10–22

Meyers T, Samson P, Acosta EP et al (2019) Pharmacokinetics and safety of Raltegravir in 2 to 12 year old children with HIV receiving rifampicin for tuberculosis. AIDS 33:2197–2203

Miele K, Bamrah Morris S, Tepper NK (2020) Tuberculosis in pregnancy. Obstet Gynecol 135: 1444–1453

Moore D, Liechty C, Ekwaru P et al (2007) Prevalence, incidence and mortality associated with tuberculosis in HIV-infected patients initiating antiretroviral therapy in rural Uganda. AIDS 21:713–719

Mukadi YD, Maher D, Harries A (2001) Tuberculosis case fatality rates in high HIV prevalence populations in sub-Saharan Africa. AIDS 15:143–152

Müller M, Wandel S, Colebunders R et al (2010) Immune reconstitution inflammatory syndrome in patients starting antiretroviral therapy for HIV infection: a systematic review and meta-analysis. Lancet Infect Dis 10:251–261

Nliwasa M, MacPherson P, Gupta-Wright A et al (2018) High HIV and active tuberculosis prevalence and increased mortality risk in adults with symptoms of TB: a systematic review and meta-analyses. J Int AIDS Soc 21:e25162

O'Donnell M, Wolf A, Werner L et al (2014) Adherence in the treatment of patients with extensively drug-resistant tuberculosis and HIV in South Africa. J Acquir Immune Defic Syndr 67(1):22–29

Oni T, Burke R, Tsekela R et al (2011) High prevalence of subclinical tuberculosis in HIV-1-infected persons without advanced immunodeficiency: implications for TB screening. Thorax 66:669–673

Pecego AC, Amancio RT, Ribeiro C et al (2016) Six-month survival of critically ill patients with HIV-related disease and tuberculosis: a retrospective study. BMC Infect Dis 16:270

Sathekge M, Maes A, Kgomo M et al (2011) Use of 18F-FDG PET to predict response to first-line tuberculostatics in HIV-associated tuberculosis. J Nucl Med 52:880– 885

Sathekge M, Maes A, Wiele C (2013) FDG-PET imaging in HIV infection and tuberculosis. Semin Nucl Med 43:349–366

Semá Baltazar C, DeLima YV, Ricardo H et al (2020) HIV prevalence and TB in migrant miners communities of origin in Gaza Province, Mozambique: the need for increasing awareness and knowledge. PLoS One 15:e0231303

Shean K, Streicher E, Pieterson E et al (2013) Drug-associated adverse events and their relationship with outcomes in patients receiving treatment for extensively drug-resistant tuberculosis in South Africa. PLoS One 8:e63057

Sileshi B, Deyessa N, Girma B et al (2013) Predictors of mortality among TB-HIV co-infected patients being treated for tuberculosis in Northwest Ethiopia: a retrospective cohort study. BMC Infect Dis 13:297

Sonnenberg P, Glynn J, Fielding K et al (2005) How soon after infection with HIV does the risk of tuberculosis start to increase? A retrospective cohort study in South African gold miners. J Infect Dis 191:150–158

Styblo K (1991) The impact of HIV infection on the global epidemiology of tuberculosis. Bull Int Union Tuberc Lung Dis 66:27–32

Swaminathan S, Padmapriyadarsini C, Narendran G (2010) HIV-associated tuberculosis: clinical update. Clin Infect Dis 50:1377–1386

Tiamiyu AB, Iliyasu G, Dayyab F et al (2020) A descriptive study of smear negative pulmonary tuberculosis in a high HIV burden patient's population in north Central Nigeria. PLoS One 15:e0238007

Tola A, Mishore KM, Ayele Y et al (2019) Treatment outcome of tuberculosis and associated factors among TB-HIV co-infected patients at public hospitals of Harar town, eastern Ethiopia. A five-year retrospective study. BMC Public Health 19:1658

Vernon A (2013) Treatment of latent tuberculosis infection. Semin Respir Crit Care Med 34:67–86

Vinnard C, Ravimohan S, Tamuhla N et al (2017) Isoniazid clearance is impaired among human immunodeficiency virus/tuberculosis patients with high levels of immune activation. Br J Clin Pharmacol 83: 801–811

Wondimeneh Y, Muluye D, Belyhun Y (2012) Prevalence of pulmonary tuberculosis and immunological profile of HIV co-infected patients in Northwest Ethiopia. BMC Res Notes 5:331

World Health Organization (2008) Anti-tuberculosis drug resistance in the world: fourth global report: the World Health Organization/International Union Against Tuberculosis and Lung Disease (WHO/UNION) Global Project on Anti-Tuberculosis Drug Resistance Surveillance. World Health Organization. https://www.who.int/tb/publications/2008/drs_report4_26feb08.pdf

World Health Organization (2018) Latent tuberculosis infection: updated and consolidated guidelines for programmatic management. World Health Organization, Geneva. https://apps.who.int/iris/handle/10665/260233

World Health Organization (2019) Updated recommendations on first line and second-line antiretroviral regimens and post-exposure prophylaxis and recommendations on early infant diagnosis of HIV. https://apps.who.int/iris/bitstream/handle/10665/325892/WHO-CDS-HIV-19.15-eng.pdf

World Health Organization (2021a) Global tuberculosis report 2021. World Health Organization, Geneva, p 1. https://www.who.int/teams/global-tuberculosis-programme/tb-reports/global-tuberculosis-report-2021

World Health Organization (2021b). Consolidated guidelines on HIV prevention, testing, treatment, service delivery and monitoring. https://www.who.int/publications/i/item/9789240031593

Zumla A, Malon P, Henderson J et al (2000) Impact of HIV infection on tuberculosis. Postgrad Med J 76: 259–268

Zürcher K, Ballif M, Kiertiburanakul S et al (2019) Diagnosis and clinical outcomes of extrapulmonary tuberculosis in antiretroviral therapy programmes in low- and middle-income countries: a multicohort study. J Int AIDS Soc 22:e25392

Diagnostic Algorithm of Tuberculosis

Guo Yuan How, Kheng Song Leow, Say Tat Ooi, and Wilfred C. G. Peh

Contents

G. Y. How (✉) · W. C. G. Peh
Department of Diagnostic Radiology, Khoo Teck Puat Hospital, Singapore, Republic of Singapore
e-mail: guoyuan.how@mohh.com.sg; wilfred.peh@gmail.com

K. S. Leow
Department of Diagnostic Radiology, Woodlands Health Campus, Singapore, Republic of Singapore
e-mail: leow_kheng_song@whc.sg

S. T. Ooi
Division of Infectious Diseases, Department of General Medicine, Khoo Teck Puat Hospital, Singapore, Republic of Singapore
e-mail: ooi.say.tat@ktph.com.sg

Abstract

Tuberculosis (TB) infection spans across multiple organ systems. Delayed or inappropriate diagnosis and treatment can result in disease spread and development of multidrug-resistant variants. Clinicians can utilize a host of serological, radiological, microbiological, and histopathological tools to diagnose TB. Using a diagnostic algorithm allows for a systematic approach to diagnosing and managing patients with TB.

Abbreviations

AFB	Acid-fast bacilli
CT	Computed tomography
MRI	Magnetic resonance imaging
TB	Tuberculosis

1 Introduction

Tuberculosis (TB) has been recognized as an infectious disease inflicting the highest number of deaths and one of the top 10 causes of mortality worldwide (World Health Organization 2020a). With approximately 10 million individuals contracting TB in 2020 and more than 1.3 million deaths, reining in this communicable

© The Author(s), under exclusive license to Springer Nature Switzerland AG 2022

M. F. Ladeb, W. C. G. Peh (eds.), *Imaging of Tuberculosis*, Medical Radiology Diagnostic Imaging,
https://doi.org/10.1007/978-3-031-07040-2_15

disease remains a pressing priority (World Health Organization 2021). TB is caused by the *Mycobacterium tuberculosis* complex, which is primarily spread via respiratory droplet nuclei, and by digestive contamination by *M. bovis* in developing countries. Following the initial inoculation, this pathogen infects the lungs and other extrapulmonary sites. Extrapulmonary TB comprises up to 21% of all tuberculous infections (Peto et al. 2009), with 50–70% of cases having concomitant human immunodeficiency virus (HIV) infection (Raviglione et al. 1992; Jones et al. 1993; Haas and Des Prez 1994). Other than by anatomical locations (pulmonary and extrapulmonary), TB can also be broadly classified into active (including primary and reactivation disease) and latent states.

2 Diagnosis of Tuberculosis

The diagnosis of TB and subsequent distinction between active and latent forms of the disease are crucial steps in treating TB. Inappropriate diagnosis of the disease (e.g., initiating treatment for latent TB in patients with active TB) could result in treatment failure and emergence of multidrug-resistant TB. The definitive diagnosis of TB requires isolation of *M. tuberculosis* in a bodily sample (Pai et al. 2016). However, a confirmatory laboratory diagnosis cannot be demonstrated in approximately 15–20% of individuals (Taylor et al. 2000). A presumptive diagnosis known as "clinically diagnosed TB" can be made, and successive treatment can be instituted on this basis (World Health Organization 2020b).

2.1 Risk Factors

Established risk factors for both contraction of TB and risk of progression to active or disseminated TB are intimately intertwined and can be classified into host and environmental factors. Host factors are defined by the inherent characteristics impacting the patient's immunological response to the pathogen, while environmental factors are characterized by the extrinsic circumstances affecting the risk of exposure to TB (Table 1) (Teweldemedhin et al. 2018). Immunosuppression has a profound impact on both the probability of being infected and disease progression. HIV infection is a well-recognized risk factor for TB, with HIV-infected individuals having a 9- to 16-fold increase in the risk of contracting TB (Guelar et al. 1993) and a heightened chance of developing active TB from reactivated latent infection (Selwyn et al. 1989).

Table 1 Risk factors for TB

Host factors
• Immunosuppressed state (e.g., HIV infection, chronic steroid use, diabetes mellitus, chronic renal disease, malnutrition)
• Substance abuse (e.g., intravenous drug user, tobacco use, chronic alcoholism)
• Other systemic conditions (e.g., malignancy, chronic obstructive pulmonary disease)
Environmental factors
• Recent close contact with a person infected with TB
• High-risk environment (e.g., immigrant community, endemic countries, healthcare workers, laboratory staff)

Deficient nutritional status and substance abuse also play crucial roles in new infections. While the relationship between impaired immunity due to malnutrition and risk of being infected is uncertain, a low body mass index of <18.5 (Palmer et al. 1957; Edwards et al. 1971) and iron deficiency (Boelaert et al. 2007) have been found to increase the risk of acquiring TB. Tobacco use has a relative risk of 1.5–2 for developing TB (Bates et al. 2007; Lin et al. 2009; Rao et al. 2014). There is a relative risk of 2.94–3.50 for progression to active TB for patients consuming >40 g of alcohol daily or having an alcohol use disorder (Lonnroth et al. 2008).

Pre-existing comorbidities, especially diabetes mellitus and chronic renal disease, are associated with an increased risk of developing TB, with the risk of developing TB rising proportionately with worsening disease. Diabetes mellitus has been shown to be an independent risk factor for TB, with the approximate risk approaching that of HIV-infected patients in certain popula-

tions (Pablos-Mendez et al. 1997). Patients with chronic renal disease have been found to have an increased risk of developing TB by a factor of 6.9–52.5 (Hussein et al. 2003). Among the environmental factors, close contact with a person who is smear positive for pulmonary TB in the household has been shown to be the most important risk factor for TB (Marks et al. 2000).

2.2 Clinical Presentation

Initial clinical suspicion of pulmonary TB begins with either symptomatic presentation or asymptomatic screening for the disease. Clinical presentation suggestive of pulmonary or extrapulmonary infection, coupled with a history of prior exposure or incidental but suggestive radiological findings, should initiate the appropriate tests for work-up of TB. Clinical manifestations of active pulmonary TB vary among individuals (Poulsen 1957). Common symptoms include prolonged cough of more than 3 weeks, hemoptysis, chest pain, fever, night sweats, and weight loss (Taylor et al. 2005). Asymptomatic screening for TB is considered in selected scenarios, such as close contact with an individual with active TB or immigrants from TB-endemic regions (de Lima Corvino et al. 2021). The 2005 American Thoracic Society guidelines suggest screening for TB in all patients with newly diagnosed HIV infection (Taylor et al. 2005). Physical examination is often non-specific and can be negative in early disease. Characteristic pulmonary findings suggestive of infection may be elicited, such as crepitations due to consolidation or decreased fremitus and breath sounds in pleural effusion.

Extrapulmonary clinical features are highly dependent on the affected organ and exhibit considerable variation, hence the moniker "the great mimicker" for extrapulmonary TB. Patients with tuberculous infection of the central nervous system manifesting as a tuberculoma can present with non-specific neurological symptoms such as headache, fever, and seizures (Weisberg 1984), while classical features of meningism, including neck stiffness, may be evident when the meninges are involved (Rock et al. 2008). Tuberculous involvement of the head and neck may be devoid of a specific pathognomonic sign or appear similar to other inflammatory and infective lesions (Pang et al. 2018).

Patients with peritoneal TB commonly present with ascites, abdominal pain, and fever (Chow et al. 2002). In contrast, patients with gastrointestinal TB can display a multitude of signs and symptoms, depending on the organ in question. Clinical presentations range from abdominal pain, chronic diarrhea, and per rectal bleeding in ulcero-constrictive disease to fever, weight loss, and night sweats due to persistent inflammatory response to intra-abdominal infection. Urogenital TB can be classified broadly into urinary or genital tract disease. Features indicative of a urinary tract infection such as increased urinary frequency, dysuria, gross hematuria, and flank pain are suggestive of urinary tract involvement (Cek et al. 2005; Figueiredo et al. 2017).

Spinal spread of TB in the form of tuberculous spondylitis (also known as Pott disease) commonly manifests as increasing local pain with neurological abnormalities. A characteristic erect stance with "alderman's gait" may also be seen in some patients (Canine et al. 2019). In the musculoskeletal system, TB can cause osteomyelitis, arthritis, or soft tissue infection. Infected patients may present with limb or joint pain, limb deformity, joint dislocation, pathological fracture, palpable mass, or draining skin sinus. Beyond localizing findings, TB has the potential to cause constitutional and non-specific clinical presentations such as weight loss, fever, night sweats, and digital clubbing (Macfarlane et al. 1979).

For people living with HIV (PLHIV), TB can occur at any stage of the disease, and its manifestations depend largely on the level of immunosuppression (Wondimeneh et al. 2012). In patients with a relatively intact immune function, pulmonary TB is more frequently seen than extrapulmonary TB (Zumla et al. 2000). During the early stage of HIV disease, symptoms and signs are similar to those without HIV infection.

2.3 Laboratory Findings

Similar to other infections, routine biochemical investigations constitute part of the initial work-up of TB. While hematological and biochemical serum markers are usually normal in pulmonary TB, a raised C-reactive protein level may be seen in up to 85% of patients and elevated erythrocyte sedimentation rate in up to 79% of patients (Breen et al. 2008). In advanced disease, non-specific laboratory findings such as normocytic normochromic anemia (Nandennavar et al. 2011), leukopenia and neutropenia (Singh et al. 2001), or hyponatremia (Lee and Ho 2010) may be found. The application of auxiliary tests such as the tuberculin skin test (TST) and interferon-gamma release assay (IGRA) is sometimes used in patients with suspicion of tuberculous infection. IGRAs consist of the commercially available QuantiFERON-TB assay and the T-SPOT.TB assay. Both TST and IGRA measure immune sensitization to mycobacterial protein antigens that may result from prior exposure. It is important to recognize their limitations, including their inability to distinguish between active and latent TB infection (Metcalfe et al. 2011; Sester et al. 2011). Both TST and IGRA should therefore not be used to diagnose active TB infection, which typically entails microbiological analysis of bodily specimens.

2.4 Imaging

Imaging plays a vital role in the diagnosis of both active and latent pulmonary TB. Chest radiography is the initial radiological investigation for patients with suspected pulmonary TB. The combination of chest radiography and clinical correlation has been reported to possess a 100% sensitivity and negative predictive value for excluding TB (World Health Organization 2018). Classical findings suggestive of active primary TB infection on a chest radiograph are consolidation, pleural effusion, mediastinal lymphadenopathy, and miliary nodules (Burrill et al. 2007). Radiographical signs of reactivation TB are consolidation with a predilection for apical and posterior segments of upper lobes, cavitation, and nodules (Leung 1999). Radiographical features such as stable fibronodularities, scarring, calcified granulomas and lymph nodes are suggestive of inactive pulmonary TB (Nachiappan et al. 2017).

The use of thoracic computed tomography (CT) offers higher sensitivity than chest radiography in evaluating parenchymal disease, mediastinal lymphadenopathy, and miliary TB (Skoura et al. 2015). Improved characterization of pulmonary lesions on CT, compared to chest radiographs, also allows exclusion of potential mimics such as malignancy. Given the concentration of activated macrophages and lymphocytes in active tuberculous lesions, the employment of ^{18}F-fluorodeoxyglucose positron-emission tomography (^{18}F-FDG PET)/CT to highlight these areas of high glucose utilization has been proposed to better delineate disease sites and monitor treatment response (Heysell et al. 2013). However, no consensus regarding the routine application of ^{18}F-FDG PET/CT in TB has been reached.

The radiological work-up of extrapulmonary TB relies largely on targeted imaging based on clinical suspicion of the anatomical organ involved in the disease. Cross-sectional imaging modalities, such as ultrasound imaging, CT, and magnetic resonance imaging (MRI), are usually used. Assessment of the head and neck, thorax, abdomen, and pelvis is commonly done by contrast-enhanced CT. Contrast-enhanced MRI is useful in evaluating the central nervous system, spine, and musculoskeletal system. Many extrapulmonary lesions share commonalities with other infective lesions, such as tuberculous spondylitis, which has similar imaging features with brucellosis, or tuberculous peritonitis, which may be mistaken for mesothelioma and other forms of nontuberculous peritonitis. Although many non-specific imaging features of TB exist, some "classic" imaging features suggestive of TB infection have been described, e.g., Fleischner sign representing thickening of ileocecal valve

lips and narrowing of the terminal ileum indicative of ileocecal TB (Balthazar et al. 1990).

3 Sputum and Organ-Specific Specimens

While biochemical and radiological examinations represent an important component of the initial work-up of TB, microbiological investigations play a key role in establishing a definitive diagnosis of TB. Histopathological features of tuberculous granulomas such as caseous necrosis, epithelioid macrophages, Langhans giant cells, and lymphocytes can serve to strongly support the diagnosis of TB but are not pathognomonic (Lewinsohn et al. 2017). Sputum sampling remains the reference standard for diagnosing pulmonary TB. The three commonly used sputum tests are acid-fast bacilli (AFB) smear, AFB culture, and molecular testing (also known as nucleic acid amplification test [NAAT]). AFB smear examination involves direct microscopic visualization of AFB in stained sputum smears and is widely accepted as the most cost-effective and rapid test. AFB culture is widely available for determining TB infection. However, it requires isolation of AFB on culture media, which may take up to 8 weeks. Molecular methods, the most sensitive tool, allow detection of *M. tuberculosis* DNA traces and further characterize mutations associated with drug resistance. The sensitivities of these three tests show considerable variation, with AFB smear (3 sets), AFB culture, and molecular testing being 72%, 85%, and 95%, respectively. In addition, all three tests have similar specificities of 95–98% (Nachiappan et al. 2017).

Under current guidelines for obtaining clinical specimens, sputum collection can be performed by spontaneous coughing or induction with at least 5 ml per specimen (Lewinsohn et al. 2017). Two consecutive sputum samples separated by intervals of at least 8 h are recommended and have the potential to detect more than 95% of sputum smear and culture-positive cases (World Health Organization 2007). When the initial two sputum specimens are negative, a third specimen has shown to increase detection by only an additional 3.1% (Caulfield and Wengenack 2016). The use of bronchoscopy with bronchoalveolar lavage and brushings can be offered in specific circumstances such as repeat unsuccessful attempts in expectoration of sputum, sputum induction, or previously negative sputum studies with high suspicion for TB infection (Lewinsohn et al. 2017). Gastric aspirates for retrieval of sputum specimens can also be performed in children, if clinically indicated (Somu et al. 1995). While not routine, attempts of gastric lavage have been performed for adult patients who are unable to expectorate (Aslam et al. 2017). In smear-negative patients, transbronchial biopsy has been shown to provide histopathological findings suggestive of pulmonary TB in 42–63% of patients (Lewinsohn et al. 2017).

The collection of tissue or bodily fluid samples for the diagnosis of extrapulmonary TB allows for both microbiological and histopathological studies. Common examples include pleural or peritoneal fluid, cerebrospinal fluid, joint effusions, and tissue obtained from various infected organs. These extrapulmonary specimens are subjected to similar microbiological processes as sputum samples to achieve a definitive diagnosis of TB. Accuracy studies indicate that histopathological examination has a sensitivity of 69–97% in pleural tissue, 79–100% in peritoneal tissue, 73–100% in pericardial tissue, and 86–94% in urological tissue (Lewinsohn et al. 2017).

4 Diagnostic Algorithms

Given the diverse presentations and manifestations of TB, a systematic approach is paramount for making the diagnosis and enabling prompt treatment. These diagnostic algorithms feature elements from available guidelines, protocols (Lewinsohn et al. 2017; Nachiappan et al. 2017), as well as our experience in diagnosing and treating patients with TB. The first diagnostic

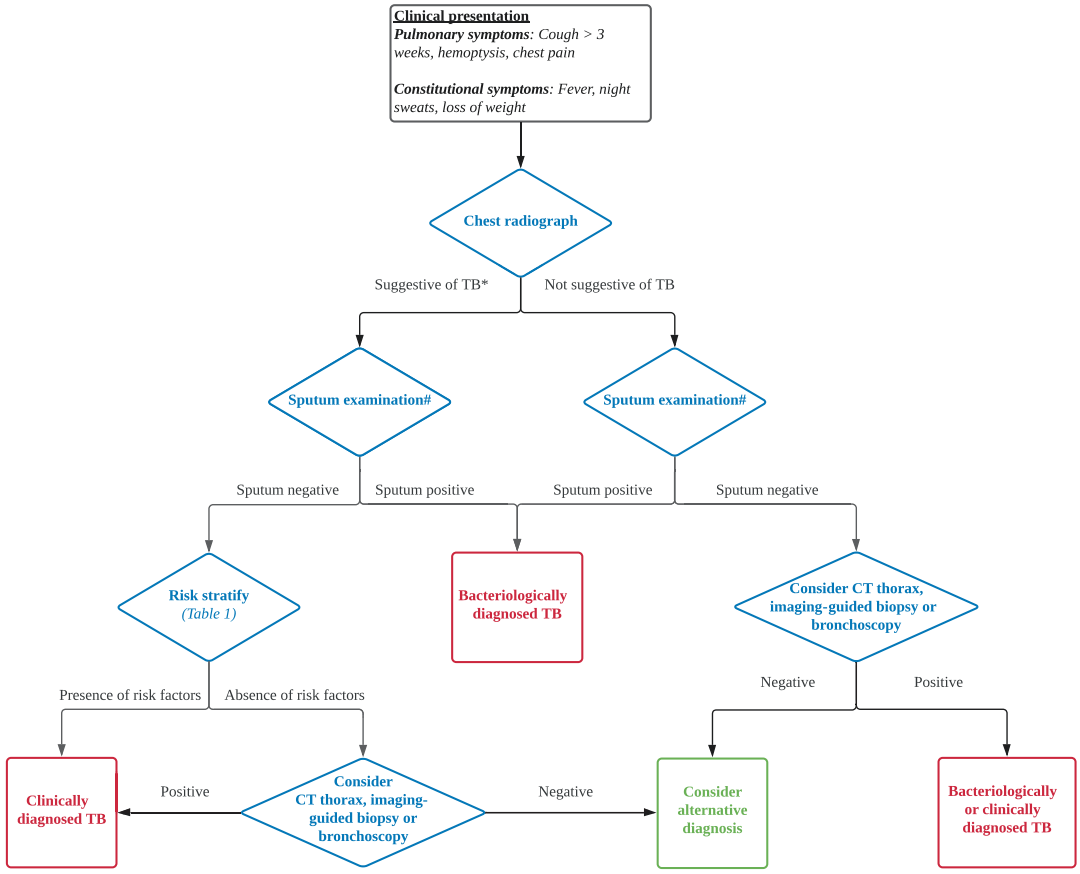

Fig 1 Symptomatic pulmonary TB. *Characteristic radiographical features: consolidation, cavitation, lymphadenopathy, miliary nodules. #2–3 AFB smears and cultures with at least 1 nucleic acid amplification test

algorithm (Fig. 1) is for patients presenting with signs and symptoms of pulmonary TB, while the second (Fig. 2) caters to patients with signs or symptoms of extrapulmonary TB. The third (Fig. 3) is a diagnostic algorithm for asymptomatic patients suspected to have latent TB. These flowcharts aim to classify all patients suspected to have TB into one of the four diagnostic categories: bacteriologically diagnosed TB, clinically diagnosed TB, latent TB, or consideration of an alternative diagnosis.

4.1 Symptomatic Pulmonary Tuberculosis (Fig. 1)

When a patient presents with pulmonary and constitutional symptoms, initial evaluation with chest radiography and sputum examination that includes 2–3 AFB smears and cultures with at least one NAAT should be performed. A chest radiograph with features suggestive of TB and a positive AFB smear or NAAT would confirm the diagnosis of TB (Ryu 2015). In the scenario where sputum AFB smears are negative and the chest radiograph features are suggestive of TB, the patient can be treated as clinically diagnosed TB with the presence of risk factors or if located in a TB-endemic region. If clinically uncertain, further imaging of pulmonary lesion(s) helps clinicians to risk stratify and guide the next step of management. For example, thoracic CT is useful, compared with radiographs, to detect subtle pulmonary findings such as centrilobular nodules and tree-in-bud opacities that could suggest TB. Imaging-guided biopsy or bronchoscopy with bronchoalveolar lavage could be used to obtain

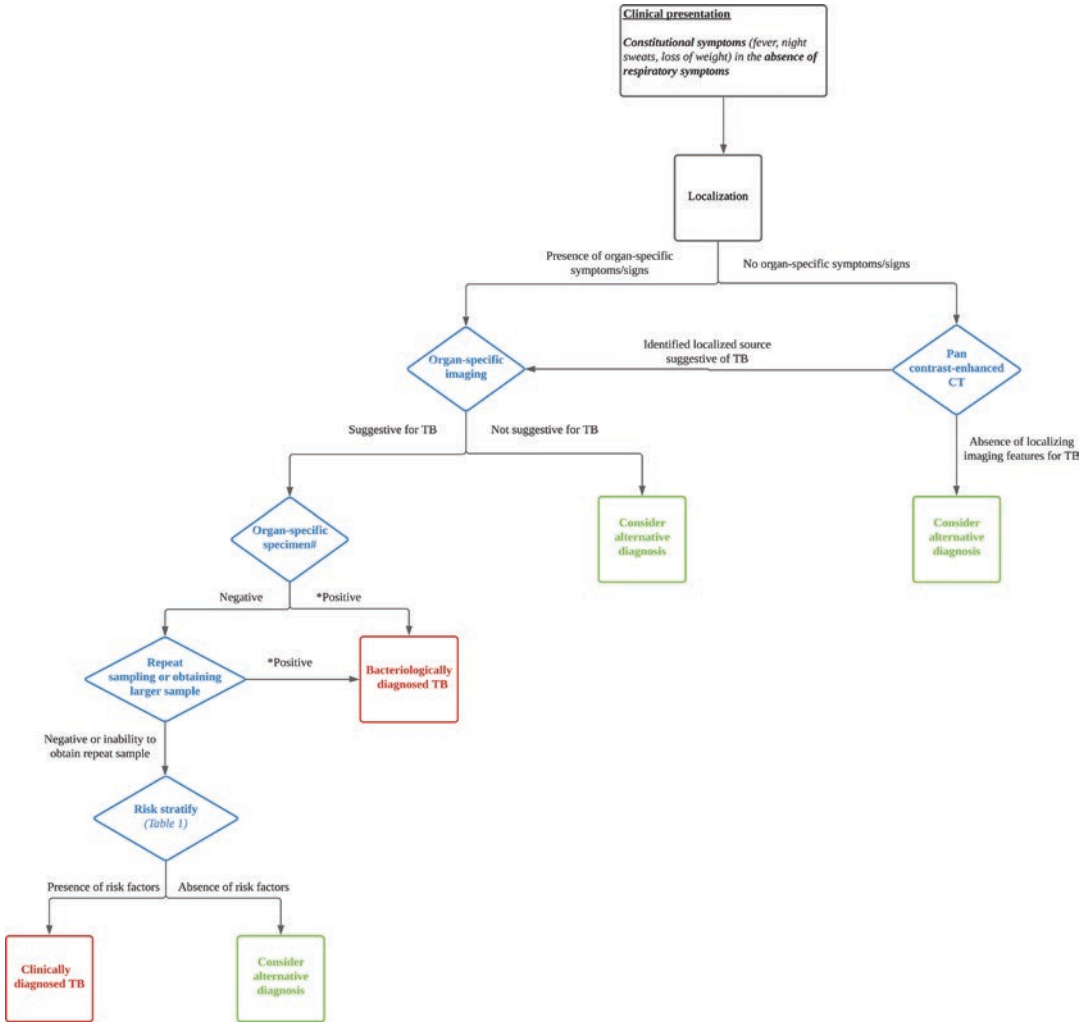

Fig 2 Symptomatic extrapulmonary TB. #Examples of organ-specific specimens include CSF (for CNS), peritoneal fluid (for abdomen), urine (for urogenital), tissues (for solid organs). *AFB smears and cultures, nucleic acid amplification tests

respiratory specimens for AFB smear, AFB culture, NAAT, and histological examination to guide the treatment decision.

4.2 Symptomatic Extrapulmonary Tuberculosis (Fig. 2)

It is not uncommon for patients with extrapulmonary TB to present with constitutional symptoms of prolonged fever, night sweats, and weight loss without respiratory symptoms. Despite this it is still recommended to look for concomitant pulmonary TB, which could be present in up to 50% of cases (Parimon et al. 2008). The imaging modalities of choice are dependent on the suspected organ system of involvement. While there are a wide variety of imaging options, contrast-enhanced CT or MRI is the most common modality of choice. "Pan-CT" (CT covering the thorax, abdomen, and pelvis) is usually used to identify the site of involvement in cases without localizing signs or symptoms. Once the site of involvement is determined, direct or imaging-guided sampling of fluid or tissue of the affected site is useful for arriving at a bacteriological and clinical diagnosis of TB.

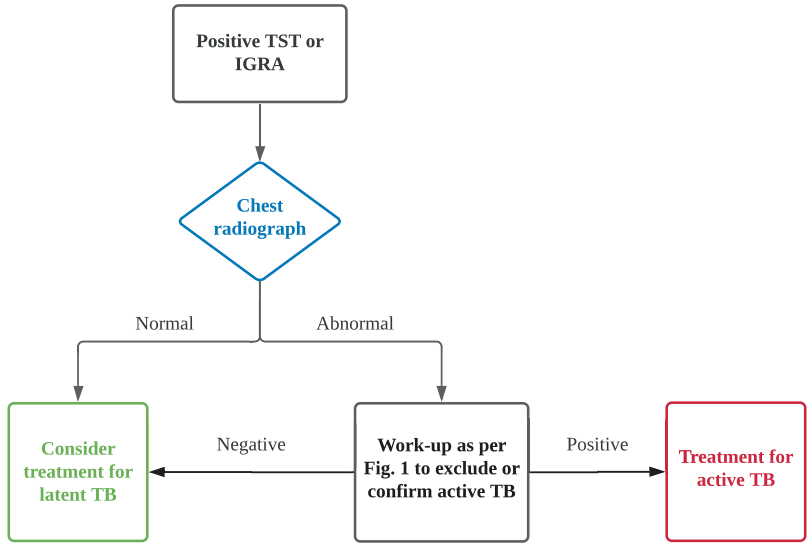

Fig 3 Asymptomatic (latent) TB

Lack of or too few bacilli in clinical samples could limit the yield of diagnostic tests in extrapulmonary TB. Repeated sampling or obtaining a larger sample has been shown to increase the yield of diagnostic tests in meningeal TB and pleural TB (Heemskerk et al. 2018; Ko et al. 2017). In the scenario where the site of involvement is inaccessible for sampling or initial diagnostic tests are negative, a clinical diagnosis of TB could be made if epidemiological and clinical features are consistent with TB. On the contrary, in the absence of a risk factor, alternative diagnoses should be considered.

4.3 Asymptomatic (Latent) Tuberculosis (Fig. 3)

TST or IGRA is commonly used as a diagnostic test for latent TB, including for PLHIV. These tests are usually performed in asymptomatic individuals with possible TB exposure or before receiving immunosuppressive therapy. A negative IGRA excludes latent TB (Klautau et al. 2018). A positive TST or IGRA should involve work-up to exclude active TB, most commonly pulmonary TB, by chest radiography. Further investigations involving sputum examination or imaging may be warranted if active TB cannot be excluded.

5 Conclusion

Patients with TB present with a diverse range of possible disease manifestations and clinical features. A high index of clinical suspicion with an understanding of the various permutations of this infection is required for the diagnosis and optimal care of these patients. The guidance provided by diagnostic algorithms allows for a structured approach to effectively diagnose and manage patients infected with TB.

References

Aslam W, Tahseen S, Schomotzer C et al (2017) Gastric specimens for diagnosing tuberculosis in adults unable to expectorate in Rawalpindi, Pakistan. Public Health Action 7:141–146

Balthazar EJ, Gordon R, Hulnick D (1990) Ileocecal tuberculosis: CT and radiologic evaluation. AJR Am J Roentgenol 154:499–503

Bates MN, Khalakdina A, Pai M et al (2007) Risk of tuberculosis from exposure to tobacco smoke: a systematic review and meta-analysis. Arch Intern Med 167:335–342

Boelaert JR, Vandecasteele SJ, Appelberg R et al (2007) The effect of the host's iron status on tuberculosis. J Infect Dis 195:1745–1753

Breen RA, Leonard O, Perrin FM et al (2008) How good are systemic symptoms and blood inflammatory markers at detecting individuals with tuberculosis? Int J Tuberc Lung Dis 12:44–49

Burrill J, Williams CJ, Bain G et al (2007) Tuberculosis: a radiologic review. Radiographics 27:1255–1273

Canine C, Medeck S, Hackett A (2019) Delayed diagnosis of spinal tuberculosis in a 44-year-old male with acute on chronic low back pain. Clin Pract Cases Emerg Med 3:107–111

Caulfield AJ, Wengenack NL (2016) Diagnosis of active tuberculosis disease: from microscopy to molecular techniques. J Clin Tuberc Other Mycobact Dis 4:33–43

Cek M, Lenk S, Naber KG et al (2005) EAU guidelines for the management of genitourinary tuberculosis. Eur Urol 48:353–362

Chow KM, Chow VC, Hung LC et al (2002) Tuberculous peritonitis-associated mortality is high among patients waiting for the results of mycobacterial cultures of ascitic fluid samples. Clin Infect Dis 35:409–413

de Lima Corvino DF, Shrestha S, Kosmin AR (2021) Tuberculosis screening. In: StatPearls (Internet). StatPearls Publishing, Treasure Island, FL. https://www.ncbi.nlm.nih.gov/books/NBK448205/

Edwards LB, Livesay VT, Acquaviva FA et al (1971) Height, weight, tuberculous infection, and tuberculous disease. Arch Environ Health 22:106–112

Figueiredo AA, Lucon AM, Srougi M (2017) Urogenital tuberculosis. Microbiol Spectr 5(1). https://doi.org/10.1128/microbiolspec.TNMI7-0015-2016

Guelar A, Gatell JM, Verdejo J et al (1993) A prospective study of the risk of tuberculosis among HIV-infected patients. AIDS 7:1345–1349

Haas DW, Des Prez RM (1994) Tuberculosis and acquired immunodeficiency syndrome: a historical perspective on recent developments. Am J Med 96:439–450

Heemskerk AD, Donovan J, Thu DDA et al (2018) Improving the microbiological diagnosis of tuberculous meningitis: a prospective, international, multicentre comparison of conventional and modified Ziehl-Neelsen stain, GeneXpert, and culture of cerebrospinal fluid. J Infect 77:509–515

Heysell SK, Thomas TA, Sifri CD et al (2013) 18-Fluorodeoxyglucose positron emission tomography for tuberculosis diagnosis and management: a case series. BMC Pulm Med 13:14. https://doi.org/10.1186/1471-2466-13-14

Hussein MM, Mooij JM, Roujouleh H (2003) Tuberculosis and chronic renal disease. Semin Dial 16:38–44

Jones BE, Young SM, Antoniskis D et al (1993) Relationship of the manifestations of tuberculosis to CD4 cell counts in patients with human immunodeficiency virus infection. Am Rev Respir Dis 148:1292–1297

Klautau GB, da Mota NVF, Salles MJC et al (2018) Interferon-γ release assay as a sensitive diagnostic tool of latent tuberculosis infection in patients with HIV: a cross-sectional study. BMC Infect Dis 18:585

Ko Y, Song J, Lee SY et al (2017) Does repeated pleural culture increase the diagnostic yield of Mycobacterium tuberculosis from tuberculous pleural effusion in HIV-negative individuals? PLoS One 12(7). https://doi.org/10.1371/journal.pone.0181798

Lee P, Ho KK (2010) Hyponatremia in pulmonary TB: evidence of ectopic antidiuretic hormone production. Chest 137:207–208

Leung AN (1999) Pulmonary tuberculosis: the essentials. Radiology 210:307–322

Lewinsohn DM, Leonard MK, LoBue PA et al (2017) Official American Thoracic Society/Infectious Diseases Society of America/ Centers for Disease Control and Prevention Clinical Practice Guidelines: diagnosis of tuberculosis in adults and children. Clin Infect Dis 64:e1–e33

Lin HH, Ezzati M, Chang HY et al (2009) Association between tobacco smoking and active tuberculosis in Taiwan: prospective cohort study. Am J Respir Crit Care Med. 180:475-480

Lonnroth K, Williams BG, Stadlin S et al (2008) Alcohol use as a risk factor for tuberculosis—a systematic review. BMC Public Health 8:289. https://doi.org/10.1186/1471-2458-8-289

Macfarlane JT, Ibrahim M, Tor-Agbidye S (1979) The importance of finger clubbing in pulmonary tuberculosis. Tubercle 60:45–48

Marks SM, Taylor Z, Qualls NL et al (2000) Outcomes of contact investigations of infectious tuberculosis patients. Am J Respir Crit Care Med 162:2033–2038

Metcalfe JZ, Everett CK, Steingart KR et al (2011) Interferon-gamma release assays for active pulmonary tuberculosis diagnosis in adults in low- and middle-income countries: systematic review and meta-analysis. J Infect Dis 204:S1120–S1129

Nachiappan AC, Rahbar K, Shi X et al (2017) Pulmonary tuberculosis: role of radiology in diagnosis and management. Radiographics 37:52–72

Nandennavar M, Cyriac S, Krishnakumar et al (2011) Immune hemolytic anemia in a patient with tuberculous lymphadenitis. J Glob Infect Dis 3:89–91

Pablos-Mendez A, Blustein J, Knirsch CA (1997) The role of diabetes mellitus in the higher prevalence of tuberculosis among Hispanics. Am J Public Health 87:574–579

Pai M, Nicol MP, Boehme CC (2016) Tuberculosis diagnostics: state of the art and future directions. Microbiol Spectr 4(5). https://doi.org/10.1128/microbiolspec.TBTB2-0019-2016

Palmer CE, Jablon S, Edwards PQ (1957) Tuberculosis morbidity of young men in relation to tuberculin sensitivity and body build. Am Rev Tuberc 76:517–539

Pang P, Duan W, Liu S et al (2018) Clinical study of tuberculosis in the head and neck region-11 years' experience and a review of the literature. Emerg Microbes Infect 7:4. https://doi.org/10.1038/s41426-017-0008-7

Parimon T, Spitters CE, Muangman N et al (2008) Unexpected pulmonary involvement in extrapulmonary tuberculosis patients. Chest 134:589–594

Peto HM, Pratt RH, Harrington TA et al (2009) Epidemiology of extrapulmonary tuberculosis in the United States, 1993-2006. Clin Infect Dis 49:1350–1357

Poulsen A (1957) Some clinical features of tuberculosis. Acta Tuberc Scand 33:37–92

Rao VG, Bhat J, Yadav R et al (2014) Tobacco smoking: a major risk factor for pulmonary tuberculosis—evidence from a cross-sectional study in central India. Trans R Soc Trop Med Hyg 108: 474–481

Raviglione MC, Narain JP, Kochi A (1992) HIV-associated tuberculosis in developing countries: clinical features, diagnosis, and treatment. Bull World Health Organ 70:515–526

Rock RB, Olin M, Baker CA et al (2008) Central nervous system tuberculosis: pathogenesis and clinical aspects. Clin Microbiol Rev 21:243–261

Ryu YJ (2015) Diagnosis of pulmonary tuberculosis: recent advances and diagnostic algorithms. Tuberc Respir Dis 78:64–71

Selwyn PA, Hartel D, Lewis VA et al (1989) A prospective study of the risk of tuberculosis among intravenous drug users with human immunodeficiency virus infection. N Engl J Med 320:545–550

Sester M, Sotgiu G, Lange C et al (2011) Interferon-gamma release assays for the diagnosis of active tuberculosis: a systematic review and meta-analysis. Eur Respir J 37:100–111

Singh KJ, Ahluwalia G, Sharma SK et al (2001) Significance of haematological manifestations in patients with tuberculosis. J Assoc Physicians India 49:790–784

Skoura E, Zumla A, Bomanji J (2015) Imaging in tuberculosis. Int J Infect Dis 32:87–93

Somu N, Swaminathan S, Paramasivan CN et al (1995) Value of bronchoalveolar lavage and gastric lavage in the diagnosis of pulmonary tuberculosis in children. Tuber Lung Dis 76:295–299

Taylor Z, Marks SM, Rios Burrows NM et al (2000) Causes and costs of hospitalization of tuberculosis patients in the United States. Int J Tuberc Lung Dis 4:931–939

Taylor Z, Nolan CM, Blumberg HM et al (2005) Controlling tuberculosis in the United States. Recommendations from the American Thoracic Society, CDC, and the Infectious Diseases Society of America. MMWR Recomm Rep 54:1–81

Teweldemedhin M, Asres N, Gebreyesus H et al (2018) Tuberculosis-human immunodeficiency virus (HIV) co-infection in Ethiopia: a systematic review and meta-analysis. BMC Infect Dis 18:676. https://doi.org/10.1186/s12879-018-3604-9

Weisberg LA (1984) Granulomatous diseases of the CNS as demonstrated by computerized tomography. Comput Radiol 8:309–317

Wondimeneh Y, Muluye D, Belyhun Y (2012) Prevalence of pulmonary tuberculosis and immunological profile of HIV co-infected patients in Northwest Ethiopia. BMC Res Notes 5:331. https://doi.org/10.1186/1756-0500-5-331

World Health Organization (2007) Proposed reduction of number of smears for the diagnosis of pulmonary TB: background document. World Health Organization, Geneva. https://www.who.int/tb/laboratory/reduction_of_smears.pdf?ua=1

World Health Organization (2018) Latent tuberculosis infection: updated and consolidated guidelines for programmatic management. World Health Organization, Geneva, pp 1–64. https://www.who.int/tb/publications/2018/latent-tuberculosis-infection/en/

World Health Organization (2020a) The top 10 causes of death. World Health Organization. https://www.who.int/news-room/fact-sheets/detail/the-top-10-causes-of-death; https://apps.who.int/iris/bitstream/handle/10665/336069/9789240013131-eng.pdf

World Health Organization (2020b) Definitions and reporting framework for tuberculosis—2013 revision. Updated December 2014 and January 2020. World Health Organization, Geneva, p 3. https://apps.who.int/iris/handle/10665/79199

World Health Organization (2021) Global tuberculosis report 2021. World Health Organization, Geneva, p 1. https://www.who.int/teams/global-tuberculosis-programme/tb-reports/global-tuberculosis-report-2021

Zumla A, Malon P, Henderson J et al (2000) Impact of HIV infection on tuberculosis. Postgrad Med J 76:259–268